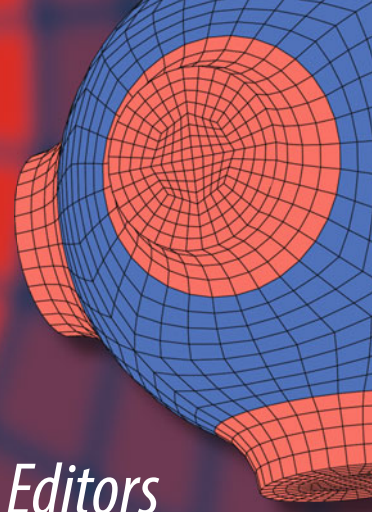Jiří Militký
Mohanapriya Venkataraman   *Editors*

Advanced Multifunctional Materials from Fibrous Structures

Springer

Advanced Structured Materials

Volume 201

Series Editors

Andreas Öchsner, Faculty of Mechanical Engineering, Esslingen University of Applied Sciences, Esslingen, Germany

Lucas F. M. da Silva, Department of Mechanical Engineering, Faculty of Engineering, University of Porto, Porto, Portugal

Holm Altenbach , Faculty of Mechanical Engineering, Otto von Guericke University Magdeburg, Magdeburg, Sachsen-Anhalt, Germany

Common engineering materials are reaching their limits in many applications, and new developments are required to meet the increasing demands on engineering materials. The performance of materials can be improved by combining different materials to achieve better properties than with a single constituent, or by shaping the material or constituents into a specific structure. The interaction between material and structure can occur at different length scales, such as the micro, meso, or macro scale, and offers potential applications in very different fields.

This book series addresses the fundamental relationships between materials and their structure on overall properties (e.g., mechanical, thermal, chemical, electrical, or magnetic properties, etc.). Experimental data and procedures are presented, as well as methods for modeling structures and materials using numerical and analytical approaches. In addition, the series shows how these materials engineering and design processes are implemented and how new technologies can be used to optimize materials and processes.

Advanced Structured Materials is indexed in Google Scholar and Scopus.

Jiří Militký · Mohanapriya Venkataraman
Editors

Advanced Multifunctional Materials from Fibrous Structures

 Springer

Editors
Jiří Militký
Department of Material Engineering
Faculty of Textile Engineering
Technical University of Liberec
Liberec, Czech Republic

Mohanapriya Venkataraman
Department of Material Engineering
Faculty of Textile Engineering
Technical University of Liberec
Liberec, Czech Republic

Preface

Fibrous materials are very important for present-day society and the society of the future, as they offer sustainable solutions to a number of practical problems by using lightweight, porous and flexible structures with plenty of special effects. Examples include electrical conductivity, EMI shielding, optical transmittance, strength and toughness, non-flammability, etc. All of these functional soft structures are related to the internal structure and macro structure of fibrous materials. The structural properties of materials include their chemical composition, local configurations of polymer chains and their arrangement into microstructures. The science of fibrous materials is therefore a broad area and can be considered an interdisciplinary field. It includes the study of the structure and properties of fibrous material, the creation of new types of materials and the design of material properties to suit the needs of specific applications.

The basis of the methodology of development of functional fibrous materials is a combination of fibers and their surface modifications, coatings and possibly a combination of different phases in a multicomponent fibrous system to achieve the desired effects. An important part are the physical properties of the fibrous materials, which usually play an important role in selecting a material for a particular application. Methods of design, modeling, simulation, prediction, evaluation, processing and production are also investigated. Research in this area uses a number of advanced methods of material characterization such as special microscopy, dynamic mechanical analysis, optoelectronic measurements, thermogravimetric analysis, FTIR, etc.

This book contains selected results and critical reviews of the TUL group of researchers focused in a broader context on the issue of materials engineering of fibrous materials focused on use of wastes and nanotechnology. Current trends in processing, microstructure and properties of materials in fibrous form with wide application for textile-oriented and technically oriented products are included. Emphasis is placed on the description of the physical and chemical nature of the processes describing the behavior and properties of the investigated materials. The chapters describing the state and expected trends in selected areas summarize not only the published works but also the results themselves and the critical evaluation

and generalization of basic knowledge. Most chapters contain the original results obtained by this group in recent years. In addition to the preparation of materials with new effects, attention is focused on the development of new measuring principles, the construction special devices and broad metrological aspects. Research activities cover all types of fibers with a clear shift towards synthetic and specialty fibers for non-clothing applications. This is in line with the current development trend in the field of high-performance materials, mainly for use as reinforcement in various composites and functional fibrous structures for smart textiles. The area of fibrous materials covered in this book is indeed very large. Compressing the basic available information in a reasonable space was therefore a difficult task. The goal in writing this book was to provide broad area of different results so that the book is suitable for anyone who is generally interested in fibrous materials and their applications for various purposes. The authors provided enough critical references to the original literature and review articles to guide readers with a particular interest in any particular area.

Contributors of the chapters in this book have a number of special knowledges in the advanced use of fibrous materials. Therefore, this book is partly interdisciplinary and also focused on the unique peculiarities of textile materials. This book is intended primarily for readers with experience in materials science, applied sciences, and product engineering in general and the textile industry in particular. The authors and editors believe that the book will also be of interest to university students, teachers and researchers who are interested in the fields of fibrous materials science, engineering and technology, and specifically in advanced materials, polymer composites, nanomaterials, biomaterials and functional materials. As it deals with many basic concepts that are of interest in their respective fields, this book can also be used as a basis for the study of materials science and engineering.

The topics covered in the book describe the latest broader or general knowledge in specific areas related to the use of fibrous materials. At the same time, there is ample evidence of previous research in this area by other researchers from around the world. The primary focus is on designing materials at the molecular level to achieve desirable properties and applications at the macroscopic level. With this broad focus, research ranges from basic scientific research into the interactions, properties, and assembly of such molecular components to applied engineering efforts that translate this basic information into futuristic technological advances. Much of the research results are highly interdisciplinary and are intended for various specialists in chemistry, biochemistry, materials science, engineering, biology and medicine.

The authors of the individual chapters are researchers and doctoral students mainly from the Department of Materials Engineering, Faculty of Textiles, Technical University of Liberec.

Liberec, Czech Republic   Jiří Militký
2023   Mohanapriya Venkataraman

Outline

Fibrous materials are very promising for the development of society, as they offer effective solutions to several practical problems using lightweight, porous and flexible materials. Examples include flexibility, thermal properties electrical conductivity, EMI shielding, optical transmittance, strength and toughness, non-flammability, etc. All these functional soft materials are related to the internal structure and macrostructure of fibrous materials. The structural properties of materials include their chemical composition, local configurations of polymer chains, and their arrangement into microstructures. The science of fibrous materials is therefore a broad area and can be considered an interdisciplinary field. It includes the study of the structure and properties of fibrous material, the creation of new types of materials, and the design of material properties to suit the needs of specific applications.

This book is focused on the description of some aspects of processing, microstructure, and properties of materials in fibrous form, or from fibres, with wide application for textile-oriented and technically oriented advanced products. Emphasis is placed on the description of the physical and chemical nature of the processes describing the behaviour and properties of the investigated materials. The chapters describing the state and expected trends in selected areas summarize not only the published works but also the original results and the critical evaluation and generalization of basic knowledge. In addition to the preparation of materials with new effects, attention is focused on the development of new testing principles, the construction of special devices, and metrological aspects. Research activities cover all types of fibres with a clear shift towards synthetic and specialty fibres for non-clothing applications. This is in line with the current development trend in the field of high-performance fibres, mainly for use as reinforcement in various composite materials and functional fibres for smart textiles. The area of fibrous materials covered in this book is indeed very large. Compressing the basic available information in a reasonable space was therefore a difficult task. The goal in writing this book was to provide a broad area

of different results so that the book is suitable for anyone who is generally interested in fibrous materials and their applications for various purposes. The authors provided enough critical references to the original literature and review articles to guide readers with a particular interest in any area.

Contents

Chapter 1
Flexible Electrically Conductive Elastomers

Azam Ali, Muhammad Faisal Nadeem, Muhammad Zaman Khan, Mohanapriya Venkataraman, Sajida Perveen, Sundaramoorthy Palanisamy, and Jiří Militký

Abstract Since new technology domains including intelligent robotics, wearable gadgets, stretchable electronics, and body-conformable systems have developed, the demand for stretchable products has been increasing significantly. For the manufacturing of such kind of composite, several rubbers and conductive polymers including ethylene–propylene–diene monomer (EPDM), nitrile, and butyl, natural are extensively applied. The present study deals with the development of electrically conductive polymers by using non-conductive rubbers and fillers. Conductive fillers including expanded graphite, carbon, carbon nano tubes, metal powders, carbon fibres, graphite, and others are used to make such rubber materials conductive. The developed materials deal with good elasticity or stretch ability as well as electrical conductivity. The low mechanical characteristics of these materials limit their widespread application. The most novel applications of developed polymers are stretchable sensors such as temperature sensors, pressure sensors and strain sensors.

1.1 Introduction

An elastomer is a material that exhibits large and rapid reversible strain under applied stress (Visakh et al. 2013). It can be distinguished from the material which possesses elastic response, a feature of various materials. The elastic response occurs where there is a proportionality relation between stress and strain based on Hooke's Law,

A. Ali · M. Z. Khan · M. Venkataraman · S. Perveen · S. Palanisamy · J. Militký (✉)
Department of Material Engineering, Faculty of Textile Engineering, Technical University of Liberec, Studentská 2, 46117 Liberec, Czech Republic
e-mail: jiri.militky@tul.cz

M. Venkataraman
e-mail: mohanapriya.venkataraman@tul.cz

M. F. Nadeem
Institute of Pharmaceutical Sciences, University of Veterinary and Animal Sciences, Lahore, Pakistan

© The Author(s), under exclusive license to Springer Nature Singapore Pte Ltd. 2023
J. Militký and M. Venkataraman (eds.), *Advanced Multifunctional Materials from Fibrous Structures*, Advanced Structured Materials 201,
https://doi.org/10.1007/978-981-99-6002-6_1

Fig. 1.1 Representative
engineering stress–strain
curve of the developed PUE
material at a strain rate of
5000/s with a reference
curve showing the static
compressive data at a strain
rate of 0.001/s (Fan and
Chen 2019)
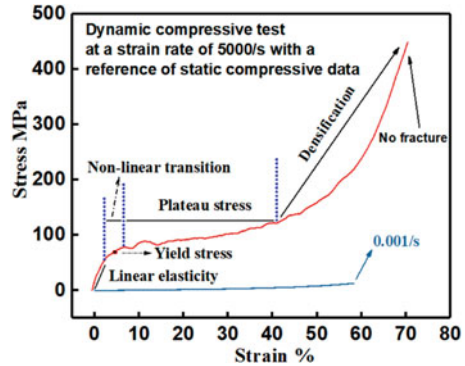
and the strain can be of a small amount like 0.001 for silicate glass. In contrast, an elastomer can exhibit a larger strain up to 5–10 and this is mostly exhibited by polymeric-based elastomers (Visakh et al. 2013; Cardarelli 2008). Using an aluminium SHPB device, dynamic compressive tests were carried out on the newly developed PUE material. The representative engineering stress–strain curve at a strain rate of 5000/s was derived to illustrate the dynamic stress–strain characteristics, as shown in Fig. 1.1. The dynamic Young's modulus refers to the initial deformation, which is linearly elastic and has a slope of approximately 1300 MPa. After that, the dynamic yield stress indicates a nonlinear transition at an intermediate stress of approximately 58 MPa. After that, a significant amount of strain is processed under plateau stress until densification and a significant stress rise occurs.

Figure 1.1 shows the stress–strain curves of co-polyether elastomer based on tetrahydrofuran and 3,3-bis(azidomethyl)oxetane at semi-crystalline phase (S0) and amorphous phase (S1). The reason for an elastic strain is stretching of the chemical bond, deformation of bond angle or crystal structure. Under strain, the bond and bond angles in elastomers are not elongated or deformed. The elastomeric stretch depends on bond rotation, which changes into dihedral angles. The unstrained elastomer exhibits random coil structure but with the increase in the strain, the uncoiling of molecules starts which changes to the linear structure. Therefore, for elastomers to be formed, there is a need for a substance which consists of macromolecules. Long molecules are required for larger strains to consider uncoiling. Whereas, the formation of random unstrained coil means that the elastomer must possess non-crystallinity since there is no contribution of regular crystalline structures into elastomeric properties (Visakh et al. 2013; Cardarelli 2008).

Elastomers being an important and unique class of polymers exhibit large and rapid reversible strains in response to applied stress. At present, researchers are focusing on the development of flexible functional structures by mixing various types of particles into elastomers. Amongst, a lot of effort is conducted to develop conductive elastomers through the incorporation of conductive fillers. Different researchers made important progress in conductive elastomers via using different types of conductive fillers. In 1493, rubber was brought firstly by Columbus from

America, however, less attention was paid to investigating the novel features of rubber for about 200 years. In 1770, it was named 'Rubber' by Joseph Priestley owing to its ability to rub out the pencil marks. Following this in the 19th century, rapid growth was observed in the technical developments and application of rubber (Klingender 2008). Thomas Hancock and Charles Macintosh introduced its application in flexible tubing, containers, waterproofing and elastic bands. With the discovery of vulcanization by Charles Goodyear's using Sulphur, it increased the durability and natural strength of rubber through cross-linking of soft gum rubber molecules into the toughest material (Cheremisinoff 1989). In contrast, technological advancement involves advanced compounding techniques which allow the utilization of accelerators and antioxidants, and carbon black incorporation for improving the strength. This leads to a widespread increase in a range of applications such as belts, seats, electrical insulators, flooring, pneumatic tyres and springs (Wankat 1994).

1.1.1 History

With the increased applications number, the demand grew rapidly for raw materials. South America especially Brazil was the major source of natural rubber till the 1900s. Afterwards, the Asian colonies in British, which used rubber trees from the seed smuggled out of the Amazon Basin, and then started competing with the traditional sources (Finch 1989). The first development of a synthetic substitute for natural rubber was witnessed during the period of World Wars I and II. The synthetic substitute includes Sodium polymerized Butadiene produced in Germany in the form of Buna rubbers and SK rubber in the USSR. In the 1930s, the emulsion co-polymerization for butadiene styrene was developed by Germany, while the major synthetic rubber in the Soviet Union remained sodium polybutadiene (Cheremisinoff 1989).

The importance of rubber was highlighted with the advent of World War II as an important raw material (Wendt 1947). When the control was gained by Axis powers of the World's overall natural rubber supplies, this leads to a fast stepping up in synthetic rubber development, especially in the USA. In 1942, the US government starts the production of SBR (styrene-butadiene) rubber, later named GR-S (Matanoski et al. 1990).Within the next three years, the fifteen SBR plants' construction was financed by the government which was helpful in the annual production of about 700,000 tons.

1.2 Fundamental Properties of Elastomers

Elastomers are complex materials that possess unique combination of excellent properties, among the most important are resilience and elasticity. All elastomers exhibit the capability to substantially deform through compression, stretching or torsion and

then after force removal, return to the original shape which causes the deformation (Smith 1963). The ability to quickly return to original shape is based on resilience which for instance enables the dynamic seal to follow changes within the sealing surface. The material's ability to return to its original size and shape after being compressed, stretched, bent or twisted is due to the reconfiguration ability of their respective long polymeric chains under the stress applied. Cross-linkages among chains make sure that the elastomer must return to its original shape upon the removal of applied stress. Due to such extreme flexibility, elastomers can extend reversibly approximately by 200–1000% which depends on the specific material used. When there is short or no cross-linkages, chains are reconfigured uneasily, then the applied stress might result in deformation permanently. The ability of elastomers to quickly return to their original shape after only temporary deflection is due to the unique property of resilience. It also indicates the recovery speed, unlike the compression set which corresponds to the recovery degree. There is an involvement of energy input when the elastomer is under deformation, where there is a part that does not return successfully to its original shape is dissipated within the elastomer as heat (Gehman 1957).

Elastomers exhibit a number of useful features like:

- Low permeability to gases, steam, water and air.
- Good thermal and electrical insulation.
- Improved mechanical properties.
- Ability to adhere to different metals, rigid plastics and fibres.

Furthermore, with proper choice of compounding constituents, products having specific or improved properties can be produced to meet a wide range of applications. This remarkable collaboration of properties is the main reason that elastomers can serve a vast variety of engineering requirements in fields that deal with shock absorption, vibration damping, sealing, thermal and electrical insulation. Mostly, the elastomers are thermosets that exhibit most of the strength after the vulcanization process, an irreversible cross-linking of the respective materials polymeric chains which occur when the compound is subjected to heat and pressure. Comparatively, thermoplastic elastomers possess weaker cross-linking and thus can be extruded, moulded and reused like plastic materials which still have the specific elastic properties of elastomers (Gehman 1957).

1.3 Types of Synthetic Rubber/Elastomers

1.3.1 Styrene-Butadiene Rubber (SBR)

Styrene-Butadiene Rubber (SBR) is used widely in the world as a synthetic elastomer. In the Germany and US, the production of SBR was set up on a larger scale during World War II. It is synthesized through the polymerization of butadiene and styrene in an emulsion or solution. The rubber can be prepared through the following methods.

- Emulsion polymerization
- Solution polymerization.

The rubber can be polymerized through solution polymerization of butadiene and styrene in hydrocarbon solvents i.e., cyclohexane or hexane using an initiator 'Butyllithium'. Solution polymerized SBR exhibit great molecular weight, reduced molecular weight distribution, and higher concentration of cis-1,4-polybutadiene (Nagata et al. 1987).

1.3.2 Polysulfide Rubber

Polysulfides are sulphur based chemical compounds with atomic chains (Foss 1960). The polysulfide polymers exhibit repeating chains containing sulphur atoms among their repetitive units. In 1929, polysulfide polymers were introduced commercially. These polymers have been utilized in different applications like adhesives, sealants or other materials. Polysulfide polymers are made through polymerization reaction of disodium polysulfides (aq.) with di or multi-halo organic compounds used commonly.

The reaction is as follows:

$$n(\mathrm{Cl-R-Cl}) + n\mathrm{Na_2S_x} \rightarrow -(\mathrm{R-S_x})n- +2n\mathrm{NaCl} \tag{1.1}$$
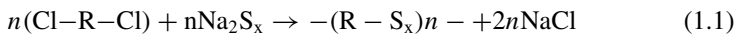
In contrast, polysulfide polymers in liquid form can be manufactured easily and then cured using different reactants. They are limited for general use as adhesives and sealants due to their expensive cost (Foss 1960).

1.3.3 Silicon Rubber (SIR)

Synthetic elastomer contains carbon, silicon, oxygen and hydrogen atoms in the polymeric form. After curing, the unreacted silicone in liquid or gel condition changes into solid. Catalysation or vulcanization can be used as curing methods for silicone. Silicon rubber vulcanizate using carbon blacks exhibit electrical conductivity of

different grades. Changes in temperature change the electrical conductivity. Mechanical properties were determined for vulcanizates like tear strength, hardness, tensile strength and elongation at break, respectively (Song et al. 2020).

1.4 Synthetic Conductive Elastomers

Rubberized materials which exhibit conductive features comes under the category of conductive rubber. They can conduct electricity in any situation and can eliminate or reduce the RFI/EMI noise (Radiofrequency interference and electromagnetic interference) often linked with electronics (Park et al. 2014). The following Fig. 1.2 is showing the embedment of conductive fillers into silica-based matrix.

Many efforts have been done to introduce electrical conductivity in synthetic rubber. Elastomers such as polyurethane (PU), poly (dimethylsiloxane) (PDMS), ethylene-propylene-diene monomer (EPDM) and styrene-butadiene rubber (SBR) exhibit low conductivity and highest reversible deformation (>200%). Traditionally, they have been used mostly for structural, home and industrial applications. Conductive additives like carbon nanotubes, graphite and carbon blacks have been employed for the conversion of rubber from insulator to conductor. This approach thus necessitates the addition of a significant filler amount which results in significant material elasticity loss, although the elasticity degradation can be lessened for elastomers based on carbon nanotubes, where the CNT conductive filtration networks can be created with only small CNTs amount. Attempts have been made by a few companies to modify the molecular structure of the elastomer for achieving strong elasticity and highest electrical conductivity at the same time. The role of the elastomer is to enhance the flexibility of materials whereas the conducting polymer contributes to the conductivity of the blend. With the increase in the fraction of conductive parts, the blend's electrical conductivity increases due to mechanical properties. To meet the required standards for specific applications, there is a need for sophisticated material design (Park et al. 2014).
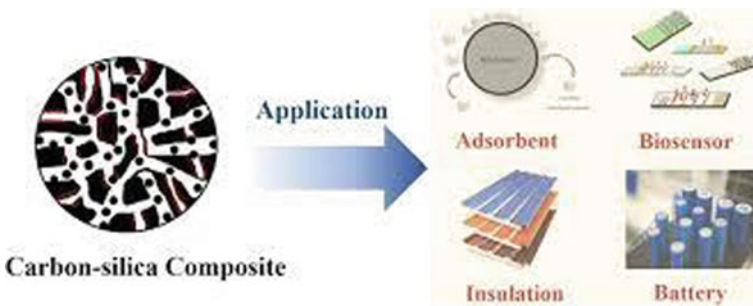
Fig. 1.2 Imbedding of conductive fillers in elastomers (Wu et al. 2022)

1.4.1 Preparation of Synthetic Conductive Based Elastomers

The conductivity of elastomers can be increased in different ways, but the methods commonly employed are.

- Addition of conductive filler into the synthetic elastomer.
- Addition of conductive material for making blends with synthetic rubber for reducing filler content.
- Coating on synthetic elastomer using a conductive material.

1.4.2 Adding Conductive Fillers into the Synthetic Elastomer

The easiest way to prepare synthetic conductive rubber is through the use of conductive fillers. Six important kinds of metallic fillers used mostly for enhanced conductivity includes silver-plated copper, silver-plated aluminium, silver, graphite plated nickel, silver plates glass and nickel aluminium. For several years, carbon black (finely divided) has been valuable addition into electrically conductive polymers which includes rubber compounds and the resultant composite materials possess a wide conductivity spectrum based on the carbon black loading. It is used for the enhancement of cost-effectiveness and conductivity. Many grades such as thermal black, channel black, acetylene black, furnace black etc. are offered from the hydrocarbon combustion of feedstocks.

The surface area and high structure of conductive carbon black help the contact probability of agglomerated carbon blacks by decreasing the distance of particle to particle. Sometimes, the hybridization of carbon black is done using carbon fibre in compounding to reach the optimized electrical conductivity, improved processability, enhanced mechanical characteristics and graphite structure exhibiting fibrous aggregate or lace-like acicular of carbon particulates. The elastomeric material exhibits the highest excellent conductivity if 70% of particles lie within 25–60 nanometric size range. Other conductive fillers include, PAN carbon fibre, carbon fibre coated with metal and Ni coated graphite fibre, aluminium fibres, stainless steel fibres, aluminium flakes, metallized glass fibres, graphite powder, metal-coated mica and glass beads (Chauhan and Bhushan 2018).

1.4.3 Adding Conductive Material for Blending to Reduce Filler Content

Rubber can be made conductive using blends. Mostly the blends used for increasing the conductivity of synthetic rubber include:

a. EPDM/NBR blend
b. HDPE/silicone rubber.

1.4.3.1   Silicone Rubber/HDPE Blend

Silicone rubber can be blended with other plastics and elastomers such as polyethylene which makes it possible to attain a needed highest electrical conductivity with decreased filler amount due to the combination of carbon black within phase among one of the polymers. By mixing polyethylene with silicone rubber, vulcanizates with good mechanical characteristics along with the highest electrical conductivity can be prepared in such a way. The feature of high chemical resistance and temperature stability are maintained within conducting vulcanizates (Zhang et al. 2001).

1.4.3.2   EPDM/NBR Blend

NBR exhibit better oil resistance but is subjective to degradation at a highest temperature where the anti-degradant is not efficient. Moreover, it is a polar rubber with fast curing as compared to EPDM. It exhibits excellent resistance towards oxygen and ozone thus improving weatherability even without the addition of antiozonants and antioxidants. EPDM/NBR blend was manufactured with the intention of generating vulcanizate having the best features of two components. Conductive fillers needed to induce conductivity to EPDM/NBR blend is very low because of selective localization of conductive filler at the interface of two constituents or in any of such phases (Botros and Tawfic 2006).

1.4.4   Coating of Conductive Material

The conductive elastomer can be coated upon its surface using resin filled with a conductive filler or a similar additive. Thus, to lower the frictional resistance on such surfaces, they may undergo UV light irradiation. The coating can be done through the application of spray or coat on the elastomer's surface. The coated elastomer can be employed like conductive rolls like development rolls, transfer rolls and charging rolls, conductive blades like blades for the formation of cleaning blades and toner layer, all of which are used in apparatus formation like electrostatic recording and electro-photographic copy machines.

1.4.5   Vulcanization by Conductive Fillers

Carbon based conductive fillers like graphite and carbon black, metallic powder like copper, nickel and silver those produced through the coating of non-conductive powder with metals like silver or metallic oxides like tin oxide and graphite. Carbon black is the preferable conductive filler as it doesn't damage any kind of photoconductive components. Graphite can be used either solely or in combined form. In a few

cases, it is preferred that electrical conductivity can be controlled using carbon black with the highest electrical conductivity and carbon black exhibit the lowest electrical conductivity in the combined form at a variable quantitative ratio (Ma et al. 2013).

Since Graphite cannot be mixed in the first step of vulcanization so it can be incorporated after the primary step of vulcanization. In contrast, the Graphite part to be added is mixed during the first step of vulcanization whereas the leftover may be incorporated additionally after the primary step. Based on these processes, the Graphite content in rubber can be improved. Similarly, in any type of process, the composition of conductive rubber includes the urethane rubber vulcanizate. Both Graphite and rubber can be attained after the first step of vulcanization. For rubber, the vulcanizing agent is incorporated within the composition to prepare conductive rubber composition. When the Graphite remainder or whole amount is added after the first step of vulcanization, then Graphite and the vulcanizing agent can be added at the same time. vulcanization can be done through kneading the rubber composition, and then shaping into the desired shape followed by its application to secondary vulcanization (formed or moulded conductive rubber product). Moreover, the conditions like heating temperature and ordinary conditions may be adopted according to the rubber type for vulcanization. Press or extrusion moulding can be utilized for shaping the composition into a desirable shape. The standard kneading process can be used for the preparation of rubber composition which contains the vulcanizing agent. By using a process like press or extrusion moulding, the composition of rubber created in this way can be either formed or moulded into the desired shape like cylindrical or plate form. The extrusion of the rubber composition is done on the peripheral surface containing a conductive blender during the manufacturing of roll covered with the conductive rubber. Vulcanization occurs on all the components of a rubber. When the conductive blade or conductive roll is produced through adopting a two-step process, then the generated rubber vulcanizate exhibit a value of electrical resistance of 10^3–10^{10} Ω in general which makes less difference in the value of electrical resistance under the condition of high humidity and temperature (35 °C). In addition, formed or moulded conductive rubber products exhibit hardness of about 20–60° using a similar two-step process (Fisher 1939).

1.5 Fillers to Impart the Electrical Conductivity in Elastomers

1.5.1 Carbon Black

Carbon Black is a stable solid formed by controlled procedures and resulted in the formation of carbon collections having different particle sizes, size, shapes, porosity and chemical surface. Typically, carbon black contains almost 95% pure carbon with oxygen, hydrogen and nitrogen present in trivial amounts (ORION Engineered Carbons 2014). During production, Carbon Black particles that range in size from 10

to 500 nm are produced. These particles blend to form chain-like aggregates, which shows the diversity of carbon black (Galli 1982) (Fig. 1.3).

In different materials, the physical, electronic and optical features are enhanced by Carbon Black. Its strengthening and performance capability is confirmed by bulk use in rubber goods. In the rubber industry, natural and synthetic elastomers are united with carbon black, sulphur, processing petroleum and different organic processing elements. The major use of Carbon Black is to enhance, the strength of tear, conductivity, and other physical attributes. Carbon Black is extensively used, low-cost (typically called Rubber Carbon Black) rubber strengthens in tire components (e.g. stranding, sidewalks and inside liner), mechanical rubber products (MRS), as well as industrial rubber products, membrane roofing, automotive rubber components (e.g. sealing systems, fins, vibration shield) and rubber goods (such as hoses, belts, gaskets and seals).

Under the electron microscope, carbon black particles appear to be a complex structure, with spherical particles. Different spherical functional groups, e.g., hydroxyl or carboxyl is the "Particle size" and known as 'surface' chemistry" if present on the black carbon surface. The basic features of carbon black are "particle size," "structure" and "surface chemistry". While combining with ink, paint or resin the practical features such as darkness and dispersibility are dependent on all three major characteristics (Gautam and Verma 2018). The diameter of the spherical particle is the basic element that mostly impacts Blackness and dispersibility while combining with resins or other carriers. Carbon blackness will be more if the size of the particle is small. However, a greater coagulation force makes dispersion difficult. Like particle sizes, structure's size also influences blackness and black dispersibility. Dispersibility is increased but darkness is reduced by the increasing structural size. There are some functional groups on a carbon black surface. Carbon black is considered good for printing inks or varnishes with a significant quantity of hydroxyl group only if the oxidation treatment and distribution are excellent. Carbon black is a major substance with extended use in history. It has been used as a colouring

agent from the days before Christ. Some carbon black uses are given below and it is a traditional yet unique material used in a new sector. The carbon black has high electrical conductivity due to its graphite-like crystalline structure. When mixed with plastic, elastomers, paints, adhesives, films and pastes carbon black acts as a lead filler such as, electrical conductivity which is also vital for preventing static fuel caps and gasoline-implementing automotive pipes (Mohammed and Simon 2006). Carbon black also provides constant strength, hence is used as an important constituent of electronic equipment related material like display, magnetic records and OA rolls. Mitsubishi Chemical has also developed carbon black having various functionalities for particular applications (Song 2017).

1.5.2 Graphene

Graphene is a wavy arrangement of carbon dioxide atoms in the form of a 2D sheet, which is atomically fine. Many desired characteristics, Mechanical force, conductivity, molecular barrier and other related things have been established (Papageorgiou et al. 2015). Consequently, a lot of research attempts were made in which graphene was assimilated to develop nano-composites based on polymers. Conversely, pure graphene was proven to be troublesome because of its complex production, low solubility rate and agglomeration interactions of van der Waals application. The molecular structure of graphite powder is shown in Fig. 1.4.

To attain benefits of graphite additionally in being the area with functional compounds comparable in structure to graphite can, in turn, be synthesized via a top-down approach using Graphite or other sources of carbon. The leads to plentiful stacking of graphite oxide layers that (GO) were obtained by the oxidation of graphite in protonating fluids (Warner et al. 2013).

Graphene has 42 Nm^{-1} breakage force, a 1,0 TPa modulus from Young, and 130,5 GPa tensile strength naturally strong. Pure monolayer graphene has thoroughly studied its mechanical properties. In Zhang et al. the fractures for graphene toughness
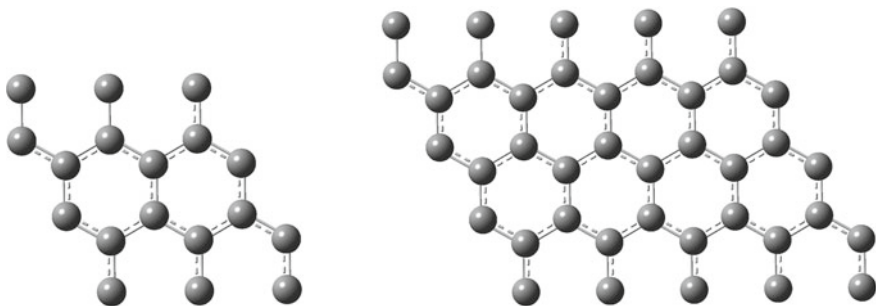

**Fig. 1.4** Molecular structure of graphite powder (Papageorgiou et al. 2015)

have also been studied revealing low graphene sheets to be 4.0 ± 0.6 MPa m1/2 fractures (Böhning et al. 2019).

Graphene is a highly mobile electrically conductive material (25 m^2 V^{-1} s^{-1}) composed of 2D layers of 1 sp2 carbohydrate thickness and an electrically conductive substance (6500 Sm-001). The electrical conductivity of low-fill polymers (e.g., 0.1 Sm-1 in polystyrene (PS) was substantially improved by Graphene with 1 volume of a percent).

The enhanced electrical features of rGO have made polymer matrices as a conducting filler a feasible material in a variety of applications. For example, Kim et al. produced extremely flexible polyaniline (PANI) super-condenser with an rGO capacity of 431 F g^{-1}. The material has maximum electricity of 24 wt. The electrical conductivity of PANI and rGO components is improved by $9.06 - 104$ Sm^{-1} per 104 Sm-1 of $5.80 - 104$ Sm-1 and $4.65 - 1$ for 103 Sm-1 for each (Chakraborty and Hashmi 2018).

1.5.3 Particulate Solids

The molecule filler has powdered materials of under 100 μm molecular size that are added to polymers for cost decrease, and improvement of handling or potentially alteration of at least one quality. Nanoparticles are those with a base one aspect inside 1–10 nm, but nanoparticles and fillers are outside the extent of this passage. Nanoparticles, metallic exfoliates in micro sizes and carbon-based particulates have been incorporated into an admixture of polymers (thermoplastics, elastomers and thermosets) from the very beginning. Indeed, the incorporation of fillers into nonconductive polymers is also a less expensive way to achieve the conductive elastomers specifically when the cost of polymeric conductive elastomers is increasing day by day. The main problem arises during the mixing of fillers into polymers, as it is necessary to achieve the homogeneous threshold for electrical conductivity. In this crucial situation, a range of different ways (suitable solvent, sonication and dispersant) have been conducted to bridge the mixing gap between the polymers and fillers (Ştiubianu et al. 2016). Checking out the commercial importance of conductive polymers where the demand and price of these polymers depend upon their stretchability, ageing and electrical conductivity. Another advantage of conductive particulate based polymers is their high electrical properties as compared to conductive polymers. When selecting the particle filler, the performance parameters for the material used must first be understood and a material is chosen or created that meets these criteria at competitive costs. There is no optimum polymer or filler; thus, the ability to mix components to enhance specific characteristics and reduce loss. In essence, by understanding the material better than its rival, the winner may make the optimal concessions (Sulaiman et al. 2019). Bloor et al. tried to make the stretchable conductive polymers by using the three different types, sizes and shapes of particles. The particles sizes and shapes were ranging from spiky micrometric-sized nickel particles (average diameter, 4.5 μm, Fig. 1.5a), to elongated multibranched copper
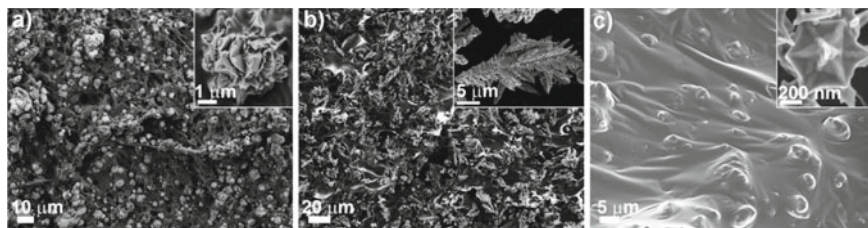
Fig. 1.5 Scanning electron microscopy images of different PDMS metal composition and nano shaped-spiky particles in the insets **a** Nickel, **b** Copper and **c** gold (Bloor et al. 2005)

ones (average diameter, 12 μm, Fig. 1.5b) up to gold nanosized stars (average diameter, 450 nm, Fig. 1.5c as shown in Fig. 1.5. He found the strong impact of shapes and size of each particle over the electrical conductivity of developed composites (Bloor et al. 2005).

1.5.4 Metallic Particle Ink

The main part of metallic design printing is the conductive ink. Various conductive materials like fine carbon powder, conductive polymers, natural/metallic precursors especially nanoparticles have been being explored for this reason (Sulaiman et al. 2019). Most driving inks are metal-based. The explanation is that their resistivity is close to that in mass (a few times more prominent) than in conductive polymers which have higher resistivity. One drawback of conductive ink is the complex procedure for its preparation. Indeed, high temperature (>250 °C) for a certain time and conductions is needed to convert the metallic precursors into organic/metallic compounds. Otherwise, the Nano dispersion can also be maintained into the inks but it is also time consumable and crucial to achieving the homogeneous suspension. The conductivity of Inks increased with an increase in viscosity of the dispersion. The main advantage of inks is highly stable on flexible structures, suitable for comfort properties, transparent facile fabricating techniques to provide a uniform electrode with bulk conductivity at mild temperatures (<100 °C) for high-performance electronic applications.

Yun et al. made highly stable silver inks for coating of highly flexible electrodes, showing conductivity of 8.2×107 S/m at 110 °C (Mou et al. 2019). In another study, Kiesar et al., reported a facial method based on an optimal chemical route to develop the viscous silver-based ink compatible with a broad range of patterning techniques such as a nozzle-jet printer and ink pen on flexible substrates (PET and PI) with low-temperature annealing at 70–100 °C (Mechanical et al. 2019). One more study was conducted to observe the annealed pattern of silver. Figures 1.1 and 1.2 show the SEM images and EDS of silver printed pattern on PET and PI substrates respectively, at 8000 mm/s nozzles moving speed and annealed at 70 °C (a1–a3), 80 °C (b1–b3),

90 °C (c1–c3) and 100 °C (d1–d3). The annealed Ag patterns are fairly smooth and uniform on both substrates. The low magnification top-view FESEM images (i.e., a1–d1 in Figs. 1.6 and 1.7) manifest the uniformly distributed and densely packed Ag nanoparticles. The high magnification top-view FESEM images (a2–d2 in Figs. 1.6 and 1.7) exhibit Ag nanoparticles grown compactly, having some voids which were formed due to the quick evaporation of low boiling point ligands. Ag NPs of different sizes were formed; the smaller ones fill up the voids to form a compact layer. The composition of the annealed Ag patterns was examined by EDS spectra analysis (a3–d3 in Figs. 1.6 and 1.7) which confirm that the annealed samples at different temperatures contain mainly silver phase with ~2 wt% carbon, which might be contributed from the substrate or the adhesive material (2% HEC) (Mechanical et al. 2019).
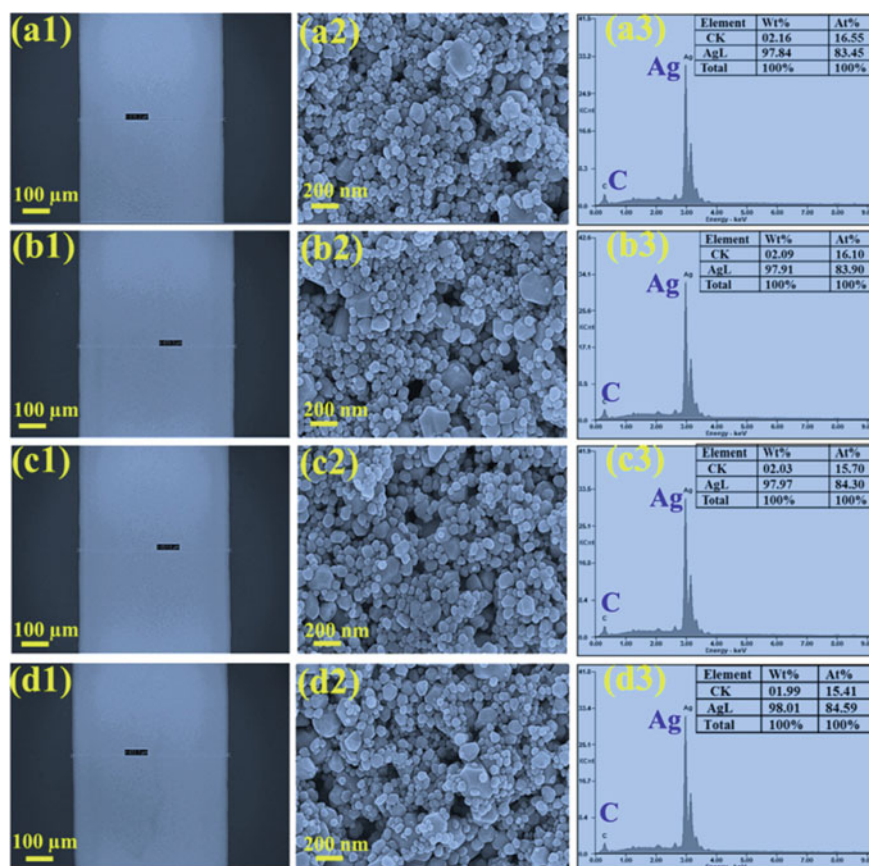
Fig. 1.6 FESEM images and EDS spectra of Ag patterns printed on PET substrate at 8000 mm/s nozzles moving speed and annealed at 70 °C (**a**1–**a**3), 80 °C (**b**1–**b**3), 90 °C (**c**1–**c**3) and 100 °C (**d**1–**d**3) in the oven (Mechanical et al. 2019)
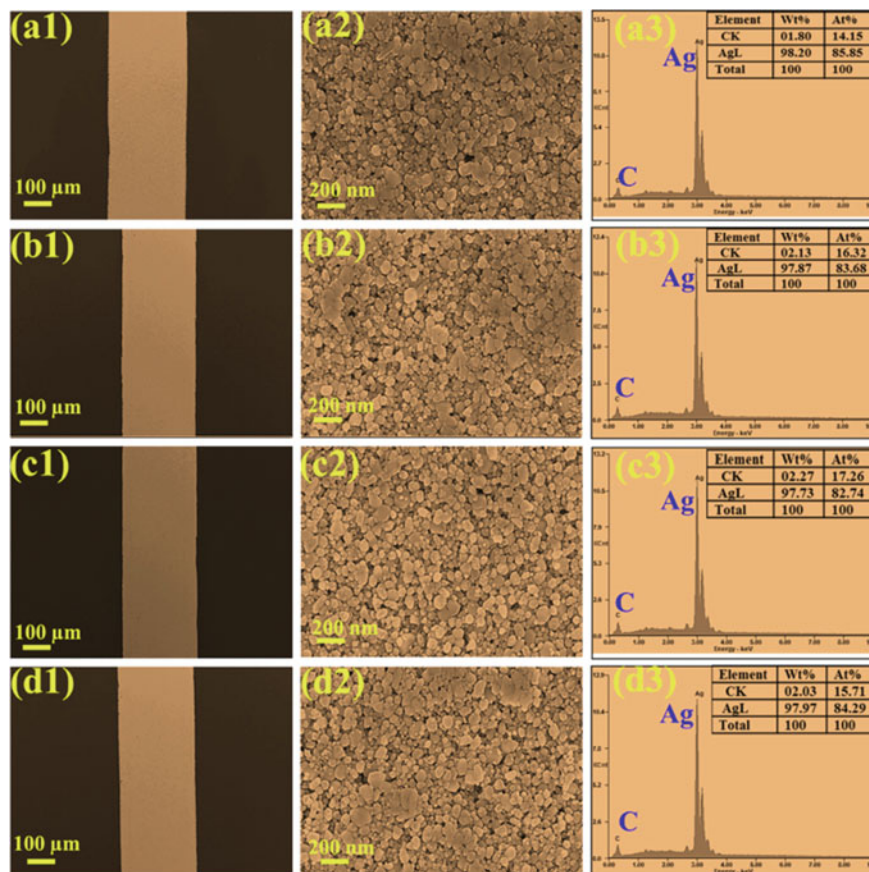
Fig. 1.7 FESEM images and EDS spectra of Ag features printed on PI substrate at 8000 mm/s nozzles moving speed and annealed at 70 °C (**a**1–**a**3), 80 °C (**b**1–**b**3), 90 °C (**c**1–**c**3) and 100 °C (**d**1–**d**3) in the oven

1.6 Conducting Nanoparticles

The metallic silverside nanoparticle dispersion with conductivities more than 107 (S/m), at a fixed temperature under 250 C, is one of the main high-conductivity inks that have been delivered at a low and adequate number of temperatures for polymers and natural substrates. Nanoscale particles have an interesting element because with scaling down the dissolving point drops significantly. The oxidation of copper is an inherent property that can never be avoided. Alternatively, it has a lot of advantages over other metallic particles such as the electrical conductivity of copper is very good and near to the most conductive silver metal. The cost of copper makes it most significant. It is less expensive and abundantly available with high electrical and thermal conductivity. Catalyst based inks were created to remove the difficulty of

storing non-noble metals and to deposit a catalytic converter to store the metal. The substrate is subsequently put into a plating bath that coats a large metallization of the catalyst.

This technique permits films equal in conductivity to be produced at a significant cost decrease with noble metal nanoparticles. The solution-oriented design also overcomes the difficulties of dust blocking and expenses of the noble metal particulate ink (Way et al. 2020; Suh et al. 2020).

1.7 Applications

The conductive elastomers are immerging in novel applications such as sensors (temperature sensors, pressure sensors and strain sensors). The elastic polymeric sensors are in demand in various applications, particularly for implantable health monitors, wearable sensory textiles, electronic skins for intelligent robots and body-conformable. Yamada et al. fabricated vertically aligned strain sensors that demonstrated high stretchability (280%) as a response to expanding and low creep of 3% at a 100% strain (Yamada et al. 2011). In another study, Xu and Zhu produced a stretchable capacitive strain sensor by incorporating silver nanowires (AgNW) into the polydimethylsiloxane. The stretching capacitance was in the range of 0%–50% (Xu and Zhu 2012). However, the same work with slight modifications was performed by Amjadi et al. They made the PDMS-AgNWs-PDMS sandwich-structured strain sensors. The fabricated samples showed reproducible resistance changes under a range of linear strain of 0–70% and even under a bending strain (Amjadi et al. 2014) (Fig. 1.8).

The polymeric pressure sensors detect the magnitude of the force acting perpendicularly on the unit area. The main method for the preparation of stretchable pressure sensors is to combine conductive matter conductive nanostructures such as metal nanoparticles/nanowires, carbon blacks, and CNTs with an elastomer in a composite. In the approaches using composite materials, conductive nanostructures such as metal nanoparticles/nanowires, carbon blacks, and CNTs are distributed through an insulating elastomer and a resistive change under a pressure is measured. Another way to achieve the uniform distribution of conductive material is the use of conductive polymers in non-conductive resins. Brady et al. coated a polyurethane foam with polypyrrole by soaking the PU foam in a solution containing a pyrrole monomer. It was quite stretchable but with low electrical conductivity (Brady et al. 2005). Choong et al. fabricated a micro-structures polydimethylsiloxane by coating the conductive PEDOT: PSS-PUD dispersion. This sensor worked fine even at a high elongation of 40% and showed a very high sensitivity of 10.32 kPa´1 (Choong et al. 2014) (Fig. 1.9).

Global warming is the current issue discussed caused using fossil fuels. Hence the researchers are focussing to find new ways of energy harvesting. Many of them have already been introduced into markets. Energy harvesting by the Piezoelectric method converts diverse mechanical stimuli to electricity. The piezoelectric energy
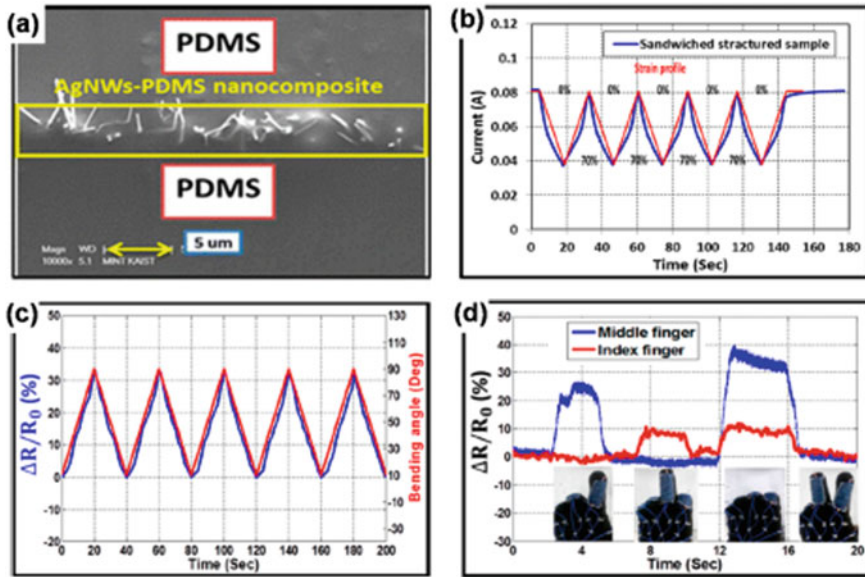
Fig. 1.8 **a** Cross-sectional SEM image of PDMS–AgNWs–PDMS sandwich-structured strain sensor. Repeated responses of the strain sensor **b** to stretching–releasing cycles at a strain of 70% and **c** to bending cycles in the bending angles of $10''–90''$. **d** Demonstration of finger motion detection using the strain sensor. Reproduced with permission from (Amjadi et al. 2014)
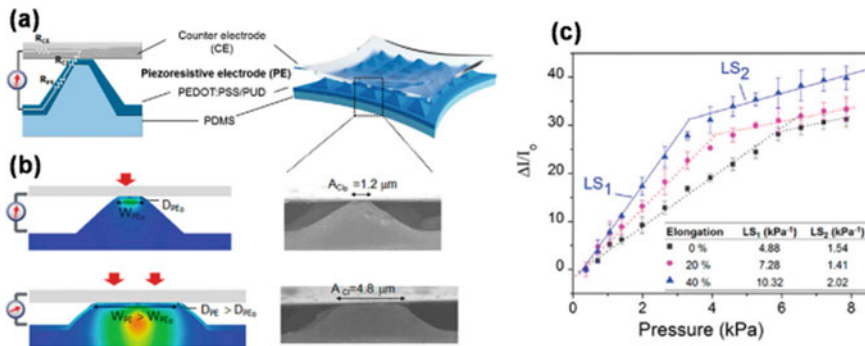
Fig. 1.9 **a** Schematic picture of a micro-pyramid PDMS array. Individual PDMS pyramids are coated with a PEDOT: PSS-PUD (Polyurethane dispersion) blend, which serves as a piezoresistive electrode; **b** Finite element analysis data showing stress distributions and SEM images at different magnitudes of pressures; **c** Relative current changes depending on the applied pressure while the sensor is stretched to a certain elongation. Here, LS1 and LS2 represent the linear sensitivities in the respective regions (Choong et al. 2014)

harvesters have been reported with various combinations such as polyvinylidene fluoride (PVDF) nanofibers on flexible substrates like polyimide, PZT nanowires/ribbons and ZnO nanorods/nanowires.

Lee et al. made a stretchable energy harvesting device that incorporated polydimethylsiloxane and carbon nanotubes PDMS–CNT as an energy harvesting layer sandwich between graphene conductive electrodes. The developed product was able to stretch up to 30% but energy harvesting capacity was much low (Lee et al. 2005). Jeong et al. demonstrated a hyper-stretchable elastic generator (SEG) by forming stretchable very long nanowire percolation (VLNP) electrodes on a piezoelectric elastic composite (PEC) composed of lead magnesium niobate–lead titanate (PMN–PT) particles and MWCNTs dispersed in silicone rubber (Fig. 1.10a). This SEG showed a large, reversible stretchability of ~200% (Fig. 1.10b) and high power output of ~4 V and ~500 nA (Fig. 1.10c) (Jeong et al. 2015a, b).
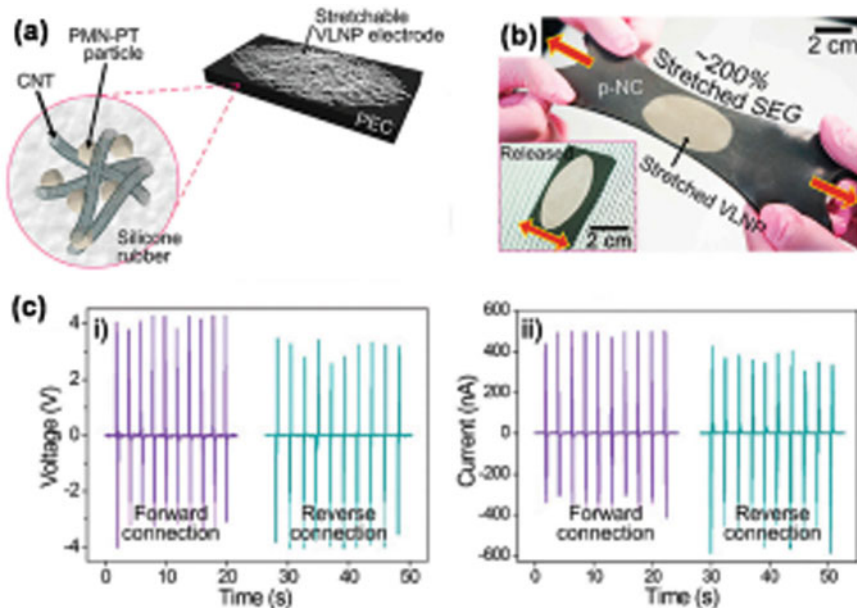
Fig. 1.10 **a** Schematic picture of the hyper-stretchable nanocomposite generator (SEG); **b** the SEG can be stretched and released without damage; **c** generated (i) open-circuit voltage and (ii) short-circuit current depending on periodic stretching–releasing cycles at a strain of 200%

1.8 Stretchable Temperature Sensors

Stretchable temperature sensors have grasped expanding heed, especially for body-attachable applications. The traditional resistance temperature detector (RTD) grabs the benefit of the principle that a conductor's resistance changes with temperature. However, good metals like Au and platinum (Pt) which are mainstream for temperature sensors do not have flexibility individually. In order to master this drawback, Chen et al. is used as the serpentine structure of Au and combined it with porous PU (Chen et al. 2015). Their temperature sensor exhibits fine linearity of resistance change, fine flexibility, and quality air-permeability. Likewise, Yan et al. used a coiled structure of graphene that was embedded inside PDMS. This graphene thermistor provided nonlinear resistance variation with temperature fluctuation in between 30 and 100 °C and tolerance to strain up to 50%. Hong et al. employed a thin film transistor (TFT) array with a stretchable PANI nanofiber temperature-sensing component. The SWCNT TFTs and PANI nanofiber sensors were initially developed on poly(ethylene terephthalate) (PET) films, and then they were implanted onto Ecoflex. This temperature sensor exhibited a high resistance sensitivity of 1.0% °C^{-1}, a response time of 1.8 s, and mechanical stability to biaxial strain up to 30%. Furthermore, Trung et al. fabricated an all elastomeric gated temperature sensor (Trung et al. 2016). For that, a PEDOT:PSS-PUD composite was consumed as source, drain, and gate material, PU as a gate dielectric, and reduced graphene oxide (R-GO)-PU composite as a temperature-sensing channel layer (Fig. 1.11a). This temperature sensor could stretch up to a strain of 70% and exhibited a high sensitivity of 1.34% °C^{-1} and stable response to temperature, even after 10,000 cycles of stretching at a 30% strain (Fig. 1.11b).
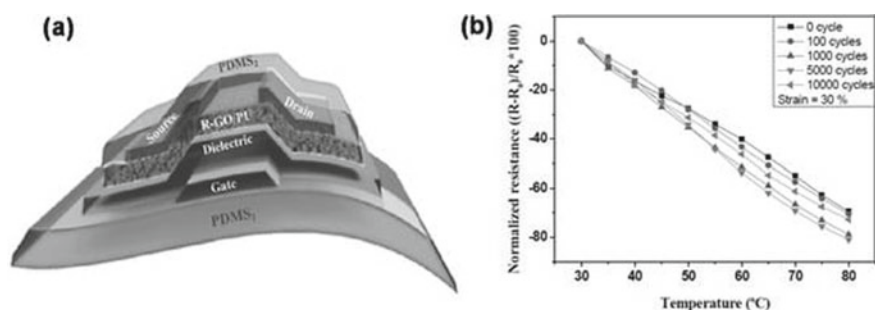
Fig. 1.11 a Schematic drawing of all elastomeric gated temperature sensor; **b** response of the temperature sensor after cyclic stretching of 0–10,000 cycles at a strain of 30%. Reproduced with permission from (Trung et al. 2016)

1.8.1 Other Stretchable Energy Harvesters

Piezoelectric energy harvesters convert diverse mechanical stimuli to electricity. Flexible piezoelectric energy harvesters have been reported, which employed various nanostructured materials such as PZT nanowires/ribbons, ZnO nanorods/nanowires, and polyvinylidene fluoride (PVDF) nanofibers on flexible substrates like polyimide and paper (Wang and Song 2006). For example, Zhou et al. have obtained a peak power density of 2.4 μW cm^{-3} using a PZT NW–PDMS nanocomposite. Although these energy harvesters proved to be highly flexible, they lacked stretchability. Lee et al. fabricated a stretchable hybrid nanogenerator (NG) that incorporated PDMS–CNT composite as the bottom electrode, poly(vinylidene fluoride-*co*-trifluoro ethylene) as the energy-harvesting layer, and graphene as the top electrode. Their NG could stretch up to a strain of 30%, but its output power was not huge enough, probably due to the inadequate piezoelectricity and pyroelectricity of the harvesting material. Jeong et al. demonstrated a hyper-stretchable elastic generator (SEG) by forming stretchable lengthy nanowire percolation (VLNP) electrodes on a piezoelectric elastic composite (PEC) composed of lead magnesio niobate–lead titanate (PMN–PT) particles and MWCNTs dispersed in a silicone rubber (Fig. 1.12a). This SEG showed a large, reversible stretchability of ~200% (Fig. 1.12b) and high power output of ~4 V and ~500 nA (Fig. 1.12c) (Jeong et al. 2015a, b).

Thermoelectric energy harvesting is a technique to make electrical power from extra heat. In current years, organic thermoelectric generators (TEGs) have obtained much awareness due to various advantages over their inorganic counterparts, such inexpensive, good processibility and flexibility, and low thermal conductivity. The major materials for the organic TEGs were conducting polymers and composites based on them. Despite numerous achievements in flexible organic TEGs, research on stretchable TEGs has been scarce. Kim et al. fabricated a wearable TEG consisting of inorganic thermoelectric components formed on glass fabric (Liang et al. 2016)Although this TEG embedded in PDMS was thin, flexible, and exhibited a high output power density of 28 mW g^{-1} at a $\Delta T = 50$ K, it was not stretchable. Liang et al. took an initial step toward a stretchable TEG (Kim et al. 2014). They prepared PPY-SWCNT nanocomposites by using an in situ oxidative polymerization method, as depicted in Fig. 1.10a. As a consequence of the reaction, SWCNTs coated with PPY were obtained, and their films were prepared by the vacuum filtration method. This nanocomposite film showed finely improved thermoelectric performance with a power factor of 19.7 μW m^{-1} K^{-2}, which is the huge value for PPY composites. In addition, it could be stretched by 2.6% (Fig. 1.13), but its stretchability still needs to be enhanced.
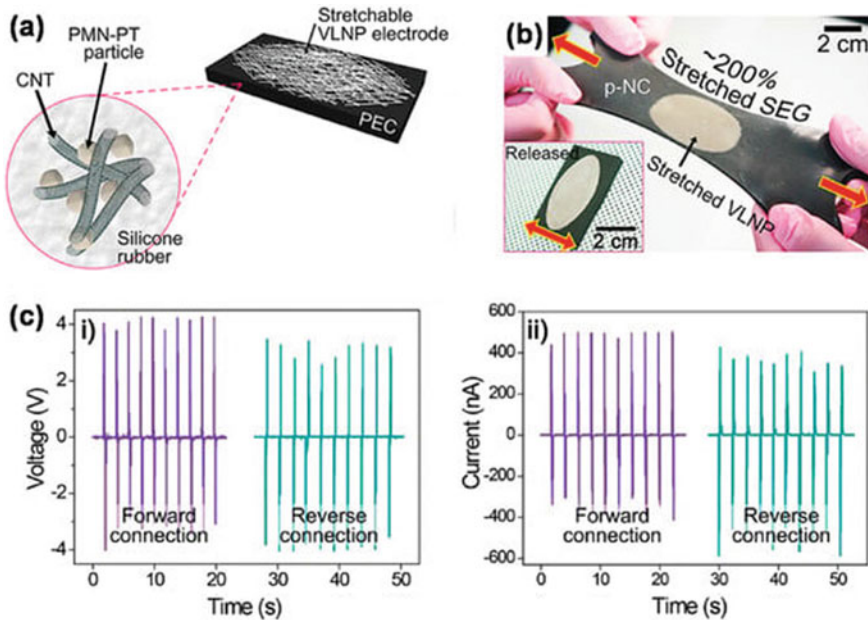
Fig. 1.12   **a** Schematic picture of the hyper-stretchable nanocomposite generator (SEG); **b** the SEG can be stretched and released without damage; **c** generated (i) open-circuit voltage and (ii) short-circuit current depending on periodic stretching–releasing cycles at a strain of 200%. Reproduced with permission from. Copyright 2015 John Wiley and Sons. VLNP: very long nanowire percolation; PMN-PT: lead magnesio niobate–lead titanate; PEC: piezoelectric elastic composite (Jeong et al. 2015a, b)

1.9   Conductive Elastomers for EMI Shielding

Electrically conductive elastomer products are ideal for both military and commercial applications requiring both environmental sealing and EMI shielding. Compounds can be provided in moulded or extruded shapes, sheet stock, custom extruded, or die-cut shapes to meet a wide variety of applications. Our conductive extrusions offer a wide choice of profiles to fit a large range of applications. The cross-sections shown on the following pages are offered as standard. Custom dies can be built to accommodate your specific design (Cheng et al. 2021).

- Available in a wide variety of conductive filler materials
- Shielding effectiveness up to 120 dB at 10 GHz.
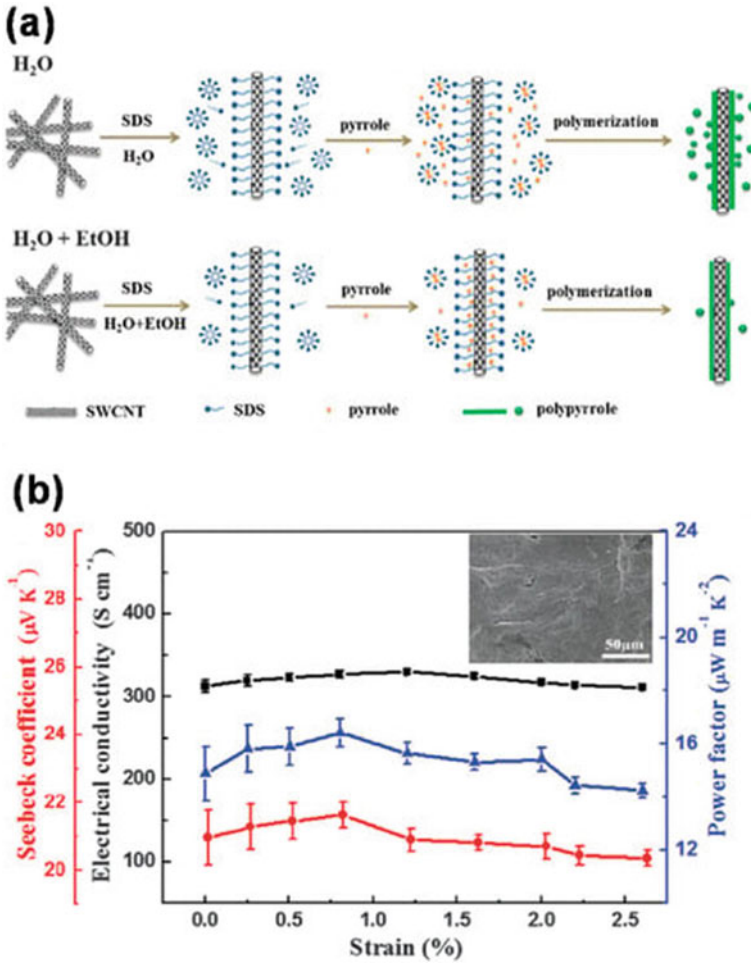
Fig. 1.13 **a** Schematic illustration for the preparation procedures of PPY–SWCNT nanocomposites; **b** dependence of thermoelectric performance of the composite on mechanical stretching. The inset is an SEM image of the composite film after a 2.5% stretching. Reproduced with permission from (Kim et al. 2014)

1.10 Conclusion

The conclusion of all the discussion is that the elastomers are generically not good conductors. The conductivity of synthetic rubber like silicon rubber conductivity can increase by adding a valuable amount of the conductive material. Three main techniques are present by which can increase conductivity, first is compounding (adding conductive fillers), second is blending (adding conductive polymer material), third is coating (spray and coat of the surface of elastomers by conductive materials).

The conductivity can be represented with the help of graph. The conductivity value of the synthetic elastomer depends upon the concentration of the conductive filler. The resistivity of the synthetic elastomers decreases with the increasing amount of conductive fillers. Furthermore, the impact of flexibility behaviour of functional elastomers over different properties has been studied. Conductive stretchable elastomeric composites can be used in EMI shielding materials, sensors and thermoelectric energy harvesting. This chapter illustrates the usefulness of any research involved with the addition of conductive fillers for making conductive elastomers. The research efforts were put into three fields of stretchable technology, which are stretchable electronics, stretchable sensors, and stretchable energy harvesters.

References

Amjadi M, Pichitpajongkit A, Lee S, Ryu S, Park I (2014) Highly stretchable and sensitive strain sensor based on silver nanowire-elastomer nanocomposite. ACS Nano 8:5154–5161

Bhat KS, Nakate UT, Yoo J-Y, Yousheng Wang TM, Hahn Y-B (2019) Cost-effective silver ink for printable and flexible electronics with robust mechanical performance. Chem Eng J 373:355–364

Bloor D, Donnelly K, Hands PJ, Laughlin P, Lussey D (2005) A metal–polymer composite with unusual properties. J Phys D: Appl Phys 38:2851–2860

Böhning M, Frasca D, Schulze D, Schartel B (2019) Multilayer graphene/elastomer nanocomposites. In: Carbon-based nanofillers and their rubber nanocomposites: fundamentals and applications. Elsevier Inc. https://doi.org/10.1016/B978-0-12-817342-8.00006-8

Botros SH, Tawfic ML (2006) Synthesis and characteristics of MAH-g-EPDM compatibilized EPDM/NBR rubber blends. J Elastomers Plast 38(4):349–365. https://doi.org/10.1177/009524 4306065889

Brady S, Diamond D, Lau KT (2005) Inherently conducting polymer modified polyurethane smart foam for pressure sensing. Sens Actuators A 119:398–404

Cardarelli F (2008) Materials handbook: a concise desktop reference. Springer.

Chakraborty M, Hashmi MSJ (2018) Graphene as a material – an overview of its properties and characteristics and development potential for practical applications. In: Reference module in materials science and materials engineering. Elsevier Ltd. https://doi.org/10.1016/b978-0-12-803581-8.10319-4

Chauhan S, Bhushan RK (2018) Improvement in mechanical performance due to hybridization of carbon fiber/epoxy composite with carbon black. Adv Compos Hybrid Mater 1(3):602–611. https://doi.org/10.1007/s42114-018-0047-0

Chen Y, Lu B, Chen Y, Feng X (2015) Breathable and stretchable temperature sensors inspired by skin. Sci Rep 5(1):11505. https://doi.org/10.1038/srep11505

Cheng HC, Chen CR, Hsu SH, Cheng KB (2021) Electromagnetic shielding effectiveness and conductivity of PTFE/Ag/MWCNT conductive fabrics using the screen printing method. Sustainability 15:2020

Cheremisinoff NP (1989) Handbook of polymer science and technology: applications and processing operations. In: Marcel Dekker.

Choong CL, Shim MB, Lee BS, Jeon S, Ko DS, Kang TH, Bae J, Lee SH, Byun KE, Im J et al (2014) Highly stretchable resistive pressure sensors using a conductive elastomeric composite on a micropyramid array. Adv Mater 26:3451–3458

Fan J, Chen A (2019) Studying a flexible polyurethane elastomer with improved impact-resistant performance. Polymers 11(3):467. https://doi.org/10.3390/polym11030467

Finch, C. (1989). *C. A. Finch, "Handbook of polymer science and technology Edited by Nicholas P. Cheremisinoff, Marcel Dekker Inc.* New York & Basel.

Fisher HL (1939) Vulcanization of rubber. Ind Eng Chem 31(11):1381–1389. https://doi.org/10.1021/ie50359a015

Foss O (1960) Structures of compounds containing chains of sulfur atoms, pp 237–278. https://doi.org/10.1016/S0065-2792(08)60191-0

Galli E (1982) Carbon blacks. Plast Compd 5(2):1–5

Gautam RK, Verma A (2018) Electrocatalyst materials for oxygen reduction reaction in microbial fuel cell. In: Biomass, biofuels, biochemicals: microbial electrochemical technology: sustainable platform for fuels, chemicals and remediation. Elsevier B.V. https://doi.org/10.1016/B978-0-444-64052-9.00018-2

Gehman SD (1957) Dynamic properties of elastomers. Rubber Chem Technol 30(5):1202–1250. https://doi.org/10.5254/1.3542759

Jeong CK, Lee J, Han S, Ryu J, Hwang G-T, Park DY, Park JH, Lee SS, Byun M, Ko SH, Lee KJ (2015a) A hyper-stretchable elastic-composite energy harvester. Adv Mater 27(18):2866–2875. https://doi.org/10.1002/adma.201500367

Jeong CK, Lee J, Han S, Ryu J, Hwang GT, Park DY, Park JH, Lee SS, Byun M, Ko SH et al (2015b) A hyper-stretchable elastic-composite energy harvester. Adv Mater 27:2866–2875

Kim SJ, We JH, Cho BJ (2014) A wearable thermoelectric generator fabricated on a glass fabric. Energy Environ Sci 7(6):1959. https://doi.org/10.1039/c4ee00242c

Klingender RC (2008) Handbook of specialty elastomers

Lee H, Seong B, Moon H, Byun D (2005) Directly printed stretchable strain sensor based on ring and diamond shaped silver nanowire electrodes. RSC Adv 5:28379–28384

Liang L, Gao C, Chen G, Guo C-Y (2016) Large-area, stretchable, super flexible and mechanically stable thermoelectric films of polymer/carbon nanotube composites. J Mater Chem C 4(3):526–532. https://doi.org/10.1039/C5TC03768A

Ma L-F, Bao R-Y, Huang S-L, Liu Z-Y, Yang W, Xie B-H, Yang M-B (2013) Electrical properties and morphology of carbon black filled PP/EPDM blends: effect of selective distribution of fillers induced by dynamic vulcanization. J Mater Sci 48(14):4942–4951. https://doi.org/10.1007/s10853-013-7275-z

Matanoski GM, Santos-Burgoa C, Schwartz L (1990) Mortality of a cohort of workers in the styrene-butadiene polymer manufacturing industry (1943–1982). Environ Health Perspect 86:107–117. https://doi.org/10.1289/ehp.9086107

Mohammed A, Simon GP (2006) Rubber-clay nanocomposites. Polym Nanocomposites 297–325. https://doi.org/10.1533/9781845691127.1.297

Mou Y, Cheng H, Wang H, Sun Q, Liu J, Peng Y, Chen M (2019) Facile preparation of stable reactive silver ink for highly conductive and flexible electrodes. Appl Surf Sci 45:75–82

Nagata N, Kobatake T, Watanabe H, Ueda A, Yoshioka A (1987) Effect of chemical modification of solution-polymerized rubber on dynamic mechanical properties in carbon-black-filled vulcanizates. Rubber Chem Technol 60(5):837–855. https://doi.org/10.5254/1.3536159

ORION Engineered Carbons (2014) What is carbon black? www.Orioncarbons.com, 7.

Papageorgiou DG, Kinloch IA, Young RJ (2015) Graphene/elastomer nanocomposites. Carbon 95:460–484. https://doi.org/10.1016/j.carbon.2015.08.055

Park M, Park J, Jeong U (2014) Design of conductive composite elastomers for stretchable electronics. Nano Today 9(2):244–260. https://doi.org/10.1016/j.nantod.2014.04.009

Smith TL (1963) Ultimate tensile properties of elastomers. I. Characterization by a time and temperature independent failure envelope. J Polym Sci Part A: Gen Papers 1(12):3597–3615. https://doi.org/10.1002/pol.1961.100011207

Song K (2017) Micro- and nano-fillers used in the rubber industry. In: Progress in rubber nanocomposites. Elsevier Ltd. https://doi.org/10.1016/B978-0-08-100409-8.00002-4

Song P, Song J, Zhang Y (2020) Stretchable conductor based on carbon nanotube/carbon black silicone rubber nanocomposites with highly mechanical, electrical properties and strain sensitivity. Compos B Eng 191:107979. https://doi.org/10.1016/j.compositesb.2020.107979

Ştiubianu G, Soroceanu A, Varganici CD, Tugui C, Cazacu M (2016) Dielectric elastomers based on silicones filled with transitional metal complexes. Compos Part B 30:3005

Suh M, Curto S, Prakash P, Van Rhoon G (2020) Wearable device for thermotherapies. In: Wearable bioelectronics. Elsevier Ltd. https://doi.org/10.1016/B978-0-08-102407-2.00007-2

Sulaiman AJH, Hissyam WNWM, Aiman MH, Ishak M, Ariga T (2019) Effect of copper based filler composition on the strength of brazed joint. J Mech Eng Sci 13:5090–5101

Trung TQ, Ramasundaram S, Hwang B-U, Lee N-E (2016) An all-elastomeric transparent and stretchable temperature sensor for body-attachable wearable electronics. Adv Mater 28(3):502–509. https://doi.org/10.1002/adma.201504441

Visakh PM, Thomas S, Chandra AK, Mathew AP (eds) (2013) Advances in elastomers II composites and nanocomposites. Springer.

Wang ZL, Song J (2006) Piezoelectric nanogenerators based on zinc oxide nanowire arrays. Science 312(5771):242–246. https://doi.org/10.1126/science.1124005

Wankat PC (1994) Crystallization from the Melt

Warner JH, Schäffel F, Rümmeli MH, Bachmatiuk A (2013) Graphene 2. https://doi.org/10.1016/C2011-0-05169-4

Way M, Willingham J, Goodall R (2020) Brazing filler metals. Int Mater Rev 65:257–285

Wendt P (1947) The control of rubber in world war II. South Econ J 13(3):201. https://doi.org/10.2307/1053336

Wu T, Ke Q, Lu M, Pan P, Zhou Y, Gu Z, Cui G, Lu H (2022) Recent advances in carbon-silica composites: preparation, properties, and applications. Catalysts 12(5):571. https://doi.org/10.3390/catal12050573

Xu F, Zhu Y (2012) Highly conductive and stretchable silver nanowire conductors. Adv Mater 24:5117–5122

Yamada T, Hayamizu Y, Yamamoto Y, Yomogida Y, Izadi-Najafabadi A, Futaba DN, Hata K (2011) A stretchable carbon nanotube strain sensor for human-motion detection. Nat Nanotechnol 6:269–301

Zhang Y, Ge S, Tang B, Koga T, Rafailovich MH, Sokolov JC, Peiffer DG, Li Z, Dias AJ, McElrath KO, Lin MY, Satija SK, Urquhart SG, Ade H, Nguyen D (2001) Effect of carbon black and silica fillers in elastomer blends. Macromolecules 34(20):7056–7065. https://doi.org/10.1021/ma010183p

Chapter 2
Phase Change Materials in Textiles for Thermal Regulation

Kai Yang, Xiuling Zhang, Mohanapriya Venkataraman, Jakub Wiener, and Jiří Militký

Abstract Phase change materials (PCMs) can have a certain temperature range during their phase transition meantime the thermal energy is adsorbed or released. PCMs are characterized to adsorb/release thermal energy during the phase transition process over a certain temperature range. PCMs have been applied in textiles for thermal regulation since the last century. The significant parameters related to thermal property and comfort of PCM-incorporated textiles as well as PCM types have been described in numerous research works. Although there has been a big progress in PCM-incorporated textiles, there are still some problems. In this book chapter, we reorganize and summarize present research work related to PCM textiles, and discuss the advantages and disadvantages of technologies for PCM textiles. We believe that this chapter can provide more alternatives for the design of PCM textiles.

2.1 Introduction

Phase change materials (PCMs) are a group of materials characterized to store/ release thermal energy according to the temperature difference between PCMs and the environment (Khan et al. 2023; Liu et al. 2021; Peng et al. 2020). PCMs have

K. Yang (✉) · X. Zhang · M. Venkataraman · J. Wiener · J. Militký
Department of Material Engineering, Faculty of Textile Engineering, Technical University of Liberec, Studentská 2, 46117 Liberec, Czech Republic
e-mail: kai.yang@tul.cz

X. Zhang
e-mail: xiuling.zhang@tul.cz

M. Venkataraman
e-mail: mohanapriya.venkataraman@tul.cz

J. Wiener
e-mail: jakub.wiener@tul.cz

J. Militký
e-mail: jiri.militky@tul.cz

been used in different fields, including building and construction, food industry, solar energy storage, electronic system, smart textiles, etc. (Cao et al. 2023; Chen et al. 2021; Gao et al. 2022; Parvate et al. 2021; Yin et al. 2022).

The textiles (e.g., fibers and fabrics) with PCMs are labelled as PCM textiles (Yang et al. 2022a, b, c, d, e, f; Zhang et al. 2019). Suitable PCMs for textiles are generally organic, which has anti-corrosion, high thermal stability, high chemical stability, etc. The organic PCMs include paraffin wax, fatty acid, polyethylene glycol and so on. For paraffin wax and fatty acid, carbon atom numbers determine their working temperature and latent heat (Bose and Amirtham 2016; Yuan et al. 2014). For polyethylene glycol, higher molecular weight contributes to higher phase transition range and latent heat. However, the organic PCMs can not be directly applied in textiles since their solid–liquid phase transition behavior can result in leakage phenomena. The supporting materials or special structure to store such PCMs are necessary. Several PCM composites without leakage have been proposed, including PCM capsules (MPCMs), form-stable PCMs, solid–solid PCMs (SSPCMs), etc. (Chen et al. 2022; Ghasemi et al. 2022; X. Lin et al. 2021; Liu et al. 2022; Yin et al. 2022). For PCM textiles, various methods have been utilized to incorporate PCMs into textiles. Correspondingly, PCM textiles have been developed for different aims, such as temperature regulation, fire protection, and so on.

In this chapter, details of suitable PCMs for textiles are first discussed. Then, current research focusing on PCM textiles is presented. Especially, a sandwich fibrous PCM encapsulation has been proposed by our research group and is totally different from current PCM textiles, which is also included. We believe that this chapter is not only beneficial for researchers but also for textile engineers.

2.2 Introduction of MPCMs

Microencapsulation is a process where PCM particles or droplets are surrounded or embedded in a homogenous matrix at a size of below 1000 μ m. The products from microencapsulation are MPCMs. The MPCMs can be classified into 5 types: simple MPCM, irregular MPCM, multi-core MPCM, multi-wall MPCM and matrix MPCM (Fig. 2.1a) (Khan et al. 2023). Generally, the produced MPCMs are spheric and applied for various fields (e.g., textiles, building, etc.).

2.2.1 Methods for MPCMs

Most common methods to prepare MPCMs are chemical methods (Giro-Paloma et al. 2016), including suspension polymerization, dispersion polymerization, emulsion polymerization, in situ polymerization, and interfacial polymerization. As shown in Fig. 2.1b, the suspension polymerization is initiated by stirring a mixture of dispersed droplets containing PCMs, monomers, initiators and surfactants in a continuous
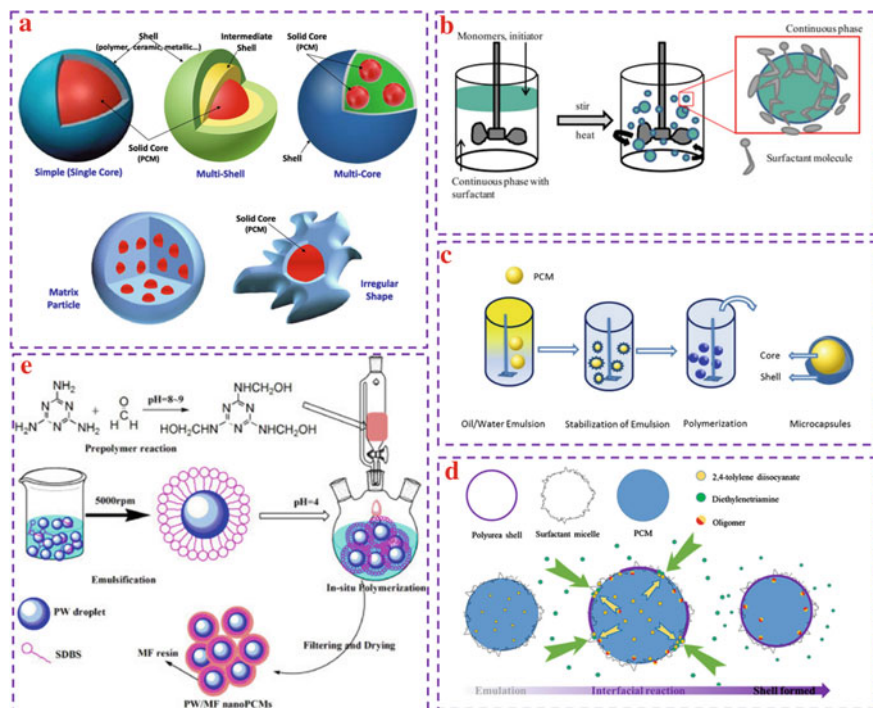
Fig. 2.1 Diagram for MPCMs with different shapes (**a**) (Reproduced with permission from (Khan et al. 2023), COPYRIGHT [2023], [Elsevier]), suspension polymerization for MPCMs (**b**) (Reproduced with permission from (Giro-Paloma et al. 2016), COPYRIGHT [2016], [Elsevier]), emulsion polymerization for MPCM (**c**) (Reproduced with permission from (Şahan and Paksoy 2018), COPYRIGHT [2018], [Wiley]), interfacial polymerization for MPCMs (**d**) (Reproduced with permission from (Cai et al. 2020), COPYRIGHT [2020], [Elsevier]), and in situ polymerization for MPCMs (**e**) (Reproduced with permission from (Zhang and Yuan 2020), COPYRIGHT [2020], [Elsevier])

aqueous process (Giro-Paloma et al. 2016). By comparing with suspension polymerization, dispersion polymerization is characterized by the monomers being soluble in the solvent. Besides, it is necessary to add the stabilizer to control the polymerization process.

The emulsion polymerization is realized by mixing polymer in an oiled system with emulsifier (Fig. 2.1c) (Şahan and Paksoy 2018). The emulsification is required to create a water/oil system and a crosslinked system. Then, the emulsion is washed to remove the oil and obtain the MPCMs. By applying emulsion polymerization, MPCMs with PMMA shell or polystyrene shell are usually obtained.

For interfacial polymerization, two reactive monomers are dissolved separately in the oil phase and the aqueous phase, and polymerization then occurs at the oil–water interface under the action of an initiator. The products via interfacial polymerization are usually the MPCMs with polyurea shell or polyurethane shell. Figure 2.1d

presented a diagram for polyurea MPCMs containing dodecanol dodecanate as core materials prepared via co-solvent-free interfacial polymermization (Cai et al. 2020).

The in-situ polymerization is also used for MPCMs, where a shell on the surface of the droplet is formed based on polymerization of the prepolymers. As shown in Fig. 2.1e, Nan Zhang et al. synthesized MPCMs with paraffin as core and melamine–formaldehyde (MF) as shell via in-situ polymerization (Zhang and Yuan 2020). The encapsulation efficiency reached 75 wt%.

Apart from chemical methods, physical–chemical methods are utilized, such as coacervation, sol–gel encapsulation, and so on. Especially, sol–gel method as economical and mild process is usually to synthesize MPCMs with inorganic shells (e.g., SiO_2, TiO_2, etc.).

Besides, some physical methods are applied for the development of MPCMs, including spray-drying, electrostatic encapsulation, etc. Especially, the spray-drying method is one of the most common physical methods. The oil/water emulsion with PCMs and shell materials is first sprayed via atomizer under controlled environment (e.g. temperature and relative humidity) and then the solid particles are obtained.

2.2.2   Classification of MPCMs

MPCMs are usually classified into polymeric MPCMs and inorganic MPCMs, which is based on type of their shells.

2.2.2.1   Polymeric MPCMs

The polymeric MPCMs are characterized as stable phase transition behavior and excellent resistance to volume change during working time. Common materials for shell of polymeric MPCMs include melamine formaldehyde resin, urea formaldehyde resin, acrylic resin and so on. For example, Rui Huang et al. prepared MPCMs with n-dodecanol as cores by using an oil-soluble melamine–formaldehyde prepolymer etherified by methanl and butanal via in-situ polymerization (Huang et al. 2017). The MPCMs had excellent stability in phase transition behavior after different pressures. Dong Xu et al. prepared paraffin-based MPCMs with PMMA (or PMMA copolymers) as shell (Xu and Yang 2019). Less than 1% leakage of MPCMs after 50 thermal cycles and encapsulation efficiency reached 70%.

Although there is significant progress in polymeric shell-based MPCMs, some disadvantages are found. The thermal conductivity of the polymeric shell-based MPCMs was found, which reduced the thermal energy storage efficiency. To dope materials with high thermal conductivity in shell materials of organic MPCMs is an alternative to increase thermal energy storage efficiency. For example, Xingang Wang et al. prepared MPCMs with capric acid as cores and graphene oxide-modified urea–formaldehyde resin as shell materials (Wang et al. 2019). The thermal conductivity

of MPCMs was higher than 0.1 W m^{-1} K^{-1}. However, the overall thermal conductivity of polymeric MPCMs is because of limited amounts of materials with high conductivity. Besides, the mechanical of polymeric shell-based MPCMs required improvement, since they were easily broken after mechanical treatment.

2.2.2.2   Inorganic MPCMs

By comparing with organic MPCMs, inorganic MPCMs have an advantage of anti-combustion, higher thermal conductivity, etc.

Silica component is usually introduced in MCMs. For preparation of silica-based MPCMs, the sol–gel process was usually applied (Tang et al. 2017). As shown in Fig. 2.2a, Fang Tang et al. prepared an MPCM consisting of silica as shell and octadecane as core. The size of silica-based MPCMs ranged from 0.5 to 2 um, and melting enthalpy value reached 227 J/g. To more precisely control volume expansion of silica-based MPCMs, nano-silica-based MPCMs were also proposed. Sagar Paneliya et al. proposed a one-step in-situ process to encapsulate paraffin wax as core with silica as shell via emulsion interfacial hydrolysis and polycondensation of silica precursor, which was based on Langmuir–Blodgett deposition technology (Fig. 2.2b) (Paneliya et al. 2021). The size of silica-based MPCMs was about 160 nm, and melting enthalpy value was about 100 J/g.

Cu components have been introduced in MPCMs to enhance thermal conductivity. Sumit Parvate et al. first made a functionalization for Cu nanoparticles (Fig. 2.3a) and then introduced into MPCMs (Parvate et al. 2021). The MPCMs with Cu nanoparticle amount of 1.0 wt% had melting enthalpy value of 132 J/g and PCM encapsulation ratio was about 60%. The thermal conductivity of Cu nanoparticle-interlocked MPCMs reached 0.34 W m^{-1} K^{-1}. Due to introduction of Cu component, the Cu nanoparticle-interlocked MPCMs were aimed for food package, which supported anti-bacterial property and temperature regulation.

Besides, TiO$_2$ components are introduced into MPCMs. For example, L. Zou et al. prepared TiO$_2$-based MPCMs by following Fig. 2.3c (Zou et al. 2022). Then, the TiO$_2$-based MPCMs were introduced into PVDF matrix to form a composite film. The hydrogen bonding between TiO$_2$-based MPCMs and PVDF is supported to avoid leakage. The TiO$_2$-based MPCMs-incorporated PVDF film had a thermal conductivity of 0.09 W m^{-1} K^{-1} and melting enthalpy value of 41 J/g. Besides, an effective photothermal behavior of TiO$_2$-based MPCMs-incorporated PVDF film was found. Since there was TiO$_2$ component, the potential applications were proposed, including anti-bacterial, anti-UV, etc.

By taking cost of metals into consideration, the usage of materials from dust had an advantage of recycling. For example, Shiyu Yu et al. prepared an MPCM consisting of n-octadecane as core and CaCO$_3$ as shell by using n-octadecane/CaCl$_2$ via a self-assembly process (Fig. 2.3b) (Yu et al. 2014). The overall thermal conductivity of the CaCO$_3$-based MPCMs was enhanced and anti-osmosis property was found. The practical cost was accepted because of low cost of calcium carbonate.
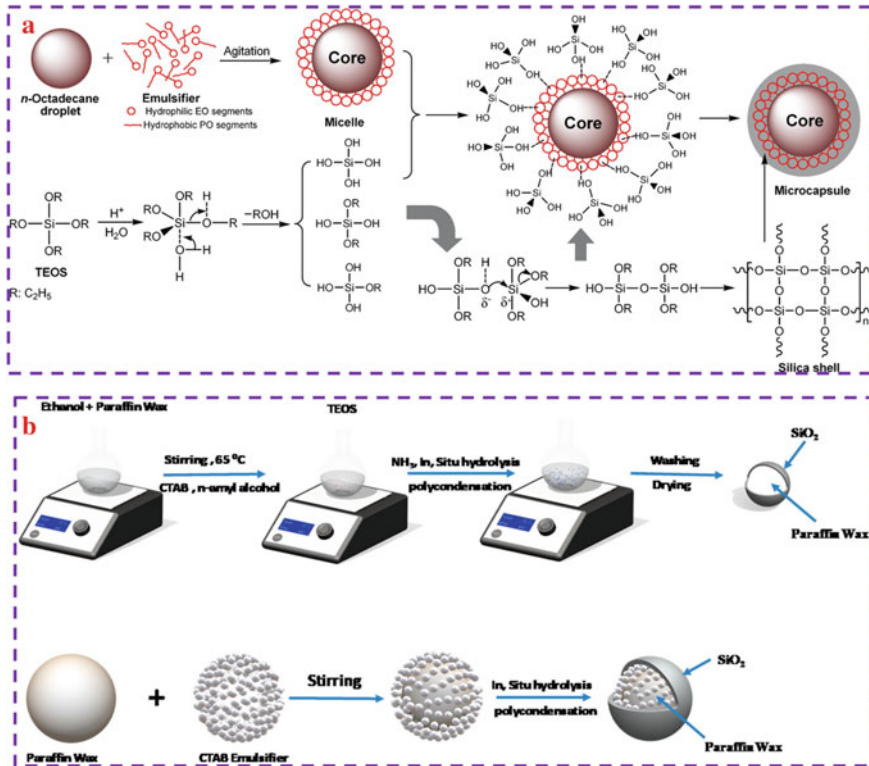
Fig. 2.2 Sol–gel process (**a**) for silica-based MPCMs (Reproduced with permission from (Tang et al. 2017), COPYRIGHT [2017], [Elsevier]), and emulsion interfacial hydrolysis and polycondensation of silica precursor (**b**) for nanoscale silica-based MPCMs (Reproduced with permission from (Paneliya et al. 2021), COPYRIGHT [2021], [Elsevier])

Recently, cenospheres have attracted more and more attention for the preparation of MPCMs. The cenospheres are fly ash particles from the byproduct of coal-burning power plants that produce hollow microspheres. The crushing strength of cenospheres ranges from 10 to 20 MPa. Especially, there is a layer of glass-crystalline nanofilm covering the hollow section of cenospheres. So, it is possible to use cenospheres to encapsulate PCMs. Based on the unique structure of cenospheres, the basic preparation of cenospheres-based inorganic MPCMs is proposed by following the steps as shown in Fig. 2.4a:

(1) The chemical etching method to destroy the glass-crystalline nanofilm is required.
(2) The etching cenospheres are then filled by PCMs.
(3) After step '2', an extra covering layer is added to cover PCM-embedded cenospheres to avoid leakage and support high stability of phase trasition, Finally, the cenospheres-based inorganic MPCMs are obtained.
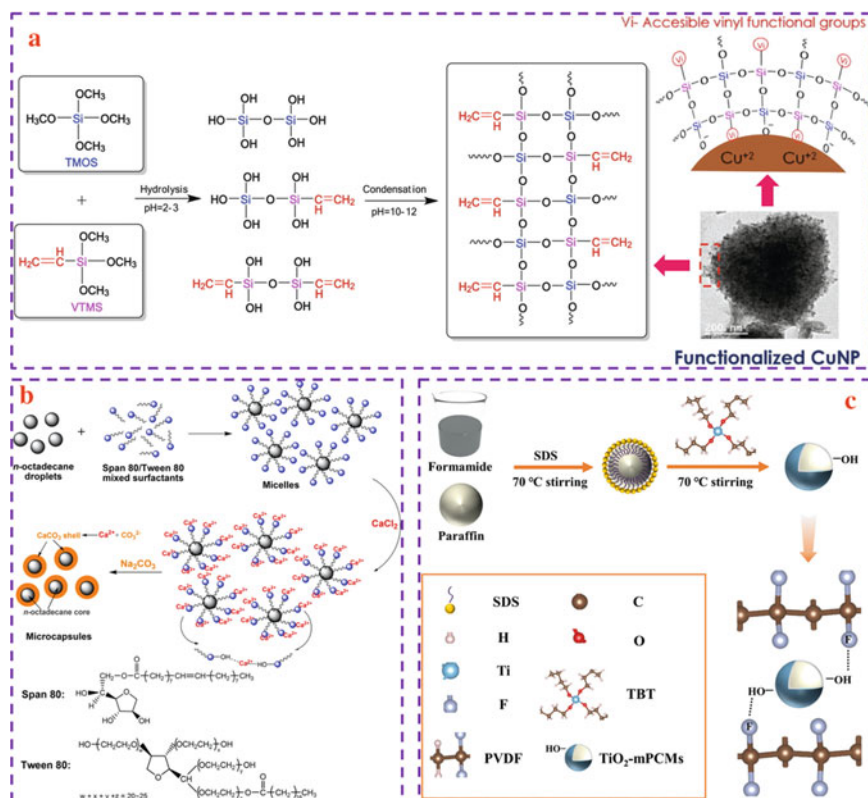
Fig. 2.3 Functionalization of Cu nanoparticles for synthesis of inorganic MPCMs (**a**) (Reproduced with permission from (Parvate et al. 2021), COPYRIGHT [2021], [Elsevier]), preparation of Ca-based MPCMs via a self-assembly process (**b**) (Reproduced with permission from (Yu et al. 2014), COPYRIGHT [2014], [Elsevier], and a diagram for preparation of TiO$_2$-based MPCMs (**c**) (Reproduced with permission from (Zou et al. 2022), COPYRIGHT [2022], [Elsevier])

For example, Fengjuan Liu et al. proposed one cenospheres-based inorganic MPCMs (Liu et al. 2017) as shown in Fig. 2.4b. In detail, the cenospheres were firstly destroyed via chemical etching with a mixture of NH$_4$F and HCl solution. The major pores size of etched cenospheres was smaller than 500 nm. Then, n-octadecane was embedded in porous etched cenospheres via vacuum-assistant melting-blending method. Then, silica sol was then to cover the n-octadecane/cenospheres composites and cenospheres-based inorganic MPCMs were obtained. As a result, the maximum loading amount of n-octadecane in the MPCMs reached 63.64 wt%. Besides, the mechanical property of the cement mortar with 3 wt% cenospheres-based inorganic MPCMs was investigated, and the compressive strength ranged from 28 to 48 MPa. In addition, the structure of cenospheres-based inorganic MPCMs was kept well after compression. Subsequently, Adam L. Brooks et al. optimized the loading amount of
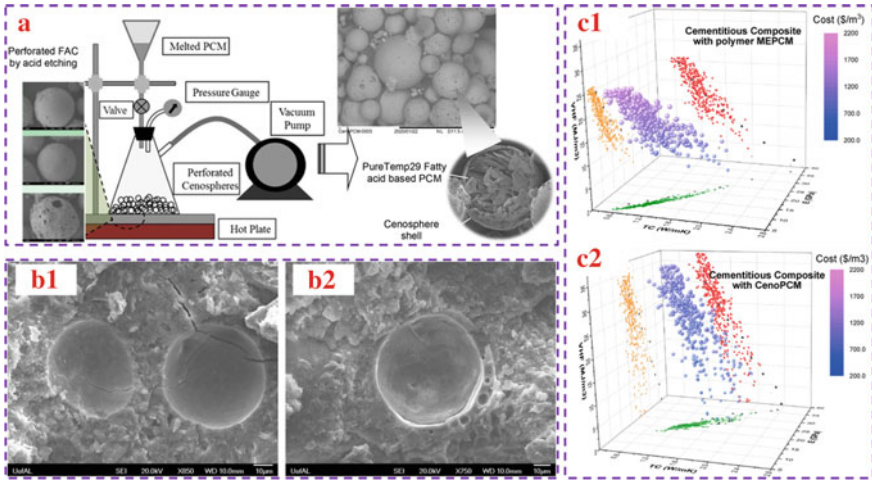
Fig. 2.4 Preparation of cenespheres-based MPCMs (**a**) (Reproduced with permission from (Brooks et al. 2021), COPYRIGHT [2021], [Elsevier]), morphology of mortar containing cenespheres-based MPCMs (**b**) (b1 and b2: hemispherical voids due to cenespheres pulled out and damaged cenespheres-based MPCMs) (Reproduced with permission from (Liu et al. 2017), COPYRIGHT [2017], [Elsevier]) and estimation for cost of cenespheres-based MPCMs (**c**) (Reproduced with permission from (Brooks et al. 2021), COPYRIGHT [2021], [Elsevier])

cenospheres-based inorganic MPCMs in cement and estimated their enormous environmental benefits and cost advantages (Fig. 2.4c) (Brooks et al. 2021). Adbulmalik Ismail et al. also prepared a novel low-cost MPCMs by using PCMs derived from refined edible vegetable oil, and high thermal stability after 10,000 thermal cycles was found (Ismail et al. 2023).

2.3   Introduction of FSPCMs

Generally, FSPCMs are a group of composites that consists of PCMs and porous materials (Huang et al. 2018). Various porous materials have been applied to store PCMs, including porous foam, porous powders, and porous membranes. Working principle of FSPCMs to encapsulate the PCM in the porous structure is based on the physical interactions (e.g. capillary force, hydrogen bonding…) between the PCMs and the porous materials during their working time. Various methods are developed for FSPCMs, including melting impregnation, vacuum impregnation, dissolving impregnation, the combined technology of dissolving impregnation and melting impregnation, and so on (Khosrojerdi and Mortazavi 2013; Shaid et al. 2016; Yang et al. 2021). Up to now, various porous materials have been used for FSPCMs.

Silica aerogels as a kind of porous material containing nanopores have been used for FSPCMs. For example, Abu Shaid et al. prepared aerogel/eicosane composites
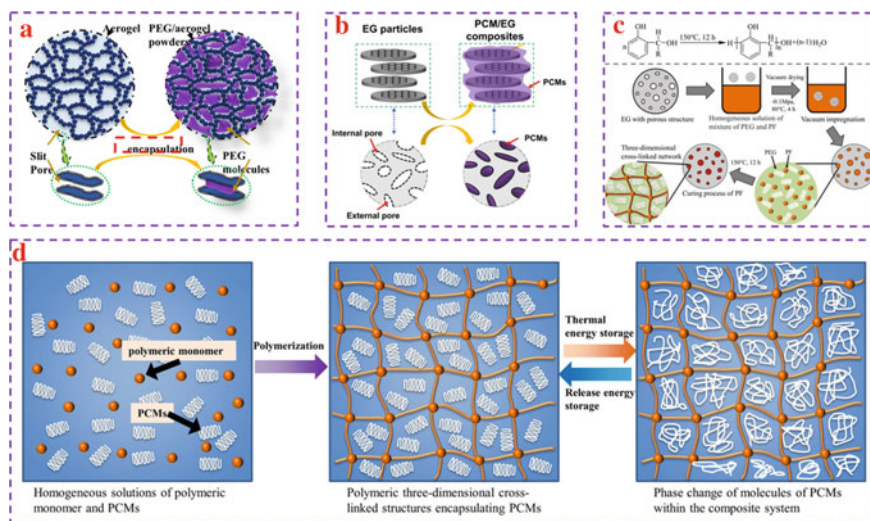
Fig. 2.5 Diagram for PEG/aerogel composites (**a**) (Reproduced with permission from (Yang et al. 2021), COPYRIGHT [2021], [Elsevier]), PCM/EG composites (**b**) (Reproduced with permission from (Yang et al. 2023a), COPYRIGHT [2023], [Wiley]), PEG/PU/EG composites (**c**) (Reproduced with permission from (Xiao et al. 2023a, b), COPYRIGHT [2022], [Wiley]) and UV-assisted PCM-based FSPCMs (D) (Reproduced with permission from (Xiao et al. 2023a, b), COPYRIGHT [2023], [Elsevier])

as FSPCMs for thermal energy storage (Shaid et al. 2016). The aerogel/eicosane composites had stable thermal behavior and could be applied in textiles. Our group also introduced PEG into aerogel and prepared an aerogel/PEG composite and the confinement of PEG in aerogel structure was revealed (Fig. 2.5a) (Yang et al. 2021).

Apart from silica aerogel, carbon-based porous materials were used to store PCMs since high thermal conductivity and free spaces for storage of PCMs were found. For example, our group recently used expanded graphite to store three common PCMs (PEG, PW and MA) (Fig. 2.5b) (Yang et al. 2023a). The confinement of PCMs in EG structure was found, which was related to phase transition behaviour of PCM/EG FSPCMs. Apart from structural analysis, the porous structure of EG was open, which was also similar to silica aerogel. So, factors of environment (e.g., humidity) could affect the phase transition behavior of such FSPCMs. By placing three FSPCMs in the environment with controlled humidity, we also revealed that higher relative humidity had a side effect on the phase transition behaviour (including phase transition range and enthalpy value) of PCM/EG FSPCMs. All the samples had smaller enthalpy values after treatment in hot and humid environment. It was proposed that the inherent chemical compatibility between PCMs and humidity accounted for such phenomena.

Although it is facial to have FSPCMs, it is argued that potential leakage and sensitivity to environment. To enhance the phase transition stability of FSPCMs, it is an alternative to use extra component to keep the whole PCMs inside. Tong Xiao et al. constructed a cross-linked porous carbon to store PEG by using phenolic

resin (Fig. 2.5c) (Xiao et al. 2023a, b). The curing process was applied after encapsulation of PEG in the porous carbon materials. After investigating leakage phenomena, the optimal resin-incorporated FSPCMs had the maximum loading amount of PEG was 87 wt% and thermal conductivity higher than 4 W m^{-1} K^{-1}. It also revealed that curing process was necessary to avoid leakage of resin-incorporated FSPCMs. Recently, UV-assistant method to enhance the stability of FSPCMs has been proposed. As shown in Fig. 2.5d, the principle of UV-assistant method to develop FSPCMs is to construct a stable network structure of porous materials by using UV and PCMs are well encapsulated (Xiao et al. 2023a, b). However, the chemical compatibility between resin and PCMs should be improved.

2.4 Introduction of SSPCMs

The SSPCMs are a group material that can keep the solid phase during their working temperature. For SSPCMs aimed to store thermal energy, the crystallizable moieties are incorporated through chemical bonding into a secondary structure that prevents them from flowing freely when they are in their liquid non-crystalline state (Fig. 2.6a) (Fallahi et al. 2017). For example, Youlong Zhao et al. proposed an SSPCM which was a polymeric PCM network based on multi-telechelic PEG-derived multimer structures (Fig. 2.6b) (Zhao et al. 2023). By applying the curing process for such SSPCMs, the storage modulus was enhanced. Besides, thermal energy storage was increased when the PEG with suitable molecular weight was used. Although the thermal stability of the SSPCMs was found, the final enthalpy of the SSPCMs was much lower than the theoretical pure PCMs, which was caused by the strong limitation of the molecular movement and the soft segment percentage (PCMs). Besides, the final SSPCMs were usually the films or the composites, which had relatively poor compatibility with textiles. To apply the SSPCMs in the textiles, the direct surface modification of the textiles or the fabrication of the PCM fibers was available.

2.5 PCM-Incorporated Textiles for Thermal Regulation

For PCM textiles, three types were included: PCM fibers, PCM yarns and PCM fabrics. Since properties of PCM yarns are mostly based on PCM fibers, here only PCM fibers and PCM fabrics are discussed.
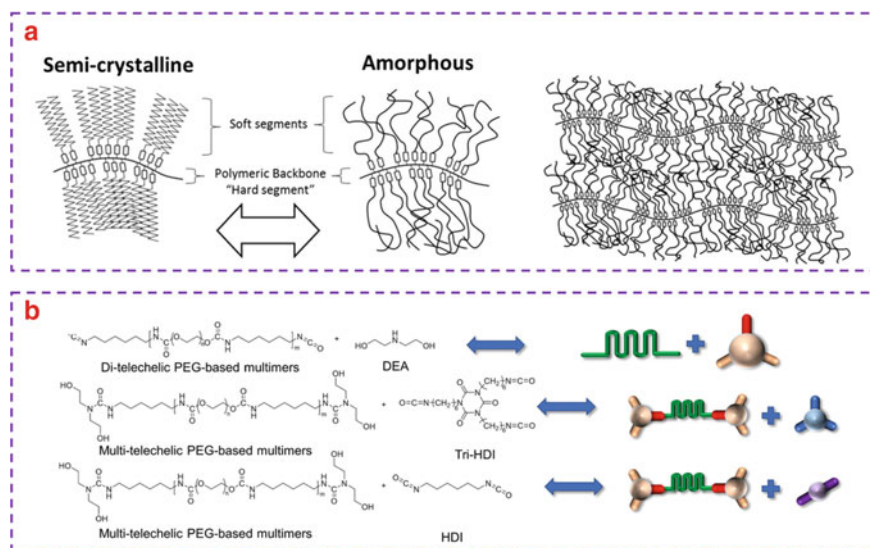
Fig. 2.6 Diagram for SSPCM (Reproduced with permission from (Fallahi et al. 2017), COPYRIGHT [2017], [Elsevier]), and multi-telechelic PEG-derived SSPCMs (Reproduced with permission from (Zhao et al. 2023), COPYRIGHT [2023], [Elsevier])

2.5.1 PCM Fibers

There are various methods for the preparation of PCM fibers, including melting polymer spinning, solution spinning, electrospinning, centrifugal spinning, etc. Especially, the ultrafine PCM fibers via electrospinning have attracted more and more attention (Wu et al. 2018). Three electrospinning technologies are included: uniaxial electrospinning, coaxial electrospinning and multifluidic electrospinning, via which various PCM fibers with different components can be fabricated (Fig. 2.7a).

Blending electrospinning is the most common method to prepare PCM fibers. For example, Nuray Kizidag fabricated paraffin/PAN PCM fibers via blending electrospinning (Kizildag 2021). The 50 wt% paraffin was able to be introduced in PAN fibers and the enthalpy value reached 57 J/g. Chao Lin et al. fabricated the IL/AlN/CoPA PCM fibers via blending electrospinning. The IL/AlN/CoPA PCM fibers had a diameter of about 1 um, and encapsulation of paraffin wax reached 57 wt% (C. Lin et al. 2021). It was included that the physical binding between PCMs and polymer matrix accounted for leakage phenomenon. However, it was unable to control the distribution of PCMs in PCM fibers and partial PCMs were on the surface, and the surface chemistry was altered. Besides, the stability of PCM fibers via blending electrospinning after washing was unideal where PCMs were removed.

In contrast to blending electrospinning, the uniaxial electrospinning (including co-electrospinning, emulsion electrospinning, etc.) provided an alternative to keep PCMs well inside of fiber matrix. For example, Aziz Babapoor et al. fabricated the
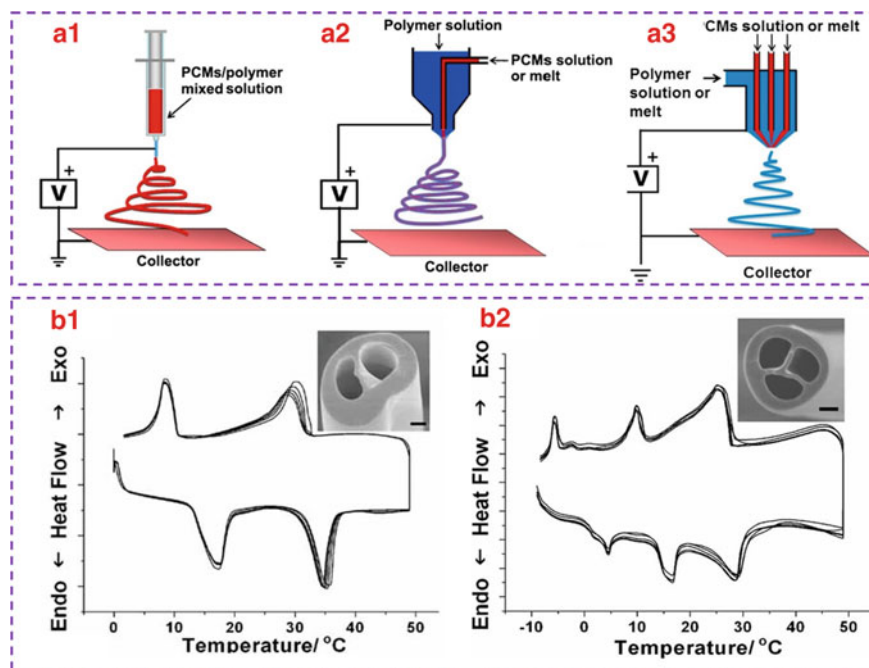
Fig. 2.7 Diagram for electrospinning technologies (a1, a2 and a3: uniaxial electrospinning, coaxial electrospinning and multifluidic electrospinning) (Reproduced with permission from (Wu et al. 2018), COPYRIGHT [2018], [Elsevier]) and multicomponent PCM fibers via multifluidic electrospinning (Reproduced with permission from (Wang et al. 2010), COPYRIGHT [2010], [Wiley])

PCM fibers with PEG as core materials and PA 6 as shell materials via uniaxial electrospinning (Babapoor et al. 2017). Higher supercooling degree of PCM fibers than pure PEG was found. Besides, Wen Feng et al. fabricated PEG/PU fiber via uniaxial electrospinning (Feng et al. 2021). The optimal latent heat of PEG/PU fibers was higher than 60 J/g. Especially, the PEG/PU fibrous membranes had shape memory.

To extend working temperature range of PCM fibers, fabrication of PCM fibers with different PCMs is an alternative, which can be realized via multifluidic electrospinning. As shown in Fig. 2.7b1 and b2, Nu Wang et al. successfully fabricated multicomponent PCM fibers and realized continuous working temperature (Wang et al. 2010).

Although there is significant progress in PCM fibers, there are some problems. The mechanical property of the fibrous webs consisting of the ultrafine PCM fibers prepared via all the electrospinning technologies is poor.

2.5.2 PCM Fabric

MPCMs or FSPCMs are usually for preparation of PCM fabrics and padding-drying-curing method is often used. For example, Yun Su et al. made a coating of MPCMs on the flame resistance fabric via the dry coating method (Su et al. 2020) (Fig. 2.8a). The coating slurry was prepared by mixing microcapsule suspension, thickener, adhesive, and water. The thickener (HEUR-B) was used to mix all components for speeding up the uniform dispersion and maintaining the surface smooth. F. Salaun et al. systematically investigated morphology of MPCM-coated fabrics by using binders. With increased binder amount, the MPCMs were well deposited on the surface while it was hard to determine the structural integrity (Fig. 2.8b). Besides, the relationship between binder amount, latent heat and melting temperature of MPCM-coated fabric was revealed as shown in Fig. 2.8c. More binders reduced overall latent heat of MPCM-coated fabrics and reduced air permeability. It was found that the binder amount and binder type affected phase transition behaviour. Apart from padding-drying-curing method, other methods have been utilized for MPCM-coated fabrics, including printing, lamination, etc. (Nejman et al. 2014). Similar to padding-drying-curing method, both MPCM amount and binder amount affected overall breathability whatever the method was applied.

Therefore, it can be included that binders are necessary for fabrics. However, there are some problems with MPCM-coated fabrics with binders as demonstrated. Here, discussions about such MPCM-coated fabrics are given here:

- Reduce breathability of fabrics because of binders

  Although the usage of binders increased MPCM loading amount on the fabric and stability of MPCMs in anti-washing cycles, the surface chemistry of fabrics was changed. Besides, the MPCM coating layer reduced breathability. To optimize breathability of MPCM-coated fabrics, several methods have been proposed, it was proposed that the PCMs were fixed on selected area of fabrics while other area of fabrics was uncoated. Then, breathability of such PCM fabric was found. However, the reduced PCM loading amount was inevitable.

- Change in surface chemistry of PCM fabrics because of binders

  It has been reported that binders affected the comfort of MPCM-coated fabrics since physical properties (e.g., wicking, etc.)) were changed. It was proposed to optimize the wicking property by modifying MPCM polymeric shell. In this case, the mass ratio between binders and MPCMs should be optimized. Besides, such MPCM-coated fabrics lacked hydrophobicity, which limited their applications.

Recently, our group proposed an MPCM-coated fabric with hydrophobicity (Yang et al. 2022a, b, c, d). As shown in Fig. 2.9, the commercial fabrics were firstly treated with hydrophobic coating, and then coated with MPCM slurry on one side. Although the binders were hydrophilic, the MPCM coating layer was very thin, and wicking supported the exposure of hydrophobic fibers outside. So, the
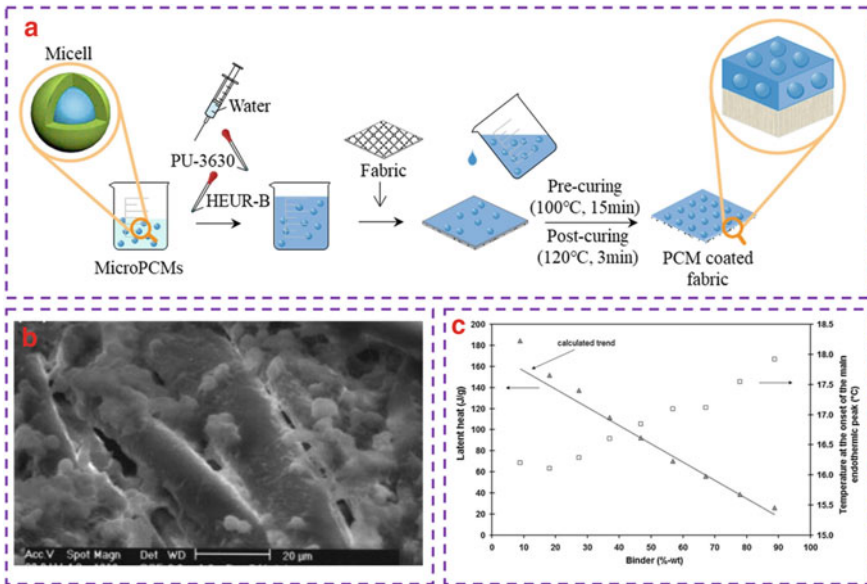
Fig. 2.8 Preparation of MPCM-coated fabric via padding-drying-curing method (**a**) Reproduced with permission from (Su et al. 2020), COPYRIGHT [2020], [Elsevier]), morphology of MPCM-coated fabric (**b**) (Reproduced with permission from (Salaün et al. 2010), COPYRIGHT [2010], [Elsevier])) and relationship between binder amount, latent heat and melting temperature of MPCM-coated fabric (**c**) (Reproduced with permission from (Salaün et al. 2010), COPYRIGHT [2010], [Elsevier])

hydrophobicity and breathability of the hydrophobic fabrics with single coating of MPCMs were found. Apart from the hydrophobicity, the thermal buffering effect of the hydrophobic fabrics with single coating of MPCMs was observed. It also proved that better thermal buffering effect was found when MPCM coating side was towards heating source. Subsequently, we reported one possibility to prepare the thermochromic MPCM-coated hydrophobic fabrics at CLOTECH 2022 conference, which was realized by making a coating of thermochromic pigments on one side of MPCM-coated hydrophobic fabrics. The thermochromic behaviour was well consistent with surface temperature change.

- Possible MPCMs destroy of coated fabrics

Various MPCMs have been coated on fabrics for thermal regulation, while the phase transition behaviour of such MPCM-coated fabrics was different from pure MPCMs (including MPCM slurry). It was argued that the difference was caused by the usage of binders, while it was one phenomenon and did not give any mechanism. We considered that some MPCMs may be destroyed during padding-drying-curing process resulting in change of phase transition behaviour. Still, it required more investigation.
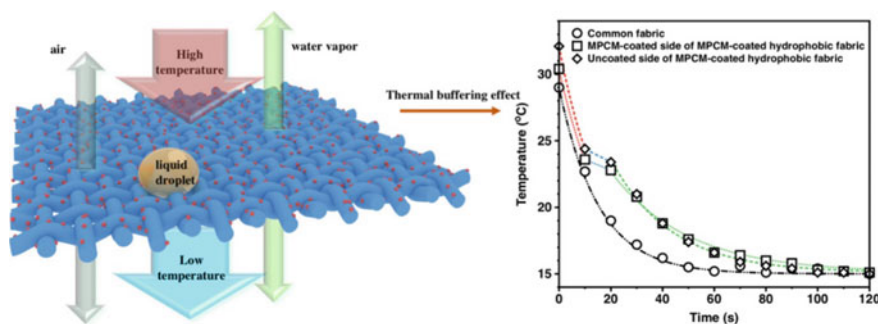
Fig. 2.9 Diagram for MPCM-coated hydrophobic fabrics and their thermal buffering effect with different directions towards heating sources (Reproduced with permission from (Yang et al. 2022b), COPYRIGHT [2022], [Elsevier])

2.5.3 Sandwich Fibrous PCM Encapsulations

From Sects. 2.5.1 to 2.5.2, both advantages and disadvantages of current PCM textiles were discussed. Although there was great progress in PCM textiles, many problems remained to be solved. It was concluded that two parameters were considered for current PCM textiles: PCM loading amount and wear comfort. The PCM loading amount in fabrics or fibers directly affected the thermal buffering effect or thermal regulation behaviour, breathability, mechanical property and so on. The wear comfort of PCM textiles was a result of breathability. So, how to optimize such PCM fabrics by controlling PCM loading amount and wear comfort was an emphasis.

Back to working principle of PCMs, the leakage phenomena of PCM textiles were caused by inherent solid–liquid phase transition. So, the leakage could be avoided by controlling the resistance of polymer film or nanofibrous membranes. Then, a concept was derived, and sandwich fibrous PCM encapsulations were proposed, which was a multi-layer PCM fabric.

Recently, a sandwich fibrous PCM encapsulation was successfully proposed by our group, was a multi-layer PCM fabric. Up to now, there have been two different sandwich fibrous PCM encapsulations.

- The laminated fabric-incorporated sandwich fibrous PCM encapsulations

The basic structure of laminated fabric-incorporated sandwich fibrous PCM encapsulations consisted of laminated fabric and PCM-loaded layer. As shown in Fig. 2.10a from our recent work (Yang et al. 2022f), the PA 6-laminated fabrics were protection layers and PEG-coated viscose fabrics were PCM-loaded layers. Then, the commercial fibrous hemming web was used to fix two layers together. Finally, the laminated fabric-incorporated sandwich fibrous PCM encapsulations were successfully fabricated. The maximum overall PEG loading amount in the laminated fabric-incorporated sandwich fibrous PCM encapsulations reached 88%, which was much higher than other PCM textiles (including PCM fabrics,

PCM fibers, etc.). The melting PEG was well kept inside during their working and no leakage was found. However, some problems remained for the laminated fabric-incorporated sandwich fibrous PCM encapsulations. Obviously, no breathability of the laminated fabric-incorporated sandwich fibrous PCM encapsulations was found. So, the microenvironment between human body and the laminated fabric-incorporated sandwich fibrous PCM encapsulations. Besides, the polymer for lamination could affect the phase transition of loaded PCMs because of their interfacial adhesion, which was still unclear. Although there are some problems, the laminated fabric-incorporated sandwich fibrous PCM encapsulations still provide an alternative for PCM textiles.

- The nanofibrous membrane-incorporated sandwich fibrous PCM encapsulations

The basic structure of nanofibrous membrane-incorporated sandwich fibrous PCM encapsulations was shown in Fig. 2.10b, consisting of a protection layer, barrier layers and PCM-loaded layer (Yang et al. 2022e, 2023b). The commercial fabrics
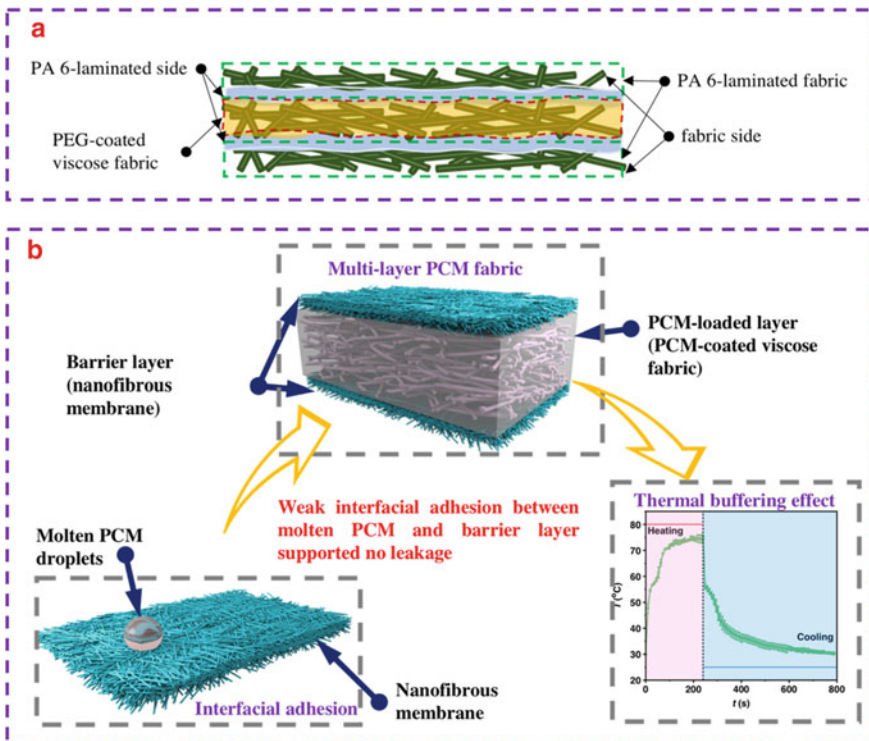
Fig. 2.10 Diagram for a laminated fabric-incorporated sandwich PCM encapsulations (**a**) (Reproduced with permission from (Yang et al. 2022f), COPYRIGHT [2022], [Lodz University of Technology Repository] and diagram for a sandwich fibrous PCM encapsulation by using nanofibrous membranes (**b**) (Reproduced with permission from (Yang et al. 2022e), COPYRIGHT [2022], [Wiley])

were protection layers, nanofibrous membranes were barrier layers and PCM-coated viscose fabric was PCM-loaded layer. The working principle of nanofibrous membrane-incorporated sandwich fibrous PCM encapsulations was that the weak adhesion between the barrier layer and melting PCMs resisted penetration of melting PCMs. Then, the leakage phenomena could be successfully avoided. In our primary stage, three organic PCMs (including PW, MA and PEG) were used, and PU nanofibrous membrane was used. By testing leakage phenomena and interfacial adhesion, only PW can be resisted by PU nanofibrous membranes. Then, nanofibrous membrane-incorporated sandwich fibrous PW encapsulations were proposed. The PW loading amount in the sandwich fibrous PW encapsulations was also high and could be adjusted by choosing a suitable protection layer with suitable areal density. However, there were some remaining problems. Similar to laminated fabric-incorporated sandwich fibrous PCM encapsulations, there was no breathability of nanofibrous membrane-incorporated sandwich fibrous PCM encapsulations. Different from laminated fabric-incorporated sandwich fibrous PCM encapsulations, there were three layers of nanofibrous membrane-incorporated sandwich fibrous PCM encapsulations. By adjusting the structure of PCM-loaded layer, the breathability could be optimized. Besides, limited PCM types were found in the nanofibrous membrane-incorporated sandwich fibrous PCM encapsulations. The possibility was to control the surface energy of the barrier layer or protection layer, then the leakage could be avoided.

2.6 Conclusion

In this chapter, we efficiently look into the recent developments of PCM textiles. In detail, the appropriate PCMs for the textiles are different, and the strategies to fabricate the PCM textiles are various. Correspondingly, the preparation of the PCM textiles is strongly with the final applications. Besides, research topics related to developing practical PCM textiles is meaningful for academic and industry, which should need more attention.

References

Babapoor A, Karimi G, Golestaneh SI, Mezjin MA (2017) Coaxial electro-spun PEG/PA6 composite fibers: fabrication and characterization. Appl Therm Eng 118:398–407. https://doi.org/10.1016/j.applthermaleng.2017.02.119

Bose P, Amirtham VA (2016) A review on thermal conductivity enhancement of paraffinwax as latent heat energy storage material. Renew Sustain Energy Rev 65:81–100. https://doi.org/10.1016/j.rser.2016.06.071

Brooks AL, Fang Y, Shen Z, Wang J, Zhou H (2021) Enabling high-strength cement-based materials for thermal energy storage via fly-ash cenosphere encapsulated phase change materials. Cement Concr Compos 120:104033. https://doi.org/10.1016/j.cemconcomp.2021.104033

Cai C, Ouyang X, Zhou L, Liu G, Wang Y, Zhu G, Yao J, Militky J, Venkataraman M, Zhang G (2020) Co-solvent free interfacial polycondensation and properties of polyurea PCM microcapsules with dodecanol dodecanoate as core material. Sol Energy 199:721–730. https://doi.org/10.1016/j.solener.2020.02.071

Cao X, Zhang R, Zhang N, Chen L, Chen D, Li X (2023) Performance improvement of lauric acid-1-hexadecanol eutectic phase change material with bio-sourced seashell powder addition for thermal energy storage in buildings. Constr Build Mater 366:130223. https://doi.org/10.1016/j.conbuildmat.2022.130223

Chen X, Cheng P, Tang Z, Xu X, Gao H, Wang G (2021) Carbon-based composite phase change materials for thermal energy storage, transfer, and conversion. Adv Sci 8(9):2001274. https://doi.org/10.1002/advs.202001274

Chen Z, Zhou J, Jiang Y, Hu Z, Yin S, Wang Q, Innocent MT, Xiang H, Zhu M (2022) Preparation of form-stable silica/polyethylene glycol composites using flash-drying for large-scale melt-spun fibers with thermal management property. Polym Eng Sci. https://doi.org/10.1002/pen.26220

Fallahi A, Guldentops G, Tao M, Granados-Focil S, Dessel SV (2017) Review on solid-solid phase change materials for thermal energy storage: molecular structure and thermal properties. Appl Therm Eng 127:1427–1441. https://doi.org/10.1016/j.applthermaleng.2017.08.161

Feng W, Zhang Y-S, Shao Y-W, Huang T, Zhang N, Yang J-H, Qi X-D, Wang Y (2021) Coaxial electrospun membranes with thermal energy storage and shape memory functions for simultaneous thermal/moisture management in personal cooling textiles. Eur Polym J 145. https://doi.org/10.1016/j.eurpolymj.2020.110245

Gao Y, Zhang W, Han N, Zhang X, Li W (2022) Cotton fabric containing photochromic microcapsules combined thermal energy storage features. Colloids Surf A 648:129249. https://doi.org/10.1016/j.colsurfa.2022.129249

Ghasemi K, Tasnim S, Mahmud S (2022) PCM, nano/microencapsulation and slurries: a review of fundamentals, categories, fabrication, numerical models and applications. Sustain Energy Technol Assess 52:102084. https://doi.org/10.1016/j.seta.2022.102084

Giro-Paloma J, Martínez M, Cabeza LF, Fernández AI (2016) Types, methods, techniques, and applications for microencapsulated phase change materials (MPCM): a review. Renew Sustain Energy Rev 53:1059–1075. https://doi.org/10.1016/j.rser.2015.09.040

Huang R, Li W, Wang J, Zhang X (2017) Effects of oil-soluble etherified melamine-formaldehyde prepolymers on in situ microencapsulation and macroencapsulation of n-dodecanol. New J Chem 41(17):9424–9437. https://doi.org/10.1039/c7nj01528c

Huang X, Chen X, Li A, Atinafu D, Gao H, Dong W, Wang G (2018) Shape-stabilized phase change materials based on porous supports for thermal energy storage applications. Chem Eng J 356:641–661. https://doi.org/10.1016/j.cej.2018.09.013

Ismail A, Zhou J, Aday A, Davidoff I, Odukomaiya A, Wang J (2023) Microencapsulation of bio-based phase change materials with silica coated inorganic shell for thermal energy storage. J Build Eng 67:105981. https://doi.org/10.1016/j.jobe.2023.105981

Khan MI, Asfand F, Al-Ghamdi SG (2023) Progress in research and development of phase change materials for thermal energy storage in concentrated solar power. Appl Therm Eng 219:119546. https://doi.org/10.1016/j.applthermaleng.2022.119546

Khosrojerdi M, Mortazavi SM (2013) Impregnation of a porous material with a PCM on a cotton fabric and the effect of vacuum on thermo-regulating textiles. J Therm Anal Calorim 114(3):1111–1119. https://doi.org/10.1007/s10973-013-3144-x

Kizildag N (2021) Smart composite nanofiber mats with thermal management functionality. Sci Rep 11(1):4256. https://doi.org/10.1038/s41598-021-83799-5

Lin C, Li W, Yan Y, Ke H, Liu Z, Deng L, Qiu Z (2021) Ultrafine electrospun fiber based on ionic liquid/AlN/copolyamide composite as novel form-stable phase change material for thermal energy storage. Solar Energy Mater Solar Cells 223.https://doi.org/10.1016/j.solmat.2020.110953

Lin X, Zhang X, Ji J, Zheng L (2021) Research progress on preparation, characterization, and application of nanoparticle-based microencapsulated phase change materials. Int J Energy Res 45(7):9831–9857. https://doi.org/10.1002/er.6538

Liu C, Zhang T, Li T, Wang Y (2022) Homogeneous-to-heterogeneous-strategy enables multifunctional phase-change materials for energy storage. Chem—A Eur J 28(29):e202200502. https://doi.org/10.1002/chem.202200502

Liu F, Wang J, Qian X (2017) Integrating phase change materials into concrete through microencapsulation using cenospheres. Cement Concr Compos 80:317–325. https://doi.org/10.1016/j.cemconcomp.2017.04.001

Liu W, Zhang X, Ji J, Wu Y, Liu L (2021) A review on thermal properties improvement of phase change materials and its combination with solar thermal energy storage. Energy Technol 9(7):2100169. https://doi.org/10.1002/ente.202100169

Nejman A, Cieślak M, Gajdzicki B, Goetzendorf-Grabowska B, Karaszewska A (2014) Methods of PCM microcapsules application and the thermal properties of modified knitted fabric. Thermochim Acta 589:158–163. https://doi.org/10.1016/j.tca.2014.05.037

Paneliya S, Khanna S, Utsav, Singh AP, Patel YK, Vanpariya A, Makani NH, Banerjee R, Mukhopadhyay I (2021) Core shell paraffin/silica nanocomposite: a promising phase change material for thermal energy storage. Renew Energy 167:591–599. https://doi.org/10.1016/j.renene.2020.11.118

Parvate S, Singh J, Vennapusa JR, Dixit P, Chattopadhyay S (2021) Copper nanoparticles interlocked phase-change microcapsules for thermal buffering in packaging application. J Ind Eng Chem 102:69–85. https://doi.org/10.1016/j.jiec.2021.06.029

Peng G, Dou G, Hu Y, Sun Y, Chen Z (2020) Phase change material (PCM) microcapsules for thermal energy storage. Adv Polym Technol 2020:1–20. https://doi.org/10.1155/2020/9490873

Şahan N, Paksoy H (2018) Developing microencapsulated 12-hydroxystearic acid (HSA) for phase change material use. Int J Energy Res 42(10):3351–3360. https://doi.org/10.1002/er.4090

Salaün F, Devaux E, Bourbigot S, Rumeau P (2010) Thermoregulating response of cotton fabric containing microencapsulated phase change materials. Thermochim Acta 506(1–2):82–93. https://doi.org/10.1016/j.tca.2010.04.020

Shaid A, Wang L, Islam S, Cai JY, Padhye R (2016) Preparation of aerogel-eicosane microparticles for thermoregulatory coating on textile. Appl Therm Eng 107:602–611. https://doi.org/10.1016/j.applthermaleng.2016.06.187

Su Y, Zhu W, Tian M, Wang Y, Zhang X, Li J (2020) Intelligent bidirectional thermal regulation of phase change material incorporated in thermal protective clothing. Appl Therm Eng 174. https://doi.org/10.1016/j.applthermaleng.2020.115340

Tang F, Liu L, Alva G, Jia Y, Fang G (2017) Synthesis and properties of microencapsulated octadecane with silica shell as shape–stabilized thermal energy storage materials. Sol Energy Mater Sol Cells 160:1–6. https://doi.org/10.1016/j.solmat.2016.10.014

Wang N, Chen H, Lin L, Zhao Y, Cao X, Song Y, Jiang L (2010) Multicomponent phase change microfibers prepared by temperature control multifluidic electrospinning. Macromol Rapid Commun 31(18):1622–1627. https://doi.org/10.1002/marc.201000185

Wang X, Chen Z, Xu W, Wang X (2019) Capric acid phase change microcapsules modified with graphene oxide for energy storage. J Mater Sci 54(24):14834–14844. https://doi.org/10.1007/s10853-019-03954-2

Wu Y, Chen C, Jia Y, Wu J, Huang Y, Wang L (2018) Review on electrospun ultrafine phase change fibers (PCFs) for thermal energy storage. Appl Energy 210:167–181. https://doi.org/10.1016/j.apenergy.2017.11.001

Xiao T, Geng L, Dai Y, Zhao J, Liu C (2023a) UV-cured polymer aided phase change thermal energy storage: Preparation, mechanism and prospects. J Energy Storage 64:107066. https://doi.org/10.1016/j.est.2023.107066

Xiao T, Liu Q, Lin Y, Lin T, Zhao J, Sun W, Chen X, Liu C (2023b) In situ encapsulation of phase-change thermal-storage material using 3D polymer-aided cross-linked porous carbon. Adv Energy Sustain Res 4(3):2200164. https://doi.org/10.1002/aesr.202200164

Xu D, Yang R (2019) Efficient preparation and characterization of paraffin-based microcapsules by emulsion polymerization. J Appl Polym Sci 136(21):47552. https://doi.org/10.1002/app.47552

Yang K, Martinkova L, Ctibor O, Venkataraman M, Wiener J, Zhang X, Zhu G, Zhang G, Yao J, Militky J (2022a) Visual textile temperature indicators by incorporating MPCMs (microencapsulation phase change materials) into thermochromic fabric. In: CLOTECH 2022 innovative materials, technologies and testing techniques for clothing improvement, 8 September 2022

Yang K, Martinkova L, Ctibor O, Zhang X, Venkataraman M, Wiener J, Zhu G, Zhang G, Yao J, Militky J (2022b) Mass transfer and thermal buffering effect of hydrophobic fabrics with single-side coating of MPCMs. Prog Org Coat 172:107151. https://doi.org/10.1016/j.porgcoat.2022.107151

Yang K, Peng Q, Venkataraman M, Novotna J, Karpiskova J, Mullerova J, Wiener J, Vikova M, Zhu G, Yao J, Militky J (2022c) Hydrophobicity, water moisture transfer and breathability of PTFE-coated viscose fabrics prepared by electrospraying technology and sintering process. Prog Org Coat 165:106775. https://doi.org/10.1016/j.porgcoat.2022.106775

Yang K, Venkataraman M, Karpiskova J, Suzuki Y, Ullah S, Kim I-S, Militky J, Wang Y, Yang T, Wiener J, Zhu G, Yao J (2021) Structural analysis of embedding polyethylene glycol in silica aerogel. Microporous Mesoporous Mater 310:110636. https://doi.org/10.1016/j.micromeso.2020.110636

Yang K, Venkataraman M, Zhang X, Wiener J, Zhu G, Yao J, Militky J (2022d) Review: incorporation of organic PCMs into textiles. J Mater Sci 57(2):798–847. https://doi.org/10.1007/s10853-021-06641-3

Yang K, Zhang X, Venkataraman M, Wiener J, Palanisamy S, Sozcu S, Tan X, Kremenakova D, Zhu G, Yao J, Militky J (2023a) Structural analysis of phase change materials (PCMs)/expanded graphite (EG) composites and their thermal behavior under hot and humid conditions. ChemPlusChem. https://doi.org/10.1002/cplu.202300081

Yang K, Zhang X, Venkataraman M, Wiener J, Tan X, Zhu G, Yao J, Militky J (2023b) Sandwich fibrous PEG encapsulations for thermal energy storage. ChemPhysChem e202300234. https://doi.org/10.1002/cphc.202300234

Yang K, Zhang X, Wiener J, Venkataraman M, Wang Y, Zhu G, Yao J, Militky J (2022e) Nanofibrous membranes in multilayer fabrics to avoid PCM leakages. ChemNanoMat 8(10). https://doi.org/10.1002/cnma.202200352

Yang K, Zhang X, Wiener J, Venkataraman M, Zhu G, Yao J, Militky J (2022f) Thermal behavior of a multi-layer laminated fabric containing PCMS. In: AUTEX 2022, 3 December 2022. https://doi.org/10.34658/9788366741751.64

Yin G-Z, López AM, Yang X-M, Ye W, Xu B, Hobson J, Wang D-Y (2022) Shape-stable and smart polyrotaxane-based phase change materials with enhanced flexibility and fire-safety. Eur Polymer J 173:111262. https://doi.org/10.1016/j.eurpolymj.2022.111262

Yu S, Wang X, Wu D (2014) Microencapsulation of n-octadecane phase change material with calcium carbonate shell for enhancement of thermal conductivity and serving durability: synthesis, microstructure, and performance evaluation. Appl Energy 114:632–643. https://doi.org/10.1016/j.apenergy.2013.10.029

Yuan Y, Zhang N, Tao W, Cao X, He Y (2014) Fatty acids as phase change materials: a review. Renew Sustain Energy Rev 29:482–498. https://doi.org/10.1016/j.rser.2013.08.107

Zhang G, Cai C, Wang Y, Liu G, Zhou L, Yao J, Militky J, Marek J, Venkataraman M, Zhu G (2019) Preparation and evaluation of thermo-regulating bamboo fabric treated by microencapsulated phase change materials. Text Res J 89(16):3387–3393. https://doi.org/10.1177/0040517518813681

Zhang H, Wang X, Wu D (2010) Silica encapsulation of n-octadecane via sol–gel process: a novel microencapsulated phase-change material with enhanced thermal conductivity and performance. J Colloid Interface Sci 343(1):246–255. https://doi.org/10.1016/j.jcis.2009.11.036

Zhang N, Yuan Y (2020) Synthesis and thermal properties of nanoencapsulation of paraffin as phase change material for latent heat thermal energy storage. Energy Built Environ 1(4):410–416. https://doi.org/10.1016/j.enbenv.2020.04.003

Zhao Y, Liu T, Wei Z, Yuan A, Chen Y, Jiang L, Lei J, Fu X (2023) Polymeric phase change material networks based on multi-telechelic polyethylene glycol-derived multimer structures for thermal energy storage. Chem Eng J 462:142164. https://doi.org/10.1016/j.cej.2023.142164

Zou L, Li S, Li L, Ji W, Li Y, Cheng X (2022) Synthesis of TiO2 shell microcapsule-based phase change film with thermal energy storage and buffering capabilities. Mater Today Sustain 18:100119. https://doi.org/10.1016/j.mtsust.2022.100119

Chapter 3
Application of Graphene in Supercapacitor and Wearable Sensor

Qingyan Peng, Xiaodong Tan, Mohanapriya Venkataraman, and Jiří Militký

Abstract The performance of energy storage devices and sensors is predominantly influenced by the microstructure and composition of the electrode materials. The two-dimensional (2D) structure of graphene has attracted significant attention in the research of supercapacitors and wearable sensors due to its remarkable electrical conductivity, mechanical properties, and large surface area surpassing that of carbon nanotubes. The inherent porous structure of graphene provides ample space for the storage and transportation of electrolyte ions, enabling fast charge/discharge kinetics. The human body is a complex system abundant with sensory organs such as fingers, nose, mouth, and more. Numerous physiological signals are continuously generated, which can reflect the body's condition. However, the interface between commercial rigid sensors and the skin is often inadequate, resulting in suboptimal signal quality. In this chapter, our objective is to review the recent advancements in graphene research and development for the applications of supercapacitors and wearable sensors. We will provide an overview of various synthesis strategies for graphene and explore their potential utilization in both asymmetric/symmetric supercapacitors and wearable sensors.

3.1 Introduction

Carbon, as the second most abundant element in the biosphere, holds significant potential for applications in various scientific, industrial, nanotechnological, and medical fields. The rapid development of carbon-based materials and their applications has made them a crucial topic in modern materials science (Titirici et al. 2015).

Q. Peng · X. Tan · M. Venkataraman (✉) · J. Militký
Department of Material Engineering, Faculty of Textile Engineering, Technical University of Liberec, Studentská 2, 46117 Liberec, Czech Republic
e-mail: mohanapriya.venkataraman@tul.cz

J. Militký
e-mail: jiri.militky@tul.cz

Carbon exhibits polymorphism, meaning it can form different allotropes due to variations in valency and morphology. The most common crystalline forms of carbon include graphite, diamond, and fullerene. The structural differences among these allotropes are attributed to the orbital overlap between carbon atoms. Graphite, for instance, has a density of approximately 2250 kg/m^2. The distance between its layers is about 0.335 nm, while the distance between two bonded carbon atoms within a layer is 0.142 nm.

In graphene, which consists of stacked layers of graphite, carbon atoms possess a trigonal planar molecular structure. They are bonded to each other in a sp2-hybridized manner, forming σ-bonds and delocalized π-bonds. The delocalization of loosely bound π-electrons leads to high electron mobility, which significantly influences the electrical conductivity of graphitic materials. The interlayer spacing in graphite, which is larger than the 0.142 nm distance of the C–C bond, is due to the absence of chemical bonds between the layers. Graphite's nanolayered structure allows adjacent graphene sheets to be bonded by weak Van der Waals forces (Fig. 3.1), enabling the layers to slide over each other and giving graphite its lubricating properties (Marsh and Reinoso 2006).

The electrical conductivity of graphite can be understood by examining its electronic energy band structure. Each carbon atom in graphite contributes 4 valence electrons, forming a unit cell with 4 carbon atoms and a total of 16 energy bands. Among these bands, 12 are σ-bands and 4 are π-bands. The 12 σ-bands are divided into bonding and antibonding orbitals, which are separated by approximately 5 eV. Between these bands, there are 2 strongly coupled bonding and antibonding π-orbitals. The valence electrons occupy 8 of these energy bands, resulting in the Fermi level being positioned in the middle of the 4 π-bands. The upper π-bands exhibit an overlap of approximately 0.03 eV along the edges of the Brillouin zone. This characteristic makes graphite a semi-metallic material, as it conducts electricity primarily through π-electrons (Marsh and Reinoso 2006). The electrical and thermal conductivity of graphite is highly anisotropic due to its layered structure. The layers
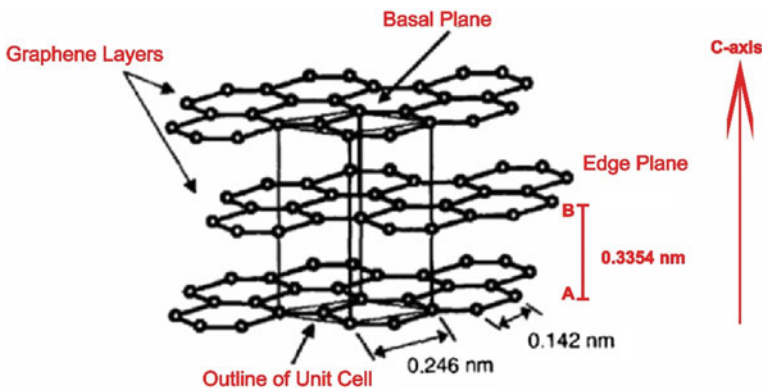
Fig. 3.1 Structure of graphite (Marsh and Reinoso 2006)

of graphene sheets in graphite allow for efficient electron and heat transfer within the plane, leading to high conductivity parallel to the layers. However, the interlayer bonding, governed by weak Van der Waals forces, hinders electron and heat transfer between the layers, resulting in lower conductivity in the perpendicular direction. Conductivity occurs in the plane of layers, σ_a, due to electron transfer compared to very low conductivity along the intrinsic c-axis σ_c where no electron transfer takes place (see Fig. 3.1). The anisotropy ratio of σa/σc for pyrolytic graphite is 10^3–10^5 (Marsh and Reinoso 2006). However, for single-crystal graphite the anisotropy ratio range is wider with values between 10^2 and 10^5 for reasons that are not well understood.

A particular type of expandable graphite serves as the initial material for producing worm-like expanded graphite (EG), which acts as an intermediate in the production of graphene (refer to Fig. 3.2). Various methods exist for exfoliating or expanding graphite, either by starting with graphene oxide (GO) or utilizing graphite intercalation compounds. Graphite intercalation compounds can be categorized into two types: electron donor reagents and electron acceptors. Electron donor reagents, such as alkali metals, function as reducing agents and result in the formation of metallic graphitides when interacting with graphite. On the other hand, electron acceptors, including halogens or oxoacids, act as oxidizing agents, leading to the formation of graphite salts through their interaction with graphite. These different intercalation compounds play a crucial role in the expansion and exfoliation of graphite, enabling the production of EG and further progression toward graphene synthesis.

Graphene, composed of thin 2D nanosheets of sp2-hybridized carbon atoms arranged in a hexagonal lattice, exhibits remarkable properties. It is utilized as a functional material due to its exceptional characteristics, including high current density, ballistic transport, high thermal conductivity, optical transparency, and superhydrophobicity at the nanoscale.

Since its discovery in 2004, graphene has garnered significant interest and has been extensively studied for its physical and chemical properties as well as its potential applications. The unique optical, mechanical, and electrical properties of graphene make it highly promising in various fields, including material science,

(a)   (b)   (c)
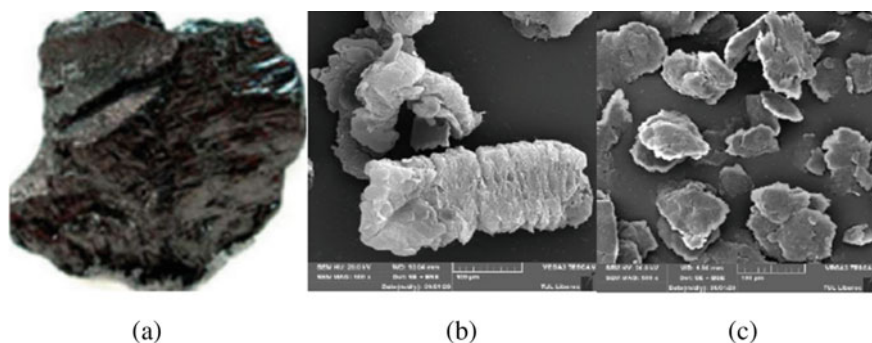
Fig. 3.2 **a** graphite **b** expanded graphite, **c** expanded graphite after 6 min ball milling

biomedicine, environmental treatment, and energy applications. Graphene is particularly recognized as a highly favorable electrode material for supercapacitors due to its exceptional characteristics such as high specific surface area, remarkable electrical conductivity, flexibility, and excellent chemical stability. Sensors, which are devices capable of converting incoming information into electrical or other output signals, play a vital role in the era of intelligence, digitization, and networking. They serve as crucial means of obtaining information. Graphene, although challenging to produce as a standalone material, is often used in the form of graphene composites, taking advantage of its remarkable features in combination with other materials. The size, number of layers, shape, and chemical groups of graphene have demonstrated significant influence on sensor performance. Moreover, the p-orbital electrons in graphene form π bonds with neighboring atoms, making them highly sensitive to environmental changes. This attribute makes graphene materials highly suitable for chemical and biosensor applications. This paper aims to explore the applications of graphene-based supercapacitors and sensors with different configurations. It also provides specific examples of their applications in various fields.

3.2 Fabrication of Graphene

3.2.1 Mechanical Exfoliation Approach

Geim et al. (Novoselov et al. 2004) from Manchester University achieved the production of a single layer of stable and highly crystalline graphene through mechanical exfoliation. The primary method involved using oxygen plasma on a 1 mm thick, strategically positioned pyrolytic graphite surface to create particle scratches. By scratching the surface with a width ranging from 20 µm to 2 mm and a depth of 5 µm, the graphene film adheres to a glass substrate and can be repeatedly peeled off using transparent tape. The excess pyrolytic graphite is then removed, and the glass substrate with a micro-cut is sonicated in acetone. Eventually, the mono-layer graphene is isolated using van der Waals or capillary force in acetone. However, this method has some limitations, such as uneven graphene thickness and low yield, which restrict its application in industrial settings.

Annett et al. employed thermodynamic forces to peel multilayer graphene, enabling the production of a large quantity of monolayer graphene. This approach facilitates self-exfoliation and self-assembly of graphene strips and holds promise for the large-scale preparation of graphene using physical techniques (Annett and Cross 2016). Xie et al. successfully produced high-density, surface-free, and high-quality graphene by peeling graphene from ball-milled graphite. This method allowed for the fabrication of a highly conductive graphene paper, providing a significant volume of graphene material (Xie et al. 2017).

3.2.2 Liquid Phase Stripping Approach

Liquid-phase stripping is a versatile and sustainable method for producing single-layer graphene. However, this approach has limitations, including low yield efficiency, severe agglomeration, and structural deformities caused by the ultrasonic process. It requires the addition of a significant amount of active agents, and the organic solvents used are highly sensitive to air and humidity, which restricts its practical application. Coleman et al. (Hernandez et al. 2008) investigated the dispersion and exfoliation of graphite in N-methyl-pyrrolidone. They successfully obtained individual graphene sheets with yields of up to 12% by mass. Hernandez et al. (Lotya et al. 2009) developed a method to disperse and exfoliate graphite using Sodium Dodecyl Benzene Sulphonate. The resulting graphene, with fewer than 5 layers, exhibited excellent conductivity, achieving a yield of approximately 40%. Drummond et al. (Bepete et al. 2017) reported a technique for preparing a single-layer graphene aqueous solution that is not sensitive to air and does not require the addition of surfactants. The preparation method is straightforward: KC8 is dispersed in a tetrahydrofuran solution, followed by the addition of degassed water and evaporation of the organic solvent. This process results in a monolayer graphene aqueous solution without the need for additional active agents.

3.2.3 Chemical Vapor Deposition

Chemical vapor deposition (CVD) is a technique used to deposit thin film materials by introducing the vapor or liquid reactant into a reaction chamber, where a chemical reaction takes place on the substrate surface to form a film. It is widely employed in the production of semiconductor films and is also utilized for graphene synthesis. CVD enables the high-quality, large-scale production of high-purity graphene. However, the conventional CVD method suffers from slow growth rates, which limits the advancement of graphene synthesis. Xu et al. (2016) addressed this issue by placing a copper foil catalyst on an oxide substrate with a distance of 15 μm. They introduced a continuous supply of oxygen to the outer layer of the copper foil catalyst through the oxide substrate, significantly reducing the energy barrier during the decomposition of carbon materials. As a result, they successfully achieved the rapid growth of single-crystal graphene, with a transverse dimension of 0.3 mm, in just 5 s, reaching a remarkable growth rate of up to 60 μm/s. This approach provides a means for large-scale production of high-quality graphene. Zheng et al. (2013). improved the speed and quality of graphene growth using CVD by subjecting the target substrate to ultrasonic treatment. This method is commonly applied in the field of laser photonics. Through AFM and Raman analysis, they demonstrated that treating the target substrate with ultrasound prior to CVD significantly reduces defects and overlayers and enhances the growth rate compared to graphene produced without sonication treatment.

Hu et al. (Xu et al. 2017) developed a static atmospheric pressure chemical vapor deposition (SAPCVD) system based on molecular thermal motion, enabling the rapid and large-scale production of high-quality graphene. The results demonstrated that the SAPCVD system could simultaneously fabricate optically homogeneous graphene on a 20-layer copper substrate. In comparison to conventional CVD techniques, the graphene produced using the SAPCVD system exhibited batch quantization, uniform optical properties, and low cost. The introduction and advancement of the SAPCVD system have accelerated the application of graphene in industrial production.

Ren et al. (Zhao et al. 2014) employed the atmospheric pressure chemical vapor deposition (APCVD) technique to fabricate large-area, multilayer graphene structures on polycrystalline copper foil surfaces. By optimizing the growth parameters, they achieved the formation of hexagonal double-layer and three-layer graphene with different stacking modes. Through a systematic investigation of the prepared double-layer and three-layer graphene, they observed a strong correlation between the energy band structure of graphene and its stacking mode. They found that graphene with a single-layer graphite stacking exhibited fewer defects compared to the multilayer stacking, making it more similar to the ideal graphene structure.

3.2.4 Oxidation Reduction Technology

Oxidation reduction technology is widely used in the preparation of graphene, with Stankovich et al. (Hernandez et al. 2008) being successful in synthesizing monolayer graphene using this approach. Since then, this technique has been extensively applied in laboratory settings.

Graphene is characterized as a zero-bandgap semiconductor with a surface that lacks reactive oxygen species, making it insoluble in water and organic solvents. As a result, researchers turned their attention to graphene oxide. Graphene oxide is a derivative of graphene that contains a significant number of oxygen functional groups on its surface. These oxygen groups readily react with organic molecules, making graphene oxide soluble in water (Nakajima and Matsuo 1994). The interlayer spacing of graphite oxide is approximately double that of untreated graphite, making it easier for small molecules and polymers to intercalate into the graphene oxide structure (Xiao-Ya 2011). There are several common methods for preparing graphene oxide, including the Brodie method (Brodie 1860), Staudenmaier method (Staudenmaier 1898) and Hummers method (Hummers and Offeman 1958). Among these, the improved Hummers method is widely used in current practice (Stankovich et al. 2007).

The general principle behind these methods is to treat graphite with strong acids and a small amount of oxidizing agent, which leads to the formation of intercalated graphite compounds. Subsequently, an excess of strong oxidant is added to obtain oxidized graphite, which is further subjected to ultrasonic treatment to obtain graphene oxide. To reduce graphene oxide back to graphene, various reduction

approaches are employed. These include the chemical liquid-phase reduction method (Stankovich et al. 2007), heat reduction approach (Yang et al. 2009), microwave reduction approach (Chen et al. 2010), and others. Each of these methods utilizes specific conditions to facilitate the reduction of graphene oxide and the restoration of graphene's structure.

3.2.5 Other Means for Fabrication of Graphene

Vecera et al. (2016) successfully prepared defect-free monolayer graphene on a silica substrate by utilizing K+ intercalation as a precursor for reductive graphite compounds. This technique offers several advantages, including controllable preparation conditions, batch production capability, cost-effectiveness, and sustainability. Li et al. (2016) introduced a wet-process fusion assembly method for the fabrication of nonwoven textures made of graphene fiber. They utilized the self-fusion property between oxidized graphite fibers, achieving the first successful production of large-scale graphene fibers with excellent performance. This breakthrough is significant for practical applications requiring high-performance graphene fibers. Sha et al. (2017) developed a simple technique to produce low-density graphene foam by 3D laser printing a mixture of nickel and sugar. This method eliminates the need for cold pressure molds or high-temperature chemical vapor deposition treatment. By directly laser-impacting a carbon-nickel mixture, they obtained graphene foam with low density and fingertip size. This approach lays the foundation for utilizing graphene in large-scale industrial applications. Yong et al. (2016) presented a rapid and straightforward strategy for graphene immobilization. They achieved one-step synthesis of graphene using a mold and oxygen plasma etching to remove ions. This method involved using a chemical vapor deposition system to produce large-area, homogeneous, and high-quality graphene, which was then directly transferred onto flexible substrates without the need for a polymer transfer layer or organic solvent. This approach offers simplicity, speed, low cost, and contamination-free graphene on various flexible substrates. The one-step molding technique holds significant potential for applications in flexible circuit components and wear-resistant electronic devices.

3.3 Graphene for Supercapacitor Applications

In our interconnected world, there is a growing need to explore enhanced energy storage and management systems in response to escalating energy demands, power shortages, and rising costs. Supercapacitors have garnered significant attention due to their impressive attributes, including high power density, fast charging capability, and long lifespan. With ongoing advancements, supercapacitors find applications in diverse fields such as personal electronics and hybrid electric vehicles. These

devices typically consist of dual electrodes separated by a porous separator in an electrolyte-based medium. When a voltage is applied, opposite charges accumulate at the electrodes, creating an electric field that enables the supercapacitor to store energy. Researchers primarily focus on energy and power densities, which determine the energy storage capacity and the duration a supercapacitor can function as a power source. The energy storage capacity can be calculated using the following equation:

$$E = \frac{1}{2}CV^2 \tag{3.1}$$

where C represents the capacitance and V is the applied voltage. The energy density of a supercapacitor is directly proportional to its capacitance, as it represents the amount of energy stored per unit volume or mass. Therefore, extensive research is focused on maximizing the capacitance of supercapacitors. Capacitance is defined as the ratio of the stored charge to the applied voltage, and it can be expressed using the following equation:

$$C = \varepsilon 0 \varepsilon r \frac{A}{D} \tag{3.2}$$

where $\varepsilon 0$ and εr refer to the dielectric constants of free space and for the insulating material flanked by the electrodes respectively, A is the electrode surface area and D is the distance between the electrodes. From the equation, it can be found that one of the main methods to enhance the capacitance would be to increase the surface area of the electrodes. The extensive surface area of graphene makes it become excellent candidate as an electrode material.

Power density is a crucial factor in supercapacitors as it governs the discharge and charging rate of energy. Higher power density in a supercapacitor-powered car, for instance, would result in significantly shorter charging times compared to conventional batteries, enabling faster acceleration. The following equation represents the maximum attainable power output of a supercapacitor:

$$p = \frac{V^2}{4ESR} \tag{3.3}$$

where V^2 refers to the voltage and ESR is the equivalent series resistance. Therefore, another incentive to improving the power density would be to reduce the resistance of the electrode.

Supercapacitors can be categorized into two types based on their capacitance generation mechanism: electric double-layer capacitance (EDLC) and pseudocapacitance (Tan and Lee 2013). EDLC-type supercapacitors derive capacitance from charge separation at the electrode–electrolyte interface. Enhancing this attribute involves optimizing pore volume and size distribution, hierarchical structure, interconnectivity between macropores and mesopores, and expanding the specific

surface area of the material. Pseudocapacitors, on the other hand, generate capacitance through rapid Faradaic reactions within the electrode material, which can include redox reactions, intercalation, and electrosorption. EDLC capacitors demonstrate good electrochemical cycling stability but tend to have lower capacitance values, while pseudocapacitors exhibit higher capacitance but relatively lower cyclic stability. To achieve high performance, comprehensive utilization of both EDLC and pseudocapacitor electrode materials has been proven effective. Graphene, with its constant surface area, pore size distribution, and favorable exposure to electrolytes, is recognized as an excellent constituent for supercapacitors (Park and Ruoff 2009). Additionally, graphene possesses remarkable properties such as high thermal conductivity (up to 5000 W m^{-1} k^{-1}) (Edwards and Coleman 2013), high strength with Young's modulus around 1 TPa, and an extensive surface area with a theoretical value of 2630 m^2 g^{-1}. Given the focus of this literature review on recent advancements in graphene science for supercapacitor applications, it is essential to discuss the key parameters that define a high-quality supercapacitor.

One crucial factor in determining the capacitance and overall performance of a supercapacitor is the effective area, which defines the electrode/electrolyte interface and the extent of the electric double-layer capacitance (EDLC). While graphene has a theoretically extensive surface area, it does not guarantee a high EDLC if the surface is not accessible to ions. Therefore, the layering and stacking configuration of graphene significantly impact its capacitance, and extensive research has been conducted to develop graphene composite structures with large ion-accessible surface areas. Porosity, pore volume, and pore size distribution also play a vital role in electrode capacitance. The size of the pores determines the types of ions that can reach the electrode surface. Optimizing this parameter is crucial to ensure that a majority of ions in the electrolyte can access the surface for optimal performance. The ideal pore size and volume depend on the specific electrolyte used. For instance, it has been demonstrated that pore sizes below 1.5 nm render the surface inaccessible to most ionic liquids. On the other hand, the total pore volume should be minimized to achieve a densely packed electrode with reduced weight.

3.3.1 Graphene–Nanoporous Carbon Supercapacitors

Recent studies have focused on combining nanoporous carbon materials with graphene to investigate the impact of porosity on supercapacitor performance. Nanoporous carbon materials, derived from carbide, exhibit varying degrees of porosity. Through careful formulation methods, researchers can create structures with different levels of microporosity and mesoporosity, as well as control the volume, size, and size distribution of pores. One study by Bandosz et al. (Seredych et al. 2012). explored the use of carbon graphene-nanoporous composites to examine the effect of porosity on supercapacitor performance. The study found that a pore volume below 0.7 nm was highly efficient for electric double-layer capacitance (EDLC) and resulted

in the highest gravimetric capacitance compared to pore volumes of 1 and 2 nm. Additionally, Na_2SO_4 exhibited superior capacitance performance at corresponding pore volumes, which can be attributed to the greater pseudocapacitance effects in Na2SO4 cells. Extensive research has also been conducted on other graphene-nanoporous carbon materials, including carbon nanotubes (CNTs) and carbon fibers (CFs) (Le et al. 2011). In many cases, the objective of developing these composites was to increase the effective surface area or introduce functional groups with oxygen on the graphene surface, as these factors play a crucial role in enhancing supercapacitor capacitance. To prevent aggregation of graphene sheets, which hinders ion access to the inner layers and reduces specific capacitance, efforts have been made to increase the surface area of graphene and maintain its dispersion.

In recent studies, the addition of carbon nanotubes (CNTs) as spacers and binders has been shown to prevent the aggregation of graphene sheets and maintain their connectivity (Cheng et al. 2011). These graphene-CNT electrodes demonstrated superior performance compared to pure CNTs or graphene electrodes. Specific capacitances of 290.4 F g-1 in KCl electrolyte and 201.0 F g-1 in TEABF4 electrolyte were calculated for the graphene-CNT electrodes. Another study addressed multiple challenges including interfacial strength, surface area, pore volume, and edge effects by utilizing graphene-like carbon fiber paper with CNTs grown on the surface (Hsu et al. 2012). The combination of good electrical conductivity, the unique structure of carbon fibers and CNTs, and the resulting increase in surface area and pore volume contributed to a reduction in resistance and an increase in specific capacitance. These free-standing structures also exhibited numerous edge effects, further enhancing the specific capacitance.

3.3.2 Graphene–Polymer Hybrids

Graphene-polymer composites play a crucial role in the advancement of supercapacitors, specifically for enhancing supercapacitor electrodes. Electrically conductive polymers alone demonstrate favorable specific capacitance, thanks to the presence of a p electron conjugation system that facilitates rapid and reversible redox reactions. However, relying solely on the polymer as an electrode material has limitations. It lacks the structural robustness of graphene and is susceptible to degradation caused by swelling and shrinkage of the polymer material. Therefore, this section emphasizes the advantages of combining graphene with electrically conductive polymers. By incorporating graphene, the composite not only exhibits excellent electrical double-layer capacitance (EDLC) but also enables faradaic reactions due to the presence of polymers. Various polymers such as polypyrrole (PPY), polyaniline (PANI), poly (3, 4-ethylenedioxythiophene) (PEDOT), polythiophene (PT), and poly (p-phenylenevinylene) (PPV) have been extensively studied for their potential as supercapacitor components. These polymers are preferred due to their

ease of production and excellent capacitance. Among them, PANI has been extensively researched, surpassing the other polymers, owing to its promising electrochemical activity and thermal stability (Ramaprabhu 2012). One study investigated the synthesis of carboxyl functionalized graphene oxide (CFGO)–PANI composites by performing in situ polymerization of PANI on the oxygenated base groups present on graphene. However, prior to this polymerization process, it was necessary to convert the oxygenated groups into carboxyl groups through chemical reactions. According to the authors, this approach maximized the utilization of naturally occurring oxygenated groups on the basal plane of graphene. Previous research studies had primarily focused on utilizing carboxyl groups located at the edges when forming PANI composites (Liu et al. 2012). At an applied current density of 0.3 A g^{-1}, the graphene–polymer composite produced in this study demonstrated remarkable capacitance (525 F g^{-1}) surpassing the capacitance achieved by previously synthesized graphene–polymer composites (323 F g^{-1}). The authors attributed this improvement in capacitance to the composite's ability to accommodate a greater number of PANI chains, which was facilitated by the utilization of oxygen-containing groups on the basal plane of graphene. In addition to the graphene–PANI composites, another interesting aspect of the research focused on graphene–PPY composites. While there has been extensive research on utilizing graphene and PPY as electrode composites, this study took a unique approach by employing PPY nanotubes instead of PPY fibers as the composite material (Biswas and Drzal 2010; Bose et al. 2011). The graphene-PPY nanotube composites demonstrated higher capacitance values (324 F g^{-1}) compared to graphene-PPY fiber composites studied previously. The researchers attributed this improvement to the larger surface area and macropore volume provided by the nanotube structures. This increased the exposure of the electrode to electrolytes and facilitated ion transfer. Furthermore, graphene has been combined with polyurethane (PU) to create supercapacitor electrodes with shape memory properties. These graphene-PU composites offer the ability to assume different shapes while retaining and recovering their original shape. This is particularly useful for flexible electrodes in non-conventional-shaped supercapacitors. The researchers aimed to synthesize graphene-PU composites using a simple bonding method. Graphene was initially produced via vacuum filtration from a graphene oxide (GO)/water solution, while PU was cast from a polyurethane/dimethylformamide (PU/DMF) solution. The resulting graphene-PU electrodes exhibited a maximum capacitance of 218 F g^{-1} at a current density of 0.5 A g^{-1}.

3.3.3 Graphene–Metal Oxide Supercapacitors

In recent years, there has been extensive research on graphene-metal oxide composites as they offer a unique approach to enhancing electrode performance in supercapacitors. Similar to graphene-polymer composites, these composites combine the advantages of graphene for high electric double-layer capacitance (EDLC) and metal oxides for pseudocapacitance. The incorporation of metal oxides into graphene

enables the composites to achieve enhanced efficiency in energy storage. To illustrate the enhanced performance of these composites, a comparison can be made between the capacitance achieved by pure graphene electrodes and metal oxide-graphene composites. Pure graphene electrodes typically exhibit an EDLC capacitance of around 135 F g^{-1}. In contrast, the introduction of metal oxides into graphene composites can significantly increase the capacitance, with values reaching as high as 135 F g^{-1}.

Mn_3O_4 has gained popularity in recent times due to its affordability, environmental compatibility, and high intrinsic capacity. In this particular approach, ethylene glycol was employed as a reducing agent, resulting in the successful dispersion of nanoparticles on the graphene surface. The final composite material exhibited a specific capacitance of 121 F g^{-1}, retaining 100% of that capacitance even after 10,000 cycles. This specific capacitance was found to be 3–4 times higher than that obtained with pure Mn_3O_4 electrodes. The improved performance can be attributed to a couple of factors. Firstly, pure Mn3O4 electrodes have lower conductivities, whereas the synthesis method used in this approach allowed for effective dispersion of the nanorods, enhancing the accessibility of the electrolytes to the composite and preventing aggregation. This facilitated better electrochemical performance. Apart from Mn oxide composites, graphene-metal oxide composites have been extensively explored for their potential as supercapacitor electrodes. For instance, the graphene-Co3O4 composite was synthesized using a simple two-step method involving sodium dodecyl sulfate (SDS). The resulting composite exhibited a unique scroll-like structure, demonstrating its suitability for supercapacitor applications (Zhou et al. 2011). Unlike many other composites that involve the intercalation of metal oxide particles onto graphene sheets, this method takes a different approach by intercalating reduced graphene wafers into Co_3O_4 scrolls. This integration process relies on the interaction between Co_3O_4 and oxygen functional groups present in the reduced graphene oxide. The resulting composite, known as reduced graphene oxide–Co_3O_4, achieved a specific capacitance of 168 F g^{-1} when discharged at a current of 1 A g^{-1}. The authors suggested that the excellent performance of the electrode could be attributed to the unique structure and synergistic effects arising from the combination of graphene and Co_3O_4.

3.3.4 Asymmetric Supercapacitors

The utilization of asymmetric supercapacitors, which employ two different types of electrodes instead of identical ones, has gained significant interest due to their ability to achieve higher energy densities while maintaining power densities. In a study by Yan and colleagues, flower-like nickel hydroxide-graphene composites were investigated as the positive electrode, while porous graphene served as the negative electrode in an asymmetric capacitor. The flower-like graphene composites were prepared using a microwave heating method, eliminating the need for templates or precipitate control agents. The choice of the flower-like structure was based on its

shorter diffusion path length for ions and electrons in electrolytes, facilitating rapid charging and discharging processes. In the asymmetric capacitor, the electrochemical potential window was varied from 0 to 1.6 V, resulting in a specific capacitance of $218.4\,F\,g^{-1}$ and an energy density of $77.8\,W\,h\,kg^{-1}$. Notably, the device demonstrated a long-term stable cycling capacity with 94% retention in capacitance after 3000 cycles (Yan et al. 2012).

3.4   Graphene for Supercapacitor Applications

Recently, graphene has garnered significant attention as an advanced functional material. It is a single-atom-thick, planar sheet composed of carbon atoms that are tightly packed in a honeycomb crystal lattice structure with sp2 bonding. Graphene's exceptional properties, such as its high current density, ability to enable ballistic transport of electrons without scattering, chemical inertness, high thermal conductivity, optical transparency, and superhydrophobicity at the nanoscale, have made it a highly sought-after material for cutting-edge applications (Chen et al. 2008). The initial extraction of graphene from graphite was achieved through a technique known as micromechanical cleavage (Novoselov et al. 2004). This method enabled the easy production of high-quality graphene crystallites and subsequently sparked extensive experimental efforts.

Graphene, in its natural form, is characterized as a semi-metal or a zero-gap semiconductor. It exhibits exceptional electronic properties, leading to a remarkably high transparency for an atomic monolayer. Interestingly, graphene has a remarkably low absorption ratio, with only 2.3% of white light being absorbed (Kuzmenko et al. 2008). Electrical portrayal has revealed an astonishingly high electron mobility at room temperature, with tentatively revealed qualities of more than $15{,}000\,cm^2\,V^-\,s^{-1}$ (Novoselov et al. 2004). The remarkable electrical properties of graphene have generated interest in its potential applications in future electronics. It can be utilized as a ballistic semiconductor, field emitter, component of integrated circuits, transparent conducting electrodes, and sensors. Graphene exhibits high electron or hole mobility and low Johnson noise, making it suitable for use as the channel in field-effect transistors (FETs). The combination of excellent electrical properties and low noise makes graphene an outstanding sensor. Its 2D structure allows the entire volume to be exposed to the surroundings, making it highly efficient in detecting adsorbed molecules. The high electrical conductivity and optical transparency of graphene also make it a promising candidate for transparent conducting electrodes, which are crucial for touchscreens, liquid crystal displays, organic photovoltaic cells, and organic light-emitting diodes (OLEDs).

3.4.1 Graphene Mechanical Sensor (Breath, Pulse, and Motion)

Due to its exceptional flexibility and mechanical strength, graphene holds tremendous potential in the field of mechanical sensors. Furthermore, its excellent piezoresistive properties make multilayer graphene and graphene-like materials highly desirable for such applications. The fractures or cracks in graphene play a crucial role in the sensing mechanism and overall measurement accuracy (El-Kady et al. 2012). Accurate measurement of mechanical signals such as pulse, breath, and heart rate requires precise detection within a limited range of pressure or strain. Yang et al. (2018) introduced a graphene-based textile sensor capable of measuring both subtle and significant human motion. This sensor exhibited the ability to accurately detect subtle pulse signals, including the percussion wave (P-wave), tidal wave (T-wave), and diastolic wave (D-wave). Additionally, the strain sensor made of graphene was placed near the mouth on the skin to effectively capture facial expressions such as crying and grinning. Qiao et al. (2018) developed a multilayer graphene-based epidermal electronic skin using laser scribing techniques. This sensor was specifically designed to be integrated onto a respirator or placed on the throat, allowing for the monitoring of respiratory signals. It effectively detected and distinguished between strong or slow breathing and weak or fast breathing. Tao et al. (2017a, b, c) presented a graphene-paper pressure sensor capable of detecting subtle variations in tension, such as heartbeat and gas pressure. This sensor demonstrated the ability to accurately distinguish changes in breathing patterns before and after exercise. Wang et al. (2014) developed a strain sensor made of graphene-woven textiles using the chemical vapor deposition (CVD) method. This sensor efficiently detects various human physiological signals and micro motions. It can be applied to the face, and the resistance of the sensor changes accordingly when the person changes facial expressions, blinks, or breathes.

SEM images of the graphene textile strain sensor in different scales are shown in Fig. 3.3. (Yang et al. 2018).

Monitoring human motion often necessitates a broad detection range, excellent flexibility, long-term durability, and high sensitivity (Shi et al. 2016). The graphene-based sensor mentioned above is capable of measuring large-scale motions such as finger bending, wrist bending, knee bending, and elbow bending.
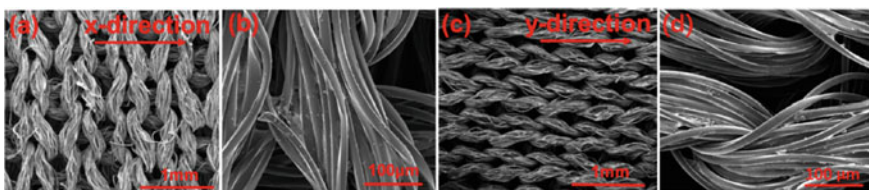
Fig. 3.3 SEM images of the graphene textile **a**, **b** the x-direction, **c**, **d** the y-direction

3.4.2   Graphene Acoustic Sensor

Sound is a form of mechanical vibration, and due to the excellent piezoresistive and thermoacoustic properties of graphene, graphene sensors are widely used for sound detection as well (Tao et al. 2017a, b, c) and sound emission (Wei et al. 2019). Furthermore, monolayer and multilayer graphene are highly suitable for use in acoustic devices. In comparison to conventional acoustic devices, graphene-based devices exhibit a broader frequency response and lower variance. A flexible sound-emitting device using reduced graphene oxide (rGO) was created through a one-step process called laser-induced graphene (LIG). A polyimide film was positioned under a 450 nm laser, resulting in the direct irradiation that transformed it into LIG. By applying an AC voltage to the device, cyclic joule heating caused the air to expand, generating sound waves. When a low bias voltage was applied, the resistance of the device changed due to the vibration of throat lines, resulting in a current variation (Tao et al. 2017a, b, c). Consequently, the devices can work as sound sources and detector simultaneously (see Fig. 3.4).

When a person coughs, hums, or screams, the vibrations of the throat cords can be detected by the laser-induced graphene (LIG) artificial throat. Subsequently, the LIG artificial throat is able to produce controlled sounds accordingly. This enables the LIG artificial throat to differentiate between arbitrary sounds and deliberate, pre-designed sounds. The morphology of the LIG produced under the optimal laser power of 290 mW is depicted in Fig. 3.5.

The image demonstrates the presence of well-organized ridges that are formed along the scanning path of the laser, extending from top to bottom. These ridges have a width of approximately 100 µm, which closely resembles the focal spot size of the laser.

Fig. 3.4 LIG with the ability of emitting and detecting sound in one device
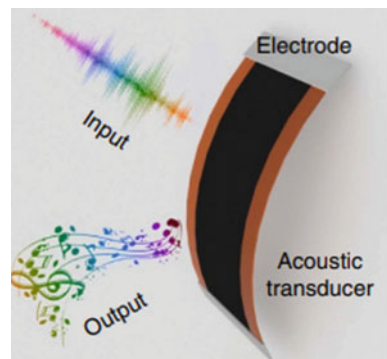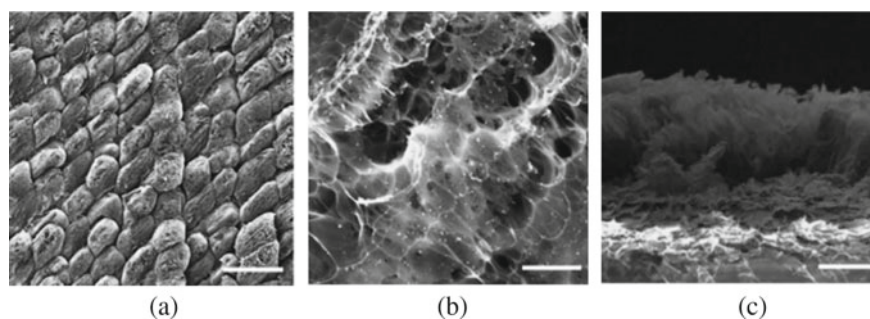
Fig. 3.5 The morphology of LIG sample produced at 290 mW **a** scale bar 150 mm, **b** scale bar 50 mm, **c** scale bar 12.5 mm (Tao et al. 2017a, b, c)

3.4.3 Graphene-Enabled Thermal Sensors

Temperature serves as a fundamental indicator of health. Thermal sensors utilizing graphene can detect internal temperature signals by measuring resistance changes resulting from transitions in the number of holes and electron pairs in the material. Graphene-enabled wearable sensors are widely applied in thermal management of human body, such as arm (Trung et al. 2016), neck (Trung et al. 2016), forehead (Ren et al. 2016), elbow (Lin et al. 2017), finger (Liu et al. 2019), belly (Lee et al. 2016), and palm (Park et al. 2015). Graphene-enabled thermal sensors have the capability to capture, process, and transmit body thermal signals to user interfaces such as smartphones or computers. This enables personal or clinical health evaluation and management. Various types of graphene-family composite materials with different structures can be utilized for thermal monitoring, catering to different application scenarios. For instance, Trung et al. (2018) integrated a temperature sensor based on reduced graphene oxide (rGO) fibers into garments or textiles. This allowed for temperature monitoring of the environment and the skin with a fast response time of 7 s and a recovery time of 20 s. The sensor remained unaffected during normal human activities. Besides, to acknowledge real-time and long-term thermal monitoring, Liu et al. (2019) produced a polyethyleneimine/rGO film-based temperature sensor by spray-dipping method, with a high sensitivity of $1.3\%°C^{-1}$ and a durability of 60 d, which can be applied for temperature checking of skin, breath, contact and blow. For 3D sponge-enabled physical sensor, a zeolite/graphene sponge is fabricated by a one-pot hydrothermal reduction method, which has a gentle exothermic methodology and superb thermal conductivity, holding incredible promise for injury treatment (Liang et al. 2019). In the context of local body temperature monitoring, 1D fiber-based thermal sensors are commonly used due to their precise tracking capabilities and space-saving nature. On the other hand, 2D film-based thermal sensors are primarily employed for monitoring temperature over a large area. 3D foam-based thermal sensors, characterized by their porous structure, are utilized for both thermal monitoring and adsorption purposes.

3.4.4 Graphene-Enabled Electrophysiological Sensors

Wearable sensors enabled by graphene technology are available for monitoring various electrophysiological signals, including electrocardiogram (ECG) measurements (Yun et al. 2017). electroencephalography (EEG) (Yun et al. 2017), electromyogram (EMG) (Kim et al. 2016), and electrooculography (EOG) (Golparvar and Yapici 2018). As an example, Yun et al. developed an epidermal sensor using reduced graphene oxide (rGO) and polydimethylsiloxane (PDMS) through a process involving electrostatic deposition of graphene oxide (GO) onto PDMS and subsequent chemical reduction. The resulting sensor exhibited remarkable properties, including the ability to withstand 150% strain and 5000 cycles of stretching. These characteristics make it highly promising for applications in emergency response, artificial intelligence, and biomedical fields (Yun et al. 2017). However, there is a mechanical mismatch between soft tissues and rigid wearable devices, resulting in low sensitivity and stability. To address this issue, Kim et al. developed a stretchable cell-sheet-graphene hybrid for electromyographical monitoring and treatment of neuromuscular disorders, both in vivo and in vitro. The combination of multifunctional sensing capabilities and therapeutic regimens offered by these graphene-based biomedical sensors holds great promise for the advancement of highly advanced multifunctional soft bioelectronics (Kim et al. 2016). Electrophysiological sensors enabled by graphene can be fabricated in various dimensional structures, including 1D, 2D, and 3D, to facilitate different types of electrophysiological monitoring. In an effort to mimic the surface morphology of the skin, Ameri et al. developed a graphene electronics tattoo using a "wet transfer, dry patterning" technique. This tattoo had a thin thickness of 463 ± 30 nm, high transparency of approximately 85%, and a stretchability of 40%. It was specifically designed for monitoring electrocardiogram (ECG), electromyogram (EMG), and electroencephalogram (EEG) signals (Ameri and Wang 2020). To achieve a relatively large contact area with the skin, a 2D film-based physical sensor composed of a graphene-coated textile electrode is employed. This sensor demonstrates excellent compatibility and exhibits a 97% cross-correlation compared to conventional silver/silver chloride electrodes. It is suitable for ECG signals and acquiring data, which can be interfaced with a computer or similar user interface (Yapici et al. 2015). However, many on-skin sensors currently available lack breathability, which can hinder sweat evaporation and potentially lead to skin inflammation. To address this issue, Sun et al. developed a 3D sponge-based wearable sensor by using laser-written graphene as the sensing unit and a sugar-templated silicone sponge as a flexible substrate. This sensor exhibited a high gas permeability of 18 mg cm^{-2} h^{-1}, allowing for enhanced breathability. It can be used for multifunctional monitoring of EEG, ECG, EMG, hydration and temperature (Sun et al. 2018).

3.4.5 Graphene-Enabled Biochemical Sensors

Graphene-enabled biochemical sensors have shown promising applications in monitoring various health-related signals, including glucose, cortisol, cytokines, gases, SpO2, hormones, and more. These signals can be detected in breath, skin sweat, blood, interstitial fluid, tears, saliva, and wound exudate. Each source has different concentrations of biomarkers that are associated with different diseases. For example, blood typically has higher concentrations of glucose compared to other sources, making blood monitoring the most reliable method for assessing glucose levels. The mechanism for detecting these biochemical stimuli involves measuring resistance changes in graphene-based materials in response to different health-related states. Sampling from sweat, tears, saliva, breath, and skin perspiration is relatively effortless and straightforward. On the other hand, sampling from wound exudate, blood, and interstitial fluid usually requires invasive procedures or optical monitoring techniques, such as using microneedles. By utilizing graphene-enabled biochemical sensors, we can assess the overall state of body health and potentially prevent the onset of diseases at an early stage. These sensors provide a non-invasive and convenient approach to monitoring and maintaining individual well-being.

3.5   Conclusion

Graphene, since its discovery, has demonstrated remarkable properties and has found widespread applications in various fields, including electrical, mechanical, electromechanical, and optical domains. It exists in different dimensional forms, such as fullerene (0D), carbon nanotube (1D), and graphite (stacked layers). Graphene is an ultrathin material with nanometer thickness and is recognized as the strongest material ever measured. Commercial synthesis methods for graphene have been developed, and significant progress has been made in utilizing graphene for electrochemical energy storage and conversion devices. Research has focused on combining graphene with metal oxides and conducting polymers to create hybrid materials with excellent electrochemical properties. However, further investigation is required to fully understand the interactions between metal oxides, polymers, and graphene that lead to synergistic effects. By systematically varying these factors and studying their impacts, a comprehensive understanding can be achieved, allowing for the optimization of graphene materials for superior electrochemical performance in supercapacitor applications. This fundamental understanding is crucial for maximizing the potential of graphene in energy storage devices. In the field of wearable sensors, graphene has demonstrated exceptional performance, resulting in significant improvements in signal quality and the successful detection of various types of signals. The flexibility and comfortable interface of graphene-based wearable sensors enable real-time monitoring, leading to a wealth of information. Combined with machine learning and big data techniques, graphene wearable sensors have the

potential to meet clinical and medical requirements. It is compelling to envision that in the future, graphene sensors and their wearable devices will greatly enhance people's quality of life. Perhaps one day, diagnosis and therapy will seamlessly integrate into our daily lives.

References

Ameri SK, Wang L (2020) Graphene electronic tattoo sensors for point-of-care personal health monitoring and human–machine interfaces In: Emerging 2D materials and devices for the internet of things. Elsevier, pp 59–86

Annett J, Cross GL (2016) Self-assembly of graphene ribbons by spontaneous self-tearing and peeling from a substrate. Nature 535(7611):271–275

Bepete G, Anglaret E, Ortolani L, Morandi V, Huang K, Pénicaud A et al (2017) Surfactant-free single-layer graphene in water. Nat Chem 9(4):347–352

Biswas S, Drzal LT (2010) Multilayered nanoarchitecture of graphene nanosheets and polypyrrole nanowires for high performance supercapacitor electrodes. Chem Mater 22(20):5667–5671

Bose S, Kim NH, Kuila T, Lau K-T, Lee JH (2011) Electrochemical performance of a graphene–polypyrrole nanocomposite as a supercapacitor electrode. Nanotechnology 22(29):295202

Brodie BC (1860) Sur le poids atomique du graphite. Ann Chim Phys 59(466):e472

Chen J-H, Jang C, Xiao S, Ishigami M, Fuhrer MS (2008) Intrinsic and extrinsic performance limits of graphene devices on SiO 2. Nat Nanotechnol 3(4):206–209

Chen W, Yan L, Bangal PR (2010) Preparation of graphene by the rapid and mild thermal reduction of graphene oxide induced by microwaves. Carbon 48(4):1146–1152

Cheng Q, Tang J, Ma J, Zhang H, Shinya N, Qin L-C (2011) Graphene and carbon nanotube composite electrodes for supercapacitors with ultra-high energy density. Phys Chem Chem Phys 13(39):17615–17624

Edwards RS, Coleman KS (2013) Graphene synthesis: relationship to applications. Nanoscale 5(1):38–51

El-Kady MF, Strong V, Dubin S, Kaner RB (2012) Laser scribing of high-performance and flexible graphene-based electrochemical capacitors. Science 335(6074):1326–1330

Golparvar AJ, Yapici MK (2018) Electrooculography by wearable graphene textiles. IEEE Sens J 18(21):8971–8978

Hernandez Y, Nicolosi V, Lotya M, Blighe FM, Sun Z, De S et al (2008) High-yield production of graphene by liquid-phase exfoliation of graphite. Nat Nanotechnol 3(9):563–568

Hsu H-C, Wang C-H, Nataraj S, Huang H-C, Du H-Y, Chang S-T et al (2012) Stand-up structure of graphene-like carbon nanowalls on CNT directly grown on polyacrylonitrile-based carbon fiber paper as supercapacitor. Diam Relat Mater 25:176–179

Hummers WS Jr, Offeman RE (1958) Preparation of graphitic oxide. J Am Chem Soc 80(6):1339–1339

Kim SJ, Cho KW, Cho HR, Wang L, Park SY, Lee SE et al (2016) Stretchable and transparent biointerface using cell-sheet–graphene hybrid for electrophysiology and therapy of skeletal muscle. Adv Func Mater 26(19):3207–3217

Kuzmenko AB, Van Heumen E, Carbone F, Van Der Marel D (2008) Universal optical conductance of graphite. Phys Rev Lett 100(11):117401

Le LT, Ervin MH, Qiu H, Fuchs BE, Lee WY (2011) Graphene supercapacitor electrodes fabricated by inkjet printing and thermal reduction of graphene oxide. Electrochem Commun 13(4):355–358

Lee H, Choi TK, Lee YB, Cho HR, Ghaffari R, Wang L et al (2016) A graphene-based electro-chemical device with thermoresponsive microneedles for diabetes monitoring and therapy. Nat Nanotechnol 11(6):566–572

Li Z, Xu Z, Liu Y, Wang R, Gao C (2016) Multifunctional non-woven fabrics of interfused graphene fibres. Nat Commun 7(1):1–11

Liang Y, Xu C, Liu F, Du S, Li G, Wang X (2019) Eliminating heat injury of zeolite in hemostasis via thermal conductivity of graphene sponge. ACS Appl Mater Interfaces 11(27):23848–23857

Lin S-Y, Zhang T-Y, Lu Q, Wang D-Y, Yang Y, Wu X-M et al (2017) High-performance graphene-based flexible heater for wearable applications. RSC Adv 7(43):27001–27006

Liu Q, Tai H, Yuan Z, Zhou Y, Su Y, Jiang Y (2019) A high-performances flexible temperature sensor composed of polyethyleneimine/reduced graphene oxide bilayer for real-time monitoring. Adv Mater Technol 4(3):1800594

Liu Y, Deng R, Wang Z, Liu H (2012) Carboxyl-functionalized graphene oxide–polyaniline composite as a promising supercapacitor material. J Mater Chem 22(27):13619–13624

Lotya M, Hernandez Y, King PJ, Smith RJ, Nicolosi V, Karlsson LS et al (2009) Liquid phase production of graphene by exfoliation of graphite in surfactant/water solutions. J Am Chem Soc 131(10):3611–3620

Marsh H, Reinoso FR (2006) Activated carbon. Elsevier

Nakajima T, Matsuo Y (1994) Formation process and structure of graphite oxide. Carbon 32(3):469–475

Novoselov KS, Geim AK, Morozov SV, Jiang D, Zhang, Y., Dubonos SV et al (2004) Electric field effect in atomically thin carbon films.Science 306(5696):666–669

Park J, Kim M, Lee Y, Lee HS, Ko H (2015) Fingertip skin–inspired microstructured ferroelectric skins discriminate static/dynamic pressure and temperature stimuli. Sci Adv 1(9):e1500661

Park S, Ruoff RS (2009) Chemical methods for the production of graphenes. Nat Nanotechnol 4(4):217–224

Qiao Y, Wang Y, Tian H, Li M, Jian J, Wei Y et al (2018) Multilayer graphene epidermal electronic skin. ACS Nano 12(9):8839–8846

Ramaprabhu S (2012) Poly (p-phenylenediamine)/graphene nanocomposites for supercapacitor applications. J Mater Chem 22(36):18775–18783

Ren X, Pei K, Peng B, Zhang Z, Wang Z, Wang X et al (2016) A low-operating-power and flexible active-matrix organic-transistor temperature-sensor array. Adv Mater 28(24):4832–4838

Seredych M, Koscinski M, Sliwinska-Bartkowiak M, Bandosz TJ (2012) Active pore space utiliza-tion in nanoporous carbon-based supercapacitors: effects of conductivity and pore accessibility. J Power Sources 220:243–252

Sha J, Li Y, Villegas Salvatierra R, Wang T, Dong P, Ji Y et al (2017) Three-dimensional printed graphene foams. ACS Nano 11(7):6860–6867

Shi J, Li X, Cheng H, Liu Z, Zhao L, Yang T et al (2016) Graphene reinforced carbon nanotube networks for wearable strain sensors. Adv Func Mater 26(13):2078–2084

Stankovich S, Dikin DA, Piner RD, Kohlhaas KA, Kleinhammes A, Jia Y et al (2007) Synthesis of graphene-based nanosheets via chemical reduction of exfoliated graphite oxide. Carbon 45(7):1558–1565

Staudenmaier L (1898) Verfahren zur darstellung der graphitsäure. Ber Dtsch Chem Ges 31(2):1481–1487

Sun B, McCay RN, Goswami S, Xu Y, Zhang C, Ling Y et al (2018) Gas-permeable, multifunctional on-skin electronics based on laser-induced porous graphene and sugar-templated elastomer sponges. Adv Mater 30(50):1804327

Tan YB, Lee J-M (2013) Graphene for supercapacitor applications. J Mater Chem A 1(47):14814–14843

Tao L-Q, Sun H, Liu Y, Ju Z-Y, Yang Y, Ren T-L (2017a) Flexible graphene sound device based on laser reduced graphene. Appl Phys Lett 111(10):103104

Tao L-Q, Wang D-Y, Tian H, Ju Z-Y, Liu Y, Pang Y et al (2017b) Self-adapted and tunable graphene strain sensors for detecting both subtle and large human motions. Nanoscale 9(24):8266–8273

Tao L-Q, Zhang K-N, Tian H, Liu Y, Wang D-Y, Chen Y-Q et al (2017c) Graphene-paper pressure sensor for detecting human motions. ACS Nano 11(9):8790–8795

Titirici M-M, White RJ, Brun N, Budarin VL, Su DS, Del Monte F et al (2015) Sustainable carbon materials. Chem Soc Rev 44(1):250–290

Trung TQ, Le HS, Dang TML, Ju S, Park SY, Lee NE (2018) Freestanding, fiber-based, wearable temperature sensor with tunable thermal index for healthcare monitoring. Adv Healthc Mater 7(12):1800074

Trung TQ, Ramasundaram S, Hwang BU, Lee NE (2016) An all-elastomeric transparent and stretchable temperature sensor for body-attachable wearable electronics. Adv Mater 28(3):502–509

Vecera P, Holzwarth J, Edelthalhammer KF, Mundloch U, Peterlik H, Hauke F et al (2016) Solvent-driven electron trapping and mass transport in reduced graphites to access perfect graphene. Nat Commun 7(1):1–7

Wang Y, Wang L, Yang T, Li X, Zang X, Zhu M et al (2014) Wearable and highly sensitive graphene strain sensors for human motion monitoring. Adv Func Mater 24(29):4666–4670

Wei Y, Qiao Y, Jiang G, Wang Y, Wang F, Li M et al (2019) A wearable skinlike ultra-sensitive artificial graphene throat. ACS Nano 13(8):8639–8647

Xiao-Ya Y (2011) Progress in preparation of graphene. J Inorg Mater 26(6):561–570

Xie X, Chen M, Liu P (2017) High hydrogen desorption properties of Mg-based nanocomposite at moderate temperatures: the effects of multiple catalysts in situ formed by adding nickel sulfides/graphene. J Power Sources 371:112–118

Xu J, Hu J, Li Q, Wang R, Li W, Guo Y et al (2017) Fast batch production of high-quality graphene films in a sealed thermal molecular movement system. Small 13(27):1700651

Xu X, Zhang Z, Qiu L, Zhuang J, Zhang L, Wang H et al (2016) Ultrafast growth of single-crystal graphene assisted by a continuous oxygen supply. Nat Nanotechnol 11(11):930–935

Yan J, Fan Z, Sun W, Ning G, Wei T, Zhang Q et al (2012) Advanced asymmetric supercapacitors based on Ni (OH) 2/graphene and porous graphene electrodes with high energy density. Adv Func Mater 22(12):2632–2641

Yang D, Velamakanni A, Bozoklu G, Park S, Stoller M, Piner RD et al (2009) Chemical analysis of graphene oxide films after heat and chemical treatments by X-ray photoelectron and Micro-Raman spectroscopy. Carbon 47(1):145–152

Yang Z, Pang Y, Han X, Yang Y, Ling J, Jian M et al (2018) Graphene textile strain sensor with negative resistance variation for human motion detection. ACS Nano 12(9):9134–9141

Yapici MK, Alkhidir T, Samad YA, Liao K (2015) Graphene-clad textile electrodes for electrocardiogram monitoring. Sens Actuators B Chem 221:1469–1474

Yong K, Ashraf A, Kang P, Nam S (2016) Rapid stencil mask fabrication enabled one-step polymer-free graphene patterning and direct transfer for flexible graphene devices. Sci Rep 6(1):1–8

Yun YJ, Ju J, Lee JH, Moon SH, Park SJ, Kim YH et al (2017) Highly elastic graphene-based electronics toward electronic skin. Adv Func Mater 27(33):1701513

Zhao H, Lin Y-C, Yeh C-H, Tian H, Chen Y-C, Xie D et al (2014) Growth and Raman spectra of single-crystal trilayer graphene with different stacking orientations. ACS Nano 8(10):10766–10773

Zheng G, Chen Y, Huang H, Zhao C, Lu S, Chen S et al (2013) Improved transfer quality of CVD-grown graphene by ultrasonic processing of target substrates: applications for ultra-fast laser photonics. ACS Appl Mater Interfaces 5(20):10288–10293

Zhou W, Liu J, Chen T, Tan KS, Jia X, Luo Z et al (2011) Fabrication of Co 3 O 4-reduced graphene oxide scrolls for high-performance supercapacitor electrodes. Phys Chem Chem Phys 13(32):14462–14465

Chapter 4
Comparison of the Synthesis, Properties, and Applications of Graphite, Graphene, and Expanded Graphite

Divan Coetzee, Jiří Militký, Jakub Wiener, and Mohanapriya Venkataraman

Abstract Carbon is one of the most abundant elements in the universe and exists in many forms. The allotropes of carbon have very different properties due to differences in their physical and electronic structures. The sp^2 hybridized allotropes of carbon are typically formed by processing graphite on commercial scale to form graphene, fullerene, and carbon nanotubes. Expanded graphite is a form of processed graphite after exfoliation and heating. This is technically not considered an allotrope of carbon since the physical structure still partly resembles that of graphite, but the material exhibits distinctly different properties.

4.1 Introduction

Carbon is one of the fundamental elements in our universe and is essential for life to exist. This importance is due to the chemical nature of carbon to form strong bonds with most other elements including itself; thus, it can form large and complex molecules. Crystalline carbon naturally has two allotropes which are sp^2 hybridized graphite and sp^3 hybridized diamond (Karthik et al. 2014). The twentieth century saw the discovery of carbon as fullerene, nanotubes, and graphene which are considered synthetic allotropes using graphite as precursor material. These synthetic allotropes of carbon are showing very promising properties for use in nano- and optoelectronics. Research in this field is deepening our knowledge of elemental bonding and optical interactions of organic structures. (Prenzel and Tykwinski 2014; Nasir et al. 2018). The allotropes of carbon are illustrated in Fig. 4.1.

D. Coetzee · J. Militký · J. Wiener · M. Venkataraman (✉)
Department of Material Engineering, Faculty of Textile Engineering, Technical University of Liberec, Studentská 2, 46117 Liberec, Czech Republic
e-mail: mohanapriya.venkataraman@tul.cz

J. Militký
e-mail: jiri.militky@tul.cz
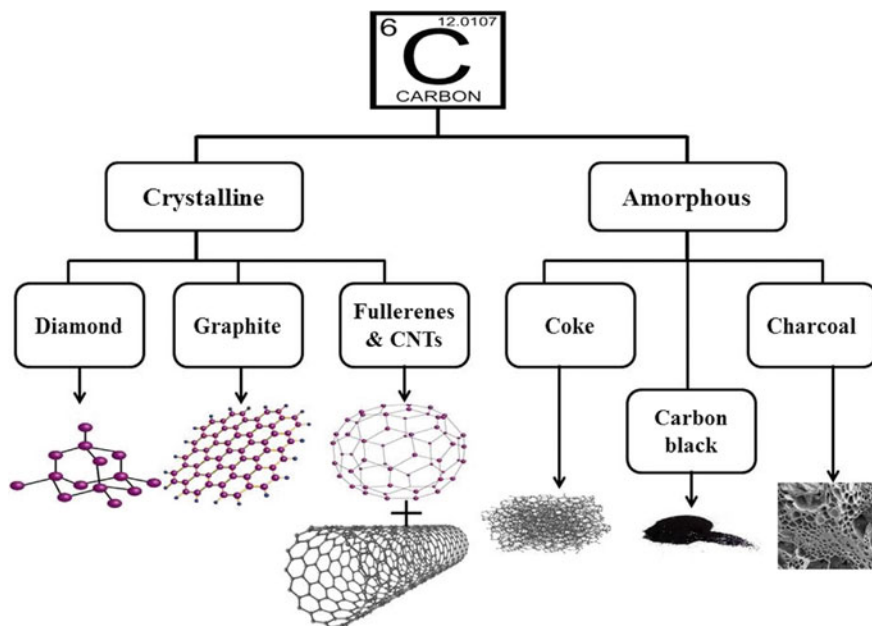
Fig. 4.1 Carbon allotropes (Dhawane et al. 2018)

Graphene and graphite can be easily distinguished using Raman spectroscopy. The Raman spectra of graphite do look close to that of graphene in terms of Raman shifts since graphite is essentially stacked layers of graphene. The distinguishing factor is therefore the difference in intensity as observed in Fig. 4.2. This intensity difference is visible on the first overtone of the second order Raman D-band around 2650 cm^{-1}. There is also an observable peak in the first Raman order G-band at around 1586 cm^{-1} (Zólyomi et al. 2011; Nasir et al. 2018). The G-band peak is common to all sp^2-hybridized carbons and can be used to estimate the thermal conductivity and expansion of carbon materials such as single-walled carbon nanotubes (Casimir et al. 2019). The D-band peak is used to identify the amount of graphene layers present in a sample since it is directly related to the peak intensity. There is also a noticeable change in the overtone shifting toward higher frequencies with an increasing amount of layers as well as a broadening of the peak possibly due to defects in the graphene layers (Budde et al. 2016; März et al. 2018). The reason for the up-field shift and peak broadening for the increasing amount of graphene is due to the change in the electronic band structure because of inter-layer coupling. The coupling results in a splitting of the bonding and antibonding π-bands leading to an increase in the number of phonon wave-vectors that can satisfy the double resonance condition. Since the splitting that occurs in the valence and conduction bands are not the same, this results in four different phonon wave vectors of different intensities in the graphene bilayers. It is these four-wave vectors that result in the observed peak broadening, and they act together to increase the peak intensity with an increase in graphene layers (Zólyomi
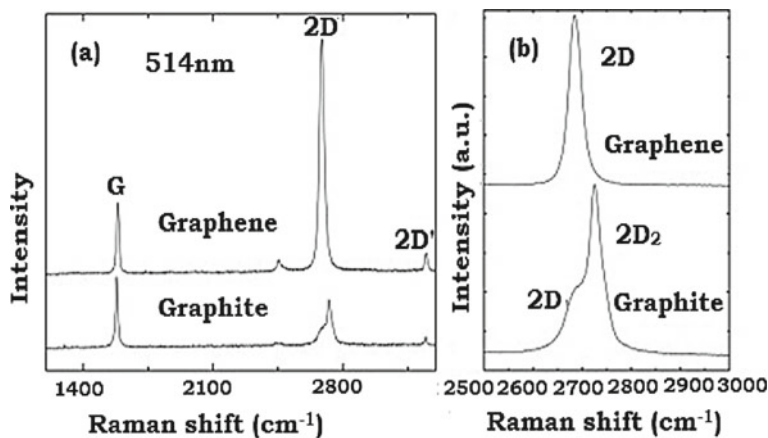
Fig. 4.2   a Raman spectra of graphene and graphite measured at 514.5 nm; **b** comparison of the 2D peaks in graphene and graphite (Ferrari et al. 2006)

et al. 2011). Other than the visual differences between expanded graphite and graphite the 2D peak intensity also increases when comparing the former with the latter due to separation of the graphene layers and defects in the graphene layers resulting in peak broadening (Liao et al. 2011; Mondal et al. 2014; Borah et al. 2014).

Typically X-ray Diffraction is used to characterise the dimensional properties of expanded graphite compared to graphite based on the difference in diffraction patterns due to changes in molecular structure and crystal lattice. Laser particle size analysis can be used to determine particle size accurately (Hu et al. 2019; Selezneva et al. 2020).

4.2   Graphite

4.2.1   Properties and Morphology

Graphite was named by the German geologist Abraham Gottlob Werner in 1789 and the material consists of multiple layers of stacked graphene sheets in a hexagonal close-packed structure. Each graphene layer is held together by weak van der Waals forces due to the unsaturated pi-bonds in the graphene sheets. Due to its natural occurrence, it was one of the first carbon allotropes to be analyzed and characterized. Graphite exhibits a very good electrical conductivity which is attributed to electron transport within each graphene layer due to the delocalized π-electrons between the carbon atoms. It is this mechanism of electron transport that also contributes to the material having a very high thermal conductivity as shown in Table 4.1. Graphite is flexible, but not elastic and is chemically inert. It has a grayish-black appearance

Table 4.1 Select reported in-plane electrical and thermal conductivity values for graphite

Material	Comment	Electrical conductivity	Thermal conductivity	References
Graphite	Surface area 3.5–2.0 m^2/g Bulk density 1–1.8 g/cm^3	10^7 S/m	100–400 W/mK	Murugan et al. (2021)
Graphite	Literature review	10^6 S/m	Not reported	Yemata et al. (2017)
Graphite	Produced from coconut coir waste	25.75 S/cm	Not reported	(Destyorini et al. (2021)

and exhibits the properties of both metals and organic materials. Due to the weak van der Waals forces between the graphene sheets in the graphite crystal structure, the graphene layers can easily slide over each other (Nasir et al. 2018). It is due to the layered structure and the non-covalent bonding between the layers that graphite has anisotropic electrical and thermal conductive properties (Tanzi et al. 2019). A scanning electron microscope (SEM) image of graphite is shown as well as the crystal structure of the material in Figs. 4.3 and 4.4, respectively.

4.2.2 Synthesis

4.2.2.1 Natural Graphite

Graphite can be found in nature and is typically mined. Depending on the geological environment of natural graphite, it may contain impurities that could alter its physical properties. This could also determine the crystal structure which can be classified as either ABA, ABC or turbostatic. The type of crystal structure will determine the most probable cleaving positions. According to ISO standards, graphite consists of more than 10 layers of stacked graphene at room temperature (Kauling et al. 2018).

4.2.2.2 Synthetic Graphite

Graphite can be synthetically prepared from any carbon rich material. Common methods involve using coal, coke or bitumen and graphitizing it by heating the fossil fuel material to temperatures of between 1000 and 2600 °C. The amount and type of impure elements present in the bulk material has an effect on the graphitization temperature and time to remove them (Ishii et al. 2017; Xing et al. 2018). More recently focus has shifted from using fossil fuels as precursor materials due to their negative environmental effects and emphasis has been placed on renewable materials and recycling. Various carbon rich renewable materials and their waste has been successfully converted into graphite such as sawdust, bamboo, algae, biomass,
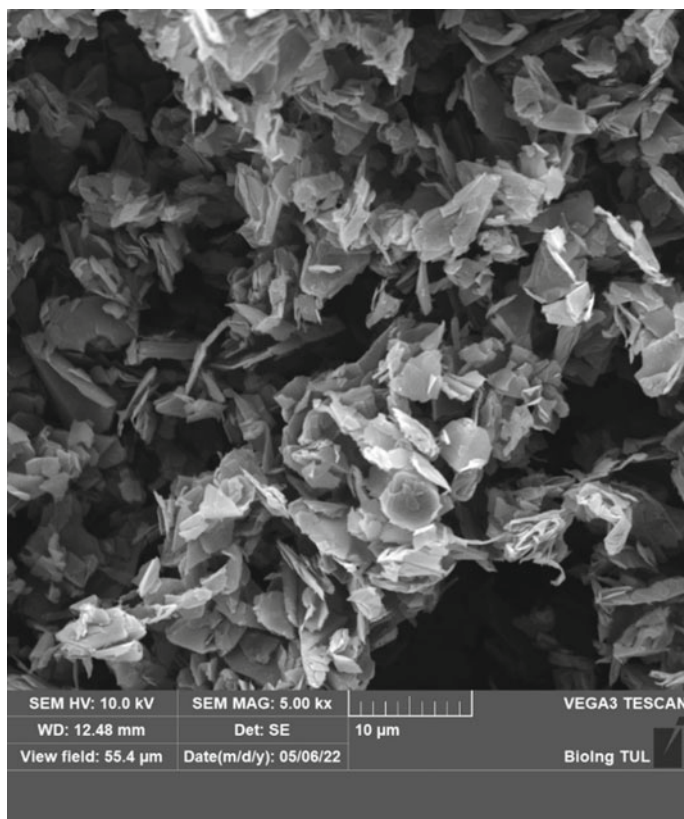
Fig. 4.3 SEM of micro graphite

Fig. 4.4 Crystal structure of graphite (Tsai and Tu 2010)
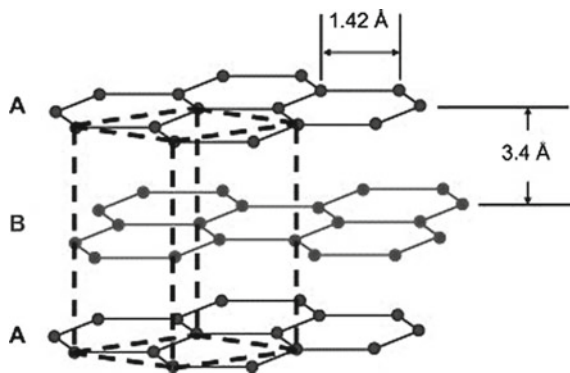
seafood waste, cellulose, sucrose, hemp grass, degreasing cotton, and cellulose. Typically, these materials require high temperatures and complicated pretreatment before graphitization however with the use of catalysts such as Nickel their conversion to graphite has become more economical (Kamal et al. 2020; Destyorini et al. 2021). In an effort to reduce plastic waste, polymeric textile waste has also been successfully converted into graphite. This has been done by heating polyethylene terephthalate fibers (PET) to 900 °C in a tube-type furnace for 1 h under an inert nitrogen atmosphere. Another used technique is grinding the waste material into a powder followed by catalytic graphitization using boron powder as a catalyst (Ko et al. 2020).

4.2.3 Applications

Due to the inter-layer weakness in the graphite crystal structure caused by the attractive part of the van der Waals forces between the graphene layers; it is possible for the layers to slide over each other with relatively little effort. It is for this reason that graphite exhibits excellent lubricating properties and is used in dynamos and electric motors (Nasir et al. 2018; Tanzi et al. 2019). This movement of the graphene layers due to friction could lead to graphite exfoliation to form graphene (Bhowmick et al. 2015). Graphite has a very high melting point of 4125 °C with an acceptable thermal conductivity which makes it a good filler to use in phase change materials (Rashidi et al. 2022). Due to its high electrical conductivity graphite is extensively used in battery technology and electrolysis reactions. Graphite has a high thermal conductivity which makes it good for phase change material applications, however this is not ideal for thermoelectric applications since it also has a low Seebeck coefficient and low ZT value at room temperature. This makes the material generate heat when current is applied in a process called Joule heating. The heating of graphite can also be beneficial for some applications as this allows for regeneration of graphite to remove adhered impurities. (Yun et al. 2018; Chen et al. 2021; Dong et al. 2022). The thermoelectric performance of graphite can be significantly improved by exfoliating the graphite into graphene or expanded graphite for electronic applications (Yemata et al. 2017).

4.3 Graphene

4.3.1 Properties and Morphology

Graphene is a densely packed monolayer of sp^2-hybridized carbon atoms. Graphene is considered one of the strongest materials known to man with a Youngs modulus of 1 TPa. This is due to strong covalent interlayer bonding between the carbon atoms. Graphene is one of the most electrically and thermally conductive materials on earth
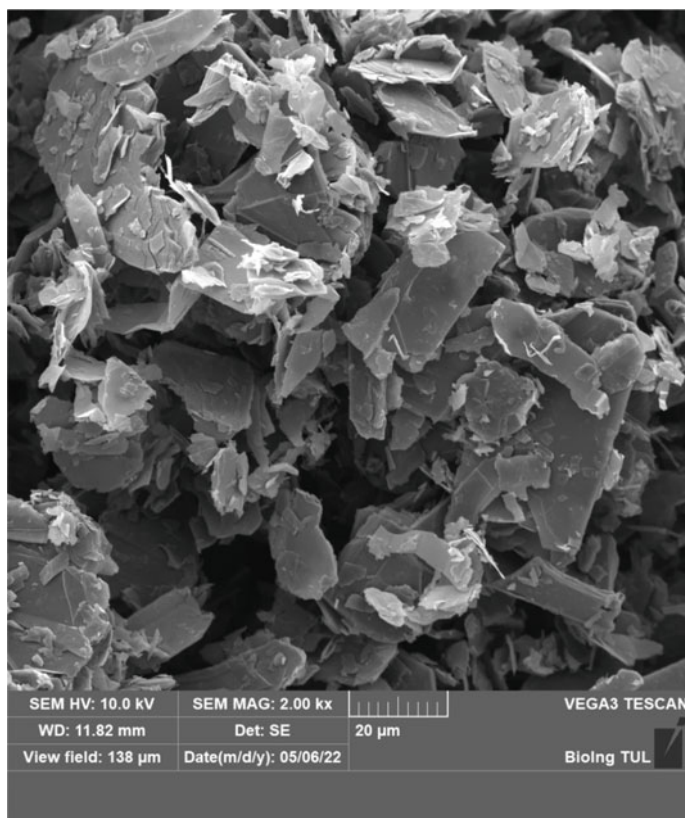
Fig. 4.5 SEM of commercial graphene particles 20–30 μm

mainly due to its high electron mobility of 200,000 cm^2v^{-1} s^{-1} (Méndez-Lozano et al. 2022). It was stated that more recently the nomenclature from graphene was established by the ISO as a single layer, monocrystal of carbon atoms organized in a hexagonal lattice with lattice symmetry *p3m1,* point group D3 (Kauling et al. 2018). A SEM image of commercial graphene is presented in Fig. 4.5. A table of select graphene and graphene containing materials is presented in Table 4.2 for comparison of their electrical and thermal conductivity.

4.3.2 Synthesis

4.3.2.1 Exfoliation by Oxidation of Graphite

The main problem in producing graphene from graphite is to overcome the van der Waals forces holding the graphene sheets together. Traditionally graphene is

Table 4.2 Electrical and thermal conductivities of selected graphene and graphene containing materials

Material	Comment	Electrical conductivity	Thermal conductivity	References
Graphene	Prepared from expandable graphite *(annealed at 2600°C, 4 h)	2104 S/m 19,200 S/m*	Not reported	Çelik et al. (2017)
Graphene	Suspended single-layer graphene	1–4 kΩ resistance	4.84×10^3 to 5.30×10^3 W/mK	Balandin et al. (2008), Méndez-Lozano et al. (2022)
Graphene composite film	EG/cellulose nanofiber/PEO composite film produced by exfoliation of expandable graphite	1226 S/cm	302.3 W/mK	Yang et al. (2019)
Graphene fiber	Wet spinning of graphene oxide and reduction	2721 S/cm	Not reported	Bong Lee et al. (2021)
Graphene	Theoretical	1×10^8 S/m	5300 W/mK	Fang et al. (2020)

produced by exfoliating graphite in what is referred to as the top-down approach. The graphite is exfoliated by mechanical, chemical or electrochemical methods to produce graphene flakes (Kauling et al. 2018). The most common method of preparing graphene is to exfoliate the graphite to form graphene oxide in a process called Hummer's method, also referred to as Hummers and Hofmann's method. This is done with a combination of sulfuric acid as intercalator, sodium nitrate which acts synergistically with sulfuric acid to oxidize the graphite, and potassium permanganate which is also an oxidant. This is followed by a second oxidation step with water and hydrogen peroxide (Kang et al. 2016; Hou et al. 2020b). The reaction mechanisms for this method are complex due to all the different reagents and steps involved. Recent research is showing that potassium permanganate may also be acting as an intercalator in a second intercalation step after the action of sulfuric or nitric acid (Chen et al. 2022). The produced graphene oxide can then be reduced to form graphene by reacting it with hydrazine hydrate at 100 °C for 24 h (Kauling et al. 2018). The conventional Hummers method can be considered dangerous and polluting due to harsh exothermic reactions, toxic exhaust gasses as well as sodium and nitrate ions released in the wastewater. Several modified approaches have been made to decrease the effects or avoid these problems, such as omitting the use of sodium nitrate (Zaaba et al. 2017; Santamaría-Juárez et al. 2020; Méndez-Lozano et al. 2022). It has been established that the method of exfoliation does have an impact on the electrochemical properties which can be also due to non-carbon elements remaining in the graphene

after oxidation. Hummer's method has shown to have an advantage over Staudenmaier and Hofmann's methods due to increased heterogeneous electron transfer between the carbon atoms, but it also leaves nitrogen in the graphene backbone (Poh et al. 2012). The formation of graphene oxide from graphite to form graphene or reduced graphene oxide makes the structure amorphous and causes scarring in the graphene backbone. This results in poorer electrical conductivity compared to graphene crystal. The defects produced by the oxidation can be easily detected using Raman spectroscopy (Kauling et al. 2018).

4.3.2.2 Liquid Phase Exfoliation (LPE) of Graphite

Liquid phase exfoliation (LPE) of graphite to graphene is a common alternative to oxidative techniques. This is a mechanical method where large crystal graphite is milled to a powder and dispersed in a solvent. The powder particles are then ultrasonicated to allow the solvent to penetrate the graphite layers and break the van der Waals forces holding it together due to sheer forces and cavitation. Particles can then be separated by conventional methods such as centrifugation (Ciesielski and Samorì 2014; Kauling et al. 2018). Research has mainly focused on modifying the LPE solvents of which N-methyl-2-pyrrolidone is the most common (NMP). NMP is still considered as one of the best solvents to use in LPE of graphite due to its low enthalpy of mixing with graphite (Wei and Sun 2015; Ng et al. 2023). N,N-dimethylformamide (DMF) is another common solvent, however similar to NMP they are considered as eye irritants and toxic to the reproductive and other organs. There are also very different sonication parameters used between experiments ranging from 30 min to 1000 h with varying results (Ciesielski and Samorì 2014). Water is seen as a more environmentally friendly and low-cost medium for exfoliation in LPE of graphite, however it has its limitations, especially for electronic applications. These limitations are being overcome by using water mixed with ethanol to improve its removal from the produced graphene. Surfactants have proven to improve the exfoliating power of water on graphite (Wei and Sun 2015; Gonçalves et al. 2022; Morton et al. 2023). Recent research has shown that isopropanol may be a more effective solvent than NMP (Ng et al. 2023).

4.3.2.3 Exfoliation of Expanded Graphite

Expanded graphite has in recent years been used as a route toward producing graphene by utilizing mechanical and chemical methods since it is easier to separate the graphene layers in expanded graphite compared to a graphite crystal. Sun and Fugetsu developed a method of producing graphene oxide from expanded graphite on a large scale using a spontaneous expansion method which can be reduced to graphene. The authors used commercially expanded graphite which was exfoliated using sulfuric acid as precursor material and oxidized using potassium permanganate. The produced graphene oxide flakes had the same diameter as the precursor expanded graphite. This

method of producing graphene or graphene oxide was stated to be much safer since the reactions are more stable compared to the Hummers method (Sun and Fugetsu 2013). Vacacela Gomez et al. used a combination of mechanical and chemical methods to further exfoliate expanded graphite. This was done by hydrothermally expanding expanded graphite in a hexadecyltrimethylammonium bromide aqueous solution at 180 °C for 15 h and ultrasonicating the mixture for 20 min at 2000 rpm to form a few layered graphene as identified by Raman spectroscopy (Vacacela Gomez et al. 2019).

4.3.2.4   Synthetic Graphene

The most common synthetic or bottom-up approach for creating graphene is by carbon vapor deposition (CVD). This is done by using a hydrocarbon gas of simple molecules such as methane to produce graphene films on a metal substrate such as copper or its alloys which can be many square meters in size. The technique is widely used, but it is known for producing graphene with defects and voids which reduces its desired conductive properties (Kauling et al. 2018; Xu et al. 2021). This method is also difficult to scale since it does not produce large quantities of material in terms of mass (Fang et al. 2020). Epitaxial growth of carbon on silica carbide (SiC) is another method of the synthetic bottom-up approach and does deliver good results. In this process, graphene is grown by sublimation of silicon under high vacuum and temperature which also makes this process expensive and difficult to scale (Borah et al. 2014).

4.3.3   Applications

Most commercially available graphene is of poor quality and not considered optimal for most applications. Commercial graphene may be classified as graphene however it may have up to 10 stacked layers such as what can be seen in the commercial graphene illustrated in Fig. 4.5 (Kauling et al. 2018). In the LPE of expanded graphite the use of water as exfoliation medium is considered simple, scalable, and environmentally friendly. This is however a problem when using the produced graphene for electronic applications since water molecules may remain trapped in the layers of non-monolayer graphene (Ciesielski and Samorì 2014). Despite being in the early stages of development green graphene produced from renewable and waste materials has shown to be comparable to conventional graphene. Green graphene produced by exfoliation typically involves producing green graphite first (Torres et al. 2021). It has been shown that expandable graphite and expanded graphite can easily exfoliate into graphene for composite material production. Yang et al. produced an expandable graphite (EG)/cellulose nanofiber (CNF)/polyethylene oxide (PEO) composite material that relied on this exfoliation process. At a ratio 95:5:3 the material exhibited an electrical conductivity of 1226 S cm^{-1} and a thermal conductivity 302.3 W m^{-1} K^{-1}.

At a thickness of 12 μm the electromagnetic interference (EMI) shielding was 44 dB. The composite tensile strength was 587% higher than that of a pure graphene film of similar thickness at 66.3 MPa. This method is seen as a more environmentally conscious way of producing graphene containing composite materials for electronic, thermal, and EMI shielding applications (Yang et al. 2019). Graphene fibers have gained interest in the past decade since its initial development in 2011 by liquid spinning graphene oxide crystals. Commercial carbon fiber filaments are prepared from carbonization and pyrolysis of organic precursor fibers such as polyacrylonitrile and rayon fibers. Therefore, the building blocks of the carbon fibers are controlled by the molecular properties of the precursor. After graphitization at temperatures above 1000 °C the polymer segments fuse into small graphene dots which build up into graphite and finally carbon fiber. This process leads to many defects in the graphite structure and therefore although carbon fibers have excellent mechanical strength, they have limited conducting performance. The wet spinning of graphene oxide into graphene fibers overcomes these problems. This is due to the highly ordered crystalline behavior of the spinning dopes and its self-healing ability to overcome defects. Due to available spinning technology graphene fibers have a high degree of freedom in terms of shape such as monofilament, hollow, core sheath, porous, etc. Since the size of the building blocks are controllable it provides a great deal of flexibility in obtaining the desired mechanical and conductive properties. All these advantages of the novel technique give graphene fibers great potential for use in electronic applications such as smart textiles, sensors, and energy storage (Fang et al. 2020; Tang et al. 2020). Graphene fibers have been shown to have electrical conductivities higher than that of copper wire at 2721 S/cm (Bong Lee et al. 2021). Synergistic effects between graphene fibers and platinum electrodes have been reported with potential for neuroscience applications (Wang et al. 2019).

4.4 Expanded Graphite

4.4.1 Properties and Morphology

Expanded graphite has the same layered graphene structure as graphite, however it has a much higher degree of exfoliation resulting in a low-density porous structure with worm-like appearance. Due to the degree of exfoliation expanded graphite also has a high thermal and electrical conductivity which is just as anisotropic as graphite (Solfiti and Berto 2020; Rashidi et al. 2022). A SEM image illustrating expanded graphite is presented in Fig. 4.6.
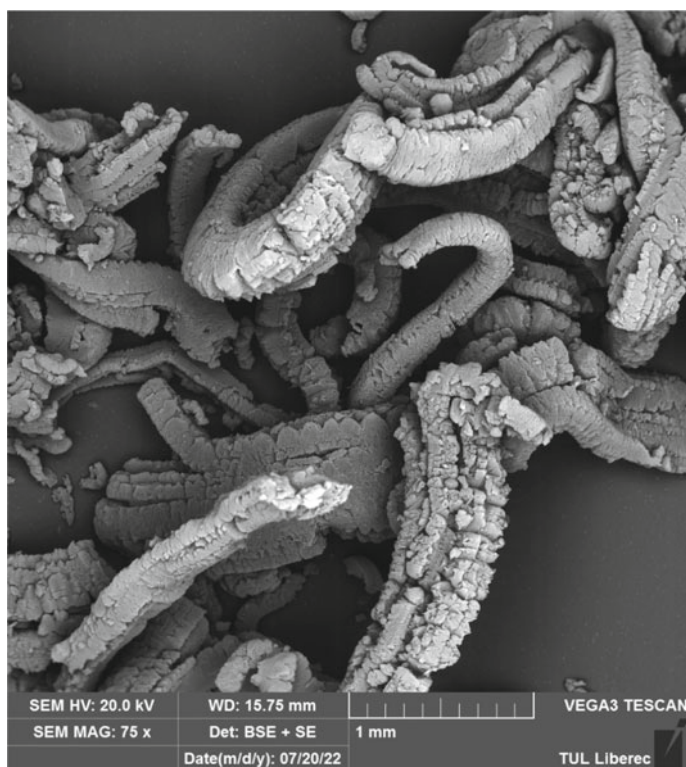
Fig. 4.6 SEM of expanded graphite

4.4.2 Synthesis

The synthesis of expanded graphite is done by either chemical or physical methods. Chemical methods include electrochemical and chemical oxidation. The electrochemical method is considered the fastest, most environmental, and efficient method. However, this method is only possible when using graphite paper or foil as electrodes and requires additional steps to treat the raw graphite material making it costly. Physical methods include ultrasonication, microwave, and low or high temperature thermal expansion of which the latter is the most used approach. This method has disadvantages such as a high thermal energy loss, gas release, and requiring equipment capable of withstanding high pressures and temperatures. The microwave method is fast, but due to its high energy consumption and scaling limitations, it is not commonly used for large scale production. Ultrasonication requires specific solvents and typically results in a low yield (Zhang et al. 2023). The porosity of the expanded graphite is strongly dependent on the method of intercalation since better intercalation would lead to greater expansion (Bannov et al. 2021). Traditionally expanded graphite

is produced using the high temperature processes where a graphite precursor material is first treated using the chemical method. This uses oxidants such as sulfuric or nitric acid and hydrogen peroxide to open the graphite structure by intercalation. This produces intercalated or expandable graphite which can then be thermally treated to 900–1000 °C to produce expanded graphite (Hou et al. 2020a). The mechanism of expansion relies on the almost instant conversion of the intercalating agent from the liquid or solid phase to the gaseous phase. This results in a sharp increase in interlayer pressure between the graphene sheets leading to the interlayer distance increasing to cause an over 100 times expansion. The interlayer distance of the pre-expanded graphene sheets is approximately 3.355 Å (Mazela et al. 2020). A diagram illustrating the basic principle of synthesizing expanded graphite using the conventional high temperature technique is illustrated in Fig. 4.7. The high temperature method of producing expanded graphite is considered harsher than the low temperature method. Hou et al. produced expanded graphite using a low temperature method by exfoliating flake graphite with potassium persulfate (1:7) and sulfuric acid (1:20) at 80 °C for 5 min. Potassium persulfate was said to act as both an intercalating agent and oxidant. The authors method resulted in expanded graphite with a volume density of 150ml/g and showed very little defects in the graphite structure after exfoliation. The authors obtained expanded graphite with a high electrical conductivity of 5.47×10^4 S/m (Hou et al. 2020a). Traditionally the low temperature method exhibited similar problems to the chemical method such as improper intercalation and the remaining of intercalating agents thus resulting in impurities (Yakovlev et al. 2006). Hou et al. proved that their low temperature method resulted in a high degree of expansion which was comparable to that produced using traditional methods with little defects in the graphite structure. The effect of impurities should also be minimized due to the negative Gibbs free energy value of the intercalating agent in the acid environment at the reaction temperature resulting in its decomposition (Hou et al. 2020a). It has been proven that with the use of programmable heating in the thermal processes of creating expanded graphite it is possible to modify the texture, yield, disorder degree, and bulk density (Steksova et al. 2016; Bannov et al. 2021). The authors Bannov et al. noted that at a lower temperature of 400 °C they were able to achieve comparable results to the traditional high temperature thermal shock technique which expands the graphite at 900–1000 °C (Bannov et al. 2021).
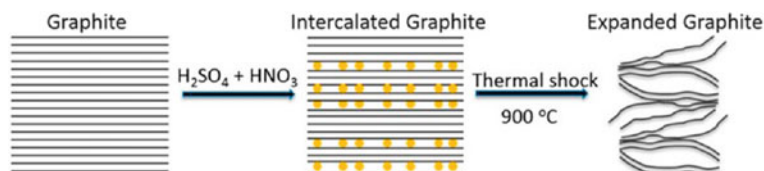
Fig. 4.7 High temperature process of producing expanded graphite (Mazela et al. 2020) reused under CC BY 4.0

4.4.3 Applications

Expanded graphite has a very high thermal conductivity and a very low density which makes it ideal for heat transfer applications in phase change materials (Rashidi et al. 2022). Due to its high electrical conductivity, it has been increasingly investigated for use in electronic equipment. It has been found to increase the thermal conductivity of polymers such as LLDPE to 19.6 Wm^{-1} K^{-1} with an electrical conductivity of up to 4000 S/m and EMI shielding effectiveness of 52.4 dB (Wei et al. 2021). The electrical conductivity of expanded graphite is essentially that of graphite, but due to the worm-like porous structure of expanded graphite, it can achieve better electrical conductivity at lower particle loading for the same applications (Yuan et al. 2016; Mokhena et al. 2018).

4.5 Conclusion

Graphite has for years been used for its electrical and thermal conductive properties which has been mostly attributed to the graphene layers making up its structure. Since the Nobel prize was won for the isolation of monolayer graphene there has been a significant uptick in research in the field. There have been many attempts to achieve the ideal properties of graphene by either trying to produce it from graphite or from its molecular elements with varying success. Commercial graphene does not hold up to the claimed theoretical properties of graphene as stated in literature, but it does have its applications. As the world is moving toward a more sustainable future recent advances have been made in producing green graphite and graphene. Expanded graphite offers a more cost-effective alternative to graphene and is also considered a route toward producing graphene. Improvements in its synthesis have been made by using better intercalators and utilizing low temperature methods of production to reduce energy costs. These carbon materials and their modifications are already used in various electrical and thermal applications. Advances in research are being made to get closer to their ideal thermal and electrical conductivity which could have a significant impact on modern life.

References

Balandin AA, Ghosh S, Bao W et al (2008) Superior thermal conductivity of single-layer graphene. Nano Lett 8:902–907. https://doi.org/10.1021/nl0731872
Bannov AG, Ukhina AV, Maksimovskii EA et al (2021) Highly porous expanded graphite: thermal shock vs programmable heating. Materials 14:7687. https://doi.org/10.3390/ma14247687
Bhowmick S, Banerji A, Alpas AT (2015) Role of humidity in reducing sliding friction of multilayered graphene. Carbon 87:374–384. https://doi.org/10.1016/j.carbon.2015.01.053

Bong Lee H, Hyun Noh S, Hee Han T (2021) Highly electroconductive lightweight graphene fibers with high current-carrying capacity fabricated via sequential continuous electrothermal annealing. Chem Eng J 414:128803. https://doi.org/10.1016/j.cej.2021.128803

Borah M, Dahiya M, Sharma S et al (2014) Few layer graphene derived from wet ball milling of expanded graphite and few layer graphene based polymer composite. Mater Focus 3:300–309. https://doi.org/10.1166/mat.2014.1185

Budde H, Coca-López N, Shi X et al (2016) Raman radiation patterns of graphene. ACS Nano 10:1756–1763. https://doi.org/10.1021/acsnano.5b06631

Casimir D, Alghamdi H, Ahmed IY et al (2019) Raman spectroscopy of graphene, graphite and graphene nanoplatelets. In: Wongchoosuk C, Seekaew Y (eds) 2D materials. IntechOpen

Çelik Y, Flahaut E, Suvacı E (2017) A comparative study on few-layer graphene production by exfoliation of different starting materials in a low boiling point solvent. FlatChem 1:74–88. https://doi.org/10.1016/j.flatc.2016.12.002

Chen W, Li JT, Wang Z et al (2021) Ultrafast and controllable phase evolution by flash joule heating. ACS Nano 15:11158–11167. https://doi.org/10.1021/acsnano.1c03536

Chen X, Qu Z, Liu Z, Ren G (2022) Mechanism of oxidization of graphite to graphene oxide by the hummers method. ACS Omega 7:23503–23510. https://doi.org/10.1021/acsomega.2c01963

Ciesielski A, Samorì P (2014) Grapheneviasonication assisted liquid-phase exfoliation. Chem Soc Rev 43:381–398. https://doi.org/10.1039/C3CS60217F

Destyorini F, Irmawati Y, Hardiansyah A et al (2021) Formation of nanostructured graphitic carbon from coconut waste via low-temperature catalytic graphitisation. Eng Sci Technol Int J 24:514–523. https://doi.org/10.1016/j.jestch.2020.06.011

Dhawane SH, Kumar T, Halder G (2018) Recent advancement and prospective of heterogeneous carbonaceous catalysts in chemical and enzymatic transformation of biodiesel. Energy Convers Manag 167:176–202. https://doi.org/10.1016/j.enconman.2018.04.073

Dong S, Song Y, Ye K et al (2022) Ultra-fast, low-cost, and green regeneration of graphite anode using flash joule heating method. EcoMat 4. https://doi.org/10.1002/eom2.12212

Fang B, Chang D, Xu Z, Gao C (2020) A review on graphene fibers: expectations, advances, and prospects. Adv Mater 32:1902664. https://doi.org/10.1002/adma.201902664

Ferrari AC, Meyer JC, Scardaci V et al (2006) Raman spectrum of graphene and graphene layers. Phys Rev Lett 97:187401. https://doi.org/10.1103/PhysRevLett.97.187401

Gonçalves RV, Maraschin TG, Koppe GC et al (2022) Cardanol surfactant/ultrasound-assisted exfoliation of graphite in a water/ethanol solution. Mater Chem Phys 290:126578. https://doi.org/10.1016/j.matchemphys.2022.126578

Hou B, Sun H, Peng T et al (2020a) Rapid preparation of expanded graphite at low temperature. New Carbon Mater 35:262–268. https://doi.org/10.1016/S1872-5805(20)60488-7

Hou Y, Lv S, Liu L, Liu X (2020b) High-quality preparation of graphene oxide via the Hummers' method: understanding the roles of the intercalator, oxidant, and graphite particle size. Ceram Int 46:2392–2402. https://doi.org/10.1016/j.ceramint.2019.09.231

Hu Z, Cai L, Liang J et al (2019) Green synthesis of expanded graphite/layered double hydroxides nanocomposites and their application in adsorption removal of Cr(VI) from aqueous solution. J Clean Prod 209:1216–1227. https://doi.org/10.1016/j.jclepro.2018.10.295

Ishii T, Kaburagi Y, Yoshida A et al (2017) Analyses of trace amounts of edge sites in natural graphite, synthetic graphite and high-temperature treated coke for the understanding of their carbon molecular structures. Carbon 125:146–155. https://doi.org/10.1016/j.carbon.2017.09.049

Kamal AS, Othman R, Jabarullah NH (2020) Preparation and synthesis of synthetic graphite from biomass waste: a review. Syst Rev Pharm 11:881–894

Kang JH, Kim T, Choi J et al (2016) Hidden second oxidation step of hummers method. Chem Mater 28:756–764. https://doi.org/10.1021/acs.chemmater.5b03700

Karthik PS, Himaja AL, Singh SP (2014) Carbon-allotropes: synthesis methods, applications and future perspectives. Carbon Lett 15:219–237. https://doi.org/10.5714/CL.2014.15.4.219

Kauling AP, Seefeldt AT, Pisoni DP et al (2018) The worldwide graphene flake production. Adv Mater 30:1803784. https://doi.org/10.1002/adma.201803784

Ko S, Kwon YJ, Lee JU, Jeon Y-P (2020) Preparation of synthetic graphite from waste PET plastic. J Ind Eng Chem 83:449–458. https://doi.org/10.1016/j.jiec.2019.12.018

Liao K, Ding W, Zhao B et al (2011) High-power splitting of expanded graphite to produce few-layer graphene sheets. Carbon 49:2862–2868. https://doi.org/10.1016/j.carbon.2011.03.021

März B, Jolley K, Marrow TJ et al (2018) Mesoscopic structure features in synthetic graphite. Mater Des 142:268–278. https://doi.org/10.1016/j.matdes.2018.01.038

Mazela B, Batista A, Grześkowiak W (2020) Expandable graphite as a fire retardant for cellulosic materials—a review. Forests 11:755. https://doi.org/10.3390/f11070755

Méndez-Lozano N, Pérez-Reynoso F, González-Gutiérrez C (2022) Eco-friendly approach for graphene oxide synthesis by modified hummers method. Materials 15:7228. https://doi.org/10.3390/ma15207228

Mokhena TC, Mochane MJ, Sefadi JS et al (2018) Thermal conductivity of graphite-based polymer composites. In: Shahzad A (ed) Impact of thermal conductivity on energy technologies. InTech

Mondal T, Bhowmick AK, Krishnamoorti R (2014) Stress generation and tailoring of electronic properties of expanded graphite by click chemistry. ACS Appl Mater Interfaces 6:7244–7253. https://doi.org/10.1021/am500471q

Morton JA, Kaur A, Khavari M et al (2023) An eco-friendly solution for liquid phase exfoliation of graphite under optimised ultrasonication conditions. Carbon 204:434–446. https://doi.org/10.1016/j.carbon.2022.12.070

Murugan P, Nagarajan RD, Shetty BH et al (2021) Recent trends in the applications of thermally expanded graphite for energy storage and sensors—a review. Nanoscale Adv 3:6294–6309. https://doi.org/10.1039/D1NA00109D

Nasir S, Hussein M, Zainal Z, Yusof N (2018) Carbon-based nanomaterials/allotropes: a glimpse of their synthesis, properties and some applications. Materials 11:295. https://doi.org/10.3390/ma11020295

Ng KL, Maciejewska BM, Qin L et al (2023) Direct evidence of the exfoliation efficiency and graphene dispersibility of green solvents toward sustainable graphene production. ACS Sustain Chem Eng 11:58–66. https://doi.org/10.1021/acssuschemeng.2c03594

Poh HL, Šaněk F, Ambrosi A et al (2012) Graphenes prepared by Staudenmaier, Hofmann and Hummers methods with consequent thermal exfoliation exhibit very different electrochemical properties. Nanoscale 4:3515. https://doi.org/10.1039/c2nr30490b

Prenzel D, Tykwinski RR (2014) New synthetic carbon allotropes. In: Kobayashi S, Müllen K (eds) Encyclopedia of Polymeric Nanomaterials. Springer, Berlin, pp 1–12

Rashidi S, Esfahani JA, Hormozi F (2022) Classifications of porous materials for energy applications. In: Encyclopedia of smart materials. Elsevier, pp 774–785

Santamaría-Juárez G, Gómez-Barojas E, Quiroga-González E et al (2020) Safer modified Hummers' method for the synthesis of graphene oxide with high quality and high yield. Mater Res Express 6:125631. https://doi.org/10.1088/2053-1591/ab4cbf

Selezneva O, Orlov V, Shustov P (2020) Oxidized thermally expanded graphite as a raw material for the production of cement composites. IOP Conf Ser: Mater Sci Eng 880:012019. https://doi.org/10.1088/1757-899X/880/1/012019

Solfiti E, Berto F (2020) A review on thermophysical properties of flexible graphite. Procedia Struct Integr 26:187–198. https://doi.org/10.1016/j.prostr.2020.06.022

Steksova YuP, Berdyugina IS, Shibaev AA et al (2016) Effect of synthesis parameters on characteristics of expanded graphite. Russ J Appl Chem 89:1588–1595. https://doi.org/10.1134/S10704427216100049

Sun L, Fugetsu B (2013) Mass production of graphene oxide from expanded graphite. Mater Lett 109:207–210. https://doi.org/10.1016/j.matlet.2013.07.072

Tang M, Wu Y, Yang J, Xue Y (2020) Hierarchical core-shell fibers of graphene fiber/radially-aligned molybdenum disulfide nanosheet arrays for highly efficient energy storage. J Alloy Compd 828:153622. https://doi.org/10.1016/j.jallcom.2019.153622

Tanzi MC, Farè S, Candiani G (2019) Organization, structure, and properties of materials. In: Foundations of Biomaterials Engineering. Elsevier, pp 3–103

Torres FG, Troncoso OP, Rodriguez L, De-la-Torre GE (2021) Sustainable synthesis, reduction and applications of graphene obtained from renewable resources. Sustain Mater Technol 29:e00310. https://doi.org/10.1016/j.susmat.2021.e00310

Tsai J-L, Tu J-F (2010) Characterizing mechanical properties of graphite using molecular dynamics simulation. Mater Des 31:194–199. https://doi.org/10.1016/j.matdes.2009.06.032

Vacacela Gomez C, Tene T, Guevara M et al (2019) Preparation of few-layer graphene dispersions from hydrothermally expanded graphite. Appl Sci 9:2539. https://doi.org/10.3390/app9122539

Wang K, Frewin CL, Esrafilzadeh D et al (2019) High-performance graphene-fiber-based neural recording microelectrodes. Adv Mater 31:1805867. https://doi.org/10.1002/adma.201805867

Wei B, Zhang L, Yang S (2021) Polymer composites with expanded graphite network with superior thermal conductivity and electromagnetic interference shielding performance. Chem Eng J 404:126437. https://doi.org/10.1016/j.cej.2020.126437

Wei Y, Sun Z (2015) Liquid-phase exfoliation of graphite for mass production of pristine few-layer graphene. Curr Opin Colloid Interface Sci 20:311–321. https://doi.org/10.1016/j.cocis.2015.10.010

Xing B, Zhang C, Cao Y et al (2018) Preparation of synthetic graphite from bituminous coal as anode materials for high performance lithium-ion batteries. Fuel Process Technol 172:162–171. https://doi.org/10.1016/j.fuproc.2017.12.018

Xu S, Zhang L, Wang B, Ruoff RS (2021) Chemical vapor deposition of graphene on thin-metal films. Cell Reports Phys Sci 2:100372. https://doi.org/10.1016/j.xcrp.2021.100372

Yakovlev AV, Finaenov AI, Zabud'kov SL, Yakovleva EV (2006) Thermally expanded graphite: synthesis, properties, and prospects for use. Russ J Appl Chem 79:1741–1751. https://doi.org/10.1134/S1070427206110012

Yang W, Gong Y, Zhao X et al (2019) Strong and highly conductive graphene composite film based on the nanocellulose-assisted dispersion of expanded graphite and incorporation of poly(ethylene oxide). ACS Sustain Chem Eng 7:5045–5056. https://doi.org/10.1021/acssuschemeng.8b05850

Yemata TA, Ye Q, Zhou H, et al (2017) Conducting polymer-based thermoelectric composites. In: Hybrid polymer composite materials. Elsevier, pp 169–195

Yuan Y, Zhang N, Li T et al (2016) Thermal performance enhancement of palmitic-stearic acid by adding graphene nanoplatelets and expanded graphite for thermal energy storage: a comparative study. Energy 97:488–497. https://doi.org/10.1016/j.energy.2015.12.115

Yun Y, Park J, Kim H et al (2018) Electrothermal local annealing via graphite joule heating on two-dimensional layered transistors. ACS Appl Mater Interfaces 10:25638–25643. https://doi.org/10.1021/acsami.8b06630

Zaaba NI, Foo KL, Hashim U et al (2017) Synthesis of graphene oxide using modified hummers method: solvent influence. Procedia Eng 184:469–477. https://doi.org/10.1016/j.proeng.2017.04.118

Zhang D, Zhang W, Zhang S et al (2023) Synthesis of expanded graphite-based materials for application in lithium-based batteries. J Energy Storage 60:106678. https://doi.org/10.1016/j.est.2023.106678

Zólyomi V, Koltai J, Kürti J (2011) Resonance Raman spectroscopy of graphite and graphene: resonance Raman spectroscopy of graphite and graphene. Phys Status Solidi B 248:2435–2444. https://doi.org/10.1002/pssb.201100295

Chapter 5
Functionalization of Cellulose-Based Materials

Xiaodong Tan, Qingyan Peng, Tereza Šubrová, Jana Šašková, Jakub Wiener, Mohanapriya Venkataraman, and Jiří Militký

Abstract Multifunctional hybrid materials based on nanocellulose have gradually emerged as a substitute for petroleum-based materials. In this chapter, we briefly present the latest technology in this field, including processing, functional properties, and areas of application. For example, the combination of cellulose nanocrystals (CNCs) with different types of organic or inorganic nanoparticles enables the study and analysis of multifunctional nanohybrids with important scientific and industrial applications and opens new horizons in materials science. In particular, technical analysis, including supercapacitors, solar cells and batteries, separation technology, and wastewater treatment, catalysis.

5.1 Introduction

Cellulose comes from a variety of sources, can be derived from plants and is a renewable, bio-based polymer. A new class of renewable crystal particles, represented by nanocellulose, can be combined with other micro- or nanomaterials, enabling the development of efficient and sustainable multifunction devices (Klemm et al. 2018). Research into CNC may require improvements in a variety of projects, from platforms or supercapacitors for biomedical applications, permeable separators for batteries, slim films for hardware and anti-counterfeiting applications, for detection, for standalone catalytic membranes or water disinfection applications (Lizundia et al. 2017a, b; Rescignano et al. 2014).

To move from the laboratory to commercial and modern applications, specialists should complete the transition from removing CNC from research facilities to modern scale creation (Reid et al. 2017). Currently, there are many organizations that are

X. Tan · Q. Peng · T. Šubrová · J. Šašková · J. Wiener · M. Venkataraman (✉) · J. Militký
Department of Material Engineering, Faculty of Textile Engineering, Technical University of Liberec, Studentská 2, 46117 Liberec, Czech Republic
e-mail: mohanapriya.venkataraman@tul.cz

J. Militký
e-mail: jiri.militky@tul.cz

able to transport kilograms to large quantities of nanocellulose per day using various flushing systems. Nevertheless, unique extraction strategies can greatly influence CNC strength and surface science, surface charge thickness, and molecular size (Foster et al. 2018). Therefore, it is essential to use key and standard testing techniques to characterize these properties to ensure reliable material execution. In general, the current level of modern production of cellulose nanocrystals is remarkable, which offers incredible potential for commercial applications.

As noted by Stratistics Market Research Consulting, the global CNC market size will reach $22.2 million annually in 2017 and $227.2 million by 2026, growing at a CAGR of 29.5% (Hamad et al. 2019). The interest in green materials, sustainable and biodegradable conventional materials in emerging markets is driving the market. Increasing interest in innovations in paper, board and plastics, materials, food bundling, beauty care and personal cleaning, pharmaceuticals, biomedicine, paints, and coatings is driving the nanocellulose market.

Depending on the technology and method, the cost of CNC varies from $3 to $25 per gram, which is the same as the cost of carbon nanotubes. Considering that cellulose is the most abundant natural polymer and processing innovations have been created to remove cellulose from various sources compared to synthetic mercury fusion techniques for carbon nanotubes, CNC costs may become critical sooner or later. Facilitate. Similarly, another variable to consider when setting up CNC usage in different applications is extraction strategy. From now on, CNC is removed from cellulose hydrolysis by using various corrosive drugs. In order to obtain maintainable bio-based nanomaterials, new and ecosystem-friendly strategies should be developed (Trache et al. 2017).

The basic commitment of this part is to talk about the impact of CNC on nanohybrid materials. The advantages and disadvantages of basic processing methods for obtaining CNC-based nanohybrid materials are mainly studied. First, a short demo and dialogue on CNC characteristics is given. Important issues related to the production, handling, and dispersion of CNC-based nanohybrids are examined in the accompanying section. Influence of CNC on nanohybrid performance. CNC is divided as an extension of the program for the production of nanohybrid materials with further development characteristics focusing on design and biomedical applications. The natural effects associated with the use of CNC nanohybrids are also summarized. Finally, conclusions and future possibilities are presented and discussed.

5.2 Hybrid Manufacturing Technology

5.2.1 Solution Casting

Solution casting is the most widely used manufacturing strategy for obtaining pure or nanohybrid CNC materials (Marchessault et al. 1959). This technique is simple and feasible because it is likely done by scattering the CNC and enriching the nanoparticles into a liquid (usually water), which is then projected onto the Petri dish to drain the soluble substance (usually within 2 days). After drying at room temperature, the film can be stripped off the substrate. Achieving uniform scattering of nanohybrid partners in liquid arrangement becomes an essential element in obtaining highly dispersed CNC and homogeneous thin films. In this sense, sulfate CNCs are preferred because the electrostatic effect between nearby nanoparticles makes them very dispersed in the liquid arrangement (Fig. 5.1).

When CNCs transport nanoparticles, new chiral materials with practical overhaul properties are created (Revol et al. 1992). Typically, nanoparticles are mixed with CNC in water, and after proper scattering of CNC and nanoparticles in an ultrasonic step, they are projected onto the substrate to enable their vaporization-induced self-assembly, resulting in a strong nanohybrid film. Some important models are plasma-gold nanorods, quantum spots, carbon nanotubes, carbon swabs or unusual earth compounds (Revol et al. 1998).

In any case, the consolidation of such nanoparticles is largely limited to low loads (about 1–1.5 wt %), since their nature often interferes with the chiral nematic long-distance requirements of the CNC (Querejeta-Fernández et al. 2015). Advanced molecular stacking serves as the basis for the creation of multifunctional materials, because the more prominent the presence of responsive nanoparticles, the faster they react in the external booster. In this particular case, the preparation of

Fig. 5.1 Surface deposition of CNC on film
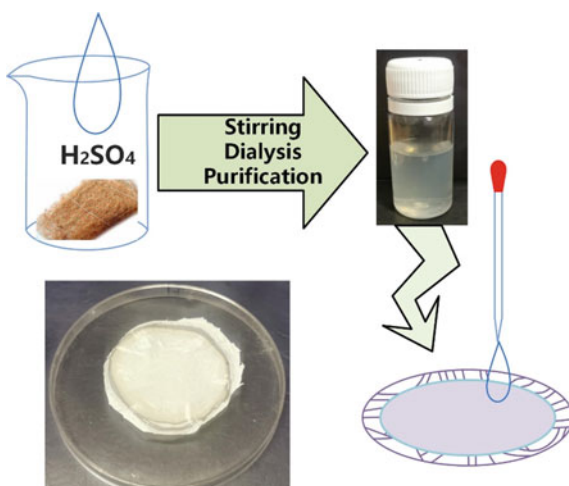
nanoparticles with suitable surface-useful aggregations to make them feasible with hydrophilic CNC is one of the main difficulties in this field (Lizundia et al. 2017a, b). Subsequently, hydrophobic nanoparticles can be surface-altered with amphiphilic stabilizers or parts such as carbonyl, hydroxyl and carboxylate aggregation can be transported.

5.2.2 Filtering Process

Using the traditional papermaking process, the aqueous CNC suspension can be quickly converted into a delicate film through a basic filtration process, including the extraction of a wet gel (called a gel/cake) and the subsequent disappearance of the water (Sehaqui et al. 2010). As the water in the gel/cake continues to disappear, a narrow power is generated that brings the CNC close to the point where the auxiliary spell is made, bringing full filaments with modulus of elasticity in the range of 5–10 GPa and rigid masses up to 70 MPa in ordinary films (Moon et al. 2011). While wet cakes can dry normally under the right conditions, several efforts have been made to reduce the time required for film making, including vacuum filtration of the CNC suspension, removal from channels, and subsequent broiler drying or autoclaving. While the cutting results are fascinating from a modern point of view, these projects, unfortunately, neglect the CNC's interesting ability to collect the self in very specific structures (Nan et al. 2017).

5.2.3 Layer by Layer Deposition

The layer-by-layer (LbL) strategy, first proposed by Iler in 1966, is a useful method for obtaining nanostructured faceted films with at least two species if they have an often attractive association (Iler 1966). While the idea was originally intended for countercharged polyelectrolytes, it has been extended to various frames, including CNC. In this production line, Martin et al. obtained diaspore trihydrate nanosheets with an absolute charge and a CNC facet film with an adverse charge. The results show that by fluctuating the ionic strength of the CNC suspension (via the expansion of monovalent salts), the layer thickness in the range of 13 to 70 nm can be controlled (Martin et al. 2017). Irradiation materials can also be obtained after LbL collection. For example, consolidation of colloidal SiO_2 and CNC, creating layers with alternative low and high refractive records, creates fragile films reflected at 550 nm (green).

With the LbL collection method, high-strength and very robust graphene oxide/CNC nanohybrids with layered morphology such as normal mother-of-pearl (7–15 nm per double layer) are obtained (Xiong et al. 2016). SA-LbL has also been extended to other nanohybrid frameworks, including multiwall carbon nanotubes (MWCNT)/CNC, aluminosilicate imogolite nanotubes/CNC, or zinc oxide/silver

(ZnO/Ag) (Trigueiro et al. 2014). Since these rely on static electricity, the robustness of faceted nanohybrids with communication as the main driving force may be slightly lower under brutal conditions, so the association between the two layers can be improved to bring various utilitarian aggregations into the CNC surface to provide a harder material (Li et al. 2018a, b).

5.2.4 Soft and Hard Templating

Given the combination of formats for CNC self-assembly, the LLC model was used to integrate mesoporous solids (porosity in the range of 2–50 nm) with large explicit surface areas and intermittent porosity (Kresge et al. 1992). CNC scattering is mixed with viable precursors, so self-aggregation delivers a nanostructured crossover material. At this point, one of the steps is specifically removed in order to obtain permeable material (Giese et al. 2015). According to this approach, controlled porosity can be brought into intermittent CNC structures, allowing CNC nanohybrids to help with applications such as drive support, enantioselective sensors, capacitor materials, or battery anodes. Using CNC as a template as a refined layout technique offers advantages, resulting in a particularly intriguing creation strategy compared to hard format strategies, as it allows good control of morphology, requires fewer manufacturing steps, and can be cultivated cost-effectively (Shopsowitz et al. 2011).

Taking into account the similarity of fast CNC autopolymerization and inorganic precursors during the sol–gel reaction, the mesoporous chiral nematic requirements obtained in CNC slimming films can also be transferred to many different materials by hard stencil strategy. For example, Shopowitz et al. used water scattering CNC as the chiral nematic stage. Free chiral nematic mesoporous carbon films with well-defined ranges up to 1465 m^2/g, meeting key instructions for mesoporous carbons with chiral requirements (CNC's EISA and TMOS, followed by pyrolysis at 900 °C followed by NaOH silica mapping in a nitrogen environment) (Shopsowitz et al. 2011). In addition, chiral nematic CNC/silica films can be calcined in air at 540 °C, leaving a silica gel film with a large surface area. The mesoporous chirality of CNC can also be transferred to various materials by unloaded mesoporous films of polymers formed by silicon dioxide, metal/metal oxides or fluorescence (Shopsowitz et al. 2010).

5.2.5 Nanoparticle Growth onto CNC

Due to the high surface energy of the nanoparticles, the overall inclination of the nanoparticles after mixing can be overwhelmed by turning into inorganic nanoparticles directly on the CNC surface (Kaushik and Moores 2016). With CNC as a strong format, nanoparticles can be developed by aqueous or decreasing techniques. For example, ZnO nanoparticles are developed on a water-scattering CNC covered with an elongated melamine–formaldehyde layer (Awan et al. 2018). At 100 °C, the

water hydration of zinc acetate derivatives is absent and NaOH and CNC produce round ZnO nanoparticles of 20–25 nm. Heat CNC, polyethylene glycol and chlorine corrosively at 80 °C for 1 h (Yan et al. 2016).

5.2.6   Sol–Gel Process

The sol–gel process involves the conversion of a "sol" (colloidal arrangement) into a "gel"-like frame with a strong and liquid phase. The morphology of these two stages can range from discrete particles to uninterrupted polymer tissue. When using water as the liquid stage (the most famous case of CNC), the sol–gel process creates a hydrogel, a three-layer, deeply penetrating hydrophilic fabric suitable for absorbing large amounts of water, thus keeping the tissue structure flawless. Using the remote-controlled chiral nematic requirements of CNCs, an improvement was made in response to photonic hydrogels in 2013, showing large color changes in the light of pH, solubility or temperature changes (Kelly et al. 2013). The chiral nematic phase is maintained by connecting the CNC to a nonionic hydrogel predecessor (acrylamide, acrylic corrosive, 2-hydroxyethyl methacrylate, macrogol methacrylate or N-isopropylacrylamide as monomer). Under ultraviolet light, the self-collected design is blocked. In addition, Hiratani et al. developed CNC hydrogels for ionic strength and strain detection. An anisotropic structure with critical birefringence was obtained by mechanical shear (Hiratani et al. 2018).

   Although these models require CNC to facilitate the gelation of polymers, there is basically less work to manage pure CNC hydrogel improvements (there is no polymer stage, only CNC and water) (Ureña-Benavides et al. 2011). The production of pure CNC hydrogels has been cultivated in many ways. In order to create a consistent organization of the detected poles from the nano to the macro scale, the simplest approach is to increase the CNC focus in the dispersion by more than 14 vol % (Heath and Thielemans 2010). Low-power ultrasound also creates the gel 3D fabric of a CNC because hydrogen remains bonded between adjacent CNCs. A finer way to deal with acquired hydrogels is to control static aversion between adjacent CNCs. Drops, which can weaken the dispersion of the charge balance. In this way, bonding the salts protects the carbonized electrical double layers, enhances their zeta potential, and reduces the electrostatic aversion between the CNC along these lines. After the salt expands, the charm becomes stronger, resulting in CNC collection and the resulting hydrogel (Dong and Gray 1997).

   A green, immediate, and effective CNC hydrogel manufacturing technology was recently announced that uses water treatment to advance the desulfurization of CNC surfaces, reducing their dispersibility and finally favoring their hydrogel arrangement. The results show that adjustable mechanical properties can be achieved by controlling the water temperature, response time, CNC focus, and pH. Similar meetings also show the production of CO_2-switchable CNC hydrogels, in which the gelation is due to the expansion of ionic strength by imidazole protonation (Bertsch et al. 2017; Oechsle et al. 2018).

5.2.7 Oven-Drying, Freeze-Drying, and Supercritical-Drying

The fluid circuit of the hydrogel can be removed by various techniques to obtain primary strong materials with deep penetration (close to 100%) and ultra-low thickness nanostructures (4–500 mg/cm^3) with a large exposed surface area (100–1000 m^2/g). Kistler first announced this permeable construction, called aerogels, in 1931 and can be obtained by various drying processes, of which freeze-drying and supercritical drying are the most popular methods (Pierre and Pajonk 2002). Previously, various aerogels made of carbon, silicon dioxide, alumina, and tin oxide were considered. The production of deep penetration CNC designs can help to improve specific adsorption properties, thermal and electrical protection properties, acoustic materials for attenuation limits and as templates/beams for various materials, thus opening new doors (Baetens et al. 2011).

The soluble evacuation step essentially influences the morphology and properties of subsequent aerogels and remains an important test for their formation. In fact, the disappearance of fluids in osmotic systems stresses fine stretches, leading to pore deformities, aerogel shrinkage, and surprising primary decompositions and fractures (Scherer 1986). Ice sublimation avoids the development of liquid-smoke interfaces and limits the presence of fine stresses that damage the structure. For example, the first hydrogel structures can be protected by submerging the fast-freezing solutes with liquid nitrogen, while slow freezing is often used as a way to create designs. In this strategy, known as the "ice template" (IT), the distribution of the propagation phases is carried out by the development of ice gemstones (Deville 2010). The construction of ice gemstones can be limited by directed warm slopes to create honeycomb 2D shapes that are compatible with the freezing process and offer interesting anisotropic mechanical properties (Munier et al. 2016).

5.2.8 Electrospinning

The innovation of electrospinning is gaining importance in the production of practical materials, as it is used to produce a layer of nano- and microfibers without interruption (Reneker and Yarin 2008). After using the electric field, the response containing the given material (broken, scattered or liquid) is removed from the spinnerets and stored with the help of electrostatic communication on the authority to provide a fiber pad of electrospinning (Ahmed et al. 2015). Boundaries such as fixed permutation, resolvable decision, applied stress, distance between tip and authority, and relative blockage fundamentally influence the morphology of the subsequent material. During electrospinning, the polar CNC adapts to the main fiber pivot point, resulting in an anisotropic material. Unfortunately, due to the difficulty of producing CNC in successive stages, CNC was mainly used as a support for the gradual relief of polymer fiber felts, and no work was announced on the development of pure CNC

electrospinning. However, given the excellent scattering of CNC in water, we recognize the extraordinary potential of electrospinning innovations in creating novel CNC nanohybrids with tendon morphology (Zhou et al. 2011).

5.3 Nanohybrid Types

5.3.1 CNC Structural, Chemical and Physical Properties

When considering the synthetic and practical properties of CNCs, it should be noted that their properties depend in particular on the strategy used for separation. CNC is removed from cellulose by controlled hydrolysis, in which less coordinated (blurred) areas endure the cleavage of their glycosidic bonds, leaving areas with safer, deep-translucent areas. In 2009, an enzymatic hydrolysis process was carried out to obtain CNCs, and most of their production was done after corrosive hydrolysis of solids (Filson et al. 2009). Typically, cellulose is immersed at 45° C for 30 min in a sulfuric acid corrosive (H_2SO_4) (64 wt.%) liquid arrangement and stably mixed, but other acids such as phosphoric acid, nitric acid, hydrobromic acid or hydrochloric acid can also be corrosive. After additional mechanical treatment by ultrasound, a water-scattering CNC was obtained (Lizundia et al. 2016).

CNC is a needle-like translucent nanoparticle of β-1,4 bonded anhydrous D-glucose units with widths of 3–20 nm, while its length can vary from 150 to 2000 nm depending on the cellulose source and mixing conditions, although usually a quality of 100–250 nm is obtained. CNCs typically have a degree of polymerization (DS or glucose units) of 500–15,000 and, due to their anisotropic properties, a specific surface area in the range of 150 and 250 m^2/g (Beck-Candanedo et al. 2005; Habibi et al. 2010).

5.3.2 CNC/Metal Oxide Nanohybrids

Oxide metal nanoparticles (NPs) such as titanium dioxide (TiO_2), zinc oxide (ZnO), copper oxide (CuO and Cu_2O), silicon dioxide (SiO_2) and iron oxides (Fe_2O_3 and Fe_3O_4) require their versatile, modulating and multifunctional properties, which are fundamental for relatively long-term technological applications, including propulsion, safety precautions, optoelectronics, attractive nanocomposites, luminescent materials, drug delivery frameworks, sensors, antimicrobial materials, imaging (Boury and Plumejeau 2015; Goikuria et al. 2017).

5.3.3 CNC/Carbonaceous Nanomaterials

Carbon nanostructures can be grouped according to their perspective ratio and nanometer size, using 1D as nanotubes or nanofibers, 2D as graphene nanosheets or graphene oxide, and 3D as fullerenes or carbon-dark nanoparticles (Iijima and Ichihashi 1993). Carbon nanotubes (CNTs) are formed by moving the graphene layer upwards in a circular and hollow manner. They are sequenced into single-walled carbon nanotubes (SWCNTs), double-layer carbon nanotubes (DWCNTs), and multi-walled carbon nanotubes (MWCNTs) as indicated by the number of layers, creating containers of different sizes and dimensions, ranging in length from about a few nanometers to millimeters, by changing interactions and boundaries.

Graphene is a two-layer carbon material consisting of a single sheet of graphite. The monolayer of carbon particles is organized in a hexagonal cross-section so that a thickness of 0.35 nm is assumed. Andre Geim and Kostya Novoselov received the Nobel Prize in Physics in 2010 for "leading the study of the double-layer material graphene" (Geim and Novoselov 2010). It is extremely conductive and robust, with a modulus of elasticity of 1 TPa and an extreme strength of 130 GPa. In fact, it is a material with excellent mechanical properties, even compared to carbon nanotubes. Fullerenes are an allotrope of carbon that is round (Zhu et al. 2010).

All carbon nanostructures have very strange electrical properties, and they are mixed with other nanomaterials to transfer this effect to the membrane material. Carbon nanostructures enable improved low-conductive layers of carbon CNC nanohybrids. Most conductive hybrids use carbon nanotubes or graphene, two new materials that often have amazing properties. Carbon black (CB) is additionally used due to its innate conductivity over a large surface area (Meng and Manas-Zloczower 2015).

5.3.4 CNC/Luminescent Nanoparticles

The resulting combination of brilliant materials and luminescence was sought as a tempting way to plan new optical devices. Quantum spots (QDs) are small semi-conductors that have tunable and elongated emission spectra induced by quantum repulsion, which is particularly useful for detection and light exchange (Alivisatos 1996). Quantum swabs are passivated with a suitable amphiphilic stabilizer to keep them away from their accumulation and ensure the development of chiral nematic phases. The photoluminescence (PL) outflow power of the film corresponds to the QD stack, which shows green to red light when irradiated with ultraviolet light (emission frequency of 490–680 nm) (Bruchez et al. 1998).

Carbon Pats (CDs) without metallic photoluminescent nanomaterials are attracting more and more attention due to their lowest cost, PL stability, and intrinsic

physicochemical properties. Contrary to what is commonly found in many semiconductor nanoparticles, the photoluminescence of CDs often relies on precursor materials used for their combination, making them useful in the fabrication of materials for detection, catalysis or design (Baker and Baker 2010).

5.4 Applications of CNC Nanohybrids

The study of CNC inorganic/natural nanohybrids is a rapidly developing interdisciplinary field in materials science and design that provides valuable properties for two parts that cannot be observed alone. In this sense, there are some licenses, progressive and commercial projects (George and Sabapathi 2015). Cellulose nanocrystals have been read and evaluated for a variety of applications, particularly in paper, polymers, plastics, chiral layout, flocculants, aerogels, hydrogels, drug delivery, detection, catalysis, high energy, and biomedicine (Fig. 5.2).

5.4.1 Energy Applications: Supercapacitors, Solar Cells, Batteries

Cellulose nanocrystals offer the benefits of high strength and adaptability for some advanced applications, providing capacitor gadgets that are less expensive than battery-powered batteries, with higher power thicknesses and faster charging capabilities (Dhar et al. 2018). Fast chargers can save critical energy because they accumulate energy when slowing down and provide energy as the speed increases. While conventional supercapacitors can actually damage the climate during assembly and dismantling, cellulose-based electroactive nanohybrids can be calibrated to make them more adaptable on the nanoscale (Pérez-Madrigal et al. 2016).

As is shown in Fig. 5.3, CNC can be used as (I) lightweight mechanical substrates with adaptability and unity to electrochemical and electroactive materials; (ii) conventional layout covered with other electrochemical dynamic anode materials or converted into other carbons by pyrolysis; (iii) the stomach between the cathodes of the supercapacitor; (iv) Materials that promote electrolyte retention, supplied as electrolytes or even as components of the actual electrolyte (Borghei et al. 2018).

5.4.2 Environmental Remediation Application

Practical cellulose-based materials are often used for separation, especially in the field of water treatment (Fig. 5.4). Biopolymers such as chitosan, chitin, and lignin are
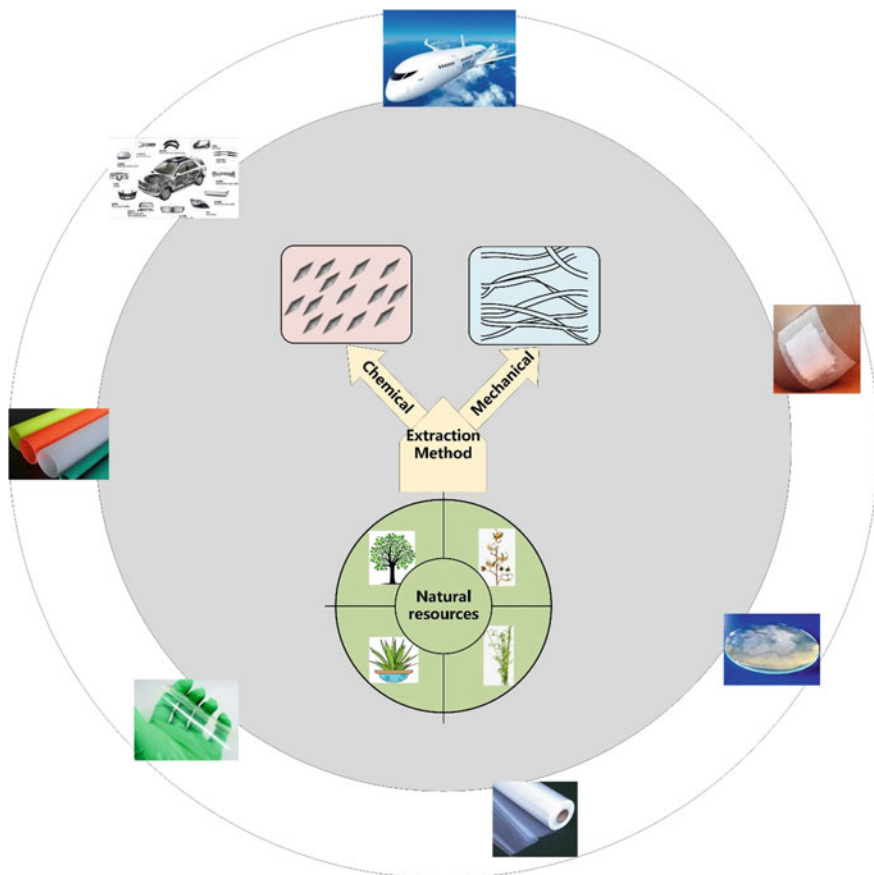
Fig. 5.2 Extraction and application of nanocellulose from lignin biomasses
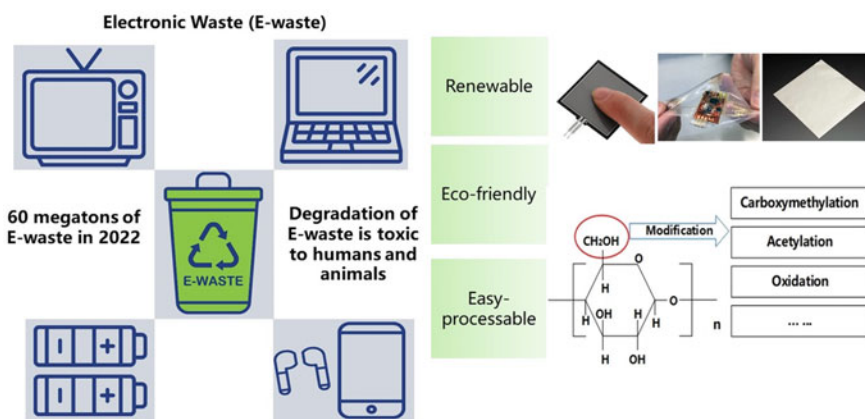
Fig. 5.3 Application of cellulose-based materials in electronic components

known to adsorb heavy metal particles from liquid arrangements. Practical cellulose-based materials offer excellent adsorption capacity for water treatment applications (Li et al. 2018a, b).

Nanotechnology is believed to be able to limit costs and further increase productivity in predicting, treating, and remediating pollution. Two applications of cellulose nanostructures in this field have aroused interest, in particular as dynamic adsorption materials for impurities and stabilizers for other dynamic particles (Carpenter et al. 2015).

Cellulose nanomaterials have an effectively functionalized surface that can limit the performance of nanocellulose impurities due to the bonding of material parts.
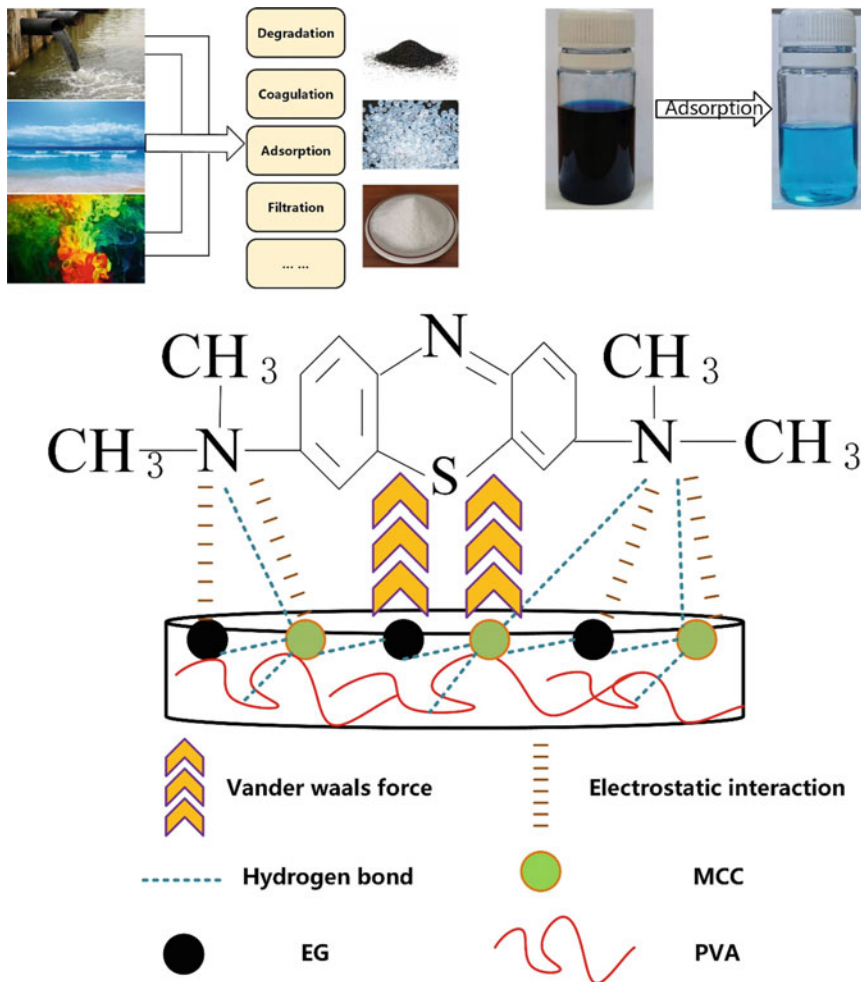
Fig. 5.4 Schematic diagram of the mechanism of physical adsorption of waste dyes on cellulose-based materials

Carboxylation is the technology that focuses most on increasing the adsorption limit. Yu et al. found that attaching succinic acid blasting to CNC significantly limits the productivity of Pb^{2+} (Yu et al. 2013).

5.4.3 Catalysis

Catalysis plays an important role in both industry and science, as it provides an effective platform for triggering various chemical reactions (Pan and Wang 2012). For example, catalysis can be used to produce materials such as polymers or for environmental remediation purposes by breaking down environmentally harmful molecules. The decomposition of organic pollutants in water offers the opportunity to reduce the widespread accumulation of pollutants in reservoirs (i.e., antibiotics, insecticides, etc.), a global challenge of the twenty-first century (Salas et al. 2014).

Since catalytic reactions often occur in the outer layers of valuable/non-valuable metallic materials, nanoscale particles are preferred because they have a larger explicit surface area and an increased number of reaction sites per unit mass (Eisa et al. 2018). Unfortunately, many people use nanoparticles to disperse synergistic reactions in liquid media, reducing their pleasantly explicit surfaces, and it is difficult to recover the propulsion particles once their capabilities are complete. To solve these difficulties, reactant nanoparticles can be fixed to various auxiliary materials such as cellulose, where the surface hydroxyl bundle provides great adhesion between the particles and the nanocellulose. Since this field has been considered recently, new light has been gained in heterogeneous catalytic processes with CNC as carrier material (Wu et al. 2013).

5.5 Conclusion

This paper provides an overview of the latest major improvements in the use of CNC in the field of nano-based nanocontamination of cellulose, including CNC design, inorganic or natural nanoparticle mixtures for the arrangement of nanopollutants and their applications. Due to its adaptability, CNC is one of the most interesting nature-based nanomaterials with a number of remarkable properties, including innate repeatability, biodegradability, business accessibility, adaptability, printability, low thickness, high porosity, optical directness, and superior mechanical, thermal, and physico-chemical properties.

Although some progress has been made in the production, characterization, and use of CNC or CNC-based nano-grown materials, there are still some problems that need to be solved from a logical and mechanical point of view.

References

Ahmed FE, Lalia BS, Hashaikeh R (2015) A review on electrospinning for membrane fabrication: challenges and applications. Desalination 356:15–30

Alivisatos AP (1996) Semiconductor clusters, nanocrystals, and quantum dots. Science 271(5251):933–937

Awan F, Islam MS, Ma Y, Yang C, Shi Z, Berry RM, Tam KC (2018) Cellulose nanocrystal–ZnO nanohybrids for controlling photocatalytic activity and UV protection in cosmetic formulation. ACS Omega 3(10):12403–12411

Baetens R, Jelle BP, Gustavsen A (2011) Aerogel insulation for building applications: a state-of-the-art review. Energy Build 43(4):761–769

Baker SN, Baker GA (2010) Luminescent carbon nanodots: emergent nanolights. Angew Chem Int Ed 49(38):6726–6744

Beck-Candanedo S, Roman M, Gray DG (2005) Effect of reaction conditions on the properties and behavior of wood cellulose nanocrystal suspensions. Biomacromol 6(2):1048–1054

Bertsch P, Isabettini S, Fischer P (2017) Ion-induced hydrogel formation and nematic ordering of nanocrystalline cellulose suspensions. Biomacromol 18(12):4060–4066

Borghei M, Miettunen K, Greca LG, Poskela A, Lehtonen J, Lepikko S, Tardy BL, Lund P, Subramanian VR, Rojas OJ (2018) Biobased aerogels with different surface charge as electrolyte carrier membranes in quantum dot-sensitized solar cell. Cellulose 25(6):3363–3375

Boury B, Plumejeau S (2015) Metal oxides and polysaccharides: an efficient hybrid association for materials chemistry. Green Chem 17(1):72–88

Bruchez M Jr, Moronne M, Gin P, Weiss S, Alivisatos AP (1998) Semiconductor nanocrystals as fluorescent biological labels. Science 281(5385):2013–2016

Carpenter AW, de Lannoy C-F, Wiesner MR (2015) Cellulose nanomaterials in water treatment technologies. Environ Sci Technol 49(9):5277–5287

Deville S (2010) Freeze-casting of porous biomaterials: structure, properties and opportunities. Materials 3(3):1913–1927

Dhar P, Gaur SS, Kumar A, Katiyar V (2018) Cellulose nanocrystal templated graphene nanoscrolls for high performance supercapacitors and hydrogen storage: an experimental and molecular simulation study. Sci Rep 8(1):1–15

Dong XM, Gray DG (1997) Effect of counterions on ordered phase formation in suspensions of charged rodlike cellulose crystallites. Langmuir 13(8):2404–2409

Eisa WH, Abdelgawad AM, Rojas OJ (2018) Solid-state synthesis of metal nanoparticles supported on cellulose nanocrystals and their catalytic activity. ACS Sustain Chem & Eng 6(3):3974–3983

Filson PB, Dawson-Andoh BE, Schwegler-Berry D (2009) Enzymatic-mediated production of cellulose nanocrystals from recycled pulp. Green Chem 11(11):1808–1814

Foster EJ, Moon RJ, Agarwal UP, Bortner MJ, Bras J, Camarero-Espinosa S, Chan KJ, Clift MJD, Cranston ED, Eichhorn SJ (2018) Current characterization methods for cellulose nanomaterials. Chem Soc Rev 47(8):2609–2679

Geim AK, Novoselov KS (2010) The rise of graphene. In Nanoscience and technology: a collection of reviews from nature journals. World Scientific, pp 11–19

George J, Sabapathi SN (2015) Cellulose nanocrystals: synthesis, functional properties, and applications. Nanotechnol Sci Appl 8:45

Giese M, Blusch LK, Khan MK, MacLachlan MJ (2015) Functional materials from cellulose-derived liquid-crystal templates. Angew Chem Int Ed 54(10):2888–2910

Goikuria U, Larranaga A, Vilas JL, Lizundia E (2017) Thermal stability increase in metallic nanoparticles-loaded cellulose nanocrystal nanocomposites. Carbohyd Polym 171:193–201

Habibi Y, Lucia LA, Rojas OJ (2010) Cellulose nanocrystals: chemistry, self-assembly, and applications. Chem Rev 110(6):3479–3500

Hamad WY, Miao C, Beck S (2019) Growing the bioeconomy: advances in the development of applications for cellulose filaments and nanocrystals. Ind Biotechnol 15(3):133–137

Heath L, Thielemans W (2010) Cellulose nanowhisker aerogels. Green Chem 12(8):1448–1453

Hiratani T, Kose O, Hamad WY, MacLachlan MJ (2018) Stable and sensitive stimuli-responsive anisotropic hydrogels for sensing ionic strength and pressure. Mater Horiz 5(6):1076–1081

Iijima S, Ichihashi T (1993) Single-shell carbon nanotubes of 1-nm diameter. Nature 363(6430):603–605

Iler RK (1966) Multilayers of colloidal particles. J Colloid Interface Sci 21(6):569–594

Kaushik M, Moores A (2016) Nanocelluloses as versatile supports for metal nanoparticles and their applications in catalysis. Green Chem 18(3):622–637

Kelly JA, Shukaliak AM, Cheung CCY, Shopsowitz KE, Hamad WY, MacLachlan MJ (2013) Responsive photonic hydrogels based on nanocrystalline cellulose. Angew Chem Int Ed 52(34):8912–8916

Klemm D, Cranston ED, Fischer D, Gama M, Kedzior SA, Kralisch D, Kramer F, Kondo T, Lindström T, Nietzsche S, Petzold-Welcke K, Rauchfuß F (2018) Nanocellulose as a natural source for groundbreaking applications in materials science: today's state. Mater Today 21(7):720–748. https://doi.org/10.1016/J.MATTOD.2018.02.001

Kresge CT, Leonowicz ME, Roth WJ, Vartuli JC, Beck JS (1992) Ordered mesoporous molecular sieves synthesized by a liquid-crystal template mechanism. Nature 359(6397):710–712

Li L, Ma W, Higaki Y, Kamitani K, Takahara A (2018a) Organic-inorganic hybrid thin films fabricated by layer-by-layer assembly of the phosphorylated cellulose nanocrystal and imogolite nanotubes. Langmuir 34(44):13361–13367

Li Y-Y, Wang B, Ma M-G, Wang B (2018b) Review of recent development on preparation, properties, and applications of cellulose-based functional materials. Int J Polym Sci 2018

Lizundia E, Maceiras A, Vilas JL, Martins P, Lanceros-Mendez S (2017a) Magnetic cellulose nanocrystal nanocomposites for the development of green functional materials. Carbohyd Polym 175:425–432. https://doi.org/10.1016/J.CARBPOL.2017.08.024

Lizundia E, Nguyen T-D, Vilas JL, Hamad WY, MacLachlan MJ (2017b) Chiroptical luminescent nanostructured cellulose films. Mater Chem Front 1(5):979–987

Lizundia E, Urruchi A, Vilas JL, León LM (2016) Increased functional properties and thermal stability of flexible cellulose nanocrystal/ZnO films. Carbohyd Polym 136:250–258

Marchessault RH, Morehead FF, Walter NM (1959) Liquid crystal systems from fibrillar polysaccharides. Nature 184(4686):632–633

Martin C, Barker R, Watkins EB, Dubreuil F, Cranston ED, Heux L, Jean B (2017) Structural variations in hybrid all-nanoparticle gibbsite nanoplatelet/cellulose nanocrystal multilayered films. Langmuir 33(32):7896–7907

Meng Q, Manas-Zloczower I (2015) Carbon nanotubes enhanced cellulose nanocrystals films with tailorable electrical conductivity. Compos Sci Technol 120:1–8

Moon RJ, Martini A, Nairn J, Simonsen J, Youngblood J (2011) Cellulose nanomaterials review: structure, properties and nanocomposites. Chem Soc Rev 40(7):3941–3994

Munier P, Gordeyeva K, Bergström L, Fall AB (2016) Directional freezing of nanocellulose dispersions aligns the rod-like particles and produces low-density and robust particle networks. Biomacromol 17(5):1875–1881

Nan F, Nagarajan S, Chen Y, Liu P, Duan Y, Men Y, Zhang J (2017) Enhanced toughness and thermal stability of cellulose nanocrystal iridescent films by alkali treatment. ACS Sustain Chem & Eng 5(10):8951–8958

Oechsle A-L, Lewis L, Hamad WY, Hatzikiriakos SG, MacLachlan MJ (2018) CO2-switchable cellulose nanocrystal hydrogels. Chem Mater 30(2):376–385

Pan K, Wang W-X (2012) Trace metal contamination in estuarine and coastal environments in China. Sci Total Environ 421:3–16

Pérez-Madrigal MM, Edo MG, Alemán C (2016) Powering the future: application of cellulose-based materials for supercapacitors. Green Chem 18(22):5930–5956

Pierre AC, Pajonk GM (2002) Chemistry of aerogels and their applications. Chem Rev 102(11):4243–4266

Querejeta-Fernández A, Kopera B, Prado KS, Klinkova A, Methot M, Chauve G, Bouchard J, Helmy AS, Kumacheva E (2015) Circular dichroism of chiral nematic films of cellulose nanocrystals loaded with plasmonic nanoparticles. ACS Nano 9(10):10377–10385

Reid MS, Villalobos M, Cranston ED (2017) Benchmarking cellulose nanocrystals: from the laboratory to industrial production. Langmuir 33(7):1583–1598

Reneker DH, Yarin AL (2008) Electrospinning jets and polymer nanofibers. Polymer 49(10):2387–2425

Rescignano N, Fortunati E, Montesano S, Emiliani C, Kenny JM, Martino S, Armentano I (2014) PVA bio-nanocomposites: a new take-off using cellulose nanocrystals and PLGA nanoparticles. Carbohyd Polym 99:47–58. https://doi.org/10.1016/J.CARBPOL.2013.08.061

Revol J-F, Bradford H, Giasson J, Marchessault RH, Gray DG (1992) Helicoidal self-ordering of cellulose microfibrils in aqueous suspension. Int J Biol Macromol 14(3):170–172

Revol J-F, Godbout L, Gray DG (1998) Solid self-assembled films of cellulose with chiral nematic order and optically variable properties. J Pulp Pap Sci 24(5):146–149

Salas C, Nypelö T, Rodriguez-Abreu C, Carrillo C, Rojas OJ (2014) Nanocellulose properties and applications in colloids and interfaces. Curr Opin Colloid Interface Sci 19(5):383–396. https://doi.org/10.1016/j.cocis.2014.10.003

Scherer GW (1986) Drying gels: I. General theory. J Non-Cryst Solids 87(1–2):199–225

Sehaqui H, Liu A, Zhou Q, Berglund LA (2010) Fast preparation procedure for large, flat cellulose and cellulose/inorganic nanopaper structures. Biomacromol 11(9):2195–2198

Shopsowitz KE, Hamad WY, MacLachlan MJ (2011) Chiral nematic mesoporous carbon derived from nanocrystalline cellulose. Angew Chem Int Ed 50(46):10991–10995

Shopsowitz KE, Qi H, Hamad WY, MacLachlan MJ (2010) Free-standing mesoporous silica films with tunable chiral nematic structures. Nature 468(7322):422–425

Trache D, Hussin MH, Haafiz MKM, Thakur VK (2017) Recent progress in cellulose nanocrystals: sources and production. Nanoscale 9(5):1763–1786

Trigueiro JPC, Silva GG, Pereira FV, Lavall RL (2014) Layer-by-layer assembled films of multi-walled carbon nanotubes with chitosan and cellulose nanocrystals. J Colloid Interface Sci 432:214–220

Ureña-Benavides EE, Ao G, Davis VA, Kitchens CL (2011) Rheology and phase behavior of lyotropic cellulose nanocrystal suspensions. Macromolecules 44(22):8990–8998

Wu X, Lu C, Zhang W, Yuan G, Xiong R, Zhang X (2013) A novel reagentless approach for synthesizing cellulose nanocrystal-supported palladium nanoparticles with enhanced catalytic performance. J Mater Chem A 1(30):8645–8652

Xiong R, Hu K, Grant AM, Ma R, Xu W, Lu C, Zhang X, Tsukruk VV (2016) Ultrarobust transparent cellulose nanocrystal-graphene membranes with high electrical conductivity. Adv Mater 28(7):1501–1509

Yan W, Chen C, Wang L, Zhang D, Li A-J, Yao Z, Shi L-Y (2016) Facile and green synthesis of cellulose nanocrystal-supported gold nanoparticles with superior catalytic activity. Carbohyd Polym 140:66–73

Yu X, Tong S, Ge M, Wu L, Zuo J, Cao C, Song W (2013) Adsorption of heavy metal ions from aqueous solution by carboxylated cellulose nanocrystals. J Environ Sci 25(5):933–943

Zhou C, Chu R, Wu R, Wu Q (2011) Electrospun polyethylene oxide/cellulose nanocrystal composite nanofibrous mats with homogeneous and heterogeneous microstructures. Biomacromol 12(7):2617–2625

Zhu Y, Murali S, Cai W, Li X, Suk JW, Potts JR, Ruoff RS (2010) Graphene and graphene oxide: synthesis, properties, and applications. Adv Mater 22(35):3906–3924

Chapter 6
Self-Cleaning Textiles and Their Applications

Muhammad Zaman Khan, Jiří Militký, Blanka Tomková, Azam Ali, Mohanapriya Venkataraman, and Dana Křemenáková

Abstract The research related to self-cleaning textiles has received considerable attention within the scientific community due to their potential applications in industry and daily life. During the last two decades research interests on self-cleaning textiles have grown tremendously. Over the past years, researchers have been working to mimic nature by inducing self-cleaning properties into fibrous materials. The self-cleaning textiles have applications in the fields, such as space, defense, automotive, medical, sensors, apparel, and so on. Currently, there are two main concepts used in developing self-cleaning textiles. The first concept (physical self-cleaning) is based on the superhydrophobic approach where water droplets attain a spherical shape and then roll off the surface carrying away the dirt particles. The second concept (chemical self-cleaning) is based on the process of photo-catalysis where the dirt/stain molecules break down to simpler species (such as CO_2 and water) on exposure to light. This chapter is about the current approaches to the self-cleaning textiles and their functional applications.

6.1 Introduction

Self-cleaning is the term that has attracted a lot of attention in recent years. When we think of any surface, three kinds of self-cleanings come to our mind; physical, chemical, and biological self-cleanings. Physical self-cleaning means physically removal of dust and dirt particles present on any surface. These surfaces are available in nature like lotus leaves, rice leaves, and duck feathers. Chemical self-cleaning refers to chemically degradation of stains present on the surface, and biological self-cleaning means killing of bacteria if they attach to the surface and prevention of their growth.

M. Z. Khan · J. Militký (✉) · B. Tomková · A. Ali · M. Venkataraman · D. Křemenáková
Department of Material Engineering, Faculty of Textile Engineering, Technical University of Liberec, Studentská 2, 46117 Liberec, Czech Republic
e-mail: jiri.militky@tul.cz

M. Venkataraman
e-mail: mohanapriya.venkataraman@tul.cz

The self-cleaning surfaces have gained great interest in the researcher and scientific society due to their potential applications in industry and daily life. For example, it is useful for textile products that are endangered by staining with heavy contaminants such as soot, oils, lubricants or those not capable of washing due to their size or water and/or detergent sensitivity (i.e., curtains, blinds, roller blinds or external sunshades) (Sobczyk-Guzenda et al. 2013). The self-cleaning textiles also hold great promise for military applications where there is a lack of time for laundering in severe conditions, and in business life when clothes get stained accidentally. Currently, there are two main concepts used in developing self-cleaning surfaces. The first concept (physical self-cleaning) is based on the anti-wetting approach where water droplets attain a spherical shape and then roll off the surface carrying away the dirt particles (Li et al. 2015). The second concept (chemical self-cleaning) is based on the process of photo-catalysis where the dirt/stain molecules break down into simpler species (such as CO_2 and water) on exposure to light (Du et al. 2018). The superhydrophobic surfaces exhibit extremely high water repellency, where water drops bead up on the surface, rolling with a slight applied force, and also water droplet bounce over the superhydrophobic surface when dropped from a height (Mohamed et al. 2015). It is well known that the surface roughness and low surface energy of materials are the two important factors to control the wettability of a surface and to obtain water contact angles greater than 150° (Hsieh et al. 2008a, b; Zhang and Wang 2013). As an inspiration from nature (e.g. lotus leaves, butterfly wings, and water strider legs), scientists have fabricated superhydrophobic textiles by creating surface roughness in combination with low surface energy materials such as organic silanes, fluorinated silanes, alkyl amines, and silicates (Yao and He 2014). For chemical self-cleaning, polycrystalline semiconductor oxides have been applied in the form of nano-coatings, leading to the successful development of a number of UV-active self-cleaning textiles (Afzal et al. 2014). In this regard, titanium dioxide (TiO_2) has become the most popular high-efficiency catalyst due to the advantages of its high refraction coefficient, absorption in the UV range, strong photocatalytic effect, biological inertness, and low cost (Ge et al. 2014; Yuenyongsuwan et al. 2018). It was reported that the particle size, crystal structure, and morphology play important roles in photocatalytic activity of TiO_2, which is mainly dependent on the synthetic method and reaction conditions including titanium salt, pH value, reaction temperature, time, additives, etc. (Li et al. 2006).

In 1997, Wilhelm Barthlott studied the self-cleaning of plant leaves, and the lotus leaf was the first, he analyzed. It was found that plant leaves had this unique characteristic due to the presence of hierarchical roughness structure (Barthlott and Neinhuis 1997). Since then, this cleaning of plant leaves has been called the lotus effect. This work opened new horizons for researchers and the focus of research activity was changed from changing surface chemistry to modifying its structure to mimic lotus leaf. This effect has been mimicked on different surfaces including textiles. Another aspect of self-cleaning which came into the limelight during the late 1990s, is the photocatalytic degradation of stains deposited on a surface. The research work was focused on degrading the color stains deposited on a surface that was not repellent to water and oil. In 2001, Pilkington Glass announced the development of

the first self-cleaning windows with the name of Pilkington Activ TM which was followed by self-cleaning glass by Saint Gobain.

In recent years several techniques and methods have been used for the fabrication of self-cleaning textiles, including hydrothermal techniques (Ashraf et al. 2013; Li et al. 2015), the sol–gel method (Xiong et al. 2011), dip coating (Khan et al. 2018a, b; Shirgholami et al. 2011), the electro-chemical method (Liu et al. 2016), the layer-by-layer method (Gustafsson et al. 2012), chemical vapor deposition (Aminayi and Abidi 2013; Boscher et al. 2014), and spray coating (Latthe and Rao 2012; Lu et al. 2015; Zhang et al. 2018). A very thin transparent layer of TiO_2 was deposited on glass surface which during sunlight irradiation, chemically degraded the organic species deposited on surface. During the last decade, photocatalytic self-cleaning has been developed on textile surfaces as well. For this, the textile surface was functionalized with TiO_2 to degrade the stains of red wine and discoloration of the dye solution. Zinc oxide (ZnO) is an n-type important semiconductor having a wide band gap (3.37 eV), and large excitation binding energy of E_g (60 meV) that can give exciton emission under low excitation energy at room temperature. This wide band gap semiconductor material has many functional properties, such as self-cleaning, antimicrobial, non-toxic, photocatalytic ability, UV resistance, antistatic, and *piezoelectric* properties. Zinc oxide nanoparticles are utilized in catalytic reaction process due to their large surface area and high photocatalytic properties. Synthesis of the ZnO nanostructures with controlled morphology is usually carried out using microwave-assisted synthesis techniques (Hasanpoor et al. 2015; Khan et al. 2023).

6.2 Self-Cleaning Textiles

The ability of a fabric to provide clean and neat surface is called self-cleaning property. Self-cleaning properties in textiles can be achieved by two different processes. By integration of nanoparticles on fabric surface that can act as photo-catalysts and have the ability to degrade stain and organic dirt. It can also degrade dye solution (Khan et al. 2020a, b). The second method is the production of superhydrophobic surfaces which can provide stain and grime repellency and provide self-cleaning function by rolling water drops that can collect dust and other debris. The potential chemical and physical self-cleaning mechanism is shown in Fig. 6.1.

6.2.1 Materials for Self-Cleaning Textiles

Due to growing market demand, the researchers have focused their attention on the development of self-cleaning textiles using non-conventional techniques. These techniques include the use of nanotechnology or nanomaterials either to deposit nanoparticles on textiles to functionalize them or to develop nanofibers which are used for manufacturing of fabrics with functional characteristics. The use of various
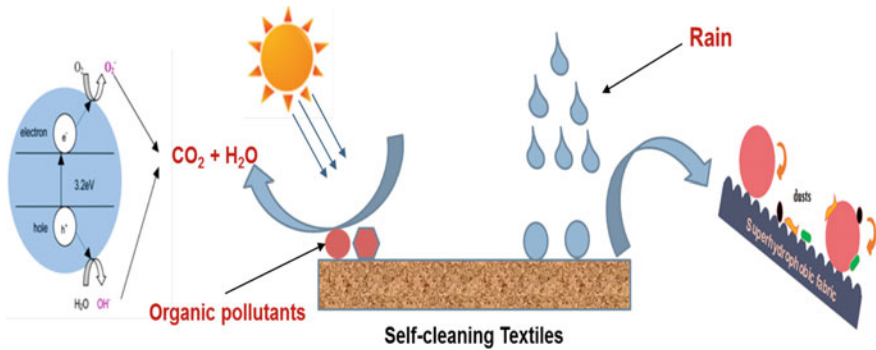
Fig. 6.1 Self-cleaning mechanism of the textiles

nanoparticles is the easiest way to fabricate self-cleaning textiles with high resistance against various environments (Bayer 2017; Boscher et al. 2014; Yao et al. 2018). The use of nanoparticles, nano finishes, and nanostructures is very useful for enhancing and developing superior performance characteristics of conventional textiles including superhydrophobicity, self-cleaning, UV blocking, antimicrobial activity, soil-resistance, anti-static, anti-infrared, and flame-retardancy. The super-hydrophobicity or superhydrophilicity of textile materials can also be enhanced by creating nanostructure surfaces (Joshi and Bhattacharyya 2011). UV protection property of a textile fabric can be achieved by dye, pigment, metal oxides or UV absorber finish. These materials can protect against UV radiation by absorbing and blocking its penetration through a fabric.

In recent years, a lot of research has been done to develop self-cleaning textiles using nanoparticles of ZnO, TiO_2, and SiO_2, etc. Excellent UV protection was achieved by deposition of TiO_2 on polyester fabric (Khan et al. 2015). TiO_2 and ZnO nanoparticles are also used for this purpose as they have good UV protection properties. They give protection by reflecting, scattering or absorbing harmful UV radiations of the sun. They are more stable when compared to organic UV-blocking agents. Nanoparticles of ZnO can be prepared by wet chemical technique followed by application on fabrics for enhanced UV protection (Becheri et al. 2008; Haydon 2012; Mao et al. 2009; Yadav et al. 2006). Antibacterial effects on textile fabric can be maximized using nanoparticles because of the increased surface area (Dastjerdi and Montazer 2010; Lee et al. 2007; Perelshtein et al. 2009; Selvam et al. 2012). Nano-rough superhydrophobic surfaces can be prepared by controlling surface topography by many processing methods which include sol–gel technique, organic/inorganic hybrid method, CVD, electrochemical deposition, embossing, plasma processing, and phase separation technique. The incorporation of TiO_2 nanoparticles by titania sol–gel coating can cause surface roughness for enhancing the superhydrophobicity of the fabric (Xue et al. 2008). Carbon fabric was coated with silica nanoparticles to make it superhydrophobic (Hsieh et al. 2008a, b). For physical and chemical self-cleaning, polycrystalline semiconductor oxides have been applied in the form

of nano-coatings, leading to the successful development of a number of UV-active self-cleaning textiles (Afzal et al. 2014). Although TiO_2 or ZnO are widely used inorganic UV blockers, but they accelerate the photodamage of human skin due to high photocatalytic activity (Wang et al. 2015). Therefore, the search on safe UV shielding agents that possess superior shielding efficiency with poor photocatalytic properties has become an urgent necessity.

6.3 Chemical Self-Cleaning

Chemical self-cleaning refers to the degradation of stains at solid surface. It also concerns the degradation of chemical species contained in solution with which the solid surface comes in contact for a longer period. Normally, this self-cleaning effect takes place under the effect of UV light. The UV light activates the photocatalyst deposited on the surface which produces active species capable of degrading organic chemicals (Wu et al. 2009).

6.3.1 Photocatalysis Process

This term is basically the combination of two words "photo" and "catalysis." Photo means light and catalysis means acceleration of chemical reaction in the presence of catalyst. Therefore, photocatalytic effect refers to the acceleration of a chemical reaction under the effect of light. The term "photocatalysis" is still the subject of some debate. For example, it is argued that the idea of a photocatalyzed reaction is fundamentally incorrect since it implies that, in the reaction, light is acting as a catalyst, whereas it always acts as a reactant that is consumed in the chemical process. Therefore, it should be called "acceleration of a photoreaction by the presence of a catalyst." All the photocatalysis-based reactions produce hydroxyl radicals which are the basic ingredients of advanced oxidation processes. These processes have emerged as a promising water and wastewater treatment technology for the degradation or mineralization of a wide range of organic contaminants (Gupta and Gulrajani 2015). The chemical self-cleaning concept is based on the process of photo-catalysis where the dirt/stain molecules break down to simpler species (such as CO_2 and water) on exposure to light. The UV radiation activates the photocatalyst deposited on the surface which generates the active species capable of degrading organic chemicals. In photocatalytic reaction, the electromagnetic radiation with phonon energy (given by its wavelength λ (nm)) at least equal to the band gap of semiconductor E_g (eV) should be used. The required wavelength for just overcoming the band gap is simply given by Eq. (6.1).

$$\lambda = \frac{1240}{E_g} \qquad (6.1)$$

For the visible light range, this is from 3.1 to 1.8 eV.

One of the most efficient materials for chemical self-cleaning (photochemical oxidation/reduction) are TiO_2 and ZnO nanoparticles of different shapes and sizes. TiO_2 is a versatile photocatalyst degrading a wide range of organic pollutants, bacteria, cancer cells, and viruses and has applications in air and water remediation, and self-sterilizing surfaces as well (Banerjee et al. 2014, 2015; Carneiro et al. 2011; Fu et al. 2017). When TiO_2 was illuminated by light energy higher than its band gaps, the electrons in TiO_2 jumped from the valence band to the conduction band and then formed electron (e^-) and electric hole (h^+) pairs on the surface of the photocatalyst. The negative electrons and oxygen combine into $\cdot O_2^-$, whereas the positive electric holes and water generate hydroxyl radicals. When the organic compound falls on the surface of the photocatalyst, it can combine with $\cdot O_2^-$ and $\cdot OH$ respectively, and turn into carbon dioxide and water (Mills and Le Hunte 1997). The hydroxyl radical is a highly oxidizing agent. The addition of hydroxyl radicals to azo bond leads to its breaking. The degradation mechanism of dye solution begins with the azo bond cleavage and is followed by the hydroxylation of the aromatic ring (Fujishima et al. 2000). The potential chemical self-cleaning mechanism of ZnO nanostructures under UV irradiation can be seen in Fig. 6.2. When the ZnO is illuminated by energy higher than its band gap (3.37 eV) the electrons in the valence band jump to the conduction band followed by the generation of electron (e^-), and electric hole (h^+) pairs on the surface of the photocatalyst. The negative electrons (e^-) and oxygen (O_2) combine into superoxide radicals ($\cdot O_2^-$), while the positive holes (h^+) and water (H_2O) produce hydroxyl radicals ($\cdot OH$). Finally, the generated hydroxyl radicals ($\cdot OH$), and superoxide radicals ($\cdot O_2^-$) are responsible for the antimicrobial activity and dye degradation (Chen et al. 2017; Kajbafvala et al. 2012). A proposed chemical reaction is shown as follows (Eqs. (6.2)–(6.5)) (Khan et al. 2021a, b, c):

$$ZnO + hv \rightarrow ZnO(e^- + h^+) \tag{6.2}$$

$$h^+ + H_2O \rightarrow H^+ + \cdot OH \tag{6.3}$$

$$O_2 + e^- \rightarrow \cdot O_2^- \tag{6.4}$$

$$\cdot OH, \cdot O_2^- + Azo\text{dye} \rightarrow \text{degradation} \tag{6.5}$$
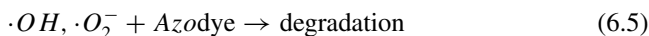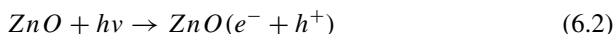
6.4 Physical Self-Cleaning (Superhydrophobicity)

Superhydrophobicity is inspired from nature and superhydrophobic surfaces are found in some plants, insect species, and animal kingdoms with water-active properties and mimesis to allow them to better survive in their environment (Celia et al.
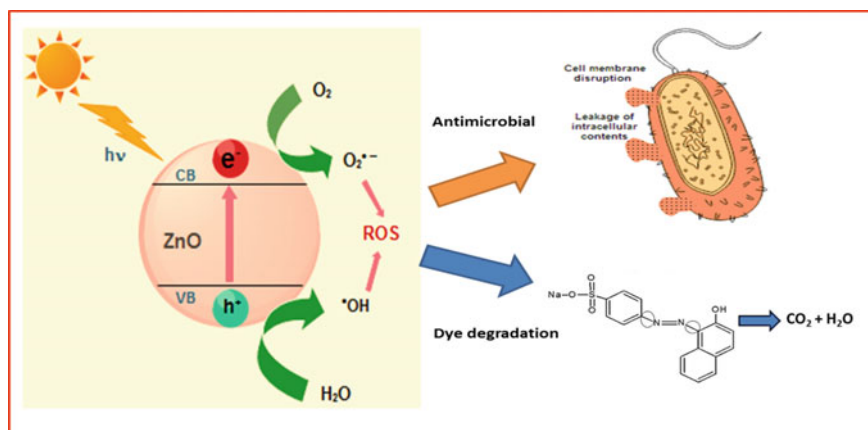
Fig. 6.2 Photocatalysis mechanism of zinc oxide

2013; Darmanin and Guittard 2015; Webb et al. 2014; Zhu et al. 2014). The natural superhydrophobic layer prevents the water accumulation, adhesion of the dirt particles and facilitates the rolling of the water droplets over the surface, and also performs the self-cleaning activity. The superhydrophobic layer on the surface of mosquito's eyes serves for anti-fogging. The self-cleaning properties in plants help to remove the dirt particles on the surface that can interfere with photosynthesis. In all-natural scenarios, the low contact angle hysteresis (CAH) contributes to the self-cleaning properties and the reduction of drag in fluid flow. The superhydrophobic property has a combination of functions possible by the material structure. The geometrical arrangement of nanostructures interacts with the light, which generates optical properties for harvesting and protection, communication, sensing, camouflage, mimesis, and mate attraction. The annual legume Melilotus siculus has a gas layer that physically separates the seawater from the leaves, which allows the plant to survive in saline water and achieve photosynthesis under complete submergence. The nanopillars in butterfly and cicada wings enhance the surface roughness and anti-wetting properties, which results in self-cleaning and anti-wetting (Bhushan 2009; Eder et al. 2018; Nguyen-tri et al. 2019). These attributes also possess photonic features with iridescent and antireflection functions. The most famous example of natural superhydrophobic surfaces is lotus leaves (Nelumbo nucifera), which are characterized by ultra-low water adhesion and self-cleaning properties (Barthlott and Neinhuis 1997) (Fig. 6.3). The self-cleaning properties (properties to remove dust and particles by the moving of water droplets) are derived from the Cassie–Baxter state (Fig. 6.3b, c). This property is the consequence of a dual (micro/nano) surface structure (Fig. 6.3d). The duality is very important to stabilize the Cassie–Baxter state even after pressures corresponding to the impact of rainfall. At the microscale (Fig. 6.3e) the leaf contains convex cell papilla, while at the nanoscale (Fig. 6.3f) epicuticular wax (lipid) crystals are observed. Since this discovery, many superhydrophobic plants have been
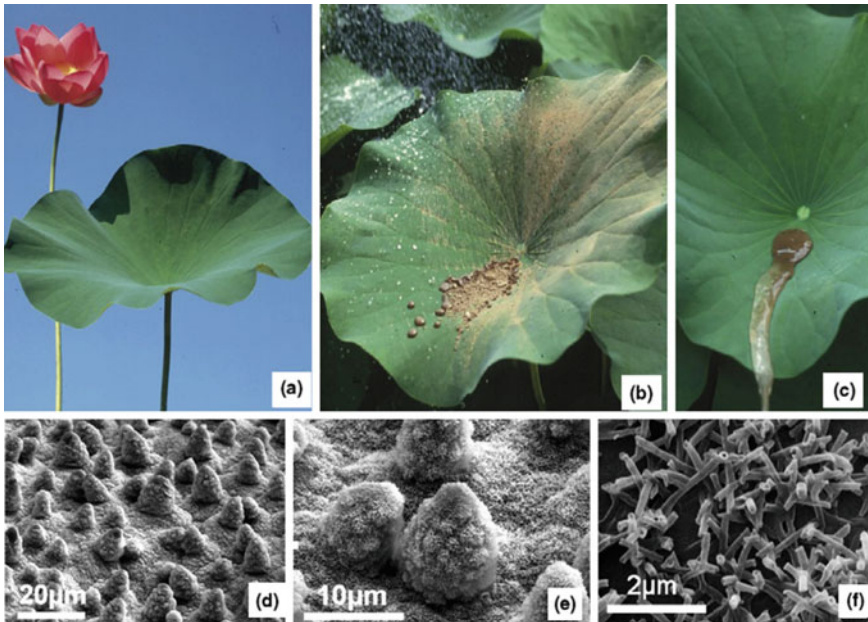
Fig. 6.3 Images of lotus leaves (Nelumbo nucifera) with self-cleaning properties at different magnifications. Reproduced with permission of Ref. (Koch et al. 2009)

investigated. Barthlott and coworkers studied the surface structures of submersed and floating water plants (Koch et al. 2008, 2009).

6.4.1 Theories and Fundamentals

The wetting of the surface can be categorized as hydrophilic, hydrophobic or superhydrophobic. The water contact angle (WCA) measurements are often used to characterize the wettability of the solid surface. A hydrophilic surface shows a strong affinity toward water, whereas a hydrophobic surface strongly repels water. The surface is known to be superhydrophilic when the water contact angle is less than 10°, hydrophilic when the WCA is less than 90°, and hydrophobic when the WCA is greater than 90°. The surfaces with WCA above 150° and a sliding angle below 10° are known as superhydrophobic surfaces (Fig. 6.4) (Zhang et al. 2022).

Young's law

Wetting is commonly characterized by the contact angle, which is defined as the angle between the tangent to the liquid/vapor interface and the solid surface at the three-phase contact line. In 1805, Thomas Young proposed a model (Eq. 6.6) to
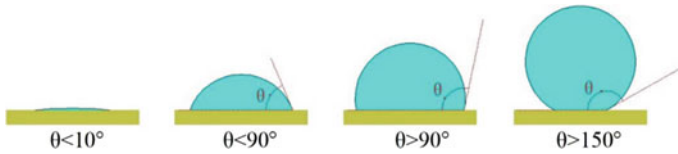
Fig. 6.4 Water droplet state of the surface. Reprinted under the terms of the Creative Commons Attribution license from MDPI Publications (Zhang et al. 2022)

determine the contact angle of the liquid on a homogeneous and perfectly smooth surface (Valipour et al. 2014).

$$\cos\theta = \frac{\gamma_{SV} - \gamma_{SL}}{\gamma_{LV}} \tag{6.6}$$

Young's equation is a basic and classical wetting model used to evaluate the wetting of a flat surface. According to his law, the droplet can only be in equilibrium if the forces acting on the triple are equal (see Fig. 6.5). By convention, the contact angle is measured from the liquid side. For a smooth and chemically homogeneous solid surface, the contact angle of a drop can be calculated theoretically by using the Young's equation (Huhtamäki et al. 2018; Khan et al. 2022).

Where; θ is the Young contact angle on ideally smooth surface, γ_{SV} and γ_{SL} refer to the solid/vapor and solid/liquid interfacial tensions, respectively, and γ_{LV} is the liquid/vapor interfacial tension (i.e., surface tension of the liquid). From the Young equation, it is well known that solid surfaces having high surface energy show a low contact angle, whereas solid surfaces with low surface energy tend to exhibit a high contact angle value. The contact angle depends on the difference of interfacial tension between solid, gas, and solid, liquid. A high quality silicon wafer is considered close to the ideal smooth surface.

Wenzel model

In 1936, Wenzel proposed a new model (Fig. 6.6a) for rough surfaces. In the Wenzel model, the liquid is in contact with the entire solid surface and completely penetrates into cavities. The Wenzel model states that a rough material has a higher surface area than a smooth one, which modifies the contact angle (Darmanin and Guittard 2015; Valipour et al. 2014).

Fig. 6.5 A drop of water on an ideal smooth surface (Young's model)
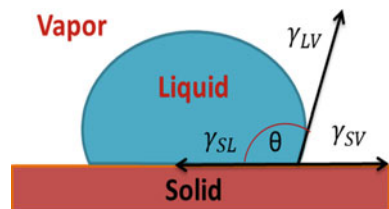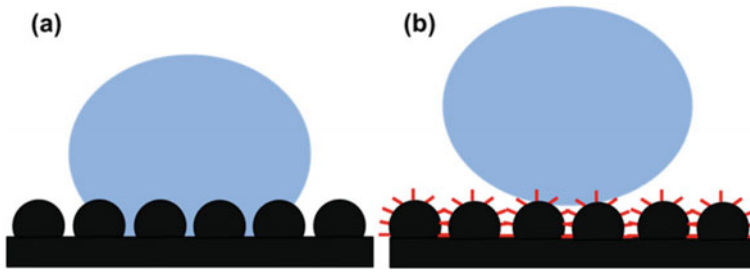
Fig. 6.6 **a** Wenzel droplet, **b** Cassie-Baxter droplet. Reprinted under the terms of the Creative Commons Attribution license from MDPI Publications (Latthe et al. 2014)

There is not a single surface in nature which is completely homogeneous and perfectly smooth. So, there is always more or less roughness present on the surface. Therefore, Young's law does not give the exact value of contact angle. In order to calculate the contact angle on rough surface, Wenzel put forward the following equation (Eq. 6.7).

$$\cos\theta_w = r\cos\theta \tag{6.7}$$

where; θ_w is the contact angle on a surface with roughness, and θ is that of on an ideal surface and r is the roughness fraction which is defined as the ratio between the contact area to projected area of the surface. The "r" is either equal to 1 or more than 1. If it is equal to 1 that means the surface is 100% homogeneous and smooth which is not possible. If the surface is already hydrophilic (WCA < 90º), the introduction of roughness to the surface will increase its hydrophilicity. The surface having a water contact angle of less than 10° is referred to superhydrophilic surface. Similarly, if the surface is already hydrophobic, the roughness of the surface will increase the hydrophobicity and the surface will become superhydrophobic, having contact angle greater than 150° (Li et al. 2007). This equation is valid only when the water droplet penetrates into the asperities of roughness as shown in Fig. 6.4a.

Cassie-Baxter model

The Cassie model (1944) is based on water contact with a composite surface of the solid and air that is trapped into the microgrooves of the rough surface. In this state, the droplet of liquid does not make complete contact with the surface that is due to the presence of air pockets underneath. The drops of liquid rest on the heterogeneous composite interface of the surface that consists of the peaks of a patterned rough surface and air pockets trapped between them, which a drop of liquid cannot penetrate as shown in Fig. 6.6b (Jeevahan et al. 2018; Ramachandran and Nosonovsky 2016). Therefore, for a surface composed of two fractions, one with the fractional area f_1 and the contact angle θ_1 and the other with f_2 and θ_2, respectively (so that $f_1 + f_2 = 1$), the contact angle for the heterogeneous interface is given by the Cassie-Baxter equation (Eq. 6.8) (Bhushan and Jung 2011).

Where; $f_2 = 1 - f_1$

$$\cos \theta^* = f_1 \cos \theta_1 + (1 - f_1)\cos \theta_2 \tag{6.8}$$

On applying this equation to air/solid composite interface, the equation becomes (Eq. 6.9).

$$\cos \theta^* = f_1(\cos \theta_1 + 1) - 1 \tag{6.9}$$

where apparent contact angle (θ^*) observed on a rough surface and the equilibrium contact angle (θ_1) obtained on a smooth surface without roughness. The f_1 is surface fraction of solid in contact with the droplet. The Cassie–Baxter model given in Eq. (6.9) can be used to estimate the area fraction of a water droplet (f_1) in contact with a surface (i.e., wetted solid fraction). The superhydrophobicity of a surface is due to roughness, when the roughness of the surface increases, the value of f_1 decreases. The air pockets can lead to the surface being superhydrophobic. As the droplet of liquid does not penetrate between the cavities of roughness, therefore, water beads up into a spherical shape and rolls off the surface.

Work of adhesion

The work of adhesion is the amount of work that is done when two adherent surfaces are parted and removed to a large distance from each other. The work of adhesion (W_{ad}) may be either positive or negative depending on the bonding of the two surfaces; if positive the two surfaces will bond or the higher the value of (W_{ad}) the stronger the bond. Conversely, if it is negative, no bonding will occur. Furthermore, the movement of liquid droplets on hydrophobic surfaces can be described by calculation of work of adhesion (W_{ad}) according to the Young–Duprè equation (Aminayi and Abidi 2013) (see Eq. 6.10).

$$W_{ad} = \gamma_L (1 + \cos \theta) \tag{6.10}$$

where γ_L is the surface tension of the liquid drops (i.e.72.8 mN/m).

6.5   Approaches to Develop Self-Cleaning Textiles

Self-cleaning can be produced in different ways; plasma etching, lithography, sol–gel process, micro-phase separation, templating, spray coating, switchable electrospinning, electrochemical deposition, nanoparticles assembly, and nano-fabrication. These approaches are based on top-down or bottom-up methodologies and the combination of them (Cohen et al. 2016; Pakdel et al. 2020; Roach et al. 2008; Zhao et al. 2010). In the last decade, studies have focused on a variety of methodologies to produce self-cleaning textiles on different solid substrates. The primary approach for creating self-cleaning textiles is based on patterning roughness on the solid surface,

followed by a thin layer of hydrophobic coating material. The hydrophobic chemistry is based on fluoropolymers or siloxanes that possess low surface energy. To obtain superhydrophobicity, low surface energy incorporation with the surface roughness is also necessary (Khan et al. 2018a, b, 2021a, b, c). Most solid material, such as elastic polymers, fiber-based materials (textiles), metals, metal oxides, and ceramics, has the ability to be superhydrophobic provided that roughness can be formed on its surface. Surface etching techniques such as chemical, laser, and plasma have the potential to generate the roughness on a solid substrate to form the required super-hydrophobicity. Many other techniques are commonly used for the development of self-cleaning textiles including photolithography, sol–gel method, Chemical bath deposition, electro-spinning, employing templates, polymer solutions evaporation, and spray techniques (Bae et al. 2009; Bu et al. 2019; Liravi et al. 2020; Wang and Wang 2019; Wei et al. 2020).

6.5.1 Top-Down Approach

The top-down approach to obtain the fundamental features and make them functional is reviewed. In the top-down approach, material size is reduced to nanometer range. Top-down reduces large pieces of materials to the nanoscale level. In top-down approach, size distribution is wide but the Shapes of the nanoparticles are difficult to control. It also contains impurities that come from milling apparatus. Top-down approaches mainly include or rely on lithographic patterning and etching materials to shape nanostructures. The process has evolved from lithographic techniques, requiring larger amounts of materials which can lead to waste from the discarding of excess material (Halim 2009). Another difference from the bottom-up approach is that in the top-down approach, the parts or chips are both patterned and built in place so that no assembly step is needed. It is a very useful process for the evolution of the electronics, computer, photonic, and microsystem industries (Yu et al. 2012). In practice, top-down approaches can be used to fabricate well-defined nanostructures. Combined bottom-up and top-down approaches will soon be the standard practice (Patra and Gouda 2013).

Nanolithography

Nanolithography is most widely used for the devolvement of nanostructures and patterns. Nanolithography name is derived from greek words which mean, small writing on rocks. Nanolithography technique involves writing, depositing, and etching on surfaces with nanometer dimensions (Madou 2018). This technique can be demonstrated by using light (optical- or photolithography), electrons (electrons beam lithography), ions (ion beam lithography), or X-ray (X-ray lithography). Lithography is useful for generating self-cleaning textiles where the shape of the features and the pattern are well-defined. For this reason, it has mostly been employed to generate surfaces allowing theories of superhydrophobicity to be tested, although more recently direct applications have been suggested. Lithographic processes are

often used to produce master surfaces, for instance in photoresist, which are then used as templates for the casting of the desired surface features in another material (Roach et al. 2008).

Surface etching

Etching is another simple and efficient method to produce self-cleaning coatings with rough surfaces. Different etching techniques, such as chemical, plasma, and laser etching have been recently used (Dong et al. 2011). Plasma etching may be the most effective and simple technique to achieve a rough surface. Currently, self-cleaning textile fabrication includes several different kinds of etching techniques such as laser, plasma or chemical etching (Teisala et al. 2014). The surface roughness is obtained by plasma etching having different etching rates depending on the crystal planes in the materials. Superhydrophobicity can be obtained, either after applying the hydrophobic coating or directly following etching (Saleh and Baig 2019).

Milling and grinding

Milling is used to convert the bigger particles into smaller ones. The milled particles are used to develop self-cleaning textiles (Kha et al. 2018a, b). During mechanical grinding and milling large quantities of fine and nanocrystalline powders can be produced. Both dry and wet milling require high energy. This process is easy for making nanoparticles but this process need more time for proper milling. Impurities produced during milling are a big disadvantage of this process. Sometimes all particles are not milled properly (Tsuzuki 2009).

6.5.2   Bottom-Up Approach

Bottom-up approaches are most commonly used for the fabrication of self-cleaning textiles. Bottom-up approaches are those techniques or methods involving growing or assembling of nanomaterials from the atomic level, for example, vapor–liquid-solid (VLS) growth, vapor–solid (VS) growth, electrochemical growth, etc. (Yu et al. 2012). In the bottom-up approach, required shape, size, and size distribution can be easily controlled. The synthesis of nanoparticles by the bottom-up method can be done by two techniques which are the thermodynamic equilibrium approach and kinetic approach. Bottom-up approach is used to develop products by building them up from atomic and molecular-scale components. The process involves manipulation or synthetic methods of biochemistry in directly assembling sub-nanoscale building blocks, such as atomic molecular and supramolecular elements into required nanoscale patterns. It is a very time-consuming process and is therefore better for biomedical, chemical, and physical sensors than large scale molecular electronics and computer parts. The fabrication strategy must occur in parallel or in arrays to self-form groups of atoms fast enough to produce useful structures of macroscopic size. Further research is being done to create self-assembling structures that will put themselves together and reduce the waste of top-down approaches (Patra and Gouda

2013). Bottom-up approach is mostly used instead of top-down approach because it's easy to start with atoms and molecules by arranging and reassembling to build large nanostructures. Diverse type of nanomaterials can be created by bottom-up approach (Daraio and Jin 2012). Many methods and techniques are used in bottom-up approach. Some techniques are described below.

Physical vapor deposition (PVD)

Physical Vapor Deposition (PVD) is a process of transferring growth species from a source or target and depositing them on a substrate to form a film. The process proceeds atomistically and mostly involves no chemical reactions. The thickness of the deposits can vary from angstroms to millimeters. A large numbers of inorganic materials, metals, and some organic materials can be deposited by using Physical Vapor Deposition. The growth species are removed from the source by thermal means. Evaporation and sputtering techniques are most commonly used for the physical vapor deposition (Mubarak et al. 2005).

Chemical vapor deposition (CVD)

Chemical vapor deposition (CVD) is a process in which chemicals react to produce very pure, fine, and high performance films. Chemical vapor deposition involves the flowing of a precursor gas or gasses into a chamber containing one or more heated objects to be coated. A chemical reaction can take place on or near the heated surfaces that results in the deposition of a thin film on the surface. CVD can be done with a variety of chemicals for a wide range of applications. Chemical vapor deposition technique depend upon the type of precursors and substrate used (Li Puma et al. 2008). The process can be enhanced with plasmas and ions to increase deposition rates or lower temperatures. Types of chemical vapor deposition include metal organic chemical vapor deposition, plasma-enhanced chemical vapor deposition, and laser chemical vapor deposition (Daraio and Jin 2012). The CVD approach is regarded as a simple and effective method to deposit self-cleaning coatings onto substrates (Kannan et al. 2009; Pour et al. 2019).

Sol–gel process

In recent years, sol–gel process has been widely used in research on self-cleaning textiles due to its unique advantages such as low temperature processing, functionalization of fiber surfaces, and high homogeneity of final products (Liu et al. 2011). The sol–gel method is based on the hydrolysis of liquid precursors and the formation of colloidal sols that can be easily applied on textile substrates. After drying the wet gel a porous xerogels (dry gel) is formed. Sol is a stable suspension of colloidal solid particles or polymers in a liquid while; gel is a porous, three-dimensional, continuous solid network surrounding a continuous liquid phase (Daraio and Jin 2012). The sol–gel process using organosilane precursors with hydrophobic moieties has been also widely employed (Fouhaili et al. 2019). Sol–gel processing is a wet chemical route for the synthesis of colloidal dispersions of inorganic and organic–inorganic hybrid

materials, particularly oxides and oxide-based hybrids. Sol–gel processing is particularly useful in making complex metal oxides, temperature-sensitive organic and inorganic hybrid materials. Sol–gel processing provides many advantages which include low processing temperature and molecular level homogeneity. Sol–gel processing precursors include metal alkoxides or inorganic and organic salts (Pokropivny et al. 2007).

Aqueous and organic solvents can be used to dissolve precursors. Catalysts are added to enhance hydrolysis and condensation reactions. In sol–gel process a sol is formed by hydrolysis and polymerization reaction of the precursors. Condensation and hydrolysis are multi-step processes. Nanoscale clusters of metal oxides or hydroxides are formed as a result of condensation (Chen and Mao 2007). The size, morphology, and microstructure of the final product can be controlled by hydrolysis and condensation reactions. Successive thermal treatments give dense ceramics, both crystalline and amorphous. The sol–gel method is very versatile, allowing to easily obtain not only bulk samples and nanoparticles but also films and fibers (Branda 2011).

Hydrothermal method

The hydrothermal method is a well-known method for the fabrication of nano/microscale materials and the creation of nano roughness. There has been considerable research on the growth of metal oxide materials with different structures on substrates to fabricate self-cleaning textiles. The hydrothermal technique may be applied to a variety of substrates, such as fibers, textiles, silicon wafers, glasses, metals, and even polymer surfaces, regardless of their irregular shapes or curved surfaces (Xue et al. 2010).

Hydrothermal synthesis is a process in which the raw material and water as solvent react under a controlled temperature and pressure in a closed system. For crystal growth hydrothermal synthesis requires a reaction and pressure vessel which is called an autoclave. The temperature is elevated above the boiling point of water. The internal pressure of the autoclave depends upon temperature and amount of solution added to the autoclave (Chen and Mao 2007). Hydrothermal method is one of the most popular and promising nanomaterials synthesis methods because particle size, morphology, and crystallinity of materials can be controlled as compared to any other techniques (Montazeri-Pour 2012). Hydrothermal synthesis offers many advantages over conventional and non-conventional synthesis methods. Some advantages of hydrothermal synthesis include, hydrothermal method is environmentally friendly because it takes place at low temperatures as compared to other methods. The uniformity and rate of growth and nucleation can be easily controlled. Many types of nanostructures can be prepared by using this method. Different materials can be used such as polymers, metals, and ceramics. Hydrothermal is a low-cost process because energy, instrumentation, and precursors have low cost. Hydrothermal processes can be used in combination with electrochemical, mechanical, microwave techniques. In a previous study, one-dimensional (1D) semiconducting ZnO nanorods were grown on a self-cleaning polyethylene terephthalate (PET) fabric using a hydrothermal method (Jeong et al. 2020). Many researchers used hydrothermal

technique for synthesis of different nanomaterials (Boulos et al. 2005; Cui et al. 2012; Ganesan and Natarajan 2005; Jia et al. 2013; Li et al. 2013; Nagaraju et al. 2013; Panasyuk et al. 2005; Suzuki and Yoshikawa 2011; Thirumurugan and Natarajan 2005; Wang et al. 2011).

6.6 Functional Applications of Self-Cleaning Textiles

The self-cleaning textiles have numerous interesting properties and functional applications, and the range of application of self-cleaning textiles is deemed very large.

6.6.1 Self-Cleaning

The ability of a fabric to provide a clean and neat surface is called self-cleaning property. Recently, numerous efforts have been made to simultaneously create superhydrophobic and photocatalytic surfaces that not only repel water but also decompose organic contaminates at the same time. However, the fabrication of self-cleaning textiles is challenging because this surface either loses its superhydrophobicity upon irradiation with light or does not show a photocatalytic property (Xu et al. 2015). It was observed that the sliding angles decrease with increasing contact angle depending on the surface roughness. The superhydrophobic approach of physical self-cleaning surfaces exhibits high water contact angle (WCA > 150°), low contact angle hysteresis and low roll-off angle. During superhydrophilic approach (WCA < 5°) where water droplets are spread, producing a film on the surface transport on the top dirt particles (Banerjee et al. 2015; Nishimoto and Bhushan 2013). One of the most efficient materials for chemical self-cleaning (photochemical oxidation/ reduction) is TiO_2 nanoparticles of different shapes and sizes. TiO_2 is a versatile photocatalyst that degrades a wide range of organic pollutants, bacteria, cancer cells, and viruses and has applications in air and water remediation, and self-sterilizing surfaces as well (Khan et al. 2021a, b, c).

6.6.2 UV-Protection

The main function of garments made for UV protection is to provide protection against the harmful ultraviolet radiations of the sun and provide wearer protection against weather conditions. UV radiation cause skin cancer and many other skin diseases. In agriculture and horticulture, UV protective textiles have much importance because they are exposed to sun and weather for long period of time. The UV protection property of a textile fabric can be achieved by dye, pigment, delustrant

(TiO$_2$) or UV absorber finish. These materials can provide protection against UV radiation by absorbing and blocking its penetration through a fabric. To achieve UV protection several nanomaterials or nanoparticles can be applied to textile fabric ("http://www.indiantextilejournal.com/articles/FAdetails.asp?id=693tle," n.d.).

Titanium dioxide and zinc oxide nanoparticles are mostly used for this purpose because they have good UV protection properties. They give protection by reflecting, scattering or absorbing harmful UV radiations of the sun. They are more stable when compared to organic UV-blocking agents. Nanoparticles of ZnO can be prepared by the wet chemical method (Khan et al. 2020a, b). Titanium dioxide nanoparticles can be imparted on textile fabric by treating in TiO$_2$ nanoparticles aqueous solution using a pad-drying-cure method (Haydon n.d.). Organic UV absorbers are mainly derivatives of O-hydroxy benzophenones, O-hydroxy phenyl triazines, O-hydroxy phenyl hydrazine's and they are less stable than inorganic UV absorbers (Saravanan 2007).

6.6.3 Anti-microbial

The humidity, sweat, and moisture provide suitable environment for the growth of many types of microbes (pathogenic or non-pathogenic) on the textile's inner or outerwear. These microbes can cause diseases, bad odor for the wearer and reduce the strength and color properties of the fabric. To avoid all these microbes, we need anti-microbial finish on the fabric. Many antibacterial finishes and disinfection techniques have been developed for all types of textiles. For anti-microbial finishing, many materials are used including nano-sized silver, titanium dioxide, and zinc oxide particles. Metallic ions and metallic compounds also show some degree of sterilizing effect. It is considered that oxygen in the air or water is turned into active oxygen by means of catalysis with the metallic ion so dissolving the organic substance to create a sterilizing effect. Anti-bacterial effects can be maximized on textile fabric by using nanoparticles because nanoparticles increase the surface area (Branch and Republic 2007; Wong et al. 2006).

6.6.4 Anti-static

An antistatic agent is a compound used for the treatment of materials or their surfaces in order to reduce or eliminate the buildup of static electricity generally caused by the triboelectric effect. Static charge mostly builds up in synthetic fibers such as nylon and polyester because they absorb little water (Siegfried 2007). Anti-static properties of synthetic fibers are very poor. The use of nanotechnology has increased in textiles to impart anti-static properties in synthetic fibers or textile fabrics. It is well determined that nanoparticles like zinc oxide, titanium dioxide, antimony-doped tin oxide (ATO), and silane nano solution could impart anti-static properties to synthetic

fibers. These material helps to dissipate the static charge which builds up on the fabric (Patra and Gouda 2013).

6.6.5 Moisture Management

Moisture management is the ability of a fabric to transport moisture away from the skin to the outer surface of the fabric. Textiles with good wicking and moisture transportation properties can provide comfort to the wearer in hot and humid conditions and keep the wearer and fabric dry and cool. Moisture management properties can be achieved by suitable hydrophilic fibers or hydrophilic finishing (Khan et al. 2018a, b). Successful results have been obtained by coating textiles with a hydrophilic coating of titanium dioxide nanoparticles which provide the desired surface functionality. Nanocoatings of titanium dioxide are applied to textiles that are changed from hydrophobic to hydrophilic by light, moving moisture from the dark side to the bright side.

6.7 Conclusion

This chapter provided an overview of the state of the art regarding the developments and applications of self-cleaning textiles. As an inspiration from nature such as lotus leaves, butterfly wings, and water strider legs, the scientists have fabricated self-cleaning fibrous structures by creating surface roughness in combination with low surface energy materials such as organic silanes, fluorinated silanes, alkyl amines, and silicates. For physical self-cleaning textiles, the surface roughness and low surface energy of materials are the two important factors to control the wettability of a surface and to obtain water contact angles greater than 150°. For chemical self-cleaning, polycrystalline semiconductor oxides have been applied in the form of nano-coatings, leading to the successful development of a number of UV-active self-cleaning textiles. The self-cleaning textiles have many applications such as hydrophobicity, self-cleaning, superhydrophobicity, anti-corrosion, antimicrobial, UV protection, water purification, photocatalytic, thermal, oil/water separation, and anti-bio adhesion applications. Future works on self-cleaning textiles should focus on the improvement of the durability and stability of the self-cleaning textiles. More investigations are needed in future on precisely controlling surface roughness and structure in both small and large scales. Moreover, in future the self-healing properties must be incorporated into self-cleaning textiles.

References

Afzal S, Daoud WA, Langford SJ (2014) Superhydrophobic and photocatalytic self-cleaning cotton. J. Mater. Chem. A 2(42):18005–18011. https://doi.org/10.1039/C4TA02764G

Aminayi P, Abidi N (2013) Imparting super hydro/oleophobic properties to cotton fabric by means of molecular and nanoparticles vapor deposition methods. Appl Surf Sci 287:223–231. https://doi.org/10.1016/j.apsusc.2013.09.132

Ashraf M, Campagne C, Perwuelz A, Champagne P, Leriche A, Courtois C (2013) Development of superhydrophilic and superhydrophobic polyester fabric by growing Zinc Oxide nanorods. J Colloid Interface Sci 394(1):545–553. https://doi.org/10.1016/j.jcis.2012.11.020

Bae GY, Min BG, Jeong YG, Lee SC, Jang JH, Koo GH (2009) Superhydrophobicity of cotton fabrics treated with silica nanoparticles and water-repellent agent. J Colloid Interface Sci 337(1):170–175. https://doi.org/10.1016/j.jcis.2009.04.066

Banerjee S, Dionysiou DD, Pillai SC (2015) Self-cleaning applications of TiO2 by photo-induced hydrophilicity and photocatalysis. Appl Catal B 176–177:396–428. https://doi.org/10.1016/j.apcatb.2015.03.058

Banerjee S, Pillai SC, Falaras P, O'shea KE, Byrne JA, Dionysiou DD (2014) New insights into the mechanism of visible light photocatalysis. J Phys Chem Lett 5(15):2543–2554. https://doi.org/10.1021/jz501030x

Barthlott W, Neinhuis C (1997) Purity of the sacred lotus, or escape from contamination in biological surfaces. Planta 202(1):1–8

Bayer IS (2017) On the durability and wear resistance of transparent superhydrophobic coatings. Coatings 7(1). https://doi.org/10.3390/coatings7010012

Becheri A, Durr M, Lo Nostro P, Baglioni P (2008) Synthesis and characterization of zinc oxide nanoparticles: application to textiles as UV-absorbers. J Nanopart Res 10(4):679–689. https://doi.org/10.1007/s11051-007-9318-3

Bhushan B (2009) Biomimetics: lessons from nature—an overview. Philos Trans A 367(1893):1445–1486. https://doi.org/10.1098/rsta.2009.0011

Bhushan B, Jung YC (2011) Natural and biomimetic artificial surfaces for superhydrophobicity, self-cleaning, low adhesion, and drag reduction. Prog Mater Sci 56(1):1–108. https://doi.org/10.1016/j.pmatsci.2010.04.003

Boscher ND, Vaché V, Carminati P, Grysan P, Choquet P (2014) A simple and scalable approach towards the preparation of superhydrophobic surfaces-importance of the surface roughness skewness. J Mater Chem A 2(16):5744–5750. https://doi.org/10.1039/c4ta00366g

Boulos M, Guillemet-fritsch S, Mathieu F, Lebey T, Bley V (2005) Hydrothermal synthesis of nanosized BaTiO3 powders and dielectric properties of corresponding ceramics. Solid State Ionics 176(13–14)

Branch A, Republic C (2007) Antibacterial agents in textile industry.

Branda F (2011) The sol-gel route to nanocomposites. In: Advances in nanocomposites—synthesis, characterization and industrial applications. InTech, p 966

Bu Y, Zhang S, Cai Y, Yang Y, Ma S (2019) Fabrication of durable antibacterial and superhydrophobic textiles via in situ synthesis of silver nanoparticle on tannic acid-coated viscose textiles. Cellulose 26(3):2109–2122. https://doi.org/10.1007/s10570-018-2183-7

Carneiro JT, Savenije TJ, Moulijn JA, Mul G (2011) How phase composition influences optoelectronic and photocatalytic properties of TiO2. J Phys Chem C 115(5):2211–2217. https://doi.org/10.1021/jp110190a

Celia E, Darmanin T, De Givenchy ET, Amigoni S, Guittard F (2013) Journal of colloid and interface science recent advances in designing superhydrophobic surfaces. J Colloid Interface Sci 402:1–18. https://doi.org/10.1016/j.jcis.2013.03.041

Chen X, Mao SS (2007) Titanium dioxide nanomaterials: synthesis, properties, modifications, and applications. Chem Rev 107(7):2891–2959. https://doi.org/10.1021/cr0500535

Chen X, Wu Z, Liu D, Gao Z (2017) Preparation of ZnO photocatalyst for the efficient and rapid photocatalytic degradation of Azo dyes. Nanoscale Res Lett 12(1):4–13. https://doi.org/10.1186/s11671-017-1904-4

Cohen N, Dotan A, Dodiuk H, Kenig S (2016) Superhydrophobic coatings and their durability superhydrophobic coatings and their durability. Mater Manuf Process 31(9):1143–1155. https://doi.org/10.1080/10426914.2015.1090600

Cui L, Hui KN, Hui KS, Lee SK, Zhou W, Wan ZP, Thuc C-NH (2012) Facile microwave-assisted hydrothermal synthesis of TiO2 nanotubes. Mater Lett 75:175–178. https://doi.org/10.1016/j.matlet.2012.02.004

Daraio C, Jin S (2012) Synthesis and patterning methods for nanostructures useful for biological applications. In Silva GA, Parpura V (eds) Nanotechnology for biology and medicine. Springer, New York, pp 27–45. https://doi.org/10.1007/978-0-387-31296-5

Darmanin T, Guittard F (2015) Superhydrophobic and superoleophobic properties in nature. Mater Today 18(5):273–285. https://doi.org/10.1016/j.mattod.2015.01.001

Dastjerdi R, Montazer M (2010) A review on the application of inorganic nano-structured materials in the modification of textiles: focus on anti-microbial properties. Colloids Surf B Biointerfaces 79(1):5–18. https://doi.org/10.1016/j.colsurfb.2010.03.029

Dong C, Gu Y, Zhong M, Li L, Sezer K, Ma M, Liu W (2011) Fabrication of superhydrophobic Cu surfaces with tunable regular micro and random nano-scale structures by hybrid laser texture and chemical etching. J Mater Process Technol 211:1234–1240. https://doi.org/10.1016/j.jmatprotec.2011.02.007

Du Z, Cheng C, Tan L, Lan J, Jiang S, Zhao L, Guo R (2018) Enhanced photocatalytic activity of Bi2WO6/TiO2composite coated polyester fabric under visible light irradiation. Appl Surf Sci 435:626–634. https://doi.org/10.1016/j.apsusc.2017.11.136

Eder M, Amini S, Fratzl P (2018) Biological composites—complex structures for functional diversity. Science 362(6414):543–547

Fouhaili BE, Ibrahim A, Dietlin C, Chemtob A, Allonas X (2019) Single-step formation of super-hydrophobic surfaces using photobase- catalyzed sol-gel process. Prog Org Coat 137:105293. https://doi.org/10.1016/j.porgcoat.2019.105293

Fu W, Li G, Wang Y, Zeng S, Yan Z, Wang J, Xin S, Zhang L, Wu S, Zhang Z (2017) Facile formation of mesoporous structured mixed-phase (anatase/rutile) TiO2 with enhanced visible light photocatalytic activity. Chem Commun 54(1):58–61. https://doi.org/10.1039/c7cc05750d

Fujishima A, Rao TN, Tryk DA (2000) Titanium dioxide photocatalysis. J Photochem Photobiol C Photochem Rev 1(1):1–21. https://doi.org/10.1016/S1389-5567(00)00002-2

Ganesan SV, Natarajan S (2005) Hydrothermal synthesis and structure of [(C4N2H12)3][P2Mo5O23] · H2O. J Chem Sci 117(3):219–226

Ge S, Wang B, Li D, Fa W, Yang Z, Yang Z, Jia G, Zheng Z (2014) Surface controlled photocatalytic degradation of RhB over flower-like rutile TiO2 superstructures. Appl Surf Sci 295:123–129. https://doi.org/10.1016/j.apsusc.2014.01.015

Gupta D, Gulrajani ML (2015) Self cleaning finishes for textiles. In: Functional finishes for textiles: improving comfort, performance and protection. Woodhead Publishing Limited. https://doi.org/10.1533/9780857098450.1.257

Gustafsson E, Larsson PA, Wågberg L (2012) Treatment of cellulose fibres with polyelectrolytes and wax colloids to create tailored highly hydrophobic fibrous networks. Colloids Surf A Physiochem Eng Aspects 414:415–421. https://doi.org/10.1016/j.colsurfa.2012.08.042

Halim N (2009) Nanotechnology's big impact. Chemmatters

Hasanpoor M, Aliofkhazraei M, Delavari H (2015) Microwave assisted synthesis of Zinc oxide nanoparticles. Procedia Mater Sci 8(11):320–325. https://doi.org/10.1016/j.mspro.2015.11.101

Haydon B (n.d.) Nanomaterials and their applications in textiles—domestic standardization for Canadian manufacturers and importers and international standardization developments, pp 1–36

Haydon B (2012) Nanomaterials and their applications in textiles—domestic standardization for Canadian manufacturers and importers and international standardization developments.

Hsieh C-T, Wu F, Yang S (2008a) Superhydrophobicity from composite nano / microstructures: carbon fabrics coated with silica nanoparticles. Surf Coat Technol 202(24):6103–6108. https://doi.org/10.1016/j.surfcoat.2008.07.006

Hsieh C-T, Wu FL, Yang SY (2008b) Superhydrophobicity from composite nano/microstructures: carbon fabrics coated with silica nanoparticles. Surf Coat Technol 202(24):6103–6108. https://doi.org/10.1016/j.surfcoat.2008.07.006

http://www.indiantextilejournal.com/articles/FAdetails.asp?id=693tle. (n.d.)

Huhtamäki T, Tian X, Korhonen JT, Ras RHA (2018) Surface-wetting characterization using contact-angle measurements. Nat Protoc 13(7):1521–1538. https://doi.org/10.1038/s41596-018-0003-z

Jeevahan J, Chandrasekaran M, Britto Joseph G, Durairaj RB, Mageshwaran G (2018) Superhydrophobic surfaces: a review on fundamentals, applications, and challenges. J Coat Technol Res 15(2):231–250. https://doi.org/10.1007/s11998-017-0011-x

Jeong S, Bolortuya S, Eadi SB, Kim S (2020) Fabrication of superhydrophobic surfaces based on PDMS coated hydrothermal grown ZnO on PET fabrics. J Adhes Sci Technol 34(1):102–113. https://doi.org/10.1080/01694243.2019.1661609

Jia X-H, Song H-J, Min C-Y (2013) Hydrothermal synthesis of flower-like TiO2 nanocrystals/graphene oxide nanocomposites. Appl Phys A 111(4):1021–1024. https://doi.org/10.1007/s00339-013-7674-7

Joshi M, Bhattacharyya A (2011) Nanotechnology—a new route to high-performance functional textiles. Text Prog 43(3):155–233. https://doi.org/10.1080/00405167.2011.570027

Kajbafvala A, Ghorbani H, Paravar A, Samberg JP, Kajbafvala E, Sadrnezhaad SK (2012) Effects of morphology on photocatalytic performance of Zinc oxide nanostructures synthesized by rapid microwave irradiation methods. Superlattices Microstruct 51(4):512–522. https://doi.org/10.1016/j.spmi.2012.01.015

Kannan AM, Kanagala P, Veedu V (2009) Development of carbon nanotubes based gas diffusion layers by in situ chemical vapor deposition process for proton exchange membrane fuel cells. J Power Sources 192:297–303. https://doi.org/10.1016/j.jpowsour.2009.03.022

Khan MZ, Ashraf M, Hussain T, Rehman A, Malik MM, Raza ZA, Nawab Y, Zia Q (2015) In situ deposition of TiO 2 nanoparticles on polyester fabric and study of its functional properties. Fibers Polym 16(5):1092–1097. https://doi.org/10.1007/s12221-015-1092-8

Khan MZ, Baheti V, Militky J, Ali A, Vikova M (2018a) Superhydrophobicity, UV protection and oil/water separation properties of fly ash/Trimethoxy(octadecyl)silane coated cotton fabrics. Carbohyd Polym 202:571–580. https://doi.org/10.1016/j.carbpol.2018.08.145

Khan MZ, Baheti V, Militky J, Wiener J, Ali A (2020a) Self-cleaning properties of polyester fabrics coated with flower-like TiO2 particles and trimethoxy (octadecyl)silane. J Ind Text 50(4):543–565. https://doi.org/10.1177/1528083719836938

Khan MZ, Hussain S, Siddique HF, Baheti V, Militky J, Azeem M, Ali A (2018b) Improvement of liquid moisture management in plaited knitted fabrics. TEKSTİL Ve KONFEKSİYON 28(3):182–188

Khan MZ, Militky J, Baheti V, Fijalkowski M, Wiener A, Volesky L, Adach K (2020b) Growth of ZnO nanorods on cotton fabrics via microwave hydrothermal method: effect of size and shape of nanorods on superhydrophobic and UV-blocking properties. Cellulose 27:10519–10539. https://doi.org/10.1007/s10570-020-03495-x

Khan MZ, Militky J, Baheti V, Wiener J, Vik M (2021a) Development of durable superhydrophobic and UV protective cotton fabric via TiO 2/trimethoxy (octadecyl) silane nanocomposite coating. J Text Inst 112(10):1639–1650. https://doi.org/10.1080/00405000.2020.1834235

Khan MZ, Militky J, Petru M, Ali A, Wang Y, Kremenakova D (2021b) Hydrothermal growth of TiO2 nanoflowers on PET fabrics for functional applications. J Fiber Bioeng Inf 14(4):199–210. https://doi.org/10.3993/jfbim00381

Khan MZ, Militky J, Petru M, Tomkov B, Ali A, Javed A, Azeem M, Kremenakova D (2021c) Ultra-fast growth of ZnO nanorods on cotton fabrics and their self-cleaning and physiological comfort properties. Coatings 11:1309. https://doi.org/10.3390/coatings11111309

Khan MZ, Militky J, Petru M, Tomkova B, Ali A, Toren E, Perveen S (2022) Recent advances in superhydrophobic surfaces for practical applications: a review. Eur Polymer J 178:111481. https://doi.org/10.1016/j.eurpolymj.2022.111481

Khan MZ, Taghavian H, Fijalkowski M, Militky J, Tomkova B, Venkataraman M, Adach K (2023) Effect of microwave power on bactericidal and UV protection properties of the ZnO nanorods grown cotton fabrics. Colloids Surf A 664:131135. https://doi.org/10.1016/j.colsurfa.2023.131135

Koch K, Bhushan B, Barthlott W (2008) Diversity of structure, morphology and wetting of plant surfaces. Soft Matter 4(10):1943–1963. https://doi.org/10.1039/b804854a

Koch K, Bhushan B, Barthlott W (2009) Progress in materials science multifunctional surface structures of plants: an inspiration for biomimetics. Prog Mater Sci 54(2):137–178. https://doi.org/10.1016/j.pmatsci.2008.07.003

Latthe SS, Rao AV (2012) Superhydrophobic SiO 2 micro-particle coatings by spray method. Surf Coat Technol 207:489–492. https://doi.org/10.1016/j.surfcoat.2012.07.055

Latthe SS, Terashima C, Nakata K, Fujishima A (2014) Superhydrophobic surfaces developed by mimicking hierarchical surface morphology of lotus leaf. Molecules 19(4):4256–4283. https://doi.org/10.3390/molecules19044256

Lee HY, Park HK, Lee YM, Kim K, Park SB (2007) A practical procedure for producing silver nanocoated fabric and its antibacterial evaluation for biomedical applications. Chem Commun 28:2959–2961. https://doi.org/10.1039/b703034g

Li M, Jiang Y, Ding R, Song D, Yu H, Chen Z (2013) Hydrothermal synthesis of anatase TiO2 nanoflowers on a nanobelt framework for photocatalytic applications. J Electron Mater 42(6):1290–1296. https://doi.org/10.1007/s11664-013-2593-0

Li S, Huang J, Ge M, Cao C, Deng S, Zhang S, Al-Deyab SS, Lai Y (2015) Robust flower-like TiO2@cotton fabrics with special wettability for effective self-cleaning and versatile oil/water separation. Adv Mater Interfaces 2(14):1500220. https://doi.org/10.1002/admi.201500220

Li X-M, Reinhoudt D, Crego-Calama M (2007) What do we need for a superhydrophobic surface? A review on the recent progress in the preparation of superhydrophobic surfaces. Chem Soc Rev 36(8):1350–1368

Li Y, Liu J, Jia Z (2006) Morphological control and photodegradation behavior of rutile TiO2prepared by a low-temperature process. Mater Lett 60(13–14):1753–1757. https://doi.org/10.1016/j.matlet.2005.12.012

Li Puma G, Bono A, Krishnaiah D, Collin JG (2008) Preparation of titanium dioxide photocatalyst loaded onto activated carbon support using chemical vapor deposition: a review paper. J Hazard Mater 157(2–3):209–219. https://doi.org/10.1016/j.jhazmat.2008.01.040

Liravi M, Pakzad H, Moosavi A, Nouri-borujerdi A (2020) A comprehensive review on recent advances in superhydrophobic surfaces and their applications for drag reduction. Prog Org Coat 140:105537. https://doi.org/10.1016/j.porgcoat.2019.105537

Liu H, Gao SW, Cai JS, He CL, Mao JJ, Zhu TX, Chen Z, Huang JY, Meng K, Zhang KQ, Al-Deyab SS, Lai YK (2016) Recent progress in fabrication and applications of superhydrophobic coating on cellulose-based substrates. Materials 9(3):124. https://doi.org/10.3390/ma9030124

Liu J, Huang W, Xing Y, Li R, Dai J (2011) Preparation of durable superhydrophobic surface by sol–gel method with water glass and citric acid. J Sol-Gel Sci Technol 58:18–23. https://doi.org/10.1007/s10971-010-2349-8

Lu Y, Sathasivam S, Song J, Crick CR, Carmalt CJ, Parkin IP (2015) Robust self-cleaning surfaces that function when exposed to either air or oil. Science 347(6226):1132–1135. https://doi.org/10.1126/science.aaa0946

Madou MJ (2018) Fundamentals of microfabrication: the science of miniaturization, 3rd edn. CRC Press, p 1992

Mao Z, Shi Q, Zhang L, Cao H (2009) The formation and UV-blocking property of needle-shaped ZnO nanorod on cotton fabric. Thin Solid Films 517(8):2681–2686. https://doi.org/10.1016/j.tsf.2008.12.007

Mills A, Le Hunte S (1997) An overview of semiconductor photocatalysis. J Photochem Photobiol A Chem 108(1):1–35. https://doi.org/10.1016/S1010-6030(97)00118-4

Mohamed AMA, Abdullah AM, Younan NA (2015) Corrosion behavior of superhydrophobic surfaces: a review. Arab J Chem 8(6):749–765. https://doi.org/10.1016/j.arabjc.2014.03.006

Montazeri-Pour M (2012) Synthesis of single-phase anatase TiO2 nanoparticles by hydrothermal treatment. Proc Int Conf Nanomater: Appl Prop 1(1):1–4

Mubarak A, Hamzah E, Toff MRM (2005) Review of physical vapour deposition (PVD) techniques for hard coating. J Mekanikal 20:42–51

Nagaraju G, Manjunath K, Ravishankar TN, Ravikumar BS, Nagabhushan H, Ebeling G, Dupont J (2013) Ionic liquid-assisted hydrothermal synthesis of TiO2 nanoparticles and its application in photocatalysis. J Mater Sci 48(24):8420–8426. https://doi.org/10.1007/s10853-013-7654-5

Nguyen-tri P, Nguyen H, Ouellet C, Tuduri L, Voe D-VN, Nanda S, Mishra A, Chao H-P, Bajpai AK (2019) Recent progress in the preparation, properties and applications of superhydrophobic nano-based coatings and surfaces: a review. Prog Org Coat 132:235–256. https://doi.org/10.1016/j.porgcoat.2019.03.042

Nishimoto S, Bhushan B (2013) Bioinspired self-cleaning surfaces with superhydrophobicity, superoleophobicity, and superhydrophilicity. RSC Adv 3(3):671–690. https://doi.org/10.1039/c2ra21260a

Pakdel E, Wang J, Kashi S, Sun L, Wang X (2020) Advances in photocatalytic self-cleaning, superhydrophobic and electromagnetic interference shielding textile treatments. Adv Coll Interface Sci 277:102116. https://doi.org/10.1016/j.cis.2020.102116

Panasyuk GP, Azarova LA, Voroshilov IL, Khaddaj MH, Budova GP, Izotov AD (2005) Hydrothermal synthesis of aluminum terephthalate. Inorg Mater 41(11):1201–1205. https://doi.org/10.1007/s10789-005-0287-6

Patra JK, Gouda S (2013) Application of nanotechnology in textile engineering. J Eng Technol Res 5:104–111

Perelshtein I, Applerot G, Perkas N, Wehrschetz-Sigl E, Hasmann A, Guebitz GM, Gedanken A (2009) Antibacterial properties of an in situ generated and simultaneously deposited nanocrystalline ZnO on fabrics. ACS Appl Mater Interfaces 1(2):361–366. https://doi.org/10.1021/am8000743

Pokropivny V, Hussainova I, Vlassov S (2007) Introduction to nanomaerials and nanotechnology. Tartu University Press, Tartu, p 138

Pour FZ, Karimi H, Avargani VM (2019) Preparation of a superhydrophobic and superoleophilic polyester textile by chemical vapor deposition of dichlorodimethylsilane for water—oil separation. Polyhedron 159:54–63. https://doi.org/10.1016/j.poly.2018.11.040

Ramachandran R, Nosonovsky M (2016) Vibrations and spatial patterns change effective wetting properties of superhydrophobic and regular membranes. Biomimetics 1(1):4. https://doi.org/10.3390/biomimetics1010004

Roach P, Shirtcliffe N, Roach P, Shirtcliffe NJ, Newton MI, Roach P (2008) Progess in superhydrophobic surface development progess in superhydrophobic surface development. Sof Mattter 4:224–240. https://doi.org/10.1039/B712575P

Saleh TA, Baig N (2019) Efficient chemical etching procedure for the generation of superhydrophobic surfaces for separation of oil from water. Prog Org Coat 133:27–32. https://doi.org/10.1016/j.porgcoat.2019.03.049

Saravanan D (2007) UV protection textile materials. AUTEX Res J 7(1):11–18

Selvam S, Rajiv Gandhi R, Suresh J, Gowri S, Ravikumar S, Sundrarajan M (2012) Antibacterial effect of novel synthesized sulfated??-cyclodextrin crosslinked cotton fabric and its improved

antibacterial activities with ZnO, TiO2 and Ag nanoparticles coating. Int J Pharm 434(1–2):366–374. https://doi.org/10.1016/j.ijpharm.2012.04.069

Shirgholami MA, Shateri Khalil-Abad M, Khajavi R, Yazdanshenas ME (2011) Fabrication of superhydrophobic polymethylsilsesquioxane nanostructures on cotton textiles by a solution-immersion process. J Colloid Interface Sci 359(2):530–535. https://doi.org/10.1016/j.jcis.2011.04.031

Siegfried B (2007) NanoTextiles Functions , nanoparticles and commercial applications, December 2007

Sobczyk-Guzenda A, Szymanowski H, Jakubowski W, Błasińska A, Kowalski J, Gazicki-Lipman M (2013) Morphology, photocleaning and water wetting properties of cotton fabrics, modified with titanium dioxide coatings synthesized with plasma enhanced chemical vapor deposition technique. Surf Coat Technol 217:51–57. https://doi.org/10.1016/j.surfcoat.2012.11.071

Suzuki Y, Yoshikawa S (2011) Synthesis and thermal analyses of TiO2-derived nanotubes prepared by the hydrothermal method. J Mater Res 19(04):982–985. https://doi.org/10.1557/JMR.2004.0128

Teisala H, Tuominen M, Kuusipalo J (2014) Superhydrophobic coatings on cellulose-based materials : fabrication, properties, and applications. Adv Mater Interfaces 1(1):1300026. https://doi.org/10.1002/admi.201300026

Thirumurugan A, Natarajan S (2005) Hydrothermal synthesis, structure and luminescent properties of one-dimensional lanthanide benzenedicarboxylates, possessing infinite M-O–M linkages. J Mater Chem 15(43):4588. https://doi.org/10.1039/b510146h

Tsuzuki T (2009) Commercial scale production of inorganic nanoparticles. Int J Nanotechnol 6(5–6):567–578

Valipour MN, Birjandi FC, Sargolzaei J (2014) Super-non-wettable surfaces: a review. Colloids Surf A Physicochem Eng Aspects 448(1):93–106. https://doi.org/10.1016/j.colsurfa.2014.02.016

Wang J, Wang H (2019) Integrated device based on cauliflower-like nickel hydroxide particles—coated fabrics with inverse wettability for highly efficient oil/hot alkaline water separation. J Colloid Interface Sci 534:228–238. https://doi.org/10.1016/j.jcis.2018.09.028

Wang Y, Mo Z, Zhang C, Zhang P, Guo R, Gou H, Hu R, Wei X (2015) Morphology-controllable 3D flower-like TiO2for UV shielding application. J Ind Eng Chem 32:172–177. https://doi.org/10.1016/j.jiec.2015.08.013

Wang Z, Tao F, Cai W, Yao L (2011) Hydrothermal synthesis of NaEuF 4 spindle-like nanocrystals. Bull Mater Sci 34(7):1371–1374

Webb HK, Crawford RJ, Ivanova EP (2014) Wettability of natural superhydrophobic surfaces. Adv Coll Interface Sci 210:58–64. https://doi.org/10.1016/j.cis.2014.01.020

Wei DW, Wei H, Gauthier AC, Song J, Jin Y, Xiao H (2020) Superhydrophobic modification of cellulose and cotton textiles: methodologies and applications. J Bioresour Bioprod 5(1):1–15. https://doi.org/10.1016/j.jobab.2020.03.001

Wong YWH, Yuen CWM, Leung MYS, Ku SKA, Lam HLI (2006) Selected applications of nanotechnology in textile water repellence 6(1):1–8

Wu D, Long M, Zhou J, Cai W, Zhu X, Chen C, Wu Y (2009) Synthesis and characterization of selfcleaning cotton fabrics modified by TiO2 through a facile approach. Surf Coat Technol

Xiong D, Liu G, Hong L, Duncan EJS (2011) Superamphiphobic diblock copolymer coatings. Chem Mater 23(19):4357–4366. https://doi.org/10.1021/cm201797e

Xu B, Ding J, Feng L, Ding Y, Ge F, Cai Z (2015) Self-cleaning cotton fabrics via combination of photocatalytic TiO2 and superhydrophobic SiO2. Surf Coat Technol 262:70–76. https://doi.org/10.1016/j.surfcoat.2014.12.017

Xue C-H, Jia S, Zhang J, Ma J-Z (2010) Large-area fabrication of superhydrophobic surfaces for practical applications: an overview. Sci Technol Adv Mater 11(3):033002. https://doi.org/10.1088/1468-6996/11/3/033002

Xue C-H, Jia S-T, Chen H-Z, Wang M (2008) Superhydrophobic cotton fabrics prepared by sol–gel coating of TiO 2 and surface hydrophobization. Sci Technol Adv Mater 9(3):035001. https://doi.org/10.1088/1468-6996/9/3/035001

Yadav A, Prasad V, Kathe AA, Raj S, Yadav D, Sundaramoorthy C, Vigneshwaran N (2006) Functional finishing in cotton fabrics using zinc oxide nanoparticles. Bull Mater Sci 29(6):641–645. https://doi.org/10.1007/s12034-006-0017-y

Yao CW, Sebastian D, Lian I, Günaydin-Şen Ö, Clarke R, Clayton K, Chen CY, Kharel K, Chen Y, Li, Q (2018) Corrosion resistance and durability of superhydrophobic copper surface in corrosive NaCl aqueous solution. Coatings 8(2). https://doi.org/10.3390/coatings8020070

Yao L, He J (2014) Recent progress in antireflection and self-cleaning technology—from surface engineering to functional surfaces. Prog Mater Sci 61:94–143. https://doi.org/10.1016/j.pmatsci.2013.12.003

Yu R, Lin Q, Leung S-F, Fan Z (2012) Nanomaterials and nanostructures for efficient light absorption and photovoltaics. Nano Energy 1(1):57–72. https://doi.org/10.1016/j.nanoen.2011.10.002

Yuenyongsuwan J, Nithiyakorn N, Sabkird P, O'Rear EA, Pongprayoon T (2018) Surfactant effect on phase-controlled synthesis and photocatalyst property of TiO 2 nanoparticles. Mater Chem Phys 214:330–336. https://doi.org/10.1016/j.matchemphys.2018.04.111

Zhang M, Wang C (2013) Fabrication of cotton fabric with superhydrophobicity and flame retardancy. Carbohyd Polym 96(2):396–402. https://doi.org/10.1016/j.carbpol.2013.04.025

Zhang Y, Zhang Z, Yang J, Yue Y, Zhang H (2022) A Review of recent advances in superhydrophobic surfaces and their applications in drag reduction and heat transfer. Nanomaterials 12(1):44

Zhang ZH, Wang HJ, Liang YH, Li XJ, Ren LQ, Cui ZQ, Luo C (2018) One-step fabrication of robust superhydrophobic and superoleophilic surfaces with self-cleaning and oil/water separation function. Sci Rep 8(1):1–12. https://doi.org/10.1038/s41598-018-22241-9

Zhao Y, Tang Y, Wang X, Lin T (2010) Applied Surface Science Superhydrophobic cotton fabric fabricated by electrostatic assembly of silica nanoparticles and its remarkable buoyancy. Appl Surf Sci 256(22):6736–6742. https://doi.org/10.1016/j.apsusc.2010.04.082

Zhu H, Guo Z, Liu W (2014) Adhesion behaviors on superhydrophobic surfaces. Chem Commun 50:3900–3913. https://doi.org/10.1039/c3cc47818a

Chapter 7
Characterization and Multifunction Application of Metalized Textile Materials

Shi Hu, Dan Wang, Dana Křemenáková, and Jiří Militký

Abstract The development of modern materials technology has drawn attention to more application possibilities for metalized fabrics. Metalized textiles not only have electrical conductivity, antibacterial properties, and electromagnetic shielding properties of metals but also significantly improve the softness and comfort of the material after combining with textiles. Under such circumstances, the application scenarios of metal-coated fabrics become very broad. For different applications, the selected technical methods are different. Traditional metal-coated fabrics are mainly achieved by blending metal fibers, metal ions reduction reaction (electroless plating or electroplating) on the surface of textiles, and controlled magnetic sputtering. Using appropriate post-processing methods, metal-coated textiles can be used as functional fabrics for electromagnetic shielding clothing. Electromagnetic interference (EMI) shielding textiles is one of the important applications for metal-coated fabrics, especially for people sensitive to electromagnetic radiation. The primary mechanism of EMI shielding textiles is reflection, absorption, and multi-reflection of the inner material. Certain metals like silver and copper have inherently good antimicrobial properties. Textiles with silver or copper elements integrated on this basis have significantly improved antimicrobial properties. Especially at the current stage of the coronavirus pandemic, the demand for anti-microbial and anti-viral textiles is very urgent. Considering the skin's sensitivity to these metals, such textiles should be suitable for outer fabrics, and the skin-friendly layer should not contain metal elements. Due to the electrical conductivity of metals, heat is generated when electricity is applied, and Joule's formula can also describe this phenomenon. Through the effective control of metal content and temperature, clothing that generates heat through Joule heat to resist cold weather has gradually entered the market. With intelligent control technology, the clothing temperature can be adjusted through mobile terminals, and the clothing temperature can be automatically adjusted after integrating temperature sensors. Good electrical conductivity also means the transmission of electrical

S. Hu · D. Wang · D. Křemenáková · J. Militký (✉)

Department of Material Engineering, Faculty of Textile Engineering, Technical University of Liberec, Studentská 2, 46117 Liberec, Czech Republic

e-mail: jiri.militky@tul.cz

signals. As an essential part of intelligent textiles, metal-coated textiles can effectively transmit electrical signals of human activities, including heartbeat, motion signals, etc., through integration with sensors. Combined with appropriate analysis software, such data can be efficiently acquired. This chapter will introduce the basic knowledge of metalized textiles, including the metallization method, essential characterization, and factors influencing the properties. Additionally, the application of metalized textiles will also be discussed.

7.1 Introduction

Metallized textiles give traditional textiles more possibilities in performance and application versatility. From the earliest application of metals in clothing decoration to modern multi-purpose metallized textiles, attempts to integrate metal elements in textile fibers have never stopped.

The application of metals to textiles was first used for decoration, especially the use of precious metal filaments in clothing. It was deduced that during 300–400 years from Qin to Eastern Han Dynasty (BC221-AC220), gold thread began to be applied to textiles in ancient China as decorations for clothing (Hu and Yu 2017) (Fig. 7.1). Especially for royal clothing, textiles containing gold threads are mostly used to show royal status and dignity. For ordinary people, the use of metal filaments as decorative applications in textiles is relatively rare. It is mostly used in the stitching of soldiers' armors or the shroud of nobles after death.

The modern application of metalized textiles started in the 1930s of fabric coated with gold and silver (Han and Min 2020). Since then, technology development in materials engineering has brought a new look to metallized fabrics. With its unique appearance and function, metallic textiles are now widely applied in both clothing and other technical textiles (Shinagawa et al. 1999). Modern incorporation of metallic materials into textiles can be classified into two basic technologies—metal material integration and textile metallization (Dong et al. 2020). Metal material integration attaches metallic materials, such as metal filaments, metallic foils, sheet metals, directly onto fabrics to achieve designed effects. Textile metallization can be realized by coating metallic particles on textile surfaces to create fine metal layer (Fathi et al. 2022)

Regarding the metal material integration method, metal fiber was mainly used. Metal fiber and its products are new industrial materials and high-tech and high-value-added products developed in the past 20 years (Yan et al. 2011). It not only presents softness like chemical fiber, synthetic fiber, but also has excellent thermal conductivity, electrical conductivity, corrosion resistance, high temperature resistance, and other characteristics of the metal itself. Blending is an effective way to combine metal staple fibers and other textile staple fibers (Cheng et al. 2003). Iron fiber, stainless steel fiber with a fineness of tens of microns can be obtained through various metal wire production processes, as well as various metallized fibers obtained by metal plating methods. Blending, interweaving, and paralleling of such

Fig. 7.1 Chinese Qing dynasty emperor Qianlong gold silk dragon Robe (Reproduced from the source: https://www.sohu.com/a/359421859_260616)

fibers are commonly used in textile processing to produce metalized textiles. Core-spun, embroidery, non-woven, etc., are relatively mature and inexpensive methods of preparing metal integration fabrics (Wu 2022). Among them, stainless steel fiber is the most widely used and studied metal fiber.

According to the different uses of textiles, the preparation methods of surface metallized functional textiles are also different. At present, the commonly used methods for mass production of surface metallized functional textiles include electroless plating, coating, vacuum plating, and electroplating (Ojstršek et al. 2021).

The functional textiles, which are metallized on the surface, exhibit multiple features, including heat preservation, antibacterial, antiviral, and antistatic properties (Nouri et al. 2023). Additionally, they offer comfort and ease of maintenance. These textiles have the potential to meet the scientific research needs in challenging environments such as aviation, aerospace, and deep sea. Notably, in personal protection for aerospace and deep-sea environments, there is a demand for multi-functional integrated textiles that comply with material mechanics, thermophilic, and medical hygiene criteria, while conforming to launch volume and load limitations. These textiles can significantly improve the protective performance of safety equipment, while also enhancing safety and comfort (Militký et al. 2023). This provides an essential guarantee for personnel engaged in specialized operations in unique environments.

(a)   (b)
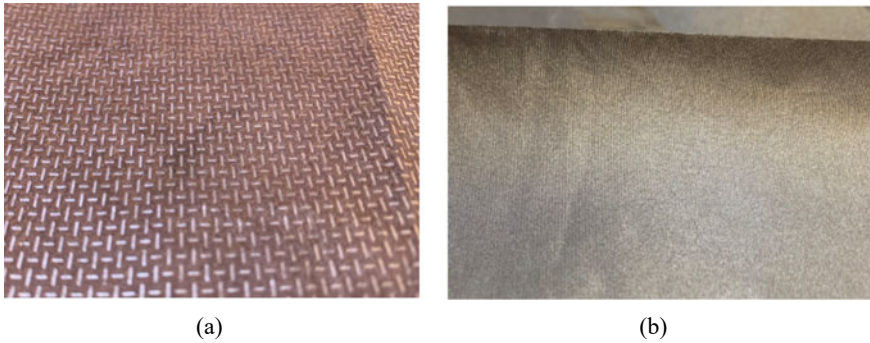
Fig. 7.2 **a** Copper coated nonwoven fabric. **b** Silver short fiber blended woven fabric

According to the morphological structure, metalized textiles can be divided into one-dimensional fiber materials; two-dimensional single-layer planar fabrics; two-dimensional multi-layer planar composite fabrics; three-dimensional structure fabrics (Chang et al. 2022). According to its use, it can be roughly divided into conductive or antistatic; electromagnetic shielding; radar absorbing; antenna, soft keyboard, and other special purposes. Based on the previous research, Hong Xiao et al. put forward the concept of electromagnetic textiles and the development technology of new electromagnetic textiles, expounds that the morphological structure parameters should be integrated into the existing metallization preparation methods, and demonstrate the impact of changes in two-dimensional periodic structures and three-dimensional periodic structures (Xiao et al. 2014). The proposal of this concept includes the previous electromagnetic shielding textiles, antistatic textiles, wave-absorbing materials, and other metal-containing or metallized textiles, as well as the electrical, magnetic, and electromagnetic properties of such textiles (Fig. 7.2).

The demand for antimicrobial properties has resulted in an increased application of metallized textile fabrics. The process involves vacuum magnetron sputtering silver plating on the surface of polyester and nylon after plasma treatment (Kiwi and Pulgarin 2010). The resulting silver-plated antibacterial fibers can be blended or interwoven with cotton, viscose, polyester, and other fibers, making them applicable to various textile and clothing products, such as underwear, shirts, bedding, towels, car seat covers, and filter materials (Qureshi et al. 2021). These fabrics exhibit strong antibacterial properties and good antibacterial persistence.

As the demand for high-comfort clothing increases, the development of functional textile finishing technology has led to the creation of multi-functional metalized fabrics. These fabrics possess several characteristics, including heat preservation, antibacterial properties, lightweight, comfortable wearing, and easy care. Researcher Pamela Miśkiewicz et al. has reviewed vacuum magnetron sputtering silver plating on fabrics made of polyester, nylon, and aramid. These fabrics have a high infrared radiation blockage capacity within the wavelength range of 8–14 μm, resulting in

reduced heat loss. Furthermore, the broad-spectrum antibacterial and strong reflection properties of silver make the fabric highly effective in preventing bacterial growth and preserving heat (Miśkiewicz et al. 2022).

The use of vacuum magnetron sputtering technology between metal and textiles combines the advantages of the two materials (Tan et al. 2018). The coating is less than 1 μm, ensuring that the original fabric's softness and comfort remain unaffected. This technique aligns with the direction of the textile industry's development, which seeks high-performance, lightweight, flexible, and multi-functional fabrics. Vacuum magnetron sputtering metal coating functional textiles possess dense and uniform coatings and stable structures. These textiles meet diverse daily life needs while also satisfying scientific research requirements in challenging environments, such as aerospace, deep sea, and desert (Chang et al. 2022; Dong et al. 2020).

7.2 Realization Method of Metallized Textiles

Metallic fiber blending fabric

Metal fibers refer to fibrous materials that have a high content of metal and a continuous distribution of metal material, with a transverse dimension in the micron range. Based on the primary metal composition, metal fibers can be made from gold, silver, copper, nickel, stainless steel, tungsten, and other materials (Zeng et al. 2014). According to the processing method and structural form, metal fibers can be formed by pure metal wire drawing or melt spinning methods with diameters in the micron range, or through composite fibers created by pure metal wire drawing and coating methods, or by metallizing organic compound fibers. Based on processing methods, metal fibers can be categorized into wire drawing, melt spinning, metal coating, film, and growth methods (Zeng et al. 2014).

Typically, metal fibers have a diameter in the micron range, with fine stainless-steel fibers available in the market having an average diameter of 4 μm. These fibers possess excellent mechanical properties, including high specific strength at break and specific tensile modulus, good toughness, and electrical conductivity, and are capable of preventing static electricity (Shabaridharan and Bhattacharyya 2016). Additionally, metal fibers exhibit properties such as anti-electromagnetic radiation and conductivity, making them essential materials for electrical signal transmission. Stainless steel and gold fibers, in particular, are highly resistant to chemical corrosion and oxidation in the air, owing to their high-temperature resistance.

Metal fibers are commonly used in smart clothing as signal and power transmission wires, as well as for antistatic materials in general functional clothing (Cho et al. 2009). The incorporation of metal wires into fabric can achieve an effective electromagnetic shielding effect. Moreover, metal fibers find wide-ranging applications in military, aviation, communications, and confidential shielding environments (Wang et al. 2010).

During the spinning process, metallic fibers can be blended with cotton fibers (Shahzad et al. 2019). However, it is difficult to achieve a suitable blend ratio due to the disparity in fiber diameter between the two types of fibers. The usual processing methods such as opening, carding, drawing, and combing are used to process the blended cotton and metal fibers. Although the combed sample is similar to usual cotton fibers, the metal fibers cannot reach the required fineness during the drawing process. In order to achieve a uniform and correct blend ratio, the sliver must be twice as thin as the metal fiber sliver. By combining and drafting, the fiber strands tend to become more uniform, resulting in a high level of fiber parallelism (Veit 2022).

It is important that the metal fibers are evenly distributed in the sliver or other semi-finished products during the spinning process to ensure the necessary mutual contact between the fibers for electrical conductivity. However, blending metal fibers with cotton fibers can lead to increased yarn fineness deviation, especially for coarse yarns. The presence of metal fibers can also lead to increased fineness unevenness and twist coefficient unevenness. However, the relationship between nominal and actual twist does not appear to depend on the metal fiber content (Veit 2022).

Similar process as cotton blending spinning process, except for the natural fiber, metallic fiber could also blend with synthetic fiber (Veit 2022). However, the mechanical properties of produced yarn could decrease caused by the metallic fiber. The relationship between yarn strength and stainless-steel fiber content is that as the content of metal fiber increases, the strength of blended yarn decreases. This is because: the properties of stainless-steel fiber and polyester fiber are very different, the breaking strength of polyester is 4.2–5.0cN/dtex, and the elongation at break can reach 35–50% (Cho and Jeong 2005); while the breaking strength of stainless-steel fiber is only 0.66–1.76cN/dtex, and the elongation at break is only 0.425% (Sun et al. 2012), which is a big difference between the two. During the tensile fracture process of the blended yarn, when the yarn begins to be stressed, the stainless-steel fiber shares more tensile force, and the polyester fiber shares less; When the elongation of the fiber reaches its own breaking elongation, it breaks first. At this time, the role of external force is changed to polyester fiber, until the whole yarn breaks. Of course, this process also includes fiber slippage. Apparently, the incorporation of stainless-steel fibers aggravates the non-simultaneity of fiber breakage in the yarn, and also reduces the tensile capacity of the yarn, and its external performance is the downward trend of strength.

In the initial stage of strength decline (stainless steel fiber content 0–10%), the strength decline of blended yarn is not significant. This is mainly because the stainless steel fiber content in the yarn is relatively small at this time, and the polyester fiber that accounts for the vast majority plays a leading role in the strength of the yarn. When the metal fiber breaks, there are still more polyester fibers that share the external force. The decrease in yarn strength is less significant. As the content of stainless steel fiber increases, the number of metal fibers in the yarn gradually increases. Due to the poor cohesion between the uncrimped and rigid stainless steel fiber and polyester fiber, when the yarn is stretched, the fiber is easy to pull out and slip off, so there is a strong downward trend is evident. However, when the stainless steel fiber continued to increase, there was a strong downward trend and a moderation (Fig. 7.3).
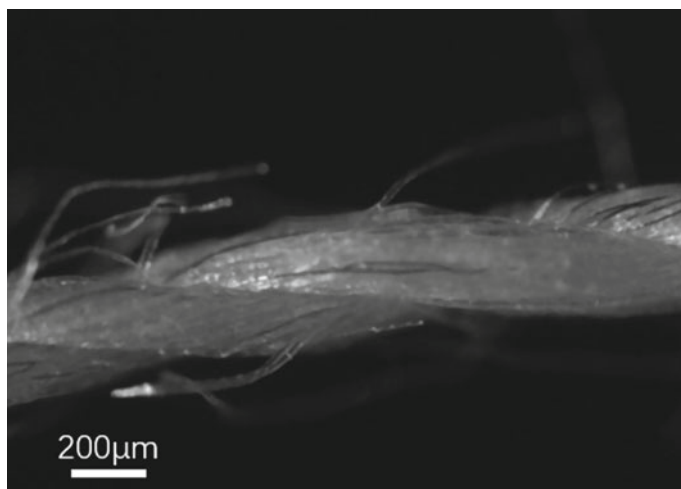
Fig. 7.3 Stainless steel blended polyester yarn

Electroplating and electroless plating

Except for blending metallic fiber into textile fabric, metal particles coated textiles also as functional material that has been produced as a mature industry production in recent years. The methods of metal coating textiles are diverse and range from traditional methods, such as electroplating and electroless plating, to more recent innovations like vacuum magnetron sputtering, physical vapor deposition (PVD), and chemical vapor deposition (CVD). In this section, electroplating, electroless plating, and vacuum magnetron sputtering method will be introduced (Yuen et al. 2006).

One of the earliest techniques for applying metal to surfaces made of various materials, including textiles, is electroplating (Liu and Liang 2001). It is a procedure where an electrolysis solution is used to deposit a metal coating onto a conductive surface (Fig. 7.4). The basic mechanism of electrolysis, which includes using an electric current to create a chemical reaction, serves as the foundation for the electroplating process (Zakeri and Zakeri 2022). An electrolytic cell is used to deposit a metal coating during electroplating onto the substrate, a conducting surface. An electrolyte solution containing the ions of the metal to be deposited is added to the solution, along with an anode, and the substrate is then submerged in it. The ions in the electrolyte and the anode are both formed of the same metal. The electrolyte's metal ions are drawn to the substrate by an electric current flowing through the solution, where they are reduced and left as a thin layer on the surface. The metal atoms from the anode disintegrate into the solution at the same time, replenishing the metal ions in the electrolyte. The current density, the amount of metal ions present in the electrolyte, and the length of time the current is applied all affect how quickly metal

Fig. 7.4 Principle of
electroplating method
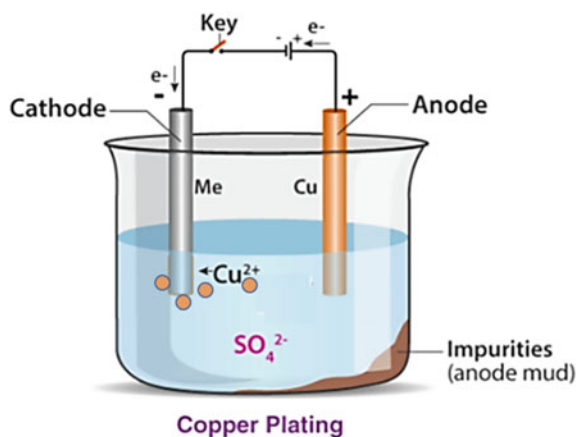
is deposited. The quality and thickness of the metal coating can be controlled by
adjusting these variables (Zakeri and Zakeri 2022).

As previously mentioned, the conductive surface is suitable for the electroplating
procedure. Since the majority of textile material is non-conductive in this situation,
the initial step of electroplating involves making the textile fabric conductive before
applying metal coatings to it. There are various ways to make textiles conductive,
such as treating them with conductive polymers or metallic coatings, or employing
metal salts that can bind to the fibers of the fabric and produce conductive sites
(Stoppa and Chiolerio 2014).

The same process used for metal deposition on other substrates can be used to
electroplate the textile fabric after it has been made conductive (Ali et al. 2021).
Copper particles were electroplated on cotton fabric with success by Ali et al. The
chemical reduction reaction facilitates the rendering process. The cotton materials
were soaked in the copper sulphate solution for around 15 min before drying. The
treated substrate was then submerged in a 10 g/L sodium hydrosulfite solution to
activate copper sulfate's reduction activity. The treated fabric can be utilized for the
electroplating procedure after 40 min.

A metallic coating can be applied to the conductive fabric by immersing the fabric
in an electrolyte solution containing ions of the metal to be deposited (You et al.
2021). For copper or silver plating, the most used electrolyte are copper (II) sulfate
pentahydrate ($CuSO_4 \cdot 5H_2O$) and silver nitrate ($AgNO_3$). The conductive fabric can
act as the cathode while an anode of the same metal is also placed in the electrolyte
solution. An electric current is then applied to the solution, causing metal ions in the
electrolyte to be attracted to the conductive fabric and deposited as a thin layer on
the surface. By controlling the current density, electrolyte composition, and process
time, it is possible to control the thickness and quality of the deposited metallic
coating. The advantage of electroplating method is the relatively low-cost and easy
to handle. However, there are some limitations, such as the pretreatment of the fabric
is necessary, the requirement for a high level of precision in the application of the

electrical current, and the need for careful control of the solution chemistry to ensure uniform metal deposition.

Another crucial technique for embedding metal particles on textile surfaces in addition to electroplating is electroless plating. By using a method called electroless plating, often referred to as autocatalytic plating, a thin layer of metal particles can be applied to a substrate like a fabric without the use of an external electric current. Instead of using an electric field, the procedure depends on a chemical reduction reaction to deposit the metal layer (Tseghai et al. 2020). Typically, the electroless plating procedure consists of three phases. The substrate must first be ready by being cleaned and activated to encourage the metal layer's adherence. One typical method of electroless plating on PET fabric is shown in Fig. 7.5, where $SnCl_2$ and $PdCl_2$ were utilized in the activation step. The electroless plating process is started by reducing the metal ions in the plating solution to their metallic state using the potent reducing chemical $SnCl_2$. $SnCl_2$ reacts with the metal ions in the plating solution to transform them into metallic forms, which then deposit onto the substrate. For metals like copper, nickel, and silver electroless plating baths, $SnCl_2$ is frequently utilized as the main reducing agent. In the process of electroless plating, $PdCl_2$ is a catalyst that is utilized to start the autocatalytic reaction. $PdCl_2$ is a very soluble salt that is quickly reduced to generate the highly effective catalyst Pd (0). $PdCl_2$ is reduced to Pd (0) when it is introduced to the plating solution, forming catalytic sites that encourage the reduction of the metal ions in the plating solution. In the electroless plating of non-conductive substrates like plastics and textiles, $PdCl_2$ and $SnCl_2$ are frequently combined (Osaka et al. 1980).

The activated substrate is placed into a plating bath that also contains a reducing agent, a metal salt, and other additives in the second stage. The metal layer is applied
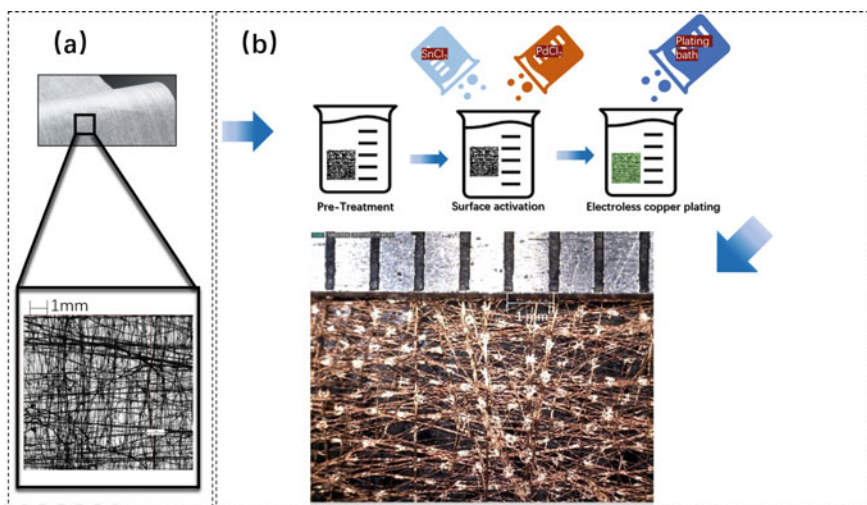
Fig. 7.5 One typical electroless plating method for coating copper on polyester nonwoven fabric

to the substrate surface as a result of the metal salt and reducing agent reacting. $CuSO_4$ was utilized as a metal salt in the example, and formaldehyde served as the reducing agent. The exact metal being deposited and the demands of the finished product can influence the choice of reducing agent when electroless plating textile surfaces. For electroless plating on textile surfaces, common reducing agents include hydrazine, sodium borohydride, dimethylamine borane, and others. The following is a representation of the reaction equation for copper sulfate ($CuSO_4$) reduction by formaldehyde in the electroless plating process (Guo 2010):

$$CuSO_4 + 4HCHO + 4NaOH \rightarrow Cu + 4HCOONa + Na_2SO_4 + 3H_2O$$

(7.1)
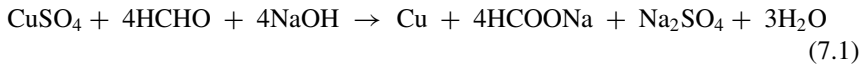
The reaction occurs in an alkaline solution, typically with a pH of around 12. In the presence of formaldehyde and sodium hydroxide, copper ions in solution are reduced to their metallic form, which deposit onto the surface of the substrate.

The third step is to rinse the substrate with water to remove any excess plating solution, and the final step involves a post-treatment process to improve the adhesion and durability of the deposited metal layer.

To use the electroless plating process on textile fabrics, it is important to carefully select the plating bath chemistry to ensure that it is compatible with the fabric material and does not cause damage or degradation to the fibers. The plating parameters, such as the temperature and the concentration of the plating solution, can also be optimized to control the thickness and quality of the deposited metal layer (Guo 2010).

Vacuum magnetron sputtering

According to the material, the method of changing from a solid state to a gaseous state, and the process of transporting coating atoms in vacuum, vacuum plating can be divided into vacuum evaporation plating, vacuum magnetron sputtering plating, vacuum ion plating, and vacuum chemical vapor deposition plating (Deng et al. 2020). However, for the purpose of producing textiles on a wide scale, only vacuum magnetron sputtering is utilized. Vacuum magnetron sputtering is the process of producing argon ions through gas discharge in a vacuum, using charged argon ions to bombard a negatively charged target, and depositing the sputtered atoms from the target on the substrate to create a metal layer. Different metals can be plated according to varied needs, and the production process is environmentally friendly and pollution-free, but the equipment is expensive and needs a lot of maintenance.

Metal films are the only thing that can be coated using vacuum magnetron sputtering. Because it is challenging to satisfy the aforementioned standards for combination fastness, additional processing is frequently needed to satisfy the performance requirements of garment textiles. It is required to treat the surface of textiles in order to give them a strong bonding force. Plasma treatment of the substrate's surface is required in addition to traditional pretreatment to guarantee that the substrate is clean and to produce free radicals, which will enhance the quality of the textiles. The surface activity can satisfy the fundamental performance standards for textiles (Depla et al. 2011).

Polymers including polyester, nylon, and aramid are primarily employed as substrates for metallization. Chemical fibers and metals fall into two groups of substrates that have poor surface qualities such hydrophilicity, antistaticity, and viscosity. The substrate fiber's surface must be changed in order to increase its surface activity because there is a weak binding force between the two materials. The surface of the fiber will be etched by plasma surface treatment, meaning that the chemically active components of the plasma will contact with the fiber's surface. Etching alters the microscopic morphology of the plasma-treated fiber surface, improving the bonding strength between the fiber and the metal layer. This increases the product's wear resistance and washing resistance, which satisfies the demands of wearability (Yuan et al. 2022).

On the cathode target's surface, a magnetic field is created in order to maximize sputtering efficiency. This magnetic field can be used to confine electrons, expand the electron route, raise the possibility that argon atoms will ionize, and achieve low-pressure stable discharge. Membrane metal plating using a magnetron is the coating technique based on this idea. Currently, this technique is frequently employed in industrial production. According to this theory, an electric field is directed from the substrate to the metal target, which is used to create a magnetic field, when the target and substrate are placed in a vacuum chamber with their backs to one another, the target connected to a negative voltage and the substrate to a positive voltage. The magnetic force lines point from the N pole of the permanent magnet to the S pole and form a closed area with the cathode target surface when the permanent magnet is placed on the back of the target. Water cooling is used to cool the target and magnet. Argon gas will glow discharge to form argon plasma when the vacuum chamber is evacuated to the proper pressure, filled with argon gas, and then sufficient voltage is applied to the cathode and anode electrodes. The argon ions in the argon plasma will then flow to the cathode target under the influence of an electric field. Target atoms and secondary electrons are sputtered out by blasting the target material as it travels and accelerates in the cathode region. The electromagnetic field's influence extends the effective running path of the electrons, increasing the likelihood of an electron–gas atom collision and enhancing the rate at which argon atoms ionize. This improves the density of argon ions impacting on the target surface and speeds up sputtering. The neutral atoms that are sputtered do not adhere to the substrate because of the magnetic field. A metal film is created by adsorption, diffusion, nucleation, and deposition on the substrate's surface. High speed and low temperature are the two key properties of vacuum magnetron sputtering metallization layer. Textile metallization offers excellent efficiency, a variety of substrates, and an environmentally benign manufacturing process (Kelly and Arnell 2000).

7.3 Characterization Methods and Main Influencing Factors of Metallized Fabrics

Metallized fabrics have been processed by coating or blending with metallic coatings, such as aluminum, copper, or silver. Characterization of metallized fabrics is significant to understand their physical and chemical structures, which offering the basic information for further investigation of properties, as well as their performance in different applications. Metallized fabrics can be characterized using various methods to evaluate their different morphology structure parameters. In this section, some of the commonly used characterization methods and examples for metallized fabrics will be introduced:

Regarding morphology characterization, scanning electron microscopy (SEM) is widely used for identifying the surface and cross-section structure of metallized textile. This method can be used to visualize the morphology and structure of the metallized layer even particles on the fabric surface. SEM can provide information on the thickness, uniformity, and distribution of the metallized layer, size of the metal particles, as well as any defects or cracks that may affect the performance of the fabric. Figure 7.6 presents the copper particles plated PET nonwoven fabric by electroless plating method.

From Fig. 7.6a the structure of metallized fabric can be identified clearly. The fabric was fabricated via thermal bonding process. The bonding points are identified. Fiber arrangement is irregular which is also one important character of nonwoven fabric. After changing the magnification, from Fig. 7.6b the copper particles could be identified clearly on the surface of PET fiber. The size of the particles is variant; however, the distribution of particles is evenly on the surface. Figure 7.7 presents the

(a)   (b)
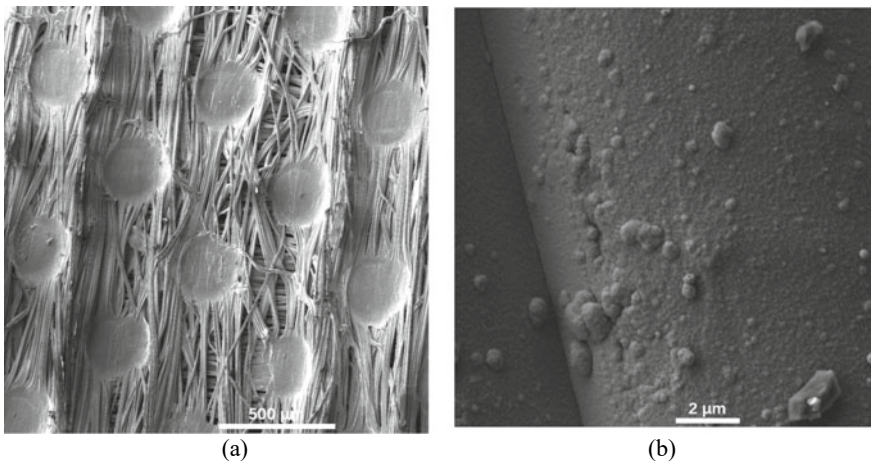
Fig. 7.6 Copper-coated PET nonwoven fabric
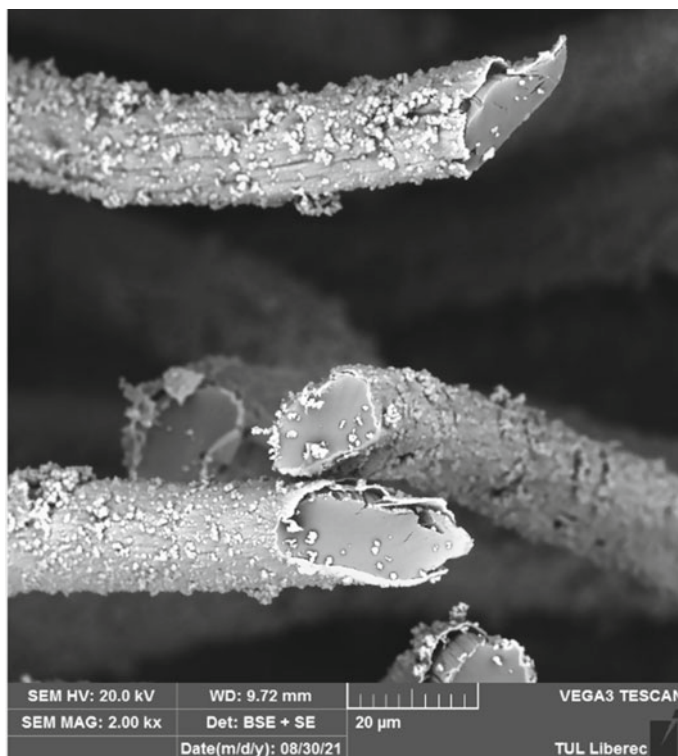
Fig. 7.7 Cross section view of copper-coated PET fiber

cross-section view of the copper-coated PET fiber. It was clear to see that the cooper particles were plated on the surface of the fiber and distribution was relatively even.

Energy dispersive X-ray spectroscopy (EDS): This method can be used to identify the elemental composition of the metallized layer on the fabric surface. EDS can provide information on the type and amount of metal deposited on the fabric, which can affect the conductivity, adhesion, and corrosion resistance of the metallized layer. Figure 7.8 presents the EDS test result of PET nonwoven fabric with copper-plated particles. The relative weight ratio of Cu occupies value can be checked from the map sum spectrum. Through the EDS method, the surface element could be identified. Normally for metallic textile material, the specific metal element could be identified. However, the relative weight ratio can not be used as the real metal mass ratio of the fabric. The value from EDS only identified very limited area of the sample, and the scanning only focus on the sample surface. In this case, calculating the metal mass ratio is more accurate by calculating the difference before and after metal plating process.

X-ray diffraction (XRD): This method can be used to analyze the crystal structure of the metallized layer on the fabric surface. XRD can provide information on the orientation, texture, and phase composition of the metallized layer, which can affect
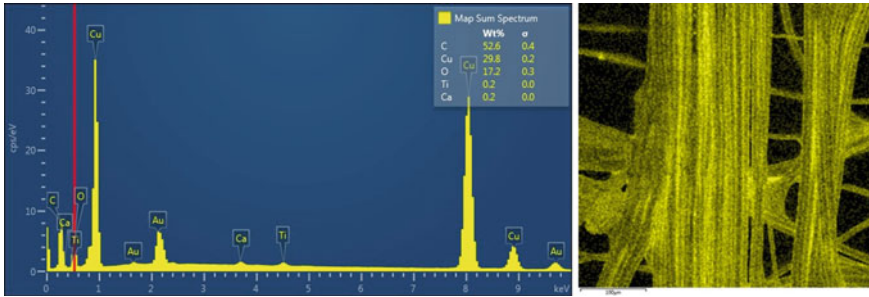
Fig. 7.8 EDS test result of copper plated PET nonwoven fabric

the mechanical and physical properties of the fabric. Even for the metalized sample with protection coating, the XRD method could still identify the crystal structure of greige fabric and plated metal component. Figure 7.9 presented the XRD test result of the copper-plated nonwoven fabric with the protection Parylene-C coating. The XRD spectrum of the sample shows no apparent shift compared to untreated copper coating PET fabric (Fig. 7.2i). Therefore, the crystal morphology of copper existing on the fibers did not change due to the chemical vapor deposition of Parylene-C, which also shows that the presence of Parylene-C does not affect the crystal morphology of copper on the surface of the fabric, thus ensuring other functionalities of the sample.

Except the above method, there are also other necessary characterization method can be selected to identify the metallic textiles, which including Fourier-transform infrared spectroscopy (FTIR): This method can be used to analyze the chemical bonding and functional groups of the metallized layer on the fabric surface. FTIR
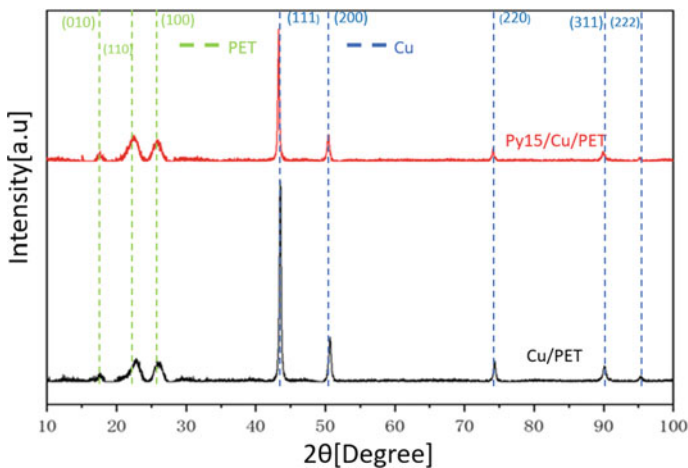
Fig. 7.9 XRD test result of copper-plated PET nonwoven fabric

can provide information on the chemical composition and structure of the metallized layer, which can affect the adhesion, stability, and functional properties of the fabric.

The conductivity measurement is one of the important factors which should be evaluated. This method can be used to measure the electrical conductivity of the metallized layer on the fabric surface. Conductivity measurement can provide information on the effectiveness of the metallized layer in shielding electromagnetic radiation and preventing static charges, which are important for applications in EMI shielding and electrostatic discharge protection.

The adhesion and abrasion tests can be used to evaluate the durability and reliability of the metallized layer on the fabric surface. Adhesion tests can measure the strength of the bond between the metallized layer and the fabric substrate, while abrasion tests can simulate the wear and tear of the metallized fabric in actual use.

Depending on the application, the main required performance of metallic fabric can be different. The performance of metallic fabric mainly depends on the parameter of the fabric, so it's important to understand which factor could impact the property of the metallic fabric. Generally, for textile fabric there are many parameters could be evaluated. Among all the parameters, there are three important influencing factors of metallized fabrics:

1. Metal content and electrical conductivity/resistance: This factor measures the amount of metal on the fabric surface or blended in the fabric, which is an important factor in determining the fabric's conductivity, reflectivity, and durability. The metal content normally has a close relationship with the specialized properties of metallized fabrics. Such as EMI shielding property, with the increase of the metal content, the fabric conductivity will be improved. According to the transmission line theory, the reflected electromagnetic radiation will be increased after adding the content of metal. In this case, the EMI shielding property can be variant when the metal content is different. Changing of the metal content of metallized fabrics will also influence many properties related to conductivity. For ohmic-heated metallized fabrics, the material conductivity is very sensitive to the changing of conductivity. For the sensor or smart textile, conductivity change may also influence the signals sending and receiving accuracy of the material. Depending on the final application and production costs, a proper metal content of metallic fabric is significant to be analyzed.

2. Morphology analysis: This method examines the surface and structure characteristics of the fabric, such as roughness, porosity, thickness, which can affect the adhesion of the metal coating, the air permeability, and the fabric's mechanical properties. Depending on the plating method and metal particle form, the morphology change of the metallic fabric can be different. After the metallization process the fabric will perform good electrical properties, but on the other hand, the influence on wearing comfort, mechanical properties should also be considered.

3. Thermal properties parameters: This mainly includes the fabric's thermal conductivity and thermal resistance, which is important in applications where the fabric is used to extreme temperatures. Basically, metal material has superior

thermal conductive properties compared to textile material. After the metallization process, the thermal conductivity of the sample should be improved. However, as we discussed before, this conclusion can not be applied for all the cases of metallic fabric. There are many parameters could influence the thermal properties of metallic fabric, such as porosity, thickness, greige fabric thermal properties. Depending on the ratio of coated metal, the difference of thermal properties changes before and after metal plating could be mathematically not significant.

The performance of metallic fabric could be influenced by many factors depending on the metallization method and structure of the fabric. In some cases, the metal-related properties could be improved after integrating the metal component, but the metallization process may bring negative impact on the textile material itself, for example, mechanical properties could drop after the electroless plating method, because the fabric may corrode during the metallization process. Additionally, the metallic fabric is sensitive to moisture and temperature, the metal particles could be oxidated and then lost the metal-related properties. That's why for industry-produced metallic fabric, the additional finishing process will be applied to protect the metal layer. Normally the metallic fabric is not suitable for washing cycles, because the washing process will separate the metal particle from the fabric. In this case, considering the technical clothing use of metallic fabric, the proper finishing method to prevent the lost of metal particle after washing cycles should be processed.

7.4 Application of Metalized Textiles

Metallic textiles have a wide range of applications in industries where properties such as reflectivity, electrical conductivity, and thermal resistance are required.

In the last century, metalized textiles were mainly used for decoration or protection as armor. However, with the enormous development of the electrical industry and telecommunication technology, metalized textiles have become an advanced material for various applications. By combining the wearing comfort properties of greige textile materials with the good electrical properties of metal, metalized textiles can now be used as wearable conductive material. Conductive clothing made from metalized textiles can perform EMI shielding, which can protect individuals who are sensitive to extra electromagnetic radiation. Additionally, conductive textiles can be used in aviation and automobiles (Jiang et al. 2006). The good antimicrobial properties of metals like silver or copper enable metal-integrated textiles to perform well as antimicrobial materials, which is particularly important in medical textiles. Regarding smart textiles, which have rapidly developed in recent years, metalized textiles can transfer bioelectric signals via conductive yarn to monitors for collecting movement or other physical activity data (Jiang et al. 2005).

Although metalized textiles have been developed in recent years, they also bring new challenges (Fig. 7.10). For most metalized textiles designed for technical
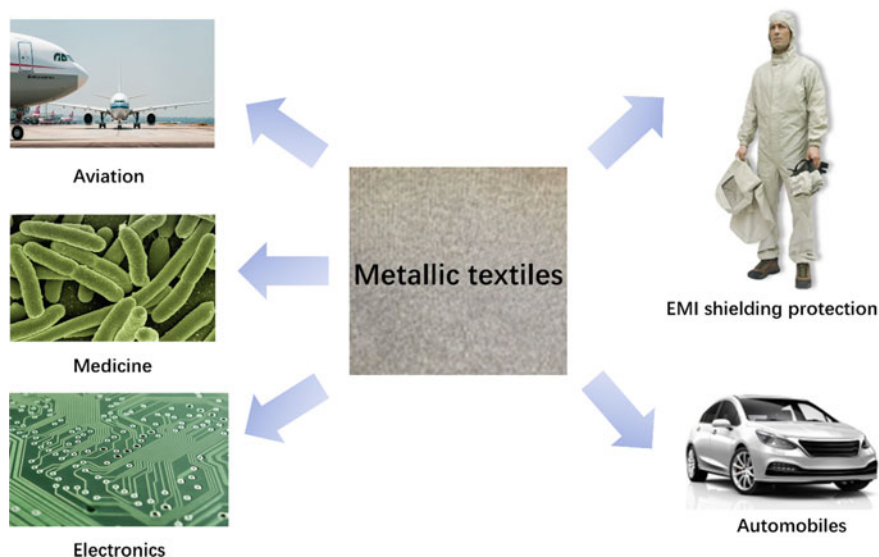
Fig. 7.10 Some applications of metallic textiles

clothing applications, washing durability is a critical problem (Ojstršek et al. 2021). The poor mechanical properties of metalized textiles can also limit their service life. Furthermore, the recycling of metalized textiles poses a significant challenge for waste processing (Zhong et al. 2021).

In this section, we focus on mainly the application of EMI shielding, antimicrobial, and smart textiles.

EMI shielding

The more common way to prepare electromagnetic shielding textiles is to blend, interweave, and parallel metal fibers or metalized fibers with ordinary fibers. This kind of textile has excellent wearing properties such as soft texture, good moisture absorption, and air permeability, and washing resistance. For example, Xinjin. Liu et al. used different proportions of blended stainless steel fiber and polyester fiber yarns to test fabrics EMI shielding property, and found that when the frequency range was 300 kHz to 3 GHz, the shielding effectiveness was 20–40 dB, and the electromagnetic shielding effect was good (Liu et al. 2020). Das et al. found that the fabric made of pure stainless steel fiber has better shielding performance than the fabric made of stainless steel fiber and polyester blended yarn (Das et al. 2014). Conductive polymer fibers are also widely used in protective textiles. The PANI nanofiber prepared by Munan Qiu et al. has an electromagnetic shielding effect of 20.7 dB when the thickness of the sample is only 0.35 mm (Qiu et al. 2018). The PTh/PET fiber prepared by Erdogan M K etc. has a shielding effect of 21 dB in the frequency range of 0-100 MHz (Erdoğan et al. 2012).

According to the principle, electromagnetic shielding can be divided into three categories (1) Electric field shielding (also known as electrostatic shielding, used for low frequency alternating electric field shielding). (2) Magnetic field shielding (also known as magnetostatic shielding, used for low frequency alternating magnetic field shielding). (3) Electromagnetic shielding (for high-frequency electromagnetic field shielding, using reflection and attenuation to isolate the coupling of electromagnetic fields) (Marciniak et al. 2019). The electromagnetic shielding materials involved in this topic are mainly for high-frequency electromagnetic fields. The electromagnetic wave energy under high-frequency electromagnetic fields is relatively vital, and a conductor (flat plate type) is generally used as the shielding material to shield the electromagnetic wave. When the electromagnetic waves in the environment reach the material's surface, most of them will be reflected, and some of the remaining electromagnetic waves will enter the material and transmit forward. Part of the electromagnetic waves is reflected and absorbed multiple times at internal interfaces. Finally, a small part of the electromagnetic waves continues to transmit forward through the shielding body (Tong 2016). These electromagnetic waves passing through the shielding body will have varying degrees of impact, affecting human health and electronics. The attenuation of electromagnetic shielding materials mainly includes reflection loss, absorption loss, and internal multiple reflection loss (*Review on Shielding Mechanism and Structural Design of Electromagnetic Interference Shielding Composites—Wang—2021—Macromolecular Materials and Engineering—Wiley Online Library* n.d.). Among them, the reflection loss mainly occurs at the interface between the surface of the highly conductive material and the free space. The movable charge carrier electrons or holes can induce electromagnetic waves and respond quickly. This process often plays a primary role in the electromagnetic shielding mechanism. The absorption loss requires the shielding material to have a high dielectric constant or permeability, and under the action of electric dipoles or magnetic dipoles, electromagnetic waves can be effectively absorbed inside the material. There are many methods to explain the electromagnetic shielding mechanism in the existing research, such as transmission line theory (Fig. 7.11), eddy current effect method, and electromagnetic field theoretical analysis method. The transmission line theory method is widely used due to its easy understanding, high precision, and convenient calculation (Jaroszewski et al. 2018). According to this theory, the electromagnetic shielding effectiveness (SE) of flat plate electromagnetic shielding materials can be calculated using the Schelkunoff formula (Militký and Šafářová 2012).

$$SE = SE_A + SE_R + SE_M \tag{7.2}$$

SE_A (dB) is the absorbing loss of the shielding materials, SE_R (dB) is the single reflection loss on the surface of the shielding materials, and SE_M (dB) is the multi-reflection loss inside the shielding materials.

There are four parameters of the metalized textile material influencing the shielding effectiveness. These are permeability, conductivity, porosity, and thickness.

Fig. 7.11 EMI shielding mechanism interpreted from transmission line theory
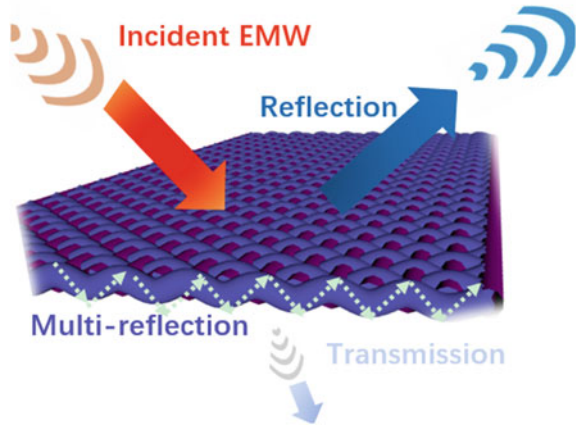
We understand that the material permeability will influence the shielding effectiveness considering the magnetic field shielding. According to the frequency selective surface theory (FSS theory), the shape of the material's apertures will also influence the shielding effectiveness (Anwar et al. 2018). For textile material, the composition of the fiber/fabric determined the conductivity. By using high conducted metal short fiber mixed with textile fiber in the spinning process or coating with conductive polymer or metal, the conductivity of treated textile material can significantly improve (Simon 1981). There is already plenty of research that can approve that with the increasing of the pore size, the shielding effectiveness of the material will reduce.

There are several methods available for shielding effectiveness (SE) measurement:

Free-space measurement techniques
Shielded room method
Coaxial transmission line method
Waveguide method—modified shielded box method.

Shielded room method is marked as the most sophisticated ones, but test specimen size is typically of the order of 2.5 m^2 in area. In general, a signal source is placed outside the test enclosure, whilst the measurement device is located inside. Frequency range is about 100 kHz to 10 GHz. It is expected (Więckowski et al. n.d.) that the test results obtained for the same material tested at different laboratories can vary, even by as much as several dB. This is because the opening in the shielded wall of the chamber also affects the measurements. This opening itself forms a type of antenna with the parameters depending of several factors, one of which is its dimension.

The main measuring method in the controlled medium is the coaxial holder method (ASTM International 1999). This method uses a holder transmission line and a vector network analyzer, as is shown in Fig. 7.12. The sample material is placed and fixed in the flanged circular coaxial transmission line holder. By measuring the S-parameters, S11 and S21—reflection and transmission coefficients, it is possible to determine the contribution of the absorption and the reflection at the total shielding effectiveness.
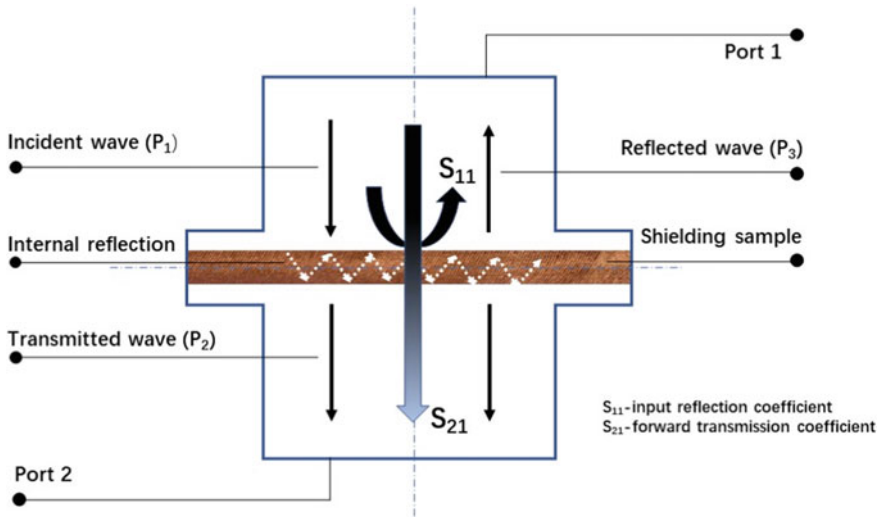
Fig. 7.12 Measurement of SE by using coaxial holder method

Generally, the maximum operating frequency is around 2 GHz. The increase of the maximum operating frequency determines the decrease of the flanged coaxial line dimensions and, of course, the sample dimensions (Hong et al. 2003).

This measuring system is compact and allows automation and data proceeding by computer control. The difficulty of this measurement method arises from the sample preparation. Thus, the dimensions of the sample must be small, especially for higher frequency measurements and the influence of the contact resistance between the sample and the coaxial holder is necessary to be considered. The SE evaluation of the sample can refer to the standard listed in Table 7.1.

Table 7.1 Classification of EM SE values on textiles for general use

Type	Grade	Shielding effectiveness (dB)	Classification	Percentage of electromagnetic shielding (%)
Class I professional use	AAAAA	SE > 60 dB	Excellent	ES > 99.9999
	AAAA	60 dB ≥ SE > 50 dB	Very good	99.9999% ≥ ES > 99.999
	AAA	50 dB ≥ SE > 40 dB	Good	99.999% ≥ ES > 99.99
	AA	40 dB ≥ SE > 30 dB	Moderate	99.99% ≥ ES > 99.9
	A	30 dB ≥ SE > 20 dB	Fair	99.9% ≥ ES > 99.0
Class II general use	AAAAA	SE > 30 dB	Excellent	ES > 99.9

Antimicrobial

With the increasing pandemic of Covid-19 in recent years, viral infection problems have become more serious compared to the past. In addition, microbial presence in the human environment poses a challenge. Certain metals have been shown to exhibit good antimicrobial properties, which have been demonstrated for centuries (Dizaj et al. 2014). Metals have played a critical role in the development of human society. The antibacterial properties of silver, copper, zinc, titanium dioxide, and other metals and metal oxides have been recognized early on. These metals possess high safety, heat resistance, durability, broad-spectrum antibacterial properties, and no drug resistance (Bekmurzayeva et al. 2018). Consequently, they have become the core of antimicrobial agent research. In recent years, various metal antibacterial products have appeared on the market, most of which use silver as the main antibacterial material. These products include antibacterial textiles, antibacterial coatings, and antibacterial plastics. The metal is prepared as nano-metal powder, and its properties change dramatically. Nano-sized metal particles can easily enter bacteria, greatly enhancing their antibacterial properties. Therefore, all metals with particle sizes at the nanometer level have a certain degree of antibacterial properties. Nano-metal powders have broad application prospects in the field of antibacterial materials (Allahverdiyev et al. 2011).

Antibacterial materials have long been the subject of research and development in the area of textiles. This trend has affected civilian bed sheets, civilian undergarments, socks, masks, even combat uniforms and tents from the military. Skin and clothes serve as a breeding environment for germs due to the sweat that the human body secretes, the dander that is shed, and the ideal body temperature. Thus, it is crucial to create clothing that has antibacterial qualities. The metal coating on the fabric plays a major role in the antibacterial characteristics of metalized textiles (Du et al. 2022). Strong antibacterial action has been demonstrated for the metal coating, such as silver or copper, against a variety of pathogens, including bacteria, fungus, and viruses. The release of metal ions from the metal coating is assumed to be the mechanism of antimicrobial action. These metal ions can interact with microbes and interfere with their biological functions.

Metal ions are discharged from the metalized textile surface and can bind to the microorganisms' cell membranes when they come into contact with it (Fig. 7.13). The cell membrane may be damaged as a result, allowing the contents of the cell to leak out and ultimately causing cell death. Moreover, the metal ions may interact with the bacteria' proteins and enzymes, leading to denaturation and function loss (Ueda et al. 2003).

The type of metal utilized, the amount of metal ions produced, and the length of time the microbes are in touch with the fabric surface all affect how effective metalized textiles are as antimicrobial agents (Yu et al. 2015). Because of their wide-spectrum activity and relatively low toxicity to human cells, silver, and copper are among the most popular metals utilized for antimicrobial coatings. In general, the antimicrobial qualities of metalized textiles are a significant feature for applications like medical textiles, protective garments, and residential textiles, where it is essential
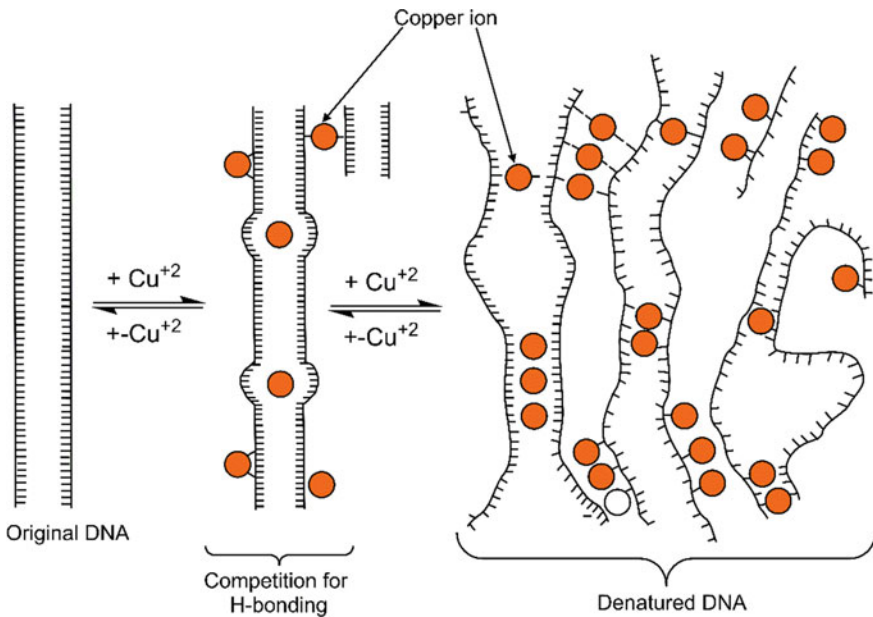
Fig. 7.13 The mechanism of copper ion denatures the structure of microbial DNA structure

to inhibit microbial development and transmission for the protection of the general public's health and safety.

Regarding the research about copper-coated textile antimicrobial properties, researcher A. Ali and his colleague studied copper-coated cotton fabrics, the zone of inhibitions presented the property against both types of bacteria S. aureus and E. coli after the copper coating. Further, S. aureus shows the highest sensitivity as compared to E. coli. The zone of inhibitions for S. aureus increased from 9.5 to 15.5 mm, for E. coli it increased from 7.5 to 12 mm with increasing number of dips (Ali et al. 2018).

After coating with copper particles, the acrylic fiber also perform good antimicrobial properties. For all samples with copper-coated acrylic fabrics, there is a visible color change, which presents the release of copper into the nutrient medium. Microbial cultures in all concentrations do not grow up to the selected material, the zone clearly corresponds to copper diffusion into the medium and ranges from 9 to 11 mm. For Cu-free control samples, Escherichia coli and Staphylococcus aureus grow to the tested material even under the material without treatment (Fig. 7.14).

Additionally, the metal coatings' antibacterial qualities can aid in lowering the development and spread of dangerous germs and other pathogens, making the textiles acceptable for usage in industries like medical, protective apparel, and home textiles.

Medical fabrics, where microbial growth and transmission must be prevented, can likewise benefit greatly from the joule heating effect also. To encourage healing while lowering the danger of infection, metal-coated fabrics, for instance, can be used as self-heating wound dressings that also have antimicrobial qualities.
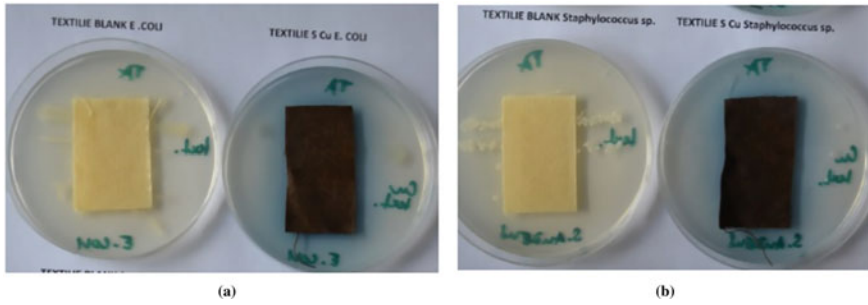
Fig. 7.14 Anti-microbial performance of copper-coated acrylic fabrics. **a** Anti Escherichia coli effect **b** anti Staphylococcus aureus effect

Heavy metal antibacterial goods that are quite mild and have few adverse effects have also entered the market as the functional textile sector has grown increasingly passionate about the development of heavy metals, particularly those based on silver. Nonetheless, it cannot be denied that the method by which heavy metal preparations work is to gradually release heavy metal ions into the environment. Also, it will deal a fatal blow to the microenvironment on the surface of the human body. It should be mentioned that a concealed risk is the accumulating effect of heavy metals in organisms. Many nations with developed technologies have banned the use of heavy metal antibacterial products out of concern for public safety. Since ancient times, mankind has employed natural antibacterial compounds. Chitin, chitosan, insect antibacterial protein, palm oil, coconut oil, juniper, aloe, and others are among the common natural antibacterial substances. The creation of natural products is growing annually along with people's comprehension of antibacterial fabrics, their awareness of environmental protection, and their demand for "green" textiles. While being safe and pollution-free, this type of antibacterial agent has only moderate antibacterial activity, and its application is severely constrained by its high extraction cost, high processing difficulty, small amount of addition, and poor durability. In this instance, the graphene-coated textile was created with the intention of being used for antibacterial purposes.

Joule heat performance

Joule heating, often referred to as Ohmic heating, is a process that takes place when an electric current travels through a conductor and some of the electrical energy is converted into heat energy as a result of the conductor's resistance (Joe et al. 2021).

The size of the current flowing through a conductor, the conductor's resistance, and the length of the current flow all affect how much heat is produced in the conductor as a result of Joule heating. The equation Eq. 7.2 can be used to compute the heat produced:

$$Q = I^2 \times R \times t \tag{7.2}$$

where Q is the heat energy produced, I is the current, R is the resistance of the conductor, and t is the time for which the current flows.

In metalized textiles, the joule heating effect can be utilized to create self-heating textiles with antimicrobial properties. By applying an electric current to the metal-coated fibers in the textile, Joule heating can be used to generate heat that can help keep the wearer warm and comfortable in cold environments (Park et al. 2021). There are generally two ways to keep clothing warm, one is passive warmth, and the other is active warmth. The warming methods of traditional clothing are basically passive warming, that is, by controlling the content of the still air layer and preventing the body's heat from losing outwards, the purpose of keeping warm is achieved. Active heat preservation is to use heat-generating fiber materials or add heat-generating devices to actively heat the human body to achieve a heat-retaining effect. In this way, the thickness and weight of clothing can be reduced, and people's aesthetic and light-weight application requirements for warm clothing can be more complied with. Because the heat that the human body itself can produce is very limited. Under the cold temperature, it is difficult to ensure the body's heat balance by only relying on the contraction of human muscles and blood vessels to regulate body temperature, especially in the case of prolonged hunger and cold, it is difficult for the human body to maintain basic body temperature. Therefore, it is very meaningful to develop a heating element that can actively provide a heat source built into clothing. At present, metalized textile are mostly used in clothing. It uses electric energy as the energy source and converts electric energy into heat energy through electric heating elements, so as to generate heat at low pressure and achieve the effect of active warmth. Electric heating clothing usually connects the power supply, heating element, automatic temperature control device, and safety protection device with wires to form a circuit (Fig. 7.15). The power supply generally uses a human body-safe DC voltage below 12 V The conductive textile could generate heat by joule heating method.

Fig. 7.15 Joule heating effect of copper-coated acrylic fiber sliver

Due to the good wearing comfort and gentle heat generated from the metalized textile, this material can also be applied for the thermotherapy treatment. Thermotherapy is a type of medical treatment that involves the application of heat to the body to alleviate pain and promote healing. In recent years, metalized textiles have been developed that can be used for thermotherapy, providing a convenient and effective way to apply heat to the body (Caya et al. 2020).

Metalized textiles for thermotherapy typically use silver or copper coatings, which have been shown to possess strong antimicrobial activity, as well as excellent thermal conductivity. These metal coatings can be applied to a range of fabrics, including cotton, polyester, and nylon.

One way that metalized textiles are used for thermotherapy is by incorporating them into wearable heating pads or wraps. These pads or wraps can be placed on specific areas of the body, such as the lower back or neck, to provide targeted heat therapy. The metal coatings in the textile conduct electricity, which can be used to generate heat through the Joule heating effect.

Metalized textiles for thermotherapy can also be used in medical settings for wound healing or pain management. For example, metal-coated wound dressings can be used to deliver heat therapy directly to a wound site, promoting healing and reducing the risk of infection.

In addition to their thermotherapy applications, metalized textiles can also provide antimicrobial properties, making them useful in a range of medical and non-medical applications, such as hospital textiles, protective clothing, and home textiles. Overall, metalized textiles for thermotherapy offer a versatile and effective way to deliver heat therapy, with the added benefit of antimicrobial properties.

Smart textiles

With the continuous development of wearable electronic products and smart textiles, and the increasing demand of consumers for advanced smart textiles, various wearable biomedical and smart sportswear textile electronics devices have emerged on the market (Cherenack and van Pieterson 2012). The popularity of rigid smart electronic devices (such as electronic skins, smart watches, and sports wristbands) has also boosted the development of wearable and flexible smart electronics. Lightweight, convenient, and comfortable flexible electronic smart textiles will have broad application prospects. At present, electronic smart textiles play an important role in health monitoring, disease prevention, electromagnetic shielding, energy conversion, storage, and human–computer interaction. Taking health monitoring as an example, the smart sports bra released by the high-end underwear brand Victoria's Secret has a built-in heart rate belt that can monitor the wearer's heartbeat (*This Victoria's Secret Sports Bra Can Hook Up With A Heart Rate Monitor|TechCrunch* n.d.); Canada's Hexoskin company has launched a new smart sports vest called "Personal Data Laboratory," which can monitor heart rate, breathing, activity intensity, and other data can provide users with monitoring data during physical training, sleep, and daily activities (Hexoskin n.d.). For flexible and wearable smart textiles, on the one hand, it is necessary to meet the requirements of miniaturization, light weight of the device, and the flexibility and extensibility of the device system itself; And under the action

of external force, the electronic device can still maintain the stability of the normal working state. Therefore, smart textiles made of conductive fibers and new textile technologies have emerged.

From the perspective of development history, the early conductive fibers were metal fibers. Since there are a large number of freely movable electrons inside the metal conductor, under the action of the electric field force, the directional movement of the electrons can form a current. When there is a potential difference in the external power supply, the originally disordered free electrons move in a directional manner, thereby realizing the conduction of the metal-type fiber, which has excellent conductivity. However, due to the bulky metal conductive fibers (such as copper fibers, etc.), and poor flexibility and bending resistance, the strain range and gauge coefficient are small, and they do not meet the relatively high mechanical properties and comfort requirements of smart textiles, so they are seldom used directly. in flexible and wearable smart textiles. Subsequently, the discovery of conductive polymers ushered in a new era of conductive fibers. In the 1970s, researchers found that the conductivity of polyacetylene (PA) was increased by 13 orders of magnitude to 103 S/cm through the redox doping of Lewis acid AsF5, comparable to the conductivity of copper and gold. The successful development of PA conductive materials has broken people's traditional concept that polymer materials are insulators. and research table.

It has been shown that various conjugated polymers can be changed into conductive polymers with different conductive properties after doping (Fou and Rubner 2002), and their conductive properties are related to doping and conjugated systems, which not only change the energy of the original electronic energy band level, which reduces the resistance of free electron migration, and at the same time, the conductive energy band formed by overlapping and crossing the π electron orbitals in the macromolecular chain and the interchain provides a channel for the transfer and transition of carriers. Under the impetus of external energy and vibration of macromolecular chains, electric current can be conducted. However, the characteristics of carriers in conductive polymers are different from those in metals, semiconductors, and ordinary polymers. Metal and semiconductor carriers (electrons or holes) are charged and have spins, while the carriers of PA are charged particles that have no spin. At room temperature, pure polymers can only conduct electricity through doping. After doping, a variety of carriers (such as solitons, polarons, electrons, ions, etc.) are drawn out, which have good electrical conductivity.

As the core of the research and development of smart textiles, flexible metalized fabric has great advantages in the field of smart wearables due to their light weight, comfort, and ease of weaving (Shi et al. 2020). At present, it is mainly used in flexible strain sensors, flexible supercapacitors, flexible nanogenerators, and other fields. In the future, smart textiles will not be limited to a single function, and wearable electronic devices with integrated functions will become the focus of research and development in the next stage.

Flexible sensors are monitoring devices attached to human skin or tissue, which can continuously monitor the physiological, physical, and chemical signals released by the human body or the environment and convert them into electrical signals. Its structural forms are flexible and diverse, and it has good flexibility and ductility. It is

one of the most mature technologies for flexible wearable devices. Among them, the fiber-based flexible sensor can use weaving, knitting, embroidery, and other textile technologies to directly construct conductive fibers into flexible electronic components, which effectively improves the integration and connection defects between traditional flexible electronic equipment and textiles, and is a high-performance, intelligent flexible sensor. The development of electronic equipment provides new ideas (Krifa 2021).

Another interesting application of conductive textiles is supercapacitors. The principle of supercapacitors is to achieve higher capacitance than conventional capacitors through high surface area electrode materials and thin dielectrics. Flexible supercapacitors are mainly composed of three parts: flexible substrate, electrode material, and solid electrolyte. Different from traditional planar supercapacitors, fibrous flexible supercapacitors have a unique one-dimensional structure, good flexibility, and a higher degree of fit with the human body, which can meet the requirements of miniaturization, integration, and flexibility of wearable devices (Gao et al. 2021).

Nanogenerator is a new type of self-powered device. At present, various forms of nanogenerators such as piezoelectric, friction, thermoelectric, electrostatic, and hybrid have been developed. Among them, the piezoelectric nanogenerator (PENG) and the triboelectric nanogenerator (TENG) have the advantages of high output voltage, small size, low cost, and environmental friendliness, and are relatively mature technologies at present (Mule et al. 2019).

References

Ali A, Baheti V, Militky J, Khan Z, Tunakova V, Naeem S (2018) Copper coated multifunctional cotton fabrics. J Ind Text 48(2):448–464. https://doi.org/10.1177/1528083717732076

Ali A, Hussain F, Kalsoom A, Riaz T, Zaman Khan M, Zubair Z, Shaker K, Militky J, Noman MT, Ashraf M (2021) Multifunctional electrically conductive copper electroplated fabrics sensitizes by in-situ deposition of copper and silver nanoparticles. Nanomaterials 11(11):Article 11. https://doi.org/10.3390/nano11113097

Allahverdiyev AM, Abamor ES, Bagirova M, Rafailovich M (2011) Antimicrobial effects of TiO2 and Ag2O nanoparticles against drug-resistant bacteria and leishmania parasites. Future Microbiol 6(8):933–940. https://doi.org/10.2217/fmb.11.78

Anwar RS, Mao L, Ning H (2018) Frequency selective surfaces: a review. Appl Sci (switz) 8(9):1–47. https://doi.org/10.3390/app8091689

ASTM International (1999) ASTM D 4935—standard test method for measuring the electromagnetic shielding effectiveness of planar materials 10(1986):1–10

Bekmurzayeva A, Duncanson WJ, Azevedo HS, Kanayeva D (2018) Surface modification of stainless steel for biomedical applications: revisiting a century-old material. Mater Sci Eng C 93:1073–1089. https://doi.org/10.1016/j.msec.2018.08.049

Caya MVC, De Pano CJR, Magpayo JGS (2020) Development of wearable wireless heating E-textile using conductive threads for thermotherapy. In: 2020 IEEE 12th international conference on humanoid, nanotechnology, information technology, communication and control, environment, and management (HNICEM), pp 1–6. https://doi.org/10.1109/HNICEM51456.2020.9400105

Chang J, Zhai H, Hu Z, Li J (2022) Ultra-thin metal composites for electromagnetic interference shielding. Compos B Eng 246:110269. https://doi.org/10.1016/j.compositesb.2022.110269

Cheng KB, Cheng TW, Lee KC, Ueng TH, Hsing WH (2003) Effects of yarn constitutions and fabric specifications on electrical properties of hybrid woven fabrics. Compos A Appl Sci Manuf 34(10):971–978. https://doi.org/10.1016/S1359-835X(03)00178-7

Cherenack K, van Pieterson L (2012) Smart textiles: challenges and opportunities. J Appl Phys 112(9):091301. https://doi.org/10.1063/1.4742728

Cho G, Lee S, Cho J (2009) Review and reappraisal of smart clothing. Int J Hum-Comput Interact 25(6):582–617. https://doi.org/10.1080/10447310902997744

Cho KH, Jeong SH (2005) Bundle strength of polyester fibers determined using a series-parallel combination model. J Mater Sci 40(20):5341–5347. https://doi.org/10.1007/s10853-005-4260-1

Das A, Krishnasamy J, Alagirusamy R, Basu A (2014) Electromagnetic interference shielding effectiveness of SS/PET hybrid yarn incorporated woven fabrics. Fibers Polym 15(1):169–174. https://doi.org/10.1007/s12221-014-0169-0

Deng Y, Chen W, Li B, Wang C, Kuang T, Li Y (2020) Physical vapor deposition technology for coated cutting tools: a review. Ceram Int 46(11, Part B):18373–18390. https://doi.org/10.1016/j.ceramint.2020.04.168

Depla D, Segers S, Leroy W, Van Hove T, Van Parys M (2011) Smart textiles: an explorative study of the use of magnetron sputter deposition. Text Res J 81(17):1808–1817. https://doi.org/10.1177/0040517511411966

Dizaj SM, Lotfipour F, Barzegar-Jalali M, Zarrintan MH, Adibkia K (2014) Antimicrobial activity of the metals and metal oxide nanoparticles. Mater Sci Eng C 44:278–284. https://doi.org/10.1016/j.msec.2014.08.031

Dong K, Peng X, Wang ZL (2020) Fiber/fabric-based piezoelectric and triboelectric nanogenerators for flexible/stretchable and wearable electronics and artificial intelligence. Adv Mater 32(5):1902549. https://doi.org/10.1002/adma.201902549

Du P, Zhang J, Guo Z, Wang H, Luo Z, Fan Z, Li B, Cai Z, Ge F (2022) A novel breathable flexible metallized fabric for wearable heating device with flame-retardant and antibacterial properties. J Mater Sci Technol 122:200–210. https://doi.org/10.1016/j.jmst.2022.01.015

Erdoğan MK, Karakişla M, Saçak M (2012) Preparation, characterization and electromagnetic shielding effectiveness of conductive polythiophene/poly(ethylene terephthalate) composite fibers. J Macromol Sci Part A 49(6):473–482. https://doi.org/10.1080/10601325.2012.676896

Fathi R, Wei H, Saleh B, Radhika N, Jiang J, Ma A, Ahmed MH, Li Q, Ostrikov KK (2022) Past and present of functionally graded coatings: advancements and future challenges. Appl Mater Today 26:101373. https://doi.org/10.1016/j.apmt.2022.101373

Fou AC, Rubner MF (2002). Molecular-level processing of conjugated polymers. 2. Layer-by-layer manipulation of in-situ polymerized p-type doped conducting polymers (world). ACS Publications; American Chemical Society. https://doi.org/10.1021/ma00125a013

Gao Y, Xie C, Zheng Z (2021) Textile composite electrodes for flexible batteries and supercapacitors: opportunities and challenges. Adv Energy Mater 11(3):2002838. https://doi.org/10.1002/aenm.202002838

Guo R (2010) A study of optimizing processes for metallized textile design application. https://theses.lib.polyu.edu.hk/handle/200/5785

Han CH, Min BG (2020) Superhydrophobic and antibacterial properties of cotton fabrics coated with copper nanoparticles through sonochemical process. Fibers Polym 21(4):785–791. https://doi.org/10.1007/s12221-020-9925-5

Hexoskin (n.d.) Hexoskin smart shirts—cardiac, respiratory, sleep & activity metrics. Hexoskin. https://www.hexoskin.com/. Accessed 27 Feb 2023

Hong YK, Lee CY, Jeong CK, Lee DE, Kim K, Joo J (2003) Method and apparatus to measure electromagnetic interference shielding efficiency and its shielding characteristics in broadband frequency ranges. Aip.scitation.org 74(2):1098–1102. https://doi.org/10.1063/1.1532540

Hu X, Yu W (2017) Specialization of gold thread for textiles from origin of metal wire. J Text Res 38(11):116–123. https://doi.org/10.13475/j.fzxb.20170101108

Jaroszewski M, Thomas S, Rane A (2018) Advanced materials for electromagnetic shielding: fundamentals, properties, and applications (Jaroszewski M (ed)). John Wiley & Sons, Inc.

https://www.google.com/books?hl=zh-CN&lr=&id=Rlt0DwAAQBAJ&oi=fnd&pg=PP15&dq=Advanced+Materials+for+Electromagnetic+Shielding&ots=L-fKA3htbK&sig=5usKMnQ9C2YXnNZEyDwmtC7unTw

Jiang SQ, Newton E, Yuen CWM, Kan CW (2005) Chemical silver plating and its application to textile fabric design. J Appl Polym Sci 96(3):919–926. https://doi.org/10.1002/app.21541

Jiang SQ, Newton E, Yuen CWM, Kan CW (2006) Chemical silver plating on cotton and polyester fabrics and its application on fabric design. Text Res J 76(1):57–65. https://doi.org/10.1177/0040517506053827

Joe SB, Gomathi T, Marshiana D, Krishnamoorthy NR (2021) Effects of joule heating on the temperature-voltage relationship in copper. In: 2021 6th international conference on inventive computation technologies (ICICT), pp 400–403. https://doi.org/10.1109/ICICT50816.2021.9358523

Kelly PJ, Arnell RD (2000) Magnetron sputtering: a review of recent developments and applications. Vacuum 56(3):159–172. https://doi.org/10.1016/S0042-207X(99)00189-X

Kiwi J, Pulgarin C (2010) Innovative self-cleaning and bactericide textiles. Catal Today 151(1):2–7. https://doi.org/10.1016/j.cattod.2010.01.032

Krifa M (2021) Electrically conductive textile materials—application in flexible sensors and antennas. Textiles 1(2):Article 2. https://doi.org/10.3390/textiles1020012

Liu PS, Liang KM (2001) Review functional materials of porous metals made by P/M, electroplating and some other techniques. J Mater Sci 36(21):5059–5072. https://doi.org/10.1023/A:1012483920628

Liu X, Yan X, Su X, Song J (2020) Study on properties of electromagnetic shielding yarns and fabrics. Int J Cloth Sci Technol 32(5):677–690. https://doi.org/10.1108/IJCST-09-2019-0134

Marciniak K, Grabowska KE, Stempień Z, Stempień S, Luiza I, Bel C-W (2019) Shielding of electromagnetic radiation by multilayer textile sets. J.Sagepub.Com 89(6):948–958. https://doi.org/10.1177/0040517518760749

Militký J, Křemenáková D, Venkataraman M (2023) Recent trends in textile structures. In Militký J, Venkataraman M, Periyasamy AP (eds) Fibrous structures and their impact on textile design. Springer Nature, pp 15–77. https://doi.org/10.1007/978-981-19-4827-5_2

Militký J, Šafářová V (2012) Numerical and experimental study of the shielding effectiveness of hybrid fabrics. Vlakna a Textil 19(1):21–27

Miśkiewicz P, Frydrych I, Cichocka A (2022) Application of physical vapor deposition in textile industry. Autex Res J 22(1):42–54. https://doi.org/10.2478/aut-2020-0004

Mule AR, Dudem B, Patnam H, Graham SA, Yu JS (2019) Wearable single-electrode-mode tribo-electric nanogenerator via conductive polymer-coated textiles for self-power electronics. ACS Sustain Chem & Eng 7(19):16450–16458. https://doi.org/10.1021/acssuschemeng.9b03629

Nouri A, Rohani Shirvan A, Li Y, Wen C (2023) Surface modification of additively manufactured metallic biomaterials with active antipathogenic properties. Smart Mater Manuf 1:100001. https://doi.org/10.1016/j.smmf.2022.100001

Ojstršek A, Plohl O, Gorgieva S, Kurečič M, Jančič U, Hribernik S, Fakin D (2021) Metallisation of textiles and protection of conductive layers: an overview of application techniques. Sensors 21(10):Article 10. https://doi.org/10.3390/s21103508

Osaka T, Takematsu H, Nihei K (1980) A study on activation and acceleration by mixed PdCl2/SnCl2 catalysts for electroless metal deposition. J Electrochem Soc 127(5):1021. https://doi.org/10.1149/1.2129810

Park C, Kim T, Samuel EP, Kim Y-I, An S, Yoon SS (2021) Superhydrophobic antibacterial wear-able metallized fabric as supercapacitor, multifunctional sensors, and heater. J Power Sources 506:230142. https://doi.org/10.1016/j.jpowsour.2021.230142

Qiu M, Zhang Y, Wen B (2018) Facile synthesis of polyaniline nanostructures with effective electro-magnetic interference shielding performance. J Mater Sci: Mater Electron 29(12):10437–10444. https://doi.org/10.1007/s10854-018-9100-6

Qureshi S, Stojanović GM, Simić M, Jeoti V, Lashari N, Sher F (2021) Silver conductive threads-based embroidered electrodes on textiles as moisture sensors for fluid detection in biomedical applications. Materials 14(24):Article 24. https://doi.org/10.3390/ma14247813

Review on Shielding Mechanism and Structural Design of Electromagnetic Interference Shielding Composites—Wang—2021—Macromolecular Materials and Engineering—Wiley Online Library (n.d.). https://onlinelibrary.wiley.com/doi/full/10.1002/mame.202100032. Accessed 27 Feb 2023

Shabaridharan K, Bhattacharyya A (2016) Metallic fibers for composite applications. In: Rana S, Fangueiro R (eds) Fibrous and textile materials for composite applications. Springer, pp 205–230. https://doi.org/10.1007/978-981-10-0234-2_6

Shahzad A, Rasheed A, Khaliq Z, Qadir MB, Khan MQ, Hamdani STA, Ali Z, Afzal A, Irfan M, Shafiq M, Kim IS (2019) Processing of metallic fiber hybrid spun yarns for better electrical conductivity. Mater Manuf Processes 34(9):1008–1015. https://doi.org/10.1080/10426914.2019.1594270

Shi J, Liu S, Zhang L, Yang B, Shu L, Yang Y, Ren M, Wang Y, Chen J, Chen W, Chai Y, Tao X (2020) Smart textile-integrated microelectronic systems for wearable applications. Adv Mater 32(5):1901958. https://doi.org/10.1002/adma.201901958

Shinagawa S, Kumagai Y, Urabe K (1999) Conductive papers containing metallized polyester fibers for electromagnetic interference shielding. J Porous Mater 6(3):185–190. https://doi.org/10.1023/A:1009619711017

Simon RM (1981) EMI shielding through conductive plastics. Polym-Plast Technol Eng 17(1):1–10. https://doi.org/10.1080/03602558108067695

Stoppa M, Chiolerio A (2014) Wearable electronics and smart textiles: a critical review. Sensors 14(7):Article 7. https://doi.org/10.3390/s140711957

Sun YC, Cheng ZH, Zhang YM (2012) Analysis on tensile properties of stainless-steel fiber and yarn quality. Adv Mater Res 399–401:176–179. https://doi.org/10.4028/www.scientific.net/AMR.399-401.176

Tan X-Q, Liu J-Y, Niu J-R, Liu J-Y, Tian J-Y (2018) Recent progress in magnetron sputtering technology used on fabrics. Materials 11(10):Article 10. https://doi.org/10.3390/ma11101953

This Victoria's Secret Sports Bra Can Hook Up With A Heart Rate Monitor|TechCrunch (n.d.). https://techcrunch.com/2014/11/25/victorias-secret-heart-rate-sports-bra/?guccounter=1&guce_referrer=aHR0cHM6Ly93d3cuZ29vZ2xlLmRlLw&guce_referrer_sig=AQAAACwXbU0wr8W3R82bRkXKiYkEQ6EYPj61slxUGrq_sF-HFw8yganKlSPC_FNQlQtOovN2ttNcsPIoaYWHPENSqt5ldlFU4NkRxHN3M5iv_BPmaNwyRy0WCI_NPwX1Zd-N50-bEwuM1GIvUYb5R86EFEXWdCLt_6g-8gADnsQTxlQS. Accessed 27 Feb 2023

Tong XC (2016) Advanced materials and design for electromagnetic interference shielding, pp 11–16.https://doi.org/10.1201/9781420073591/ADVANCED-MATERIALS-DESIGN-ELECTROMAGNETIC-INTERFERENCE-SHIELDING-XINGCUN-COLIN-TONG

Tseghai GB, Malengier B, Fante KA, Nigusse AB, Van Langenhove L (2020) Integration of conductive materials with textile structures, an overview. Sensors 20(23):Article 23. https://doi.org/10.3390/s20236910

Ueda EKM, Gout PW, Morganti L (2003) Current and prospective applications of metal ion–protein binding. J Chromatogr A 988(1):1–23. https://doi.org/10.1016/S0021-9673(02)02057-5

Veit D (2022) Metal fibers. In: Veit D (ed) Fibers: history, production, properties, market. Springer International Publishing, pp 941–956. https://doi.org/10.1007/978-3-031-15309-9_46

Wang L, Wang X, Lin T (2010) 6—Conductive coatings for textiles. In: Smith WC (ed) Smart textile coatings and laminates. Woodhead Publishing, pp 155–188. https://doi.org/10.1533/9781845697785.2.155

Więckowski TW, Janukiewicz JM (2006, undefined. (n.d.)) Methods for evaluating the shielding effectiveness of textiles. Fibres Text Eastern Europe. Infona.Pl. https://www.infona.pl/resource/bwmeta1.element.baztech-526445db-c2ba-4d2a-befd-39db288c61dd. Accessed 23 Nov 2020

Wu S (2022) An overview of hierarchical design of textile-based sensor in wearable electronics. Crystals 12(4):Article 4. https://doi.org/10.3390/cryst12040555

Xiao H, Shi MW, Wang Q, Liu Q (2014) The electromagnetic shielding and reflective properties of electromagnetic textiles with pores, planar periodic units and space structures. Text Res J 84(16):1679–1691. https://doi.org/10.1177/0040517514527371

Yan Y, Yang H, Li J, Lu X, Wang C (2011) High value-added textiles: Nanotechnology and microsystems technology leading the way. Mater Technol 26(3):109–110. https://doi.org/10.1179/175355511X13032908978395

You J-L, Chen Y-S, Chang C-P, Wu M-Z, Ger M-D (2021) Utilizing a pH-responsive palladium nanocomposite to fabricate adhesion-enhanced and highly reliable copper coating on nylon 6 fabrics. J Market Res 15:3983–3994. https://doi.org/10.1016/j.jmrt.2021.10.053

Yu D, Kang G, Tian W, Lin L, Wang W (2015) Preparation of conductive silk fabric with antibacterial properties by electroless silver plating. Appl Surf Sci 357:1157–1162. https://doi.org/10.1016/j.apsusc.2015.09.074

Yuan X, Yin W, Ke H, Wei Q, Huang Z, Chen D (2022) Properties and application of multi-functional and structurally colored textile prepared by magnetron sputtering. J Ind Text 51(8):1295–1311. https://doi.org/10.1177/1528083719900671

Yuen CWM, Jiang SQ, Kan CW, Tung WS (2006) Textile metallisation. Textile Asia 37:33–35

Zakeri R, Zakeri R (2022) Bio inspired general artificial muscle using hybrid of mixed electrolysis and fluids chemical reaction (HEFR). Sci Reports 12(1):Article 1. https://doi.org/10.1038/s41598-022-07799-9

Zeng W, Shu L, Li Q, Chen S, Wang F, Tao X-M, Zeng W, Shu L, Li Q, Chen S, Wang F, Tao X-M (2014) Fiber-based wearable electronics: a review of materials, fabrication, devices, and applications. Adv Mater 26(31):5310–5336. https://doi.org/10.1002/ADMA.201400633

Zhong S, Yi L, Zhang J, Xu T, Xu L, Zhang X, Zuo T, Cai Y (2021) Self-cleaning and spectrally selective coating on cotton fabric for passive daytime radiative cooling. Chem Eng J 407:127104. https://doi.org/10.1016/j.cej.2020.127104

Chapter 8
Effect of Textile Structure on Heat Transfer Performance

Dan Wang, Shi Hu, Dana Křemenáková, Jiří Militký, and Guocheng Zhu

Abstract With the improvement in people's quality of life, the requirements for clothing are becoming more and more comprehensive. In the past, people paid more attention to the durability of clothing and the beauty of style. Nowadays, more and more people pay attention to the function and comfort of clothing, especially its thermal comfort performance. The thermal comfort of clothing is an interdisciplinary subject that studies the relationship between the human body, clothing, and the environment. The heat transfer performance of the clothing is an important indicator to describe the heat exchange between the human body and the environment. The main directions of clothing heat transfer performance research include textile materials, clothing styles, human body factors, and the influence of environmental factors on its heat transfer performance. This article will mainly analyze how textile materials' structure affects the heat transfer performance of clothing. Due to the diversity and complexity of textile materials, this paper only analyzes and discusses the structure of textile materials that affect the heat transfer performance of clothing. It will include the fineness of the fiber, the cross-sectional shape of the fiber, the fineness of the yarn, the twist turns of the yarn, the loop length of yarn, the structure of the fabric, and the structural parameters of the fabric.

D. Wang · S. Hu · D. Křemenáková · J. Militký (✉)
Department of Material Engineering, Faculty of Textile Engineering, Technical University of Liberec, Studentská 2, 46117 Liberec, Czech Republic
e-mail: jiri.militky@tul.cz

G. Zhu
Zhejiang-Czech Joint Laboratory of Advanced Fiber Materials, Zhejiang Sci-Tech University, Hangzhou 310018, China

8.1 Introduction

Heat transfer is the transfer of energy due to temperature differences, also known as heat transfer. Heat transfer is a complex phenomenon (Karamanos et al. 2004). From the second law of thermodynamics, it is known that whenever there is a temperature difference, heat is bound to be transferred from a high temperature to a low temperature, so heat transfer is an extremely common transfer phenomenon in nature and engineering technology (Carey et al. 2008). In essence, as long as there is a temperature difference within a medium or between two media, heat transfer must occur (Wooldridge and Luebbers 2020). We refer to different types of heat transfer processes as "heat transfer modes." The heat transfer process of an object is divided into three basic modes: heat conduction, heat convection, and heat radiation (Kaviany and Kanury 2002). The intermediate medium through which heat transfer takes place includes water, steam, oil, brine, glycol, etc. According to the temperature of heat transfer, they can be divided into two categories: high-temperature heat transfer media and low-temperature heat transfer media (Couper et al. 2005) (Fig. 8.1).

The phenomenon of heat transfer is ubiquitous, and its influence is present in almost all modern industrial sectors and also permeates many technical sectors such as agriculture and forestry (*Heat Transfer Fluids Applications Overview|Therminol*, n.d.). It can be said that it is difficult to find an industry, sector, or industrial process that has nothing at all to do with heat transfer, except in very rare cases. Not only traditional industrial fields, such as energy power, metallurgy, chemical industry, transportation, construction and building materials, machinery, as well as food, light industry, textile, medicine, etc., use a lot of knowledge about heat transfer, but also many high-tech fields, such as aerospace, nuclear energy, microelectronics, materials, biomedical engineering, environmental engineering, new energy, and agricultural engineering, also rely on the latest achievements of applied heat transfer research to varying degrees (Edreis and Petrov 2020). In some aspects, the development of heat transfer technology and related materials and equipment has even become a key factor in the success or failure of the whole system (Kazi 2015). Among the studies in textile science, heat transfer properties are a very important part of the research. Textiles are not only a necessity for human life but also a symbol of human progress and civilization (Bakola 2016). Its main function is to adapt to the natural environment, that is, to resist changes in the external temperature, and at the same time prevent various hazards from the outside to protect the human body. In addition, it also has the function of adapting to the social environment, such as the decoration function, the wearing function, the identification function, the decoration function, and so on (Kang et al. 2013). However, the basic function of textiles is to keep people

Fig. 8.1 Heat transfer sketch

warm when the ambient temperature is low, prevent heatstroke when the temperature is high, play a role in climate regulation, and maintain the thermal balance and thermal comfort of the human body in a thermal environment. With the continuous expansion of the geographical space that humans are involved in, the natural and man-made climate conditions that people are exposed to are more severe, which requires the development of special purpose work clothes and protective clothing under the guidance of the correct physiology and hygiene theory (Van Langenhove and Hertleer 2004). And with the development of the economy and the improvement of people's living standards, people's pursuit of clothing comfort is becoming increasingly intense. In addition to wearing comfortable work clothes and protective clothing at work, comfortable casual clothes are also required for leisure and sports. Therefore, the development of various casual wear and sportswear with different usage requirements can ensure people's physical and mental happiness and personal safety (Tabor et al. 2020). Therefore, an in-depth study of the relationship between textile structure and heat transfer performance can guide the development of clothing with excellent thermal and moisture comfort.

8.2   Basic Concept of Heat Transfer

Heat transfer is the process of energy exchange between objects due to a temperature difference (Guo et al. 2007). Heat transfer has three ways, including conduction, convection, and radiation. In conduction, heat flows through a material from a region of higher temperature to a region of lower temperature. This occurs because molecules in the warmer region are more energetic and collide with adjacent molecules, transferring their energy to them. This transfer of energy continues until the entire material reaches thermal equilibrium (Narasimhan 1999). Convection occurs when heat is transferred through a fluid, such as air or water, due to the movement of the fluid. This can happen through natural convection, which is the result of buoyancy forces caused by temperature differences, or forced convection, which occurs when a fluid is forced to move by an external means, such as a fan (Xu et al. 2019). Radiation occurs when energy is transferred through electromagnetic waves. Unlike conduction and convection, radiation can occur in a vacuum and does not require a medium for energy transfer. This type of heat transfer is responsible for the transfer of energy from the sun to the earth and the transfer of thermal energy between objects separated by a distance (Howell et al. 2020) (Fig. 8.2).

The heat exchange between the human body and the environment includes two parts: the heat exchange caused by the "temperature difference" between the environments, and the body energy exchange caused by the difference in vapor pressure or water vapor content between the environments. The sum of these two types of heat is the metabolic heat of the human body (Havenith et al. 2002). In the complex heat exchange process between the human body, clothing, and environment, clothing has both thermal resistance and thermal conductivity between the human skin and the environment (Khromova 2017). It means that the human body dissipates heat into or

Fig. 8.2 Methods of heat flow between the body and the environment
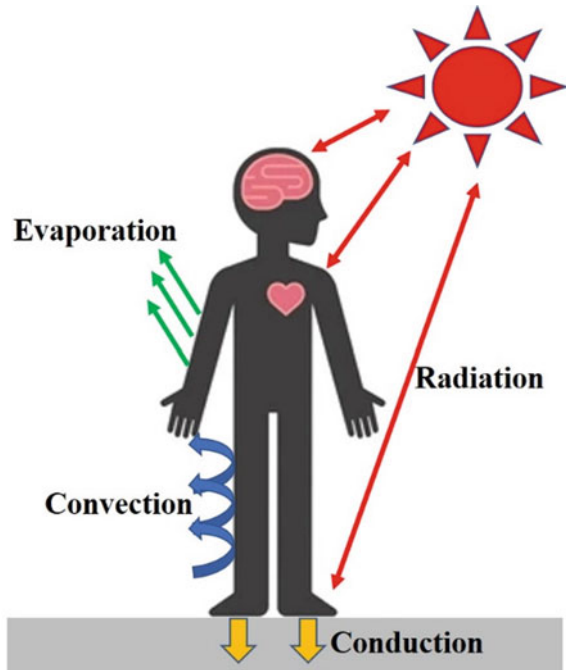
receives heat from the surrounding environment. While the human body produces radiant heat, it dissipates the heat outside the body in various ways so as to maintain the dynamic heat balance of the human body and maintain a constant body temperature (Fengzhi and Yi 2005). If people's metabolic heat production cannot dissipate in time after a hot summer or intense exercise, then the body temperature will increase by 2.5° in 2 h, and this consequence is conceivable (Maloney and Forbes 2011). There are several main pathways for heat flow from the body to the environment, or vice versa: conduction, convection, radiation, and evaporation (Ullah et al. 2022).

8.2.1 Heat Conduction

Heat conduction is the phenomenon of energy transfer through microscopic vibrations, displacements, and mutual collisions of molecules, atoms, and electrons inside an object when there is a temperature difference between different objects or within the same object. The mechanism of internal heat conduction varies in different phases of matter. The thermal conductivity inside a gas is mainly the result of its internal molecules doing irregular thermal motion as a result of mutual collisions. In non-conducting solids, vibration near the equilibrium position of their lattice structure transfers energy to neighboring molecules, thus achieving thermal conduction. Thermal conduction in metallic solids is accomplished by virtue of the movement

of free electrons between the lattice structures. The mechanism of heat conduction in liquids is similar to that of nonconductive solids (John n.d.). The heat conduction processes can be expressed as a diffusive process of phonons, i.e., energy-carrying particles. Let the phonons of density ρ_p, travel at velocity v along all directions, and are carrying energy u. They travel with time τ before the collision. Then the thermal conductivity λ can be described below:

$$\lambda = \frac{1}{3}\rho_p c \tau v^2 \tag{8.1}$$

where, c is the phonon heat capacity. The phonon velocity is often assumed to be sound velocity and τ is called phonon relaxation time. Macroscopically, heat conduction complies with Fourier's laws of heat conduction ("Thermal Conduction," 2023). One-dimensional steady flow of heat through an idealized circular solid homogeneous fiber with a length L, cross-sectional area A in the direction of the x-axis identical to the direction of the fiber axis due to the temperature difference ΔT is expressed by first Fourier's law:

$$q = -\lambda A \frac{\Delta T}{L} \tag{8.2}$$

where, q is the heat flux in the direction of the fiber axis x and λ is the thermal conductivity of the fiber. Thermal conductivity is an intensive property of materials characterizing their ability to transport heat. The negative sign means that the direction of the heat flux always follows the direction of temperature decrease (Fig. 8.3).

In the unsteady state, the one-dimensional heat flow is the heat flow (for the case of constant thermal conductivity independent of direction) expressed by a partial differential equation (modified second Fourier's law):

$$\frac{\partial T}{\partial t} = D_T \left(\frac{\partial^2 T}{\partial x^2} + \frac{\partial^2 T}{\partial y^2} + \frac{\partial^2 T}{\partial z^2} \right) + \frac{\O}{\rho c} \tag{8.3}$$

where, $\O$ is the internal heat source; x, y, z are coordinates; D_T is thermal diffusivity; c is specific heat at constant pressure; and t is time. In general, the thermal conductivity of solids is considerably higher than that of liquids. The thermal conductivity of most polymers is around 0.2–0.5 W·m^{-1}·K^{-1}. The thermal conductivity of water at 20 °C is 0.6 W·m^{-1}·K^{-1}, the thermal conductivity of ice at 0 °C is 2.24 W·m^{-1}·K^{-1} and the thermal conductivity of dry air at 0 °C is 0.024 W·m^{-1}·K^{-1}. More convenient

Fig. 8.3 Heat transport
through an idealized fiber
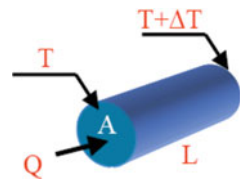
is characterization of textile structures heat conductivity by other variable thermal resistance directly connected with comfort. The thermal resistance of the material R is the reciprocal value of the amount of heat that passed per unit of time through the unit area at a unit temperature difference:

$$R = \frac{\Delta T}{Q} = \frac{h}{\lambda} \tag{8.4}$$

where, Q is the specific heat flow, λ is the thermal conductivity and h is the material thickness. Thermal resistance is typically an extensive quantity dependent on the thickness of the fabric. It is directly related to thermal comfort. To quantify thermal comfort, Gagge et al. proposed quantity *clo* (Gagge et al. 1941). One *clo* defines insulation thanks to a clothing system that provides comfort to a person sitting calmly in a normally ventilated room (air flow speed is 0.1 m/s) at a temperature $Ta = 21$ °C and a relative air humidity RH less than 50%. It is estimated that under these conditions 24% of metabolic heat is lost by evaporation from the skin surface. The total metabolic heat under these conditions is 1 *Met,* which is equivalent to 50 kcal·m^{-2}·h^{-1}, i.e., 58.153 W·m^{-2}. The remaining 76% of the metabolic heat, i.e., $Q_e = 44.1963$ W·m^{-2} (38 kcal·m^{-2}·h^{-1}), must be removed through the clothing by radiation, convection and conduction mechanisms. The temperature of the skin in a comfortable state is estimated as $Ts = 33$ °C. The total thermal resistance R_T (insulation) of the clothing and the surrounding insulating layer is then given by the relation:

$$R_T = \frac{T_s - T_a}{Q_e} = \frac{33 - 21}{44.1963} = 0.2715 (\text{K} \cdot \text{m}^2 \cdot \text{W}^{-1}) \tag{8.5}$$

The insulation of the air layer under the above conditions is $R_a = 0.12$ K·m^2·W^{-1}. Air conductivity $\lambda_a = 0.024$ W·m^{-1}·K^{-1} is an intensive variable. So, the thickness of the surrounding insulating air layer h_I is equal to:

$$h_I = \lambda_a R_a = 0.12 * 0.024 = 0.0028 \, [m] \tag{8.6}$$

Therefore, the insulation of the clothing system only is $R_O = R_T - R_a = 0.1515$, i.e., approximately 0.155 Km^{2}W^{-1}, i.e., 1 *clo.* The clothing insulation determined in this way is actually an effective insulation of the entire body. Knowing the *clo* value, the corresponding thermal conductivity can then be easily determined from the relationship as below:

$$\lambda = \frac{h}{R} = \frac{h}{0.155 \, clo} \tag{8.7}$$

Another thermal comfort unit *tog* is equal to 0.1 K·m^2·W^{-1}. One *clo* is equal to 1.55 *tog*, i.e., 0.155 K·m^2·W^{-1}. In general, thermal resistance $R = 0.155$ *clo.* Clothing intended for standard winter conditions has a *clo* of more than 1 and for

summer clothing the *clo* is around 0.5. Total value clo_{Tot} of multilayer clothing system is equal to sum of individual layers clo_i, i.e., $clo_{Tot} = \sum_i clo_i$.

8.2.2 Heat Convection

Heat convection refers to the internal molecular movement of the fluid, often occurring in the fluid or fluid and solid between the temperature difference occurs. Because the difference in temperature will make the different density between the fluid. When the liquid or gas is heated, the volume expansion causes the density to decrease. Then the material gradually rises, and the original position is supplemented by the surrounding low-temperature and high-density material. The material is then heated up again, and the surrounding material is supplemented. So, the cycle of heat from the fluid spreading everywhere is called heat convection (Li and Guo 2011). Heat convection is divided into natural convection and forced convection according to the different causes of flow. Natural convection is due to temperature differences caused by the different densities of different parts of the fluid and the natural up-and-down movement of convective heat transfer. Therefore, there is a temperature difference that does not necessarily occur in natural convection, and we should also consider whether the relative position of the surface can be formed due to temperature differences caused by the density difference in a fluid motion. When the temperature of a solid surface is higher than the ambient air temperature, the air above that surface becomes less dense when heated and rises freely, thus causing natural convection to occur. Below the surface, air immediately below the surface becomes less dense when heated, and it is difficult to produce free movement of air because it is blocked from accumulating under the surface so that no natural convection occurs. If the temperature of the solid surface is lower than the temperature of the ambient air, the air above is cooled and becomes denser, accumulating on the upper surface and preventing the free movement of air and natural convection. While the surface below is cool and the air is free to sink after being cooled, natural convection can occur. Forced convection is the convective heat transfer caused by the flow of fluid under the push of external forces. The degree of forced convection is much more intense than natural convection, and the vast majority of industrial applications are forced convection (Cooper and Kingery 1964). According to Newton's law of cooling, the heat flow by heat convection on the body surface when naked can be expressed as:

$$Q = h * A * (t' - t'') \tag{8.8}$$

where, h is convective heat transfer coefficient, A is body surface area, t' is average body surface temperature, and t'' is ambient temperature. The convective heat transfer coefficient is related to the convection method. When the air velocity is small, it is a function of temperature difference (natural convection); When the wind speed is large, it is a function of wind speed (forced convection). In addition, when the human body is dressed, the heat flow by heat convection can be expressed as:

$$Q_c = h * A_c * (t_c - t'')$$ (8.9)

where, h is convective heat transfer coefficient, A_c is clothing coverage area, t_c is external surface temperature of clothing, and t'' is ambient temperature. At ambient temperatures below $35°$, the above equation shows that the clothing acts as a barrier to convective heat transfer between the body and the environment. The clothing covers the body and restricts the flow of air on the body surface, and heat convection is necessarily reduced (Zhou and Zhang 2006). According to the above analysis, the structure of the clothing, including openings, slits, and looseness, all have an effect on heat convection (McQuerry et al. 2016).

8.2.3   Heat Radiation

Heat radiation is electromagnetic radiation generated by the thermal motion of particles in matter. All matter with a temperature greater than absolute zero emits heat radiation. Since electromagnetic waves propagate without any medium, heat radiation is the only way to transfer heat in a vacuum. In the concept of heat radiation, there is a special ideal surface called "blackbody." It absorbs all incident radiation, regardless of wavelength and direction; For a prescribed temperature and wavelength, no surface can emit more energy than a blackbody; The wavelength and temperature of a blackbody's radiation determine it, but its direction is unrelated. That is, the blackbody is a diffuse emitter. As the perfect absorber and diffuse emitter, the blackbody serves as a standard against which the radiative properties of actual surfaces are compared (Brewster 1992). The concept of emissive power is introduced to quantify the rate of radiation emitted per unit of surface area. The total emissive power, E (W/ m^2), is the rate at which radiation is emitted per unit area in all possible directions and at all possible wavelengths.

$$E = \int_0^\infty E_\lambda(\lambda)d\lambda$$ (8.10)

And the total emissive power of a blackbody can be expressed as:

$$E_b = \int_0^\infty E_{\lambda,b}d\lambda = \int_0^\infty \frac{C_1}{\lambda^5[\exp(\frac{C_2}{\lambda T}) - 1]}d\lambda$$ (8.11)

The result obtained from performing the integration is termed the Stefan–Boltzmann law having the form:

$$E_b = \sigma T^4$$ (8.12)

where the Stefan–Boltzmann constant has the numerical value $\sigma = 5.67*10^{-8}$ W/m^{2}K^4. This simple but important law enables the calculation of the amount of radiation emitted in all directions and over all wavelengths based on the knowledge of the blackbody temperature. In addition to this, to calculate the total emissive power of an actual object, it is necessary to know the emissivity of such an object. Emissivity is a physical quantity that describes the characteristics of a surface radiation source. The total emissivity, ε, is defined as the ratio of the total emissive power of a surface to that of a blackbody at the same temperature.

$$\varepsilon(T) \equiv \frac{E(T)}{E_b(T)} \tag{8.13}$$

Objects in the outward emission of radiation energy at the same time, but also will continue to absorb other objects around the emission of radiation energy and will be re-transformed into heat, this object between the mutual emission of radiation energy and absorption of radiation energy heat transfer process is called radiation heat transfer. If the radiation heat transfer is carried out between two objects with different temperatures, the result of the heat transfer is that the high-temperature object will be heated by the low-temperature object; if the temperature of the two objects is the same, the amount of radiation heat transfer between objects is equal to zero, but the radiation and absorption process between objects is still in progress (Bergman et al. 2011). Heat flow by heat radiation between naked human body and environment can be expressed as:

$$Q = \sigma * \varepsilon_\alpha * \varepsilon_\beta * \left(T_\alpha^4 - T_\beta^4\right) * A \tag{8.14}$$

where, σ is the Stefan–Boltzmann constant, ε_α is the emissivity of human body, ε_β is the emissivity of environment, T_α is the thermodynamic temperature of human body, T_β is the thermodynamic temperature of environment, and A is the effective radiation area. When the human body wears the garment, there is a change in the effective radiation area, and at this time the heat flow by heat radiation between the surface of the garment and the environment can be expressed as:

$$Q_c = \sigma * \varepsilon_c * \varepsilon_\beta * \left[(t_c + 273.15)^4 - \left(t_\beta + 273.15\right)^4\right] * A_c * f_c \tag{8.15}$$

where, σ is the Stefan–Boltzmann constant, ε_c is the emissivity of garment, ε_β is the emissivity of environment, t_c is the temperature of garment, t_β is the temperature of environment, A_c is the effective radiation area, and f_c is the effective radiation area coefficient (0.7 when standing, 0.65 when sitting still). In addition, when the ambient temperature is lower than 35 degrees, the surface temperature of the garment will be lower than the skin temperature, and the garment on the skin emits radiation plays a blocking role. On the contrary, when the ambient temperature is higher than 35 degrees, the surface temperature of the garment will be higher than the body surface

temperature, garment on the human body absorbs radiation heat also plays a role in blocking (Zhou and Zhang 2006).

8.3 Thermal Conductivity of Textile Structures

Based on the presentation of the above theory, the indices indicating the heat transfer properties of the textile material will be discussed in turn, including the thermal conductivity and thermal resistance. Thermal conductivity is defined as the heat transfer through one square meter area in a given time for a material with one-meter thickness and a temperature difference of one degree on both sides under stable heat transfer conditions. The measurement unit is watt/meter·degree. Different substances have different thermal conductivities; the thermal conductivity of the same substance is affected by its structure, density, humidity, temperature, pressure, and other factors. In general, solids have higher thermal conductivity than liquids, and liquids have higher thermal conductivity than gases. The difference between these two states is largely due to differences in molecular spacing. Special tests are used to determine the coefficient values used in engineering calculations. For textile materials, thermal conductivity indicates its ability to conduct heat. The lower the thermal conductivity, the worse the thermal conductivity, but the better the thermal insulation. The calculation of the thermal conductivity of textiles is also varied, and many mathematical models of thermal conductivity will be based on the geometry structure of different textile materials, which include fibers, yarns, and fabrics (Militkỳ and Křemenáková 2008, 2014). Thermal resistance is the ability of an object to resist heat transfer when temperatures differ. Generally, the higher the thermal conductivity of the textile material, the lower the thermal resistance. Thermal resistance is the resistance encountered when heat is transferred inside an object via thermal conduction. It is the reciprocal of the amount of heat passed through the unit cross-section of textiles with the unit temperature gradient in a unit of time. In general, the thermal resistance of a piece of fabric is h/λ. Where h is the fabric's thickness and λ is the fabric's thermal conductivity (Bivainytė et al. 2012; Majumdar et al. 2010).

8.3.1 Thermal Conductivity of Fibrous Polymers

The general theory for predicting the thermal conductivity of polymers has not yet been fully developed. A simple model based on the so-called phonon model of thermal conductivity of polymers is described by Krevelen and Hoftyzer (Van Krevelen and Te Nijenhuis 2009). Heat transport is realized in quanta of energy from one layer to another with the speed of sound. The amount of heat transferred is directly proportional to the density and heat capacity. The Debye equation is then commonly used to express the thermal conductivity (Sakiadis and Coates 1956):

$$\lambda = C_p * \rho * u * L \tag{8.16}$$

where, L is the distance between molecules in adjacent isothermal layers, and u is the speed of elastic waves (speed of air propagation). Assuming that L is approximately constant and independent of temperature, it follows that there is a direct relationship between the thermal diffusivity D_T and the air velocity u. The thermal conductivity of materials is temperature-dependent and can be expressed by a two-branch model (Bicerano 2002):

$$\frac{\lambda(T)}{\lambda(T_g)} = \left(\frac{T}{T_g}\right)^{0.22} \text{ for } T \leq T_g$$

$$\frac{\lambda(T)}{\lambda(T_g)} = 1.2 - 0.2\left(\frac{T}{T_g}\right) \text{ for } T > T_g \tag{8.17}$$

This model describes the experimental data relatively well. For amorphous polyethylene terephthalate, a value of 0.218 $W \cdot m^{-1} \cdot K^{-1}$ was found and for amorphous polypropylene a value of 0.172 $W \cdot m^{-1} \cdot K^{-1}$ was found. Thermal conductivity of crystalline polymers increases due to intense interaction between chain sections. Thermal conductivity of highly crystalline polymers are strongly dependent on temperature (Eiermann 1964) found for highly crystalline polymers such as polyethylene and polypropylene (100% crystalline) a simple relationship:

$$\lambda = \frac{210}{T} \tag{8.18}$$

The thermal conductivity of these highly regular crystalline polymers at room temperature is then around 0.71 $W \cdot m^{-1} \cdot K^{-1}$ and for the same amorphous polymers, the thermal conductivity is only around 0.17 $W \cdot m^{-1} \cdot K^{-1}$. For regular polymers, a simple relationship can also be used as below:

$$\frac{\lambda_c}{\lambda_{am}} = \left(\frac{\rho_c}{\rho_a}\right)^6 \tag{8.19}$$

The thermal conductivity of crystalline polymers can therefore be determined if the density ratio $\rho c/\rho a$ is known. For less regular crystalline polymers, it is possible to use the relation (Van Krevelen and Te Nijenhuis 2009):

$$\frac{\lambda_c}{\lambda_{am}} = 1 + 5.8\left(\frac{\rho_c}{\rho_a} - 1\right) \tag{8.20}$$

The calculated thermal conductivity of semi-crystalline polyethylene terephthalate with a degree of crystallinity of 0.4 correlates well with the experimental value of 0.272 $W \cdot m^{-1} \cdot K^{-1}$ (Bicerano 2002).

8.3.2   Thermal Conductivity of Fibres

The thermal conductivity of textile fibers is generally directionally dependent due to special morphology as a result of drawing and thermal treatment. Thermal conductivity along the fiber axis is much higher due to the orientation and close arrangement of polymeric chains (refer to Table 8.1).

The thermal conductivity of textile fibers is generally related to their chemical composition, preparation technology, porosity, and moisture content. For a standard atmosphere with a relative humidity of RH 65%, there are changes in the moisture content of hydrophilic fibers. For cotton fibers, the relationship between wetness RE%, the moisture content in the air RH%, and temperature T is expressed approximately in the form below:

$$RE = (0.8067 + 0.02912RH)\sqrt[4]{100 - T} \tag{8.21}$$

This relationship can be used for the $RE < 85\%$ range. The wetness RE is defined as the relative weight of water (the difference between the weight at a given humidity W of the air and the dry weight D) related to the weight of the dried material D:

$$RE = 100\frac{W - D}{D} \tag{8.22}$$

Wetness is directly related to the water content of MC fibers defined as the weight of water relative to the total weight at a given air humidity:

$$MC = 100\frac{W - D}{W} \tag{8.23}$$

It is easy to determine the relation as following:

Table 8.1   Thermal conductivity along the fiber axis and fiber radial

Name of fiber	Thermal conductivity along the fiber axis [W/m·K]	Thermal conductivity along the fiber radial [W/m·K]
Cotton	1.13	0.16
Ramie	1.66	0.21
Mulberry silk	0.83	0.16
Mohair	0.35	0.17
Polyester	0.97	0.19
Polyamide	0.59	0.27
Acrylic	0.74	0.22
Viscose	0.72	0.19

$$MC = \frac{RE}{1 + (\frac{RE}{100})} \qquad (8.24)$$

For standard laboratory conditions, it is cotton wetness equal to 8.0734%. Due to the high thermal conductivity of water, the thermal conductivity of cotton under standard laboratory conditions is higher than in the dry state. Haghi published thermal conductivities for a number of typical fibers. He found a value of $0.518 \text{ W·m}^{-1}\text{·K}^{-1}$ for non-porous polypropylene fibers and $0.288 \text{ W·m}^{-1}\text{·K}^{-1}$ for porous acrylic fibers (Haghi 2003). For hydrophilic fibers, the thermal conductivity depends on the wetness $RE\%$. Haghi proposed a linear relationship between thermal conductivity and wetness for cotton fibers. However, this model has an order of magnitude errors, as Rengasamy and Kawabata found a value of $0.352 \text{ W·m}^{-1}\text{·K}^{-1}$ for dry cotton fibers (Rengasamy and Kawabata 2002). A simple linear mixing rule was used to predict the thermal conductivity of cotton fibers as a function of moisture content as below:

$$\lambda_{cot}(MC) = \left(1 - \frac{MC}{100}\right)\lambda_{cot} + \frac{MC}{100}\lambda_{water} \qquad (8.25)$$

where, λ_{cot} is the thermal conductivity of dry cotton determined in work and λ_{water} is the thermal conductivity of water. If different fibers are mixed, when fiber A has a mass fraction of b_r and fiber B has a mass fraction of $1 - b_r$, the upper limit of the thermal conductivity of the mixture of fibers can be determined from a simple relation:

$$\lambda_{AB} = b_r\lambda_A + (1 - b_r)\lambda_B \qquad (8.26)$$

If the fiber mixture consists of wet components, the thermal conductivities of the wet fibers must first be determined.

8.3.3 Thermal Conductivity of Yarns

Yarns are the basic component of fabrics and knitwear. Fabrics are composed of warp (fineness T_C) and weft (fineness T_M) yarns. For idealized circular yarns with constant packing density, it is possible to determine the diameter of the yarn from the relation as following:

$$d_C = \frac{2\sqrt{T_C}}{\sqrt{10^6 \pi \rho_C}} \qquad (8.27)$$

$$d_M = \frac{2\sqrt{T_M}}{\sqrt{10^6 \pi \rho_M}} \qquad (8.28)$$

where, ρ_C and ρ_M are warp and weft yarn densities. These densities are a combination of fiber density ρ_F and air density ρ_A with regard to yarn packing density or the arrangement of fibers in yarns. For a known packing density of warp yarns μ_M, ρ_M equal to $\mu_M \rho_F$ and a similar relationship is valid for weft yarns. The values of yarn densities ρ_C and ρ_M are therefore a function of twist and yarn production technology. For the mid-level twist, it was found to be approximately:

$$\frac{\rho_C}{\rho_F} = \mu_C \approx 0.525 \tag{8.29}$$

This correction can be used to calculate d_C and d_M. The porosity of yarn P_Y can be simply expressed by the relation as below:

$$P_Y = 1 - \mu_c \tag{8.30}$$

To calculate the thermal conductivity of yarns λ_Y, models based on the combination of the thermal conductivity of air and fibers with the introduction of a correction for their orientation are used:

$$\lambda_Y = \lambda_f + \frac{\lambda_a - \lambda_f}{1 + \frac{1 - P_Y}{P_Y}\left[1 + z\frac{\lambda_a - \lambda_f}{\lambda_a + \lambda_f}\right]} \tag{8.31}$$

where, $z = 1$ for all fibers are oriented perpendicularly to the heat flow direction, $z = 2/3$ for random fiber orientation, and $z = 5/6$ for the half of the fibers are randomly oriented and half are perpendicular to the heat flow direction. Based on preliminary tests, it is appropriate to choose $z = 1$. The calculation of the thermal conductivity of the yarns can be omitted if the density definition of the porosity of flat textiles is used (Militký and Křemenáková 2008).

8.3.4 Thermal Conductivity of Fabrics

To calculate the thermal conductivity of flat textiles, the thermal conductivity of yarns and the porosity of planar textiles can be used, or only the density definition of the porosity of planar textiles and the thermal conductivity of fibers are sufficient. Especially for fabrics, the basic structural parameters are the weft sett D_C and the warp sett D_M, the areal weight W_P, and the fabric thickness t_W. For an idealized arrangement of yarns in a fabric, the thickness t_I is equal to d_C plus d_M, where d_C is the diameter of the weft threads and d_M is the diameter of the warp threads. If $t_W \approx t_I$, the yarns in the fabric have an approximately circular cross-section. Fabric porosity can be divided into three categories: Macro-porosity related to the spaces between warp and weft yarns; Meso-porosity related to the arrangement of fibers in yarns; Micro porosity related to voids and pores in fibers. The volumetric porosity is partly

Fig. 8.4 Idealized
projection of the surface of
fabrics
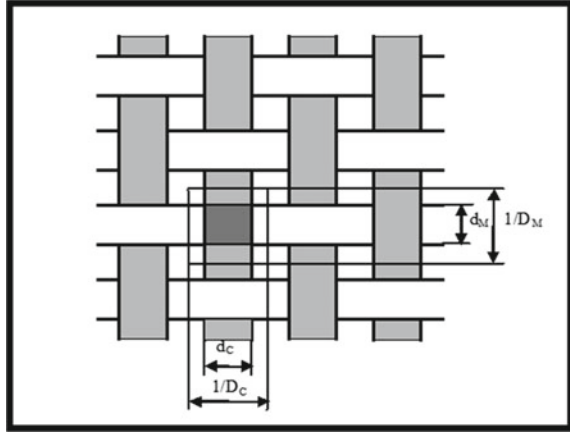
based on the idealized structure of the textile surface as shown in the projection in
Fig. 8.4.

A fabric unit cell (structural element) contains sections of curved weft and warp
yarns. The volumes and lengths of these sections of yarn are calculated from the
relationships given in the work (Militký and Havrdová 2001). The corrected volume
porosity is calculated from the relation as follows:

$$P_V = 1 - \frac{\pi\left[d_C^2 D_C \sqrt{1.16 d_C^2 D_C^2 + 1} + d_M^2 D_M \sqrt{1.16 d_M^2 D_M^2 + 1}\right]}{4(d_M + d_c)} \qquad (8.32)$$

Based on the Fig. 8.4, the surface macro-porosity of P_S can be easily defined
using the relation (Cay et al. 2007):

$$P_S = 1 - CF \qquad (8.33)$$

where CF is the fabric coverage defined by the relation:

$$CF = D_C d_C + D_M d_M - d_C d_M D_C D_M \qquad (8.34)$$

The total porosity can be determined for all types of surface textiles using only
their areal weight W_P and thickness t_W according to the relationship (Militký and
Havrdová 2001):

$$P_D = 1 - \frac{W_P}{\rho_F t_W} \qquad (8.35)$$

For the case of wet fabrics, the areal weight and thickness of the fabric in the
wet state must be used. For these purposes, the wet fiber density must be calculated

Fig. 8.5 Limit arrangement
of yarns (black) and air
(grey) in thermal
conductivity models
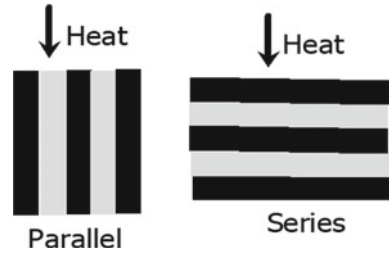
from the dry fiber density and the water density. The thermal conductivity of planar
textiles can be easily predicted on the basis of two-phase models consisting of yarns
with thermal conductivity λ_Y and air with thermal conductivity λ_a. The proportion
of the air phase corresponds to the P_V porosity and the proportion of the yarn phase
is $1 - P_V$. The lower limit of the thermal conductivity then corresponds to the
serial arrangement of the phases, and the upper limit of the thermal conductivity
corresponds to the parallel arrangement (refer to Fig. 8.5).

The upper limit of the thermal conductivity λ_P corresponding to the parallel
arrangement is calculated from the relation:

$$\lambda_P = P_V \lambda_Y + (1 - P_V)\lambda_a \tag{8.36}$$

The lower limit of the thermal conductivity λ_s corresponding to the series
arrangement is calculated from the relation:

$$\lambda_s = \frac{\lambda_a \lambda_Y}{P_V \lambda_a + (1 - P_V)\lambda_Y} \tag{8.37}$$

In real textiles, it is advantageous to calculate the effective thermal conductivity
as a linear combination of upper and lower limits:

$$\lambda_{PS} = \frac{\lambda_P + \lambda_S}{2} \tag{8.38}$$

In many cases it is advantageous to calculate the effective thermal conductivity
as a geometric mean:

$$\lambda_G = \lambda_Y^{P_V} \lambda_a^{1-P_V} \tag{8.39}$$

Equations (8.36), (8.37) and (8.39) are special cases of general mixing rule for
the selected parameter n ($n = 1, 0, -1$).

$$\lambda_O = \sqrt[n]{P_V \lambda_Y^n + (1 - P_V)\lambda_a^n} \tag{8.40}$$

Fig. 8.6 Dependence of thermal conductivity of PES fabric on its P_d porosity predicted by different mixing models
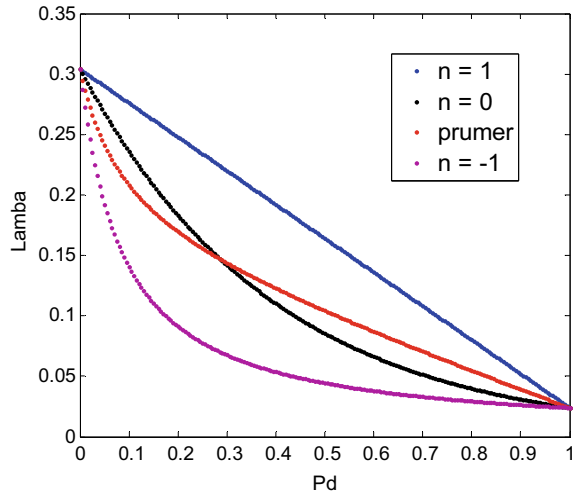
The simulated dependence of the thermal conductivity of PES fabric on its porosity predicted using different mixing models is shown in Fig. 8.6. In this figure, the upper limit of the thermal conductivity is shown in blue, the lower limit is shown in purple, and the geometric mean is shown the black and red lines correspond to the arithmetic mean of the lower and upper limits. It can be seen that these are monotonically convex decreasing functions and for porosities above 0.5 the thermal conductivity decreases by more than 2/3.

An overview of other multiphase models is given in a paper (Wang and Pan 2008). For the case of all types of planar textiles, all the above-mentioned mixing models can be used. With the fact that instead of volume porosity P_V, density porosity P_D is used, and instead of yarn conductivity λ_Y, fiber conductivity λ_f. This makes it possible to easily calculate the effect of hollow fibers or moisture on the effective thermal conductivity of planar textiles.

8.4 Relationship Between Textile Structure and Heat Transfer

The factors affecting the heat transfer properties of textiles have been explored in depth by an increasing number of scholars. Broadly speaking, it consists of two factors, one is the performance of the textile itself, and the other is the environmental factor. For the performance of the textile itself, which contains the thermal conductivity of the fibers and the structure of the fibers, yarns, and fabrics. It is of practical importance to study and measure the thermal conductivity of fiber aggregates. It should be noted that the thermal conductivity of fiber aggregates is the combined value of the irregularly arranged aggregate state, i.e., the value of the mixture of fiber,

air, and moisture. Table 8.2 shows the thermal conductivity of several fiber aggregates measured at an ambient temperature of 20 degrees and a relative humidity of 65%. As can be seen from Table 8.2, the thermal conductivity of water is the largest and the thermal conductivity of still air is the smallest, so air is the best thermal insulator. Therefore, the warmth of the fiber material aggregate depends mainly on the amount of still air and water maintained between the fibers, i.e., the more still air, the better the warmth, and the more water, the worse the warmth (Pang 2013). The influence of the structure of the textile on its heat transfer properties is the focus of this article. It will include the fineness of the fiber, the cross-sectional shape of the fiber, the linear density of the yarn, the loop length of the yarn, the twist turns of the yarn, the structure of the fabric, and the structural parameters of the fabric. This part will be analyzed and discussed in the subsequent sections.

In addition, environmental factors also affect the heat transfer performance of textiles, including ambient temperature and humidity, wind speed, and atmospheric pressure. The thermal conductivity of still air increases by 0.00009 W/m·K for every 1-degree increase in ambient temperature. The study shows that when the ambient temperature increases by 8 degrees, the thermal resistance of a down jacket with a basic thermal resistance of 0.95 clo increases by 0.015 clo, which is only equivalent to the increase in the thermal resistance of a small undershirt. Therefore, the change in ambient temperature does not have a significant effect on the thermal resistance of the garment and can be completely ignored in practical applications. This conclusion mentioned above can be authenticated from the studies of scholars such as Mohanapriya Venkataraman. This group of researchers observed the changes in the thermal conductivity as well as the thermal resistance of the fabric samples by varying the ambient temperature. The results showed that the thermal conductivity of the samples increased by only 0.0012 W/m·K and the thermal resistance decreased by only 0.0063 m^2·K/W when the ambient temperature was increased from -25 to 25 degrees Celsius (Mohanapriya et al. 2014). Determining the thermal resistance of heat protective clothing under room temperature conditions, if used in a high temperature environment, the thermal resistance increases with the rise of the external temperature, which can reduce the heat transfer from the environment to the human body, which is beneficial to the thermal protection of the human body. In the determination of the anticold clothing under normal temperature conditions, the thermal resistance value decreases due to the low temperature of the actual use environment, but the decrease is small. It is found that there are two kinds of moisture in textile materials: one is hygroscopic moisture, which is due to the hygroscopicity

Table 8.2 Thermal conductivity of different fibres

Name	Thermal conductivity [W/m·K]	Name	Thermal conductivity [W/m·K]
Cotton	0.071–0.073	Polyester	0.084
Wool	0.052–0.055	Polyamide	0.244–0.337
Silk	0.050–0.055	Acrylic	0.051
Still air	0.026	Water	0.697

of textile fibers in the atmosphere to absorb water vapor gathered on the surface of the fiber, usually expressed in terms of moisture regain; the other is intermediate moisture, which is filled with water droplets in the space between yarns and spreads along the yarn fiber due to capillary phenomena, thus forming capillary moisture. The hygroscopic moisture is often present, and the intermediate moisture exists only when the textile is soaked by sweat or rain and when the ambient humidity is high. The hygroscopic moisture in textile fibers does not actually change the volume of voids between yarns, but the effect of intermediate moisture on textile materials can be significant. This is because it will fill the voids between the yarns and squeeze out the still air or even dead cavity air in them, thus making the textile lose its insulating properties. Wind speed is also a major factor affecting the heat transfer performance of textiles. In an outdoor environment, winds of 1 to 5 m/s are frequent, and it makes the thermal resistance of the air layer on the outer surface of the textile 50% to 70% lower than when it is indoors. Secondly, wind can also penetrate directly into the porous and loose textile interior, disturbing the still air between the yarns. Wind can also compress the textile locally and change the thickness of its air layer, all of which will result in lower thermal resistance. In highland areas and at high altitudes, as the atmospheric pressure decreases, the air density decreases, the air density between textile fibers and yarns also decreases, the thermal conductivity decreases, and thus the thermal resistance increases. This situation is beneficial to the plateau area to prevent cold and keep warm. And the next sections will elaborate on the influence of the structure of textile materials on their heat transfer properties (Huang 2008).

8.4.1 Fiber Fineness

Fiber fineness refers to the degree of fiber thickness expressed by the diameter of the fiber or the size of the cross-sectional area. In more cases, often due to the irregular shape of the fiber cross-section and the existence of cavities, gaps, and pores that cannot be accurately expressed in terms of diameter, cross-sectional area, or other indicators, the customary use of mass per unit length or length per unit mass to express the fiber fineness is appropriate. The important indicators to express fiber fineness are linear density, denier, metric count, and imperial count. When using the linear density and geometric thickness to express fiber fineness, the larger the value, the thicker the fiber; when using the length per unit mass of fiber to express fiber fineness, the larger the value, the finer the fiber (Geng et al. 2022). It can be found that an increase in the linear density results in higher thermal resistance, lower thermal conductivity, and lower thermal absorptivity in the study of R. K. Varshneya et al. In the course of the experiment, this group of researchers used polyester fibers in circular cross-sections of four different fineness, i.e., 1.33, 1.55, 1.66, and 2.22 dtex. This is caused by an increase in the size of the air gaps that are trapped inside the fabric sample, which reduces the amount of heat that passes through the fabric (Varshney et al. 2010).

8.4.2 Fiber Cross-Sectional Shape

The cross-sectional shape of fibers varies with the type of fiber, with natural fibers having various forms and chemical fibers obtaining variously shaped cross-sections depending on the spinnerets. As the cross-sectional shape of fibers varies, their mechanical properties, thermal properties, optical properties, and comfort level will also change. For example, the modulus of elasticity of profiled fibers is higher than that of round cross-sections, so it is more resistant to deformation and has a good anti-wrinkle effect. Fiber luster also has a greater relationship with fiber cross-sectional shape. When a parallel beam of light is irradiated on the surface of fibers with different cross-sectional shapes, different luster effects will occur. For a triangular cross-section, when the light shines on it, that can be transmitted out onto the prism inside the fiber, so the luster at the prism that produces total reflection is weak, while the luster outside the other prism is strong. When the angle of incidence changes, the prism that produces total reflection also changes, resulting in a shimmering effect. In addition, the profiled fibers can also reduce the pilling phenomenon and enhance the dyeing effect. After fiber deformation, the pilling phenomenon is greatly reduced because the surface area of the fiber increases, and the holding force between fibers in the filament increases. Due to the larger surface area, the coloring speed is accelerated, and the dyeing rate increases significantly (Karaca and Ozcelik 2007; Wang et al. 2012; Zhang et al. 2021) (Fig. 8.7).

In the study of R. K. Varshneya et al., four cross-sectional shapes (circular, trilobal, scalloped oval, and tetrakelion) of the polyester fiber were selected to test the heat transfer performance. According to the findings, more noncircular fibers are being used in place of circular fibers, which results in fabrics with higher porosity and more internal still air. Lead to higher thermal resistance, poorer thermal conductivity and absorptivity, and a warmer overall feel (Varshney et al. 2010). A similar study occurred in an experiment by Guocheng Zhu and other researchers. This group of researchers investigated the effect of inclusion shape on the effective thermal conductivity of heterogeneous materials, which included square, rectangular, circular, and elliptical shapes. The results showed that the heterogeneous materials with elliptical
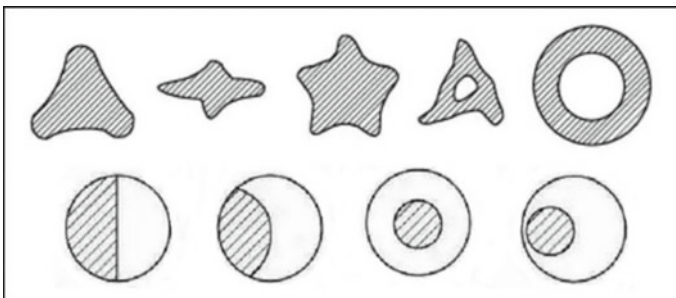

Fig. 8.7 Illustration of the profiled fiber cross-section

inclusions had the smallest effective thermal conductivity and the heterogeneous materials with rectangular inclusions had the largest effective thermal conductivity. Therefore, it can be shown that the shape of the inclusions is an important factor influencing effective thermal conductivity (Zhu et al. 2014). In another study by a group of Uludag University scholars, they compared the heat transfer properties of solid as well as hollow fibers. When compared to fabrics made with solid fibers, the heat conductivity was higher in fabrics made with hollow fibers. As a result, the fabrics made from hollow fibers had inferior thermal insulation properties. In comparison to fibers with the same fiber count, hollow fibers have a larger outer dimension. It is generally known that hollow fibers display strong insulation qualities when utilized in a random manner insulation materials. The current study, however, demonstrated that the covering and total porosity features of the woven textiles outweighed the impacts of inter-fiber pores in the yarn when the hollow fibers were spun into yarns and later used in the fabrication of woven fabrics. As a result, the hollow fibers' anticipated insulating characteristics were not seen, and even the opposite outcomes in terms of thermal properties were obtained (Karaca et al. 2012). But the opposite result was obtained in the test results of another group of researchers. Guocheng Zhu and other researchers tested the thermal conductivity of fibers with the same fiber diameter but different hollow diameters, and the results showed that the effective thermal conductivity of their fibers decreased as the hollow diameter of the fibers increased. Simulation of predicted thermal conductivity of fabric composed from hollow polyester fibers with porosities P_o is shown in Fig. 8.8. It is clear that the hole (central cavity) in the fibers is of practical importance only for textiles with a density porosity of less than approx. 0.65 and for cases where a material with relatively high thermal conductivity is used. For density porosities above 0.7, the volume of the hole in the fibers has practically no effect on the change in total thermal conductivity, i.e., the total thermal conductivity of the textile is close to the thermal conductivity of air. This result demonstrates the expected insulating properties of hollow fibers. Based on the results of the above two cases, it can be seen that the heat transfer properties of the hollow fiber itself and its thermal conductivity when woven into fabric cannot be generalized (Zhu et al. 2013).

8.4.3 Yarn Fineness

It is also known as linear density or yarn count and refers to the thickness or thinness of a yarn. It is usually expressed as the number of length units per unit mass of the yarn. The most commonly used units for yarn fineness are tex, denier, cotton count, and worsted count. The "tex" system is based on the weight in grams of 1,000 m of yarn. A yarn with a tex count of 10, for example, would weigh 10 g per 1,000 m of length. The "denier" system is based on the weight in grams of 9,000 m of yarn. A yarn with a denier count of 100, for example, would weigh 100 g per 9,000 m of length. The "cotton count" system is used for cotton yarns and is based on the number of hanks of 840 yards each that weighs one pound. A higher cotton count
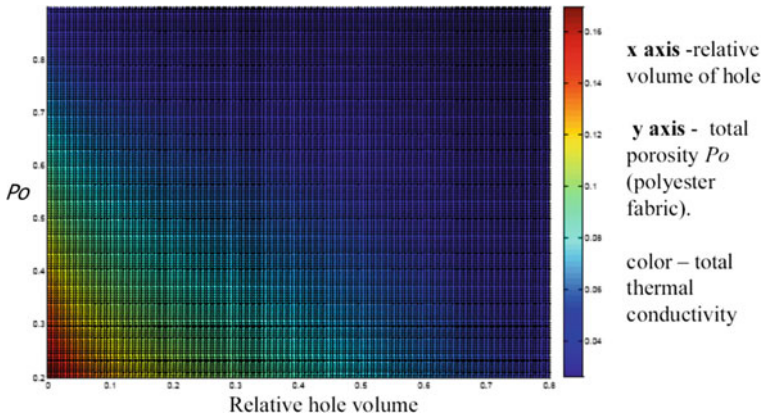
Fig. 8.8 Predicted thermal conductivities of fabric from hollow fibers

indicates a finer yarn, with more hanks of 840 yards required to make a pound of yarn. For example, a cotton count of 40 means that 40 hanks of 840 yards each weigh one pound. The "worsted count" system is used for wool yarns and is based on the number of hanks of 560 yards each that weighs one pound. A higher worsted count indicates a finer yarn, with more hanks of 560 yards required to make a pound of yarn. For example, a worsted count of 80 means that 80 hanks of 560 yards each weigh one pound (Woodhouse 2021). The fineness of yarn affects the characteristics of the fabric made from it, such as its drape, strength, texture, and appearance. Finer yarns produce smoother, softer, and more lustrous fabrics, while coarser yarns create more textured and durable fabrics. The appropriate yarn fineness depends on the intended use of the fabric and the desired properties of the final product (Akgun 2015; Aydoğdu and Yilmaz 2020). In the study of Nilgün Özdil et al., a kind of 1 × 1 rib structure was knitted using 100% combed cotton yarns in three different yarn counts (Ne 20, Ne 30, and Ne 40) and with the same twist coefficient to test the heat transfer performance. The thermal resistances of the fabrics knit with Ne 20/1–Ne 40/1 and Ne 30/1–Ne 40/1 differed significantly, per statistical analysis, from one another. In order to compare the thermal resistance properties of different materials, it was discovered that as the yarn gets finer, both thermal resistance and thermal conductivity decline. In fact, it was generally anticipated that thermal resistance and thermal conductivity would exhibit an inverse relationship. Yet, the test findings showed that thermal conductivity also diminishes as much as thermal resistance does. The fabric's thickness may provide an explanation for this paradox. Fabric thickness reduces as yarn diameter increases when finer yarn is used. The thermal resistance also decreases if the thickness loss is greater than the loss in thermal conductivity (Özdil et al. 2007). In addition to the researchers mentioned above who reached this conclusion, there are other groups of researchers who also obtained the same results. For example, researchers from Bahir Dar University also obtained these results using different counts of cotton yarn. And there are also scholars from India, Chidambaram

Prakash and Govindan Ramakrishnan, who have also studied the effect of the linear density of yarn on thermal comfort properties. In their study, cotton, bamboo fibers, and blends of both fibers (100% cotton, 50:50 bamboo/cotton, 100% bamboo) were spun into yarns with linear densities (the 20 s, 25 s, and 30 s Ne), and the above results were also obtained in the end (Atalie et al. 2022).

8.4.4 Loop Length

It is a term used in textile manufacturing to describe the length of a loop in a knitted fabric or a pile fabric. It is measured from the base of the loop to the point where the yarn re-enters the fabric. Loop length can vary depending on the type of fabric being produced, the yarn being used, and the knitting or weaving process. In general, loop length can affect the texture, appearance, and properties of the fabric. For example, fabrics with shorter loop lengths may have a smoother texture and be more compact, while fabrics with longer loop lengths may have a more open, fluffy texture. In textile manufacturing, loop length is controlled through various techniques, such as adjusting the tension on the knitting or weaving machine, changing the gauge of the machine, or using different yarns. The desired loop length depends on the intended use of the fabric and the desired properties of the final product (Chidambaram et al. 2011; Pavko-Cuden et al. 2013). In the study of several scholars from the National Textile University of Pakistan, it can be found that the loop length of yarn is directly proportional to the thermal resistance and thermal conductivity of the fabric. This is due to the increase in air gap due to the increase in the loop length of the yarn, the result is a decrease in stationary air and an increase in flowing air. This ultimately leads to an increase in the thermal conductivity of the fabric. The increase in fabric thermal resistance is due to the increase in loop length resulting in an increase in fabric thickness and a decrease in fabric porosity, caused by the combined effect of the above two aspects (Afzal et al. 2017). And scholars from India, Chidambaram Prakash, and Govindan Ramakrishnan have also studied the effect of the loop length of yarn on thermal comfort properties. In their study, cotton, bamboo fibers, and blends of both fibers were spun into yarns with loop lengths (2.7, 2.9, and 3.1 mm), and the same results were obtained as above (Prakash and Ramakrishnan 2013).

8.4.5 Yarn Twist

It refers to the spiral arrangement of fibers in a yarn. It is created by twisting individual fibers or plies of yarn together, causing them to interlock and form a cohesive strand. The number of twists in a yarn can affect its strength, durability, appearance, and texture. There are different methods for measuring yarn twists, but one common approach is to count the number of twists per unit length of the yarn. The unit of twist can vary depending on the system being used, but common units include turns

per inch or turns per meter. The number of twists in yarn can affect its properties in different ways. In general, a higher twist level can increase the strength and durability of the yarn, as well as its resistance to abrasion and pilling. However, a higher twist can also make the yarn stiffer and less pliable, which may affect its drape and feel. Conversely, a lower twist can create a softer, more pliable yarn, but it may also be weaker and more prone to pilling. The appropriate level of twist for a yarn depends on the intended use of the fabric or textile product and the desired properties of the final product. For example, a high-twist yarn may be more suitable for sturdy, durable fabrics such as denim or corduroy, while a lower-twist yarn may be more appropriate for softer, more delicate fabrics such as silk or cashmere (Kolte et al. 2017; Ozkaya et al. 2010). Five different varieties of plain-woven cotton fabrics were created using weft yarns with 900, 905, 910, 915, and 920 twists per meter in the study by Desalegn Atalie et al. The samples' other parameters, including count, thread density, and fabric structures, were left unchanged. Thermal conductivity and thermal resistance measurements were used to assess the fabric's thermal characteristics. The result shows that thermal conductivity increased with the increase in twist turns. This could be due to the higher twist turns, more flowing air available in the fabric, and thus more heat transfer through convection. The fabrics with lower twist turn, leading to more still air will be entrapped inside, then reducing the thermal conductivity of the fabrics. As still air has the lowest thermal conductivity value compared to any fiber, it is the still air included in the fabric structure that has the most impact on the thermal conductivity value in textile materials. The fabric's thermal resistance dropped as the twist turns rose from 900 to 920 twists per meter, demonstrating significantly the twist turns of the yarn influences the fabric's thermal resistance. This may be because the yarns are more compact at higher twist turns, resulting in less thickness and reduced thermal resistance (Atalie et al. 2018).

8.4.6 Woven and Knit Fabric

Woven fabric and knit fabric are two types of textiles that are commonly used in the fashion and apparel industry. They differ in terms of their structure, production method, appearance, and properties. Woven fabric is made by interlacing two sets of yarns at right angles to each other, creating a stable and structured fabric. The two sets of yarns are known as the warp and the weft, and they are interlaced by a machine known as a loom. Woven fabrics tend to be more durable and stable than knit fabrics, and they can have a wide range of textures, patterns, and finishes. Knit fabric, on the other hand, is made by interlocking loops of yarn together, creating a stretchy and flexible fabric. Knit fabrics are made using knitting machines, which can produce different types of knit structures, such as jersey, rib, and cable knits. Knit fabrics tend to be more comfortable and breathable than woven fabrics, and they are often used for garments that require stretch and flexibility, such as activewear, underwear, and socks (Kiron 2021). The influence of fabric structure on heat transfer is mainly that the fabric structure will affect the structure of the void, that is, the

content of still air, thus affecting heat conduction. In addition, for clothing fabrics, the convective transfer of heat transfer through the microclimate under the fabric will also be affected by the difference in the pores in the fabric. In the pure dry state, when the fabric density and thickness are the same, the heat transfer performance of woven and knitted fabrics is basically the same. However, during use, since the human skin is constantly removing sweat, even in a comfortable environment, there will be no obvious sweat discharge, and the discharged sweat needs to be diffused into the surrounding air through the fabric. Especially in hot summer, the microclimate under the fabric has a lot of sweat to keep it in a humid state. The heat transfer performance of woven fabrics is better than that of knitted fabrics. This is because: woven fabrics are interwoven with warp and weft yarns, with compact structure, less static air, and high thermal conductivity; The pores are large, there is more static air, and the thermal conductivity is small. When the water vapor is wet, the yarn expands, and the thickness increases, so the warmth retention of knitted fabrics is better than that of woven fabrics. This is why people wear cool woven fabrics in summer and warm knitted fabrics in winter (Pang 2013).

8.4.7 Thickness of Fabric

The fabric's thickness is measured in millimeters and represents the fabric's actual thickness when put under a specific amount of pressure. The use of the fabric and technical specifications mostly define the fabric's thickness. Wearability characteristics are greatly influenced by the fabric's thickness. For instance, the fastness, thermal performance, air permeability, wind resistance, rigidity, and drape are all influenced by the fabric's thickness (Kamalha et al. 2013). The fabric will be squeezed to varying degrees when the inspector touches it. Hence, when gauging the fabric's thickness, the measurement parameters must be precisely defined. The characteristics, size, presser foot pressure, presser foot drop speed, reading duration, etc., of the thickness meter, for instance, will all have an impact on the test findings for fabric thickness. More thought should go into selecting a smaller pressure when measuring some highly flexible textiles (Yao 2015). Researchers from Dalian Polytechnic University 2015, led by Ju Wei, used the KES-F7 thermal Lab II equipment to investigate the relationship between the thickness and heat transfer performance of woven and knitted fabrics, including cotton, ramie, wool, and polyester. The value of fabrics' thermal resistance exhibits a trend that initially rises and then tends to hold steady as thickness increases (Wei et al. 2015). Similar tests were carried out in 1998 by the University of Otago scholars C. A. Wilson et al. They discovered that thermal resistance followed suit when fabric thickness increased. Yet, once fabric thickness increased to a certain point, the thermal resistance actually began to drop somewhat (Wilson et al. 1999). These both serve as examples of the thickness-based law of thermal resistance. The thickness of the conduction medium is inversely correlated with conduction heat, according to thermophysical theory. Only the predicted fabric thickness is used when the influence of materials is not taken into account.

Fig. 8.9 Dependence of
fabric thermal conductivity
on thickness for various
planar mass
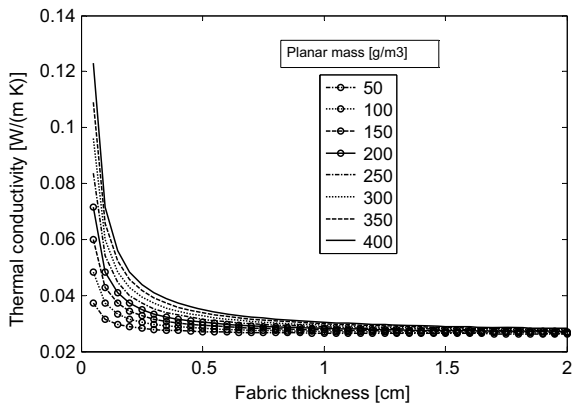
The estimation relationship can be expressed as h/λ. Yet, the fabric's thermal resistance actually significantly diminishes when its thickness rises to a certain point. This is due to the fact that thicker fabrics contain more still air. Since still air has a significantly lower thermal conductivity than fibers, the thermal resistance will rise as the fabric's thickness does. However, as fabric thickness increases, two things happen: on the one hand, flowing air within the fabric increases, and flowing air has a much higher thermal conductivity than still air; on the other hand, the fabric's voids expand, and the effect of convective heat transfer on total heat transfer becomes more pronounced. As a result, the fabric's ability to provide thermal insulation starts to decline as its thickness grows (Shi 2001). Researchers from Technical University of Liberec, simulated the dependence of polyester fabric thermal conductivity on thickness for various planar masses is shown in Fig. 8.9 (Militky et al. n.d.). It is visible that for sufficient fabric thickness are thermal conductivities of fabric are very low and approaching the thermal conductivity of air. For low planar mass are thermal conductivities of fabric relatively low for small thickness as well. They also researched the influence of fabric geometric parameters, i.e., planar mass *GSM* and thickness on the thermal conductivity of polyester fabric is shown in Fig. 8.10 (Militky et al. n.d.). It is visible that for the sufficient thickness of the fabric is thermal conductivity very low independent of planar mass. Therefore, the insulation properties can be simply tuned by the thickness of the fibrous layer.

8.4.8 Density of Fabric

The mass per unit area of a two-dimensional object is used to determine its area density, which is also referred to as areal density, surface density, mass thickness, density thickness, and other terms. Kilogram per square meter (kg/m^2) is the unit derived from the SI (International System of Units). It is known as grammage in the textile industry and is measured in grams per square meter (g/m^2) ("Area Density,"
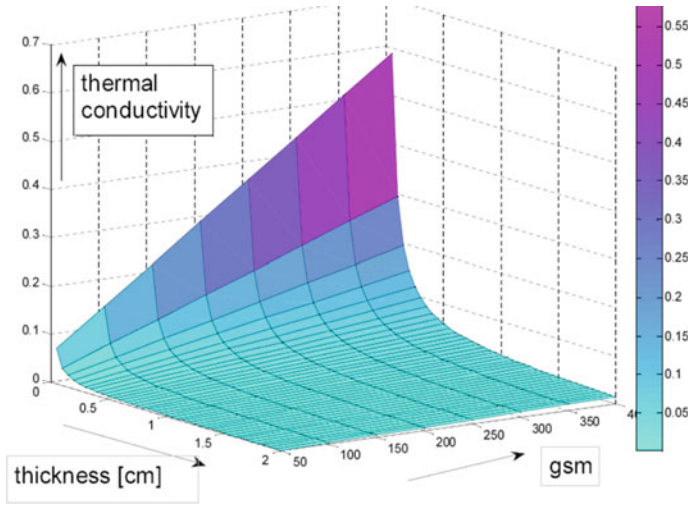
Fig. 8.10 Influence of fabric planar mass GSM and thickness on thermal conductivity

2022). The primary fabric design criterion and a crucial component of fabric cost accounting is the fabric's areal density. The following formula is the calculation method of fabric areal density:

$$\text{Areal density} = \text{Weight (g)}/\text{Length} \times \text{Width (m}^2) \tag{8.41}$$

The mass per unit volume of a substance is referred to as volume density. Grams per cubic centimeter (g/cm^3) is the unit of measurement used in the textile industry. It is associated with fabric thickness and has an impact on a variety of fabric characteristics, including bulkiness, thermal qualities, and breathability, among others ("Density," 2023). The following formula is the calculation method of fabric volume density:

$$\text{Volume density} = \text{Weight (g)}/\text{Length} \times \text{Width} \times \text{Thickness} \left(cm^3\right) \tag{8.42}$$

The relationship between areal density and the heat transfer performance of fabrics has also been the subject of extensive research by academics. Three of them, from the University of Monastir, have investigated the connection between the areal density and thermal resistance of woven materials. The trapped air in the woven structure explains why the woven fabric's ability to increase areal density also increases thermal resistance. As a result, the structure's air volume increases as the woven surface area increases. The air has significant insulating qualities, and as its volume increases, its structure becomes more thermally resistant and its heat conductivity decreases (Halaoua et al. 2019). In addition to the aforementioned instance, a number of other academics from the University of Zagreb have worked in a similar direction, however, their research items were knitted fabrics instead of other materials

Fig. 8.11 Dependence of
fabric thermal conductivity
on planar mass for various
small fabric thicknesses
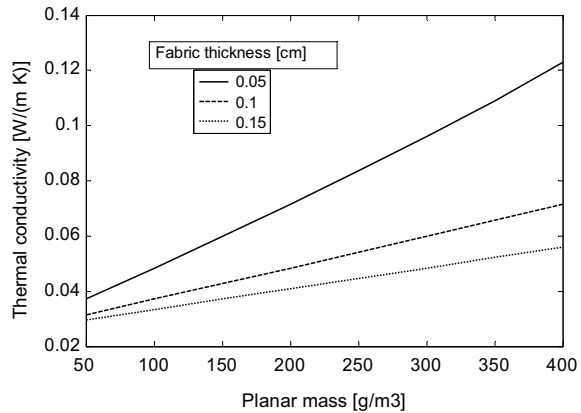
(Čubrić et al. 2012). By experimentation, they also came to the same conclusion
as in the previous experiment: Heat resistance increases along with areal density.
It can be inferred from some past research that, within a specific range, there is a
positive link between the fabric's areal density and its heat resistance. The relation-
ship between areal planar mass and the heat transfer performance of fabrics has also
been researched by the researchers from Technical University of Liberec. The simu-
lated dependence of PES fabric thermal conductivity on planar mass for selected
fabric thicknesses is shown in Fig. 8.11. For the same thickness sample, the thermal
conductivities of fabric became higher following the planar mass higher (Militky
et al. n.d.).

8.4.9 Porosity of Fabric

Porosity, also known as pore fraction, is a physical property that describes a material's
pores. The volume of pores to the overall volume of the material is represented as a
percentage, ranging from 0 to 100%. Openings or pores related to apertures are more
useful in the application since they can let liquid in. The effective porosity is therefore
frequently described as the volume of the openings divided by the material's total
volume, and it is either lower or equal to the total porosity. There are numerous ways
to gauge a material's porosity and effective porosity. Optical porosity and volume
porosity are the two categories into which porosity in textile engineering is always
classified. This characteristic will rely on the caliber of the photos captured and is
more suited for transparent textiles. Since the optical porosity parameters are two-
dimensional, the thickness and length of the pores are disregarded, and only the
smallest transparent portion of the pores is seen. It will provide details on porosity,
including the quantity, size, and dispersion of pores. There is currently a large range
of imaging equipment, such as microscopes and scanners, that can be employed in a
variety of settings. Moreover, software for image processing is available separately, as

open-source software, or as a component of microscope software, including Image analysis and Image J. The percentage of air in a material body's total volume is known as volume porosity. The equation listed below can be used to express it. The air volume in the body can either be made up of a portion of larger pores or a portion of smaller pores, therefore it cannot provide enough criteria to compare various materials, particularly with regard to their permeability (Kostajnšek et al. 2021; Angelova 2012). As a result, additional porosity-related factors including pore numbers, diameters, and dispersion must be taken into account. These variables relate to the fabric's permeability and offer specific details on the interior geometry of the material. The following formula is the calculation method of fabric volume porosity:

$$\text{Volume porosity} = \frac{V_{\text{air}}}{V_{\text{fabric}}} = 1 - \frac{V_{\text{fiber}}}{V_{\text{fabric}}} = 1 - \frac{\rho_{\text{fabric}}}{\rho_{\text{fiber}}} \tag{8.43}$$

Several academics studied the relationship between the fabric's porosity and its heat transfer properties. In 2015, Matthew P. Morrissey and Rene M. Rossi, two researchers from the EMPA Swiss Federal Materials Laboratory for Materials science and technology, carried out related tests. When the optical porosity of the mid-layer was appropriately high, they discovered that the rise in thermal resistance was the largest. They then examined the thermal resistance of various combinations of commercial fabrics (Morrissey and Rossi 2015). Many academics from Malaysia and Singapore examined the same topic in 2021, but their findings differed slightly. Several knitted materials and non-woven fabrics were used in their investigation. The experimental findings demonstrate that as porosity rises, most textiles' thermal resistance will generally decrease. One type of needle-punched cotton nonwoven, however, demonstrated the opposite outcome; it has both a high thermal resistance and a high porosity (Al-Hakimi et al. 2021). Researchers like Dragana Kopitar of the University of Zagreb researched the heat resistance of another polypropylene nonwoven structure in 2014, and their investigation produced the finding that the fabric's thermal resistance increases as the porosity decreases. It goes against the findings of the two earlier investigations (Kopitar et al. 2014). It is possible to conclude that the relationship between porosity and heat resistance cannot be generalized based on the findings of the three sets of experiments mentioned above. Porosity is first separated into optical and volume porosities. Based on the correlation between two porosities and thermal resistance, the same fabric can have various properties. Second, the connection between porosity and heat resistance can be radically opposite for fabrics made from different raw materials but using the same processing method, or from the same raw material but using various processing methods. Finally, the principles governing the relationship between porosity and thermal resistance can also vary greatly depending on the type of fabric. There is a correlation between heat resistance and the still air held in the pores, even if it is too tough to determine the rules between porosity and thermal resistance. The fabric's heat resistance will rise as the porosity does if the pores are filled with still air. On the other hand, convective air forms in the fabric's pores, and as the porosity rises, so does its thermal resistance. In conclusion, it is important to investigate the relationship between porosity and heat

resistance based on the amount of air present in the pores (Shi 2001; Křemenáková et al. 2017). In addition to this, Guocheng Zhu and other researchers used mathematical models to calculate the effect of the effective pore size of nonwoven fabrics on their thermal performance. As the pore size inside the nonwoven increases, the radiation heat transfer becomes stronger. The effective thermal conductivity increases with increasing pore size while keeping the thickness of the nonwoven constant. The increased effective thermal conductivity is due to the increased radiative heat transfer. When the effective pore diameter is greater than 2 mm, the conduction and radiation heat transfer ratios are almost the same (Zhu, Křemenáková, et al. 2015a, b). At the same time, they obtained similar experimental results in real tests. As the pore size in the fabric increases, the thermal resistance of the fabric decreases (Zhu, Kremenakova, et al. 2015a, b). But when the porosity is the same, the pore size and pore distribution don't play significant roles in thermal performance (Guocheng et al. 2012).

8.4.10 Evenness of the Fabric Surface

The front and back surfaces of woven, knitted, and non-woven materials are flat when viewed macroscopically. But, when viewed in detail, they exhibit unevenness and certain regular patterns on both sides. These lumps are scattered in many directions, some of which are radial, some of which are latitudinal, and some of which are irregular. Furthermore, differences are its height and period. Surface evenness for woven and knitted materials typically ranges between 0.1 and 0.3 mm (Yao 2015). The fabric will also be generally uneven when it shrinks to varied degrees in specific localized areas. This occurrence is categorized as having an uneven appearance. The majority of the time, two-dimensional image processing technology is used to measure fabric evenness. With the advancement of three-dimensional scanning technology, scanner costs are now decreasing and accuracy is rising, offering a new approach to the objective assessment of fabric evenness (Liu et al. n.d.). In response to this circumstance, a number of Ph.D. students from Pakistan's National Textile University completed two relevant studies. In the initial study, flat and seersucker textiles with differing surface appearances were woven using the same basic materials. The thermal resistance experiment was then conducted, and the findings revealed that seersucker had nearly twice the thermal resistance of flat clothing (Shaker et al. 2019). The only fabric used in the second trial was seersucker, but it had different tube courses and puckered stripe heights. The outcome demonstrates that seersucker cloth gains insulation as tube courses or puckered stripe height are increased. The likelihood of the tube's two plies being farther apart and having more trapped air increases with tube size. More gaps and a looser structure will increase the thermal resistance of the fabric because the thermal conductivity values of fibers are higher than those of trapped air. Less puckered cloth has lower thermal resistance, which may be explained by the presence of air spaces between the fabric and the skin. As a good heat insulator,

air contributes to improved thermal insulation (Basra et al. 2020). From the afore-mentioned two examples, it is clear that a fabric's surface irregularity on a regular basis can enhance the material's thermal resistance, which in turn affects the fabric's thermal performance.

8.5 Conclusion

The heat transfer performance of fabrics is an important factor related to human comfort. Through the analysis of the factors affecting the heat transfer performance of fabrics, it can provide important technical references for textile companies to develop new products, and improve the warmth retention of fabrics. From the above research and investigation, it can be found that an increase in the linear density of fiber results in higher thermal resistance, and lower thermal conductivity. This is caused by an increase in the size of the air gaps that are trapped inside the fabric sample, which reduces the amount of heat that passes through the fabric. In contrast, the yarn is finer, its thermal resistance and thermal conductivity are lower. In fact, it was generally anticipated that thermal resistance and thermal conductivity would exhibit an inverse relationship. Yet, the test findings showed that thermal conductivity also diminishes as thermal resistance does. The fabric's thickness may provide an explanation for this paradox. Fabric thickness reduces as yarn diameter increases when the finer yarn is used. The thermal resistance also reduces if the thickness loss is greater than the loss in thermal conductivity. The effect of fiber cross-sectional shape on its thermal transfer performance is a very complex issue. Since the shape of the fiber cross-section varies, it is difficult to find the relevant law, so it is necessary to analyze the specific problem. In addition to that, it can be found that the loop length of yarn is directly proportional to the thermal resistance and thermal conductivity of the fabric. This is due to the increase in air gap due to the increase in the loop length of the yarn, the result is a decrease in stationary air and an increase in flowing air. This ultimately leads to an increase in the thermal conductivity of the fabric. The increase in fabric thermal resistance is due to the increase in loop length resulting in an increase in fabric thickness and a decrease in fabric porosity, caused by the combined effect of the above two aspects. It also shows that thermal conductivity increased with the increase in the twist turns. This could be due to the higher twist turns, the more flowing air available in the fabric, and thus more heat transfer through convection. The fabrics with lower twist turn, leading to more still air will be entrapped inside, then reducing the thermal conductivity of the fabrics. As still air has the lowest thermal conductivity value compared to any fiber, it is the still air included in the fabric structure that has the most impact on the thermal conductivity value in textile materials. On the contrary, the fabric's thermal resistance dropped as the twist turns increased demonstrating significantly that the twist turns of the yarn influence the fabric's thermal resistance. This may be because the yarns are more compact at higher twist turns, resulting in less thickness and reduced thermal resistance. Additionally, it can be deduced that the thermal resistance of the fabric increases as the fabric's

thickness increases, but the increase rate exhibits a trend of rapid increase followed by slow increase; after a particularly critical point, the thermal resistance of the fabric will exhibit a slight downward trend as the fabric's thickness increases. It can be inferred from some past research that, within a specific range, there is a positive link between the fabric's areal density and its heat resistance. The relationship between the fabric porosity and thermal resistance can't be summed up. The porosity is divided into optical porosity and volume porosity. The same texture of the fabrics can be distinctive of thermal resistance depending on two kinds of porosities. Furthermore, for fabrics with different raw materials but the same processing method or the same raw material but different processing methods, the relationship between porosity and thermal resistance can be completely different. And the relationship between porosity and thermal resistance can likewise be very complicated guidelines for the various texture's fabrics. It very well may be viewed as too hard to even consider tracking down the relationship between porosity and thermal resistance. When the porosity is the same, the pore size and pore distribution don't play significant roles in thermal performance. If the porosity is not considered, the thermal resistance of the fabric will decrease as the pore size becomes larger. The association between the evenness of the fabric and the heat resistance is the most obvious from the study findings that are currently known. As can be observed, the regular unevenness of the fabric surface can make it more thermally resistant than fabric with a flat surface, which in turn affects the fabric's thermal performance. Based on the analysis of all the above elements and the summary, it can be seen that the study of the heat transfer theory of textiles has been an important branch of research in textile, material, and thermal-related disciplines. It helps to explain the thermal phenomena of textiles and is also important for the development of textiles.

References

Afzal A, Ahmad S, Rasheed A, Ahmad F, Iftikhar F, Nawab Y (2017) Influence of fabric parameters on thermal comfort performance of double layer knitted interlock fabrics. Autex Res J 17(1):20–26

Akgun M (2015) Effect of yarn filament fineness on the surface roughness of polyester woven fabrics. J Eng Fibers Fabr 10(2):155892501501000220

Al-Hakimi MTA, Hani AA, Didi GMQ, Amirah NA (2021) Porosity and thermal resistance properties of needle-punched nonwovens cotton and polyester. AIP Conf Proc 2347(1):020115

Angelova R (2012) Determination of the pore size of woven structures through image analysis. Open Eng 2(1):129–135

Area density (2022) Wikipedia. https://en.wikipedia.org/w/index.php?title=Area_density&oldid=1118955473

Atalie D, Gideon R, Melesse G, Ferede E, Getnet F, Nibret A (2022) Thermo-physiological comfort of half bleached woven fabrics made from different cotton yarns parameters. J Nat Fibers 19(13):5034–5049

Atalie D, Tesema AF, Rotich GK (2018) Effect of weft yarn twist level on thermal comfort of 100 per cent cotton woven fabrics. Res J Text Appar 22(3):180–194. https://doi.org/10.1108/RJTA-11-2017-0049

Aydoğdu SHÇ, Yilmaz D (2020) Effect of yarn fineness and core/sheath fibre types on the physical properties of dual-core yarns and fabrics. Cellul Chem Technol 54(3–4):381–394

Bakola E (2016) Textile symbolism and the "wealth of the earth": Creation, production and destruction in the "tapestry scene" of Aeschylus' Oresteia (Ag. 905–78). In: Harlow M, Nosch M-L, Fanfani G (eds) Spinning fates and the song of the loom: the use of textiles, clothing and cloth production as metaphor, symbol and narrative. Oxford, pp 115–136.

Basra SA, Azam Z, Asfand N, Anas S, Iftikhar K, Irshad MA (2020) Development of interlock knitted seersucker fabric for better comfort properties. J Eng Fibers Fabr 15:1558925020963009

Bergman TL, Bergman TL, Incropera FP, DeWitt DP, Lavine AS (2011) Fundamentals of heat and mass transfer. Wiley

Bicerano J (2002) Prediction of polymer properties. CRC Press

Bivainytė A, Mikučionienė D, Kerpauskas P (2012) Investigation on thermal properties of double-layered weft knitted fabrics. Mater Sci 18(2):Article 2. https://doi.org/10.5755/j01.ms.18.2.1921

Brewster MQ (1992) Thermal radiative transfer and properties. Wiley

Carey VP, Chen G, Grigoropoulos C, Kaviany M, Majumdar A (2008) A review of heat transfer physics. Nanosc Microscale Thermophys Eng 12(1):1–60. https://doi.org/10.1080/15567260801917520

Cay A, Atav R, Duran K (2007) Effects of warp-weft density variation and fabric porosity of the cotton fabrics on their colour in reactive dyeing. Fibres Text East Europe 15:91–94

Chidambaram P, Govind R, Venkataraman KC (2011) The effect of loop length and yarn linear density on the thermal properties of bamboo knitted fabric. AUTEX Res J 11(4):102–105

Cooper AR Jr, Kingery WD (1964) Dissolution in ceramic systems: i, molecular diffusion, natural convection, and forced convection studies of sapphire dissolution in calcium aluminum silicate. J Am Ceram Soc 47(1):37–43. https://doi.org/10.1111/j.1151-2916.1964.tb14638.x

Couper JR, Penney WR, Fair JR, Walas SM (eds) (2005) Heat transfer and heat exchangers (Chap. 8). In: Chemical process equipment, Second edn. Gulf Professional Publishing, pp 165–224. https://doi.org/10.1016/B978-075067510-9/50040-1

Čubrić IS, Skenderi Z, Mihelić-Bogdanić A, Andrassy M (2012) Experimental study of thermal resistance of knitted fabrics. Exp Thermal Fluid Sci 38:223–228

Density (2023) Wikipedia. https://en.wikipedia.org/w/index.php?title=Density&oldid=1140142021

Edreis E, Petrov A (2020) Types of heat exchangers in industry, their advantages and disadvantages, and the study of their parameters. IOP Conf Ser: Mater Sci Eng 963(1):012027. https://doi.org/10.1088/1757-899X/963/1/012027

Eiermann K (1964) Thermal conductivity of high polymers. J Polym Sci Part C: Polym Symp 6(1):157–165

Fengzhi L, Yi L (2005) Effect of clothing material on thermal responses of the human body. Modell Simul Mater Sci Eng 13(6):809

Gagge AP, Burton AC, Bazett HC (1941) A practical system of units for the description of the heat exchange of man with his environment. Science (New York, N.Y.) 94(2445):428–430. https://doi.org/10.1126/science.94.2445.428

Geng Q, Zhou C, Nie K, Lv W, Ben H, Han G, Jiang W (2022) Relationship between fiber fineness and diameter of three bast fibers. J Nat Fibers 19(13):5496–5503. https://doi.org/10.1080/15440478.2021.1877233

Guo Z-Y, Zhu H-Y, Liang X-G (2007) Entransy—a physical quantity describing heat transfer ability. Int J Heat Mass Transf 50(13):2545–2556. https://doi.org/10.1016/j.ijheatmasstransfer.2006.11.034

Guocheng Z, Jiri M, Yan W, Mishra R, Sayed I, Dana K (2012) The effect of the pore size and pores distribution on the thermal insulation of fibers and fiber bundles. In: 19th International Conference Structure and Structural Mechanics of Textiles, Liberec, Czech Republic, December 2012

Haghi AK (2003) Factors effecting water-vapor transport through fibers. J Theor Appl Mech 30:277

Halaoua S, Romdhani Z, Jemni A (2019) Effect of textile woven fabric parameters on its thermal properties. Ind Text 70(1):15–20

Havenith G, Holmér I, Parsons K (2002) Personal factors in thermal comfort assessment: clothing properties and metabolic heat production. Energy Build 34(6):581–591. https://doi.org/10.1016/S0378-7788(02)00008-7

Heat Transfer Fluids Applications Overview|Therminol (n.d.). https://www.therminol.com/applications

Howell JR, Mengüç MP, Daun K, Siegel R (2020) Thermal radiation heat transfer, 7th edn. CRC Press. https://doi.org/10.1201/9780429327308

Huang J (2008) Clothing comfort. China Science and Technology Publishing and Media Co., Ltd. https://book.sciencereading.cn/shop/book/Booksimple/show.do?id=B251419C63937438BAB4B536537EF0C2C000

Kamalha E, Zeng Y, Mwasiagi JI, Kyatuheire S (2013) The comfort dimension; a review of perception in clothing. J Sens Stud 28(6):423–444

Kang J-YM, Johnson KKP, Kim J (2013) Clothing functions and use of clothing to alter mood. Int J Fash Des Technol Educ 6(1):43–52. https://doi.org/10.1080/17543266.2012.762428

Karaca E, Kahraman N, Omeroglu S, Becerir B (2012) Effects of fiber cross sectional shape and weave pattern on thermal comfort properties of polyester woven fabrics. Fibres & Text East Europe 3(92):67–72

Karaca E, Ozcelik F (2007) Influence of the cross-sectional shape on the structure and properties of polyester fibers. J Appl Polym Sci 103(4):2615–2621. https://doi.org/10.1002/app.25350

Karamanos A, Papadopoulos A, Anastaselos D (2004) Heat transfer phenomena in fibrous insulating materials

Kaviany M, Kanury A (2002) Principles of heat transfer. Appl Mech Rev 55(5):B100–B102. https://doi.org/10.1115/1.1497490

Kazi SN (2015) Heat transfer: studies and applications. BoD – Books on Demand

Khromova IV (2017) Heat exchange in "human body—thermal protection—environment" system. J Phys: Conf Ser 891(1):012084. https://doi.org/10.1088/1742-6596/891/1/012084

Kiron MI (2021). Difference between woven and knitted fabric. Textile Learner, 17 November 2021. https://textilelearner.net/difference-between-woven-and-knitted-fabric/

Kolte P, Patil KR, Sing K, Daberao A (2017) Effect of twist on yarn properties. Int J Text Eng Process 3:19

Kopitar D, Skenderi Z, Mijović B (2014) Study on the inuence of calendaring process on thermal resistance of polypropylene nonwoven fabric structure. J Fiber Bioeng Inf 7(1):1–11. https://doi.org/10.3993/jfbi03201401

Kostajnšek K, Zupin Ž, Hladnik A, Dimitrovski K (2021) Optical assessment of porosity parameters in transparent woven fabrics. Polymers 13(3):408

Křemenáková D, Militký J, Venkataraman M, Mishra R (2017) Thermal insulation and porosity—from macro- to nanoscale. In Šesták J, Hubík P, Mareš JJ (eds) Thermal physics and thermal analysis: from macro to micro, highlighting thermodynamics, kinetics and nanomaterials. Springer International Publishing, pp 425–448. https://doi.org/10.1007/978-3-319-45899-1_20

Lienhard JH (n.d.) A heat transfer textbook, 5th edn. https://ahtt.mit.edu/

Li Z-X, Guo Z-Y (2011) Optimization principles for heat convection. In Wang L (ed) Advances in transport phenomena 2010. Springer, pp 1–91. https://doi.org/10.1007/978-3-642-19466-5_1

Liu C, Gan M, Zheng W (n.d.) Comparative study of feature extraction for fabric smoothness

Majumdar A, Mukhopadhyay S, Yadav R (2010) Thermal properties of knitted fabrics made from cotton and regenerated bamboo cellulosic fibres. Int J Therm Sci 49(10):2042–2048. https://doi.org/10.1016/j.ijthermalsci.2010.05.017

Maloney SK, Forbes CF (2011) What effect will a few degrees of climate change have on human heat balance? Implications for human activity. Int J Biometeorol 55(2):147–160. https://doi.org/10.1007/s00484-010-0320-6

McQuerry M, Denhartog E, Barker R, Ross K (2016) A review of garment ventilation strategies for structural firefighter protective clothing. Text Res J 86:727–742. https://doi.org/10.1177/0040517515595029

Militký J, Havrdová M (2001) Porosity and air permeability of composite clean room textiles. Int J Cloth Sci Technol 13(3/4):280–289. https://doi.org/10.1108/09556220110396533

Militkỳ J, Křemenáková D (2008) Thermal conductivity of wool/pet weaves. In: HEFAT 2008

Militky J, Kremenakova D (2014) Prediction of thermal comfort of multilayer protective clothing. In: 7th international textile, clothing & design conference, Dubrovnik, Croatia, 10 August 2014

Militky J, Zhu G, Kremenakova D (n.d.) Thermal conductivity of textiles containing advanced fibres. In: Proceedings of 8th international conference on TEXSCI 2013. TEXSCI 2013, Liberec, Czech Republic

Mohanapriya V, Rajesh M, Jakub W, Ahmed MA, Jiří M, Arumugam V (2014) Innovative techniques for characterization of nonwoven insulation materials embedded with aerogel. Int J Mater Metall Eng 8(9). World Academy of Science, Engineering and Technology. https://doi.org/10.5281/zenodo.1094545

Morrissey MP, Rossi RM (2015) The effect of metallisation, porosity and thickness on the thermal resistance of two-layer fabric assemblies. J Ind Text 44(6):912–923

Narasimhan TN (1999) Fourier's heat conduction equation: history, influence, and connections. Rev Geophys 37(1):151–172. https://doi.org/10.1029/1998RG900006

Özdil N, Marmaralı A, Kretzschmar SD (2007) Effect of yarn properties on thermal comfort of knitted fabrics. Int J Therm Sci 46(12):1318–1322. https://doi.org/10.1016/j.ijthermalsci.2006.12.002

Ozkaya YA, Acar M, Jackson MR (2010) Yarn twist measurement using digital imaging. J Text Inst 101(2):91–100. https://doi.org/10.1080/00405000802263476

Pang F (2013) Factors affecting heat transfer properties of fabrics. Text Ind Technol 2:21–24

Pavko-Cuden A, Hladnik A, Sluga F (2013) Loop length of plain single weft knitted structure with elastane. J Eng Fibers Fabr 8(2):155892501300800220

Prakash C, Ramakrishnan G (2013) Effect of blend ratio, loop length, and yarn linear density on thermal comfort properties of single jersey knitted fabrics. Int J Thermophys 34(1):113–121

Rengasamy R, Kawabata S (2002) Computation of thermal conductivity of fibre from thermal conductivity of twisted yarn. Indian J Fibre Text Res 27:342–345

Sakiadis BC, Coates J (1956) Prediction of specific heat of organic liquids. AIChE J 2(1):88–93

Shaker K, Umair M, Jabbar M, Baitab DM, Nawab Y, Afzal A, Ahmad S (2019) Effect of fabric structural design on the thermal properties of woven fabrics. Therm Sci 23(5 Part B):3059–3066

Shi H (2001) The review of heat transmisson mechanism of the textiles. J Nantong Inst Technol 17(4):44–47

Tabor J, Chatterjee K, Ghosh TK (2020) Smart textile-based personal thermal comfort systems: current status and potential solutions. Adv Mater Technol 5(5):1901155. https://doi.org/10.1002/admt.201901155

Thermal conduction (2023) Wikipedia. https://en.wikipedia.org/w/index.php?title=Thermal_conduction&oldid=1140734954

Ullah HMK, Lejeune J, Cayla A, Monceaux M, Campagne C, Devaux É (2022) A review of noteworthy/major innovations in wearable clothing for thermal and moisture management from material to fabric structure. Text Res J 92(17–18):3351–3386

Van Krevelen DW, Te Nijenhuis K (eds) (2009) Properties of polymers, Fourth edn. (1972). In: Properties of polymers, Fourth edn. Elsevier, p vii. https://doi.org/10.1016/B978-0-08-054819-7.00047-9

Van Langenhove L, Hertleer C (2004) Smart clothing: a new life. Int J Cloth Sci Technol 16(1/2):63–72. https://doi.org/10.1108/09556220410520360

Varshney RK, Kothari VK, Dhamija S (2010) A study on thermophysiological comfort properties of fabrics in relation to constituent fibre fineness and cross-sectional shapes. J Text Inst 101(6):495–505

Wang M, Pan N (2008) Predictions of effective physical properties of complex multiphase materials. Mater Sci Eng R Rep 63(1):1–30. https://doi.org/10.1016/j.mser.2008.07.001

Wang Z, Zhong Y, Wang S (2012) A new shape factor measure for characterizing the cross-section of profiled fiber. Text Res J 82(5):454–462

Wei J, Xu S, Liu H, Zheng L, Qian Y (2015) Simplified model for predicting fabric thermal resistance according to its microstructural parameters. Fibres & Text East Europe

Wilson CA, Niven BE, Laing RM (1999) Estimating thermal resistance of the bedding assembly from thickness of materials. *International* J Cloth Sci Technol

Woodhouse T (2021) Yarn counts and calculations. Read Books Ltd.

Wooldridge M, Luebbers RH (2020) Heat transfer [Text]. AccessScience|McGraw Hill's AccessScience; McGraw Hill. https://doi.org/10.1036/1097-8542.311100

Xu HJ, Xing ZB, Wang FQ, Cheng ZM (2019) Review on heat conduction, heat convection, thermal radiation and phase change heat transfer of nanofluids in porous media: Fundamentals and applications. Chem Eng Sci 195:462–483. https://doi.org/10.1016/j.ces.2018.09.045

Yao M (2015) Textile materials science, 1st edn. China Textile Press

Zhang H, Shen Y, Edgar KJ, Yang G, Shao H (2021) Influence of cross-section shape on structure and properties of Lyocell fibers. Cellulose 28(2):1191–1201. https://doi.org/10.1007/s10570-020-03605-9

Zhou Y, Zhang J (2006) Clothing comfort and evaluation. Beijing Arts and Crafts Publishing House

Zhu G, Křemenáková D, Wang Y, Militky J, Mazari F (2014) An analysis of effective thermal conductivity of heterogeneous materials. Autex Res J 14. https://doi.org/10.2478/v10304-012-0044-2

Zhu G, Kremenakova D, Wang Y, Militky J, Mishra R (2015a) Study on air permeability and thermal resistance of textiles under heat convection. Text Res J 85(16):1681–1690

Zhu G, Křemenáková D, Wang Y, Militky J, Mishra R (2015b) Study on the thermal property of highly porous nonwoven fabrics. Industria Textilă 66:74–79

Zhu G, Militký J, Wang Y, Huang J, Křemenáková D (2013) Comparison of effective thermal conductivity of hollow fibers by prediction models and FE method. D-Scopus. https://doi.org/10.4028/www.scientific.net/AMM.440.3

Chapter 9
Flexible Carbon-Based Nanocomposites

Yuanfeng Wang, Mohanapriya Venkataraman, and Jiří Militký

Abstract The demand for stretchable strain sensors is increasing due to their potential applications in emerging fields such as human motion detection, wearable electronics, and electronic skins. This review paper provides an overview of the latest developments and advanced applications of flexible carbonous conductive polymer composite strain sensors. Various sensing mechanisms for strain sensors, including the tunneling effect, the disconnection mechanism, and the cracking effect, are described and analyzed. Additionally, the differences in fabrication methods and sensing performance of different sensors are compared from the perspective of different morphological structures of conductive polymer composite strain sensors. The applications of flexible carbon-based strain sensors in detecting motion signals, vital signs, and other areas, such as elbow and knee flexion, gesture recognition, voice recognition, pulse, respiration, and human–computer interaction, are also discussed. Finally, the paper summarizes the current challenges that need to be overcome in the practical application of flexible conductive polymer composite strain sensors.

9.1 Introduction

The advancement of artificial intelligence and electronic technology has led to an increasing use of flexible sensors in various aspects of our lives (Lee et al. 2019). Wearable devices based on flexible sensors, including flexible strain sensors, electrochemical sensors, humidity sensors, and temperature sensors, have been developed rapidly (Chen et al. 2021a, b; Cui et al. 2019; Delipinar et al. 2021; Li and Bo 2022;

Y. Wang · M. Venkataraman (✉) · J. Militký
Department of Material Engineering, Faculty of Textile Engineering, Technical University of Liberec, Studentská 2, 46117 Liberec, Czech Republic
e-mail: mohanapriya.venkataraman@tul.cz

J. Militký
e-mail: jiri.militky@tul.cz

Thakur et al. 2022; Wu et al. 2020; Zhao et al. 2022). Among these sensors, flexible strain sensors are rapidly developing with outstanding characteristics for full-range strain monitoring. Flexible and wearable electronic devices are designed to detect and quantify external signals and respond accordingly in a smart and practical manner. The recent rapid development of flexible wearable technology has provided wearability, comfort, teleoperability, and real-time response to many devices. The key component of these wearable electronics is the sensor, which converts various physiological signals, such as subtle movements caused by breathing, vocalization, and heartbeat, and large body movements caused by joint flexion, into quantifiable electrical signals (Wang et al. 2017). Furthermore, their non-invasive and real-time monitoring of vital signs provides important clinical information for preventing and rehabilitating relevant diseases. Additionally, they demonstrate great potential for human–computer interaction and robot control.

Flexible strain sensors can be fabricated using various materials, such as metal, inorganic semiconductors, and conductive polymer composites (CPCs). However, metal and inorganic semiconductor strain sensors have limitations in terms of their detection range, complex processing, and high manufacturing costs (Rahimi et al. 2015; Zhao et al. 2018; Kirubasankar et al. 2018; Lou et al. 2017). In contrast, CPCs, which consist of conductive particles in an insulating polymer matrix, have become a popular research topic due to their easy processing, adjustable electrical properties, and wide range of applications. The electrical conductivity of the polymer is determined by the conductive network created by the conductive filler (Chen, Zhu, and Jiang 2020b). Research has shown that the resistance of conductive polymers can vary with changes in the conductive network within the polymer matrix, making them suitable for use as multifunctional sensors that can monitor external stimuli such as strain and temperature (Li et al. 2020a, b, c; Li et al. 2019; Chen et al. 2020c, a, b; Arman Kuzubasoglu and Kursun Bahadir 2020; Chen et al. 2021a, b; Yu et al. 2020).

CPC-based strain sensors are ideal because of their unique combination of properties. The low-density and flexible polymer matrix allows for superior flexibility and stretchability, while the conductive fillers provide high thermal and conductive conductivity, magnetic properties, and excellent mechanical properties. The resulting strain sensors are skin-attachable, wearable, and can be arbitrarily deformed, making them superior to conventional sensors (Li et al. 2018a, b; Tang et al. 2018; Park et al. 2021; Bu et al. 2021). The wide range of potential applications for flexible strain sensors includes human motion detection, vital sign monitoring, and human–computer interaction. These sensors can detect subtle movements caused by breathing, vocalization, and heartbeat, as well as large body movements caused by joint flexion. In addition, they can provide important clinical information for the prevention and rehabilitation of relevant diseases (Kim et al. 2021; Li et al. 2021a, b, c; Wang et al. 2021a, b, c, d, e, f, g, h). Despite the advantages of CPC-based strain sensors, there are still challenges that need to be addressed before they can be practically applied. These challenges include improving the sensitivity and repeatability of the sensors, increasing their durability, and optimizing their performance

under various environmental conditions. Continued research in this field is needed to overcome these challenges and fully realize the potential of flexible strain sensors.

Appropriate material selection and preparation methods are essential to obtain flexible strain sensors with optimum performance. Currently, conductor materials used to fabricate flexible strain sensors are mainly classified into carbon materials (Xiao et al. 2021; Wang et al. 2021a, b, c, d, e, f, g, h; Feng et al. 2021, conductive polymers (Luo et al. 2022; Liu et al. 2021a, b; Wu et al. 2021), and metal nanoparticles (Liu et al. 2021a, b; Sun et al. 2022; Zhang et al. 2021a, b). Among them, carbon-based materials, including carbon nanotubes (CNTs) (Qaiser et al. 2021; Wang et al. 2021a, b, c, d, e, f, g, h), graphene (Wang et al. 2021a, b, c, d, e, f, g, h; Niu et al. 2021), carbon nanofiber (Peng et al. 2021), and carbon black (Hu et al. 2021a, b), have shown prominent prospects for development. In terms of the choice of flexible substrates, elastomers with high elongation and good flexibility, including rubber (Liu et al. 2019; Lam et al. 2021), thermoplastic polyurethane (TPU) (Wang et al. 2021a, b, c, d, e, f, g, h; Tang et al. 2022), polydimethylsiloxane (PDMS) (Soe et al. 2021; Zhang et al. 2021a, b), and polyimide (PI) (Li et al. 2021a, b, c; Pu et al. 2021), have been extensively reported in the literatures. A stable interaction between the carbon filler and the elastomeric matrix is essential for the sensing performance of the CPCs. Typically, CPC is obtained by incorporating a conductive filler with an insulating polymer matrix using suitable processing techniques such as spin-coating (Soe et al. 2021), spray-coating (Hu et al. 2021a, b; Hu et al. 2021a, b) and solution mixing (Zheng et al. 2021). Continuous conductive networks are established based on interconnections of neighboring conductive fillers as the filler loading increases. The transition of the resulting material from insulator to conductor can occur at a threshold content of filler, which is known as the percolation threshold (Pc). The lesser amount of filler, i.e. lower Pc, can maintain the good electrical properties of CPC while preserving the inherent processability and mechanical properties of the polymer (Mei et al. 2021; Lv et al. 2021). The percolation threshold is typically determined experimentally by measuring the electrical conductivity of a composite material as a function of the concentration of the conductive filler. A common method is to prepare a series of samples with different filler loadings and measure their conductivity using a four-point probe or other suitable method. The percolation threshold is then identified as the concentration at which the conductivity starts to increase rapidly.

In recent years, there have been numerous studies on the development of methods for combining carbon-based materials with polymers to improve the strain-sensing properties of the resulting composites. These methods can be broadly classified into two categories based on the distribution morphology of the carbon-based materials: homogeneous blends and ordered arrangements. Homogeneous blends refer to the uniform dispersion of materials throughout the polymer matrix, while ordered arrangements involve the controlled alignment of materials within the polymer matrix. Different assembly methods endowed the conductive polymer composites with different structures, including membranes Li et al. 2021a, b, c; Yang et al. 2021), fibers (Sheng et al. 2021; Zeng et al. 2021a), yarns (Tang et al. 2022; Jang et al. 2021; Zhao and Xu 2022), sponges (Xu et al. 2021; Bai et al. 2022; Huang et al.

2021), and foams (Wang et al. 2021a, b, c, d, e, f, g, h; Veeralingam et al. 2022), which had an impact on the resulting strain sensor performance.

This paper aims to provide an in-depth and comprehensive review of recent advances in carbon-based CPC flexible strain sensors. This review covers a wide range of topics, including the sensing mechanisms of strain sensors, the use of various carbon conductive materials in strain sensors, the impact of different sensor structures and assembly methods on sensing performance, and the latest applications of flexible strain sensors for signal monitoring. Furthermore, the paper not only summarizes the current state of the art in flexible strain sensors but also predicts future trends in this field. Through presenting the latest research on carbon-based flexible strain sensors and offering a comprehensive reference, the main aim of this paper is to facilitate a more profound and extensive understanding of this promising and increasingly popular research area.

9.2 Strain Sensing Mechanism

The sensing mechanism of strain sensors is the fundamental principle underlying the detection of strain-induced changes in electrical conductivity within the CPC material. To accurately measure the degree of strain, it is necessary to adjust the conductive network within the material in a manner that is both responsive and reliable. This section will comprehensively discuss various mechanisms that describe the strain sensing behavior of CPC strain sensors, including the tunneling effect, disconnection of a coupled conductive network, and crack extension mechanisms.

9.2.1 Tunneling Effect

In general, the conductivity of CPC is determined by the formation of a conductive network from the conductive filler. The formation of a conductive network can be divided into two main types, one is the tunneling effect and the other is the physical contact of the conductive filler. Tunneling effect, also known as quantum tunneling, refers to the phenomenon in which particles can pass through a barrier that, according to classical physics, they should not be able to overcome. This occurs because of the wave-like nature of particles at the quantum level. In classical mechanics, if a particle encounters a barrier that is higher than its kinetic energy, it will bounce off the barrier and be unable to penetrate it. However, in quantum mechanics, particles have a wave-like nature and are described by a probability wave function. This means that a particle can actually pass through a barrier that it doesn't have enough energy to surmount, by tunneling through the barrier (Lantada et al. 2010; Hu et al. 2008).

Tunneling effect provides the possibility for insulating matrix with low filler content to be transformed into a conductor. In the electrical behavior of CPCs, the tunneling effect mainly exists in CPCs with low filler content. Typically, there are

insulating polymer barriers between the fillers in these CPCs, which are located above the level of free electrons and can prevent the flow of electrical current. When the filler particles are sufficiently separated from each other, there is usually no electrical current in the CPCs. However, when the distance between the filler particles is small enough, tunneling current may occur. The total resistance R of the CPC is calculated according to the available models as follows (Chen et al. 2007; Zhang et al. 2000),

$$R = \left(\frac{L}{N}\right)\left(\frac{8hs}{3a^2e^2\gamma}\right)\exp(\gamma s) \tag{9.1}$$

where L is the number of filler particles forming a single conducting path, N is the number of conducting paths, h is Planck constant, s is the distance between filler particles, a^2 is the effective cross-section at which tunneling occurs, e is the electron charge, and γ is calculated as follows,

$$\gamma = \frac{4\pi}{h}\sqrt{2m\varphi} \tag{9.2}$$

where m is the mass of the electron, φ is the height of the potential barrier between adjacent particles.

It is evident that R is proportional to s, making s a crucial parameter that influences the tunneling effect between adjacent conductive fillers. It is widely accepted that s decreases with the increasing quantity of conductive fillers, resulting in a lower R of the CPC. As the filler content increases further, until the Pc is reached, the interconnected fillers will establish an even lower resistance conductive network within the polymer matrix. At this point, the interconnected conductive network gradually replaces the tunneling effect as the main conducting mechanism.

In the case of a CPC under stress, the resistance changes as the distance of the filler particles changes. Assuming that the distance between the filler particles is s_0 in the initial state, changes to s after the applied strain and the number of conductive paths changes from N_0 to N, the relative resistance (R/R_0) can be calculated from Eqs. (9.3), (9.4) and (9.5) (Chen et al. 2019).

$$\frac{R}{R_0} = \left(\frac{Ns}{N_0s_0}\right)\exp\left[\gamma(s - s_0)\right] \tag{9.3}$$

$$s = s_0(1 + C\varepsilon) = s_0\left[1 + C\left(\frac{\Delta l}{l_0}\right)\right] \tag{9.4}$$

$$N = \frac{N_0}{\exp\left(M\varepsilon + W\varepsilon^2 + U^3 + V^4\right)} \tag{9.5}$$

where R_0 and s_0 are the initial resistance and the initial particle distance, ε is the tensile strain of the CPC, Δl and l_0 refer to the deformation and the initial length of the CPC, respectively. M, W, U, and V are constants.

This mechanism is suitable for relatively small strain amplitudes where a varying tunneling distance results in a change in resistance and thus a small induced signal. Some literature has validated the accuracy of the tunnel conduction model from experimental test data on different types of CPC strain sensors (Ji et al. 2014; Luo et al. 2018; Lin et al. 2013).

9.2.2 Network Disconnection Mechanism

As mentioned above, with an increase in filler content, the conductive mechanism of CPC changes from a tunneling effect to the formation of an interconnected conductive network, i.e. the percolation theory. According to the classical statistical percolation model, when the filler loading exceeds Pc, the relationship between the filler loading and the conductivity of the CPC can be expressed as (Bershtein et al. 2002),

$$\sigma = \sigma_0 (p - p_c)^t \tag{9.6}$$

where σ is the conductivity of the CPC, σ_0 is the conductivity of conductive fillers, p is the volume fraction of the conductive filler in the CPC, p_c is the percolation threshold, and t is the exponent.

In general, two-dimensional conductive networks can be realized with a t of 1.1–1.3, and three-dimensional (3D) conductive networks are considered possible when the t is in the range 1.6–2.0.

When the CPC is under strain, the large stiffness mismatch between the conductive fillers and the flexible polymer due to weak interfacial bonding and the conductive nanomaterial slips, leads to an overlap disconnection and consequently an increase in resistance. The strain-sensing mechanism of CPCs constructed from flexible polymers and multidimensional conductive fillers is commonly explained by a disconnection mechanism (Alamusi et al. 2011; Desai and Haque 2005; Li et al. 2018a, b).

On removal of the external strain, the conductive network within the CPC returns to its initial state in conjunction with the polymer matrix. However, the hysteresis effect of the polymer molecular chains and the irrecoverable damage to a few of the conductive paths result in the resistance of the CPC not being recovered to its initial value. This phenomenon above the initial resistance is known as residual resistance and is apparently one of the factors affecting the stability of the CPC strain sensing performance.

9.2.3 Network Crack Mechanism

It is widely recognized that tunneling conduction and disconnection mechanisms can be used to describe the strain-sensing behavior of homogeneous CPC strain

Fig. 9.1 The resistance model of a sensing unit
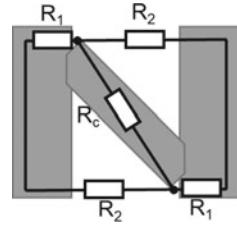
sensors. Recently, a new sensing mechanism, called network crack mechanism, has been discovered by researchers studying the strain sensing properties of sandwich structure CPC (Wang et al. 2018a, b).

The sandwich structure CPC consists of at least one conductive layer and one high elasticity polymer layer. Due to the difference in stiffness between the two layers, when a strain is applied to the CPC, the conductive layer is not able to sustain the strain and produces cracks perpendicular to the direction of stretch. Within a limited range of strain stretching, such cracks are evenly distributed in the conductive layer, rather than penetrating the entire material leading to the fracture of the material and the conductive network. There is no doubt that the formation of cracks destroys part of the conductive network and leads to an increase in the resistance of the CPC. After strain removal, the crack will re-close as the elastic layer recovers its initial state. Such reproducible disconnections and connections of the cracks enable a large sensing range and excellent repeatability. Several scholars have already designed strain sensors with a high detection range based on this mechanism (Yang et al. 2018; Wang et al. 2014).

It has been shown that most cracks will break at 60% strain, but bridges between adjacent cracks can effectively prevent the conductive network from rupturing monolithically. A simplified resistance model based on the network crack has also been proposed (Wang et al. 2018a, b), as shown in Fig. 9.1.

The resistance can be calculated by as,

$$R = \frac{R_1 R_C + 2R_1 R_2 + R_2 R_C}{R_1 + 2R_C + R_2} \tag{9.7}$$

where R_1, R_2, and R_c are the resistances of the island, crack gap, and bridge, respectively.

In conclusion, the sensing mechanism of strain sensors is complex and highly determined by the composition of the CPCs and the structure of the internal conductive network. Excellent strain sensing performance is often the result of a synergy of various sensing mechanisms. In general, the tunneling effect imparts sensitivity to a small range of strains, the disconnection mechanism ensures repeatability and the network crack mechanism extends the effective strain sensing range.

9.3 Carbon-Based Strain Sensors with Special Structure Design

The morphological structure of CPCs plays a critical role in their sensing performance, as it governs the distribution and connectivity of conductive fillers within the polymer matrix. To achieve the desired sensing performance, it is crucial to design and fabricate CPC sensors with specific structures that enable effective strain sensing. Currently, there is significant research focused on designing a range of sensor structures through the synergistic conformation of micro/nanostructures, which has proven to be an effective approach to creating functional CPCs. In this section, we will classify the current carbon-based CPC strain sensor structures and provide detailed discussions on the preparation methods of each structure and their effects on sensing performance, providing insights into the optimization of CPC sensor design for improved sensing performance.

9.3.1 Carbon-Based Film Strain Sensors

Thin films, due to their high sensitivity and flexibility, have gained great interest as a promising structure in the field of developing strain sensors. Thin film CPC sensors can be prepared using various methods, including wet and dry methods, which offer distinct advantages and disadvantages.

Wet methods are, by definition, the manufacture of thin films from a liquid phase dispersion of carbon material. Wet methods include solution casting, spin coating, spray coating, dip coating, vacuum filtration, compression moulding, electrophoretic deposition, and layer-by-layer self-assembly. The fabrication of CPC films by solution casting involves casting a dispersion consisting of fillers and polymers into the substrate mould, followed by drying and curing to obtain a film that adheres to the surface of the substrate. Based on this, the uniformity of the film can be further improved by using the spin coating method. In this way, the same dispersion is deposited in the center of the substrate and the dispersion is uniformly diffused by the centrifugal force of the high-speed rotation of the base. Spraying coating is the process of applying the dispersion to the substrate by using a sprayer. The involvement of the sprayer enables a thinner film to be created, also as a way of improving uniformity. Compression molding entails casting the CPC dispersion into a mold and curing it under pressure and heat within the mold. Under the influence of an electric field, the charged filler particles in a dispersed solution migrate toward the electrodes, forming a homogenous film during the electrophoretic deposition process (Fu and Yu 2014). For example, a simple and effective compression mold method, as shown in Fig. 9.2a, was reported for the preparation of natural rubber/primitive graphene film sensors. The composite had a graphene loading of 5 wt% and a conductivity of 0.005 S/m, which was significantly higher than other methods (Liu et al. 2019).
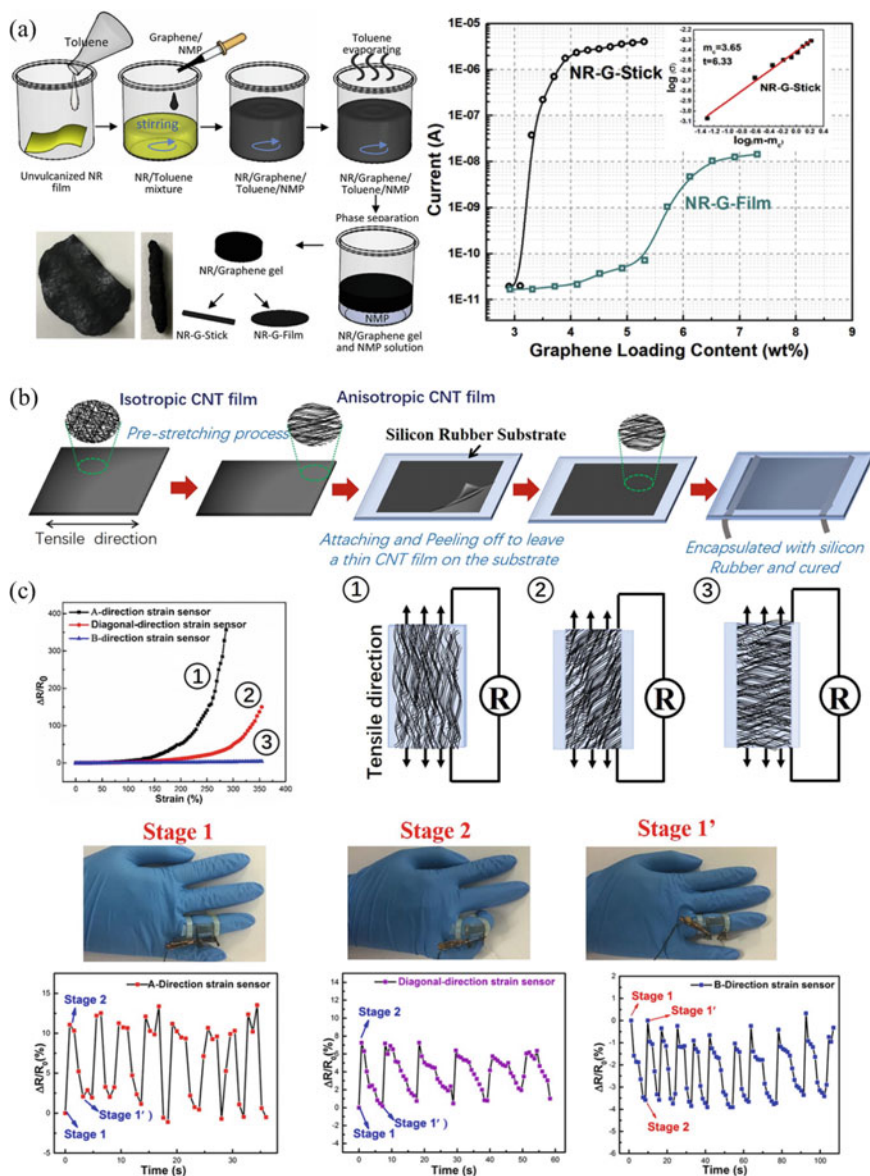
Fig. 9.2 **a** Preparation process and conductivity of natural rubber/primitive graphene film (Liu et al. 2019). **b** Schematics of the fabrication process of the aligned CNT film. **c** The anisotropic feature of CNT film-based strain sensors (Ma and Lu 2020) (Reprinted from references, with kind permission of Elsevier Publications)

Dry methods involve the formation of thin films directly from filler arrays including chemical vapor deposition (CVD) growth and direct dry transfer. Typically, the CVD process allows hydrocarbon gases to pass through a tubular reactor at high temperatures, where the hydrocarbon gases thermally decompose on the surface of a substrate coated with a metal catalyst to form graphene films. Direct dry transfer is the transfer of conductive fillers onto a polymeric substrate under hot pressing and mechanical peeling. Layer-by-layer self-assembly processes use electrostatic interactions, hydrogen bonding, or covalent bonding to alternately deposit oppositely charged components (polymers and fillers) on a substrate. The several layers that make up the film overlap and interpenetrate one other (Zhang et al. 2018). Numerous carbon-based film strain sensors based on these methods have been reported in the literature. The pre-stretching process has been reported to align the CNT film prepared by CVD on a silicone rubber substrate to prepare a highly sensitive and flexible bi-directional strain sensor (Fig. 9.2) (Ma and Lu 2020). The results indicate that the arrangement of CNTs in the axial direction and their entanglement in the transverse direction contribute to providing strain-sensing capabilities in different directions. The authors also highlighted the demonstration of joint motion detection as evidence of the potential of this flexible, bi-directional strain sensor in detecting complex large deformations, as shown in Fig. 9.2c. The fabrication of reduced graphene oxide-TiO2 composite films by spraying methods is proposed to develop a multifunctional material for strain sensing and photodegradation applications. The obtained multifunctional composite films show high optical transmittance and excellent strain sensing properties with a gauge factor (GF) of 12–23 (Liu and Zhang 2016). Moreover, a similar approach was used by Yu et al. to prepare a strain sensor by direct coating of aligned CNT films on a PDMS substrate (Yu et al. 2017). The strain sensors are extremely durable, with a strain capacity of up to 400% and a response time of 98 ms, thanks to their superior mechanical qualities. However, the GF of the sensors resulting in the above work was poor, which is attributable to the thickness of the conductive film. These results show that by simply attaching fillers to the surface of an elastic substrate it is difficult to obtain superior sensors. Sandwich-structured films obtained by embedding filler films into polymers are considered to be a better way to fabricate strain sensors. Zhou et al. (2017), prepared strain sensors by embedding fragmented SWCNT paper into PDMS and demonstrated that a GF of more than 107 was guaranteed even at 50% strain. The sensors obtained by this technique possess unprecedented robustness and sensitivity.

A flexible polyurethane/graphene sheet composite film was manufactured by the layer-by-layer method for wearable strain sensors. It exhibited an excellent conductivity of 1430 ± 50 S/cm and a GF of up to 150 (Meng et al. 2019). In addition, rapid assembly of graphene films at the liquid/gas interface via the Marangoni effect has been reported (Li et al. 2016a, b). These graphene-based strain sensors exhibited extremely high sensitivity at 2% strain, with GF as high as 1037. These sensors can be utilized in electrodynamic systems to monitor large-scale bodily movements.

9.3.2 Carbon-Base Foam Strain Sensor

Porous foam structures can be designed for use in carbon-based strain sensors to detect varying degrees of compression and tension. The unique porous structure of the composite foam material gives it excellent elasticity and recoverability, a characteristic that ensures an excellent strain range and stability of the strain sensor. Strain sensors with porous foam structures are prepared by template-assisted methods, freeze-drying, and CVD. The size of these pores can be tuned by varying the template structure and the preparation process.

In the preparation of CPCs using template-assisted methods, sugar is the most commonly used template due to its low cost and ease of removal (Hwang et al. 2021; Sun et al. 2018; Wan et al. 2020; González-Rivera et al. 2018). For example, a carbon black/polydimethylsiloxane (PDMS) foam (CPF) was fabricated using a templating method combined with ultrasound technology for use as a stretchable sensor, as shown in Fig. 9.3a. The CPF, featuring a robust 3D conductive network, exhibits excellent linearity and a wide strain range. Owing to the strong interaction between the conductive nanofillers and the PDMS matrix, the fabricated CPF possesses negligible electrical hysteresis (Xia et al. 2021). Iglio et al. (2018), reported a piezoresistive flexible foam sensor that can simultaneously detect ultralow strain less than 0.1% and pressure of 20 Pa in compression mode. This PDMS/CNT foam sensor was prepared using a low-cost and scalable process by the molding of a sugar template and subsequent drop-casting of CNT ink. The good stability and limited hysteresis were evident by performing 255 compression release cycles at different strain rates of up to 10 mm/min over a strain range of 0–60%. The same method was used to prepare a 3D microporous graphene-coated PDMS sponge for highly elastic and wearable piezoresistive strain sensors suitable for attachment to human skin (Jung et al. 2019). The obtained graphene-coated PDMS sponges showed highly stable mechanical properties in various tensile stress–strain tests. When various strains were applied, the resistance of the device varied in a highly stable, repeatable, and reversible manner. Besides, the use of other chemicals as pore-forming agents is also a simple and effective way to obtain porous CPC strain sensors. For instance, Long et al. (2018), reported a chemical foaming method using ammonium bicarbonate powder to prepare porous CPCs using PDMS as a matrix and graphene as a conductive filler for the detection of tensile and compressive strains.

Freeze-drying can also be used to prepare three-dimensional carbon foams. By using the freeze-drying process, porous CNT/TPU and graphene/TPU nanocomposites were prepared by Liu's group (Liu et al. 2018). The density of the two carbon-based TPU conductive foams was only 0.1 g/cm^3, and the compression rate exceeded 90%. The resistance of the porous CNT/TPU showed a decreasing trend during compression due to the densification of the porous structure and the opposite piezoresistive behavior was observed due to the disruption of the defective cell walls. After cyclic load stabilization, both porous foams showed excellent recoverability and reproducibility when cyclically compressed at wide strains of up to 90%. Similarly, Li et al. (2016a, b) provided a self-assembly method to form graphene hydrogels
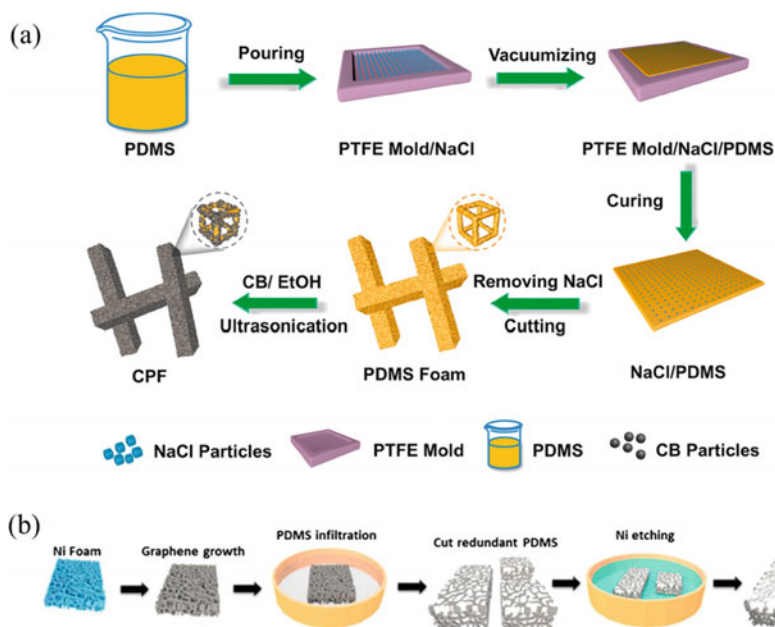
Fig. 9.3 **a** Fabrication of carbon black/PDMS foam through a sacrificial template method (Xia et al. 2021). **b** Fabrication process of graphene foam/PDMS sensor (Pang et al. 2016) (Reprinted from references, with kind permission of Elsevier and ACS Publications)

and obtained graphene foams by a freeze-drying process. Due to its friability, the foam was inserted into a PDMS to be used as a strain sensor. The sensors obtained by embedding the foam into PDMS elastomers showed a strain range of more than 20% and the relative resistance change showed a high degree of superposition with the strain curve during the stretch-relaxation cycle.

Graphene foams are prepared by the CVD method, typically using nickel and copper foams as templates (Ma et al. 2017). In the preparation process, graphene oxide was first grown on the metal foam by the CVD method, followed by the reduction of the graphene oxide to graphene. Finally, the metal skeleton was removed by etching to retain the porous structure of the template. Graphene foam has ultra-lightweight properties. This material needs to be combined with an elastic polymer in order to form a stable structure during compressive strain. As a compressive strain sensor, the higher the raw resistance of the conductive material, the higher the sensitivity. A graphene foam/PDMS/PET CPC strain sensor was also reported, which was fabricated by infiltrating PDMS into 3D graphene foam and introducing a thin layer of PET as a substrate (Xu et al. 2014). However, the performance did not show advantages in terms of sensing performance, with a maximum strain of approximately 16% and a GF of only 6.24. A strain sensor combining graphene porous foam with PDMS was also demonstrated by Pang et al. (2016), as shown in Fig. 9.3b. Using nickel foam as a template and a chemical etching method, graphene foam sensors

can be prepared in PDMS-nickel foams coated with graphene, which can achieve both pressure and strain-sensing properties. Graphene foam-based sensors exhibited a wide pressure sensing range and highest sensitivity as pressure and strain sensors respectively. Generally, the strain range of carbon-based foams was lower than that of carbon-based films, typically below 50%, and there was no significant advantage in sensing sensitivity. The primary reason for such results is the fact that the conductive network within the foam structure is more difficult to vary during the deformation process (Yan et al. 2018).

9.3.3 Carbon-Base Textile Strain Sensor

Textiles, due to their naturally flexible structure and wearability, are more suitable for use as strain sensors to monitor the physiological signals emitted by the human body. A great deal of work has been done to develop textile-based sensors and apply them to monitor the human body in real-time and to detect various other signals (Li et al. 2020a, b, c; Lu et al. 2019; Yue et al. 2020; Sun et al. 2019; Gao et al. 2020; Wang et al. 2020; Zheng et al. 2020; Feng et al. 2020). Textiles are usually divided into three categories: fibers, yarns, and fabrics. Fibers are the most basic unit form that constitutes a textile and have a very high length-to-diameter ratio. The twisting of fiber bundles results in yarns, while further techniques such as weaving and knitting produce fabrics. In this section, carbon-based strain sensors based on textile structures realized using various manufacturing methods are presented.

The slender morphological structure of fibers gives them a natural advantage for use in detecting tensile deformation. As biomass fibers, natural silk, and hair fibers can be used alone as strain-sensing substrates due to their sufficient length and natural elasticity. The active groups on their surfaces facilitate the bonding to carbon-based materials. By incorporating ultra-fine graphite flakes on the surface of the silk fibers, researchers have developed a strain sensor with a GF of 14.5 and a strain range of 15% (Zhang et al. 2016). The flexible and elastic characteristics of the silk fibers guaranteed that the sensor could maintain its performance after 3000 cycles of loading and releasing. Yuan et al. (2015) have developed strain sensors based on rGO-coated hairs. These sensors can detect tensile, bending, and compression deformations. They have excellent mechanical stability and repeatability, with moderate sensitivity. The excellent mechanical properties of chemical fibers, including high stress and elasticity, enable them to be used as a base material for carbon-based strain sensors. Wang et al. (2018a, b) reported the preparation of TPU and MWCNT-based fibrous strain sensors by wet-spinning method. In tensile tests, the MWCNTs/TPU fibrous sensors showed an effective strain range of up to 320% and a strain coefficient of 97.1 in the high tensile range. The durability of the MWCNTs/TPU fibrous sensors was also examined by means of a 100% tensile cycle test at 9700 cycles. In the same way, Zeng et al. (2021b) developed polystyrene-block-poly (ethylene butylene)-block polystyrene (SEBS)/CNT hybrid fibers with high electrical conductivity, high strength, and elongation at break. The hybrid fiber-based strain sensors

have an ultra-wide sensing range of 471%, a high GF of 368, and excellent reliability and stability. To overcome the challenges of the adhesive properties of elastic polymers, researchers have developed a novel self-healing carbon nanotube/ethylene vinyl acetate (CNTs/EVA) fiber strain sensor by embedding CNTs into the surface of an expandable shape memory EVA fiber using ultrasound. The CNTs/EVA fiber strain sensor exhibits significant response capabilities, including high stretchability, a large linear working range, excellent dynamic durability, and a fast response time. Furthermore, the mechanism of CNTs/EVA fiber conductive network changes at the stretched state and unstretched state was discussed, as shown in Fig. 9.4a (Li et al. 2020a, b, c). The strain sensors obtained using this hybrid fiber can accurately detect subtle muscular and large-scale body movements due to their excellent performance. Meanwhile, the fibers traditionally have a feature for use in clothing, satisfying their use in garments and other flexible electronic devices to monitor human movement signals.

Compared to fibers, yarns are structurally more stable due to the twisting effect and are ideal for strain sensors. Wang et al. (2016a, b) have produced a composite yarn for strain sensors by coating highly conductive SWCNT with an elastic cotton/PU core yarn. Thanks to the cotton/PU yarn covering structure and the reinforcing effect of the SWCNTs, the composite yarn can withstand strains of up to 300% and can be cycled nearly 300,000 times at 40% strain without significant breakage. A CNT and PU nanofiber composite spiral yarn with electrical conductivity, hyperextension, and high tensile sensitivity has been developed (Gao et al. 2020). The spring-like microscopic geometry and the good elasticity of the PU molecules give the spiral yarn excellent stretching properties (Fig. 9.4b). CNTs/PU spiral yarns achieve good recovery up to 900% and maximum tensile elongation of up to 1700% due to the interlaced conductive network at the micro level and the spiral structure at the macro level. In addition, Park et al. (2015) developed various yarn strain sensors by dip-coating polyvinyl alcohol and graphene nanosheets layer by layer onto rubber, nylon-covered rubber, and wool yarns, respectively. Due to the yarn structure, these sensors were highly stretchable (up to 150%) and versatile, and capable of detecting human motion on both large and small scales.

Fabrics obtained by weaving or knitting yarns allow further integration of strain sensors into wearable devices. In other words, fabric sensors can be worn without any supporting substrate or additional accessories. Different fabric tissues also provide adjustability in the sensing range, sensitivity, and stability of the fabric sensor. The early fabric strain sensors were fabricated from tubular plain knitted fabrics woven from steel or carbon fiber yarns (Park et al. 2015). Although the resulting fabrics were highly conductive, the strain-sensing range was only 20%. Ren et al. (2017) prepared graphene/cotton fabrics by depositing graphene oxide onto cotton fabrics by vacuum filtration and then hot pressing the material to reduce the graphene oxide. However, due to its compact structure, the graphene layer could not stretch large strains. In order to increase the sensing range, a study was carried out to create a fabric strain sensor by continuously winding CNT around a spandex yarn during the knitting process (Foroughi et al. 2016). The developed fabric showed a strain-sensing range of up to 100%. After 1000 stretch-release cycles at 100% strain, the
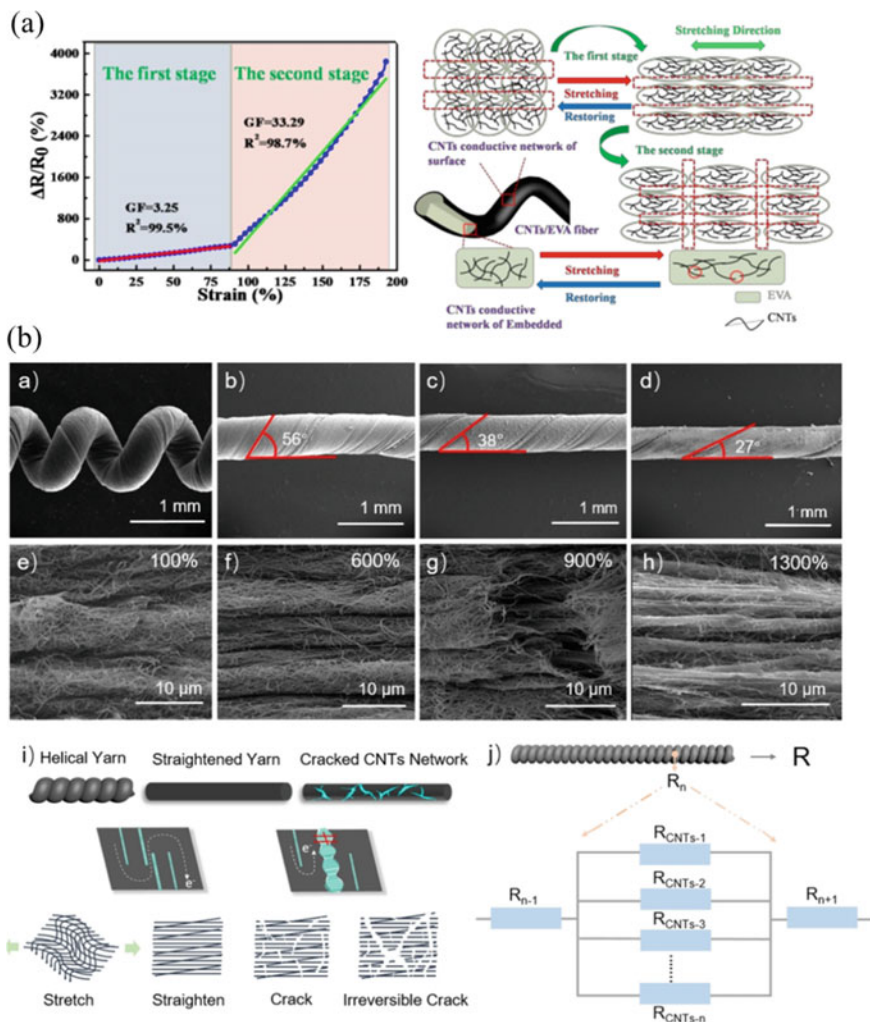
Fig. 9.4 **a** The relative resistance change of CNTs/EVA fiber strain sensors and the mechanism of CNTs/EVA fiber conductive network changes at different states (Li et al. 2020a, b, c). **b** SEM images and mechanism illustration of the conductive network of the helical CNTs/PU yarn (Gao et al. 2020) (Reprinted from references, with kind permission of ACS Publications)

sensitivity was still largely maintained. Wang et al. (2016a, b) developed an ultra-highly stretchable and extremely sensitive strain sensor derived from a carbonized silk fabric. Thanks to the hierarchical structure of the fabric, these fabric-based strain sensors have a large sensing range of up to 500% and long-term stability. In addition, a new graphene woven fabric sensor with an ultra-high GF of approximately 103 and a detection range of 6% strain was developed by the CVD method (Wang et al. 2014). In addition to conventional textile knitted and woven structures, non-woven

fabrics can also be used as sensor substrates. For example, nonwoven sensor has been prepared by integrating graphene directly onto a nonwoven fabric and reducing it in HI acid (Du et al. 2016). The prepared sensor exhibited a negative strain coefficient at small strains and the signal was reproducible in response to tension, bending, and pressure.

In summary, woven fabric-based strain sensors offer ultra-low detection limits, high sensitivity, excellent cycling stability, and durability due to the high dimensional stability of the woven structure. Knitted fabric-based strain sensors, on the other hand, offer excellent sensing sensitivity and a customizable sensing range. Different fabric constructions offer options for sensor design and manufacture, allowing for a greater variety of strain sensor construction forms.
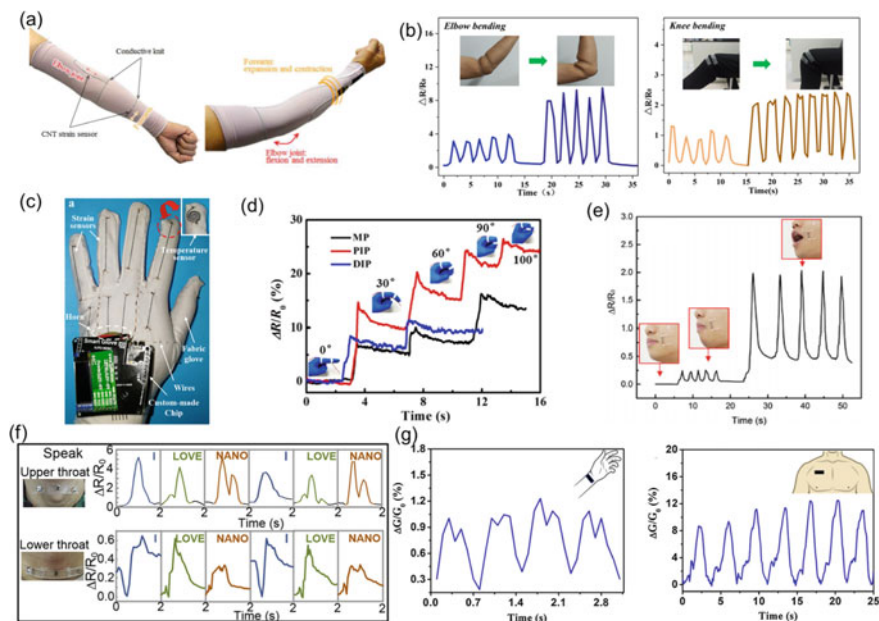
9.3.4 Applications of the Carbon-Based Strain Sensors

As discussed above, carbon-based CPCs were developed into flexible strain sensors with varying morphological structures and excellent performance. By attaching these carbon-based sensors directly or indirectly to the body, various signals generated by the human body can be effectively detected. This section describes the various applications of carbon-based CPC strain sensors.

9.3.5 Human Motion Detection

In general, human motion can be divided into two categories, the first being strenuous movements such as running, walking, and limb flexion, and the second being subtle movements such as, for example, blinking, speaking, and facial expressions. The performance requirements for strain sensors for detecting these two forms of motion signals are different, with the former requiring a greater operating range and the latter requiring exceptionally high sensitivity at low strain (Yin et al. 2017). For the monitoring of strenuous movements, flexible strain sensors with a wide operating range and reliability can be assembled into wearable textiles. For example, by attaching flexible CPC strain sensors to sleeves and trousers, elbow and knee flexion can be sensitively detected (Suzuki et al. 2016; Zhang et al. 2020a, b), as shown in Fig. 9.5a, b. Moreover, it is possible to ultimately recognize different gestures by attaching flexible sensors to the fingers, by outputting different signals of resistance changes, as shown in Fig. 9.5c, d (Suzuki et al. 2016; Li et al. 2020a, b, c).

For the monitoring of small movement signals, flexible strain sensors with excellent low-strain sensitivity are required. For instance, the different movement signals generated by the corners of the mouth when a person chews and speaks can be captured and analyzed by a flexible sensor attached to the cheek, as in Fig. 9.5e (Chen et al. 2020a). Similarly, the changes in throat movement produced when different words are spoken can be monitored with flexible strain sensors (Fig. 9.5f) (Xue et al.

Fig. 9.5 Application of the carbon-based CPC strain sensors. **a** Sleeve with a CNT strain sensor (Suzuki et al. 2016). **b** Monitoring of human motions using flexible strain sensors: elbow bending and knee bending (Zhang et al. 2020a, b). **c** Data glove with CNT strain sensors. **d** MWNTs/PDMS sensor for finger bend detection (Li et al. 2020a, b, c). **e** Responses of the PDMS/CNTs/PDMS motions of cheek (chewing and yawning) (Chen et al. 2020a). **f** The changes in throat movement when saying different words are monitored by sensor (Xue et al. 2019). **g** Real-time human bio-signals monitoring: pulse beat and respiration (Yin et al. 2019) (Reprinted from references, with kind permission of Elsevier and ACS Publications)

2019). In addition, facial expressions such as crying, laughing, and blinking can be monitored by mounting flexible strain sensors on the cheeks, forehead, or around the eyes (Meng et al. 2019; Zhao et al. 2019).

9.3.6 Detection of the Information on Human Vital Signs

In addition to monitoring motion signals, strain sensors can also be used to detect information on human vital signs, including blood pressure, heartbeat, and respiration. Such signals are much weaker than motion and therefore smart, flexible sensors with high sensitivity to small deformations need to be prepared. Flexible carbon-based strain sensors proved to be suitable for the detection of vital signs.

Numerous reports have been made of high-performance strain sensors placed on the chest for monitoring respiratory rate, a deformation created by changes in the undulation of the chest acting on the sensor during breathing (Zhang et al. 2020a, b;

Zhao et al. 2019; Yin et al. 2019). Strain sensors can also detect pulses to assess the physiological status of the cardiovascular system for health monitoring. Similarly, by fixing a flexible carbon-based strain sensor to the wrist, the weak deformation generated by the pulse was recognized and recorded, allowing information about the heart rate to be monitored and output (Yin et al. 2019; Zu et al. 2020). Flexible strain sensors can also be implanted in the body and wrapped around blood arteries during surgery to continuously monitor vascular pressure and flow (Majerus et al. 2018). In conclusion, highly sensitive carbon-based strain sensors are making tremendous progress in the detection of physiological information in the human body.

9.3.7   Other Applications

The low strain range sensitivity of strain sensors can also make them candidates for structural damage monitoring, which can be applied to the monitoring of internal damage in structural materials. For example, PVA/CNT fibers were embedded in glass fiber-reinforced composites to enable monitoring of damage to the composite when subjected to external loads (Alexopoulos et al. 2010). Real-time monitoring has shown that micro-cracks and fractures within the composite can generate signals of changes in electrical resistance, thereby preventing further damage. Moreover, future intelligent robots will rely heavily on flexible strain sensors (Zhang et al. 2020a, b). When the strain sensing system is configured as a multi-channel structure, precise strain detection for each of the intelligent robot's fingers is possible, either concurrently or sequentially. Furthermore, highly compliant, low-modulus, and lightweight stretchable sensors can be integrated with machine learning technologies, offering unlimited prospects for bioelectrical signal recognition, tactile sensing, and multimodal integration (Wang et al. 2021a, b, c, d, e, f, g, h).

9.3.8   Conclusion and Outlook

This review presented the latest developments in flexible carbon-based CPC strain sensors and their advanced applications in various aspects. Firstly, we analyze the various sensing mechanisms of strain sensors, mainly including the tunneling effect, the disconnection mechanism, and the cracking effect. Despite the existence of different sensing mechanisms, all can be attributed to changes in resistance due to material deformation at a macroscopic level. Subsequently, the fabrication methods and sensing performance of different sensors are compared in terms of different morphological structures of CPC strain sensors. There is no doubt that the operating range and sensitivity of the sensors can be tuned by the choice of substrate material and the design of the morphological structure. Furthermore, applications of flexible carbon-based strain sensors in the detection of motion signals, vital signs, and other

areas are cited, including elbow and knee flexion, gesture recognition, voice recognition, pulse, respiration, and human–computer interaction. So far, a number of flexible CPC-based strain sensors have been developed and have demonstrated a wide strain range, high sensitivity, and good repeatability.

In terms of current flexible strain sensors in practical applications, there are still many areas for improvement. In the future, the production costs for reducing carbon-based fillers need to be further reduced, effective communication between the sensors and other electronic devices needs to be established, and the sensors need to be given the ability to accurately analyze and capture strain signals under complex environmental conditions. In summary, high performance carbon-based materials, optimized structural design, manufacturing methods, and working mechanisms pave the way for the preparation of carbon-based strain sensors with excellent sensing performance. When the current challenges are overcome, we expect CPC-based strain sensors to show greater potential for health monitoring, wearable electronics, human–computer interaction, and more.

References

Alamusi, Hu N, Fukunaga H, Atobe S, Liu Y, Li J (2011) Piezoresistive strain sensors made from carbon nanotubes based polymer nanocomposites. Sensors 11(11):10691–10723. https://doi.org/10.3390/S111110691

Alexopoulos ND, Bartholome C, Poulin P, Marioli-Riga Z (2010) Damage detection of glass fiber reinforced composites using embedded PVA–carbon nanotube (CNT) fibers. Compos Sci Technol 70(12):1733–1741. https://doi.org/10.1016/J.COMPSCITECH.2010.07.004

Arman Kuzubasoglu B, Kursun Bahadir S (2020) Flexible temperature sensors: a review. Sens Actuators A 315:112282. https://doi.org/10.1016/j.sna.2020.112282

Bai Y, Qin F, Lu Y (2022) Lightweight Ni/CNT decorated melamine sponge with sensitive strain sensing performance for ultrahigh electromagnetic absorption in both GHz and THz bands. Chem Eng J 429:132393. https://doi.org/10.1016/j.cej.2021.132393

Bershtein VA, Egorova LM, Yakushev PN, Pissis P, Sysel P, Brozova L (2002) Conductive mechanism of polymer/graphite conducting composites with low percolation threshold. J Polym Sci Part B: Polym Phys 40(10):954–963. https://doi.org/10.1002/POLB.10141

Bu Y, Shen T, Yang W, Yang S, Zhao Y, Liu H, Zheng Y, Liu C, Shen C (2021) Ultrasensitive strain sensor based on superhydrophobic microcracked conductive Ti3C2T MXene/paper for human-motion monitoring and E-skin. Sci Bull 66(18):1849–1857. https://doi.org/10.1016/j.scib.2021.04.041

Chen J, Yu Q, Cui X, Dong M, Zhang J, Wang C, Fan J, Zhu Y, Guo Z (2019) An overview of stretchable strain sensors from conductive polymer nanocomposites. J Mater Chem C 7(38):11710–11730. https://doi.org/10.1039/c9tc03655e

Chen J, Zhu Y, Guo Z, Nasibulin AG (2020a) Recent progress on thermo-electrical properties of conductive polymer composites and their application in temperature sensors. Eng Sci. https://doi.org/10.30919/es8d1129

Chen J, Zhu Y, Jiang W (2020b) A stretchable and transparent strain sensor based on sandwich-like PDMS/CNTs/PDMS composite containing an ultrathin conductive CNT layer. Compos Sci Technol 186:107938. https://doi.org/10.1016/j.compscitech.2019.107938

Chen J, Zhu Y, Jiang W (2020c) A stretchable and transparent strain sensor based on sandwich-like PDMS/CNTs/PDMS composite containing an ultrathin conductive CNT layer. Compos Sci Technol 186:107938. https://doi.org/10.1016/j.compscitech.2019.107938

Chen L, Chen G, Lu L (2007) Piezoresistive behavior study on finger-sensing silicone rubber/ graphite nanosheet nanocomposites. Adv Func Mater 17(6):898–904. https://doi.org/10.1002/ ADFM.200600519

Chen Q, Yao Y, Huang X, Liu D, Mao K (2021a) Simulation analysis and experimental verification for sensitivity of IDE-QCM humidity sensors. Sens Actuators B Chem 341:129992. https://doi. org/10.1016/j.snb.2021.129992

Chen Z, Zhao D, Ma R, Zhang X, Rao J, Yin Y, Wang X, Yi F (2021b) Flexible temperature sensors based on carbon nanomaterials. J Mater Chem B 9(8):1941–1964. https://doi.org/10.1039/D0T B02451A

Cui Z, Poblete FR, Zhu Y (2019) Tailoring the temperature coefficient of resistance of silver nanowire nanocomposites and their application as stretchable temperature sensors. ACS Appl Mater Interfaces 11(19):17836–17842. https://doi.org/10.1021/acsami.9b04045

Delipinar T, Shafique A, Gohar MS, Yapici MK (2021) Fabrication and materials integration of flexible humidity sensors for emerging applications. ACS Omega 6(13):8744–8753. https://doi. org/10.1021/acsomega.0c06106

Desai AV, Haque MA (2005) Mechanics of the interface for carbon nanotube–polymer composites. Thin-Walled Struct 43(11):1787–1803. https://doi.org/10.1016/J.TWS.2005.07.003

Du D, Li P, Ouyang J (2016) Graphene coated nonwoven fabrics as wearable sensors. J Mater Chem C 4(15):3224–3230. https://doi.org/10.1039/C6TC00350H

Feng J, Tian Y, Wang S, Xiao M, Hui Z, Hang C, Duley WW, Zhou YN (2021) Femtosecond laser irradiation induced heterojunctions between carbon nanofibers and silver nanowires for a flexible strain sensor. J Mater Sci Technol 84:139–146. https://doi.org/10.1016/j.jmst.2020. 12.060

Feng J, Wang X, Lv Z, Qu J, Lu X, Wei Q, Wang Q (2020) Multifunctional wearable strain sensor made with an elastic interwoven fabric for patients with motor dysfunction. Adv Mater Technol 5(11):2000560. https://doi.org/10.1002/ADMT.202000560

Foroughi J, Spinks GM, Aziz S, Mirabedini A, Jeiranikhameneh A, Wallace GG, Kozlov ME, Baughman RH (2016) Knitted carbon-nanotube-sheath/spandex-core elastomeric yarns for arti- ficial muscles and strain sensing. ACS Nano 10(10):9129–9135. https://doi.org/10.1021/ACS NANO.6B04125/SUPPL_FILE/NN6B04125_SI_005.PDF

Fu L, Yu AM (2014) Carbon nanotubes based thin films: fabrication, characterization and applications. Rev Adv Mater Sci 36(1):40–61

Gao Y, Guo F, Cao P, Liu J, Li D, Wu J, Wang N, Su Y, Zhao Y (2020) Winding-locked carbon nanotubes/polymer nanofibers helical yarn for ultrastretchable conductor and strain sensor. ACS Nano 14(3):3442–3450. https://doi.org/10.1021/ACSNANO.9B09533/SUPPL_FILE/NN9B09 533_SI_001.PDF

González-Rivera J, Iglio R, Barillaro G, Duce C, Tinè MR (2018) Structural and thermoanalytical characterization of 3D porous PDMS foam materials: the effect of impurities derived from a sugar templating process. Polymers 10(6):616. https://doi.org/10.3390/POLYM10060616

Hu M, Gao Y, Jiang Y, Zeng H, Zeng S, Zhu M, Xu G, Sun L (2021a) High-performance strain sensors based on bilayer carbon black/PDMS hybrids. Adv Compos Hybrid Mater 4(3):514–520. https://doi.org/10.1007/s42114-021-00226-z

Hu N, Karube Y, Yan C, Masuda Z, Fukunaga H (2008) Tunneling effect in a polymer/carbon nanotube nanocomposite strain sensor. Acta Mater 56(13):2929–2936. https://doi.org/10.1016/ j.actamat.2008.02.030

Hu X, Yang F, Wu M, Sui Y, Guo D, Li M, Kang Z, Sun J, Liu J (2021b) A super-stretchable and highly sensitive carbon nanotube capacitive strain sensor for wearable applications and soft robotics. Adv Mater Technol 2100769. https://doi.org/10.1002/admt.202100769

Huang L, Chen J, Xu Y, Hu D, Cui X, Shi D, Zhu Y (2021) Three-dimensional light-weight piezoresistive sensors based on conductive polyurethane sponges coated with hybrid CNT/CB nanoparticles. Appl Surf Sci 548:149268. https://doi.org/10.1016/j.apsusc.2021.149268

Hwang J, Kim Y, Yang H, Oh JH (2021) Fabrication of hierarchically porous structured PDMS composites and their application as a flexible capacitive pressure sensor. Compos B Eng 211:108607. https://doi.org/10.1016/J.COMPOSITESB.2021.108607

Iglio R, Mariani S, Robbiano V, Strambini L, Barillaro G (2018) Flexible polydimethylsiloxane foams decorated with multiwalled carbon nanotubes enable unprecedented detection of ultralow strain and pressure coupled with a large working range. ACS Appl Mater Interfaces 10(16):13877–13885. https://doi.org/10.1021/acsami.8b02322

Jang J, Kim S, Lee K, Park S, Park G-Y, Kim B-J, Oh J, Lee MJ (2021) Knitted strain sensor with carbon fiber and aluminum-coated yarn, for wearable electronics. J Mater Chem C 9(46):16440–16449. https://doi.org/10.1039/D1TC01899J

Ji M, Deng H, Yan D, Li X, Duan L, Fu Q (2014) Selective localization of multi-walled carbon nanotubes in thermoplastic elastomer blends: an effective method for tunable resistivity–strain sensing behavior. Compos Sci Technol 92:16–26. https://doi.org/10.1016/J.COMPSCITECH.2013.11.018

Jung Y, Jung K, Park B, Choi J, Kim D, Park J, Ko J, Cho H (2019) Wearable piezoresistive strain sensor based on graphene-coated three-dimensional micro-porous PDMS sponge. Micro Nano Syst Lett 7(1):1–9. https://doi.org/10.1186/S40486-019-0097-2/FIGURES/6

Kim JH, Cho KG, Cho DH, Hong K, Lee KH (2021) Ultra-sensitive and stretchable ionic skins for high-precision motion monitoring. Adv Func Mater 31(16):2010199. https://doi.org/10.1002/adfm.202010199

Kirubasankar B, Murugadoss V, Lin J, Ding T, Dong M, Liu H, Zhang J, Li T, Wang N, Guo Z, Angaiah S (2018) In situ grown nickel selenide on graphene nanohybrid electrodes for high energy density asymmetric supercapacitors. Nanoscale 10(43):20414–20425. https://doi.org/10.1039/C8NR06345A

Lam TN, Lee GS, Kim B, Dinh Xuan H, Kim D, Yoo SI, Yoon J (2021) Microfluidic preparation of highly stretchable natural rubber microfiber containing CNT/PEDOT:PSS hybrid for fabric-sewable wearable strain sensor. Compos Sci Technol 210:108811. https://doi.org/10.1016/j.compscitech.2021.108811

Lantada AD, Lafont P, Sanz JLM, Munoz-Guijosa JM, Otero JE (2010) Quantum tunnelling composites: characterisation and modelling to promote their applications as sensors. Sens Actuators a: Phys 164(1–2):46–57. https://doi.org/10.1016/j.sna.2010.09.002

Lee S, Shi Q, Lee C (2019) From flexible electronics technology in the era of IoT and artificial intelligence toward future implanted body sensor networks. APL Mater 7(3):031302. https://doi.org/10.1063/1.5063498

Li G, Dai K, Ren M, Wang Y, Zheng G, Liu C, Shen C (2018a) Aligned flexible conductive fibrous networks for highly sensitive, ultrastretchable and wearable strain sensors. J Mater Chem C 6(24):6575–6583. https://doi.org/10.1039/C8TC01924J

Li H, Chen J, Chang X, Xu Y, Zhao G, Zhu Y, Li Y (2021a) A highly stretchable strain sensor with both an ultralow detection limit and an ultrawide sensing range. J Mater Chem A 9(3):1795–1802. https://doi.org/10.1039/D0TA10990H

Li J, Bo X (2022) Laser-enabled flexible electrochemical sensor on finger for fast food security detection. J Hazard Mater 423:127014. https://doi.org/10.1016/j.jhazmat.2021.127014

Li J, Zhao S, Zeng X, Huang W, Gong Z, Zhang G, Sun R, Wong CP (2016a) Highly stretchable and sensitive strain sensor based on facilely prepared three-dimensional graphene foam composite. ACS Appl Mater Interfaces 8(29):18954–18961. https://doi.org/10.1021/ACSAMI.6B05088/SUPPL_FILE/AM6B05088_SI_001.PDF

Li M, Chen X, Li X, Dong J, Zhao X, Zhang Q (2021b) Wearable and robust polyimide hydrogel fiber textiles for strain sensors. ACS Appl Mater Interfaces 13(36):43323–43332. https://doi.org/10.1021/acsami.1c10055

Li Q, Liu H, Zhang S, Zhang D, Liu X, He Y, Mi L, Zhang J, Liu C, Shen C, Guo Z (2019) Super-hydrophobic electrically conductive paper for ultrasensitive strain sensor with excellent anti-corrosion and self-cleaning property. ACS Appl Mater Interfaces 11(24):21904–21914. https://doi.org/10.1021/acsami.9b03421

Li Q, Yin R, Zhang D, Liu H, Chen X, Zheng Y, Guo Z, Liu C, Shen C (2020a) Flexible conductive MXene/cellulose nanocrystal coated nonwoven fabrics for tunable wearable strain/pressure sensors. J Mater Chem A 8(40):21131–21141. https://doi.org/10.1039/D0TA07832H

Li W, Zhou Y, Wang Y, Jiang L, Ma J, Chen S, Zhou F (2021c) Core-sheath fiber-based wearable strain sensor with high stretchability and sensitivity for detecting human motion. Adv Electron Mater 7(1):2000865. https://doi.org/10.1002/aelm.202000865

Li X, Yang T, Yang Y, Zhu J, Li L, Alam FE, Li X, Wang K, Cheng H, Lin C-T, Fang Y, Zhu H (2016b) Large-area ultrathin graphene films by single-step marangoni self-assembly for highly sensitive strain sensing application. Adv Funct Mater 26(9):1322–1329.https://doi.org/10.1002/ADFM.201504717

Li Y, Zheng C, Liu S, Huang L, Fang T, Li JX, Xu F, Li F (2020b) Smart glove integrated with tunable MWNTs/PDMS fibers made of a one-step extrusion method for finger dexterity, gesture, and temperature recognition. ACS Appl Mater Interfaces 12(21):23764–23773. https://doi.org/10.1021/ACSAMI.0C08114/SUPPL_FILE/AM0C08114_SI_005.MP4

Li Y, Zhou B, Zheng G, Liu X, Li T, Yan C, Cheng C, Dai K, Liu C, Shen C, Guo Z (2018b) Continuously prepared highly conductive and stretchable SWNT/MWNT synergistically composited electrospun thermoplastic polyurethane yarns for wearable sensing. J Mater Chem C 6(9):2258–2269. https://doi.org/10.1039/C7TC04959E

Li Z, Qi X, Xu L, Lu H, Wang W, Jin X, Md ZI, Zhu Y, Fu Y, Ni Q, Dong Y (2020c) Self-repairing, large linear working range shape memory carbon nanotubes/ethylene vinyl acetate fiber strain sensor for human movement monitoring. ACS Appl Mater Interfaces 12(37):42179–42192. https://doi.org/10.1021/ACSAMI.0C12425/SUPPL_FILE/AM0C12425_SI_002.AVI

Lin L, Liu S, Zhang Q, Li X, Ji M, Deng H, Fu Q (2013) Towards tunable sensitivity of electrical property to strain for conductive polymer composites based on thermoplastic elastomer. ACS Appl Mater Interfaces 5(12):5815–5824. https://doi.org/10.1021/AM401402X/SUPPL_FILE/AM401402X_SI_002.PDF

Liu H, Gao H, Hu G (2019) Highly sensitive natural rubber/pristine graphene strain sensor prepared by a simple method. Compos B Eng 171:138–145. https://doi.org/10.1016/j.compositesb.2019.04.032

Liu H, Li Q, Zhang S, Yin R, Liu X, He Y, Dai K, Shan C, Guo J, Liu C, Shen C, Wang X, Wang N, Wang Z, Wei R, Guo Z (2018) Electrically conductive polymer composites for smart flexible strain sensors: a critical review. J Mater Chem C 6(45):12121–12141. https://doi.org/10.1039/C8TC04079F

Liu H, Zhang S, Li Z, Lu TJ, Lin H, Zhu Y, Ahadian S, Emaminejad S, Dokmeci MR, Xu F, Khademhosseini A (2021a) Harnessing the wide-range strain sensitivity of bilayered PEDOT:PSS films for wearable health monitoring. Matter 4(9):2886–2901. https://doi.org/10.1016/j.matt.2021.06.034

Liu Y, Zhang D (2016) The preparation of reduced graphene oxide-TiO2 composite materials towards transparent, strain sensing and photodegradation multifunctional films. Compos Sci Technol 137:102–108. https://doi.org/10.1016/J.COMPSCITECH.2016.10.025

Liu Z, Li Z, Zhai H, Jin L, Chen K, Yi Y, Gao Y, Xu L, Zheng Y, Yao S, Liu Z, Li G, Song Q, Yue P, Xie S, Li Y, Zheng Z (2021b) A highly sensitive stretchable strain sensor based on multi-functionalized fabric for respiration monitoring and identification. Chem Eng J 426:130869. https://doi.org/10.1016/j.cej.2021.130869

Long Y, Zhao X, Jiang X, Zhang L, Zhang H, Liu Y, Zhu H (2018) A porous graphene/ polydimethylsiloxane composite by chemical foaming for simultaneous tensile and compressive strain sensing. FlatChem 10:1–7. https://doi.org/10.1016/J.FLATC.2018.07.001

Lou X, Lin C, Luo Q, Zhao J, Wang B, Li J, Shao Q, Guo X, Wang N, Guo Z (2017) Crystal structure modification enhanced FeNb 11 O 29 anodes for lithium-ion batteries. ChemElectroChem 4(12):3171–3180. https://doi.org/10.1002/celc.201700816

Lu L, Zhou Y, Pan J, Chen T, Hu Y, Zheng G, Dai K, Liu C, Shen C, Sun X, Peng H (2019) Design of helically double-leveled gaps for stretchable fiber strain sensor with ultralow detection

limit, broad sensing range, and high repeatability. ACS Appl Mater Interfaces 11(4):4345–4352. https://doi.org/10.1021/ACSAMI.8B17666/SUPPL_FILE/AM8B17666_SI_001.PDF

Luo Q, Ma H, Hou Q, Li Y, Ren J, Dai X, Yao Z, Zhou Y, Xiang L, Du H, He H, Wang N, Jiang K, Lin H, Zhang H, Guo Z (2018) All-carbon-electrode-based endurable flexible perovskite solar cells. Adv Func Mater 28(11):1706777. https://doi.org/10.1002/ADFM.201706777

Luo R, Li X, Li H, Du B, Zhou S (2022) A stretchable and printable PEDOT:PSS/PDMS composite conductors and its application to wearable strain sensor. Prog Org Coat 162:106593. https://doi.org/10.1016/j.porgcoat.2021.106593

Lv Z, Huang X, Fan D, Zhou P, Luo Y, Zhang X (2021) Scalable manufacturing of conductive rubber nanocomposites with ultralow percolation threshold for strain sensing applications. Compos Commun 25:100685. https://doi.org/10.1016/j.coco.2021.100685

Ma L, Lu W (2020) Carbon nanotube film based flexible bi-directional strain sensor for large deformation. Mater Lett 260:126959. https://doi.org/10.1016/J.MATLET.2019.126959

Ma Y, Yu M, Liu J, Li X, Li S (2017) Ultralight interconnected graphene-amorphous carbon hierarchical foam with mechanical resiliency for high sensitivity and durable strain sensors. ACS Appl Mater Interfaces 9(32):27127–27134. https://doi.org/10.1021/ACSAMI.7B05636/SUPPL_FILE/AM7B05636_SI_001.PDF

Majerus SJA, Chong H, Ariando D, Swingle C, Potkay J, Bogie K, Zorman CA (2018) Vascular graft pressure-flow monitoring using 3D printed MWCNT-PDMS strain sensors. In: Proceedings of the annual international conference of the IEEE engineering in medicine and biology society, EMBS, July 2018, pp 2989–2992. https://doi.org/10.1109/EMBC.2018.8512997

Mei S, Zhang X, Ding B, Wang J, Yang P, She H, Cui Z, Liu M, Pang X, Fu P (2021) <scp>3D-Printed</scp> thermoplastic polyurethane/graphene composite with porous segregated structure: toward ultralow percolation threshold and great strain sensitivity. J Appl Polym Sci 138(14):50168. https://doi.org/10.1002/app.50168

Meng Q, Liu Z, Han S, Xu L, Araby S, Cai R, Zhao Y, Lu S, Liu T (2019) A facile approach to fabricate highly sensitive, flexible strain sensor based on elastomeric/graphene platelet composite film. J Mater Sci 54(15):10856–10870. https://doi.org/10.1007/S10853-019-03650-1/TABLES/2

Niu S, Chang X, Zhu Z, Qin Z, Li J, Jiang Y, Wang D, Yang C, Gao Y, Sun S (2021) Low-temperature wearable strain sensor based on a silver nanowires/graphene composite with a near-zero temperature coefficient of resistance. ACS Appl Mater Interfaces 13(46):55307–55318. https://doi.org/10.1021/acsami.1c14671

Pang Y, Tian H, Tao L, Li Y, Wang X, Deng N, Yang Y, Ren TL (2016) Flexible, highly sensitive, and wearable pressure and strain sensors with graphene porous network structure. ACS Appl Mater Interfaces 8(40):26458–26462. https://doi.org/10.1021/ACSAMI.6B08172/SUPPL_FILE/AM6B08172_SI_001.PDF

Park H, Song C, Jin SW, Lee H, Keum K, Lee YH, Lee G, Jeong YR, Ha JS (2021) High performance flexible micro-supercapacitor for powering a vertically integrated skin-attachable strain sensor on a bio-inspired adhesive. Nano Energy 83:105837. https://doi.org/10.1016/j.nanoen.2021.105837

Park JJ, Hyun WJ, Mun SC, Park YT, Park OO (2015) Highly stretchable and wearable graphene strain sensors with controllable sensitivity for human motion monitoring. ACS Appl Mater Interfaces 7(11):6317–6324. https://doi.org/10.1021/ACSAMI.5B00695/SUPPL_FILE/AM5B00695_SI_003.AVI

Peng S, Wu S, Yu Y, Sha Z, Li G, Hoang TT, Thai MT, Do TN, Chu D, Wang CH (2021) Carbon nanofiber-reinforced strain sensors with high breathability and anisotropic sensitivity. J Mater Chem A 9(47):26788–26799. https://doi.org/10.1039/D1TA08521B

Pu L, Liu Y, Li L, Zhang C, Ma P, Dong W, Huang Y, Liu T (2021) Polyimide nanofiber-reinforced Ti 3 C 2 T x aerogel with "lamella-pillar" microporosity for high-performance piezoresistive strain sensing and electromagnetic wave absorption. ACS Appl Mater Interfaces 13(39):47134–47146. https://doi.org/10.1021/acsami.1c13863

Qaiser N, Al-Modaf F, Khan SM, Shaikh SF, El-Atab N, Hussain MM (2021) A robust wearable point-of-care CNT-based strain sensor for wirelessly monitoring throat-related illnesses. Adv Func Mater 31(29):2103375. https://doi.org/10.1002/adfm.202103375

Rahimi R, Ochoa M, Yu W, Ziaie B (2015) Highly stretchable and sensitive unidirectional strain sensor via laser carbonization. ACS Appl Mater Interfaces 7(8):4463–4470. https://doi.org/10.1021/am509087u

Ren J, Wang C, Zhang X, Carey T, Chen K, Yin Y, Torrisi F (2017) Environmentally-friendly conductive cotton fabric as flexible strain sensor based on hot press reduced graphene oxide. Carbon 111:622–630. https://doi.org/10.1016/J.CARBON.2016.10.045

Sheng N, Ji P, Zhang M, Wu Z, Liang Q, Chen S, Wang H (2021) High sensitivity polyurethane-based fiber strain sensor with porous structure via incorporation of bacterial cellulose nanofibers. Adv Electron Mater 7(4):2001235. https://doi.org/10.1002/aelm.202001235

Soe HM, Abd Manaf A, Matsuda A, Jaafar M (2021) Performance of a silver nanoparticles-based polydimethylsiloxane composite strain sensor produced using different fabrication methods. Sens Actuators a: Phys 329:112793. https://doi.org/10.1016/j.sna.2021.112793

Sun B, McCay RN, Goswami S, Xu Y, Zhang C, Ling Y, Lin J, Yan Z (2018) Gas-permeable, multifunctional on-skin electronics based on laser-induced porous graphene and sugar-templated elastomer sponges. Adv Mater 30(50):1804327. https://doi.org/10.1002/ADMA.201804327

Sun H, Dai K, Zhai W, Zhou Y, Li J, Zheng G, Li B, Liu C, Shen C (2019) A highly sensitive and stretchable yarn strain sensor for human motion tracking utilizing a wrinkle-assisted crack structure. ACS Appl Mater Interfaces 11(39):36052–36062. https://doi.org/10.1021/ACSAMI.9B09229/SUPPL_FILE/AM9B09229_SI_005.AVI

Sun J, Yuan Y, Lu G, Xue T, Nie J, Lu Y (2022) Highly stretchable and sensitive strain sensor based on Ionogel/Ag synergistic conductive network. Adv Mater Interfaces 2102245.https://doi.org/10.1002/admi.202102245

Suzuki K, Yataka K, Okumiya Y, Sakakibara S, Sako K, Mimura H, Inoue Y (2016) Rapid-response, widely stretchable sensor of aligned MWCNT/elastomer composites for human motion detection. ACS Sens 1(6):817–825. https://doi.org/10.1021/ACSSENSORS.6B00145/SUPPL_FILE/SE6B00145_SI_005.MPG

Tang J, Wu Y, Ma S, Yan T, Pan Z (2022) Flexible strain sensor based on CNT/TPU composite nanofiber yarn for smart sports bandage. Compos B Eng 232:109605. https://doi.org/10.1016/j.compositesb.2021.109605

Tang Z, Jia S, Wang F, Bian C, Chen Y, Wang Y, Li B (2018) Highly stretchable core-sheath fibers via wet-spinning for wearable strain sensors. ACS Appl Mater Interfaces 10(7):6624–6635. https://doi.org/10.1021/acsami.7b18677

Thakur N, Mandal D, Nagaiah TC (2022) A novel NiVP/Pi-based flexible sensor for direct electrochemical ultrasensitive detection of cholesterol. Chem Commun. https://doi.org/10.1039/D1CC07115G

Veeralingam S, Praveen S, Vemula M, Badhulika S (2022) One-step synthesis of carbon-doped PPy nanoparticles interspersed in 3D porous melamine foam as a high-performance piezoresistive pressure, strain, and breath sensor. Mater Chem Front. https://doi.org/10.1039/D1QM01427G

Wan Y, Qin N, Wang Y, Zhao Q, Wang Q, Yuan P, Wen Q, Wei H, Zhang X, Ma N (2020) Sugar-templated conductive polyurethane-polypyrrole sponges for wide-range force sensing. Chem Eng J 383:123103. https://doi.org/10.1016/J.CEJ.2019.123103

Wang C, Li X, Gao E, Jian M, Xia K, Wang Q, Xu Z, Ren T, Zhang Y, Wang CY, Jian MQ, Xia KL, Wang Q, Zhang YY, Li X, Ren TL, Gao EL, Xu ZP (2016a) Carbonized silk fabric for ultrastretchable, highly sensitive, and wearable strain sensors. Adv Mater 28(31):6640–6648. https://doi.org/10.1002/ADMA.201601572

Wang F, Liu S, Shu L, Tao X-M (2017) Low-dimensional carbon based sensors and sensing network for wearable health and environmental monitoring. Carbon 121:353–367. https://doi.org/10.1016/j.carbon.2017.06.006

Wang H, Li J, Yu X, Yan G, Tang X, Sun Y, Zeng X, Lin L (2021a) Cellulose nanocrystalline hydrogel based on a choline chloride deep eutectic solvent as wearable strain sensor for human motion. Carbohyd Polym 255:117443. https://doi.org/10.1016/j.carbpol.2020.117443

Wang H, Zhou R, Li D, Zhang L, Ren G, Wang L, Liu J, Wang D, Tang Z, Lu G, Sun G, Yu H-D, Huang W (2021b) High-performance foam-shaped strain sensor based on carbon nanotubes and Ti 3 C 2 T x MXene for the monitoring of human activities. ACS Nano 15(6):9690–9700. https://doi.org/10.1021/acsnano.1c00259

Wang L, Xu T, Fan C, Zhang X (2021c) Wearable strain sensor for real-time sweat volume monitoring. Iscience 24(1):102028. https://doi.org/10.1016/j.isci.2020.102028

Wang M, Wang T, Luo Y, He K, Pan L, Li Z, Cui Z, Liu Z, Tu J, Chen X, Wang M, Wang T, Luo Y, He K, Pan L, Li Z, Cui Z, Liu Z, Tu J, Chen X (2021d) Fusing stretchable sensing technology with machine learning for human-machine interfaces. Adv Func Mater 31(39):2008807. https://doi.org/10.1002/ADFM.202008807

Wang S, Ning H, Hu N, Liu Y, Liu F, Zou R, Huang K, Wu X, Weng S, Alamusi (2020) Environmentally-friendly and multifunctional graphene-silk fabric strain sensor for human-motion detection. Adv Mater Interfaces 7(1):1901507. https://doi.org/10.1002/ADMI.201901507

Wang S, Xiao P, Liang Y, Zhang J, Huang Y, Wu S, Kuo SW, Chen T (2018a) Network cracks-based wearable strain sensors for subtle and large strain detection of human motions. J Mater Chem C 6(19):5140–5147. https://doi.org/10.1039/C8TC00433A

Wang X, Li Q, Tao X (2021e) Sensing mechanism of a carbon nanocomposite-printed fabric as a strain sensor. Compos A Appl Sci Manuf 144:106350. https://doi.org/10.1016/j.compositesa.2021.106350

Wang X, Sun H, Yue X, Yu Y, Zheng G, Dai K, Liu C, Shen C (2018b) A highly stretchable carbon nanotubes/thermoplastic polyurethane fiber-shaped strain sensor with porous structure for human motion monitoring. Compos Sci Technol 168:126–132. https://doi.org/10.1016/J.COMPSCITECH.2018.09.006

Wang Y, Gao G, Ren X (2021f) Graphene assisted ion-conductive hydrogel with super sensitivity for strain sensor. Polymer 215:123340. https://doi.org/10.1016/j.polymer.2020.123340

Wang Y, Li W, Li C, Zhou B, Zhou Y, Jiang L, Wen S, Zhou F (2021g) Fabrication of ultra-high working range strain sensor using carboxyl CNTs coated electrospun TPU assisted with dopamine. Appl Surf Sci 566:150705. https://doi.org/10.1016/j.apsusc.2021.150705

Wang Y, Wang F, Yazigi S, Zhang D, Gui X, Qi Y, Zhong J, Sun L (2021h) Nanoengineered highly sensitive and stable soft strain sensor built from cracked carbon nanotube network/composite bilayers. Carbon 173:849–856. https://doi.org/10.1016/j.carbon.2020.11.025

Wang Y, Wang L, Yang T, Li X, Zang X, Zhu M, Wang K, Wu D, Zhu H (2014) Wearable and highly sensitive graphene strain sensors for human motion monitoring. Adv Func Mater 24(29):4666–4670. https://doi.org/10.1002/ADFM.201400379

Wang Z, Huang Y, Sun J, Huang Y, Hu H, Jiang R, Gai W, Li G, Zhi C (2016b) Polyurethane/cotton/carbon nanotubes core-spun yarn as high reliability stretchable strain sensor for human motion detection. ACS Appl Mater Interfaces 8(37):24837–24843. https://doi.org/10.1021/ACSAMI.6B08207/SUPPL_FILE/AM6B08207_SI_001.PDF

Wu H, Chen H, Yao P, Wang R (2021) Stretchable and highly sensitive strain sensor based on conductive polymer aerogel for human physiological information detection. Nano Select 2(4):802–809. https://doi.org/10.1002/nano.202000215

Wu J, Wu Z, Wei Y, Ding H, Huang W, Gui X, Shi W, Shen Y, Tao K, Xie X (2020) Ultrasensitive and stretchable temperature sensors based on thermally stable and self-healing organohydrogels. ACS Appl Mater Interfaces 12(16):19069–19079. https://doi.org/10.1021/acsami.0c04359

Xia Q, Wang S, Zhai W, Shao C, Xu L, Yan D, Yang N, Dai K, Liu C, Shen C (2021) Highly linear and low hysteresis porous strain sensor for wearable electronic skins. Compos Commun 26:100809. https://doi.org/10.1016/j.coco.2021.100809

Xiao T, Qian C, Yin R, Wang K, Gao Y, Xuan F (2021) 3D printing of flexible strain sensor array based on UV-curable multiwalled carbon nanotube/elastomer composite. Adv Mater Technol 6(1):2000745. https://doi.org/10.1002/admt.202000745

Xu B, Ye F, Chen R, Luo X, Chang G, Li R (2021) A wide sensing range and high sensitivity flexible strain sensor based on carbon nanotubes and MXene. Ceram Int. https://doi.org/10.1016/j.ceramint.2021.12.235

Xu R, Lu Y, Jiang C, Chen J, Mao P, Gao G, Zhang L, Wu S (2014) Facile fabrication of three-dimensional graphene foam/poly(dimethylsiloxane) composites and their potential application as strain sensor. ACS Appl Mater Interfaces 6(16):13455–13460. https://doi.org/10.1021/AM502208G

Xue P, Chen C, Diao D (2019) Ultra-sensitive flexible strain sensor based on graphene nanocrystallite carbon film with wrinkle structures. Carbon 147:227–235. https://doi.org/10.1016/J.CARBON.2019.03.001

Yan T, Wang Z, Pan ZJ (2018) Flexible strain sensors fabricated using carbon-based nanomaterials: a review. Curr Opin Solid State Mater Sci 22(6):213–228. https://doi.org/10.1016/j.cossms.2018.11.001

Yang Y, Yang YF, Tao LQ, Pang Y, Tian H, Ju ZY, Wu XM, Ren TL (2018) An ultrasensitive strain sensor with a wide strain range based on graphene armour scales. Nanoscale 10(24):11524–11530. https://doi.org/10.1039/C8NR02652A

Yang Z, Wu Z, Jiang D, Wei R, Mai X, Pan D, Vupputuri S, Weng L, Naik N, Guo Z (2021) Ultra-sensitive flexible sandwich structural strain sensors based on a silver nanowire supported PDMS/PVDF electrospun membrane substrate. J Mater Chem C 9(8):2752–2762. https://doi.org/10.1039/D0TC04659K

Yin B, Wen Y, Hong T, Xie Z, Yuan G, Ji Q, Jia H (2017) Highly stretchable, ultrasensitive, and wearable strain sensors based on facilely prepared reduced graphene oxide woven fabrics in an ethanol flame. ACS Appl Mater Interfaces 9(37):32054–32064. https://doi.org/10.1021/ACSAMI.7B09652/SUPPL_FILE/AM7B09652_SI_004.AVI

Yin F, Li X, Peng H, Li F, Yang K, Yuan W (2019) A highly sensitive, multifunctional, and wearable mechanical sensor based on RGO/synergetic fiber bundles for monitoring human actions and physiological signals. Sens Actuators B Chem 285:179–185. https://doi.org/10.1016/J.SNB.2019.01.063

Yu Y, Luo Y, Guo A, Yan L, Wu Y, Jiang K, Li Q, Fan S, Wang J (2017) Flexible and transparent strain sensors based on super-aligned carbon nanotube films. Nanoscale 9(20):6716–6723. https://doi.org/10.1039/C6NR09961K

Yu Y, Peng S, Blanloeuil P, Wu S, Wang CH (2020) Wearable temperature sensors with enhanced sensitivity by engineering microcrack morphology in PEDOT:PSS–PDMS sensors. ACS Appl Mater Interfaces 12(32):36578–36588. https://doi.org/10.1021/acsami.0c07649

Yuan W, Zhou Q, Li Y, Shi G (2015) Small and light strain sensors based on graphene coated human hairs. Nanoscale 7(39):16361–16365. https://doi.org/10.1039/C5NR04312C

Yue X, Jia Y, Wang X, Zhou K, Zhai W, Zheng G, Dai K, Mi L, Liu C, Shen C (2020) Highly stretchable and durable fiber-shaped strain sensor with porous core-sheath structure for human motion monitoring. Compos Sci Technol 189:108038. https://doi.org/10.1016/J.COMPSCITECH.2020.108038

Zeng J, Ma W, Wang Q, Yu S, Innocent MT, Xiang H, Zhu M (2021a) Strong, high stretchable and ultrasensitive SEBS/CNTs hybrid fiber for high-performance strain sensor. Compos Commun 25:100735. https://doi.org/10.1016/j.coco.2021.100735

Zhang D, Jiang C, Tong J, Zong X, Hu W (2018) Flexible strain sensor based on layer-by-layer self-assembled graphene/polymer nanocomposite membrane and its sensing properties. J Electron Mater 47(4):2263–2270. https://doi.org/10.1007/S11664-017-6052-1

Zhang D, Xu S, Zhao X, Qian W, Bowen CR, Yang Y, Zhang D, Xu S, Zhao X, Qian W, Yang Y, Bowen CR (2020a) Wireless monitoring of small strains in intelligent robots via a joule heating effect in stretchable graphene-polymer nanocomposites. Adv Func Mater 30(13):1910809. https://doi.org/10.1002/ADFM.201910809

Zhang K, Zhang J, Liu Y, Wang Z, Yan C, Song C, Gao C, Wu Y (2021a) A NIR laser induced self-healing PDMS/gold nanoparticles conductive elastomer for wearable sensor. J Colloid Interface Sci 599:360–369. https://doi.org/10.1016/j.jcis.2021.04.117

Zhang M, Wang C, Wang Q, Jian M, Zhang Y (2016) Sheath-core graphite/silk fiber made by dry-meyer-rod-coating for wearable strain sensors. ACS Appl Mater Interfaces 8(32):20894–20899. https://doi.org/10.1021/ACSAMI.6B06984/SUPPL_FILE/AM6B06984_SI_001.PDF

Zhang P, Chen Y, Li Y, Zhang Y, Zhang J, Huang L (2020b) A flexible strain sensor based on the porous structure of a carbon black/carbon nanotube conducting network for human motion detection. Sensors 20(4):1154. https://doi.org/10.3390/S20041154

Zhang X-W, Pan YI, Zheng Q, Yi X-S (2000) Time dependence of piezoresistance for the conductor-filled polymer composites. J Polym Sci B: Polym Phys 38:2739–2749. https://doi.org/10.1002/1099-0488

Zhang X, Zhang Y, Zhang W, Dai Y, Xia F (2021b) Gold nanoparticles-deranged double network for Janus adhesive-tough hydrogel as strain sensor. Chem Eng J 420:130447. https://doi.org/10.1016/j.cej.2021.130447

Zhao G, Wang X, Liu G, Thuy NTD (2022) A disposable and flexible electrochemical sensor for the sensitive detection of heavy metals based on a one-step laser-induced surface modification: a new strategy for the batch fabrication of sensors. Sens Actuators B: Chem 350:130834. https://doi.org/10.1016/j.snb.2021.130834

Zhao W, Xu S (2022) A facile structural strategy for a wearable strain sensor based on carbon nanotube modified helical yarns. Nanoscale Adv 4(1):250–257. https://doi.org/10.1039/D1NA00215E

Zhao Y, Deng S, Liu H, Zhang J, Guo Z, Hou H (2018) First-principle investigation of pressure and temperature influence on structural, mechanical and thermodynamic properties of Ti3AC2 (A = Al and Si). Comput Mater Sci 154:365–370. https://doi.org/10.1016/j.commatsci.2018.07.007

Zhao Y, Huang Y, Hu W, Guo X, Wang Y, Liu P, Liu C, Zhang Y (2019) Highly sensitive flexible strain sensor based on threadlike spandex substrate coating with conductive nanocomposites for wearable electronic skin. Smart Mater Struct 28(3):035004. https://doi.org/10.1088/1361-665X/AAF3CE

Zheng H, Lin N, He Y, Zuo B (2021) Self-healing, self-adhesive silk fibroin conductive hydrogel as a flexible strain sensor. ACS Appl Mater Interfaces 13(33):40013–40031. https://doi.org/10.1021/acsami.1c08395

Zheng Y, Li Y, Zhou Y, Dai K, Zheng G, Zhang B, Liu C, Shen C (2020) High-performance wearable strain sensor based on graphene/cotton fabric with high durability and low detection limit. ACS Appl Mater Interfaces 12(1):1474–1485. https://doi.org/10.1021/ACSAMI.9B17173/SUPPL_FILE/AM9B17173_SI_001.PDF

Zhou J, Yu H, Xu X, Han F, Lubineau G (2017) Ultrasensitive, stretchable strain sensors based on fragmented carbon nanotube papers. ACS Appl Mater Interfaces 9(5):4835–4842. https://doi.org/10.1021/ACSAMI.6B15195/SUPPL_FILE/AM6B15195_SI_001.PDF

Zu G, Wang X, Kanamori K, Nakanishi K (2020) Superhydrophobic highly flexible doubly cross-linked aerogel/carbon nanotube composites as strain/pressure sensors. J Mater Chem B 8(22):4883–4889. https://doi.org/10.1039/C9TB02953B

Chapter 10
Carbon-Based Functional Materials Derived from Fibrous Wastes

Daniel Karthik, Jiří Militký, Izabela Gallus, Gramoz Çubreli, Mohanapriya Venkataraman, and Vivek Remadevi Jayan

Abstract The accumulation of feedstock fibrous materials as wastes for industries has led to the growing need for techno-economic and sustainable methods to utilize these fibrous wastes in various forms, towards favorable areas of applications. Over the years, numerous efforts have been taken to obtain carbon-based materials in its various allotropic forms from both natural and synthetic sources of fibrous wastes. Fibrous wastes are processed through varying conditions of pyrolysis, stabilization (if required), carbonization, or graphitization to obtain carbon rich materials, which then may be activated (physical or chemical activation) to obtain activated carbon fibers, with multifunctional properties such as high surface area, variable pore size and volume, chemical inertness and stability, electrical and thermal conductivity; envisioned for potential scope in various applications such as adsorption of contaminants, supercapacitors and batteries, water filters (removal of chlorine, organic matter, etc.), surface treatment liquid cleaning, and gas phase applications (deodorization/volatile organic compound (VOC) adsorption). Fibrous adsorbents have the advantages of fast adsorption rate and ease of handling when compared with granular adsorbents and powdered adsorbents. Activated carbon fiber (ACF) is a promising microporous material with a fiber shape and well-defined porous structure. In general, ACF can be commercially manufactured from synthetic carbon fiber (CF) with an additional activation process. Processing of activated carbon fibers from various precursors involves the same steps as conducted in the preparation of traditional carbon fiber except for an additional step of activation of carbon fibers, where pore distribution of the precursor is further developed and matured. In this chapter, we potentially review

D. Karthik · J. Militký · M. Venkataraman (✉) · V. Remadevi Jayan
Department of Material Engineering, Faculty of Textile Engineering, Technical University of Liberec, Studentská 2, 46117 Liberec, Czech Republic
e-mail: mohanapriya.venkataraman@tul.cz

J. Militký
e-mail: jiri.militky@tul.cz

I. Gallus · G. Çubreli
Institute of Mechatronics and Computer Engineering, Faculty of Mechatronics, Informatics and Interdisciplinary Studies, Technical University of Liberec, Liberec, Czech Republic

the utilization of fibrous wastes to develop carbonaceous materials with promising functionalities.

10.1   Introduction

The augmented awareness towards ecological growth and the increased focus on resolving the issue of waste management over time has led to sustainable measures for the utilization of materials resources, with a techno-economic approach (Celep et al. 2022; Todor et al. 2019). Textile wastes can be classified as pre-consumer (includes manufacturing waste) and post-consumer wastes. Environmental imbalance is facilitated by the excessive accumulation of textile and fibrous waste in landfills. In direction with this, the utilization of fibrous wastes, that include wastes sourced from industrial sectors to household wastes, brings forth immediate attention. One of the many possibilities that has been cogitated in the recent times is of utilizing fibrous wastes (natural and synthetic) to obtain carbon-based materials with favourable properties and thriving potential for various applications (Jagdale et al. 2017; Khan et al. 2018). Carbon-based materials from fibrous sources are obtained in various forms and allotropes that majorly include activated carbon fibers, graphite, graphene, CNTs, fullerenes, and carbon quantum dots (CQDs) (Abou-Hadid et al. 2022; Cheng et al. 2019; Yaqoob et al. 2022).

Globally, an estimated 92 million tons of textile waste is generated, and in addition to the incredible amount of clothing being discarded each year, only 15% of it is recycled and 85% ends up in landfills or is incinerated (*A European Policy Framework for a Climate-Neutral Textile Industry*, n.d.; *The Most Surprising Clothing Waste Statistics And Trends in 2023 • GITNUX* 2023). Approximately, 5.8 million tons of textiles are discarded every year in the EU, and only a quarter of which is recycled (ELENA PAPPAS n.d.). In Europe, more than 15 kg of textile waste is generated per person (*Circular Fashion in Europe: Turning Waste into Value|McKinsey* n.d.) and the consumption of clothing and footwear is expected to increase by 63% by 2030 (*Circular Fashion in Europe: Turning Waste into Value|McKinsey* n.d.).

The advantages of polymeric fibers for the world's rapidly expanding population have led to an increase in their consumption for versatile area of application. However, regardless of how polymeric fibrous materials have improved the standard of our living, it is extremely difficult to manage fibrous wastes. Recycling, landfills (including discarded ones), and incineration are all options for managing polymeric fibrous wastes. However, toxic gases are produced when polymers are burned. Additionally, conventional recycling has some drawbacks because the recycled polymer has diminished durability and flexibility. In contrast to the conventional recycling mechanism, the most innovative and cutting-edge approach to managing fibrous wastes is 'upcycling' into solid carbonaceous materials. The primary method of upcycling is carbonization, or pyrolysis, which calls for high heat (>800 °C), a variable heating rate, and an inert environment. The carbonized materials created by upcycling polymeric fibrous wastes are used as adsorbents for waste purification,

Fig. 10.1 Upcycling of fibrous wastes to carbon-based functional materials (Choi et al. 2022)

energy and the environment, and electrical energy storage (EES) devices. The goal of the upcycling process is to create carbon-rich solid residues instead of oils or volatile compounds, as shown in Fig. 10.1 (Choi et al. 2022).

The significant combination of favourable chemical and physical properties found in carbon-based functional materials, including their excellent electrical conductivity, excellent heat conductivity, high mechanical strength, front-line optical properties, and chemical stability has drawn much attention. In recent years, a trend has emerged for the production of low cost, useful carbonaceous materials from various natural fiber biomasses to industrial synthetic fibers. These include cotton (Duman 2021; Kawasaki et al. 2012), lignin (Braun et al. 2005), wool (Hassan et al. 2015; Kawasaki et al. 2012), Sisal (Li et al. 2019a, b, c), Polyethylene terephthalate (PET) (Duman 2021; Kawasaki et al. 2012), polyethylene (PE) (Kaneko et al. 2004; Kim and Lee 2015; Xie et al. 2016), polypropylene (PP) (Karacan and Benli 2012), Poly(p-phenylene benzobisthiazole) (PBZT) (Jiang et al. 1991), poly(p-phenylene terephthalamaide) (Kevlar®) (Karthik et al. 2021), poly(p-phenylene-2,6-benzobisoxazole) (PBO) (Zhang et al. 2020a, b, c), poly(vinylacetylene) (Mavinkurve et al. n.d.), chitosan fibers (Bengisu and Yilmaz 2002), to mention a few.

The importance of synthesizing new carbon-based materials from waste sources has been drawing more attention by researchers and industrialists, considering its multifunctional properties and cost-effectiveness. This is reflected in Fig. 10.2 (Abd Elkodous et al. 2022), which shows the increase in published research carried out in this area.

10.2   Carbon-Based Functional Materials

In this section, we categorize and describe the most common carbon-based functional materials from waste sources, for potential use in versatile areas of applications, highlighted in Fig. 10.3.
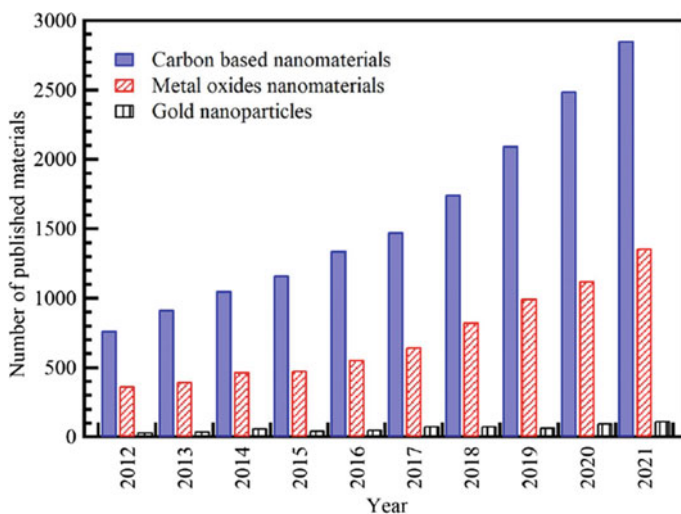
Fig. 10.2 Distribution of the cumulative number of publications on waste-derived carbon-based nanomaterials per year (Abd Elkodous et al. 2022)

10.3 Activated Carbon Fibers

Activated carbon (AC) or activated charcoal (known conventionally) is the material highly porous in nature and is characterized by its complex structure of carbon atoms (Marsh and Rodríguez-Reinoso 2006b; Hassan et al. n.d.). High surface area and improved porosity make AC an outstanding adsorbent, especially for the adsorption of liquids and gasses (Marsh and Rodríguez-Reinoso 2006a).

The value and effectiveness of ACF for adsorption applications are marked by its high packing density and excellent volumetric capacity. ACF is also potentially useful for a variety of applications, including the removal of dyes and heavy metal contamination in wastewater treatment, the capture of volatile organic compounds (VOCs), supercapacitors, electrochemical and energy storage applications, refrigeration, catalysis, ohmic heating applications, and electromagnetic shielding material.

Activated carbon obtained from fibrous sources, also known as activated carbon fibers (ACF), have shown to have higher specific surface area, adsorption rate, and adsorption efficiency than granular activated carbon obtained from petroleum pitch or coal, which is traditionally used as precursors (Kawasaki et al. 2012; Suzuki 1994). Processing of ACFs from carbon-rich precursors involves the same steps as involved in the preparation of traditional carbon fiber but for an additional step of activation, where pore distribution is developed further. Moreover, the costs involved additionally to manufacture fibrous structures particularly for the production ACFs is sidestepped (Hassan et al. n.d.).

Apart from its porous nature, which is similar with ACs, ACFs offer several other advantages owing to its fibrous shape with high surface area, trivial mesoporosity
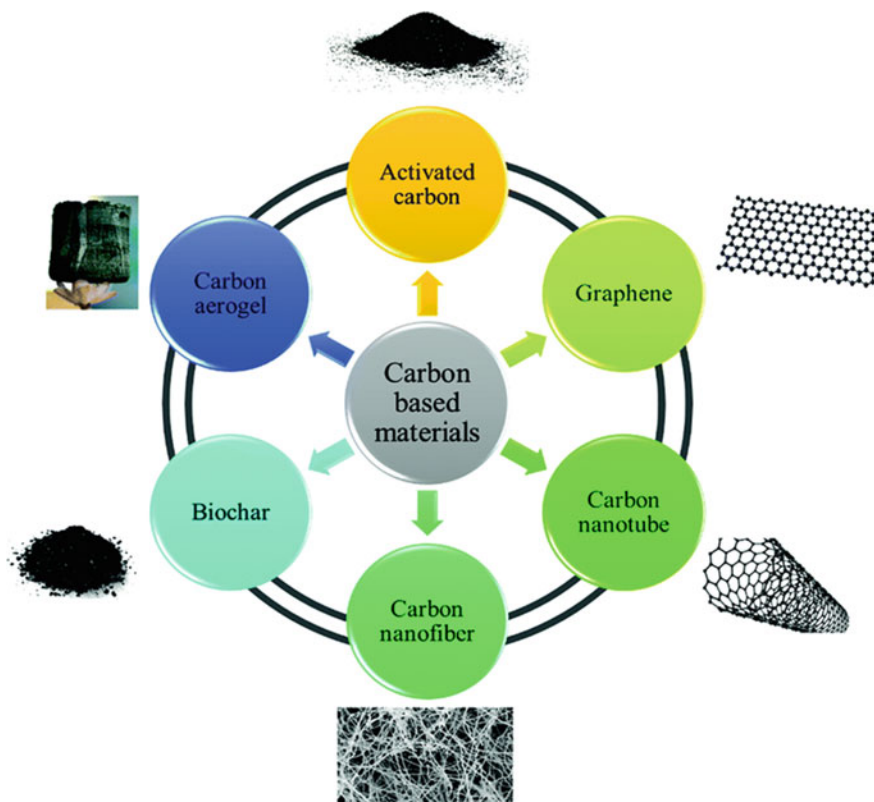
Fig. 10.3 Carbon-based materials. Reprinted with the permission from Ref (Mehdi Sabzehmeidani et al. 2021)

and nearly no microporosity (shown in Fig. 10.4), high accessible porosity, improved contact efficiencies with media which enables it to have potential applications in predominant fields of research i.e., natural gas storage, adsorbent in heavy metal industry, treatment and purification of water and air, hydrogen storage as a fuel, and electrochemical applications such as supercapacitors. Meanwhile, the versatility of ACFs allows its utilization in the textile industry, that includes personal protective clothing, domestic fabrics, medical masks, filtration, and catalytic support to mention a few. There are various that factors that influence the choice of precursor used to obtain ACF such as availability of resources, ease in activation, inorganic content, and carbon yield, keeping in mind the costs involved (Hassan et al. n.d.).

The prevailing steps involved in the production of ACFs from fibrous sources include stabilization, pre-treatment for-instance, acid impregnation (prior to carbonization), carbonization/pyrolysis, and in some cases activation (physical or
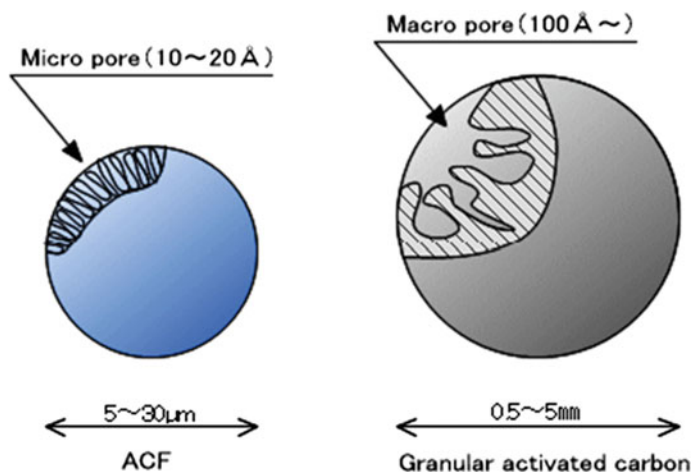
Fig. 10.4 Pore of ACF and granular activated carbon (SO-EN.CO)

chemical activation). However, it must be mentioned that pre-treatment and stabilization steps depend on the type of precursor and are not necessarily included in the preparation of ACF.

10.4 Graphene

It is known that the hexagonal structure of graphene serves as the fundamental building block for the sp2 hybridization of the 2 s orbital and two 2p orbitals of the carbon atom, which gives it interesting characteristics, including high surface area, high thermal conductivity, strong Young's modulus, and fast charge carrier mobility, which make it suitably versatile for numerous applications, such as adsorption of hazardous organic compounds, gas sensors, batteries and optoelectronic devices, drug delivery, photocatalysts, etc.

Biomass wastes have been used to synthesize graphene and its derivatives. This includes sugarcane, chitosan, glucose, etc. With hydrothermal treatment, fungus can produce porous graphene materials (Abd Elkodous et al. 2022). Green synthesis using plant extracts, grapefruit extract, agricultural waste, etc. (Saikia et al. 2020) has been employed as an environment friendly option to obtain graphene and CNTs, with reduced toxicity, greenhouse gases, and cost. PET waste was used to obtain high quality graphene, without the need of any catalyst (El Essawy et al. 2017a, b).
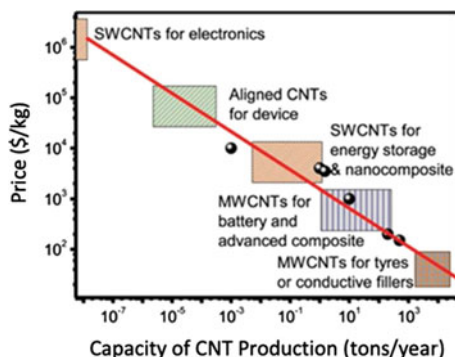
10.5   Carbon Nanotubes (CNTs)

CNTs are cylinder-shaped allotropes of carbon molecules that belong to the fullerene family and have exceptional strength as well as distinct electrical, mechanical, and thermal properties. The majority of the methods used to make CNTs encounter challenges like high energy consumption and expensive equipment requirements that restrict their approach to making CNTs. In this regard, obtaining CNTs from waste sources may be a suitable, affordable, and environmentally friendly substitute. Prior research has been done on high-value carbon CNTs made from used plastics (Wu et al. 2014). According to the estimate in Fig. 10.5, the widespread use of CNTs will not be made possible until their cost approaches that of conductive carbon black (Zhuo and Levendis 2014).

10.6   Fullerenes

Another possible form of carbon recovery is fullerenes, which can, for example, be recovered from waste PET bottles (El Essawy et al. 2017a, b). One example of the use of fullerenes is the sorption of various dyes. Elessawy et al. (2020) obtained magnetic fullerene nanocomposite (FMFNc) by catalytic thermal decomposition of sustainable PET bottle wastes.

Nanostructured fullerenes, thanks to their unique capabilities such as excellent optoelectronic features, high affinity for electrons, and the ability to rapidly transfer charge, have found applications in photovoltaics, photocatalysis, polymer solar cells, electrocatalysis, photodynamic therapy, environmental remediation, and in medicine for drug delivery. Figure 10.6 shows possible routes for the acquisition, functionalization, and applications of nanofullerenes (Baskar et al. 2022).

Fig. 10.6 Potential routes for acquisition, functionalization and applications of nanofullerenes (Baskar et al. 2022)

Fullerene unit cell
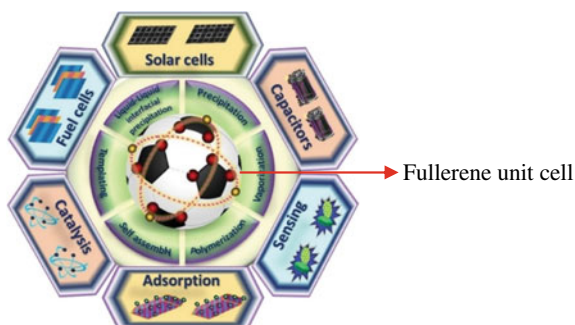
10.7 Carbon Aerogel

Yang et al. (2015) obtained a multifunctional carbon fiber (MCF) aerogel from disposable bamboo chopsticks and tested its use in adsorbing oils and organic solvents. The authors claim that the material has shown average sorption capacity, but the way it is regenerated is much better than currently available products.

10.8 Fibrous Waste Sources as Precursors for Carbon-Based Functional Materials

The following essential criteria should be considered when choosing raw materials for the production of carbon-based materials: high carbon content; low inorganic matter content for a low ash outcome; high density and content of volatile matter; available in abundance, ensuring that the cost of the raw material is constantly very low; potential activation range; low rate of deterioration during storage; and the potential for producing activated carbon with a high yield. Based on these factors, some of the fibrous sources that have been utilized for the purpose of obtaining carbon-based functional materials have been mentioned here, in two categories—natural fibrous waste sources and synthetic fibrous waste sources.

10.8.1 Natural Fibrous Waste Sources

The sustainable development of humanity depends greatly on the high value utilization of the abundantly available sources of renewable fibrous biomasses (agricultural and industrial). Furthermore, biomass is a rich source of carbon, making it a prime candidate for the production of carbon fibers and biochar. Cotton fibrous wastes are a promising precursor to activated carbon because they are a rich source of cellulose. There is no ideal method for recycling used cotton textiles. The waste hierarchy

should serve as a benchmark for all solutions. These factors make thermal transformation processes of cellulosic wastes to carbon fibers and activated carbon fibers a commercially viable solution, when cheaper primary materials and simpler recycling processes are in competition (Hemati et al. 2023; Liu et al. 2022). Table 10.1 displays the functional properties and versatile areas of application contributed by carbon-based materials from natural fibrous waste sources.

10.8.2   Synthetic Fibrous Waste Sources

Typically, synthetic polymeric wastes are recycled, downcycled into inferior products, or dumped in landfills. Plastics are adaptable for commercial and residential uses due to their wide range of characteristics, including their light weight, strength, heat resistance, high level of convenience, and low cost. These substances are, however, high molecular weight organic polymers made of substances like carbon, hydrogen, oxygen, nitrogen, and sulfur. Their potential as a secondary carbon resource has been underrated, despite their appealing hydrocarbon makeup. Only a small number of researchers have attempted to use polymer materials, such as polypropylene (PP), polycarbonate (PC), acrylonitrile butadiene styrene (ABS), polyethylene (PE), and polyurethane (PU), as an additional source of carbon in the manufacturing and metallurgical industries (Hemati et al. 2023).

Different applications produce different kinds of polymeric waste. Numerous studies using different kinds of plastic waste have been conducted. Each type of waste polymer has a unique range of carbonized products when it is transformed into invaluable carbon materials. Here, we list the various plastic types and their corresponding upcycled carbonaceous materials, as shown in Fig. 10.7.

Polyethylene Terephthalate (PET). Activated carbon is the most common upcycled PET. However, other types of carbonaceous materials have also been derived from PET. Mu et al. (2020) selectively carbonized waste PET plastic into three-dimensional porous carbon nanosheets with a high yield of 36.4 wt%. Kamali and Yang (2020), examined the thermal processing of PET waste using molten salts to create carbon materials with various properties, including porous nanostructures and nanosheets that resemble graphene. Ko et al. (2020) described a synthetic method that involved pyrolysis at 900 °C followed by boron-assisted catalytic graphitization at 2400 °C to create graphite from PET wastes. Additionally, graphite derived from PET was successfully exfoliated to yield graphene sheets. An innovative method for creating multiwalled carbon nanotubes and nanochanneled ultrafine carbon tubes from PET wastes using rotating cathode arc discharge is another possibility. Based on solvent-free and catalyst-free methods, Pol et al. (2011) suggested converting PET into carbon microspheres. Duman (2021), demonstrated that using hydrothermal carbonization as a pre-treatment can enhance the activation performance of fibrous wastes made of polyester and cotton-polyester mixtures, producing activated carbon with greater surface area and micropore volume while using less activating agent.

Table 10.1 Carbon-based materials from natural fibrous waste sources

Naturally occurring fibrous wastes/ biomass	Carbon-based material	Method of synthesis	Properties and applications
Jute biomass	Advanced biocarbon (Tripathi et al. 2022)	Waste burlap biomass carbonized at various temperatures (325–1000 °C), followed by ball-milling	High thermal stability
Jute thread	Nanoporous carbon (Ahmadi et al. 2021)	Carbonization and Chemical Activation with KOH, heated to 900 °C	High surface area and high pore volume
Jute fibers	1. Porous carbon (Sharma et al. 2017) 2. Activated carbon (Pantrangi et al. 2020) 3. arboxycellulose nanofibers (Sharma et al. 2017)9/6/2023 5:51:00 PM	1. Activation by $CuCl_2$ under 800 °C for 2 h under argon atmosphere 2. Hydrothermal approach and activation by KOH 3. Nitric acid-sodium nitrite method	1. Excellent electrochemical performance, high BET surface area 2. High surface area, high charge storage capacity 3. Nanofibers with low crystallinity
Woven cotton	Activated carbon fiber (Zheng et al. 2014)	Heated to 700–800 °C under CO_2 atmosphere	Carbon fiber with very high surface area of $789 m^2/g$
Cotton linter	Carbon fiber (Zhou et al. 2016)	CarbaCell method using a wet-spinning technology and carbonization process	Relatively smooth surface and approximately round compact morphology in cross-section
Cotton, viscose and Avicel fibers	Carbon microsphere (Zhang et al. 2020a, b, c)	Hydrothermal Carbonization	Carbon microspheres with high crystallinities of 60.35 and 60.24%, respectively, for cotton and Avicel
Coconut coir pith	Activated carbon (Sesuk et al. 2019)	Combined physical and chemical activation by using NaOH	Good capability, high surface area, high micropore volume
Hemp Bast fiber	Activated carbon (Hossain et al. 2018)	Hydrothermal processing—hot water processing (390–500 °C) followed by activation by KOH and NaOH	High surface area and mesoporosity

Table 10.1 (continued)

Naturally occurring fibrous wastes/ biomass	Carbon-based material	Method of synthesis	Properties and applications
Lignin fibers (Braun et al. 2005)	Carbon fiber	Carbonization of dry-spun fibers from lignin dissolved in an alkali solution with poly (vinyl alcohol)	Carbon fibers suitable for General performance grades
Lignocellulosic biomass	Activated carbon fiber (Hassan et al. n.d.)	Pre-oxidation, carbonization, and chemical activation with dehydrating agents	Well-defined porous structure and narrow pore size distribution
Bamboo cellulose fibers (Zhang et al. 2018)	Activated biomass carbon	Carbonization and KOH activation	High surface area, a large capacitance, excellent rate capability, mesoporous structure
Wool fibers	1. Activated carbon (Gao et al. 2013) 2. N-doped porous carbon (Li et al. 2019a, b, c) 9/6/ 2023 5:51:00 PM	1. Muffle furnace (MFAC) and microwave (MAC) heating methods with phosphoric acid activation 2. Pre-carbonization under N_2, activation with KOH, calcination at 600 °C	1. High surface area 2. Good pore structure, excellent adsorption properties
Silk fibers	Porous activated carbon (Xu et al. 2022)	Activation by $KHCO_3$ at 800 °C followed by carbonization	High electrothermal efficiency
Palm fibers (Ayinla et al. 2019)	Activated carbon	Carbonization and chemical activation (300–800 °C)	Water purification, gas storage, air purification, medicine sewage treatment, metal extraction, decaffeination, active material for energy storage devices

Table 10.1 (continued)

Naturally occurring fibrous wastes/ biomass	Carbon-based material	Method of synthesis	Properties and applications
Palm leaves (*Borassus flabellifer*) (Ahammad et al. 2019)	Carbon nanosheets	Activation with $NaHCO_3$ at 850 °C for 5 h under N_2 atmosphere	Developing Electrochemical sensor for simultaneous detection of dopamine and uric acid Large surface area, pore-size distribution, sensibility for dopamine and uric acid
Cicada slough (Jia et al. 2019)	Heteroatom incorporated porous carbon	Carbonization at 600 °C under N_2 atmosphere	High potency of naturally derived heteroatom functionalities, well-developed microporosity and high specific surface area (1676 m^2 g^{-1}),
Anaerobic digestor residue from cattle manure (Wang et al. 2019)	Activated carbon (lignocellulosic biomass)	KOH activation followed by pyrolysis under nitrogen atmosphere	High specific surface area, good pore size distribution, high specific capacitance, and excellent cycle stability in the aqueous electrolytes
Rotten carrots (Ahmed et al. 2018)	Porous activated carbon	$ZnCl_2$ activation and thermal treatment at 900 °C under N_2 atmosphere	Cost-effective, eco-friendly AC-based electrode, for energy storage devices
Black wattle bark waste (Lütke et al. 2019)	Activated carbon	$ZnCl_2$ activation and carbonization	Large specific surface area

Polypropylene (PP): PP has been shown suitable to be utilized for the upcycling of graphene, CNTs, and carbon dots (Li et al. 2015; Sharon et al. 2015). Tang et al. (2005) and Song et al. (2007) both confirmed novel catalytic degradation methods to synthesize multiwalled carbon nanotubes from PP, as the precursor for carbon source. Figure 10.8 shows a one-pot approach to convert PP into CNTs, by combined catalysis of AC and Ni_2O_3, where the combination of AC with Ni_2O_3 showed a synergistic effect on the catalytic conversion of PP to form CNTs (Gong et al. 2012). In another study, cup-stacked carbon nanotubes were efficiently produced through the carbonization of PP (Gong et al. 2013a, b).
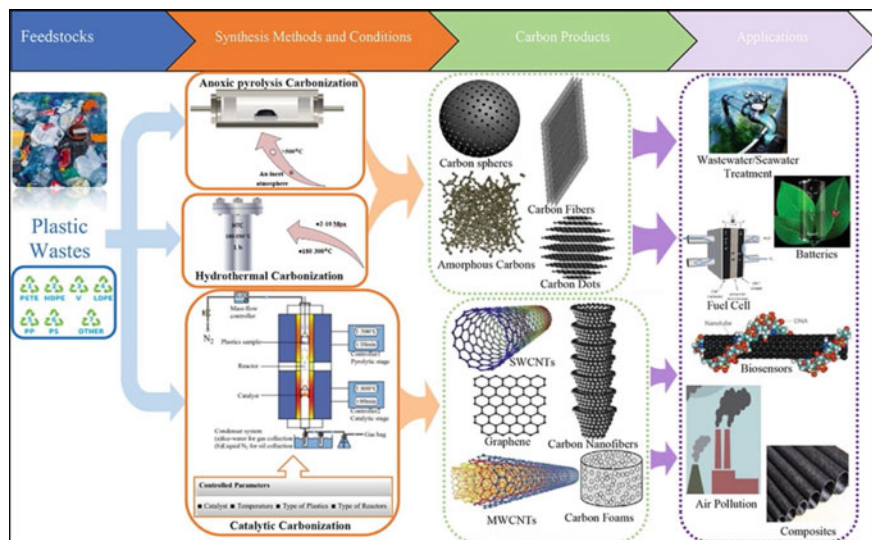
Fig. 10.7 Upcycling process of plastic wastes to obtain carbon-based functional materials (Dai et al. 2023)
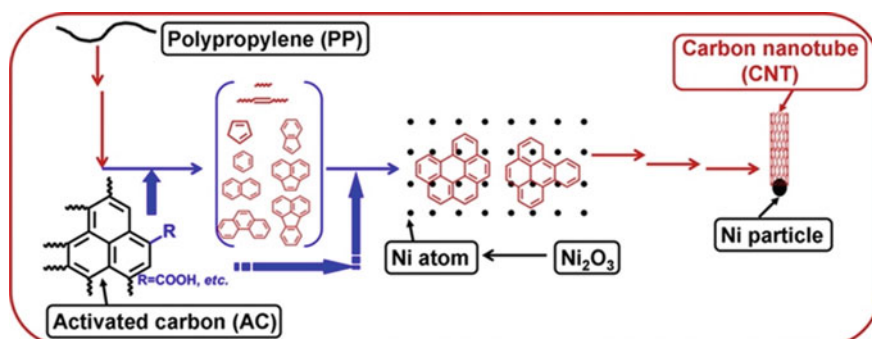
Fig. 10.8 Synthesis of CNT from PP wastes/AC (Gong et al. 2012)

Polyethylene (PE): Carbon-based functional materials are also produced from waste PE. Polyethylene has great potential as a precursor material for carbon fiber production, considering its high carbon content, large-scale and low-cost melt-spinning production. An environmentally progressive approach to synthesize modified carbon-based materials, such as spherical carbon particles, carbon nanotubes and porous carbon, obtained from PE wastes, has been reported (Lian et al. 2019; Pol et al. 2009; Younker et al. 2013).

Instead of the more conventionally used pitch or polyacrylonitrile-based precursor, Kim and Lee (2015) were able to produce carbon fibers from linear low-density PE that had the best mechanical properties (tensile strength and tensile modulus of 1.65

GPa and 110 GPa, respectively). These fibers are comparable to commercial-grade carbon fiber. In another study, high-density PE was used as the precursor to obtain carbon fibers (Wortberg et al. 2015).

Using an adaptable fabrication technique, Hunt et al. (2012) created patterned, continuous carbon fibers from PE carbon precursor with controlled surface geometries and properties. The carbon fibers, which have different cross-sectional geometries (as shown in figure), display ordered graphitic structures close to the surface and porous disordered carbon close to the core. Compared to solid fibers of similar construction, these hollow, porous fibers have a larger surface area.

Aramids or Aromatic polyamides: Aramids, prevalently referred to as Kevlar and Nomex, have proven to be suitable precursors for producing carbon fibers using a variety of carbonization and activation processes. Numerous studies concentrated on the physical activation of Nomex and Kevlar fibers using CO_2 or steam, as well as the chemical activation in the presence of trace amounts of phosphoric acid (Choma et al. 2016; Suárez-García et al. 2004). Daniel et al. (Karthik et al. 2021) demonstrated a novel single stage cost-effective method (shown in Fig. 10.9.) of simultaneous carbonization and physical activation of fibrous Kevlar wastes to produce activated carbon fabric with enhanced surface area and electrical conductivity, which significantly influenced the electromagnetic shielding ability (Karthik et al. 2021, 2023; Mosquera et al. 2002).

Polystyrene (PS): One of the white pollutants that is difficult to degrade is waste polystyrene. By catalytically carbonizing PS pellets, Nie et al. (2020) and Gong et al. (2013a, b) created porous hollow carbon nanospheres. Using the Friedel–Crafts reaction, Gatti et al. (2019) created a porous carbonaceous material from commercially available expanded polystyrene and investigated its gas adsorption characteristics. Wen et al. (2019) created porous carbon sheets from PS by carbonizing a MgO template and activating it with KOH. In a different study, metal Ni was used to catalyze the pyrolysis of polystyrene to produce graphitized carbons (Lei et al. 2008).

Polyacrylonitrile (PAN): PAN-based fibers, also referred to as acrylic fibers, as industrial wastes are available in abundance and make the perfect precursor for the production of carbon-based materials. Studies have demonstrated the utilization of Acrylic fibrous wastes to obtained porous carbon fibers with high carbon yield and
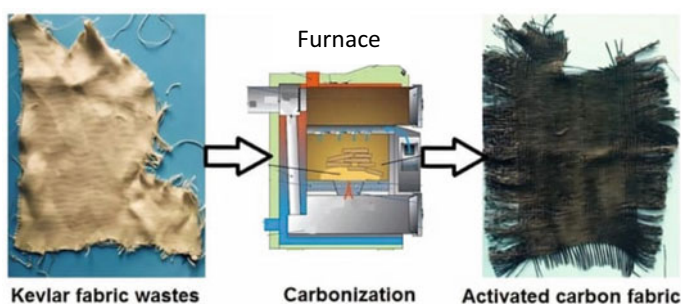
Fig. 10.9 Carbonization of Kevlar to AC fabric (Karthik et al. 2021)

improved thermal and electrical properties, also making it suitable to be used in multifunctional composites (Naeem et al. 2017, 2019) and as novel adsorbents for dye removal (Rabbi et al. 2020) and *p*-cresol removal (Alkathiri et al. 2020).

10.9   Applications of Carbon-Based Functional Materials from Waste Sources

10.9.1   Adsorption: Water and Air Purification

One of the primary uses of carbon recovered from various wastes, due to its high porosity, large specific surface area, and low apparent density, is adsorption for the purification of various media (Yang et al. 2015; Zhang et al. 2020a, b, c). Examples of its use in sorption include air purification, water filtration and purification, sorption of metals, and rare elements (Alcaraz et al. 2021; Smith et al. 2016; Yang et al. 2015). Carbon obtained from waste and used for its property of adsorption can take many forms, including carbon black (Smith et al. 2016), carbon fibers (Kumari et al. 2022; Ni et al. 2022; Pullas Navarrete and de la Torre 2022), carbon aerogels (Yang et al. 2015), carbon nanotubes, and others.

Adsorption of Oils: One of the common problems in the industry is the purification of water–oil mixtures (Gupta et al. 2017). For many years, attempts have been made to develop a low-cost technique for separating these elements. The inherently hydrophobic nature of carbon in various carbon-based aerogels such as CNT sponge, graphene/CNT hybrid foam, graphene sponge, and carbon nanofiber (CNF) sponge have been obtained for this purpose (Yang et al. 2015).

Another application and sourcing of carbon fiber were presented by Ni et al. (2022). In their work, they obtained carbon fibers by pyrolysis of waste from aerospace production. They used the extracted fibers to produce a filter membrane for separating oil-in-water emulsions. They produced the membrane by using a cellulose paper filter as a substrate, tannic acid and (3-Aminopropyl) triethoxysilane as reactants in a one-pot reaction. As a result, they obtained a super hydrophilic membrane with an oil separation efficiency of up to 99.8% [Ni].

Adsorption of dyes: Different forms of carbon have also found applications in liquid purification that are used to adsorb various pollutions, for example, dyes such as thymol blue (TB) (Kumari et al. 2022), methylene blue (MB) (El Essawy et al. 2017a, b), or 1-naphthol (Wu et al. 2015). Thymol blue is one of the most commonly used dyes in the fiber industry and poses a risk to humans and aquatic ecosystems. The search is, therefore, on for an economical and environmentally friendly sorbent that can be easily sourced. Activated carbon (AC), which can be easily obtained from natural biomass and has high porosity and surface reactivity, has proven to be an alternative. Agricultural, vegetable, and fruit wastes, as well as wood biomass, can serve as its source. Kumari et al. (2022) proposed obtaining active carbon fibers from single-use solid plastic waste such as cups, bottles, and polyethylene bags

and then tested the sorption properties of the resulting material. The results they obtained seem promising and solve the problem of polluting the environment with dyes and dealing with plastic waste. Another example of the processing and reuse of bottles, mainly consisting of PET, was proposed by El Essawy et al. (2017a, b). They obtained graphene from this waste through thermal dissociation, which they then tested for sorption of alkaline and acid dyes, i.e., methylene blue (MB) and acid blue 25 (AB25). The performance of sorption processes always depends on process parameters such as initial dye concentration, pH, temperature, the concentration of sorbent used, sorption time, etc. Under optimal conditions, they were able to remove 91–99% of MB and 70–97% of AB25 (shown in Fig. 10.7.) (Fig. 10.10).

In another study, magnetic fullerene nanocomposite (FMFNc) was obtained by catalytic thermal decomposition of sustainable PET bottle waste in combination with ferrocene as a catalyst and magnetite nanoparticles. The best separation efficiency was achieved when the dye concentration was 50 mg/l and at 35 °C. At this condition, 99.61% of methylene blue (MB) and 97.01% of acid blue (AB25) were removed. The experiment and its procedure are shown in Fig. 10.11 (Elessawy et al. 2020).

Adsorption of Rare Earth Elements (REEs): Smith et al. (2016) used the black carbon from recycled tires (RTCB) to sorb rare earth elements (REEs) such as Y, La, Ce, Nd, and Sm from liquids. These elements play a key role in current technologies like magnets, catalysis or display technologies. The advantage of this method is that the elements can be recovered from sources where their concentration is not high, as opposed to solvent extraction or precipitation, where the starting concentration of REEs must be high. In this case, carbon black derived from whole-used tires is procured by pyrolysis. This sourcing process entails a number of benefits in terms of cost reduction, energy and environmental impact. Gases produced during the pyrolysis of tires are used to provide the energy required for the process. The mechanism of REEs sorption on RTCB is based on cation and ion exchange. In the future, the

Fig. 10.10 Active carbon from single-use solid plastic waste (El Essawy 2017a)
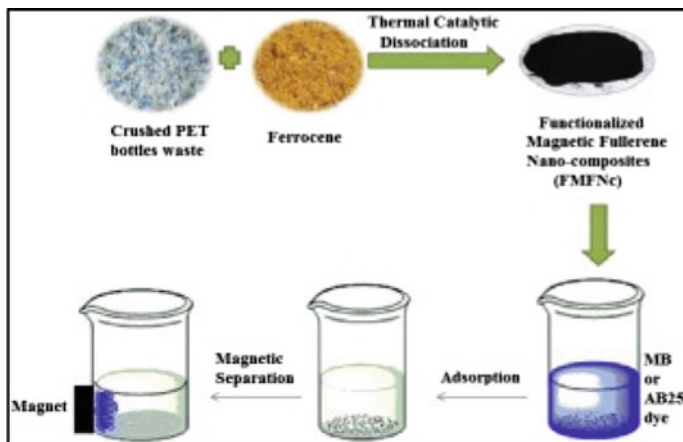
Fig. 10.11 Synthesis of magnetic fullerene nanocomposites for adsorption of MB or AB25 dyes (Elessawy et al. 2020)

regenerative issue of the product should be considered so that the method can be used on a large scale. In another study, Alcaraz et al. (2021) used activated carbon recovered from spent coffee grounds to recover terbium from liquid solutions. Their research showed that the sorption capacity increased with increasing temperature and pH value (from 2 to 5). Terbium recovery was performed under acidic conditions, where the desorption percentage was 87%.

Water purification. Another widely occurring contaminant in wastewater is antibiotics. To adsorb a mixture of antibiotics composed of cephalexin and cefradine, Li et al. (2019a, b, c) prepared activated charcoal from herbal residues. At low concentrations of these antibiotics, they were able to remove 84% of the antibiotic from the solution; 90% of the antibiotic was desorbed using the ultrasonic treatment, and the reuse capacity was 80%.

In contrast, Navarrete et al. (2022) obtained activated carbon fibers from cotton-woven wastes and impregnated them with metallic silver particles to acquire antibacterial properties. These properties are essential to prevent biofouling and bacterial proliferation inside filter pores when filtering air or water. Using a chemical activation method with phosphoric acid, they succeeded in obtaining ACF with a carbon content of 65.6% and thus proved that woven cotton waste can be a good precursor for obtaining ACF due to its high content of lignocellulosic particles. These fibers could find their application in filtration, deodorization, and catalytic support processes.

By combining and creating composites consisting of different forms of carbon, even more unique properties of the designed product can be obtained. Wu et al. (2018) described how, using carbonization and pre-impregnation of fullerene, they created a porous additive through which they increased the performance of forward osmosis (FO) water purification membranes. The additive they developed significantly increased the flow rate and water permeability for the thin film nanocomposite

(TFN) membrane they tested. Also, the photocatalytic properties of fullerenes can be used in water filtration, for example, in water disinfection.

Ouyang et al. (2017) developed an efficient and safe photocatalyst that exhibited bactericidal properties under visible light. In their work, they described the antibacterial properties of the metal-free catalysts they obtained by co-wrapping fullerenes (C60, C70) with carbon nitride (C3N4) through a hydrothermal process. The enhanced photocatalytic capabilities were due to interactions between C_3N_4 and fullerene. C60/C70 inhibited the recombination of electrons and holes located on the surface of C_3N_4. The generated pairs of electrons and holes on the surface in contact with water molecules and oxygen formed $\bullet O_2^-$ and $\bullet OH$ radicals, which damaged the bacterial cell wall under the visible light irradiation. Disinfection efficiencies for C70/C2N4 and C70/C2N4 against *E. coli* 0157:H7 were 99% and 86% after 4 h of exposure, respectively.

Air purification: In addition to the filtration of aqueous solutions, carbon is also widely used in the filtration and separation of gaseous media. Mashhadimoslem et al. (2022) verified $O_2/N_2/CO_2$ sorption properties for functionalized and not modified granular activated carbon (GAC). Functionalization with $ZnCl_2$ helped improve oxygen sorption by 19.75%, and the sorbent's affinity for gases had the following order $O_2 > N_2 > CO_2$. The effectiveness of the sorbent they prepared dropped from 100 to 97% after 20 cycles.

Miscellaneous: An interesting and innovative way of obtaining carbon fibers was demonstrated by Robertson et al. (2022), where they used disposable masks as a source of fibrous carbon. Their consumption has been greatly increased in recent years during the COVID-19 pandemic, and nowadays, there are now problems related to their storage and management. Their processing involves the simple processing steps of thermal stabilization and pyrolysis. The authors claim that from the fibrous structure of polypropylene masks through simple thermal stabilization and pyrolysis steps, carbon structures with high carbon yields can be obtained, which is characterized by porosity and natural sulfur content. Potential applications for these fibers include the removal of organic contaminants from aqueous environments, Joule heating, and oil adsorption (shown in Fig. 10.12.).

10.9.2   Energy Storage Devices

Energy consumption is increasing, and with it increases the need for new energy harvesting and storage technologies to meet such demands, while respecting the environment. The energy market, in which fossil fuels serve as the primary energy source, has a significant impact on both the environment and the global economy. The massive structure of capacitors is a drawback for their incorporation into newer technologies, which are on the horizon. The following charts highlight the main difference between different energy storage sources. It can be seen in Fig. 10.13 that supercapacitors are high-power systems while fuel cells are high-energy systems.

Fig. 10.12 Potential applications of carbon fibers obtained from waste facemask (Robertson et al. 2022)
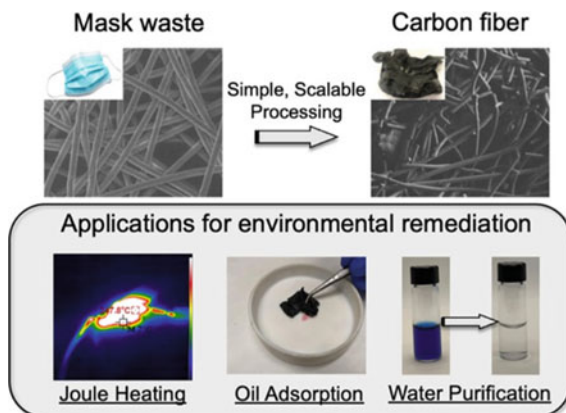
Fig. 10.13 Ragone plot of different electrochemical energy conversion systems, combustion engine, turbines, and traditional capacitors (Poonam et al. 2019)
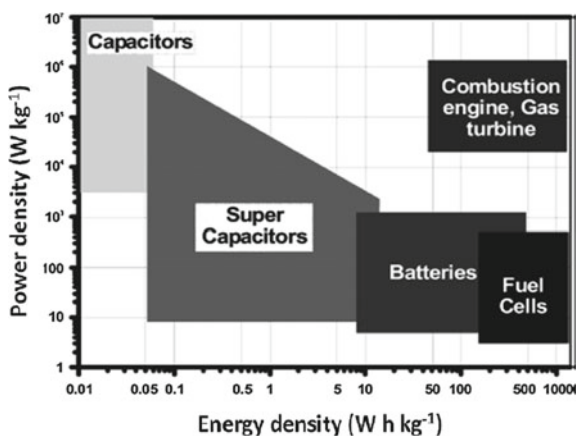
The main electrical properties of interest when it comes to energy storage devices are long life cycles combined with high power densities, high specific capacitance, no memory effect, etc. For multifunctional consumer electronics, key mechanical characteristics like flexibility, transparency, and lighter weight are prerequisites (Jiang et al. 2012; Poonam et al. 2019; Stein et al. 2009).

Supercapacitors: A type of storage that falls between a capacitor and a traditional battery is the supercapacitor. Because of their higher power density, longer lifespan, wider operating temperature range, environmental friendliness, and quick charging and discharging capabilities, supercapacitors outperform batteries. According to different reports, supercapacitors have 500,000 life cycles, compared to 400–1200 load cycles for Li–ion batteries. However, their low energy density, lower than lithium-ion batteries, poses a barrier for supercapacitors to be employed in a wider range of applications (Ding et al. 2015; Bhattacharyya et al. 2013).

The first ever supercapacitor to be patented was the one by General Electric in the year 1957, using activated charcoal as the building material of the electrodes. Nowadays, nanoporous carbon nanomaterials such as activated carbon, graphene, carbide-derived carbon, carbon nanotubes, etc. due to their good electrical conductivity, high specific area, coupled with their mechanical and chemical properties, are the main materials used for supercapacitors. Apart from these, electrodes must be chemically stable and resistant to corrosion. Flexible devices make use of carbon nanotubes and graphene as electrode materials (Li et al. 2019a, b, c; Zhai et al. 2022). In the case of hybrid capacitors, carbon-based materials can be used together with conductive polymers.

Graphene is an ideal material for supercapacitor, especially linear supercapacitors (in the form of graphene fibers) (Yu et al. 2017), coming from the fact that it has excellent electrical conductivity and high specific area (theoretical value of 2630 m^2g^{-1} which provided a specific capacitance of 550 Fg^{-1}), coupled with its chemical stability and other properties. It is also used in flexible wearable electronics and is the most thermally conductive carbon material (Poonam et al. 2019; Saikia et al. 2020; Zhai et al. 2022). A green approach to synthesis, using aloe vera leaves to obtain reduced graphene oxide with large surface area and remarkable physical properties was attempted, according to which the usage of plant extracts promotes high current density compared to graphene oxide (Bhattacharya et al. 2017).

Despite the excellent electrochemical properties of various carbon materials, activated carbon is currently the most commonly used carbon electrode material in commerce due to the low cost (Zhai et al. 2022), high specific surface area (1000–2000 m^2/g) (Hou et al. 2012), and are indispensable in wide range of applications.

Supercapacitors can be classified as electric double-layer supercapacitors (EDLCs) and pseudo-supercapacitors based on the various energy storage techniques[G2]. The electrostatic interaction at the electrode–electrolyte interface of pure carbon materials causes charges to build up, which is how EDLCs store their energy (Kim et al. 2016; Zhang and Zhao 2009). The capacitance can be enhanced by self-doping (defects, vacancies etc.) (Zhou and Yao 2022). Consequently, accessible surface area of the electrode material has a big impact on EDLC's capacitance. EDLCs have higher power density and better cycling stability than pseudo-supercapacitors due to the fact that there is no chemical reaction involved in the charging-discharging process, but they exhibit lower capacitance than pseudo-supercapacitors. Self-healing and highly stretchable supercapacitors made of graphene fibers have been reported (Wang et al. 2017).

Pseudo-supercapacitors get their capacitance by the rapid and reversible intercalation or redox reactions of electroactive species on the electrode surface. This includes, for example, conducting polymers or transition metal oxides/hydroxides. Pseudo-capacitance can also be a result of the many defects inside carbon materials, heteroatom doping, for example, or different functional groups (Wang et al. 2017; Zhai et al. 2022).

Based on the material electrodes are built of, there are also hybrid capacitors. A carbon electrode and a Li–ion electrode were combined in these capacitors, increasing
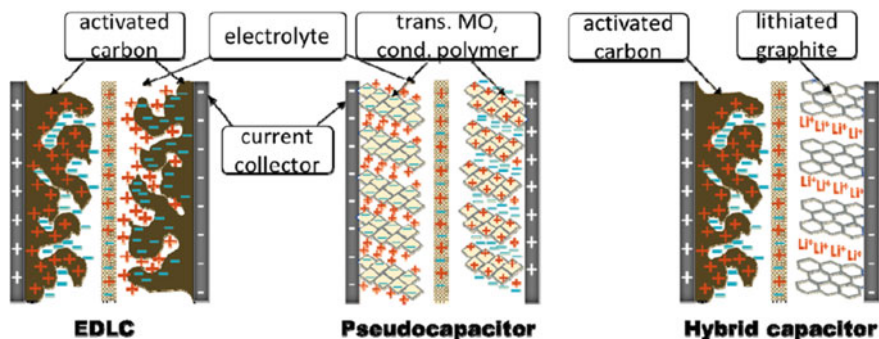
Fig. 10.14   Schematic diagram of different types of supercapacitors (Saikia et al. 2020)

the capacitance, lowering the anode potential with higher cell voltage, and thus raising the Ed. In such setups, the non-faradaic electrode generates greater Pd and the higher Ed is generated by the faradaic electrode with a high Cs. Here, carbon materials are coupled with CPs/TMOs (Poonam et al. 2019). The three types of supercapacitors are shown in Fig. 10.14.

10.9.3   Conclusion and Outlook

In summary, this review attempts to highlight different carbon-based functional materials like activated carbon fibers, CNTs, graphene, and others from various sources of fibrous wastes, their various properties and key applications. With the global temperatures rising and the efforts to reduce the emission of carbon dioxide in the atmosphere, adding to the fact that our fossil fuel sources are depleting, environmentally friendly approaches to effectively utilize industrial, agricultural, and household fibrous waste sources have gained a great deal attention. Innumerable amounts naturally available biomass wastes, as well as industrially accumulated fibrous plastic wastes, paired with disposal issues thereof, is only escalating by the hour. Providentially, these carbon-rich wastes have shown to be suitable precursor materials to produce carbon-based materials with multi-functional properties, potentially making them sustainable and cost-effective alternatives in various areas of applications.

References

A European policy framework for a climate-neutral textile industry: The Policy Hub—Circularity for Apparel and Footwear supports the EU Strategy for Sustainable and Circular Textiles (n.d.). https://www.policyhub.org/articles/a-european-policy-framework-for-a-climate-neutral-textile-industry-the-policy-hub-circularity-for-apparel-and-footwear-supports-the-eu-strategy-for-sustainable-and-circular-textiles. Accessed 24 Mar 2023

Abd Elkodous M, Hamad HA, Abdel Maksoud MIA, Ali GAM, El Abboubi M, Bedir AG, Eldeeb AA, Ayed AA, Gargar Z, Zaki FS, Farage DAM, Matsuda A, Abdelnour MR, Sabra BA, Elsayed A, Abdelrazek ST, Abdelhameed ST, Gharieb MA, Rabee MM, Aboeldiar SA, Abdo NA, Elwakeel AM, Mahmoud AS, Elsaid MMM, Omar WM, Hania RA, Mahmoud NG, Elsayed ASS, Mohamed TM, Sewidan MA, Sayed MAM, Abbas AA, Elsayed AH, Alazab AM, Basyooni MA, Magdy M, Mashaly EA, Salem OM, Saber S, Hafez AA, Tan WK, Kawamura G (2022) Cutting-edge development in waste-recycled nanomaterials for energy storage and conversion applications. Nanotechnol Rev 11(1):2215–2294. https://doi.org/10.1515/ntrev-2022-0129

Abou-Hadid AF, El-Behairy UA, Elmalih MM, Amdeha E, El Naggar AMA, Taha MH, Hussein AEM (2022) Production of efficient carbon fiber from different solid waste residuals for adsorption of hazardous metals from wastewater samples. Biomass Convers Biorefinery. https://doi.org/10.1007/s13399-022-03097-6

Ahammad AJS, Odhikari N, Shah SS, Hasan MM, Islam T, Pal PR, Qasem MAA, Aziz MA (2019) Porous tal palm carbon nanosheets: preparation, characterization and application for the simultaneous determination of dopamine and uric acid. Nanoscale Adv 1(2):613–626. https://doi.org/10.1039/C8NA00090E

Ahmadi R, Alivand MS, Haj Mohammad Hossein Tehrani N, Ardjmand M, Rashidi A, Rafizadeh M, Seif A, Mollakazemi F, Noorpoor Z, Rudd J (2021) Preparation of fiber-like nanoporous carbon from jute thread waste for superior CO2 and H2S removal from natural gas: experimental and DFT study. Chem Eng J 415:129076. https://doi.org/10.1016/j.cej.2021.129076

Ahmed S, Ahmed A, Rafat M (2018) Supercapacitor performance of activated carbon derived from rotten carrot in aqueous, organic and ionic liquid based electrolytes. J Saudi Chem Soc 22(8):993–1002. https://doi.org/10.1016/j.jscs.2018.03.002

Alcaraz L, Saquinga DN, Alguacil FJ, Escudero E, López FA (2021) Application of activated carbon obtained from spent coffee ground wastes to effective terbium recovery from liquid solutions. Metals 11(4):Article 4. https://doi.org/10.3390/met11040630

Alkathiri DSS, Sabri MA, Ibrahim TH, ElSayed YA, Jumean F (2020) Development of activated carbon fibers for removal of organic contaminants. Int J Environ Sci Technol 17(12):4841–4852. https://doi.org/10.1007/s13762-020-02808-8

Ayinla RT, Dennis JO, Zaid HM, Sanusi YK, Usman F, Adebayo LL (2019) A review of technical advances of recent palm bio-waste conversion to activated carbon for energy storage. J Clean Prod 229:1427–1442. https://doi.org/10.1016/j.jclepro.2019.04.116

Baskar AV, Benzigar MR, Talapaneni SN, Singh G, Karakoti AS, Yi J, Al-Muhtaseb AH, Ariga K, Ajayan PM, Vinu A (2022) Self-assembled fullerene nanostructures: synthesis and applications. Adv Func Mater 32(6):2106924. https://doi.org/10.1002/adfm.202106924

Bengisu M, Yilmaz E (2002) Oxidation and pyrolysis of chitosan as a route for carbon ®ber derivation. Carbohydr Polym

Bhattacharyya NK, Das M, Das I, Mukherjee D, Saha H (2013) Application of supercapacitor to power small electronic appliances. IOSR J Electr Electron Eng 4(3):28–32. https://doi.org/10.9790/1676-0432832

Bhattacharya G, Sas S, Wadhwa S, Mathur A, McLaughlin J, Roy SS (2017) Aloe vera assisted facile green synthesis of reduced graphene oxide for electrochemical and dye removal applications. RSC Adv 7(43):26680–26688. https://doi.org/10.1039/C7RA02828H

Braun JL, Holtman KM, Kadla JF (2005) Lignin-based carbon fibers: oxidative thermostabilization of kraft lignin. Carbon 43(2):385–394. https://doi.org/10.1016/j.carbon.2004.09.027

Celep G, Tetik GD, Yilmaz F, Celep G, Tetik GD, Yilmaz F (2022) Limitations of textile recycling: the reason behind the development of alternative sustainable fibers. In: Next-generation textiles. IntechOpen. https://doi.org/10.5772/intechopen.105118

Cheng Y, Zhang Q, Fang C, Huang Z, Chen J, Wu L, Wang H (2019) Synthesis of N-doped porous carbon materials derived from waste cellulose acetate fiber via urea activation and its potential application in supercapacitors. J Electrochem Soc 166(6):A1231. https://doi.org/10.1149/2.1081906jes

Choi J, Yang I, Kim S-S, Cho SY, Lee S (2022) Upcycling plastic waste into high value-added carbonaceous materials. Macromol Rapid Commun 43(1):2100467. https://doi.org/10.1002/marc.202100467

Choma J, Osuchowski L, Marszewski M, Dziura A, Jaroniec M (2016) Developing microporosity in Kevlar®-derived carbon fibers by CO2 activation for CO2 adsorption. J CO2 Util 16:17–22. https://doi.org/10.1016/j.jcou.2016.05.004

Circular fashion in Europe: Turning waste into value|McKinsey (n.d.). https://www.mckinsey.com/industries/retail/our-insights/scaling-textile-recycling-in-europe-turning-waste-into-value. Accessed 24 Mar 2023

Dai L, Karakas O, Cheng Y, Cobb K, Chen P, Ruan R (2023) A review on carbon materials production from plastic wastes. Chem Eng J 453:139725. https://doi.org/10.1016/j.cej.2022.139725

Ding J, Wang H, Li Z, Cui K, Karpuzov D, Tan X, Kohandehghan A, Mitlin D (2015) Peanut shell hybrid sodium ion capacitor with extreme energy–power rivals lithium ion capacitors. Energy Environ Sci 8(3):941–955. https://doi.org/10.1039/C4EE02986K

Duman G (2021) Preparation of novel porous carbon from hydrothermal pretreated textile wastes: effects of textile type and activation agent on structural and adsorptive properties. J Water Process Eng 43:102286. https://doi.org/10.1016/j.jwpe.2021.102286

El Essawy NA, Ali SM, Farag HA, Konsowa AH, Elnouby M, Hamad HA (2017a) Green synthesis of graphene from recycled PET bottle wastes for use in the adsorption of dyes in aqueous solution. Ecotoxicol Environ Saf 145:57–68. https://doi.org/10.1016/j.ecoenv.2017.07.014

El Essawy NA, Konsowa AH, Elnouby M, Farag HA (2017b) A novel one-step synthesis for carbon-based nanomaterials from polyethylene terephthalate (PET) bottles waste. J Air Waste Manag Assoc 67(3):358–370. https://doi.org/10.1080/10962247.2016.1242517

ELENA PAPPAS (n.d.) Latest trend keeps clothes out of landfill|Research and Innovation. https://ec.europa.eu/research-and-innovation/en/horizon-magazine/latest-trend-keeps-clothes-out-landfill. Accessed 24 Mar 2023

Elessawy NA, El-Sayed EM, Ali S, Elkady MF, Elnouby M, Hamad HA (2020) One-pot green synthesis of magnetic fullerene nanocomposite for adsorption characteristics. J Water Process Eng 34:101047. https://doi.org/10.1016/j.jwpe.2019.101047

Gao Q, Liu H, Cheng C, Li K, Zhang J, Zhang C, Li Y (2013) Preparation and characterization of activated carbon from wool waste and the comparison of muffle furnace and microwave heating methods. Powder Technol 249:234–240. https://doi.org/10.1016/j.powtec.2013.08.029

Gatti G, Errahali M, Tei L, Mangano E, Brandani S, Cossi M, Marchese L (2019) A porous carbon with excellent gas storage properties from waste polystyrene. Nanomaterials 9(5):Article 5. https://doi.org/10.3390/nano9050726

Gong J, Liu J, Chen X, Wen X, Jiang Z, Mijowska E, Wang Y, Tang T (2013a) Synthesis, characterization and growth mechanism of mesoporous hollow carbon nanospheres by catalytic carbonization of polystyrene. Microporous Mesoporous Mater 176:31–40. https://doi.org/10.1016/j.micromeso.2013.03.039

Gong J, Liu J, Jiang Z, Wen X, Chen X, Mijowska E, Wang Y, Tang T (2013b) Effect of the added amount of organically-modified montmorillonite on the catalytic carbonization of polypropylene into cup-stacked carbon nanotubes. Chem Eng J 225:798–808. https://doi.org/10.1016/j.cej.2013.03.112

Gong J, Liu J, Wan D, Chen X, Wen X, Mijowska E, Jiang Z, Wang Y, Tang T (2012) Catalytic carbonization of polypropylene by the combined catalysis of activated carbon with Ni2O3 into

carbon nanotubes and its mechanism. Appl Catal a: Gen 449:112–120. https://doi.org/10.1016/j.apcata.2012.09.028

Gupta RK, Dunderdale GJ, England MW, Hozumi A (2017) Oil/water separation techniques: a review of recent progresses and future directions. J Mater Chem A 5(31):16025–16058. https://doi.org/10.1039/C7TA02070H

Hassan M, Schiermeister L, Staiger M (2015) Sustainable production of carbon fiber: effect of cross-linking in wool fiber on carbon yields and morphologies of derived carbon fiber. ACS Sustain Chem & Eng 3:151002102858004. https://doi.org/10.1021/acssuschemeng.5b00994

Hassan MF et al (n.d.) Recent trends in activated carbon fibers production from various precursors and applications—a comparative review. Elsevier Enhanced Reader. https://doi.org/10.1016/j.jaap.2019.104715

Hemati S, Udayakumar S, Wesley C, Biswal S, Nur-A-Tomal MS, Sarmadi N, Pahlevani F, Sahajwalla V (2023) Thermal transformation of secondary resources of carbon-rich wastes into valuable industrial applications. J Compos Sci 7(1):Article 1. https://doi.org/10.3390/jcs7010008

Hossain MZ, Wu W, Xu WZ, Chowdhury MBI, Jhawar AK, Machin D, Charpentier PA (2018) High-surface-area mesoporous activated carbon from hemp bast fiber using hydrothermal processing. C 4(3):Article 3. https://doi.org/10.3390/c4030038

Hou C-H, Huang J-F, Lin H-R, Wang B-Y (2012) Preparation of activated carbon sheet electrode assisted electrosorption process. J Taiwan Inst Chem Eng 43(3):473–479. https://doi.org/10.1016/j.jtice.2011.12.003

Hunt MA, Saito T, Brown RH, Kumbhar AS, Naskar AK (2012) Patterned functional carbon fibers from polyethylene. Adv Mater 24(18):2386–2389. https://doi.org/10.1002/adma.201104551

Jagdale P, Koumoulos EP, Cannavaro I, Khan A, Castellino M, Dragatogiannis D, Tagliaferro A, Charitidis CA (2017) Towards green carbon fibre manufacturing from waste cotton: a microstructural and physical property investigation. Manuf Rev 4:10. https://doi.org/10.1051/mfreview/2017008

Jia H, Sun J, Xie X, Yin K, Sun L (2019) Cicada slough-derived heteroatom incorporated porous carbon for supercapacitor: ultra-high gravimetric capacitance. Carbon 143:309–317. https://doi.org/10.1016/j.carbon.2018.11.011

Jiang H, Desai P, Kumar S, Abhiraman AS (1991) Carbon fibers from poly (p-phenylene benzobisthiazole) (pbzt) fibers: conversion and morphological aspects. Carbon 29(4):635–644. https://doi.org/10.1016/0008-6223(91)90131-2

Jiang H, Ma J, Li C (2012) Mesoporous carbon incorporated metal oxide nanomaterials as supercapacitor electrodes. Adv Mater 24(30):4197–4202. https://doi.org/10.1002/adma.201104942

Kamali AR, Yang J (2020) Effect of molten salts on the structure, morphology and electrical conductivity of PET-derived carbon nanostructures. Polym Degrad Stab 177:109184. https://doi.org/10.1016/j.polymdegradstab.2020.109184

Kaneko M, Kumagai S, Nakamura T, Sato H (2004) Study of sulfonation mechanism of low-density polyethylene films with fuming sulfuric acid. J Appl Polym Sci 91(4):2435–2442. https://doi.org/10.1002/app.13404

Karacan I, Benli H (2012) Use of sulfonation procedure for the development of thermally stabilized isotactic polypropylene fibers prior to carbonization. J Appl Polym Sci 123(1):234–245. https://doi.org/10.1002/app.34454

Karthik D, Baheti V, Militky J, Naeem M, Tunakova V, Ali A (2021) Activated carbon derived from carbonization of kevlar waste materials: a novel single stage method. Materials 14:6433. https://doi.org/10.3390/ma14216433

Karthik D, Militky J, Wang Y, Venkataraman M (2023) Joule heating of carbon-based materials obtained by carbonization of para-aramid fabrics. C 9(1):Article 1. https://doi.org/10.3390/c9010023

Kawasaki N, Tominaga H, Ogata F, Inoue K, Kankawa M (2012) Development of novel carbon fiber produced from waste fiber by cabonization. J Oleo Sci 61(10):593–600. https://doi.org/10.5650/jos.61.593

Khan A, Jagdale P, Castellino M, Rovere M, Jehangir Q, Mandracci P, Rosso C, Tagliaferro A (2018) Innovative functionalized carbon fibers from waste: how to enhance polymer composites properties. Compos B Eng 139:31–39. https://doi.org/10.1016/j.compositesb.2017.11.064

Kim H-K, Bak S-M, Lee SW, Kim M-S, Park B, Lee SC, Choi YJ, Jun SC, Han JT, Nam K-W, Chung KY, Wang J, Zhou J, Yang X-Q, Roh KC, Kim K-B (2016) Scalable fabrication of micron-scale graphene nanomeshes for high-performance supercapacitor applications. Energy Environ Sci 9(4):1270–1281. Scopus. https://doi.org/10.1039/c5ee03580e

Kim JW, Lee JS (2015) Preparation of carbon fibers from linear low density polyethylene. Carbon 94:524–530. https://doi.org/10.1016/j.carbon.2015.06.074

Ko S, Kwon YJ, Lee JU, Jeon Y-P (2020) Preparation of synthetic graphite from waste PET plastic. J Ind Eng Chem 83:449–458. https://doi.org/10.1016/j.jiec.2019.12.018

Kumari M, Chaudhary GR, Chaudhary S, Umar A (2022) Transformation of solid plastic waste to activated carbon fibres for wastewater treatment. Chemosphere 294:133692. https://doi.org/10.1016/j.chemosphere.2022.133692

Lei Z, Xiao Y, Dang L, Bai S, An L (2008) Graphitized carbon with hierarchical mesoporous structure templated from colloidal silica particles. Microporous Mesoporous Mater 109(1):109–117. https://doi.org/10.1016/j.micromeso.2007.04.035

Li M, Xiao H, Zhang T, Li Q, Zhao Y (2019a) Activated carbon fiber derived from sisal with large specific surface area for high-performance supercapacitors. ACS Sustain Chem & Eng 7(5):4716–4723. https://doi.org/10.1021/acssuschemeng.8b04607

Li Q, Yao K, Zhang G, Gong J, Mijowska E, Kierzek K, Chen X, Zhao X, Tang T (2015) Controllable synthesis of 3D hollow-carbon-spheres/graphene-flake hybrid nanostructures from polymer nanocomposite by self-assembly and feasibility for lithium-ion batteries. Part Part Syst Charact 32(9):874–879. https://doi.org/10.1002/ppsc.201500037

Li S, Huang S, Xu F, Xiao H, Zhang F, Zhang G (2019b) Preparing polyester/carbon multifunctional fabrics by phosphoric acid carbonization. Cellulose 26(16):8907–8917. https://doi.org/10.1007/s10570-019-02699-0

Li Y, Xu R, Wang B, Wei J, Wang L, Shen M, Yang J (2019c) Enhanced N-doped porous carbon derived from KOH-activated waste wool: a promising material for selective adsorption of CO2/CH4 and CH4/N2. Nanomaterials 9(2):Article 2. https://doi.org/10.3390/nano9020266

Lian Y, Ni M, Huang Z, Chen R, Zhou L, Utetiwabo W, Yang W (2019) Polyethylene waste carbons with a mesoporous network towards highly efficient supercapacitors. Chem Eng J 366:313–320. https://doi.org/10.1016/j.cej.2019.02.063

Liu F, Wang Q, Zhai G, Xiang H, Zhou J, Jia C, Zhu L, Wu Q, Zhu M (2022) Continuously processing waste lignin into high-value carbon nanotube fibers. Nat Commun 13(1):Article 1. https://doi.org/10.1038/s41467-022-33496-2

Lütke SF, Igansi AV, Pegoraro L, Dotto GL, Pinto LAA, Cadaval TRS (2019) Preparation of activated carbon from black wattle bark waste and its application for phenol adsorption. J Environ Chem Eng 7(5):103396. https://doi.org/10.1016/j.jece.2019.103396

Marsh H, Rodríguez-Reinoso F (2006a) Introduction to the scope of the text (Chap. 1). In Marsh H, Rodríguez-Reinoso F (eds) Activated carbon. Elsevier Science Ltd., pp 1–12. https://doi.org/10.1016/B978-008044463-5/50015-7

Marsh H, Rodríguez-Reinoso F (2006b) Activated carbon (origins) (Chap. 2). In Marsh H, Rodríguez-Reinoso F (eds) Activated carbon. Elsevier Science Ltd., pp 13–86. https://doi.org/10.1016/B978-008044463-5/50016-9

Mashhadimoslem H, Safarzadeh Khosrowshahi M, Jafari M, Ghaemi A, Maleki A (2022) Adsorption equilibrium, thermodynamic, and kinetic study of o2/n2/co2 on functionalized granular activated carbon. ACS Omega 7(22):18409–18426. https://doi.org/10.1021/acsomega.2c00673

Mavinkurve A, Visser S, Pennings AJ (n.d.) An initial evaluation of poly(vinylacetylene) as a carbon fiber precursor

Mehdi Sabzehmeidani M, Mahnaee S, Ghaedi M, Heidari H, Roy VAL (2021) Carbon based materials: a review of adsorbents for inorganic and organic compounds. Mater Adv 2(2):598–627. https://doi.org/10.1039/D0MA00087F

Mosquera MEG, Jamond M, Martinez-Alonso A, Tascon JMD (2002) Thermal transformations of kevlar aramid fibers during pyrolysis: infrared and thermal analysis studies (world) [Research-article]. ACS Publications; American Chemical Society. https://doi.org/10.1021/cm00047a006

Mu X, Li Y, Liu X, Ma C, Jiang H, Zhu J, Chen X, Tang T, Mijowska E (2020) Controllable carbonization of plastic waste into three-dimensional porous carbon nanosheets by combined catalyst for high performance capacitor. Nanomaterials 10(6):Article 6. https://doi.org/10.3390/nano10061097

Naeem S, Baheti V, Militky J, Ali A (2019) Multifunctional polylactic acid composites filled with activated carbon particles obtained from acrylic fibrous wastes. Polym Compos 40(2):578–590. https://doi.org/10.1002/pc.24695

Naeem S, Baheti V, Tunakova V, Militky J, Karthik D, Tomkova B (2017) Development of porous and electrically conductive activated carbon web for effective EMI shielding applications. Carbon 111:439–447. https://doi.org/10.1016/j.carbon.2016.10.026

Ni T, You Y, Xie Z, Kong L, Newman B, Henderson L, Zhao S (2022) Waste-derived carbon fiber membrane with hierarchical structures for enhanced oil-in-water emulsion separation: performance and mechanisms. J Membr Sci 653:120543. https://doi.org/10.1016/j.memsci.2022.120543

Nie T, Yuan Z, Yin S, Tu W, Yan W, Gao J, Jiang X (2020) Thermal behavior of crosslinking polystyrene resin to carbon material by one-step carbonization. J Porous Mater 27(1):249–261. https://doi.org/10.1007/s10934-019-00808-9

Ouyang K, Dai K, Chen H, Huang Q, Gao C, Cai P (2017) Metal-free inactivation of E. coli O157:H7 by fullerene/C3N4 hybrid under visible light irradiation. Ecotoxicol Environ Saf 136:40–45. https://doi.org/10.1016/j.ecoenv.2016.10.030

Pantrangi M, Lei Z, Ran F (2020) Biomass waste derived low cost activated carbon from carchorus olitorius (jute fiber) as sustainable and novel electrode material. J Energy Storage 30:101494. https://doi.org/10.1016/j.est.2020.101494

Pol SV, Pol VG, Sherman D, Gedanken A (2009) A solvent free process for the generation of strong, conducting carbon spheres by the thermal degradation of waste polyethylene terephthalate. Green Chem 11(4):448–451. https://doi.org/10.1039/B819494G

Pol VG, Thackeray MM (2011) Spherical carbon particles and carbon nanotubes prepared by autogenic reactions: evaluation as anodes in lithium electrochemical cells. Energy Environ Sci 4(5):1904–1912. https://doi.org/10.1039/C0EE00256A

Poonam, Sharma K, Arora A, Tripathi SK (2019) Review of supercapacitors: materials and devices. J Energy Storage 21:801–825. https://doi.org/10.1016/j.est.2019.01.010

Pullas Navarrete J, de la Torre E (2022) Preparation of activated carbon fibers (ACF) impregnated with metallic silver particles from cotton-woven wastes and its performance as an antibacterial agent. Mater Today Commun 33:104598. https://doi.org/10.1016/j.mtcomm.2022.104598

Rabbi A, Dadashian F, Soleimani M (2020) Evaluation of microporous acrylic-based activated carbon fibers as novel adsorbents for methylene blue removal. Desalin Water Treat 179:288–301. https://doi.org/10.5004/dwt.2020.24981

Robertson M, Güillen Obando A, Emery J, Qiang Z (2022) Multifunctional carbon fibers from chemical upcycling of mask waste. ACS Omega 7(14):12278–12287. https://doi.org/10.1021/acsomega.2c00711

Saikia BK, Benoy SM, Bora M, Tamuly J, Pandey M, Bhattacharya D (2020) A brief review on supercapacitor energy storage devices and utilization of natural carbon resources as their electrode materials. Fuel 282:118796. https://doi.org/10.1016/j.fuel.2020.118796

Sesuk T, Tammawat P, Jivaganont P, Somton K, Limthongkul P, Kobsiriphat W (2019) Activated carbon derived from coconut coir pith as high performance supercapacitor electrode material. J Energy Storage 25:100910. https://doi.org/10.1016/j.est.2019.100910

Sharma PR, Joshi R, Sharma SK, Hsiao BS (2017) A simple approach to prepare carboxycellulose nanofibers from untreated biomass. Biomacromol 18(8):2333–2342. https://doi.org/10.1021/acs.biomac.7b00544

Sharon M, Mishra N, Patil B, Mewada A, Gurung R, Sharon M (2015) Conversion of polypropylene to two-dimensional graphene, one-dimensional carbon nano tubes and zero-dimensional C-dots, all exhibiting typical sp2-hexagonal carbon rings. IET Circuits Devices Syst 9(1):59–66. https://doi.org/10.1049/iet-cds.2014.0117

Smith YR, Bhattacharyya D, Willhard T, Misra M (2016) Adsorption of aqueous rare earth elements using carbon black derived from recycled tires. Chem Eng J 296:102–111. https://doi.org/10.1016/j.cej.2016.03.082

Song R, Jiang Z, Bi W, Cheng W, Lu J, Huang B, Tang T (2007) The combined catalytic action of solid acids with nickel for the transformation of polypropylene into carbon nanotubes by pyrolysis. Chem—A Eur J 13(11):3234–3240. https://doi.org/10.1002/chem.200601018

Stein A, Wang Z, Fierke MA (2009) Functionalization of porous carbon materials with designed pore architecture. Adv Mater 21(3):265–293. https://doi.org/10.1002/adma.200801492

Suárez-García F, Martínez-Alonso A, Tascón JMD (2004) Activated carbon fibers from Nomex by chemical activation with phosphoric acid. Carbon 42(8–9):1419–1426. https://doi.org/10.1016/j.carbon.2003.11.011

Suzuki M (1994) Activated carbon fiber: fundamentals and applications. Carbon 32(4):577–586. https://doi.org/10.1016/0008-6223(94)90075-2

Tang T, Chen X, Meng X, Chen H, Ding Y (2005) Synthesis of multiwalled carbon nanotubes by catalytic combustion of polypropylene. Angew Chem Int Ed 44(10):1517–1520. https://doi.org/10.1002/anie.200461506

The Most Surprising Clothing Waste Statistics And Trends in 2023 • GITNUX, 24 March 2023. (2023). https://blog.gitnux.com/clothing-waste-statistics/

Todor MP, Bulei C, Kiss I, Cioată VG (2019) Recycling of textile wastes into textile composites based on natural fibres: the reinforcement type and the architecture. IOP Conf Ser: Mater Sci Eng 477:012055. https://doi.org/10.1088/1757-899X/477/1/012055

Tripathi N, Uribe AR, Weldekidan H, Misra M, Mohanty AK (2022) Upcycling of waste jute biomass to advanced biocarbon materials: the effect of pyrolysis temperature on their physicochemical and electrical properties. Mater Adv 3(24):9071–9082. https://doi.org/10.1039/D2MA00678B

Wang C, Wang J, Wu W, Qian J, Song S, Yue Z (2019) Feasibility of activated carbon derived from anaerobic digester residues for supercapacitors. J Power Sources 412:683–688. https://doi.org/10.1016/j.jpowsour.2018.11.092

Wang S, Liu N, Su J, Li L, Long F, Zou Z, Jiang X, Gao Y (2017) Highly stretchable and self-healable supercapacitor with reduced graphene oxide based fiber springs. ACS Nano 11(2):2066–2074. https://doi.org/10.1021/acsnano.6b08262

Wen Y, Wen X, Wenelska K, Chen X, Mijowska E (2019) Novel strategy for preparation of highly porous carbon sheets derived from polystyrene for supercapacitors. Diam Relat Mater 95:5–13. https://doi.org/10.1016/j.diamond.2019.03.015

Wortberg G, De Palmenaer A, Beckers M, Seide G, Gries T (2015) Polyethylene-based carbon fibers by the use of sulphonation for stabilization. Fibers 3(3):Article 3. https://doi.org/10.3390/fib3030373

Wu C, Nahil MA, Miskolczi N, Huang J, Williams PT (2014) Processing real-world waste plastics by pyrolysis-reforming for hydrogen and high-value carbon nanotubes. Environ Sci Technol 48(1):819–826. https://doi.org/10.1021/es402488b

Wu X, Shaibani M, Smith SJD, Konstas K, Hill MR, Wang H, Zhang K, Xie Z (2018) Microporous carbon from fullerene impregnated porous aromatic frameworks for improving the desalination performance of thin film composite forward osmosis membranes. J Mater Chem A 6(24):11327–11336. https://doi.org/10.1039/C8TA01200H

Wu Z-L, Yang H, Jiao F-P, Liu Q, Chen X-Q, Yu J-G (2015) Carbon nanoparticles pillared multi-walled carbon nanotubes for adsorption of 1-naphthol: thermodynamics, kinetics and isotherms. Colloids Surf A 470:149–160. https://doi.org/10.1016/j.colsurfa.2015.01.069

Xie B, Hong L, Chen P, Zhu B (2016) Effect of sulfonation with concentrated sulfuric acid on the composition and carbonizability of LLDPE fibers. Polym Bull 73(3):891–908. https://doi.org/10.1007/s00289-015-1525-y

Xu Q, Si Y, He R, Qi X, Su X, Fu Y (2022) Silk-waste-derived porous carbon for fast electric heating under safe voltage. ACS Appl Mater Interfaces 14(4):6005–6015. https://doi.org/10.1021/acsami.1c21874

Yang S, Chen L, Mu L, Hao B, Ma P-C (2015) Low cost carbon fiber aerogel derived from bamboo for the adsorption of oils and organic solvents with excellent performances. RSC Adv 5(48):38470–38478. https://doi.org/10.1039/C5RA03701H

Yaqoob L, Noor T, Iqbal N (2022) Conversion of plastic waste to carbon-based compounds and application in energy storage devices. ACS Omega 7(16):13403–13435. https://doi.org/10.1021/acsomega.1c07291

Younker JM, Saito T, Hunt MA, Naskar AK, Beste A (2013) Pyrolysis pathways of sulfonated polyethylene, an alternative carbon fiber precursor. J Am Chem Soc 135(16):6130–6141. https://doi.org/10.1021/ja3121845

Yu J, Wang M, Xu P, Cho S-H, Suhr J, Gong K, Meng L, Huang Y, Byun J-H, Oh Y, Yan Y, Chou T-W (2017) Ultrahigh-rate wire-shaped supercapacitor based on graphene fiber. Carbon 119:332–338. https://doi.org/10.1016/j.carbon.2017.04.052

Zhai Z, Zhang L, Du T, Ren B, Xu Y, Wang S, Miao J, Liu Z (2022) A review of carbon materials for supercapacitors. Mater Des 221:111017. https://doi.org/10.1016/j.matdes.2022.111017

Zhang G, Chen Y, Chen Y, Guo H (2018) Activated biomass carbon made from bamboo as electrode material for supercapacitors. Mater Res Bull 102:391–398. https://doi.org/10.1016/j.materresbull.2018.03.006

Zhang J, Chevali VS, Wang H, Wang C-H (2020a) Current status of carbon fibre and carbon fibre composites recycling. Compos B Eng 193:108053. https://doi.org/10.1016/j.compositesb.2020.108053

Zhang L, Kowalik M, Gao Z, Ashraf CM, Rajabpour S, Bumgardner C, Schwab Y, Damirchi B, Zhu J, Akbarian D, Klett JW, van Duin ACT, Li X (2020b) Converting PBO fibers into carbon fibers by ultrafast carbonization. Carbon 159:432–442. https://doi.org/10.1016/j.carbon.2019.12.067

Zhang LL, Zhao XS (2009) Carbon-based materials as supercapacitor electrodes. Chem Soc Rev 38(9):2520–2531. https://doi.org/10.1039/B813846J

Zhang Y, Dai J, Guo H, Shi S, Yan Z, Hou W (2020c) A comparative study of carbon microsphere preparation by the hydrothermal carbonization of waste cotton fibers, viscose fibers and avicel. New Carbon Mater 35(3):286–294. https://doi.org/10.1016/S1872-5805(20)60490-5

Zheng J, Zhao Q, Ye Z (2014) Preparation and characterization of activated carbon fiber (ACF) from cotton woven waste. Appl Surf Sci 299:86–91. https://doi.org/10.1016/j.apsusc.2014.01.190

Zhou Q, Yao H (2022) Recent development of carbon electrode materials for electrochemical supercapacitors. Energy Rep 8:656–661. https://doi.org/10.1016/j.egyr.2022.09.167

Zhou X, Wang P, Zhang Y, Zhang X, Jiang Y (2016) From waste cotton linter: a renewable environment-friendly biomass based carbon fibers preparation. ACS Sustain Chem & Eng 4(10):5585–5593. https://doi.org/10.1021/acssuschemeng.6b01408

Zhuo C, Levendis YA (2014) Upcycling waste plastics into carbon nanomaterials: a review. J Appl Polym Sci 131(4). https://doi.org/10.1002/app.39931

Chapter 11
Flexible Textile Structures for Strain Sensing Applications

Sundaramoorthy Palanisamy, Veronika Tunáková, Jana Ornstová, Mohanapriya Venkataraman, Azam Ali, and Jiří Militký

Abstract The strain sensors are the sensors widely used for many applications, and the measurement of change in strain is called as strain sensors. Conventional metal- and semiconductor-based strain sensors are rigid, fragile, and opaque, restricting their applications in wearable electronics. Flexibility, stretchability, biocompatibility, and comfortability are all on the wish list for future wearable electronics. In recent years, apparels integrated with wearable sensors have achieved many smart functions, such as motion sensing, vital sign monitoring, and gesture recognition. Sensors for these applications require rapid response, high sensitivity, wide sensing range, and stable data acquisition capabilities. Textile fabrics have been widely used to fabricate flexible strain sensors owing to their high flexibility. However, the elasticity of ordinary textile fabrics is low, which limits their strain sensing range. E-textile consisting of natural fabrics has become a promising material to construct wearable sensors due to its comfortability and breathability on the human body. However, the fabric-based e-textile materials, such as conductive materials-treated textiles, generally suffer from the electrical and mechanical instability in long-term wearing. In particular, fabrics on the human body have to endure heat variation, moisture evaporation from metabolic activities, and even the immersion with body sweat. This chapter studied the knitted fabric material for wireless strain sensor application and its requirement.

S. Palanisamy · V. Tunáková · M. Venkataraman · A. Ali · J. Militký (✉)
Department of Material Engineering, Faculty of Textile Engineering, Technical University of Liberec, Studentská 2, 46117 Liberec, Czech Republic
e-mail: jiri.militky@tul.cz

M. Venkataraman
e-mail: mohanapriya.venkataraman@tul.cz

J. Ornstová
Department of Technologies and Structures, Faculty of Textile Engineering, Technical University of Liberec, Studentská 2, 46117 Liberec, Czech Republic

11.1 Introduction

Flexible strain sensors that can be comfortably attached onto the skin for real-time and accurate detection of physiological signals are particularly important for the realization of healthcare, soft robotics and human–machine interfacing. It is still challenging to develop strain sensors that satisfy both high stretch ability and high sensitivity. Here, the sensitivity or gauge factor (GF) in resistive-type sensors is defined as GF = (ΔR/R0)/ε, where ΔR/R0 is the relative resistance change under an applied strain ε. There are three main types of strain sensors which are resistive, capacitive and piezoelectric. The piezoelectric type sensors are the more sensible and having highest gauge factor (GF) and slight change in geometry even make good change in electrical resistance. The capacitive type sensors have good sensibility with lower energy and easy to adapt, and they are commonly used in touch screen technologies. Resistive sensors are responding to change in stress or strain of the material, and the external environment is not much affecting this sensor; the sensitivity is depending on the electrical conductivity and geometry of the material used.

Force sensing resistors (FRS) are developed for precise strain sensor applications. The FSR works by measuring the change in resistance by an increase in force. It detects physical pressure, squeezing, and weight by a change in resistive value. The applications of FRS are in the medical field (Akkermans et al. 2016), shoe insoles to detect the pressure of our foot (Rana 2009), video games, electrical automobiles, sporting equipment, etc. The textile spacer fabrics coated with silver on both sides act as a capacitor, whose capacitance helps measure snowboarding sock pressure during skiing (Holleczek et al. 2010). The highly elastic fabric was coated with polypyrrole (PPy) polymer to measure strain in urinary bladder dysfunction. The resistance is influenced by stretching the fabric and measuring strain variation (Rajagopalan et al. 2008). A conductive PPy-coated electrospun poly (vinylidene fluoride) (PVDF) fiber mat is developed for pressure sensor application; the compression stress is significantly changing the relative conductivity of PVDF/PPy mat (Merlini et al. 2014). The SS yarn knitted fabric was tested for strain sensing application, the elongation of the fabric decreased 90% of electrical resistance, and time-dependent resistance decreased by 30%. The full cardigan with a medium stitch has the best result for elongation-dependent resistance in the course direction (Ehrmann et al. 2014).

11.1.1 Electrical Resistance of Textile Structures

It is known from theory that the electrical resistance of a wire increases with the increasing distance of the probes in a relaxed state. The same phenomenon can be observed in textile structures containing a conductive component continuously throughout the length of the yarn. As per Ohm's law ($R = \rho L/A$), the resistance

(R) is directly proportional to the yarn length (L) and indirectly proportional to the cross-section area of the yarn (A), and ρ is the resistivity (Li et al. 2012).

The electrical properties of yarns were studied in several papers (Simegnaw et al. 2022; Weizman et al. 2020; Yun et al. 2017; Souri and Bhattacharyya 2018). In paper (Šafářová et al. 2014), the antistatic yarn (containing bi-component fibers with carbon part) was studied, and a linear relationship between the electrical resistance and clamping length was confirmed. On the other hand, the nonlinear behavior of the electrical resistance on the clamping length was observed for yarns containing 20% of stainless-steel fibers of staple length in their structure. Therefore, the method of conductive yarn production influences the length-resistance results. During extension, the length of the conductor (wire, single fiber, or single yarn) increases its diameter decreases and the resulting electric resistance increases.

Contact resistance is another interesting phenomenon that may affect the resulting electrical conductivity of the textile structure. The contact resistance is generated at yarn—the yarn interface. According to the contact resistance theory (Holm and Holm 1967), contact resistance factors are material resistivity, material hardness, number of contact points, and contact pressure between yarns.

The stretching of the knitted fabric is influencing the structure of the knit. The courses and wales were disturbed, as shown in Fig. 11.1. During wale-wise stretching (Fig. 11.1a), the contraction of wale to a minimum (Wmin) and expansion of course, to a maximum (Cmax), was noticed. During the course-wise stretching (Fig. 11.1b), the course contraction to a minimum (Cmin) and wale extension until maximum (Wmax) was noticed. During biaxial stretching of the knitted fabric, both the course and wale were expanded and represented as course bias (Cb) and wale bias (Wb). The yarn contact points are shifting, while a biaxial stretching of the fabric is seen in Fig. 11.1c (Mihailovic and Simovic 1998; Popper 1966; Demboski and Bogoeva-Gaceva 2001). The 1×1 rib fabric is the highest elastic textile structure, easily stretching in uniaxial and biaxial directions. This structure has more easily stretched in the course-wise direction because of loosely constructed courses. In wale-wise stretching, the elongation occurs in the side limbs of the loop and contraction in the head and sinker loop, as noticed in this work (Spencer 1998). In a study (Demboski and Bogoeva-Gaceva 2001), the glass and polypropylene yarns were co-knitted with a 1×1 rib structure, and the fabric was stretched in uniaxial and biaxial directions to test its tensile, bending, and impact. The wale-wise stretching has more stress compared with the course-wise stretching. In bias (biaxial) stretching, the wale-wise exhibited more stress than the course-wise. From the above, it can be assumed that the length-related resistance will increase with increasing uniaxial force, whereas the contact resistance will decrease with increasing contact points and contact force (Li et al. 2012).

A survey of the electro-mechanical behavior of electro-conductive fabrics can be found in several professional publications. For example, in paper (Šafářová et al. 2014), three different forms of conductive yarn, single yarn, two overlapped yarn, and knit stitch yarn, were taken for study. Unidirectional tensile force is applied to those samples, and the electrical resistance reading is taken. It was observed that the single yarn and overlapped yarn have an increase in electrical resistance with
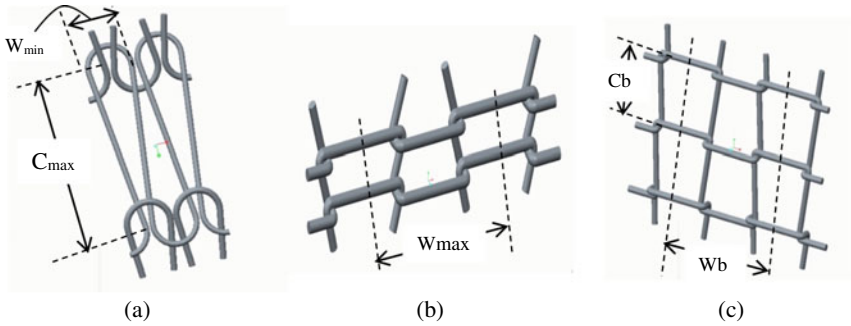
Fig. 11.1 Yarn contact point shifting during **a** wale-wise stretching, **b** course-wise stretching, and **c** biaxial stretching or both ways stretching

increasing tensile, but the knit stitch yarn has a decrease in electrical resistance during increasing tensile. The contact resistance in knit stitch form has decreased with an increase in unidirectional stretching. The conductive yarn in knit form has lesser resistance values than single-strand and overlapped yarn. In fabric form, the contact resistance affects the total resistances more than the length resistance.

The electrical conductivity of the CNT-coated nylon6/spandex yarn was investigated in the study (Ali et al. 2020). It was reported that the CNT yarn can elongate until 100% lengthwise, whereas it was noticed that the yarn's electrical resistance increases with elongation.

The linear relationship between the electrical resistance and the elongation was noticed until 70% elongation. After that, the electrical resistance was increased drastically, up to 100 times at 100% elongation. Authors reported that the drastically increased resistance after 70% elongation is because of rupture and break in the CNT coating.

Another study (Wang et al. 2014a, b) explains the contact resistance of the knit stitch made of silver-coated yarn. It was found that electrical resistance decreases while an increase in elongation and force. The authors reported that the linear fitting of the dependence of electrical resistance on elongation has a R^2 of 0.90; therefore, the statistically significant linear relationship between electrical resistance and applied force was proved. So, the contact resistance of the yarns plays an important role during fabric extension.

Three different silver-coated threads were studied for electrical resistance versus extension in work (Ruppert-stroescu and Balasubramanian 2018). The electrical resistance of all studied threads increased with increasing elongation. Studied threads were used to sew chain stitches and zig-zag stitches on the fabric substrate, and the electrical resistance was measured against the elongation of the fabric. The author noticed that the stitch electrical resistance was decreased with the elongation of the fabric because of multiple contacts in the stitch. Most of the studies confirmed that the multiple contacts of conductive yarns in the fabric structure cause a decrease in electrical resistance during fabric elongation.

The unidirectional stretching of the Ag-coated PA yarn intarsia knit fabric at wale way was studied in work (Li et al. 2012). It was noticed that the electrical resistance was decreased with increasing extensile force. An increase in the number of wales caused a decrease in the fabric's electrical resistance values. Another study (Wang, Long, Soltanian, Servati, and ko 2014a, b) also proves that the contact resistance and contact force on knitted fabric have an influence on electrical fabric resistance. The hexagonal resistance model for knitted structure validates the simulation of the resistance sensing mechanism. An increase in contact force decreases the contact resistance of the knitted fabric, which was proved by Holm's electric contact theory.

Article (Ehrmann et al. 2014) shows knitted fabric's elongation-dependent and time-dependent electrical resistance in course direction. It was reported that the full cardigan with medium stitch density is more suitable for resistance stretch sensors among various knit structures.

The Ag-coated nylon 66 blended with merino wool yarn single pique knitted structure was taken with a tuck stitch to study the resistance of the knitted fabrics in work (Liu et al. 2017). The increase in the number of courses with constant wales and increases in the number of wales with constant courses leads to decreased electrical resistance. Also, the tuck stitch reduces the electrical resistance of the single-pique fabric. Both the theoretical model and practical model confirmed the electrical resistance results.

A study (Eltahan et al. 2016) developed the copper-coated Lyocell plain-woven fabric with an electroless deposition method. The developed conductive fabric was tested for flex testing until 6000 cycles, and the resistance was measured with two probes and four probes. It can be concluded from both measuring methods that the fabric resistance increases with increasing flexing cycles. The change in resistance was explained by the partial damage of copper coating on the fabric surface after 6000 flex cycles. The decrease in resistance is caused by the damage to the copper coating due to swelling and expansion of the fabric. So, the elongation and flex of fabric cause damage to surface coating, leading to reduced electrical resistance.

From above, it is visible that the major portion of developed textile sensors is based on the change of electrical conductivity of the textile structure during external stimulus using traditional wired methods. Only a few papers describe wireless strain sensing mechanisms using electromagnetic radiation, but usually, those are for the civil engineering field. In the study (Gregori et al. 2019), the wireless measurement of the strain gauge for large metal structures is presented with the radio frequency method. It was presented that the wireless radiation measurement method's accuracy is higher than wired measurement by the traditional resistance method.

There are lots of studies about the electrical resistance on stretching of textile conductive fabrics (Ehrmann et al. 2014) (Li et al. 2012) and conductive thread stitch fabrics (Ruppert-stroescu and Balasubramanian 2018), but very few studies about the conductive yarns on electro-mechanical behaviors are reported (Zhang et al. 2005). Especially, the yarn resistance has the main influence on the fabric resistance, so it is necessary to analyze it.

It follows from the performed literature search that the influence of contact and longitudinal resistance on both electrical conductivity and electrical resistance, as

well as on electromagnetic shielding, especially during mechanical stress, needs to be further investigated to create wireless strain sensor technology using electro-conductive fabrics.

11.1.2 Electromechanical Property of the Conductive Knitted Fabric

Ohm's law states that the voltage, V is directly proportional to the current, I (amp), passes through the circuit and resistance, R (Ω), created by the circuit.

$$V = IR, \tag{11.1}$$

The electrical resistance (R) of the conductive material is written as:

$$R = V/I, \tag{11.2}$$

R depends on the length, L [m], cross-sectional area, A [m^2], and resistivity, ρ [Ω/m] of the conductor.

$$R = \rho L/A, \tag{11.3}$$

The surface-coated conductive material has an exponential constant, k, for its effective area written as:

$$R = \rho L/A^k, \tag{11.4}$$

As per the contact resistance theory, the contact resistance as:

$$R_c = \frac{\rho}{2}\sqrt{\frac{\pi H}{nP}}, \tag{11.5}$$

where H [N/m^2], n, and P [N] are material hardness, number of contact points, and contact pressure between the conductive yarns, respectively. The hardness and resistivity are related to the material properties, and it is constant. Contact resistance is indirectly proportional to the contact pressure and the number of contact points.

During the extension of the knit structure, the resistance of the fabric varies with related to yarn length, R_l and yarn contact points, R_c.

11.1.3   Conductive Yarn Extension Mechanism

During the stretching of the yarn, the cross-section area, A, decreases, and the length, L, of the yarn increases, so the length resistance, R_l is not linearly proportional to the yarn length. Conductive yarn length and cross section are a function of applied tensile force, F [N]. The force, F included in Eq. 11.6, with initial length, L_0 is written as follows:

$$R_l = f(F, L_0) = \frac{L(F, L_0)}{A(F, L_0)^k},\tag{11.6}$$

The nonlinear length-related resistance is dependent on extensile force and yarn length. The Nth order effect and cross-correlation effect between the yarn length and extensile force to the resultant resistance as in the model equation below:

$$R_l = \sum_{n=0}^{N} \sum_{m=0}^{N} C_{mn} F^n L_0^m,\tag{11.7}$$

where C_{mn} is the coefficient to be determined in the experiment.

11.1.4   Extension Mechanism of the Overlapped Yarns

The overlapped yarn contact resistance decreases with the increase in length or extension of the yarn or fabric. The decrease in contact pressure during the extension is due to torsion in the yarn twist releasing. The relationship between the tensile force, F, and contact pressure, P, is as follows:

$$P = P_0 + a_0 F,\tag{11.8}$$

where P_0 is the initial contact pressure, and a_0 is a constant coefficient. The contact resistance, R_c, is indirectly proportional to the contact pressure, P. P is required to reflect the resistance arising from the twist of the yarn. The equivalent resistance on overlapped conductive yarn is as follows:

$$R(F, L_0) = \sum_{n=0}^{N} \sum_{m=0}^{N} C_{mn} F^n L_0^m + \frac{a_1}{P_0 + a_0 F},\tag{11.9}$$

From Eq. 11.19, the contact resistance increases with the initial stretch, and thereafter, the length-related resistance plays an important role in total resistance. These constants will be determined in the experiment.

11.1.5 Yarn Resistance Model

The yarn's electrical resistance R changes with increasing tensile, elongation, or strain; the conventional resistance law is used to calculate the change in resistance as (Wang et al. 2014a, b; Murray and Miller 1992):

$$\frac{dR}{R} = \frac{d\rho}{\rho} + \frac{dl}{l} - \frac{dA}{A} \tag{11.10}$$

where ρ, l, and A are the yarn resistivity, length, and cross-sectional area, respectively. Here, the elongation (ε) of the conductive yarn in the longitudinal and radial directions with a cylindrical structure with an initial radius of r can be written as:

$$\varepsilon_l = \frac{dl}{l}, \text{and} \varepsilon_r = \frac{dr}{r} = -v\frac{dl}{l} = -v\varepsilon_l \tag{11.11}$$

Equation 11.1 uses the Poisson's ratio is v. Using this equation, the changes in the volume (V) and cross-sectional area (A) of the yarn can be written as:

$$\frac{dV}{V} = \frac{dl}{l} + \frac{dA}{A} = \varepsilon_l - 2v\varepsilon l + v^2\varepsilon_l^2 = v^2\varepsilon_l^2 + (1 - 2v)\varepsilon_l \tag{11.12}$$

and

$$\frac{dA}{A} = (1 + \varepsilon_r)^2 - 1 = 2\varepsilon_r + \varepsilon_r^2 = -2v\frac{dl}{l} + v^2\left(\frac{dl}{l}\right)^2 \tag{11.13}$$

By assuming the electrical resistivity, $\rho = cV$ for the conductive material, where c is the number of free electrons per atom constant and the atomic density, then

$$\frac{d\rho}{\rho} = c\frac{dV}{V} = cv^2\varepsilon_l^2 + c(1 - 2v)\varepsilon_l \tag{11.14}$$

From Eqs. (11.10) to (11.14), the change in resistance of the conductive material is written as:

$$\frac{dR}{R} = v^2(c - 1)\varepsilon_l^2 + [2(1 - c)v + c + l]\varepsilon_l \tag{11.15}$$

For the resistance of the yarn is written as:

$$R = v^2(c - 1)\varepsilon_l^2 R_0 + [2(1 - c)v + c + l]\varepsilon_l R_0 + R_0 \tag{11.16}$$

where R_0 is the yarn resistance at no strain. For a given material, the strain sensitivity, or gauge factor K, can be written as:

$$K = \frac{dR/R}{dl/l} = v^2(c-1)\varepsilon_l + [2(1-c)v + c + l] \tag{11.17}$$

$$R = 2(1-c)v + c + l]\varepsilon_l R_0 + R_0 \tag{11.18}$$

The yarn's electrical resistance is the main factor in the fabric's total electrical resistance; the distance between the yarn's contact points in the fabric structure also influences the fabric resistance. During the elongation of the fabric sample, the change in electrical resistance is noticeable, especially in knitted structures, as shown in the literature search above.

11.1.6 Fabric Resistance Model

The knitted loop consists of a needle loop, which has one head, two limbs, and a sinker loop in its natural state, as shown in Fig. 11.2a. While unidirectional tension is applied on the conductive knitted fabrics, the contact points are tightened and moving. The length of the head, limbs, and sinker loop has extended and may change the contact point. The increase in tensile force has further extended the contact point, and pressure creates between the head and sinker loop. The shape of the loop extended during the tensile force is shown in Fig. 11.2b. The breaking of the fabric occurs when the tensile force exceeds the breaking force of the yarn (Spencer 1998).

The resistance of the conductive fabric among wale direction extension is modeled by superposition of the length-related resistance and contact resistance with the fabric length, L. Resistance is inversely proportional to the total number of wales (Eq. 11.19) as:

$$R(F, L_0) = \frac{1}{W}\left(\sum_{n=0}^{N}\sum_{m=0}^{N} C_{mn}F^n L_0^m + \frac{a_1}{P_0 + a_0 F}\right) + W.b_0, \tag{11.19}$$

(a)   (b)
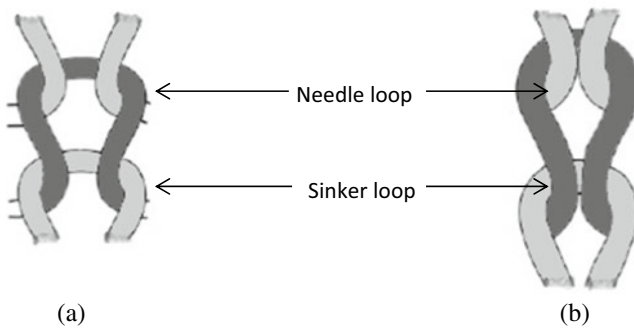
Fig. 11.2 Knitted loops with sinker loop and needle loop at **a** relaxed state and **b** extended state

where b_0 is an offset coefficient to account for the terminal resistance between the connector and the fabric under test, and W is the total number of conductive yarn wales of knitted fabric.

The electrically conductive knitted and woven fabric structures can be assumed as resistance circuits, meaning the woven fabric is similar to a square circuit with four resistors and contact points. The plain weft knitted fabric matches to hexagonal resistance circuit model (see Fig. 11.3a). There are two types of electrical resistance in this fabric structure: contact resistance (Rc), representing the contact points of overlapped yarn loop, and intrinsic resistance (RL), representing resistance between two contact points (Fig. 11.3b). The fabric structure is described by one sinker loop (La), two-loop legs (Lb), and two interloped contacts (c). Based on the fabric structure, the resistance circuit is represented with RL, R c, resistance at needle loop and sinker loop (RLa), and two-loop leg resistance (RLb) (Wang, Long, Soltanian, Servati, and ko 2014a, b) (Murray and Miller 1992). Kirchhoff's rule is used to model the network for deriving equivalent resistance of the fabric. While applying tension to the fabric, the knit structure is disturbed, as shown in Fig. 11.2. In this case, the Rc and RL values change according to the applied tension, and Eq. 11.18 also explains the single yarn resistance change during stress.

As per the pierce model (Spencer 1998), the La and Lb under no strain are represented as $La_0 = \pi w/4$ and $Lb_0 = l - 2La_0/2 = 2l - \pi w/4$, where l is loop length, and w is single loop width. The fabric under strain ε_w in course direction, loop length, $l = La_0(1 + \varepsilon_w)$; RLa and RLb in Eqs. 11.20 and 11.21 as:

$$RLa = \rho_l La = \frac{\rho_l \pi w(1 + \varepsilon_w)}{4}, \tag{11.20}$$

$$RLb = \rho_l Lb = \frac{\rho_l[2l - \pi w(1 + \varepsilon_w)]}{4}, \tag{11.21}$$

(a) (b)
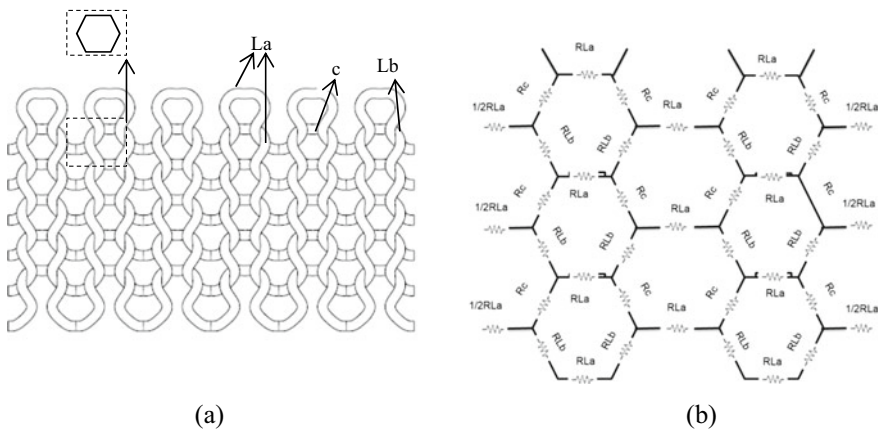
Fig. 11.3 Graphical images of **a** plain knitted fabric structure and **b** the hexagonal resistance circuit model

Fig. 11.4 Electrical resistance circuit for 2×1 unit loops for knitted fabric
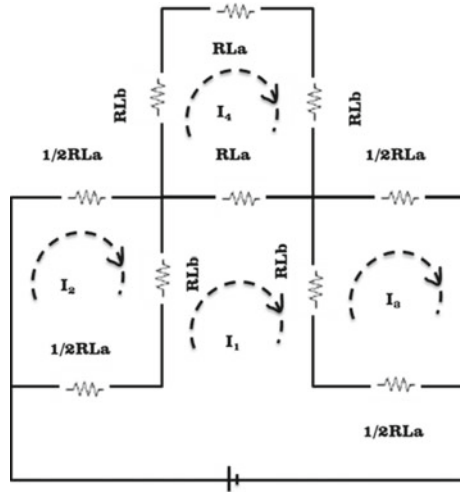
where ρ_l is the yarn resistivity per unit length, and the contact resistance is eliminated because of complications in measuring under stress.

$$R_e(2, 1) = \frac{V}{I_1(2, 1)} = \frac{RLa(RLa + 2RLb)}{RLa + RLb} \tag{11.22}$$

Figure 11.4 shows the electrical resistance circuit for 2×1 unit loops of knitted fabric, and it shows the interior loop current. Equation 11.22 is obtained from Kirchhoff's voltage law and the loop current method. $I_1, I_2, I_3,$ and I_4 are total current and equivalent resistance $Re = V/I_1$, and V is voltage (Murray and Miller 1992).

11.2 Materials and Methods

Knitted fabric with single jersey structure was developed for strain sensing ability. The knitted fabric is developed at three different densities for detailed analysis. The fabric properties like stitch density, porosity, thickness, electrical resistance, and EM SE were analyzed during the fabric elongation. SE is a crucial technique used for measuring strain sensing as a wireless technology.

11.2.1 Electrically Conductive Fabrics

Conductive silver AgPA yarn was used to knit single jersey (SJ) on a 14-gauge flat needle bed knitting machine (Shima Seiki Ltd., Japan, and Model SRY 123LP). In

(a)

(b)

(c)
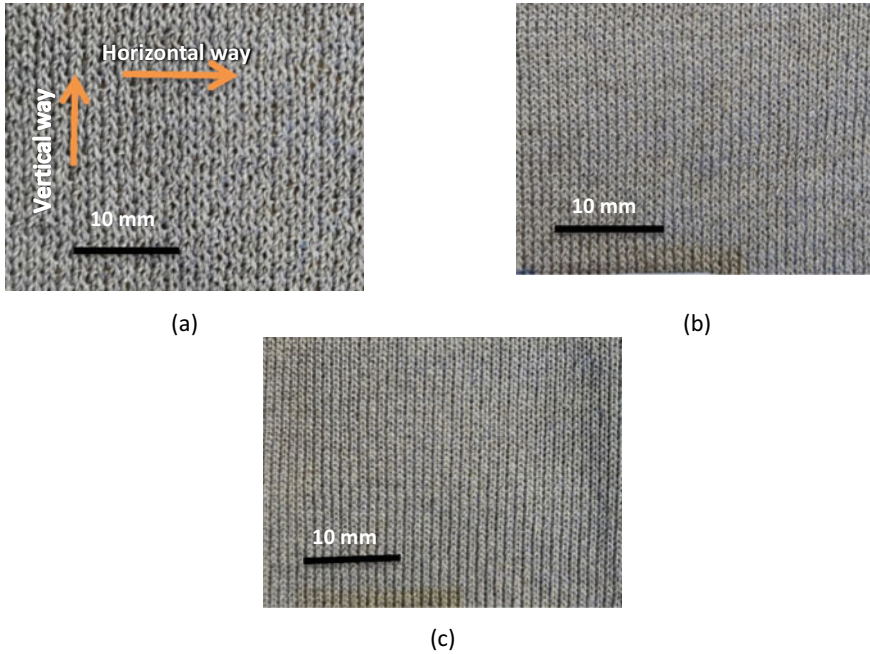
Fig. 11.5 Images of **a** SJL, **b** SJM, and **c** SJH

addition, SJ structure of the fabric is widely in use of wearable applications. The knitted fabrics are prepared at three different densities; low (L), medium (M), and high (H). The SJ fabric images are shown in Fig. 11.5. All the images are captured as per ISO 125 with 4.73 focal lengths and a 64 MP camera. The knitted fabrics were used for the examination of electrical resistance and electromagnetic shielding under unidirectional as well as biaxial extension.

11.2.2   Basic Properties of Fabrics

The fabric mass per unit area (w) [g/m^2] was measured using the standard ASTM D 3776, and the sample size was 100 cm^2. Fabric thickness (t) was measured using the thickness gauge [mm], as per the standard ASTM D1777 (knitted samples). The loop length of the fabric samples was calculated with the Dalidovich method (Eltahan et al. 2016). Ten readings per each test were taken to statistically analyze measured datasets.

11.2.3 Electrical Properties of the Fabrics

The surface resistance of the sample set was measured according to the standard ASTM D257, under a DC power supply, using two probe electrodes at the temperature $T = 21\ °C$ and the relative humidity $RH = 54\%$. Sample resistance is measured by applying a voltage potential between two probes of specified configuration, which are in contact with the same side of the tested material. Sample resistivity ρ [Ω.mm] was calculated from the below-mentioned equation:

$$\boldsymbol{\rho = R(A/L)},\tag{11.23}$$

here, R [Ω] is the sample resistance reading, A is the area of the sample [mm^2], and L is the distance between the two probes [mm]. Ten readings per each test were taken to statistically analyze the measured datasets.

11.2.4 Electromagnetic Shielding Effectiveness of Fabrics

SE of the sample set was measured according to the ASTM D4935-18 for the planar materials using a plane wave, the far-field EM wave at the temperature $T = 21\ °C$, and the relative humidity $RH = 54\%$. SE of the samples was measured over the frequency range of 30 MHz to 1.5 GHz. The setup consisted of a sample holder with its input and output connected to the network analyzer. A shielding effectiveness test fixture (Electro-Metrics, Inc., model EM-2107A) was used to hold the sample. The design and dimension of the sample holder follow the ASTM method mentioned above. A vector analyzer, Rohde and Schwarz ZN3, was used to generate and receive the electromagnetic signals. The standard mentioned above determines the shielding effectiveness of the fabric using the insertion-loss method. A reference measurement for the empty cell was required for the shielding effectiveness assessment. A "through" calibration with the help of the reference sample was made first. A load measurement was performed on a solid disk shape sample subsequently. The reference and load specimens must be of the same material and thickness. Both the reference and load samples geometries are according to the ASTM D 4935-18. The measurements were performed at five different places of the textile samples because of the subsequent statistical analysis. The mean values and 95% confidence intervals for means of the *SE* for 1.5 GHz frequency are summarized.

11.2.5 Electromechanical Properties of Fabrics

To study the effect of fabric strain on ER and SE, a biaxial device was used. Figure 11.6 shows the experimental setup of the biaxial stretching device with fabric

to measure electrical resistance using two probe method (Fig. 11.6a), and electromagnetic shielding measuring apparatus as per ASTM D4935-18 method (Fig. 11.6b). Figure 11.6b shows the knitted fabric image marked with horizontal and vertical ways; the horizontal way represents the coarse wise, and the vertical way represents the wale wise. This designation (horizontal, vertical) will be used later in the text to show which direction of loading was used.

The continuous measurement of the electrical resistance of the knitted fabric sample is done with an Arduino resistance setup, as shown in Fig. 11.6a. The edges of the fabric samples were connected with two probes from the resistance circuit board at a distance of 14 cm, and the sample was stretched at a speed of 3.5 mm/s to measure electrical resistance until 30% fabric elongation. It was found that the elongation of the fabric until 30% was not causing any damage to the knit structure. The fabric structure was disturbed by unraveling and breaking after exceeding 30% elongation. During uniaxial stretching, the probes are connected to the stretching direction for a measurement. During biaxial stretching, the probes are connected in the vertical direction of the sample, and only wale way resistance is measured. The resistance readings were recorded online using MATLAB software and then saved in a data file for further analysis.

The electromagnetic shielding effectiveness (EM SE) of the sample was measured using the coaxial transmission line method, as shown in Fig. 11.6b. The coaxial holder is placed on the surface of the fabric sample and attached with a biaxial device. The stretching cycle is programmed with Fabris 5 K software. The stretching speed was 3.5 mm/s, and for every 5% elongation of fabric, the holders were paused for 30 s to measure the EM SE. The stretching process is continued until 30% elongation of the sample.

The pore area of the fabric sample during the biaxial stretching process is measured using the Nikon NIS element software as per internal standard number 23-107-01/

(a)   (b)
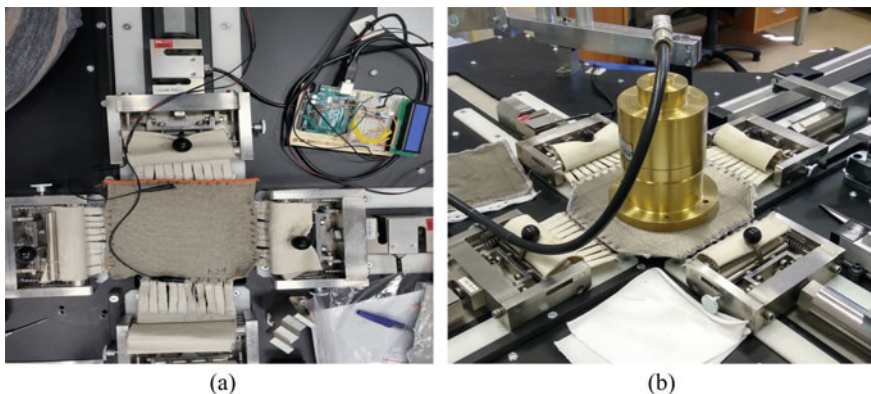
Fig. 11.6 Experimental setup of fabric attached in the biaxial device to measure **a** electrical resistance and **b** electromagnetic shielding effectiveness

01. The fabric's total open pore area value, called porosity, was obtained by the NIS element image analysis and used for plotting graphs.

All three types of experiments were conducted on the sample set: uniaxial deformation at both ways and biaxial deformation. Output values were: electrical resistance, EM SE, and sample porosity. All tests were performed at the temperature $T = 21\ °C$, and the relative humidity $RH = 54\%$ and three readings were taken for each test.

11.3 Results and Discussions

11.3.1 Mechanical Properties of Knitted Fabrics

The tensile-elongation curve of sample is important to know the stress–strain behavior of knitted fabrics, and it was necessary to know it in order to plan further electromechanical experiments. SJM sample was chosen for this experiment. The tensile strength of the SJM fabric is tested with a biaxial device at 3.5 mm/min holder speed, gauge length of 15 cm, and fabric width of 10 cm. SJM knitted fabric is tested for tensile strength at wale-wise and course-wise directions. Figure 11.7 shows the tensile strength result of the SJM fabric, whereas the wale-wise tensile strength of the sample is in Fig. 11.7a. The strain increases with increasing stress; after 154 mm elongation, the fabric tensile loses its strength from 115 N/m by breaking its loop structures. In the course-wise tensile shown in Fig. 11.7b, the strain increases with increasing stress; after 200 mm elongation, the fabric tensile loses its strength from 500 N/10 cm by breaking its loop structures. The wale-wise direction strength of fabric is higher than the course-wise direction strength. The breaking of the fabric occurs slowly that the reason the peak is not dropped suddenly, especially wale-wise. The course-wise elongation is more compared with wale-wise, which is because of loosely constructed loops in course direction, as already discussed. Based on this experiment, it was decided that both knitted samples will be deformed in the range from 0 to 25% (indicated in the graph and it corresponds to 37.5 mm) so that the elastic region of the curve was explored. It is also visible from these results that the wale-wise has more elastic recovery than course-wise. The elastic recovery of the fabric is identified as 60 and 140 mm for wale-wise and course-wise, respectively. It was noticed that the deformation of fabric in one direction is higher and it is much needed for strain sensing application.
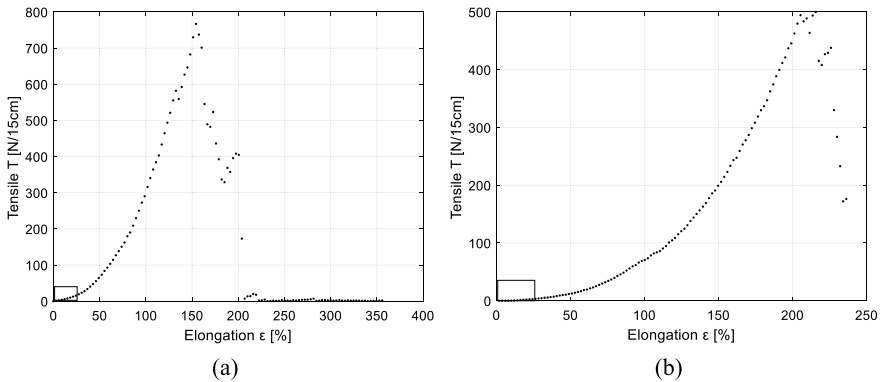
Fig. 11.7 Stress–strain curve of the SJM fabric tested with the biaxial device at **a** wale-wise and **b** course-wise directions

11.3.2 Effect of Knitted Fabric Elongation on Its Electrical Resistance

The electrical resistance (ER) is indirectly proportional to the electromagnetic shielding effectiveness if other variables are held constant, which means higher the resistance lowers the shielding and vice versa. EM SE is therefore related to the ER and total ER is mainly affected by the number of contact points between the conductive yarns causing a conductive path. While elongating the knitted fabric, the change in resistance with respect to the number of contact points is derived in Eq. (11.20) and (11.21). During both way elongation measurements, the ER is measured in a vertical way only because the wale-wise has more influence on ER than course-wise.

The SJ sample's ER behavior is different for different densities; mostly, the ER is decreased while stretching the fabrics. ER for SJ lies between the 1 and 2.5 ohms range for all the samples and there is an observable decrease in electrical resistivity with increasing density of the knitted fabric. During the increasing horizontal way of fabric elongation, the ER is slightly decreasing for all densities of samples. When increasing vertical way fabric elongation, ER is decreasing more steeply. During both ways of fabric elongation, ER is deviating moderately between horizontal and vertical ways results. ER of SJL sample has decreased with an increase in elongation at all directions of loading, as shown in Fig. 11.8a. At both ways of stretching of SJL, the ER increases slightly and then decreases drastically; from 2 to 5% elongation, the ER increases suddenly because of the relaxation of fabric. SJM sample has decreased in resistance with an increase in elongation at the horizontal way; at vertical and both ways stretching, the resistance increases initially until 7.5% elongation and then decreases drastically, as shown in Fig. 11.8b. SJM is constructed with moderate stitch density so that the ER is increased vertically as well as both ways of elongation of the fabric and fabric loops loosen in this direction. SJH sample ER slightly decreased with an increase in elongation of the sample, as shown in Fig. 11.8c.
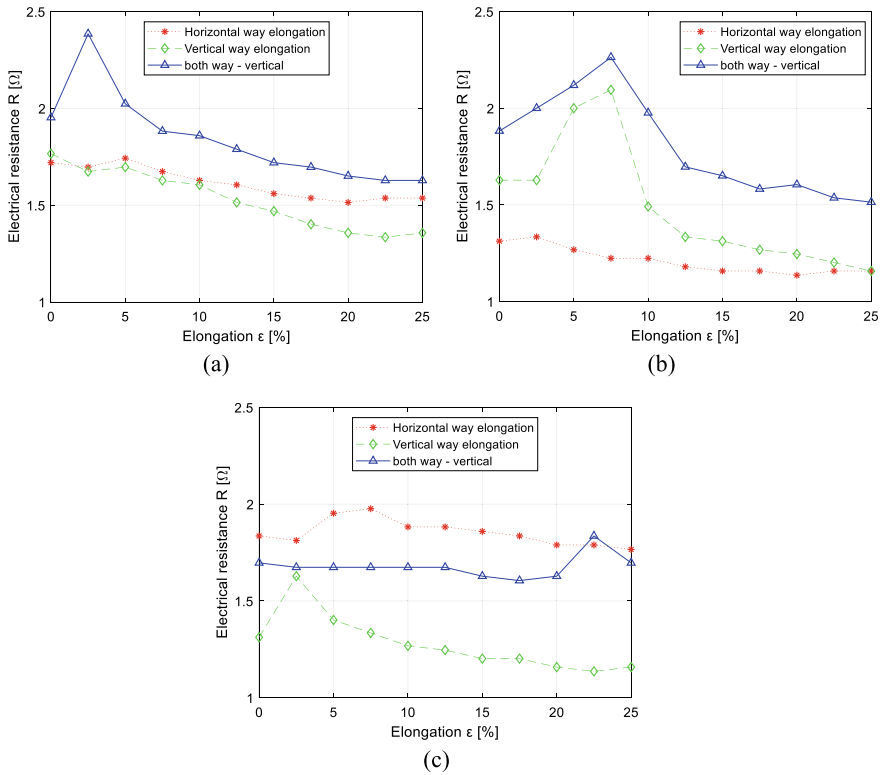
Fig. 11.8 Dependence of electrical resistance R [Ω] on elongation of fabric ε [%] for single jersey fabrics having **a** low, **b** medium, and **c** high density

SJH vertical way elongation causes increase in ER initially due to fabric relaxation or pre-tension, but in horizontal way elongation, the resistances increase after 2.5% to 7.5% elongation, proving the loose connection between the loops at this point. Based on the stitch densities, the ER results vary with fabric elongation. The loose structure has constantly decreased in ER, but the tight structure has slightly decreased in ER against the elongation. ER trend is somehow similar to the SE results of the SJ fabrics.

11.3.3 Effect of Knitted Fabric Elongation on Its Porosity

The porosity or aperture of the shielding material has significantly affected the SE results, as stated by the theory and also as confirmed in the work Palanisamy et al. (Palanisamy et al. 2021). That is why the porosity of the fabric during elongation and its SE are studied in this part.
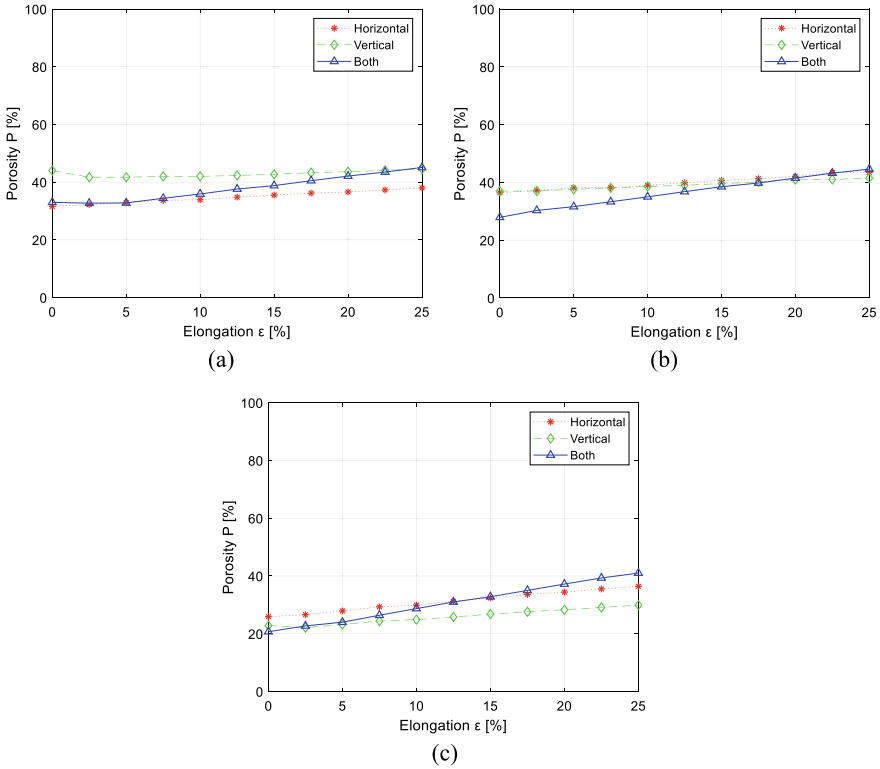
Fig. 11.9 Dependence of open pore area P on fabric elongation ε [%] for single jersey having: **a** low, **b** medium, and **c** high density

The elongation versus porosity of the SJ fabric is shown in Fig. 11.9. It is visible that the porosity at 0% loading (P_0) decreases with higher sample density. The extension of the fabric causes increase in the porosity in most cases, and increasing porosity could affect the shielding effectiveness. SJL, SJM, and SJH fabric's porosity increase with an increase in elongation at vertical, horizontal, and both ways, as shown in Fig. 11.9a–c, whereas the trend is almost linear. At both ways of elongation, the samples porosity increased much higher than in other ways, and the slope of the approximation line would have the highest slope.

11.3.4 Effect of Knitted Fabric Elongation on Its SE

The stretching of the fabric in a uniaxial and biaxial direction changes the fabric geometry, as discussed in the literature review. Equations 11.30 and 11.31 determine

the change in resistance with a change in fabric strain values. If the electrical resistance changes, then the EM SE also changes because those are indirectly proportional to each other.

In case of knitted fabric extension, the increase in electrical conductivity is expected during the initial extension process as shown during electromechanical analysis of crochet chain, which is caused by an increase in the number of contacts between the yarns in the knit structure. This phenomenon could increase the EM SE. On the other hand, it is expected that the porosity of the sample could increase with sample loading, which could have a negative effect on the SE level. That is why SE of knitted sample set (single jersey having 3 different densities) will be studied during all types of elongation experimentally.

The elongation of the SJ fabrics in a horizontal way, vertical way, and both ways versus EM SE at 1.5 GHz frequency is shown in Fig. 11.10. Studied is SE response during the extension of sample to 25% elongation. The SJ fabrics are produced at three densities: low, medium, and high, based on their stitch density. All three densities of SJ fabrics increase in SE with an increase in fabric elongation at all directions of stretches, as shown in Fig. 11.10. In Fig. 11.10a, the SJL fabric SE results are shown, and SE increases with all directions of the elongation. Especially, the vertical direction of the stretch has increased the SE value higher compared with horizontal and both ways stretching with increases in elongation.

In both ways, points lie in between vertical and horizontal points. The deviation in the SE is higher in the vertical direction and lowest in the horizontal direction. For SJM and SJH, fabric samples also have higher SE differences at vertical way stretch, but at horizontal and both ways stretching of the samples also increases the SE value with increases in elongation (Fig. 11.10b, c). In the vertical direction elongation of the fabric, the wales are expanding, and courses are contracting; wales are tightly constructed, and contact between the yarns increases with elongation; that is the reason why the SE increases much. The SJL, SJM, and SJH have the SE of 50 dB, 53 dB, and 57 dB at 25% vertical way elongation. SE is higher for high-density fabric, and the difference between the initial and final elongated SE values also had more difference than other densities. For the creation of sensors, it seems that the most interesting stretching mode is the vertical stretching of the sample, when a linear increase in SE with elongation is observed for all densities of samples and also during vertical stretch the highest ΔSE (SE-SE$_0$) is achieved, namely approx. 5 dB for a sample with low and medium density and approx. 7 dB for a sample with high density.

11.3.5 Effect of Knitted Fabric Elongation on SE Sensitivity

The SE sensitivity (SES) or gauge factor is the important parameter for describing the fabrics strain sensitivity results. The gauge factor (GF) is used to indicate the strain sensitivity of the fabric and its formula is given in Eq. 11.24.
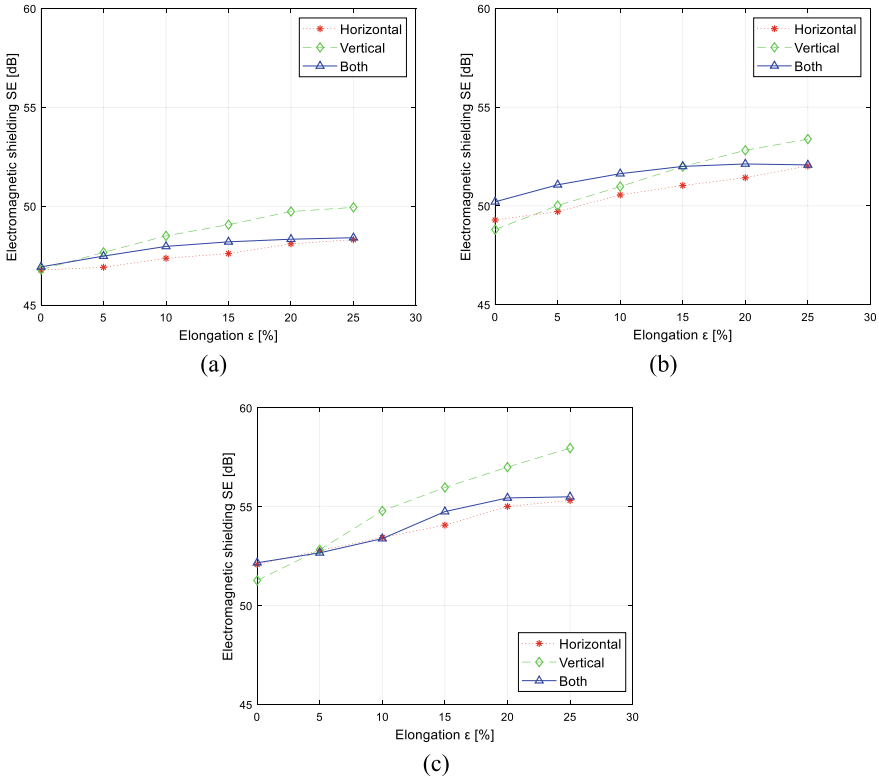
Fig. 11.10 Dependence of SE [dB] at 1.5 GHz frequency on elongation ε [%] for sample: **a** SJL, **b** SJM, and **c** SJH

Here, the sensitivity based on SE values is shown against the vertical elongation of the fabric samples (Fig. 11.11), because one directional change was noticed at vertical elongation for SJ fabric:

$$GF = SES = \frac{SE_x - SE_0}{SE_0} = \frac{\Delta SE}{SE_0}, \tag{11.24}$$

where SE_x is the SE value at x % elongation, SE_0 is SE value at 0% elongation, and ΔSE is difference between SE_x and SE_0. The elongation of the SJ fabrics versus EM SE with respect to SE at 0% elongation (SE_0) as also called as SE sensitivity (SES) was shown in Fig. 11.11. The SES of the SJ fabrics increases with the increase in elongation at vertical direction. The dependence of SES on elongation has very good correlation and its R^2 is 0.79.

The vertical elongation of the fabrics results are taken further for regression analysis to find out the correlation between explanatory variables. The model has the form:

Fig. 11.11 Dependence of
SE sensitivity SE/SE$_0$ [−] at
1.5 GHz frequency for
vertical direction of
elongation ε [%] of SJ
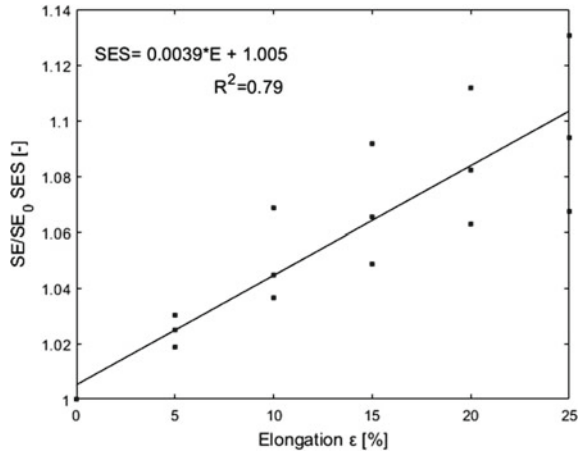
$$SE = b0 + b1 \cdot x1 + b2 \cdot \sqrt{x2} \tag{11.25}$$

The corresponding coefficient of determination is 0.91 for single jersey. The relation between predicted and measured SE for this model is shown in Fig. 11.12. The regression model coefficients are shown in Table 11.1. The model with square root for x_2 variable or P/P_0 has higher predictability and it is recommended for modelling of the sensors made of electrically conductive knitted fabrics.

Fig. 11.12 SE measured
versus SE predicted at 1.5
GHz frequency using
Eq. 11.25 of SJ
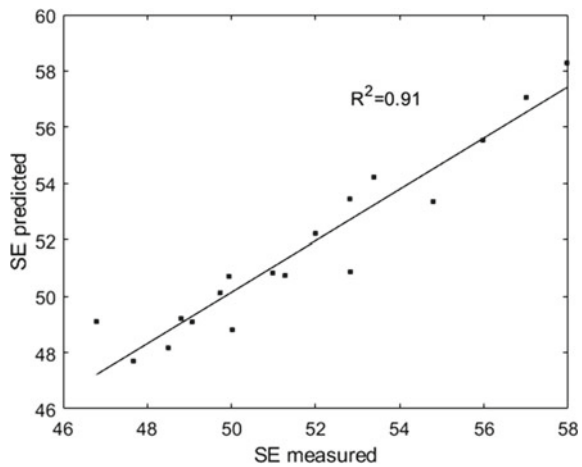
Table 11.1 Regression coefficients for regression model (Eq. 11.25) for SJ

Coefficients	Single jersey
b0	73.57
b1	7.51
b2	-0.76
R^2	0.91
Adj. R^2	0.90

11.4 Conclusions

The conductive knitted fabrics were developed successfully for the deformation characteristic. The electromagnetic shielding during the deformation at biaxial stretching of the fabrics is measured. The Ag-coated PA yarn was used for preparing the knitted fabric which was initially analyzed for its electrical properties during its extension.

The SJ fabrics' SE versus elongation results reflect deformation sensitivity. For uniaxial and biaxial elongation of the samples, the biaxial device was used equipped with four independent jaws. SE of SJ samples increased with increasing fabric elongation at all directions, and the change in SE was more significant for higher-density fabrics. On the basis of this research, for the creation of sensors, it is recommended to use SE changes in the wale wise direction of the knitted fabric, where a linear trend was observed under uniaxial tensile stress.

The electrical resistance is indirectly proportional to the SE, which also influences the fabric results. ER is decreased with an increase in elongation at all directions for SJ fabric. It was noticed that the wale-wise elongation has a significant difference in SE values, and this way of fabric strain measurement will be suitable for sensor applications. SE increases with an increase in gauge porosity of the SJ fabric samples. The pore sizes of studied fabrics are in units of micrometers, and the wavelength of 1.5 GHz is 0.19 m, so it expected that the electromagnetic wave of his frequency cannot penetrate through the fabric. According to the conductance results of wale-wise elongation, the SE increases with SJ elongation.

During the modelling of SE depending on the uniaxial tensile stress of knitted samples, regression models were introduced. Based on the partial regression graph analysis, the nonlinearity in the gauge porosity was identified and that is why optimal regression model was created using transformation of this variable. The corresponding coefficients of determination R^2 of this model are shown in Tables 11.1 which is satisfactory. The wireless strain sensor is created successfully with the electrically conductive knitted fabric.

References

Akkermans O, Spronck M, Kluskens T, Offerein F, Saralidze K, Aarts J, Keshaniyan P et al (2016) Application of electrodeposited piezo-resistive polypyrrole for a pressure-sensitive bruxism sensor. Phys Status Solidi (a) 213(6):1505–1509. https://doi.org/10.1002/pssa.201532793

Ali A, Sattar M, Riaz T, Khan BA, Awais M, Militky J, Noman MT (2020) Highly stretchable durable electro-thermal conductive yarns made by deposition of carbon nanotubes. J Text Inst 1–10. https://doi.org/10.1080/00405000.2020.1863569

Demboski G, Bogoeva-Gaceva G (2001) Properties of weft knitted composites affected by preform stretching. Appl Compos Mater 8(6):371–384. https://doi.org/10.1023/A:1012603500481

Ehrmann A, Heimlich F, Brücken A, Weber MO, Haug R (2014) Suitability of knitted fabrics as elongation sensors subject to structure, stitch dimension and elongation direction. Text Res J 84(18):2006–2012. https://doi.org/10.1177/0040517514548812

Eltahan EA, Elzaher MS, Mito AB (2016) Determination of loop length, tightness factor and porosity of single jersey knitted fabric. Alex Eng J 55(2):851–856. https://doi.org/10.1016/j.aej.2016.02.006

Gregori A, Di Giampaolo E, Di Carlofelice A, Castoro C (2019) Presenting a new wireless strain method for structural monitoring: experimental validation. J Sens 2019:1–12. https://doi.org/10.1155/2019/5370838

Holleczek T, Rüegg A, Harms H, Tröster G (2010) Textile pressure sensors for sports applications. Proc IEEE Sens 732–737.https://doi.org/10.1109/ICSENS.2010.5690041

Holm R, Holm E (1967) Electric contacts : theory and application. Springer, Berlin; New York. http://books.google.com/books?id=RBwIAQAAIAAJ

Li L, Liu S, Ding F, Hua T, Au WM, Wong K-S (2012) Electromechanical analysis of length-related resistance and contact resistance of conductive knitted fabrics. Text Res J 82(20):2062–2070. https://doi.org/10.1177/0040517512447519

Liu S, Tong J, Yang C, Li L (2017) Smart e-textile: resistance properties of conductive knitted fabric—single pique. Text Res J 87(14):1669–1684. https://doi.org/10.1177/0040517516658509

Merlini C, Dos Santos Almeida R, D'Ávila MA, Schreiner WH, De Oliveira Barra GM (2014) Development of a novel pressure sensing material based on polypyrrole-coated electrospun poly(vinylidene fluoride) fibers. Mater Sci Eng B: Solid-State Mater Adv Technol 179(1):52–59. https://doi.org/10.1016/j.mseb.2013.10.003

Mihailovic T, Simovic L (1998) Geometry and deformation properties of plain loops made of spun cotton yarns. Tekstilna Industrija 46:23–28

Murray WM, Miller WR (1992) The bonded electrical resistance strain gage. Oxford University Press Inc., New York, USA

Palanisamy S, Tunakova V, Hu S, Yang T, Kremenakova D, Venkataraman M, Petru M, Militky J (2021) Electromagnetic interference shielding of metal coated ultrathin nonwoven fabrics and their factorial design. Polymers 13(4):484. https://doi.org/10.3390/polym13040484

Popper P (1966) The theoretical behavior of a knitted fabric subjected to biaxial stresses. Text Res J 36(2):148–157. https://doi.org/10.1177/004051756603600208

Rajagopalan S, Sawan M, Ghafar-Zadeh E, Savadogo O, Chodavarapu VP (2008) A polypyrrole-based strain sensor dedicated to measure bladder volume in patients with urinary dysfunction. Sensors 8(8):5081–5095. https://doi.org/10.3390/s8085081

Rana NK (2009) Application of force sensing resistor (FSR) in design of pressure scanning system for plantar pressure measurement. In: 2009 second international conference on computer and electrical engineering. IEEE, pp 678–685. https://doi.org/10.1109/ICCEE.2009.234

Ruppert-stroescu M, Balasubramanian M (2018) Effects of stitch classes on the electrical properties of conductive threads. Text Res J 88(21):2454–2463. https://doi.org/10.1177/0040517517725116

Šafářová V, Hes L, Militký J (2014) An approach to electrical resistance measurement eliminating contact resistance problem. In: International conference on applied electronics, pp 259–262.https://doi.org/10.1109/AE.2014.7011715

Simegnaw, Ahmmed A, Malengier B, Tadesse MG, Rotich G, Van Langenhove L (2022) Study the electrical properties of surface mount device integrated silver coated vectran yarn. Materials 15(1). https://doi.org/10.3390/ma15010272

Souri H, Bhattacharyya D (2018) Electrical conductivity of the graphene nanoplatelets coated natural and synthetic fibres using electrophoretic deposition technique. Int J Smart Nano Mater 9(3):167–183. https://doi.org/10.1080/19475411.2018.1476419

Spencer DJ (1998) Knitting technology. knitting technology, Third edn. Woodhead Publishing Limited, Cambridge, England

Wang J, Long H, Soltanian S, Servati P, Ko F (2014a) Electromechanical properties of knitted wearable sensors: part 1—theory. Text Res J 84(1):3–15. https://doi.org/10.1177/004051751 3487789

Wang J, Long H, Soltanian S, Servati P, Ko F (2014b) Electro-mechanical properties of knitted wearable sensors: part 2—parametric study and experimental verification. Text Res J 84(2):200–213. https://doi.org/10.1177/0040517513490057

Weizman O, Mead J, Dodiuk H, Kenig S (2020) Electrical properties enhancement of carbon nanotube yarns by cyclic loading. Molecules 25(20). https://doi.org/10.3390/molecules252 04824

Yun, Ju Y, Ah CS, Hong WG, Kim HJ, Shin JH, Jun Y (2017) Highly conductive and environmentally stable gold/graphene yarns for flexible and wearable electronics. Nanoscale 9(32):11439–11445. https://doi.org/10.1039/c7nr04384h

Zhang H, Tao X, Wang S, Yu T (2005) Electro-mechanical properties of knitted fabric made from conductive multi-filament yarn under unidirectional extension. Text Res J 75(8):598–606. https://doi.org/10.1177/0040517505056870

Chapter 12
Flame Retardancy of Textiles—New Strategies and Mechanisms

Sajid Faheem, Nazia Nahid, Jakub Wiener, Blanka Tomková, Miroslava Pechočiaková, Jiří Militký, and Adnan Mazari

Abstract Textile substrates are pervasive in our everyday life as apparel, industrial and technical textile goods, etc., and are made up of polymers; natural, semi-synthetic, or synthetic though most of them are inherently flammable. The considerable amounts of toxic gases, smoke, heat, ashes, and melt drips produced during their burning cause immeasurable damage to human life and property every year. Hence, among different functional properties, flame retardancy of these textile polymeric materials has been a subject matter of prime significant concern due to the requisites to minimize fire risks and meet fire safety requirements. Meanwhile, the art of flame retardant applications is taking a new shape globally considering the modification of textile surfaces as well as the structure of applied flame retardant compounds. However, numerous efficient traditional flame retardants based on organo-halogenated, organo-phosphorous, organo-nitrogen compounds, minerals, other compounds, etc., have been developed to impart flame retardancy in textile materials. Nevertheless, some of these compounds have been observed to have adverse effects on living beings and the environment because of inherent high toxicity risks, and ultimately their use has been restricted and/or banned. With existing flame retardant chemicals, various new substituted active materials, finishing agents, and potential technologies including cleaner and greener approaches based on intrinsic char formation, intumescence, nanotechnology, sol–gel, plasma treatment, biomimetic coatings, etc., are being discovered, processed, and developed to encounter the challenges and requirements of ever-changing safety regulations.

S. Faheem · J. Wiener · B. Tomková · M. Pechočiaková · J. Militký (✉)
Department of Material Engineering, Faculty of Textile Engineering, Technical University of Liberec, Studentská 2, 46117 Liberec, Czech Republic
e-mail: jiri.militky@tul.cz

N. Nahid
Department of Bioinformatics and Biotechnology, Government College University, Faisalabad, Faisalabad, Pakistan

A. Mazari
Department of Clothing Technology, Faculty of Textile Engineering, Technical University of Liberec, Studentská 2, 46117 Liberec, Czech Republic

279

Indeed, these are interdisciplinary developments that include rather a lot of scientific and engineering research implements.

12.1   Introduction

From different functional properties, the field of flame retardancy for textiles (i.e., fibers, yarns, and fabrics) has always been considered a major hazard. The flammability of textile materials/products signifies an area of the safety issue, which evinces that textiles are the first thing to be ignited even by small flames (such as matchsticks, cigarettes, candles, etc.) thus resulting in the most common fire (Kundu et al. 2020), and therefore, the desired need is required for the quality and safety of textile materials that aims to prevent fires and loss of life. As far as the burning of textiles is concerned, one main drawback refers to their primitive matter. Such as they are mostly based on organic polymers, which are usually flammable contrarily if not inherently flame retarded (Price and Horrocks 2010). The desire to improve flame retardant properties of textile materials for the reduction of fire hazards has been a major preoccupation over the years for the safety of ultimate consumers under many circumstances. As a consequence of the ease of textile flammability, additives/chemicals/finishes have been suggested, designed, and synthesized/developed that are so-called flame and/or fire retardants. They are adept, to suppress/delay the appearance of a flame or reduce the flame spread (flame retardants), and/or, delay the ignition or reduce the rate of combustion (fire retardants) as required (Morgan and Wilkie 2009).

The flame retardant formulations and chemicals are numerous and include halogens, phosphorous, nitrogen, Sulphur, antimony, boron, and other elements in many forms and combinations. Flame retardants are commonly applied to different kinds of materials to make them non-flammable or self-extinguishing, as the principle of flame retardants is to reduce their propensity to ignite/burn when subjected to a heating source or open flame (Gordon 1981), which is a requirement of civilians, firefighters, and emergency personnel, e.g., upholstery, drapery, floor coverings, household, and the airline sector. Therefore, a flame retardant fabric does not stimulate to propagate the flame, although it may burn and/or char when it is exposed to any form of heat source. Char formation confines the amount of flammable volatiles and gases acting as a diffusion barrier and reduces heat transmission into textile material providing a thermally insulating layer at the surface (Lyon 1998). The basic parameter for a successful commercially acceptable flame retardant is to have little or no adverse effects on the physiological and aesthetic properties of textile materials, ease the application, and possess durability against severe washing or cleaning and drying cycles.

According to statistics, about 50% of fires in the world are particularly caused by textiles as well as textile sources contribute to the largest percentage of deaths in residential fires. Response to these alarms together with an ever-growing demand for enhanced flame retardant performance has led both researchers and industries

to increase the efficiency of presently used flame retardants and to replace those where concerns lie with other existing formulations or to use known chemistry in novel ways, that not only ensure favorable ecological profiles but also durable and cost-effective options. The use of flame retardants to reduce the combustibility of materials and smoke or toxic gas production, therefore, has become a fundamental part of the developments and applications of new materials (Lu and Hamerton 2002).

12.2 Flammability and Thermal Behavior of Textile Materials

According to ISO 13943 and ASTM E176-18a standards, a material is said to be flammable if it is susceptible to easy ignition and rapid flaming combustion (American Society for Testing and Materials 2021; International Organization for Standardization 2017). Textile flammability is a composite concept involving materials, chemistry, and physics, as well as, the nature of the environment, and the potential hazards to human life in terms of burns and burning/combustion products toxicology (Horrocks et al. 1988). Fiber is the basic building block of any textile product and that may be a natural, regenerated (i.e., derived from natural polymers) or synthetic polymers (Grishanov 2011). All of these polymers are suitable for use in textiles because of their excellent fiber-forming properties and requirements. But most of the fibers have an important common issue in that they are flammable under normal ambient conditions and cause serious fire hazards in case of fire accidents. The main reason is that a major part of these fibers is organic polymers, representing a bountiful source of hydrocarbons that act as an excellent source of fuel for burning processes (Gaan et al. 2011).

The flammability of textiles is a critical aspect with respect to their end uses and application areas. The term "flame retardant textiles" usually alludes to textiles or textile-based materials that resist the flame and/or inhibit the spread of fire. Flame retardant textiles aid to save lives, obviate injuries and property losses, and protect the environment by facilitating to prevent of fires from starting and limiting fire damages. Flame retardant textiles are requisite and have been used in several application areas (consumer and industrial) such as; apparel, uniforms for firefighters, military/police personnel, and industrial workers, high-performance sports applications, upholstery for home furnishing, office/commercial infrastructure, and transportation systems, sleepwear for children and elderly people, architectural fabrics, etc. (Neisius et al. 2014). Flame resistant/flame-retardant textiles can be manufactured by using any one or combination of the following different techniques, methods, and/or routes (S Bourbigot 2008; S Gaan et al. 2011):

- By using inherent flame-resistant fibers:

  - *Fibers that contain inherently flame-resistant polymers;* such as wool, polyaromatic amides/aramids, polyimide, polybenzimidazole, melamine, glass, basalt,

halogen-containing olefins, polyvinyl chlorides, polyphenylene benzobisox-
azole, oxidized polyacrylonitrile, and polyphenylene sulfide-based fibers
are some examples of inherently flame resistant polymers. These kinds of
flame-resistant fibers owe their property to the textile materials.

– *Fibers from polymers that contain special flame-resistant co-monomers;* such
as Trevira CS (modified polyester) and modacrylics are common examples of
fibers that contain special monomers with flame-resistant characteristics.

- By using manufactured/synthesized flame-resistant fibers:

Fibers that contain special non-reactive flame-resistant additives; such as Viscose
FR® and Visil® are flame-retardant cellulosic fibers (melt/wet spun viscose fibers)
that contain a high concentration of flame-resistant additives, which are usually
incorporated in polymer bulk before the spinning process.

- By using surface treatments with flame-resistant compounds:

Chemicals/finishes with various chemistries can be applied and/or deposited on the
surface of textiles (also known as chemical finishing) by using different finishing/
coating and subsequent fixation processes/routes.

The flammability of textile materials is a very complex phenomenon and mainly
depends on various factors such as the polymer nature of the textile fibers, additives
in the textile fibers, fabric construction of the textiles, the type of chemical treat-
ments, the testing conditions, etc. (Nair 2000; Ozcan et al. 2003). The fiber polymer
composition of textile materials is the most important factor for determining their
flammability. Understanding the thermal behavior of fiber polymers alone and in
the presence of additives is very useful in designing an efficient and effective flame
retardant system.

The flammability properties of textile fibers vary and hence can be grouped
together based on their burning characteristics as follows (Bourbigot 2008):

- *Readily flammable;* the fibers that ignite readily and burn quickly, leaving behind
a slight ash residue (e.g., cotton, ramie, rayon, acetate, and triacetate).
- *Moderately flammable;* the fibers that are comparatively more difficult to ignite.
The synthetics tend to melt and drip, however sometimes self-extinguishing on
the removal of the ignition source (e.g., silk, olefin, polyester, nylon, and acrylic).
- *Relatively non-flammable;* in general the fibers that do not support combustion on
the removal of the ignition source (e.g., wool, modacrylic, aramids, and vinyon).

When any solid polymer material including textile fibers is heated, several physical
and chemical changes take place at different specific thermal transition temperatures
and thermodynamic parameters depending on the chemical nature and structure of
the solid, thus ultimately affecting its flammability (Horrocks and Alongi 2013). The
four thermal transition temperatures such as; softening/glass transition temperature
(T_g), melting temperature (T_m), pyrolysis temperature (T_p), and combustion (T_c),
are very important while considering the burning behavior and flame retardancy of
fibers. Usually, the lower the value of T_c, the more flammable is the fiber However,
for thermoplastic fibers, the values of T_p and/or T_c are higher than T_g and/or T_m,

while, for non-thermoplastic fibers, the values of T_p and/or T_c are lower than T_g and/or T_m. Hence, when natural fibers (i.e., non-thermoplastic fibers) are exposed to a heat/ignition source, pyrolysis and combustion temperatures are encountered before softening and melting temperatures and eventually they ignite (Horrocks and Alongi 2013; Tomasino 1992). Contrarily, thermoplastic fibers will melt and drip away from the flame before pyrolysis and combustion temperatures are reached. However, if the melt does not shrink away from the flame front, pyrolysis and combustion temperatures are eventually reached and ignition will occur (Horrocks 1986; Tomasino 1992). Natural fibers can be made flame retardant and like some flame retardant synthetic fibers can offer protection to wearers because they do not shrink away from a flame. Thermoplastic fibers may appear to offer protection because they pass the ignition test by shrinking away from the flame, however, in reality; this exposes the wearers to direct heat and burns caused by contact of molten mass with the body.

Another related factor that is considered important in burning is the limiting oxygen index (LOI) value; the minimum volumetric amount of oxygen, required by any material to support combustion and usually expressed in percentage (Fenimore 1975; Fenimore and Martin 1966). It has been used to specify the relative flammability and/or flame retardancy of different polymeric materials (Camino et al. 1988) and has also broadly been applied to textile materials (Horrocks et al. 1988). In general, the textile fibers that have LOI values $\leq 21\%$ are very flammable, burn easily and rapidly in the air (as the oxygen content of natural air is ~20.8%). The fibers with LOI values of 21–25%, become moderately flammable, ignite and burn more slowly. But, if LOI values are >25%, the fibers show limited flammability and commence to pass several national and international standard test methods for flame retardant textiles (Horrocks 1983; Horrocks et al. 1988). All cellulose-based fibers have very low LOI values and are thus easy to burn. Among the natural fibers, wool has a relatively high LOI value and is a common component in manufacturing flame-retardant clothing for firefighters in some countries. Moreover, the heat release rates of fibers (PHHR), i.e., the speed at which the heat is released during thermal decomposition of fibers is also another significant criterion that determines the flammability properties of fibers (Horrocks 1986; Yang et al. 2010). The peak heat release rates of some commonly used fibers such as cotton, viscose rayon, cellulose acetate, silk, polyester, nylon, polypropylene, acrylic, and aramids have been measured by using micro-scale combustion calorimetry. Cellulose-based, polypropylene, polyester, and nylon fibers have comparatively high peak heat release rates (i.e., >200 W/g) while m-aramid (Nomex; a commonly used fiber in manufacturing flame retardant fabrics) has a very low value (i.e., ~80 W/g) (Yang et al. 2010). The thermal transition temperatures and LOI values of some commonly available fibers are enlisted in Table 12.1.

The availability of oxygen is a crucial factor in defining the flammability of textile fabrics. The construction of fabrics (i.e., yarn structure, weave/knit, weight, cover factor, and thickness) can play a significant role as it regulates active surface area, amount of air present, and flow of air through fabric (Hendrix et al. 1972). Fabrics with open constructions may be more combustible and flame propagation may also be faster. Fabrics with a raised surface (highly brushed) and containing fiber protruding

Table 12.1 Thermal transitions of commonly used fibers (Horrocks 1983)

Fiber	T_g (softens)	T_m (melts)	T_p (pyrolysis)	T_c (combustion)	LOI (limiting oxygen index)
	(°C)	(°C)	(°C)	(°C)	(%)
Wool	–	–	245	600	25
Cotton	–	–	350	350	18.4
Viscose rayon	–	–	350	420	18.9
Triacetate	172	290	305	540	18.4
Nylon 6	50	215	431	450	20–21.5
Nylon 6.6	50	265	403	530	20–21.5
Polyester	80–90	255	420–447	480	20–21
Acrylic	100	>220	290	>250	18.2
Polypropylene	−20	165	469	550	18.6
Modacrylic	<80	>240	273	690	29–30
Polyvinyl chloride	<80	>180	>180	450	37–39
Polyvinylidene chloride	−17	180–210	>220	523	60
Polytetrafluoroethylene	126	≥327	400	560	95
Oxidized acrylic	–	–	≥640	–	55
Nomex	275	375	410	>500	28.5–30
Kevlar	340	560	>590	>550	29
Polybenzimidazol	>400	–	≥500	>500	40–42

out to the surface require some special care during processing and use. The flammability hazards with raised surface fabrics involve a phenomenon called 'surface flash' where the flame can travel quickly over a fabric surface singeing the fiber ends. In itself, this flash may not be perilous unless the flame intensity is high enough to ignite the base fabric. The twist level of yarns may also affect the porosity of fabrics. A tightly woven fabric with higher areal density, fabricated from yarns with high twist levels, will provide better flame protection. Fabric blends can also play a critical role in determining the flammability of fabrics. The blended fabrics constructed from two different fiber polymers may exhibit flammability characteristics quite different from that demonstrated by each component of the blend independently. For example, fabrics constructed from polyester are less flammable as compared to cotton fabrics but cotton/polyester blended fabrics burn more quickly. This is due to the 'scaffolding effect' where the charred cotton fibers in the blend serve as a support for the polyester fibers. The melting polyester in the blend does not drip away as it may do in 100% pure polyester fabrics and remains to continue burning due to the 'wicking effect'. The flammability and thermal shrinkage of fabrics are primarily dependent on the thermal stability of component/blended fibers and relatively independent of the fabric

weave design and weight (Stepniczka and Dipietro 1971). As far as the flammability of textile materials is concerned, the inherent resistance of fiber polymers to burning is the major factor affecting fabric performance with weave, weight, and thickness being secondary. Fabric structure, weight, and thickness are more important while measuring thermal protective performance. A combination of non-flammable fiber and optimum fabric structure can be used to achieve maximum non-flammability with the lightest weight for the specific fabric application (Barker and Brewster 1982).

12.3   Combustion or Burning Process of Textile Materials

In order to comprehend the mechanism(s) of effective flame retardant(s) in a better way, it is first necessary to clarify the mechanism of combustion. The burning of materials, including textiles, generally involves two thermal degradation/decomposition processes (D. Price, Horrocks et al. 1997), such as:

- Pyrolysis, and
- Combustion.

Overall at the macro-scale, the burning/combustive process is an exothermic process (oxidation) that involves three essential components (i.e., fire triangle components) (Pelzl et al. 2018; Sutker 2000), such as:

- a fuel; a combustible substance
- an oxidant; an oxidizing gas, i.e., primarily oxygen
- an ignition/heating source; an external or from a combustion process itself.

The mechanism of combustion was previously believed to be based upon a fire triangle but further research work found that a fourth element, i.e., a chain reaction, is an essential component of combustion.

Textile materials are combustible but actually not volatile since they are not directly involved in the instigation of fire. All textiles can combust/burn provided they are exposed to the right conditions of flame, heat, air/oxygen concentration, and time of exposure to flame. However, at the initial stage for burning, through the availability and support of an ignition source, these materials encounter endothermic degradation reactions in which larger polymeric molecules are broken into smaller, volatile species and combustible compounds as fuel. Then, these pyrolysis products diffuse to the fiber/yarn/fabric surface and break down further to finally release hydroxyl (OH˙) and hydrogen (H˙) radicals, which then mix with the oxygen from the air so that flame can propagate and combustion can take place releasing heat and light. This combustion then becomes exothermic, and the heat and fumes so generated partially transfer back to fiber/yarn/fabric surfaces, so maintaining voluntarily a continuous quick supply/feedback of volatile gaseous fuel to sustain polymer pyrolysis and/or combustion (Horrocks 1983, 1986). It can be concluded that the overall burning of textile materials may be modeled and exhibited as a cyclic process
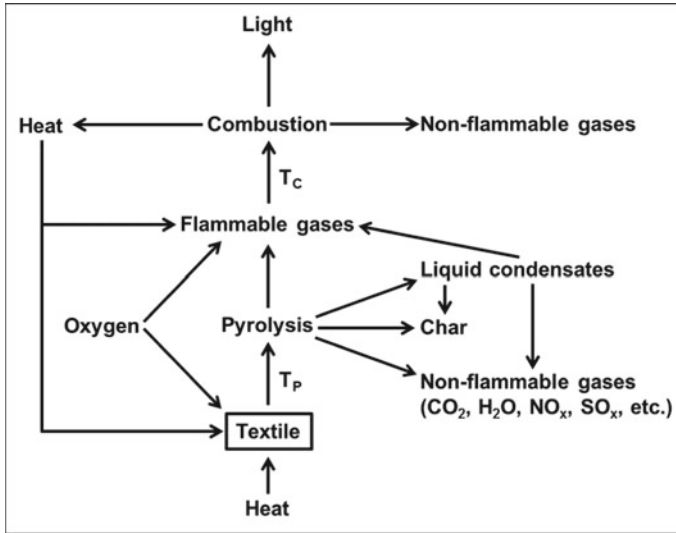
Fig. 12.1 Schematic description of combustion cycle for textile fibers, yarns, and fabrics

as shown in Fig. 12.1, maintaining a continuous supply of gaseous fuel for further flame propagation.

The absence of oxygen and/or the presence of flame retardant additives could disrupt this feedback-cyclic process. The thermal decomposition of fiber polymers is a very complex phenomenon and could lead to the generation of several products such as flammable volatiles, non-flammable volatiles, tars/liquid-condensates, and solid residues. The flammable volatiles could be carbon monoxide, hydrogen, and many oxidizable organic molecules such as low molecular weight alkanes, alkenes, alkynes, aldehydes, ketones, ethers, etc. Water vapors, carbon dioxide, and higher oxides of nitrogen and sulfur are commonly generated non-flammable gases. The solid residues in nature could be carbonaceous, inorganic, or even a combination of both (Horrocks 2001). Some fiber polymers such as cellulose, protein, and aramids tend to produce carbonaceous chars upon heating, while some, such as olefins, polyester, and polyamides do not leave behind any residues. The presence of additives may affect the amount of residues formed during the thermal decomposition process. For example, phosphorus-based compounds can react with the substrate to accelerate the production of char residues and inorganic compounds such as silica derivatives can create glassy protective layers that could insulate the inner substrate layers from further decomposition.

Thermal decomposition of fiber polymers can ensue through one or more of the following routes (Hirschler 2000):

- *Random chain-scission;* chain breakage occurs along the chain length of the polymer at random places.

- *End-scission;* breakage of the polymer occurs at the chain ends primarily in the form of monomers.
- *Chain-stripping;* main polymer chain remains more or less intact with the removal of atoms and/or functional groups attached to the backbone chain.
- *Cross-linking;* new bonds are formed between functional groups of adjacent polymer chains.

12.4 Flame Retardants and Flame Retardancy General Aspects and Theory

"Flame retardants are chemicals that are added or applied to materials in order to prevent or slow the start or growth of fire" (Gordon 1981; National Institute of Environmental Health Sciences, n.d.), and usually composed of organic and inorganic compounds of phosphorous (P), nitrogen (N), sulfur (S), halogens (X; Br, Cl, F), silicon (Si), aluminum (Al), magnesium (Mg), antimony (Sb), tin (Sn), boron (B), zinc (Zn), carbon (C; graphite), zirconium (Zr), titanium (Ti) and calcium (Ca). The flame retardants could comprise one or more of these elements and their effectiveness is usually a direct function of the fraction of an active element present in the flame retardants (Hirschler 1982; Neisius et al. 2014). For ease of understanding, flame retardants have been classified into different groups/classes under different situations/ conditions as follows, according to several different ways based on (Hull et al. 2014; Kandola et al. 1996; Vladimirtseva et al. 2016).

- *Origin/source*: such as; natural, synthetic/manmade.
- *Nature of textile material*: such as; for natural, for synthetic/manmade.
- *Way/means of incorporation to textile materials*: such as; reactive, additive.
- *End-uses/application-areas of textile materials*: such as; for non-technical textiles, for technical textiles.
- *Chemical-composition/elemental-constituents*: such as; the presence of an element or a combination of elements (i.e., phosphorus, nitrogen, halogen, etc.).
- *General chemical nature*: such as; inorganic, organic (i.e., halogenated, organo-phosphorus, halogenated phosphates, nitrogen-based, metal hydroxides or carbonates, etc.).
- *Chemical type*: such as acids, bases, ethers, esters, oxides, hydroxides, salts, etc.
- *Mode of action*: such as; physical and/or chemical mode of action.
- *Working mechanism*: such as; condensed/solid phase and/or gas/vapor *phase.*
- *Working efficiency*: such as; primary flame retardants, synergistic retardancy enhancers, adjunctive retardancy promoters.
- *Durability to fastness*: such as; non-durable, semi-durable, durable to laundry, light, heat, chemicals, etc.

Unfortunately, all of these classification groups cannot be unambiguously applied to particular flame retardants. Because, most of the flame retardants in all these classification classes, interfere with any particular stage of the combustion process
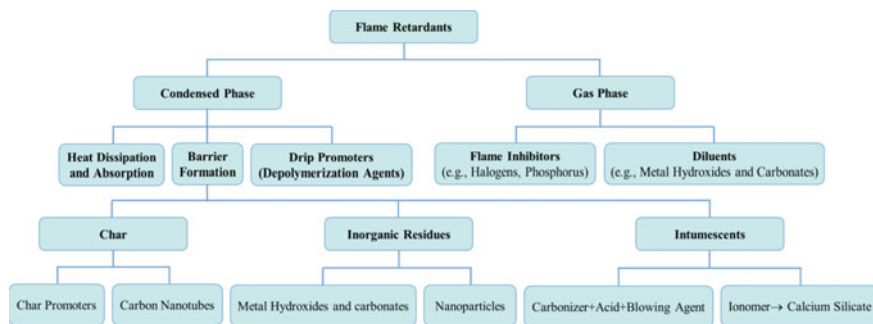
Fig. 12.2 Classification of flame retardants based on working mechanisms

(i.e., during heating, decomposition, pyrolysis, ignition, or sustained burning, etc.), and also have some common aspects such as chemistries, ultimately mode of action, and nature/kind of fibers for which these have to be used. Thus in scientific literature, flame retardants are mostly discussed and classified by considering these basic facts. The most widely used common flame retardant additives are mineral compounds, halogenated compounds, phosphorus-based compounds, nitrogen-based compounds, silicon-based compounds, and nanometric particles. Figure 12.2 illustrates how the major flame retardants could be subdivided based on their working mechanisms.

As the particular hazards associated with quick burning/combustibility of textiles, especially cellulosic materials (such as cotton and flax) were recognized during ancient civilizations (see Fig. 12.3) (Grayson 1997). Salts such as alums have been used since those times to suppress/reduce their combustibility and so confer flame retardancy. In 1735, borax, vitriol (a metal sulfate; ferrous sulfate), and some other mineral substances (alum) were then patented by Obadiah Wyld (Wyld 1735) for flame retarding canvas and linen. The state of the art for different commercially available flame retardants for textile materials has been reviewed, summarized, and classified into different periods (from almost 1735 to onward) according to their key research and development findings (Horrocks 1986, 2011; Horrocks et al. 2005).

Most of the potential and successful additives, formulations, and treatments are derived from chemistry developed in the 1950–1980 period, which is usually considered the "Golden Period" for flame retardant research and developments (Horrocks 2011). That period was particularly remarkable and interesting for the development of two important flame retardants, which are still currently being used. These represent two major and commercially dominant main generic types of durable flame retardants for cotton and cotton-rich blends, specifically those based on tetrakis(hydroxymethyl) phosphonium-urea (THPX) condensates, epitomized by Proban® (Rhodia now Solvay), and those based on N-methylol dimethylphosphonopropionamide (N-MDMPE) derivatives, epitomized by Pyrovatex® (Ciba now Huntsman).
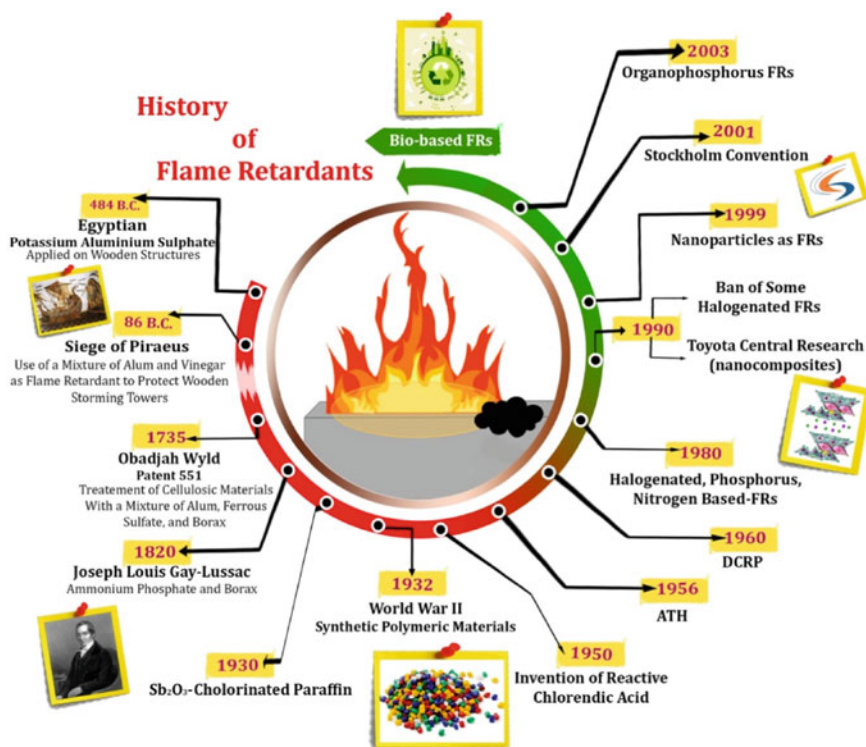
History of Flame Retardants

Bio-based FRs

2003 Organophosphorus FRs

2001 Stockholm Convention

1999 Nanoparticles as FRs

Ban of Some Halogenated FRs

1990 Toyota Central Research (nanocomposites)

1980 Halogenated, Phosphorus, Nitrogen Based-FRs

1960 DCRP

1956 ATH

1950 Invention of Reactive Chlorendic Acid

1932 World War II Synthetic Polymeric Materials

1930 Sb₂O₃-Cholorinated Paraffin

1820 Joseph Louis Gay-Lussac Ammonium Phosphate and Borax

1735 Obadjah Wyld Patent 551 Treatement of Cellulosic Materials With a Mixture of Alum, Ferrous Sulfate, and Borax

86 B.C. Siege of Piraeus Use of a Mixture of Alum and Vinegar as Flame Retardant to Protect Wooden Storming Towers

484 B.C. Egyptian Potassium Aluminium Sulphate Applied on Wooden Structures

Fig. 12.3 Evolution of flame retardants (Vahabi et al. 2021)

Flame retardant chemicals and finishes for cotton fabrics have been reviewed in a large number of research publications, encyclopedia articles, and books (Bourbigot 2008; Calamari and Harper 2000; Islam and van de Ven 2021; Kandola 2009; Kozłowski and Muzyczek 2020; Lazar et al. 2020; Lewin 2018; Lewin and Sello 2012; Samanta et al. 2015; Soliman and Hassabo 2021; Tesoro 1978; Weil and Levchik 2008; Yang 2013). Flame retardant chemical and/or finishing treatments for cotton cellulose and cellulose-based textiles, i.e., flame retardancy can be generally achieved through and/or categorized as non-durable flame retardants, semi-durable flame retardants, and durable flame retardants. Definitely, a large number of different compounds and formulations, from simple processes including deposition of inorganic salts to sophisticated processes involving modifications of cellulose molecules and/or in situ polymerization of suitable monomers, have been proposed (Alongi and Malucelli 2015; Gaan et al. 2011). Although many of these compounds, formulations, and processes are documented in scientific and/or patent literature to improve flame retardancy of cotton cellulose and cellulose-based materials and products, their utilization has been limited due to undesirable side effects and high costs (Horrocks 1986, 2011, 2003; Horrocks et al. 2005). However, phosphorus-containing materials
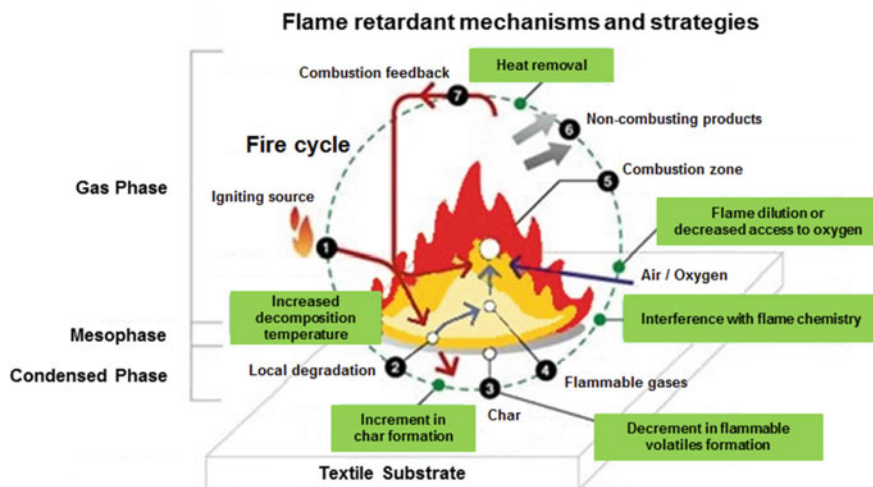
Fig. 12.4 Flame retardant working mechanisms and strategies

are so far the most significant class of compounds commonly used to impart flame resistance to cotton cellulose.

On exposure to flame, fire, or heating source, flame retardants become active depending on their nature as well as their chemical interaction with the polymers/fibers and can interfere with or disrupt the combustion process/cycle in the solid, liquid, or gas phase (see Fig. 12.4 and Fig. 12.5) during a particular stage of burning (i.e., heating, decomposition, ignition or flame propagation) through physical actions, and/or chemical actions (Bourbigot and Duquesne 2007; Horrocks 1983). They do not happen individually but should be considered as composite/complex processes in which many single distinct stages occur simultaneously with one dominating.

There are several physical phenomena that may interfere with the combustion process:

- *By formation of protective layer*: The combustible/flammable material (polymer/fiber) and its components in the condensed phase can be protected with a protective solid layer (with a low thermal conductivity) that prevents heat transfer from the heat source as well as from the gas phase and inhibit oxygen flow. It then helps to reduce the degradation rate of polymer and also the supply of pyrolysis gases to materials' surfaces. It is also a basic principle of the intumescence phenomenon (Bourbigot et al. 2004; Vandersall 1971). This same mechanism can be experienced by using phosphorus- and silicon-containing compounds, boric acid-based additives, inorganic borates, or low melting glasses (Jimenez et al. 2006; Kroenke 1986).
- *By cooling*: The combustible/flammable substrate can be cooled down to a temperature below that required for ignition and sustaining the combustion process by triggering endothermic processes such as decomposition/degradation of additives,
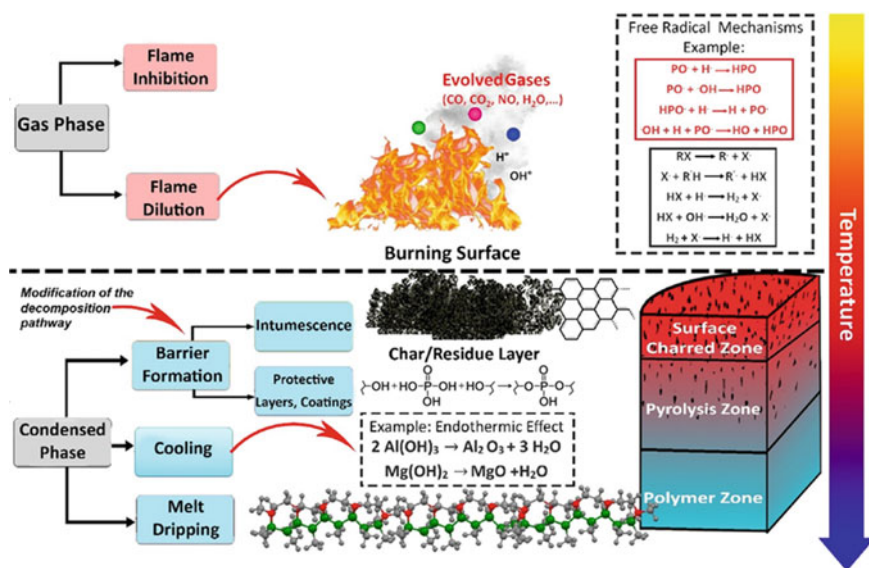
Fig. 12.5 Possible action mechanisms of flame retardants in condensed and gas phases (Vahabi et al. 2021)

e.g., inorganic/organic phosphorus-containing agents, aluminum hydroxide, or alumina trihydrate (Bourbigot et al. 1999a, b).

- *By dilution*: The concentration of flammable gases in the condensed and gas phase can be lowered by using inert substances/additives, e.g., fillers (such as talc, chalk) (Hornsby and Rothon 2005) as well as hydrates, char-promoting, and halogen-containing compounds. They release non-flammable gases on decomposition and dilute the fuel in both phases, ultimately the flammable gases concentration falls under the ignition limit.

There are some important chemical reactions that may interfere with the combustion process:

- *Reactions in the gas/vapor phase*: The free radical reactions that usually take place in the gas phase of the combustion process can be interrupted by flame retardants. The concentration of free radicals drops down to a critical value, thus flaming cannot occur. The exothermic processes and resulting thermal feedback to the condensed phase are then also declined due to less release of flammable volatiles that ultimately is completely suppressed. The halogenated and some phosphorous-based compounds can interfere with chain reactions (free radical reactions/exothermic oxidative flame chemical processes) by preventing the reaction of hydroxide and hydrogen free radicals with oxygen and carbon monoxide (Lewin 1984; Lewin and Weil 2001).
- *Reaction in the solid/condensed phase*: The amount of volatile species produced in the condensed phase can be reduced by changing the pyrolytic path using

flame retardants. Consequently, instead, carbonaceous char, carbon dioxide, and water are then often produced (Lewin 1984; Lewin and Weil 2001). Most of these phenomena occur in the case of nitrogen and phosphorous-based compounds as well as heavy metal complexes. These both are recognized to take place in cellulosic as well as synthetic fibers. In the case of synthetic fibers usually, two types of reactions can take place in this phase. First, the polymer breakdown can be accelerated by flame retardants causing a pronounced flow of polymer and, thence, enabling it to ebb from the flame influence sphere usually by dripping. Second, the formation of a layer of carbonaceous char, a ceramic-like structure, and/or a glass on the polymer surface can be produced by flame retardants. This inert insulating material/layer acts as a heat and mass flow barrier that serves to protect polymers/fibers. Whereas, in the case of cellulosic, these corresponding significant reactions are dehydration and crosslinking.

12.5 Role of Char Formation and Intumescence for Flame, Fire and Heat Protection

When polymeric materials ignite, their thermal degradation usually occurs accompanying competitive reactions such as volatilization, crosslinking, and polymer chain unsaturation. The last two responses can lead to the formation of a carbonaceous structure commonly known as char that may be either non-tumescent (non-cellular/ unexpanded) or tumescent (cellular/expanded/layered) (Horrocks et al. 1996). Char formation during polymer decomposition/degradation, with heat and/or on flame/fire exposure, is very important as it directly affects the degree of flame retardancy of the polymer. Van Krevelen (1975) has shown that the inherent flammability tendency of any polymer decreases as its char-forming propensity increases as char formation always happens at the expense of volatile fuel. During burning, char formation acts as a thermal insulating layer at the surface to reduce heat transmission into the material and also provides a diffusion barrier to combustible volatiles and gases (fuel) emanating to extinguish the fire in most cases (Lyon 1998). Additionally, char formation also accompanies the release of water condensates that can dilute combustible volatiles (Horrocks and Price 2001). Char residues are mostly composed of noncombustible carbon derivatives that proffer protection from flaming (Horrocks and Price 2001). Chars are complex materials and their structural properties can be attributed to a number of considerable parameters, such as weight, density, volume, crush, resilience, toughness, hardness, adherence, coherence, permeability, heat capacity, thermal conductivity, insulation, etc. (Lewin 2005). Open (non-ideal or poor) char structures consist of channels/fissures that allow volatile species to access flame and hence offer only limited heat protection. While, the contrary, closed (ideal) char structures consist of air pockets that entrap combustible gases further fueling flame (Horrocks and Price 2001).

In general, for flammable cotton cellulose, most of the effective and efficient flame retardants are ones that stimulate and promote the transformation of polymeric chains

into carbonaceous char (Horrocks 1996). Such as, it is notable, that the phosphorus-containing flame retardants may wield different modes of action for flame retardancy. They may ensue through the condensed phase or vapor phase or as a combination of both. The condensed phase action generally results in an increased non-tumescent char formation, and in some cases, tumescent char formation through a mechanism known as intumescence (Hirschler 2014). Intumescence or expanded carbonaceous char formation is one of the most efficient ways of imparting flame/fire retardancy to combustible materials (Horrocks 1996). Intumescent coatings (ICs) and intumescent flame retardants (IFRs) systems/technologies have emerged and attracted attention progressively and have been considered the most promising materials to displace halogen-containing flame retardants because they generate low smoke and no toxic and/or corrosive gases.

The intumescence phenomenon was observed and reported by Gay Lussac in 1821, with reference to flame retardancy of textiles, but the word "intumescence" was not used at that time. The intumescent flame/fire retardant systems have been employed widely and successfully for almost sixty years for different combustible materials such as for coatings of building structures (mainly on wood boards and steel structures) to facilitate protection against flame/fire. Though, it was the first time reported in the literature, on a fire retardant intumescent coating material mainly applied to wood for fire protection in 1938; a patent by Heinrich et al. (1938), and first reviewed in the 1970s by Vandersall (1971) and updated later by Kay et al. (1979). However, Olsen and Bechle (1948) used the term "intumescent" for the first time in this field, in 1948. In the 1980s, it was the comprehensive pioneer work of Camino et al., who successfully applied and permitted this basic concept to bulk polymers (mainly thermoplastics) (Camino and Costa 1986, 1988, 1998, 1989; Camino et al. 1991). In more recent years this approach was experienced to apply for polymers and flexible structures such as textiles and is acquiring considerable attention (Kozlowski et al. 2007).

On the basis of new chemical synthesis, several efforts at academic and industrial levels have been proposed and carried out in the last twenty years by reconsidering conventional perceptions of intumescent formulations and intumescence phenomenon (Ellard 1973; Vandersall 1971). Available detailed review articles/papers (Alongi et al. 2015; Bourbigot 2021; Hao and Chow 2003; Le Bras et al. 1998; Malucelli et al. 2014; Puri and Khanna 2017; Weil 2011), cover and present core concepts of intumescence (formulations and developments), highlighting innovations for intumescent flame retardants and their application methods, accompanying the most significant results achieved in flame retardancy of polymeric materials (such as wood, steel, metals, plastics as well as foams, films, and textiles), in last fifteen to twenty years.

The intumescent flame retardant system most commonly comprises the integration of three components, although only one single material can have more than one role. Other components that may also be used include binders, resins, viscosity modifiers, fillers, pigments, and fibers as required (Alongi et al. 2015; Bourbigot and Duquesne 2007; Kozlowski et al. 2007). The three main components are:

- *a carbonific; carbonizing agent*—supply raw material for char formation, substances with a large number of carbon atoms (as a source of carbon; either provides its own carbon or uses polymer substrate as a carbon source such as cellulose), thermal degradation of which results in the formation of carbonaceous material, and/or, having a huge number of hydroxyl groups, able to be esterified with acids such as polyols, polyphenols, saccharides, polysaccharides.
- *a catalyst; dehydrating agent*—supply acid for dehydration, accelerate the process, substances that release acid during their thermal decomposition (at a temperature between 100 and 250 °C), and then acid esterifies hydroxyl groups of carbonizing agents (at slightly above the temperature of acid release), often an inorganic acid and/or its thermal precursors such as phosphoric acid and/or its ammonium, aminic salt and esters (ammonium polyphosphate; APP), boric acid and its derivatives.
- *a spumific; blowing agent*—supply evolving gases for foam formation or char expansion, substances able to release a large amount of nonflammable gases during its thermal decomposition to form the foamed structure of carbonaceous char layers such as nitrogen- and halogen-containing compounds.

The most basic and earliest intumescent flame retardant system is; pentaerythritol (carbon source), ammonium polyphosphate (acid-releasing source), and melamine (gases forming source) which has been thoroughly and systematically studied by Camino et al. (1984a, b, c, d; 1985a, b). Flame retardancy exhibited by polymers and/or textiles through intumescence is principally a special case of condensed phase mechanism (Bourbigot et al. 2004). Intumescent flame retardants certain compounds (either initially incorporated into or merely coated onto polymeric material), on heating beyond a critical high temperature, either decompose or react with other materials in the condensed phase (Camino et al. 1990; Delobel et al. 1990; Guan et al. 2003). The intumescence phenomenon happens due to the combined effect of charring and foaming of the surface of the burning polymer. The intumescent coatings cover the polymer/textile surface and interfere with thermal degradation and self-sustained combustion at its very earlier stages with the formation and/or evolution of gaseous fuels aiding to insulating polymer/textile surface from heat and gaseous oxidant (usually air/oxygen) as shown in Fig. 12.6 (Camino et al. 1990; Horrocks 1996). The protection mechanism is based on the foamed cellular charred layer that serves as a physical barrier and slows down the heat and mass transfer between gas and condensed phases (Le Bras et al. 1998). The formation of foamed char depends on a series of complex chemical reactions and physical processes in the condensed phase of polymer/textile burning. The proposed several distinct processes/reactions that occur simultaneously but sequentially at an appropriate time via respective liquid stages in the development of the intumescence phenomenon can be described as follows (Alongi et al. 2015; Bourbigot and Duquesne 2007; Camino et al. 1991):

- the acid-producing source disintegrates to produce an inorganic/mineral acid usually at a temperature between 100 and 250 °C depending on its source and
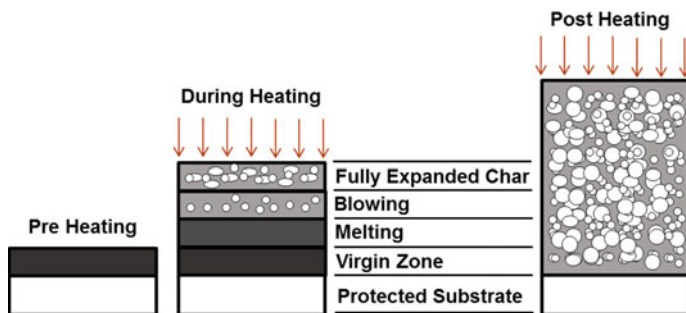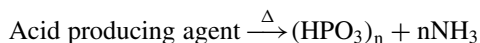
Fig. 12.6 Schematic representation of intumescence process

other components.

$$\text{Acid producing agent} \xrightarrow{\Delta} (HPO_3)_n + nNH_3$$

- the acid plays a part in the esterification of carbonizing agent (i.e., to catalyze char formation) at temperatures slightly above acid release temperature, the constituents of the mixture melt before or during esterification, the esters decompose through dehydration (carbonization of char forming agents) resulting in a matrix/residue formation of carbon-inorganic.

$$\text{Char forming agent} + (HPO_3)_n \xrightarrow{\Delta} [-\overset{|}{\underset{|}{C}}-] + H_3PO_4 + mH_2O$$
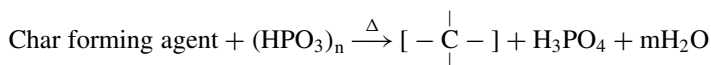
- the gases release (gasification) from the decomposition of a blowing agent as well as from the above decomposition reactions or degradation products, the released gases get entrapped by melted matrix (semi-liquid) and cause it to tumid and then expand, as the reaction nears to complete, gelation and then solidification occurs lastly through crosslinking and condensation reactions. The resultant solid procures the form of multicellular foam.

$$\text{Gas releasing agent} \xrightarrow{\Delta} NH_3 \xrightarrow{O_2} N_2 + H_2O$$
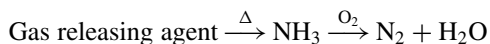
Consequently, the produced foamed cellular stable charred layer (protective barrier) on the polymer/textile surface protects the underlying substrate from the action of heat flux/flame and further excessive rise of temperature and oxygen penetration, thus ultimately thermal degradation and combustion (Vandersall 1971). Furthermore, intumescence also fills up interstices between fibers and yarns of textile fabrics as it chars. After that, it also interjects with adjacent charring fibers and yarns, if compatible liquefied phases are present in the course of initial pyrolysis stages (Kandola and Horrocks 1999, 2000). As a part of the overall flame retardancy of

polymeric materials, the formation of intumescent chars also stimulates to reduce the toxic fire gases and smoke emissions (Alongi et al. 2015; Hao and Chow 2003).

12.6   Chemistry of Flame Retardant Additives for Textile Materials

Mineral-based flame retardants

Mineral-based flame retardants represent the largest segment of flame retardant additives in the market. Some minerals (also known as inorganic fillers) are more peculiarly used as flame retardant additives owing to their specific behavior at high temperatures. The most commonly used mineral flame retardants are metal hydroxides (e.g., aluminum tri-hydroxide, magnesium di-hydroxide), hydroxy carbonates (e.g., natural magnesium carbonate (magnesite), synthetic magnesium hydroxycarbonate (hydromagnesite)), boric acid and borates (e.g., sodium borate, zinc borate,), and inert fillers. In general, the incorporation of any type of inorganic filler can influence the reaction of polymers toward flame/fire such as; can decrease the content of combustible products, as well as, can modify the thermal conductivity, thermoplastic properties, and melt viscosity of the resulting material. However, inert fillers are sometimes utilized in combination with other flame retardants such as metallic hydroxides; specifically aluminum tri-hydroxide (ATH) and magnesium di-hydroxide (MDH). These inorganic fillers can work in both gas and condensed phase of combustion and have a direct physical flame-retardant action. At high temperatures, they decompose endothermically and absorb energy, and therefore, cool down the degrading polymeric material, and consequently, retard the thermal degradation. Moreover, they release nonflammable gas molecules (e.g., H_2O, CO_2) on decomposition that dilute the combustible gas mixture and can prevent or delay ignition. The non-flammable solid filler residues can also promote the formation of a protective ceramic/vitreous char layer in the condensed phase (Hornsby 2001; Hornsby and Rothon 2005).

Halogen-based flame retardants

Halogen-based flame retardants represent the second largest segment of flame retardant additives. Halogen-based flame retardants can either be blended with polymers (i.e., additive pathway) or structurally added as units of polymer backbone chains during the progression of polymerization reaction (i.e., reactive pathway). Theoretically, chemical compounds of four element classes can be used as halogenated flame retardants containing fluorine, chlorine, bromine, or iodine. The effectiveness of halogenated flame retardants usually depends on the type of halogen atom and increases in the order of F < CI < Br < I. Halogenated flame retardants are generally recognized to act in the gas phase. During combustion, the flame retardants release halogen radicals ($X^{\bullet}$) that then form hydrogen halides (HX) by eliminating a hydrogen atom from degrading polymers (Georlette 2001). Hydrogen halides react with the highly

reactive gaseous free-radical species (e.g., hydrogen and hydroxyl radicals) that are considered responsible for sustaining combustion by a cascade-chain mechanism in the gas phase. Hydrogen radicals (H$^•$) are expended for chain-branching free-radical reactions during thermal degradation (Beyler and Hirschler 2002), and hydroxyl radicals (OH$^•$) are expended for highly exothermic oxidation of carbon monoxide (CO) to carbon dioxide (CO$_2$) (Levchik 2007). Halogenated flame retardants dilute the combustible gas mixture by scavenging free-radical species and preventing flame propagation. The hydrogen halides react with hydrogen or hydroxyl radicals to form hydrogen gas (H$_2$) and water (H$_2$O). The produced halogen radicals can then be reutilized to further prevent radical propagation. The most commonly used halogenated flame retardants are chlorine- and bromine-containing compounds due to their low bonding energy with carbon atoms (Georlette 2001). Fluorinated compounds are generally more stable than any other commercial polymers and do not release fluorine radicals and/or hydrogen fluoride. In comparison, iodinated compounds have very low thermal stability and cannot be processed with most commercial polymers. Additionally, fluorine and iodine are more expensive than chlorine or bromine (Levchik 2007). It has also been speculated that halogenated flame retardants can also act in the condensed phase through the enhancement of char formation (Green 1996). In spite of their remarkable flame retardant properties, halogenated flame retardants are however undertaking worldwide investigation since they liberate toxic gases/smoke and leach into the environment (Darnerud 2003; Watanabe and Sakai 2003).

Phosphorus-based flame retardants

Phosphorus-based compounds represent the third most used but the fastest-growing segment of flame retardant additives. They are significantly beneficial and considered to be the best substituted due to their lack of toxicity in comparison to that of halogenated flame retardants. Likewise halogenated flame retardants, they can also be used in both additive and reactive pathways. Phosphorus-based flame retardants can be divided into two classes; inorganic and organic compounds covering numerous compounds in which phosphorus exists in different oxidation states from 0 to 5. The range of phosphorus-based flame retardants is immensely wide comprising red phosphorus, phosphates, phosphonates, phosphinates, phosphine oxides, and phosphates. Phosphorus-based flame retardants can perform as gas and condensed phase active compounds at high temperatures (Levchik and Weil 2006). The active radicals (HPO$_2$$^•$, PO$^•$, PO$_2$$^•$, and HPO$^•$, in decreasing order of significance) liberated from phosphorus-based flame retardants enter the gas phase of the combustion cycle and react with (H$^•$) and (OH$^•$) radicals restraining the exothermic oxidation reactions. Phosphorus-based flame retardants prevent flame propagation in the condensed phase by releasing phosphoric acid on thermal degradation. The released phosphoric acid further reacts with either another phosphoric acid molecule to generate pyrophosphate through condensation (Laoutid et al. 2009) or a hydroxyl-containing polymer through phosphorylation (Gaan et al. 2008; Horrocks 1996; Horrocks et al. 2005) to liberate water. The released water vapors then dilute the combustible gas

phase and limit the exothermic reactions. Particularly, phosphorus-based flame retardants are effective for high oxygen-containing polymers (e.g., cellulose, polyester, polyamide, etc.) owing to their high efficiency in conditions where they can react with the polymers to create a P-O covalent bond that usually involves charring of polymeric materials (Levchik 2014; Morgan and Gilman 2013). Organo-phosphorus compounds have been extensively investigated as flame retardants, especially for cellulose-based materials. It has been well-recognized that most phosphorus-based flame retardants act by phosphorylation of cellulose at primary hydroxyls preventing the formation of levoglucosan and subsequent flammable gases by pyrolyzing the cellulose (Levchik 2014). Many of these studies have specified that phosphorus-based flame retardants are principally effective when nitrogen is used in conjunction with phosphorus (Lawler et al. 1985). Moreover, phosphoric acid can favor char formation in the condensed phase by catalyzing the dehydration reaction. A thermally stable carbonaceous char layer separates the condensed phase from the gas phase and subsequently suppresses the release of flammable volatiles as well as air/oxygen diffusion. More specifically, the condensed phase char formation phenomenon in the condensed phase has been scrutinized as an intumescent flame retardant system (G Camino et al. 1989; Vandersall 1971).

Nitrogen-based flame retardants

Nitrogen-based flame retardants exist as an interesting and varied segment of flame retardant additives. Basically, they involve compounds such as melamine and melamine derivatives (Klatt 2014), but other nitrogen-containing compounds such as N-alkoxyamines and azoalkanes also possess alluring flame-retardant effects. During thermal degradation, the melamine-containing flame retardants act in a manner similar to that of a mixture of halogen-based flame retardants and inorganic flame retardants. Melamine is an inexpensive, nitrogen-rich, and thermally stable crystalline organic compound that contains 67 wt.% nitrogen and presents a melting point of ~345 ∘C and sublimating point of ~350 ∘C (Levchik 2007). At high temperatures, non-flammable volatiles (e.g., ammonia) evolve from the decomposition of melamine diluting the combustible gas mixture and leading to the formation of thermally stable condensates (Bann and Miller 1958). Melamine salts also act as condensed-phase flame retardants (Levchik 2007). The advantages of nitrogen-based flame retardants are their low smoke release, low toxicity, and recyclability (Horacek and Grabner 1996). They are often used in combination with other flame retardants such as phosphorus-based flame retardants in order to exploit the phosphorous-nitrogen synergism (Horacek and Grabner 1996).

Silicon-based flame retardants

Silicon-containing compounds (e.g., silicones, silicas, organosilanes, silsesquioxanes, and silicates) have generally been considered co-additives in flame retardant systems (Kilinc 2014). For example, naturally occurring inexpensive silicates are utilized in large quantities as fillers resulting in a reduction in the required amount of flame retardants. Silicon-based flame retardants can also be utilized as the main

polymer matrix and as copolymers (Nodera and Kanai 2006). In particular, silicones can be utilized as flame retardants owing to their remarkably high thermal stability and heat resistance properties (Laoutid et al. 2009). The flame retardant phenomenon for silicon-based flame retardant additives is due to the migration of silicone derivatives toward the surface of the degrading material during combustion to create a thermally stable char layer partially protecting the underlying material (Gaan et al. 2011; Kilinc, 2014). The resultant viscosity of the degrading polymer and the silicon-based flame retardant complex is the main factor in the creation of a protective char layer (Kilinc 2014; Laoutid et al. 2009; Levchik 2007). The combination of organosilicon flame retardants with phosphorus-based flame retardants, through simple blending or designing new compounds containing both silicon and phosphorus elements, is an effective approach for attaining superior flame retardant performances owing to the combined effect of both ceramic and char layers.

Nanoparticles-based flame retardants

Nanocomposites have obtained much attraction as novel alternative developments in the field of polymer flame retardancy owing to their low or non-toxic environmental impact. Nanocomposites characteristically provide many advantages over traditional formulations that often demand a higher loading quantity to attain the desired performance (Kandola 2001). Nanocomposites generally consist of a polymer matrix and nanometer-sized reinforcing elements (e.g., nanoclay, carbon nanotubes, oligosilsesquioxane, silica nanoparticles, etc.) (Laoutid et al. 2009), which can be processed by using different techniques such as extrusion, injection molding, and casting (Beyer and Lan 2014; Kandola 2001).

Nanometric particle size elements when individualized and appropriately dispersed in polymer matrices are recognized to contribute to the improvement of properties such as mechanical, thermal as well as flame/fire retardant. They facilitate a substantial reduction of loading rate owing to a significant increment of the interfacial area between polymers and nano-fillers. More precisely, the involvement of each type of nanoparticle in flame retardant performance differs, and, strictly depends on its chemical structure and geometry. Three widely investigated nanoparticles are as follows (Laoutid et al. 2009):

- *Particulate materials*: such as polyhedral oligosilsesquioxane (POSS) and spherical silica nanoparticles and that are characterized by three nano-metric dimensions and are sometimes referred to as 0D nanoparticles.
- *Fibrous materials*: such as carbon nanotubes and sepiolite that are characterized by elongated structures with two nano-metric dimensions and are referred to as 1D nanoparticles.
- *Layered materials*: such as nanoclays (e.g., montmorillonite (MMT)) that are characterized by one nano-metric dimension and referred to as 2D nanoparticles.

Flame retardant features of nanocomposites can be characterized as condensed phase active. The incorporation of nanoparticles such as organoclay, carbon nanotubes, metal oxides, silica, or polyhedral oligomeric silsesquioxane reduces polymer flammability by several mechanisms such as; limiting fuel transfer to the

flame, formation of a protective char layer, etc. The surface properties of polymeric materials play a vital role in polymer flame retardancy since the surface separates the condensed phase from the gas phase and regulates the combustion cycle by obstructing heat and mass transfer. Therefore, considerable research has been concentrating on tailoring the surface properties of polymeric materials by using nanotechnology in order to induce flame-retardant properties without altering any bulk properties of polymeric materials (Malucelli et al. 2014).

Bio-based flame retardants

Biobased materials generally refer to compounds that can be obtained and/or derived from biomass. Biomass exists on earth in the form of biological matter including plants, animals, and microorganisms. Vassilev et al. presented an overview of the chemical composition of biomass (Vassilev et al. 2010). Their analysis depends on the general organization of biomass in groups, sub-groups, varieties, and species. Thus, four main families of compounds can be distinguished: carbohydrates, proteins, lipids, and phenolic compounds. They were able to pinpoint the most abundant elements which are C, H, N, Ca, K, Si, Mg, Al, S, Fe, P, Cl, Na, Mn, and Ti in decreasing order. It is worth mentioning that some of these elements are also known to have flame-retardant effects.

Up to almost ten years ago, utilization of these biopolymers/biomacromolecules was absolutely allocated for other application fields and have been used as edible films, food emulsifiers, adhesives, papermaking, printing, leather finishing systems, as well as, for the design of biosensors and environmental monitoring systems (Babu et al. 2013; Imam et al. 2013). In very recent years, continuous efforts have been expended by researchers, pursuing and looking for novel cost-effective, and environmentally sustainable flame retardants for textiles based on the use of biomacromolecules due to enhanced awareness of environmental protection.

Very recently, bio-based natural materials (i.e., biopolymers) have attracted considerable attention and exploded interest in the field of flame retardancy because of their low environmental impact and toxicity (Basak and Ali 2016; Costes et al. 2017; Kovačević et al. 2021; Malucelli 2019; Sonnier et al. 2018; Villamil Watson and Schiraldi 2020). Their effectiveness in conferring flame retardancy is quite significant because they usually consist of elements that are recognized to have flame retardant features and, in some cases, are comparable to conventional phosphorus-based flame retardants.

All the biobased flame retardant systems that have been used (e.g., starch, phytic acid, chitosan, alginates, hydrophobins, whey protein, casein, deoxyribonucleic acid, chicken feathers, chicken egg shells, vegetable oils, lignins, tannins, banana pseudostem sap, spinach leaves juice, pomegranate rind extract, coconut shell extract, etc.), report the way renewable resources were used as flame retardants systems (i) as a unique component of the flame retardant system, (ii) in combination with traditional phosphorus or nitrogen flame retardant, (iii) after chemical modification, (iv) after chemical modification and insertion in the polymer chain. It is noteworthy that the improvement of the fire behavior was essentially achieved through one preferential mode of action the so-called charring effect. The effect of charring may be

further enhanced if an expanded layer is formed; this is the so-called intumescence phenomenon. In this case, it is necessary that a gas acting as a blowing agent was released simultaneously with the charring process.

12.7 Flame Retardant Chemicals/Finishes Application to Textile Materials

Meanwhile, in parallel to the development of new flame retardants, processing technology for flame retardancy has evolved significantly and is still being developed. Flame retardants and processing methods have mutually adapted to each other from simple coating treatment in Ancient Egypt to new 3D and 4D printing technologies (Vahabi et al. 2021). The flame retardant treatment of textiles is one of the oldest forms of textile finishing. Traditionally flame retardants are normally applied to textile substrates through padding, coating, spraying, etc., techniques. A number of advanced techniques like plasma deposition, physical and chemical vapor deposition, layer by layer and sol–gel, etc., have also attracted increasing attention for coating applications in the flame retardant domain (Alongi et al. 2014; Malucelli 2016). These flame-retardant techniques generally have some inherent strengths and weaknesses (see tab 12.2), and, research and developments must continue to leverage their strengths and seek to circumvent their weaknesses. These novel coatings may exhibit a complete inorganic or hybrid organic–inorganic composition and all provide microscale or nanoscale protection against flame/fire. Durability properties, specifically to laundering/washing, remain a challenge for almost all types of flame-retardant surface treatments (Cheng et al. 2018; Feng et al. 2017; Giraud et al. 2005; Haile et al. 2016; Horrocks et al. 2011). Most of these surface treatments vanish or substantially diminish after fewer or fifty washing cycles. In many cases, washing fastness was improved through chemical crosslinking, but a large number of crosslinking treatments depend on hydrolytically unstable functional groups (such as esters, amides, or phosphonate esters), which are intended to deteriorate on subjecting to alkaline conditions experienced during laundering with washing detergents in laundering machine.

Back coating

Back-coating is one of the earliest surface treatments for flame retardancy of textile substrates. Back coatings were developed to fight flame/fire from behind the substrate rather than evolving new surface treatments that could not change aesthetic aspects such as appearance, texture, hand feel, etc. of fabrics. Back-coating formulations have involved some form of active ingredients that are employed on the unused side of textile substrates (e.g., the inner side of furniture upholstery) preventing the outer side maximally unchanged in aesthetic properties (Dombrowski 1996). These coatings typically include an active flame-retardant ingredient thoroughly dispersed within a resin. From the heat of flame/fire, the resin melts and ensures good contact

Table 12.2 Strengths and weaknesses of various flame-retardant surface treatments (Lazar et al. 2020)

Trearments	Strengths	Weaknesses
Covalent surface modification	Large variety of possible chemistries; can be applied to any substrate; can be implemented in commercial coating equipment (for textiles)	Energy-intensive or time intensive curing; often use organic solvents; poor wash durability (regardless of crosslinking)
Plasma-aided surface modification	Very effective with the addition of a low weight of flame retardant; scalable and solvent-free; can be wash durable	Limited choice of components; substrate damage is possible during treatment
Sol–gel treatments	Few processing steps; wash durable; substrate maintains desirable hand	Thermal treatment necessary; limited number of commercially available precursors
Layer-by-layer assembly	Large number of ingredient combinations (many naturally sourced and/or biodegradable); works on a variety of substrates; ambient processing	High number of processing steps; large volumes of solution required; poor wash durability
Polyelectrolyte complexes	Few processing steps; ambient processing	Limited choice of components (pKa dependent); wash durability unproven

between the active flame retardant component and the invading flame. Although, back-coating is no longer a specifically active research area it still procures extensive commercial applications due to the diversity of compliant chemistries. The earliest used back coatings were based on halogenated compounds, with antimony-halogen-based systems being the most common. This flame-retardant system was deliberated as particularly problematic because it was composed of pairing a toxic heavy metal with a toxic organic compound (Dombrowski 1996; Wang et al. 2000). Later onward 2000, the viability of implementing phosphorus-based chemistries for back coatings was thoroughly investigated (Horrocks et al. 2000, 2007; Wesolek and Gieparda 2014).

Covalent surface modification

Covalent attachment of flame retardant chemicals/finishes to textile substrates has an old long history regarding flame retardant surface treatments, which is confined to two kinds of surface modification through the covalent bond formation. In the first instance, polymerization is prompted after the impregnation of a substrate with flame retardant monomer(s) or oligomer(s) that directs to the creation of a polymer coating around the substrate. In the second case, pendant flame retardant groups or entire polymers are covalently bound to available and accessible functional groups of substrate. The first large-scale implementation of the former approach was experienced several decades ago through the application of a pad-dry-cure method to

polymerize a mixture of tetrakis(hydroxymethyl) phosphonium chloride (THPC) and amines on cotton fabrics (Cashen and Reinhardt 1976; Reeves and Guthrie 1956).

Impregnation approaches that are not based on THPC are usually attributed as flame retardant finishes, which implicate the polymerization of either small or large molecules around the substrate typically through phosphorus-containing oligomers or polymers (Charles and Wu 2003; Liu et al. 2012; Wu and Yang 2006; Yang and Wu 2003; Yang and Yang 2008; Yuan et al. 2012). These systems are often crosslinked which induces washing resistance/durability to the finish without impairing the flame retardant performance. The systems that involve crosslinking chemistry characteristically start with a hydroxyl-functional organophosphorus oligomer (HFPO) (Charles and Wu 2003), and HFPO can then be crosslinked with nitrogen-rich molecules containing methylol groups such as trimethylolmelamine or dimethyloldihydroxyethyleneurea through condensation reactions. Integration of these nitrogen-containing moieties also facilitates a synergistic effect for the phosphorous groups of HFPO, as well as, carries out crosslinking network process and confers washing resistance (Wu and Yang 2006; Yang and Chen 2019). The range of HFPO derivatives investigated as flame retardant coatings has since immensely expanded. More precisely, the co-monomers and substrates can be differed thus designating HFPO-based coatings as a versatile technique that can be easily applied through commercial scale pad-dry-cure method (Wu and Yang 2006; Yang and Chen 2019; Yang and Yang 2008).

Flame retardant finishes can also be added to substrates (usually fabrics) by fixing small or large molecules to the available and accessible functional groups of the substrate through covalent functionalization. In the case of smaller molecules, research works have been conducted to attach high phosphorus content moieties (normally in the form of phosphonic acid groups to free hydroxyl groups of cellulose in fabric substrate. This unification of phosphorus-containing compounds to cellulose in the fabric is assisted by dicyandiamide (also known as cyanoguanidine) that helps to condense the P–OH group of the phosphonic acid with the hydroxyl group of cellulose yielding a cellulose–O–P bond and removing water (Blanchard and Graves 2003; Feng et al. 2017; F. Xu et al. 2019).

The impregnation of textile substrates with small molecules or large polymers embraces the high potential for the field of flame retardancy. Particularly, many of these impregnations and surface functionalizations have good washing durability that is critically significant for practical use. These covalent strategies are supported by compliance of pad-dry-cure processing in their application. Future work regarding this field is to develop an aptitude toward UV-aided promotion of polymerization to optimally minimize the necessity of energy-intensive thermal-curing methods (Kim and Jang 2017; Xu et al. 2017; Yuan et al. 2012). Furthermore, a largely uncharted area of work in this field is the utilization of surface-initiated polymerization of the flame retardant component onto fabrics (Wang et al. 2016). Impregnations and surface functionalization is an effervescent field of flame retardant research owing to these several opportunities for improvement.

Plasma-aided surface modification

Plasma is a gaseous media consisting of electrons, ions, and neutral moieties in both ground and excited states, which has attracted considerable attention in recent years as it has become more achievable at ambient conditions (Tendero et al. 2006). So-called atmospheric-plasma has gathered much interest because its use is attainable both economically and industrially as it needs no vacuum. Moreover, plasma treatments often avoid energy-intensive thermal curing necessary either to track reactions to completion or to remove solvent after impregnation-based treatments. Plasma induces flame-retardant properties in substrates owing to generated ions and radicals. These radicals instigate reactions at the surface either to introduce new functionality or to instigate the polymerization of monomers that are put in contact with the plasma-treated substrate. The ionization of the substrate also facilitates better adhesion with charged polymers and nanoparticles. Unlike other surface treatments, surface modification of substrates by using plasma techniques is attained in the vapor phase rather than that in the liquid phase.

Plasma-aided surface modifications were first experienced in 1990 for flame retardant properties (Akovali and Gundogan 1990). In this study, polymers of hexamethyldisiloxane (HMDSO) and two different phosphate-based monomers were polymerized on the surface of polyacrylonitrile fibers and their properties were compared. This treatment only moderately enhanced the flame-retardant properties of fibers but it was an important step for the development of this class of surface treatments. In a subsequent study, plasma was used to polymerize a siloxane on the surface of polyamide-6 (Bourbigot et al. 1999a, b). The peak HRR was decreased but the treatment caused the treated substrate to ignite earlier as compared to that of an untreated substrate. It was also observed that the argon ions and radicals leading to surface functionalization and polymerization can also cause damage to the substrate resulting in easier degradation. Currently, a number of plasma-based treatments for flame retardant coatings have been studied (Carosio et al. 2011; Horrocks et al. 2011, 2018). The commercialization of plasma-aided treatments has been achieved by integrating additional energy sources into plasma-treatment techniques enabling the modification and formation of covalent bonds. For example, multiplexed laser surface enhancement (MLSE) systems have become available that contain a UV laser capable of breaking covalent bonds (such as C–C bonds, C–N bonds, etc.) common in textile fibers. The scale-up of MLSE techniques has been attained for the industrial production of fabrics with other functional finishing (e.g., hydrophobicity, antimicrobial) or to improve dye uptake. These MLSE techniques can also apply flame retardant finishes to fabrics in absence of liquid-processing steps (Horrocks et al. 2018). This result signifies a major advancement in prevalent use of plasma-aided surface treatments for flame retardant coatings and proposes that this will continue to be a rich-field of research for some time.

Sol–gel treatment

Although sol–gel treatment has been a well-known approach to induce functional properties in textile substrates since the 1950s, it has recently been exploited for

flame retardancy (Alongi and Malucelli 2012). This two-step chemical process depends on silicon-based chemistry and comprises the hydrolysis/condensation of alkoxide precursors in water to generate a colloidal dispersion of particles, usually known as sol (Hench and West 1990). The most commonly used precursors include tetraethyl orthosilicate, tetramethyl orthosilicate, (3-aminopropyl)triethoxysilane, and 3-glycidoxypropyltriethoxysilane. The sol converts to gel-like moiety upon enough agitation through condensation reactions. The substrate is then immersed into the sol–gel and after thermal treatment, it provides a ceramic coating on the substrate surface. The thermal barrier developed by these inorganic networks inhibits the substrate from contributing to the combustion/bunring. Sol–gel coatings can be tailored by adjusting the pH, precursor ratio, curing time and temperature, and the use of various co-solvents (Esposito 2019). Among conditions used for gelation, most employ a mixed solvent of water and ethanol under acidic conditions to catalyze hydrolysis, with the most significant differences originating from different precursors used to produce the sols.

The first reported sol–gel coating with flame retardant performance was developed using tetraethyl orthosilicate precursors on regenerated cellulose fibers (Hribernik et al. 2007), Pretreatment of the fibers in base, prior to depositing the silica coating, highly improved coating adhesion and increased its thermal-oxidative stability as compared to the fibers that were not base pretreated. In a later study, the influence of tetraethyl orthosilicate and water ratios on the fabrication of flame retardant coatings for cotton, polyester, and their blends was examined (Alongi et al. 2011). Regardless of tetraethyl orthosilicate and water ratios used, the fabricated sol–gel coatings were unable to improve the flame retardancy of polyester but were fruitful in increasing the time to ignition (98%) and reducing the peak heat release rate (34%) of a cotton-polyester blend containing 65% polyester. At present several studies as sol–gel treatments for flame retardant coatings have been explored under different formulations of sol-gels as conventional sols (Alongi et al. 2012a, b), sol–gel dopants (Brancatelli et al. 2011; Grancaric et al. 2017), hybrid precursors (Bentis et al. 2019; Vasiljević et al. 2013).

Layer-by-layer assembly

The most dynamic area of the field of flame retardancy research is formulations of flame retardant coatings via layer-by-layer assembly. Unlike sol–gel, layer-by-layer assembly principally depends on electrostatic interactions between polyelectrolytes and/or charged nanoparticles and is approachable to a variety of acceptor/donor interactions (Decher and Hong 1991). The sequential process primarily encompasses alternate immersion of a charged substrate (e.g., through the corona, plasma, and/or chemical treatment) in aqueous solutions comprising components necessary for enhancing flame retardancy. This process can be modified to involve three-component trilayers or four-component quadlayers of flame-retardant moieties. The thickness of the coating typically ranges from 100 nm to 1 μm and can also be adjusted using aqueous solutions of varying pH and/or ionic strength. Although an unlimited combination of chemistries subsists for layer-by-layer assembly, which already employed to construct multilayer fire-protective coatings, can be classified by the

distinct flame retardant mechanisms, i.e., passive barriers (Carosio et al. 2018; Laufer et al. 2012), (Jimenez et al. 2016; Pan et al. 2015), or combination of passive barrier and intumescent (Liu et al. 2018; Yan et al. 2017).

Polyelectrolyte complexes

A drawback of layer-by-layer assembly is the number of processing steps essential to deposit a flame retardant coating, which researchers are attempting to overcome through polyelectrolyte complexes. On the other hand, polyelectrolyte-complex coatings have taken advantage of the ability to be deposited quickly (Cheng et al. 2019; Haile et al. 2016). An important future course for polyelectrolyte complex coatings is the incorporation of clay or other nanoparticles (Carosio and Alongi 2018). This progression will hopefully enable the development of more particle-containing polyelectrolyte complex systems.

12.8 Environmental Impact of Flame Retardant Chemicals and Finishes

Chemical finishing has always been an essential part of textile processing that requires complete knowledge and consideration of several important factors (Schindler and Hauser 2004; Whewell 1970). During the last few decades, apart from the inevitable pressure of all these factors, knowledge about the toxicity and environmental impact of chemicals has been growing rapidly and people have become more conscious of potential hazards associated with them (Bajaj 2002; Chen and Burns 2006; Oulton 1995). Nowadays, the major and most important highlighted issue and challenge throughout the textile and/or chemical finishing industry is the ever-increasing influence of environmental and ecological factors and in general associated present concerns leveled at the use of flame retardants (Holme 1994; Horrocks et al. 1997; Roberts et al. 1992; Samani and van der Meer 2020; Segev et al. 2009; Šehić et al. 2016). The flame retardancy future is obstructed significantly by the eco-toxicological and environmental considerations, the flame retardants used, and the toxic nature of products released on combustion of textiles.

At present, a major part of commercially available potent flame retardants is petrochemical-based organic compounds (e.g., organo-halogenated, organo-phosphorous, organo-nitrogen compounds). Phosphorus-based flame retardant counterparts seem real as a suitable, potential, and efficient alternative to halogen-based compounds for different types of fibers/fabrics (Lu and Hamerton 2002). Though, it is not overall a general case that all phosphorus-based flame retardants are nontoxic, as the development of new flame retardants based on phosphorus compounds has revealed that they have lower toxicity profiles as compared to halogen-based counterparts (Du et al. 2019; Xu et al. 2018). However, considering the pros and cons, and according to very strict proclamations/directives concerning the chemistry of flame retardants used, a large number of flame retardant compounds including some of the

currently used halogenated and phosphorous-based compounds received a bad press. They have been limited, are no longer produced, and have been removed from the market or even banned. They are on special lists of national and/or international environmental concerns committees, as they are suspected to stimulate specific health and environmental issues. Because they release toxic products (furans, dioxins, ammonia, formaldehyde, other volatile organic compounds, etc.) during; manufacturing, application to textiles, upon combustion of textiles, etc. (Horrocks 2003). They also have certainly divulged high toxicity for both animals and humans as they do not easily break down, can build up in animals and humans over time (bioaccumulation), and can remain persistent in the environment for years (Segev et al. 2009).

Environmental benefits require terms/labels such as; green, sustainable, environmentally responsible, environmentally friendly, eco-safe, and recyclable materials and have often been used to describe, advertise, and promote materials/products that are supposedly and/or evidently considered to have nominal negative environmental impacts (Chen and Burns 2006). However, there are many concerns about the use of flame retardants in all kinds of textiles. Exposures (namely pathways exposure and route exposure) may occur at numerous points in the whole life-cycle of a flame retardant typified by; occupational exposure (during manufacturing/industrial operations), consumer exposure (during end use), and public and environment exposure to releases (during product disposal or from manufacturing/industrial facilities). Any type of products that humans can be exposed to either by direct contact, dermal adsorption, inhalation, or oral ingestion and through a breakdown in the environment as well as ingestion by animals is of concern (Wakelyn 2008). In general, ideal flame retardant chemicals and finishes should not be persistent, bioaccumulative, and/or toxic to humans, animals, and/or ecosystems. They should not cause adverse health effects to ultimate consumers and/or adversely affect the overall environment such as air, water, soil, etc. (Holme 1994; Wakelyn 2008). Therefore, it stimulated both the academic and industrial scientific communities to endow continuous efforts toward research and development in order to find out worthy alternatives and counterparts to traditional flame retardants. In the last few years, extensive consideration and attention have been concentrated on biomass-based (bio-based, i.e., biopolymers; biomacromolecules) natural products due to their renewable resources and environmental friendliness (Frenzel et al. 2014; Sheldon 2014; Tuck et al. 2012; Tursi 2019).

12.9 Assessment of Flame Retardancy of Textiles

There are a number of tests that facilitate the assessment of flammability behavior and/ or fire performance behavior as a function of heat release, ignitability, flame spread, toxicity/corrosivity, smoke production, and fire resistance (Kundu et al. 2020). These tests can be categorized by sector of activity such as aviation, railway, cables, etc., by industry standards such as EN, ISO, ASTM, etc., or simply by the scale of measurement such as small-, bench-, and large-scale tests. Some of these tests are limiting

oxygen index, UL-94, cone calorimetry, pyrolysis combustion flow calorimetry, single-flame source, single-burning item, panel tests, flame-spread tests (Sonnier et al. 2012; Troitzsch and Antonatus 2021). Some other characterization techniques are specially used to explicate the mechanism of action of flame retardants in the gas and/or condensed phase. Additionally, the characterization of mineral residue, char, and intumescent char are also beneficial, but quite often challenging due to their complex physical and chemical structures. Furthermore, their homogeneity and the choice of zone analyzed (top, middle, or bottom of remaining residue,) can be crucial.

12.9.1 Conclusions and Future Viewpoints

All textile materials including fibers, yarns, fabrics, and blends have been extensively used in our day-to-day life and are enriched with several valuable properties. However, these materials abundantly possess low flame retardancy and require further additional chemical processing toward inducing flame retardancy. Flame retardancy of textile polymeric materials is a subject of major concern due to the need to minimize fire risk and meet fire safety requirements. Nevertheless, most flame retardants have been observed to have bad impacts/effects on organisms, human beings, and the environment. With existing flame retardant materials, various new substituted technologies, finishing agents, and active materials are being developed to encounter the needs and challenges of continually changing safety regulations. It is an interdisciplinary development that comprises quite a lot of scientific and engineering tools. Novel technologies and innovative products are being under consideration to bottom down the present challenges and issues. This would help to make cleaner substitutes for sincerely unsafe and/or harmful traditionally used conventional flame retardant finishing agents and to explore new opportunities in the field of flame retadancy research and development sector as well as in the textile industry.

References

Akovali G, Gundogan G (1990) Studies on flame retardancy of polyacrylonitrile fiber treated by flame-retardant monomers in cold plasma. J Appl Polym Sci 41(9–10):2011–2019

Alongi J, Carosio F, Malucelli G (2014) Current emerging techniques to impart flame retardancy to fabrics: an overview. Polym Degrad Stab 106:138–149. https://doi.org/10.1016/j.polymdegradstab.2013.07.012

Alongi J, Ciobanu M, Malucelli G (2012a) Sol–gel treatments on cotton fabrics for improving thermal and flame stability: effect of the structure of the alkoxysilane precursor. Carbohydr Polym 87(1):627–635. https://doi.org/10.1016/j.carbpol.2011.08.036

Alongi J, Ciobanu M, Malucelli G (2012b) Thermal stability, flame retardancy and mechanical properties of cotton fabrics treated with inorganic coatings synthesized through sol–gel processes. Carbohydr Polym 87(3):2093–2099. https://doi.org/10.1016/j.carbpol.2011.10.032

Alongi J, Ciobanu M, Tata J, Carosio F, Malucelli G (2011) Thermal stability and flame retardancy of polyester, cotton, and relative blend textile fabrics subjected to sol–gel treatments. J Appl Polym Sci 119(4):1961–1969. https://doi.org/10.1002/app.32954

Alongi J, Han Z, Bourbigot S (2015) Intumescence: tradition versus novelty. A comprehensive review. Prog Polym Sci 51:28–73. https://doi.org/10.1016/j.progpolymsci.2015.04.010

Alongi J, Malucelli G (2012) State of the art and perspectives on sol–gel derived hybrid architectures for flame retardancy of textiles. J Mater Chem 22(41):21805–21809. https://doi.org/10.1039/C2JM32513F

Alongi J, Malucelli G (2015) Cotton flame retardancy: state of the art and future perspectives. RSC Adv 5(31):24239–24263. https://doi.org/10.1039/C5RA01176K

American Society for Testing and Materials (2021) Standard terminology of fire standards, ASTM E176 - 21a. ASTM International Standards

Babu RP, O'connor K, Seeram R (2013) Current progress on bio-based polymers and their future trends. Prog Biomater 2(1):1–16

Bajaj P (2002) Finishing of textile materials. J Appl Polym Sci 83(3):631–659. https://doi.org/10.1002/app.2262

Bann B, Miller SA (1958) Melamine and derivatives of melamine. Chem Rev 58(1):131–172. https://doi.org/10.1021/cr50019a004

Barker RL, Brewster EP (1982) Evaluating the flammability and thermal shrinkage of some protective fabrics. J Ind Fabr 1:7–17

Basak S, Ali SW (2016) Sustainable fire retardancy of textiles using bio-macromolecules. Polym Degrad Stab 133:47–64. https://doi.org/10.1016/j.polymdegradstab.2016.07.019

Bentis A, Boukhriss A, Grancaric AM, El Bouchti M, El Achaby M, Gmouh S (2019) Flammability and combustion behavior of cotton fabrics treated by the sol gel method using ionic liquids combined with different anions. Cellulose 26:2139–2153

Beyer G, Lan T (2014) Polymer nanocomposites: a nearly universal FR synergist. In: Morgan AB (ed) Non-halogenated flame retardant handbook. Wiley Online Library, pp 243–292. https://doi.org/10.1002/9781118939239.ch7

Beyler CL, Hirschler MM (2002) Thermal decomposition of polymers. In: SFPE handbook of fire protection engineering, vol 2. National Fire Protection Association Quincy, MA, pp 110–131

Blanchard EJ, Graves EE (2003) Phosphorylation of cellulose with some phosphonic acid derivatives. Text Res J 73(1):22–26

Bourbigot S (2008) Flame retardancy of textiles: new approaches. In Horrocks AR, Price D (eds) Advances in fire retardant materials. Woodhead Publishing and CRC Press, pp 9–40. https://doi.org/10.1533/9781845694701.1.9

Bourbigot S (2021) Intumescence-based flame retardant. In: Morgan AB (ed) Non-halogenated flame retardant handbook. Wiley, pp 169–238

Bourbigot S, Duquesne S (2007) Fire retardant polymers: recent developments and opportunities. J Mater Chem 17(22):2283–2300

Bourbigot S, Jama C, Le Bras M, Delobel R, Dessaux O, Goudmand P (1999b) New approach to flame retardancy using plasma assisted surface polymerisation techniques. Polym Degrad Stab 66(1):153–155

Bourbigot S, Le Bras M, Leeuwendal R, Shen KK, Schubert D (1999a) Recent advances in the use of zinc borates in flame retardancy of EVA. Polym Degrad Stab 64(3):419–425. https://doi.org/10.1016/S0141-3910(98)00130-X

Bourbigot S, Le Bras M, Duquesne S, Rochery M (2004) Recent advances for intumescent polymers. Macromol Mater Eng 289(6):499–511. https://doi.org/10.1002/mame.200400007

Brancatelli G, Colleoni C, Massafra MR, Rosace G (2011) Effect of hybrid phosphorus-doped silica thin films produced by sol-gel method on the thermal behavior of cotton fabrics. Polym Degrad Stab 96(4):483–490. https://doi.org/10.1016/j.polymdegradstab.2011.01.013

Calamari TA, Harper RJ (2000) Flame retardants for textiles. Kirk-Othmer Encyclopedia of Chemical Technology

Camino G (1998) Flame retardants: intumescent systems. In: Pritchard G (ed) Plastics additives. Springer Nature, pp 297–306. https://doi.org/10.1007/978-94-011-5862-6_33

Camino G, Costa L (1986) Mechanism of intumescence in fire retardant polymers. Rev Inorg Chem 8(1–2):69–100

Camino G, Costa L (1988) Performance and mechanisms of fire retardants in polymers-a review. Polym Degrad Stab 20(3–4):271–294

Camino G, Costa L, Casorati E, Bertelli G, Locatelli R (1988) The oxygen index method in fire retardance studies of polymeric materials. J Appl Polym Sci 35(7):1863–1876

Camino G, Costa L, Luda di Cortemiglia MP (1991) Overview of fire retardant mechanisms. Polymer Degrad Stab 33(2):131–154. https://doi.org/10.1016/0141-3910(91)90014-I

Camino G, Costa L, Martinasso G (1989) Intumescent fire-retardant systems. Polym Degrad Stab 23(4):359–376. https://doi.org/10.1016/0141-3910(89)90058-X

Camino G, Costa L, Trossarelli L (1984a) Study of the mechanism of intumescence in fire retardant polymers: part I-thermal degradation of ammonium polyphosphate-pentaerythritol mixtures. Polym Degrad Stab 6(4):243–252. https://doi.org/10.1016/0141-3910(84)90004-1

Camino G, Costa L, Trossarelli L (1985a) Study of the mechanism of intumescence in fire retardant polymers: part V-mechanism of formation of gaseous products in the thermal degradation of ammonium polyphosphate. Polym Degrad Stab 12(3):203–211. https://doi.org/10.1016/0141-3910(85)90089-8

Camino G, Costa L, Trossarelli L, Costanzi F, Landoni G (1984b) Study of the mechanism of intumescence in fire retardant polymers: part IV-evidence of ester formation in ammonium polyphosphate-pentaerythritol mixtures. Polym Degrad Stab 8(1):13–22

Camino G, Costa L, Trossarelli L (1984c) Study of the mechanism of intumescence in fire retardant polymers: part II-mechanism of action in polypropylene-ammonium polyphosphate-pentaerythritol mixtures. Polym Degrad Stab 7(1):25–31

Camino G, Costa L, Trossarelli L (1984d) Study of the mechanism of intumescence in fire retardant polymers: part III-effect of urea on the ammonium polyphosphate-pentaerythritol system. Polym Degrad Stab 7(4):221–229

Camino G, Costa L, Trossarelli L, Costanzi F, Pagliari A (1985b) Study of the mechanism of intumescence in fire retardant polymers: Part VI-Mechanism of ester formation in ammonium polyphosphate-pentaerythritol mixtures. Polym Degrad Stab 12(3):213–228

Camino G, Martinasso G, Costa L (1990) Thermal degradation of pentaerythritol diphosphate, model compound for fire retardant intumescent systems: part I-overall thermal degradation. Polym Degrad Stab 27(3):285–296

Carosio F, Ghanadpour M, Alongi J, Wågberg L (2018) Layer-by-layer-assembled chitosan/phosphorylated cellulose nanofibrils as a bio-based and flame protecting nano-exoskeleton on PU foams. Carbohyd Polym 202:479–487

Carosio F, Alongi J (2018) Flame retardant multilayered coatings on acrylic fabrics prepared by one-step deposition of chitosan/montmorillonite complexes. Fibers 6(2):36

Carosio F, Alongi J, Frache A (2011) Influence of surface activation by plasma and nanoparticle adsorption on the morphology, thermal stability and combustion behavior of PET fabrics. Eur Polymer J 47(5):893–902

Cashen NA, Reinhardt RM (1976) Flame-retardant coating based on THPOH-dimethylolurea-NH3 for cellulosic and cellulosic-blend fabrics. Text Res J 46(12):899–903

Charles QY, Wu WD (2003) Combination of a hydroxyfunctional organophosphorus oligomer and a mulfunctional carboxylic acid as a flame retardant finishing system for cotton: part I. The chemical reactions. Fire Mater 27(5):223–237

Chen HL, Burns LD (2006) Environmental analysis of textile products. Cloth Text Res J 24(3):248–261. https://doi.org/10.1177/0887302X06293065

Cheng X-W, Guan J-P, Yang X-H, Tang R-C, Yao F (2019) A bio-resourced phytic acid/chitosan polyelectrolyte complex for the flame retardant treatment of wool fabric. J Clean Prod 223:342–349

Cheng X-W, Liang C-X, Guan J-P, Yang X-H, Tang R-C (2018) Flame retardant and hydrophobic properties of novel sol-gel derived phytic acid/silica hybrid organic-inorganic coatings for silk fabric. Appl Surf Sci 427:69–80

Costes L, Laoutid F, Brohez S, Dubois P (2017) Bio-based flame retardants: when nature meets fire protection. Mater Sci Eng: R: Reports 117:1–25. https://doi.org/10.1016/j.mser.2017.04.001

Darnerud PO (2003) Toxic effects of brominated flame retardants in man and in wildlife. Environ Int 29(6):841–853. https://doi.org/10.1016/S0160-4120(03)00107-7

Decher G, Hong JD (1991) Buildup of ultrathin multilayer films by a self-assembly process: II. Consecutive adsorption of anionic and cationic bipolar amphiphiles and polyelectrolytes on charged surfaces. Berichte Der Bunsengesellschaft Für Physikalische Chemie 95(11):1430–1434

Delobel R, Bras ML, Ouassou N, Alistiqsa F (1990) Thermal behaviours of ammonium polyphosphate-pentaerythritol and ammonium pyrophosphate-pentaerythritol intumescent additives in polypropylene formulations. J Fire Sci 8(2):85–108

Dombrowski R (1996) Flame retardants for textile coatings. J Coat Fabr 25(3):224–238

Du J, Li H, Xu S, Zhou Q, Jin M, Tang J (2019) A review of organophosphorus flame retardants (OPFRs): occurrence, bioaccumulation, toxicity, and organism exposure. Environ Sci Pollut Res 26(22):22126–22136

Ellard JA (1973) Performance of intumescent fire barriers. In: Abstracts of papers of the American chemical society, division of organic coatings and plastics chemistry, ACS 165th meeting. Dallas, Texas, USA, pp 531–545

Esposito S (2019) "Traditional" sol-gel chemistry as a powerful tool for the preparation of supported metal and metal oxide catalysts. Materials 12(4):668

Feng Y, Zhou Y, Li D, He S, Zhang F, Zhang G (2017) A plant-based reactive ammonium phytate for use as a flame-retardant for cotton fabric. Carbohyd Polym 175:636–644. https://doi.org/10.1016/j.carbpol.2017.06.129

Fenimore CP (1975) Candle-type test for flammability of polymers. In: Flame-retardant polymeric materials. Springer, pp 371–397

Fenimore CP, Martin FJ (1966) Flammability of polymers. Combust Flame 10(2):135–139

Frenzel P, Hillerbrand R, Pfennig A (2014) Increase in energy and land use by a bio-based chemical industry. Chem Eng Res Des 92(10):2006–2015. https://doi.org/10.1016/j.cherd.2013.12.024

Gaan S, Salimova V, Rupper P, Ritter A, Schmid H (2011) Flame retardant functional textiles. In: Pan N, Sun G (eds) Functional textiles for improved performance, protection and health. Woodhead Publishing, pp 98–130. https://doi.org/10.1533/9780857092878.98

Gaan S, Sun G, Hutches K, Engelhard MH (2008) Effect of nitrogen additives on flame retardant action of tributyl phosphate: phosphorus–nitrogen synergism. Polym Degrad Stab 93(1):99–108. https://doi.org/10.1016/j.polymdegradstab.2007.10.013

Georlette P (2001) Applications of halogen flame retardants. In: Horrocks AR, Price D (eds) Fire retardant materials. Woodhead Publishing, pp 264–292

Giraud S, Bourbigot S, Rochery M, Vroman I, Tighzert L, Delobel R, Poutch F (2005) Flame retarded polyurea with microencapsulated ammonium phosphate for textile coating. Polym Degrad Stab 88(1):106–113

Gordon PG (1981) Flame retardants and textile materials. Fire Saf J 4(2):109–123

Grancaric AM, Colleoni C, Guido E, Botteri L, Rosace G (2017) Thermal behaviour and flame retardancy of monoethanolamine-doped sol-gel coatings of cotton fabric. Prog Org Coat 103:174–181

Grayson M (1997) Encyclopedia of textiles fibers and nonwoven fabrics, 1st edn. Wiley Interscience

Green J (1996) Mechanisms for flame retardancy and smoke suppression-a review. J Fire Sci 14(6):426–442. https://doi.org/10.1177/073490419601400602

Grishanov S (2011) Structure and properties of textile materials. In: Clark M (ed) Handbook of textile and industrial dyeing; principles, processes and types of dyes, vol 1. Woodhead Publishing, pp 28–63. https://doi.org/10.1533/9780857093974.1.28

Guan Y, Zheng BJ, He YQ, Liu XL, Zhuang ZX, Cheung CL, Luo SW, Li PH, Zhang LJ, Guan YJ, Butt KM, Wong KL, Chan KW, Lim W, Shortridge KF, Yuen KY, Peiris JSM, Poon LLM (2003) Isolation and characterization of viruses related to the SARS coronavirus from animals in southern China. Science 302(5643):276–278

Haile M, Leistner M, Sarwar O, Toler CM, Henderson R, Grunlan JC (2016) A wash-durable poly-electrolyte complex that extinguishes flames on polyester–cotton fabric. RSC Adv 6(40):33998–34004

Hao J, Chow WK (2003) A brief review of intumescent fire retardant coatings. Archit Sci Rev 46(1):89–95

Heinrich T, Carl C, Paul K, Walter S (1938) Fireproofing of wood. U.S. Patent 2,106,938

Hench LL, West JK (1990) The sol-gel process. Chem Rev 90(1):33–72

Hendrix JE, Drake GL, Reeves WA (1972) Effects of fabric weight and construction on OI values for cotton cellulose. J Fire Flamm 3:38–45

Hirschler M (2014) Flame retardants: background and effectiveness. In: Fire protection engineering magazine, 3rd Quarter, pp 32–42

Hirschler MM (1982) Recent developments in flame-retardant mechanisms. In: Gerald S (ed) Developments in polymer stabilisation, vol 5. Elsevier and Applied Science Publishers, pp 107–152

Hirschler MM (2000) Chemical aspects of thermal decomposition of polymeric materials. In: Grand AF, Wilkie CA (eds) Fire retardancy of polymeric materials. Marcel Dekker Inc., pp 27–79

Holme I (1994) Flammability—the environment and the green movement. J Soc Dyers Colour 110(11):362–366. https://doi.org/10.1111/j.1478-4408.1994.tb01598.x

Horacek H, Grabner R (1996) Advantages of flame retardants based on nitrogen compounds. Polym Degrad Stab 54(2–3):205–215. https://doi.org/10.1016/S0141-3910(96)00045-6

Hornsby PR (2001) Fire retardant fillers for polymers. Int Mater Rev 46(4):199–210. https://doi.org/10.1179/095066001771048763

Hornsby PR, Rothon RN (2005) Fire retardant fillers for polymers. In: Le Bras M, Wilkie CA, Bourbigot S, Duquesne S, Jama C (eds) Fire retardancy of polymers: new applications of mineral fillers. The Royal Society of Chemistry, pp 19–41

Horrocks AR (1996) Developments in flame retardants for heat and fire resistant textiles-the role of char formation and intumescence. Polym Degrad Stab 54(2–3):143–154. https://doi.org/10.1016/S0141-3910(96)00038-9

Horrocks AR (1983) An introduction to the burning behaviour of cellulosic fibres. J Soc Dyers Colour 99(7–8):191–197. https://doi.org/10.1111/j.1478-4408.1983.tb03686.x

Horrocks AR (1986) Flame-retardant finishing of textiles. Rev Prog Color Relat Top 16(1):62–101. https://doi.org/10.1111/j.1478-4408.1986.tb03745.x

Horrocks AR (2001) Textiles. In: Horrocks AR, Price D (eds) Fire retardant materials Woodhead Publishing and CRC Press LLC, pp 128–181

Horrocks AR (2003) Flame-retardant finishes and finishing. In: Heywood D (ed) Textile finishing. Society of Dyers and Colourists, pp 214–250

Horrocks AR (2011) Flame retardant challenges for textiles and fibres: new chemistry versus innovatory solutions. Polym Degrad Stab 96(3):377–392. https://doi.org/10.1016/j.polymdegradstab.2010.03.036

Horrocks AR, Alongi J (2013) Fundamental aspects of flame retardancy. In: Alongi J, Horrocks AR, Carosio F, Malucelli G (eds) Update on flame retardant textiles: state of the art, environmental issues and innovative solutions. Smithes Rapra, pp 19–52

Horrocks AR, Anand SC, Sanderson D (1996) Complex char formation in flame retarded fibre-intumescent combinations: 1. Scanning electron microscopic studies. Polymer 37(15):3197–3206

Horrocks AR, Davies PJ, Kandola BK, Alderson A (2007) The potential for volatile phosphorus-containing flame retardants in textile back-coatings. J Fire Sci 25(6):523–540

Horrocks AR, Eivazi S, Ayesh M, Kandola B (2018) Environmentally sustainable flame retardant surface treatments for textiles: the potential of a novel atmospheric plasma/UV laser technology. Fibers 6(2):31

Horrocks AR, Hall ME, Roberts D (1997) Environmental consequences of using flame-retardant textiles—a simple life cycle analytical model. Fire Mater 21(5):229–234. https://doi.org/10.1002/(SICI)1099-1018(199709/10)21:5%3c229::AID-FAM614%3e3.0.CO;2-U

Horrocks AR, Kandola BK, Davies PJ, Zhang S, Padbury SA (2005) Developments in flame retardant textiles—a review. Polym Degrad Stab 88(1):3–12. https://doi.org/10.1016/j.polymdegradstab.2003.10.024

Horrocks AR, Nazaré S, Masood R, Kandola B, Price D (2011) Surface modification of fabrics for improved flash-fire resistance using atmospheric pressure plasma in the presence of a functionalized clay and polysiloxane. Polym Adv Technol 22(1):22–29

Horrocks AR, Price D (eds) (2001) Fire retardant materials. Woodhead Publishing and CRC Press

Horrocks AR, Tune M, Cegielka L (1988) The burning behaviour of textiles and its assessment by oxygen-index methods. Text Prog 18(1–3):1–186. https://doi.org/10.1080/00405168908689004

Horrocks AR, Wang MY, Hall ME, Sunmonu F, Pearson JS (2000) Flame retardant textile back-coatings. Part 2. Effectiveness of phosphorus-containing flame retardants in textile back-coating formulations. Polym Int 49(10):1079–1091

Hribernik S, Smole MS, Kleinschek KS, Bele M, Jamnik J, Gaberscek M (2007) Flame retardant activity of SiO2-coated regenerated cellulose fibres. Polym Degrad Stab 92(11):1957–1965. https://doi.org/10.1016/j.polymdegradstab.2007.08.010

Hull TR, Law RJ, Bergman Å (2014) Environmental drivers for replacement of halogenated flame retardants. In Papaspyrides CD, Kiliaris P (eds) Polymer green flame retardants. Elsevier, pp 119–179. https://doi.org/10.1016/B978-0-444-53808-6.00004-4

Imam SH, Bilbao-Sainz C, Chiou B-S, Glenn GM, Orts WJ (2013) Biobased adhesives, gums, emulsions, and binders: current trends and future prospects. J Adhes Sci Technol 27(18–19):1972–1997

International Organization for Standardization (2017) Fire safety—vocabulary, ISO 13943. ISO Standards Catalogue

Islam M, van de Ven T (2021) Cotton-based flame-retardant textiles: a review. BioResources 16(2):4354–4381

Jimenez M, Duquesne S, Bourbigot S (2006) Intumescent fire protective coating: toward a better understanding of their mechanism of action. Thermochim Acta 449(1–2):16–26. https://doi.org/10.1016/j.tca.2006.07.008

Jimenez M, Guin T, Bellayer S, Dupretz R, Bourbigot S, Grunlan JC (2016) Microintumescent mechanism of flame-retardant water-based chitosan–ammonium polyphosphate multilayer nanocoating on cotton fabric. J Appl Polym Sci 133(32)

Kandola BK (2001) Nanocomposites. In: Horrocks AR, Price D (eds) Fire retardant materials. Woodhead Publishing, pp 204–2019

Kandola BK (2009) Flame retardancy design for textiles. In: Wilkie CA, Morgan AB (eds) Fire retardancy of polymeric materials. Taylor & Francis and CRC Press

Kandola BK, Horrocks AR (1999) Complex char formation in flame-retarded fiber/intumescent combinations: physical and chemical nature of char1. Text Res J 69(5):374–381

Kandola BK, Horrocks AR (2000) Complex char formation in flame-retarded fibre-intumescent combinations-IV. Mass loss and thermal barrier properties. Fire Mater 24(6):265–275

Kandola BK, Horrocks AR, Price D, Coleman GV (1996) Flame-retardant treatments of cellulose and their influence on the mechanism of cellulose pyrolysis. J Macromol Sci Part C 36(4):721–794. https://doi.org/10.1080/15321799608014859

Kay M, Price AF, Lavery I (1979) Review of intumescent materials, with emphasis on melamine formulations. J Fire Retard Chem 6(2):69–91

Kilinc M (2014) Silicon based flame retardants. In Morgan AB (ed) Non-halogenated flame retardant handbook. Wiley Online Library, pp 169–199. https://doi.org/10.1002/9781118939239.ch5

Kim SJ, Jang J (2017) Synergistic UV-curable flame-retardant finish of cotton using comonomers of vinylphosphonic acid and acrylamide. Fibers Polym 18:2328–2333

Klatt M (2014) Nitrogen-based flame retardants. In: Morgan AB (ed) Non-halogenated flame retardant handbook. Wiley Online Library, pp 143–168. https://doi.org/10.1002/9781118939239.ch4

Kovačević Z, Flinčec Grgac S, Bischof S (2021) Progress in biodegradable flame retardant nano-biocomposites. Polymers 13(5):741

Kozłowski RM, Muzyczek M (2020) Improving the flame retardancy of natural fibres. In: Handbook of natural fibres. Woodhead Publishing, pp 355–391

Kozlowski R, Wesolek D, Wladyka-Przybylak M, Duquesne S, Vannier A, Bourbigot S, Delobel R (2007) Intumescent flame-retardant treatments for flexible barriers. In: Duquesne S, Magniez C, Camino G (eds) Multifunctional barriers for flexible structure. Springer Nature, pp 39–61

Kroenke WJ (1986) Low-melting sulphate glasses and glass-ceramics, and their utility as fire and smoke retarder additives for poly (vinyl chloride). J Mater Sci 21(4):1123–1133

Kundu CK, Li Z, Song L, Hu Y (2020) An overview of fire retardant treatments for synthetic textiles: from traditional approaches to recent applications. Eur Polymer J 137:109911. https://doi.org/10.1016/j.eurpolymj.2020.109911

Laoutid F, Bonnaud L, Alexandre M, Lopez-Cuesta JM, Dubois P (2009) New prospects in flame retardant polymer materials: from fundamentals to nanocomposites. Mater Sci Eng: R: Reports 63(3):100–125. https://doi.org/10.1016/j.mser.2008.09.002

Laufer G, Kirkland C, Cain AA, Grunlan JC (2012) Clay-Chitosan nanobrick walls: completely renewable gas barrier and flame-retardant nanocoatings. ACS Appl Mater Interfaces 4(3):1643–1649. https://doi.org/10.1021/am2017915

Lawler TE, Drews MJ, Barker RH (1985) Pyrolysis and combustion of cellulose. VIII. Thermally initiated reactions of phosphonomethyl amide flame retardants. J Appl Polym Sci 30(5):2263–2277. https://doi.org/10.1002/app.1985.070300537

Lazar ST, Kolibaba TJ, Grunlan JC (2020) Flame-retardant surface treatments. Nat Rev Mater 1–17

Le Bras M, Bourbigot S, Camino G, Delobel R (eds) (1998) Fire retardancy of polymers: the use of intumescence, vol 224. The Royal Society of Chemistry

Levchik S (2014) Phosphorus-based FRs. In: Morgan AB (ed) Non-halogenated flame retardant handbook. Wiley Online Library, pp 17–74. https://doi.org/10.1002/9781118939239.ch2

Levchik SV (2007) Introduction to flame retardancy and polymer flammability. In: Morgan AB, Wilkie CA (eds) Flame retardant polymer nanocomposites, vol 1. Wiley, pp 1–29

Levchik SV, Weil ED (2006) A review of recent progress in phosphorus-based flame retardants. J Fire Sci 24(5):345–364. https://doi.org/10.1177/0734904106068426

Lewin M (1984) Flame Retardance of Fabrics. In: Lewin M, Sello SB (eds) Handbook of fiber science and technology volume II: chemical processing of fibers and fabrics, functional finishes part B. Marcel Dekker Inc., pp 1–142

Lewin M (2005) Unsolved problems and unanswered questions in flame retardance of polymers. Polym Degrad Stab 88(1):13–19. https://doi.org/10.1016/j.polymdegradstab.2003.12.011

Lewin M (2018) Flame retardance of fabrics. In: Handbook of fiber science and technology: chemical processing of fibers and fabrics. Routledge, pp 1–141

Lewin M, Weil E (2001) Mechanisms and modes of action in flame retardancy. In: Richard Horrocks A, Price D (eds) Fire retardant materials. Woodhead Publishing and CRC Press, pp 31–68

Lewin M, Sello SB (2012) Technology and test methods of flameproofing of cellulosics. In: Lewin M, Atlas SM, Pearce EM (eds) Flame-retardant polymeric materials. Springer Nature, pp 19–136

Liu W, Chen L, Wang Y-Z (2012) A novel phosphorus-containing flame retardant for the formaldehyde-free treatment of cotton fabrics. Polym Degrad Stab 97(12):2487–2491

Liu Y, Wang Q-Q, Jiang Z-M, Zhang C-J, Li Z-F, Chen H-Q, Zhu P (2018) Effect of chitosan on the fire retardancy and thermal degradation properties of coated cotton fabrics with sodium phytate and APTES by LBL assembly. J Anal Appl Pyrol 135:289–298

Lu SY, Hamerton I (2002) Recent developments in the chemistry of halogen-free flame retardant polymers. Prog Polym Sci 27(8):1661–1712. https://doi.org/10.1016/S0079-6700(02)00018-7

Lyon RE (1998) Pyrolysis kinetics of char forming polymers. Polym Degrad Stab 61(2):201–210

Malucelli G (2016) Surface-engineered fire protective coatings for fabrics through sol-gel and layer-by-layer methods: an overview. Coatings 6(3):33. https://doi.org/10.3390/coatings6030033

Malucelli G (2019) Biomacromolecules and bio-sourced products for the design of flame retarded fabrics: current state of the art and future perspectives. Molecules 24(20):3774. https://doi.org/10.3390/molecules24203774

Malucelli G, Carosio F, Alongi J, Fina A, Frache A, Camino G (2014) Materials engineering for surface-confined flame retardancy. Mater Sci Eng R Reports 84:1–20. https://doi.org/10.1016/j.mser.2014.08.001

Morgan A, Gilman J (2013) An overview of flame retardancy of polymeric materials: application, technology, and future directions. Fire Mater 37. https://doi.org/10.1002/fam.2128

Morgan AB, Wilkie CA (2009) An introduction to polymeric flame retardancy, its role in materials science, and the current state of the field. In Wilkie CA, Morgan AB (eds) Fire retardancy of polymeric materials, 2nd edn.. Taylor & Francis and CRC Press, pp 1–14

Nair GP (2000) Flammability in textiles and routes to flame retardant textiles—II. Important factors in fabric flammability studies - decomposition and burning of textile fibers; complex nature of fabric flammability; variety and multiplicity of flammability and burni. Colourage 39–40:42–44

National Institute of Environmental Health Sciences (n.d.) Flame retardants. https://www.niehs.nih.gov/health/materials/flame_retardants_508.pdf

Neisius M, Stelzig T, Liang S, Gaan S (2014) Flame retardant finishes for textiles. In: Paul R (ed) Functional finishes for textiles: Improving comfort, performance and protection. Woodhead Publishing, pp 429–461

Nodera A, Kanai T (2006) Flame retardancy of a polycarbonate–polydimethylsiloxane block copolymer: the effect of the dimethylsiloxane block size. J Appl Polym Sci 100(1):565–575. https://doi.org/10.1002/app.23331

Olsen JW, Bechle CW (1948) Anaconda wire and cable. U.S. Patent 2,442,706

Oulton DP (1995) Environmental impacts of the textiles industry. In: Carr CM (ed) Chemistry of the textile industry. Springer Science and Business Media, pp 333–354

Ozcan G, Dayioglu H, Candan C (2003) Effect of gray fabric properties on flame resistance of knitted fabric. Text Res J 73(10):883–891. https://doi.org/10.1177/004051750307301006

Pan H, Wang W, Pan Y, Song L, Hu Y, Liew KM (2015) Formation of self-extinguishing flame retardant biobased coating on cotton fabrics via Layer-by-Layer assembly of chitin derivatives. Carbohyd Polym 115:516–524. https://doi.org/10.1016/j.carbpol.2014.08.084

Pelzl B, Wolf R, Kaul BL (2018) Plastics additives. In: Ullmann's encyclopedia of industrial chemistry. Wiley-VCH Verlag GmbH & Co. KGaA, Weinheim, pp 1–57. https://doi.org/10.1002/14356007.a20_459.pub2

Price D, Horrocks AR (2010) Polymer degradation and the matching of FR chemistry to degradation. In Wilkie CA, Morgan AB (eds) Fire retardancy of polymeric materials, 2nd edn. Taylor & Francis and CRC Press, pp 15–42

Price D, Horrocks AR, Akalin M, Faroq AA (1997) Influence of flame retardants on the mechanism of pyrolysis of cotton (cellulose) fabrics in air. J Anal Appl Pyrol 40–41:511–524. https://doi.org/10.1016/S0165-2370(97)00043-0

Puri RG, Khanna AS (2017) Intumescent coatings: a review on recent progress. J Coat Technol Res 14(1):1–20

Reeves WA, Guthrie JD (1956) Intermediate for flame-resistant polymers-reactions of tetrakis (hydroxymethyl) phosphonium chloride. Ind Eng Chem 48(1):64–67

Roberts DL, Hall ME, Horrocks AR (1992) Environmental aspects of flame-retardant textiles-an overview. Rev Prog Color Relat Top 22(1):48–57. https://doi.org/10.1111/j.1478-4408.1992.tb00089.x

Samani P, van der Meer Y (2020) Life cycle assessment (LCA) studies on flame retardants: a systematic review. J Clean Prod 274:123259

Samanta KK, Basak S, Chattopadhyay SK (2015) Sustainable flame-retardant finishing of textiles: advancement in technology. In: Muthu SS (ed) Handbook of sustainable apparel production. Taylor & Francis and CRC Press, pp 66–91

Schindler WD, Hauser PJ (2004) Introduction to chemical finishing. In: Schindler WD, Hauser PJ (eds) Chemical finishing of textiles. Woodhead Publishing and CRC Press, pp 1–6

Segev O, Kushmaro A, Brenner A (2009) Environmental impact of flame retardants (persistence and biodegradability). Int J Environ Res Public Health 6(2):478–491

Šehić A, Tavčer PF, Simončič B (2016) Flame retardants and environmental issues—Ognjevarna sredstva in okoljski vidiki. Environment 3:20–26

Sheldon RA (2014) Green and sustainable manufacture of chemicals from biomass: state of the art. Green Chem 16(3):950–963

Soliman MY, Hassabo AG (2021) Environmentally friendly inorganic materials for anti-flammable cotton fabrics. J Text Color Polym Sci 18(2):97–110

Sonnier R, Vahabi H, Ferry L, Lopez-Cuesta J-M (2012) Pyrolysis-combustion flow calorimetry: a powerful tool to evaluate the flame retardancy of polymers. Fire Polym VI: New Adv Flame Retard Chem Sci 361–390. https://doi.org/10.1021/bk-2012-1118.ch024

Sonnier R, Taguet A, Ferry L, Lopez-Cuesta JM (2018) Biobased flame retardants. In: Towards bio-based flame retardant polymers. Springer Nature, pp 33–72

Stepniczka H, Dipietro J (1971) Flammability characteristics of cotton and polyester fibers. J Appl Polym Sci 15(9):2149–2172. https://doi.org/10.1002/app.1971.070150909

Sutker BJ (2000) Flame retardants. In: Ullmann's encyclopedia of industrial chemistry. Wiley-VCH Verlag GmbH & Co. KGaA, Weinheim

Tendero C, Tixier C, Tristant P, Desmaison J, Leprince P (2006) Atmospheric pressure plasmas: a review. Spectrochim Acta Part B 61(1):2–30

Tesoro GC (1978) Chemical modification of polymers with flame-retardant compounds. J Polym Sci: Macromol Rev 13(1):283–353

Tomasino C (1992) Flame retardant finishes. In: Chemistry and technology of fabric preparation and finishing. Department of Textile Engineering, Chemistry & Science College of Textiles North Carolina State University, Raleigh, North Carolina, USA, pp 189–208

Troitzsch J, Antonatus E (2021) Plastics flammability handbook: principles, regulations, testing, and approval. Carl Hanser Verlag GmbH Co KG.

Tuck CO, Pérez E, Horváth IT, Sheldon RA, Poliakoff M (2012) Valorization of biomass: deriving more value from waste. Science 337(6095):695–699

Tursi A (2019) A review on biomass: importance, chemistry, classification, and conversion. Biofuel Res J 6(2):962–979

Vahabi H, Laoutid F, Mehrpouya M, Saeb MR, Dubois P (2021) Flame retardant polymer materials: an update and the future for 3D printing developments. Mater Sci Eng R Rep 144:100604. https://doi.org/10.1016/j.mser.2020.100604

Van Krevelen DW (1975) Some basic aspects of flame resistance of polymeric materials. Polymer 16(8):615–620

Vandersall HL (1971) Intumescent coating system, their development and chemistry. J Fire Flamm 2:97–140. https://cir.nii.ac.jp/crid/1572543024441086336

Vasiljević J, Hadžić S, Jerman I, Černe L, Tomšič B, Medved J, Godec M, Orel B, Simončič B (2013) Study of flame-retardant finishing of cellulose fibres: organic–inorganic hybrid versus conventional organophosphonate. Polym Degrad Stab 98(12):2602–2608

Vassilev SV, Baxter D, Andersen LK, Vassileva CG (2010) An overview of the chemical composition of biomass. Fuel 89(5):913–933. https://doi.org/10.1016/j.fuel.2009.10.022

Villamil Watson DA, Schiraldi DA (2020) Biomolecules as flame retardant additives for polymers: a review. Polymers 12(4):849. https://doi.org/10.3390/polym12040849

Vladimirtseva EL, Smirnova SV, Odintsova OI, Vinokurov MV (2016) Flame-retardant finishing of different textiles. Russ J Gen Chem 86(2):460–469

Wakelyn PJ (2008) Environmentally friendly flame resistant textiles. In: Advances in fire retardant materials. Woodhead Publishing and CRC Press, pp 188–212

Wang L-H, Ren Y-L, Wang X-L, Zhao J-Y, Zhang Y, Zeng Q, Gu Y-T (2016) Fire retardant viscose fiber fabric produced by graft polymerization of phosphorus and nitrogen-containing monomer. Cellulose 23:2689–2700

Wang MY, Horrocks AR, Horrocks S, Hall ME, Pearson JS, Clegg S (2000) Flame retardant textile back-coatings. Part 1: antimony-halogen system interactions and the effect of replacement by phosphorus-containing agents. J Fire Sci 18(4):265–294

Watanabe I, Sakai S (2003) Environmental release and behavior of brominated flame retardants. Environ Int 29(6):665–682. https://doi.org/10.1016/S0160-4120(03)00123-5

Weil ED (2011) Fire-protective and flame-retardant coatings—a state-of-the-art review. J Fire Sci 29(3):259–296

Weil ED, Levchik SV (2008) Flame retardants in commercial use or development for textiles. J Fire Sci 26(3):243–281

Wesolek D, Gieparda W (2014) Single-and multiwalled carbon nanotubes with phosphorus based flame retardants for textiles. J Nanomater 2014:15

Whewell CS (1970) The finishing of textile fabrics. Text Prog 2(3):1–72. https://doi.org/10.1080/00405167008688970

Wu W, Yang CQ (2006) Comparison of different reactive organophosphorus flame retardant agents for cotton: part I. The bonding of the flame retardant agents to cotton. Polym Degrad Stab 91(11):2541–2548. https://doi.org/10.1016/j.polymdegradstab.2006.05.010

Wyld O (1735) Making or preparing of paper linen canvass and such like substances which will neither flame nor retain fire and which have also a property in it of resisting moisture and damps. British Patent 551:17

Xu F, Zhong L, Xu Y, Zhang C, Zhang F, Zhang G (2019) Highly efficient flame-retardant and soft cotton fabric prepared by a novel reactive flame retardant. Cellulose 26:4225–4240

Xu H, Wang Z, Zhang S, Guo M, Chen M, Shi L (2018) Research progress on toxicity effects of organophosphate flame retardants. Asian J Ecotoxicol 3:19–30

Xu L, Wang W, Yu D (2017) Durable flame retardant finishing of cotton fabrics with halogen-free organophosphonate by UV photoinitiated thiol-ene click chemistry. Carbohyd Polym 172:275–283

Yan H, Zhao L, Fang Z, Wang H (2017) Construction of multilayer coatings for flame retardancy of ramie fabric using layer-by-layer assembly. J Appl Polym Sci 134(48):45556

Yang CQ (2013) Flame resistant cotton. In: Handbook of fire resistant textiles. Woodhead Publishing, pp 177–220

Yang CQ, Chen Q (2019) Flame retardant finishing of the polyester/cotton blend fabric using a cross-linkable hydroxy-functional organophosphorus oligomer. Fire Mater 43(3):283–293. https://doi.org/10.1002/fam.2699

Yang CQ, He Q, Lyon RE, Hu Y (2010) Investigation of the flammability of different textile fabrics using micro-scale combustion calorimetry. Polym Degrad Stab 95(2):108–115. https://doi.org/10.1016/j.polymdegradstab.2009.11.047

Yang CQ, Wu W (2003) Combination of a hydroxy-functional organophosphorus oligomer and a multifunctional carboxylic acid as a flame retardant finishing system for cotton: part II. Formation of calcium salt during laundering. Fire Mater 27(5):239–251

Yang H, Yang CQ (2008) Flame retardant finishing of nylon/cotton blend fabrics using a hydroxy-functional organophosphorus oligomer. Ind Eng Chem Res 47(7):2160–2165

Yuan H, Xing W, Zhang P, Song L, Hu Y (2012) Functionalization of cotton with UV-cured flame retardant coatings. Ind Eng Chem Res 51(15):5394–5401